Oxidative Medicine and Cellular Longevity

Oxidative Stress, Senescence, and Nutrition in Age-Related Diseases

Lead Guest Editor: Stefania D'Adamo
Guest Editors: Cristina Cosentino and Cecile Jacovetti

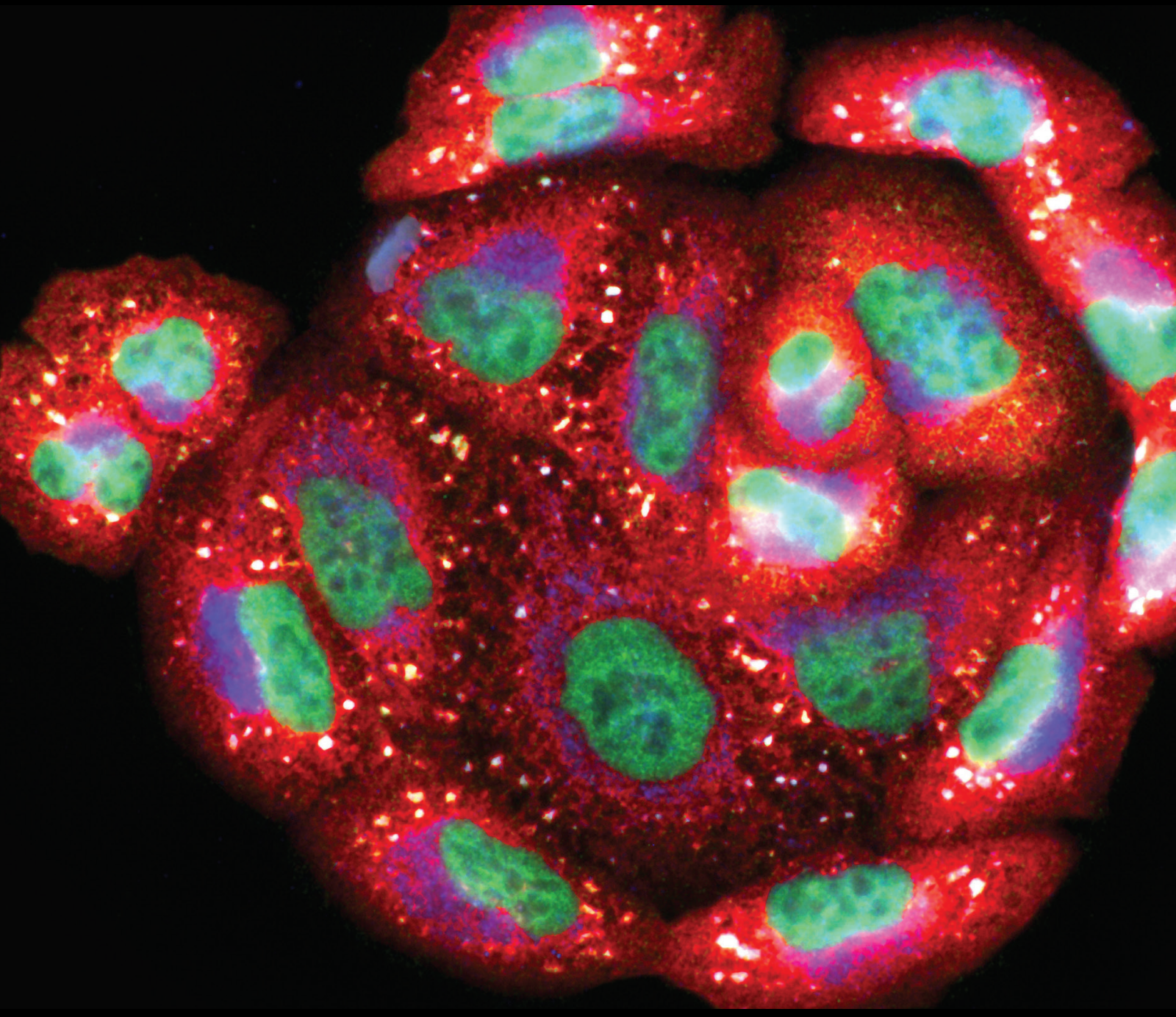

Oxidative Stress, Senescence, and Nutrition in Age-Related Diseases

Oxidative Medicine and Cellular Longevity

Oxidative Stress, Senescence, and Nutrition in Age-Related Diseases

Lead Guest Editor: Stefania D'Adamo
Guest Editors: Cristina Cosentino and Cecile Jacovetti

Contents

Hindawi
Oxidative Medicine and Cellular Longevity
Volume 2022, Article ID 1835900, 24 pages
https://doi.org/10.1155/2022/1835900

Research Article

USP7 Attenuates Endoplasmic Reticulum Stress and NF-κB Signaling to Modulate Chondrocyte Proliferation, Apoptosis, and Inflammatory Response under Inflammation

Xiaofei Dong,[1,2] Chang Yang,[1] Yao Luo,[1] Wei Dong,[1] Xiaoxiao Xu,[1] Yanru Wu,[1] and Jiawei Wang[1]

[1]*The State Key Laboratory Breeding Base of Basic Science of Stomatology (Hubei-MOST) & Key Laboratory of Oral Biomedicine Ministry of Education, School & Hospital of Stomatology, Wuhan University, Wuhan, Hubei 430079, China*
[2]*Nanjing Stomatological Hospital, Medical School of Nanjing University, Nanjing, Jiangsu 210000, China*

Correspondence should be addressed to Jiawei Wang; wb000238@whu.edu.cn

Received 2 November 2021; Revised 5 January 2022; Accepted 9 March 2022; Published 6 April 2022

Academic Editor: Stefania D'Adamo

The purpose of this research was to observe the functions and mechanisms of ubiquitin-specific peptidase 7 (USP7) on chondrocytes under tumor necrosis factor alpha- (TNF-α-) induced inflammation. Knee osteoarthritis (OA) models of mice were constructed by anterior cruciate ligament transection. The knee joint of mice was observed by histological staining, and the expression of USP7 was measured by immunohistochemistry staining. After knocking down or inhibiting USP7, chondrocyte proliferation was measured by histological staining and the CCK-8 assay; apoptosis was measured by western blot, flow cytometry, Caspase-3 activity, and TUNEL staining; and inflammatory response was measured by qRT-PCR and ELISA. The 4-phenylbutyric acid (4-PBA), siRNA of CHOP (si-CHOP), and QNZ were used to verify the signaling pathways. It was found that USP7 was reduced in the knee joint cartilage of OA mice. The knockdown of USP7 or its inhibitor decreased chondrocyte proliferation and accelerated apoptosis and inflammatory response under inflammation. The USP7 inhibitor exacerbated cartilage destruction in mice with OA. The knockdown of USP7 or its inhibitor activated the BiP-eIF2α-ATF4-CHOP signaling of endoplasmic reticulum stress (ERS) and NF-κB/p65 signaling. 4-PBA, si-CHOP, and QNZ partly reversed chondrocyte proliferation, apoptosis, and inflammatory response caused by USP7 knockdown. In conclusion, through inhibiting the BiP-eIF2α-ATF4-CHOP signaling of ERS and NF-κB/p65 signaling, USP7 promotes chondrocyte proliferation and suppresses the apoptosis and inflammatory response under TNF-α-induced inflammation.

1. Introduction

Deubiquitinases play essential roles in various diseases by modulating the posttranslational modification of related proteins. There are six families of deubiquitinases, and the largest one is the ubiquitin-specific peptidase (USP) family. Among the nearly 60 members of the USP family, ubiquitin-specific peptidase 7 (USP7) is researched extensively [1]. Increasing researches have confirmed that USP7 regulates multifaceted key protein deubiquitination to affect cell differentiation, tissue development, and disease occurrence [2, 3].

As a chronic degenerative disease of articular cartilage, osteoarthritis (OA) is commonly found with pain and dysfunction of joints and is increasing in incidence worldwide [4]. Although OA is often considered as a noninflammatory arthropathy, increased secretion of inflammatory cytokines has been observed in many patients and animal models [5]. Increasing evidence has found that proinflammatory cytokines secreted by the synovium and chondrocytes link closely to the cartilage destruction, and inflammatory pathways are vital in the progression of OA [6, 7].

Chondrocytes are the target of the inflammatory stimulation since they are the principal cells in the articular

cartilage. The inflammation from OA induces chondrocyte apoptosis, which accelerates the progression of OA [8, 9]. It was found that hypoxia-inducible factor-1 alpha (HIF-1α) stabilization inhibited chondrocyte apoptosis and alleviated cartilage degradation in a surgical OA model [10]. Previous research has indicated that USP7 inhibits HIF-1α ubiquitinatioin [11]. Moreover, the activation of inflammasome plays an important role during the progression of OA, and USP7 was reported to regulate the inflammasome activation in macrophages [12, 13]. Therefore, it is reasonable to suggest that USP7 may regulate chondrocytes under inflammation, but how USP7 exerts its effect is still unknown. A previous study has found that USP7 modulated nuclear factor-kappa B (NF-κB) signaling [14]. The aberrant activation of NF-κB signaling was often observed in OA, and the inhibition of NF-κB signaling suppressed chondrocyte apoptosis and delayed the progression of OA [15–17]. Collectively, USP7 may modulate NF-κB signaling and be an important adjustor of chondrocytes under inflammation.

On the other hand, inflammation-induced endoplasmic reticulum stress (ERS) acts a key role in OA and is positively related to the cartilage degradation [18]. PERK is one of three ERS sensors involved in the BiP-PERK-eIF2α-ATF4-CHOP signaling of ERS [19]. Under pathological conditions, BiP binds to misfolded proteins and dissociates with PERK, which further promotes eIF2α phosphorylation and the subsequent high expression of ATF4 and CHOP [20]. Curcumin attenuated OA via inhibiting PERK-eIF2α-CHOP signaling in rats [21]. Cartilage-specific autophagy promoted PERK-ATF4-CHOP signaling to hinder the growth plate development in vivo and increase chondrocyte apoptosis and decrease chondrocyte proliferation in vitro [22]. In addition, Sirtuin-1 (SIRT1) has been reported to promote the chondrogenesis of growth plate by inhibiting the PERK-eIF2α-CHOP pathway, and USP7 was found to stabilize SIRT1 [23, 24]. Therefore, it was hypothesized that USP7 might modulate chondrocytes under inflammation through BiP-eIF2α-ATF4-CHOP signaling.

To confirm this hypothesis, the expression of USP7 in the knee articular cartilage of OA mice, caused by the anterior cruciate ligament transection (ACLT), was measured. Functions of USP7 on chondrocyte proliferation, apoptosis, and inflammatory response both in vitro and in vivo were tested, and the underlying mechanisms were explored.

2. Materials and Methods

2.1. Construction of an OA Mouse Model. The animal study was approved by the Institutional Animal Care and Use Committee of Huazhong Agricultural University (HZAUMO-2020-0014). Male C57BL/6 mice were housed in specific pathogen-free facilities and randomly divided into sham and OA groups. Knee OA models were constructed by ACLT as previously described [25]. Briefly, mice were anesthetized with pentobarbital sodium (70 mg/kg) by intraperitoneal injection. Mice in the OA group received a parapatellar skin incision at the medial side of the right knee joint, the dislocation of the patella, and the ACLT. Mice in the sham group received the joint incision without ACLT.

2.2. Haematoxylin-Eosin (HE) Staining, Safranin O-Fast Green Staining, and Immunohistochemical Analysis. Eight weeks later, the knee cartilage tissues were fixed in 4% paraformaldehyde, decalcified in 10% EDTA for 4 weeks, and then sectioned (5 μm). The sections were stained with HE and Safranin O-Fast Green and incubated with of USP7 (1 : 250, Bethyl, AL, USA). Density was measured by Image-Pro Plus software 6.0.

2.3. Cell Culture and Induction. ATDC5 cell line was obtained from the Type Culture Collection of the Chinese Academy of Sciences (Shanghai, China). Cells were firstly cultured in a growth medium and then in a chondrogenic-induced medium after 80-90% confluence as our previous study described [26]. Various concentrations of tumor necrosis factor alpha (TNF-α) (Novoprotein, Shanghai, China) were added. HBX41108 was from Toris (MN, USA). 4-Phenylbutyric acid (4-PBA) and QNZ were from MCE (NJ, USA).

2.4. Cell Transfection of Lentivirus. pLVX-USP7-nc, pLVX-USP7-sh1, and pLVX-USP7-sh2 plasmids were acquired from Miaoling Bioengineering (Wuhan, China). ATDC5 cells were transfected with the three collected lentiviral supernatants as our previous study described [26].

2.5. Alcian Blue Staining and Toluidine Blue Staining. Cells were stained by toluidine blue (Aspenbio, Wuhan, China) and alcian blue 8GX (Biosharp, Hefei, China) according to the manufacturer's instructions and observed under the microscope.

2.6. CCK-8 Cell Proliferation Assay. Cell proliferation was determined by CCK-8 staining (Dojindo Laboratories, Shanghai, China) according to the manufacturer's instructions.

2.7. Quantitative Real-Time Polymerase Chain Reaction (qRT-PCR). Total RNA was extracted with TRIzol Reagent (Kangwei, Beijing, China). cDNA was harvested with HiScript® III RT SuperMix for qPCR (+gDNA wiper) (Vazyme, Nanjing, China) and measured with ChamQ SYBR qPCR Master Mix (Vazyme, Nanjing, China) in QuantStudio™ 6 Flex Real-Time PCR System (Applied Biosystems, MA, USA). Primer sequences were present in Table 1. The relative mRNA expression was calculated with the $2^{-\Delta\Delta Ct}$ method by normalizing with glyceraldehyde 3-phosphate dehydrogenase (GAPDH).

2.8. Western Blot. Cells were lysed with RIPA lysis buffer (Beyotime, Shanghai, China) and phosphate protease inhibitor. Protein samples were harvested, boiled, separated with 12% sodium dodecyl sulphate-polyacrylamide gel electrophoresis, and transferred to polyvinylidene fluoride (PVDF) membranes. The PVDF membranes were blocked with 5% milk and incubated overnight at 4°C with primary antibodies against GAPDH (1 : 2000, ZSGBBIO, Beijing, China), USP7 (1 : 1000, HUABIO, Hangzhou, China), collagen type II alpha 1 chain (Col2a1, 1 : 1000, HUABIO, Hangzhou, China), sex-determining region Y-box 9 (Sox9, 1 : 2000,

Table 1: Primer sequences for qRT-PCR.

Genes	Forward primer sequence (5′–3′)	Reverse primer sequence (5′–3′)
GAPDH	TTGCAGTGGCAAAGTGGAGA	GATGGGCTTCCCGTTGATGA
USP7	GCCCTTTGGCCTGTAAATGAG	AGTCTGAGCAACCCCAACAAA
Sox9	TGAAGAACGGACAAGCGGAG	CTTGCACGTCGGTTTTGGG
Col2a1	CCCGCCTTCCCATTATTGAC	GGGAGGACGGTTGGGTATCA
IL-6	AAGACAAAGCCAGAGTCCTTC	TCTGTGACTCCAGCTTATCTGTTA
COX	TGCAGAATTGAAAGCCCTCT	CCCCAAAGATAGCATCTGGA
NOS2	CTCACTGGGACAGCACAGAA	TGGTCAAACTCTTGGGGTTC
MMP13	TGTTTGCAGAGCACTACTTGAA	CAGTCACCTCTAAGCCAAAGAAA
BiP	ACTTGGGGACCACCTATTCCT	GTTGCCCTGATCGTTGGCTA
CHOP	GCGACAGAGCCAGAATAACAGC	TTCTGCTTTCAGGTGTGGTGGT

Abcam, Cambridge, UK), Cleaved Caspase-3 (1 : 1000, CST, MA, USA), Bcl-2 (1 : 1000, ABclonal, Wuhan, China), Bcl-2-associated X (Bax, 1 : 1000, ABclonal, Wuhan, China), eIF2α (1 : 1000, ABclonal, Wuhan, China), eIF2α phosphorylation (p-eIF2α, 1 : 1000, ABclonal, Wuhan, China), activating transcription factor 4 (ATF4, 1 : 1000, HUABIO, Hangzhou, China), CHOP (1 : 300, Santa Cruz, CA, USA), p65 (1 : 1000, CST, MA, USA), p65 phosphorylation (p-p65, 1 : 1000, CST, MA, USA), and proliferating cell nuclear antigen (PCNA, 1 : 1000, HUABIO, Hangzhou, China). Then, they were incubated in horseradish peroxidase-conjugated secondary antibodies (1 : 10000, Biosharp, Hefei, China) and visualized with an electrochemiluminescence reagent.

2.9. Immunofluorescence Staining. Cells were harvested and incubated at 4°C overnight with anti-p65 antibodies (1 : 400, CST, MA, USA). Samples were incubated with secondary antibodies conjugated to FITC (ThermoFisher, MA, USA) and DAPI (Beyotime, Shanghai, China) and observed with a fluorescence microscope.

2.10. Flow Cytometry. Cell apoptosis was identified with Annexin V-FITC/PI or Annexin V-APC/PI apoptosis detection kits (KeyGEN BioTECH, Nanjing, China) according to the manufacturer's instructions and measured by a flow cytometry (Beckman Coulter, USA).

2.11. Transfection of Small Interfering RNA (siRNA). Cells were transfected with si-CHOP (forward primer 5′-AGCG GAAAGUGGCACAGCUTT-3′, reverse primer 5′-AGCU GUGCCACUUUCCGCUTT-3′) (GenePharma, Suzhou, China) using GP-transfect-Mate (GenePharma, Suzhou, China) and then cultured in the chondrogenic-induced medium and 20 ng/mL TNF-α for 48 hours.

2.12. Caspase-3 Activity. Caspase-3 activity was detected using the Caspase-3 colorimetric assay kit (KeyGEN BioTECH, Nanjing, China) according to the manufacturer's instructions.

2.13. Enzyme-Linked Immunosorbent Assay (ELISA). IL-6 in the ATDC5 cell supernatant was quantitated by the mouse IL-6 ELISA kit (Neobioscience, Shenzhen, China) according to the manufacturer's instructions.

2.14. TUNEL Staining. Cell apoptosis was measured using a TUNEL staining kit (Beyotime, Shanghai, China) according to the manufacturer's instructions and observed with a fluorescent microscope.

2.15. Statistical Analysis. All experiments were repeated three times independently. The data were presented as means ± standard deviations (SDs). Data were analyzed by Student's *t*-tests or one-way ANOVAs. $p < 0.05$ was considered statistically significant.

3. Results

3.1. Decreased Expression of USP7 in OA Mice after ACLT. Eight weeks after ACLT, all mice in both groups were alive, although those in the OA group showed symptoms of claudication. The HE staining showed that mice in the OA group had fewer chondrocytes, while the sham group had normal morphology (Figure 1(a)). Safranin O-Fast Green staining also showed decreased cartilage thickness and chondrocytes in the OA group (Figures 1(b) and 1(c)), suggesting that OA mouse models were successfully constructed.

Immunohistochemical staining showed that USP7 was mainly situated in the nuclei of the mouse knee joint chondrocytes, and USP7 was decreased in the OA group (Figures 1(d) and 1(e)).

3.2. Decreasing ATDC5 Cell Proliferation and Increasing Apoptosis and Inflammatory Response with Increasing TNF-α. To mimic OA in vitro, different concentrations of TNF-α were added into a chondrogenic-induced medium. Alcian blue and toluidine blue stainings showed that the staining intensities decreased with increasing TNF-α (Fig. S1A). ATDC5 cell proliferation was gradually slower with increasing TNF-α; however, there was no difference between 20 ng/mL and 40 ng/mL TNF-α by CCK-8 assay (Fig. S1B). Cartilage-specific markers, *Col2a1* and *Sox9* mRNA, also decreased with increasing TNF-α (Fig. S1C). Western blot revealed that increasing TNF-α downregulated Col2a1 protein but upregulated Cleaved Caspase-3 protein (Figs. S1D and E). Caspase-3 activity and the cell apoptosis rate were also upregulated with increasing TNF-α, with no difference between 20 ng/mL and 40 ng/mL TNF-α (Figs. S1F–H). Proinflammatory cytokines,

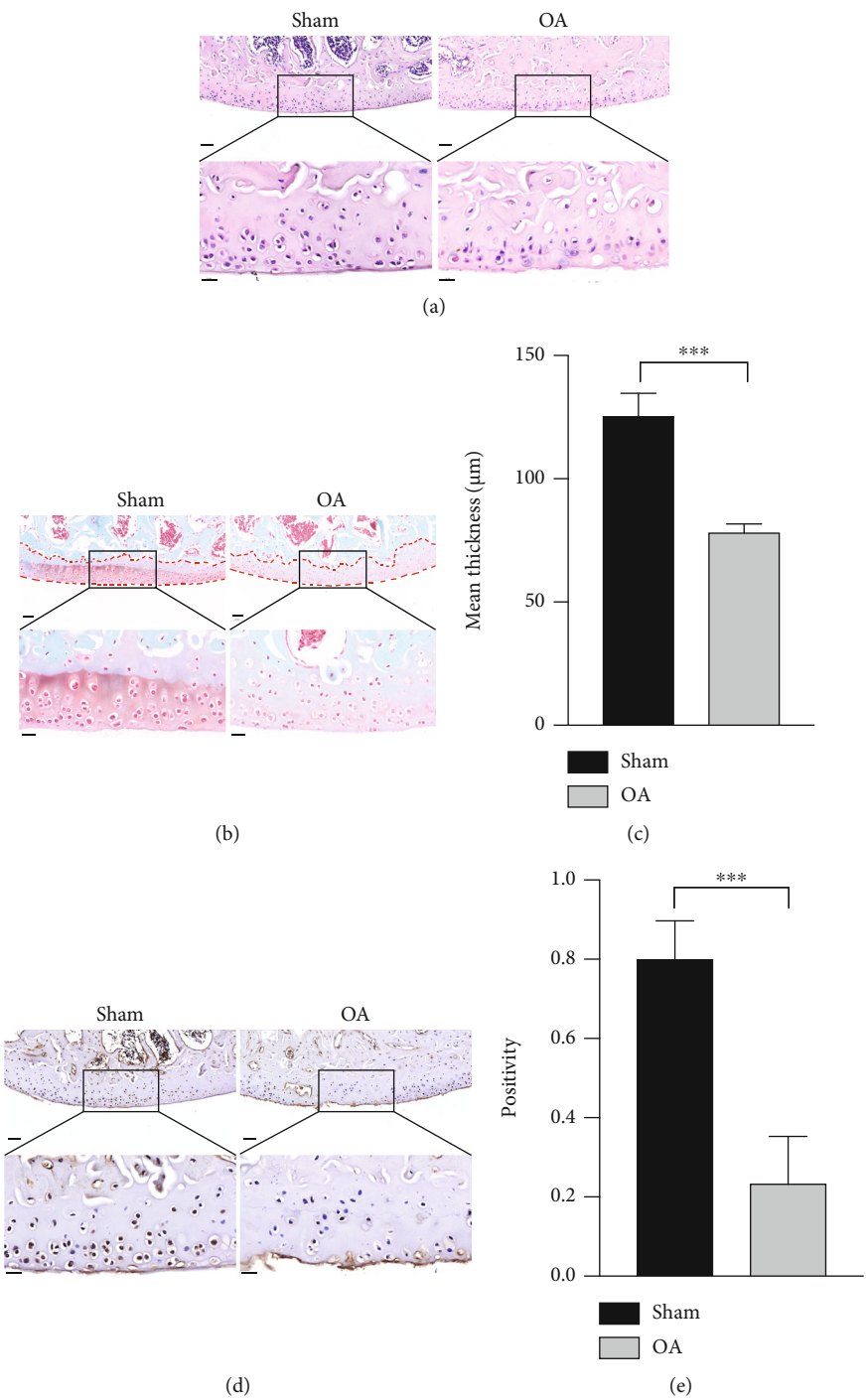

Figure 1: Decreased expression of USP7 in OA mice after ACLT. (a) HE staining of the mouse knee joint after ACLT in the sham and OA groups. (b) Safranin O-Fast Green staining of the mouse knee joint after ACLT in the sham and OA groups. The red dotted line indicates the cartilaginous region of the tibia. (c) Quantitative measurement of (b). (d) Immunohistochemistry staining of the mouse knee joint after ACLT in the sham and OA groups. (e) Quantitative measurement of (d). Scale bars of the upper panels = 50 μm and scale bars of the lower panels = 20 μm. $^{*}p < 0.05$, $^{**}p < 0.01$, $^{***}p < 0.001$, and $^{****}p < 0.0001$.

IL-6, *COX*, *NOS2*, and *MMP13* mRNA, had higher expression with increasing TNF-α (Fig. S1I). ELISA of IL-6 revealed the same result (Fig. S1J). Considering that 20 ng/mL and 40 ng/mL TNF-α showed no obvious differences on chondrocyte proliferation and apoptosis, 20 ng/mL TNF-α was selected to mimic OA in the following in vitro experiments.

3.3. USP7 Knockdown Inhibits ATDC5 Cell Proliferation and Enhances Apoptosis and Inflammatory Response under TNF-α-Induced Inflammation. The USP7 mRNA was reduced under 20 ng/mL TNF-α after 48 h chondrogenic induction (Figure 2(a)). USP7 was then knocked down by lentiviral transfection. Positive green fluorescent proteins (GFPs) of

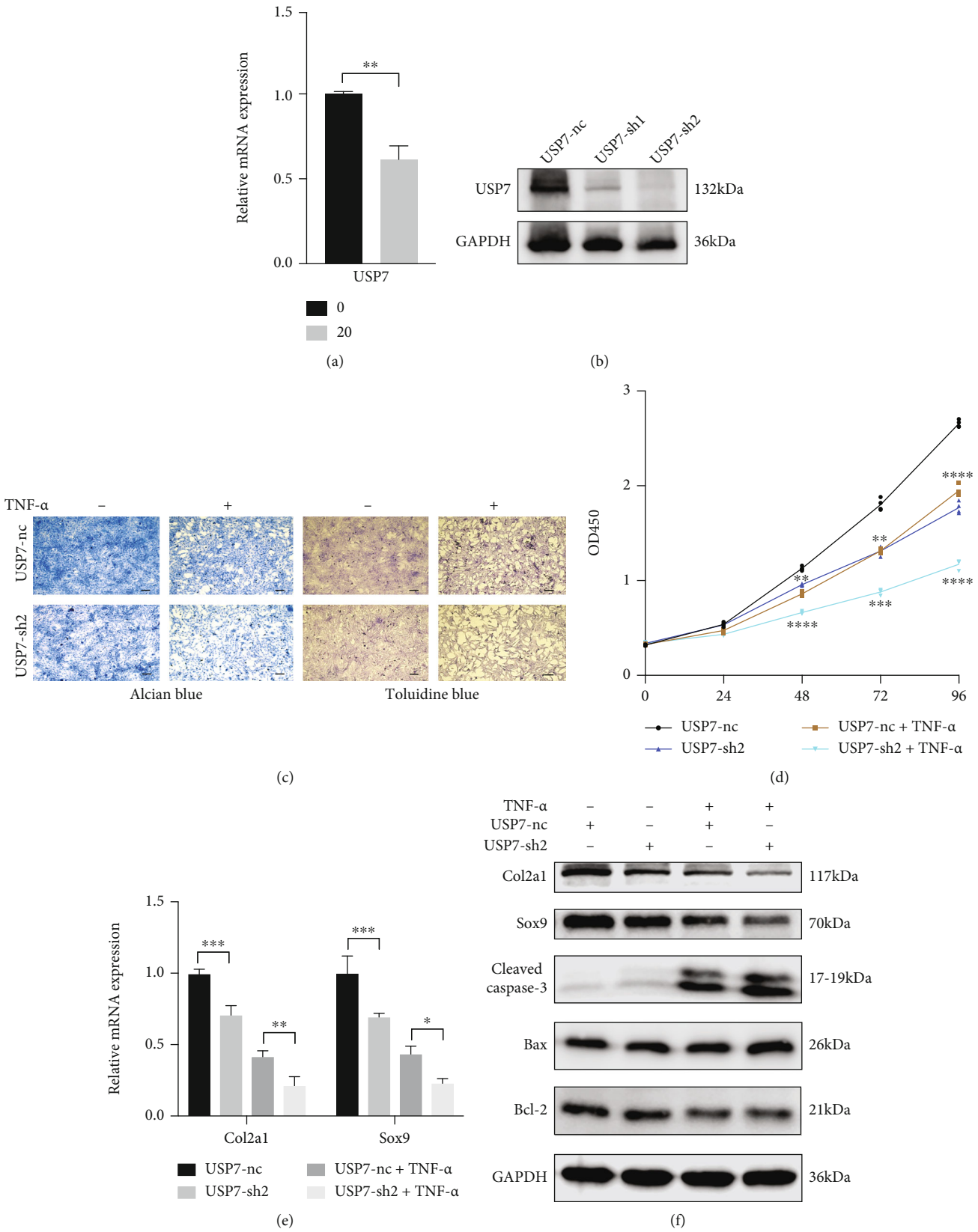

Figure 2: Continued.

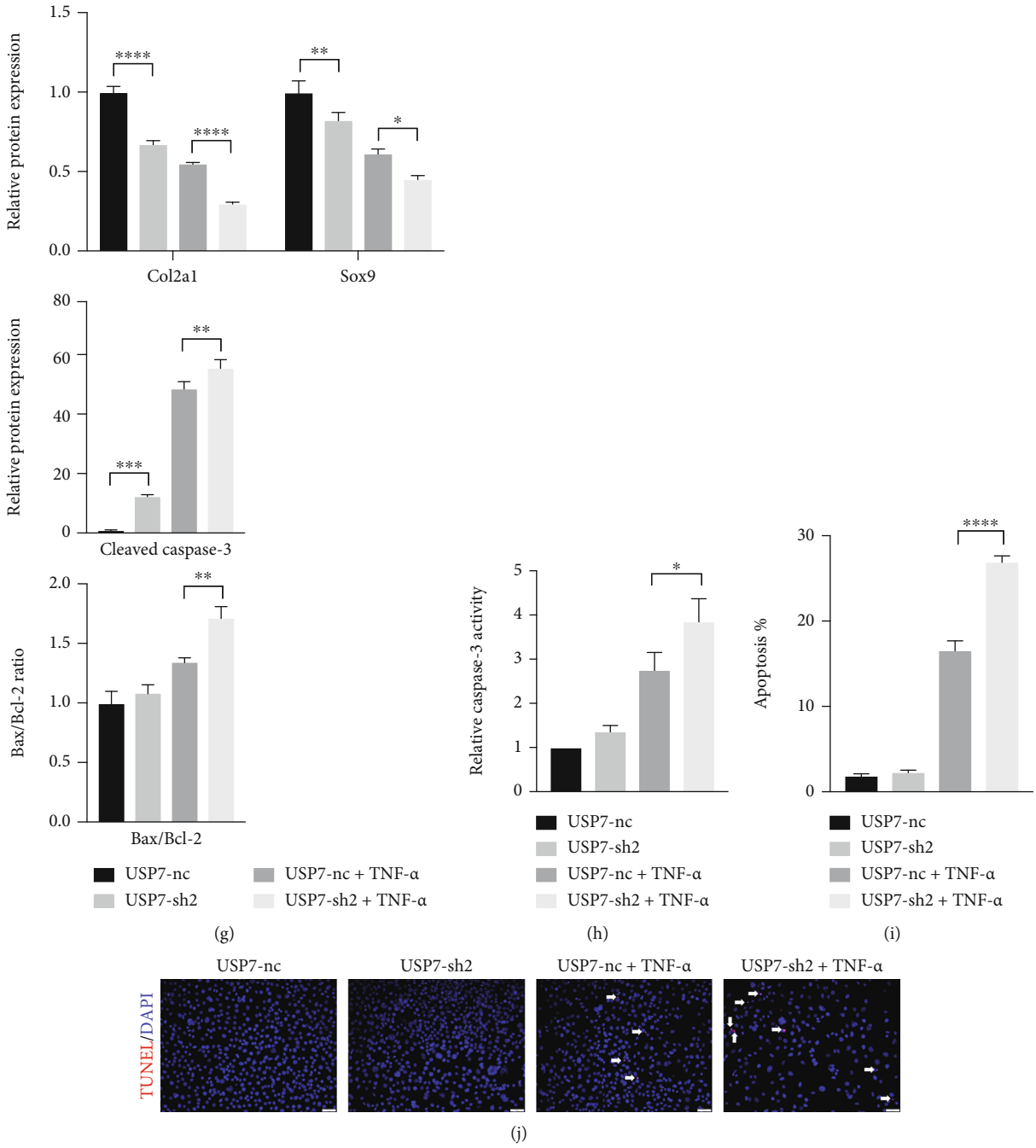

Figure 2: Continued.

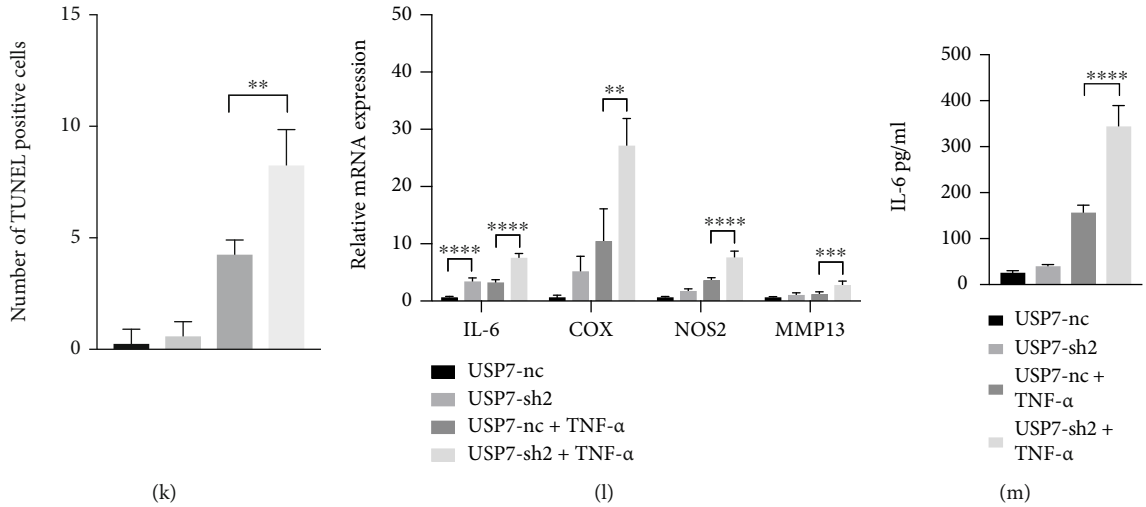

Figure 2: USP7 knockdown inhibits ATDC5 cell proliferation and increases apoptosis and inflammatory response after 48 h chondrogenic induction under TNF-α-induced inflammation. (a) Relative *USP7* mRNA expression under 20 ng/mL TNF-α. (b) Relative USP7 protein expression in USP7 knockdown and its control groups. (c) Alcian blue and toluidine blue staining in USP7 knockdown and its control groups under TNF-α-induced inflammation after 48 h chondrogenic induction. Scale bars = 100 μm. (d) Growth curves in USP7 knockdown and its control groups under TNF-α-induced inflammation after 48 h chondrogenic induction measured by CCK-8 assay. (e) Relative *Col2a1* and *Sox9* mRNA expression of in USP7 knockdown and its control groups under TNF-α stimulation after 48 h chondrogenic induction. (f) Col2a1, Sox9, Cleaved Caspase-3, Bax, and Bcl-2 protein expression of in USP7 knockdown and its control groups under TNF-α-induced inflammation after 48 h chondrogenic induction. (g) Quantitative measurement of (f). (h) Relative Caspase-3 activity in USP7 knockdown and its control groups under TNF-α-induced inflammation after 48 h chondrogenic induction. (i) Quantitative measurement of cell apoptosis measured by flow cytometry in the USP7-nc and USP7-sh2 groups under TNF-α-induced inflammation after 48 h chondrogenic induction. (j) TUNEL staining in USP7 knockdown and its control groups under TNF-α-induced inflammation after 48 h chondrogenic induction. White arrows indicated TUNEL-positive cells. Scale bars = 50 μm. (k) Quantitative measurement of (j). (l) Relative *IL-6*, *COX*, *NOS2*, and *MMP13* mRNA expression in USP7 knockdown and its control groups under TNF-α-induced inflammation after 48 h chondrogenic induction. (m) IL-6 expression in USP7 knockdown and its control group supernatant under TNF-α-induced inflammation after 48 h chondrogenic induction. $^{*}p < 0.05$, $^{**}p < 0.01$, $^{***}p < 0.001$, and $^{****}p < 0.0001$.

ATDC5 cells were over 95%, indicating that they were successfully transfected (Fig. S2). Western blot revealed that USP7 protein was successfully knocked down (Figure 2(b)). Since USP7-sh2 had better knockdown efficiency than USP7-sh1, it was used in the following experiments to determine whether USP7 regulates chondrocyte proliferation, apoptosis, and inflammatory response under TNF-α-induced inflammation.

Alcian blue and toluidine blue stainings showed that USP7 knockdown reduced the staining intensities under TNF-α-induced inflammation (Figure 2(c)). USP7 knockdown delayed ATDC5 cell proliferation under TNF-α (Figure 2(d)). Besides, Col2a1 and Sox9 were lower in the USP7-sh2 group under TNF-α (Figures 2(e)–2(g)). To observe functions of USP7 on cell apoptosis, the expression of apoptosis-related proteins, cell apoptosis rate, and TUNEL staining were tested. Western blot showed that USP7 knockdown improved the expression of the Cleaved Caspase-3 protein and the ratio of Bax/Bcl-2 under TNF-α-induced inflammation (Figures 2(f) and 2(g)). Caspase-3 activity displayed the same result (Figure 2(h)). Moreover, the ATDC5 cell apoptosis rate was higher in the USP7-sh2 group under inflammation (Figure 2(i) and Fig. S3). TUNEL staining also displayed the same trend (Figures 2(j) and 2(k)). These results indicate that USP7 knockdown upregulated ATDC5 cell apoptosis under TNF-α-induced inflammation.

USP7 knockdown also increased the expression of *IL-6*, *COX*, *NOS2*, and *MMP13* mRNA (Figure 2(l)). ELISA showed the same trend of IL-6 (Figure 2(m)), revealing that USP7 knockdown exacerbated the inflammatory response of ATDC5 cells under inflammation.

3.4. USP7 Inhibitor HBX41108 Inhibits ATDC5 Cell Proliferation and Enhances Apoptosis and Inflammatory Response under TNF-α-Induced Inflammation. HBX41108 was a small molecular inhibitor of USP7. The alcian blue and toluidine blue staining intensities decreased gradually with increasing HBX41108 under TNF-α (Fig. S4A). HBX41108 also inhibited ATDC5 cell proliferation at equal or greater than 1 μM in a dose-independent manner (Fig. S4B). Flow cytometry suggested that HBX41108 accelerated chondrocyte apoptosis at a dose-independent manner, except 0.5 μM (Figs. S4C and S4D). Considering that 0.5 μM HBX41108 had no obvious effect on chondrocyte proliferation and apoptosis, 1 μM and 2 μM HBX41108 were selected for use in the following experiment.

HBX41108 inhibited the expression of Col2a1 and Sox9 (Figs. S4E–S4G), upregulated ATDC5 cell apoptosis, and improved the expression of proinflammatory cytokines (Figs. S4F-S4J). These results were consistent with USP7 knockdown. Collectively, USP7 inhibitor HBX41108 reduced chondrocyte proliferation and aggravated apoptosis and the inflammatory response under TNF-α-induced inflammation.

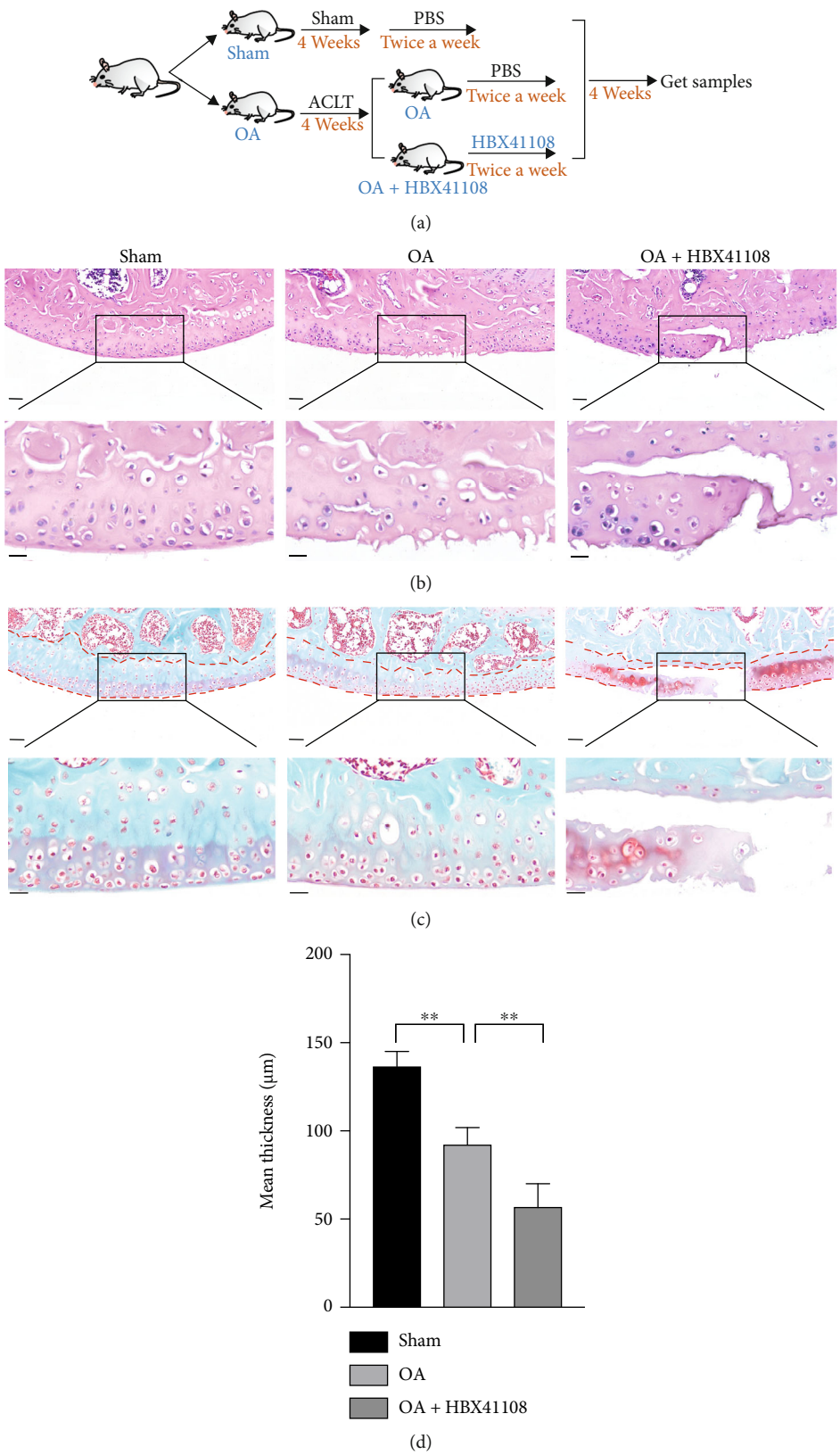

Figure 3: USP7 inhibitor HBX41108 aggravated cartilage destruction of OA mice. (a) Flow chart of the in vivo experiment with HBX41108. (b) HE staining of the mouse knee joint after ACLT in the sham, OA, and OA with HBX41108 groups. (c) Safranin O-Fast Green staining of the mouse knee joint after ACLT in the sham, OA, and OA with HBX41108 groups. The red dotted line indicates cartilaginous region of the tibia. (d) Quantitative measurement of (c). Scale bars of the upper panels = 50 μm and scale bars of the lower panels = 20 μm. $^{*}p < 0.05$, $^{**}p < 0.01$, $^{***}p < 0.001$, and $^{****}p < 0.0001$.

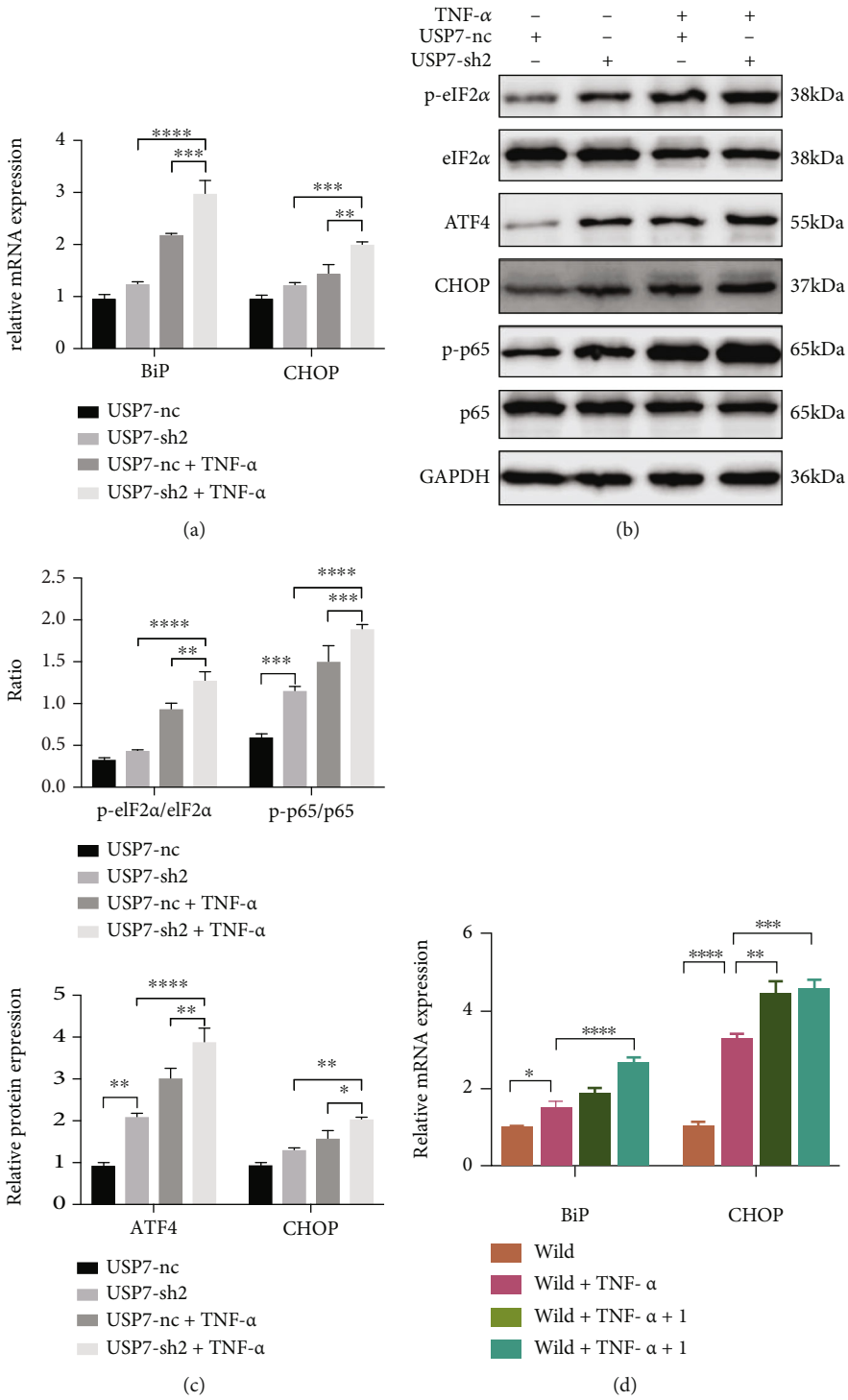

Figure 4: Continued.

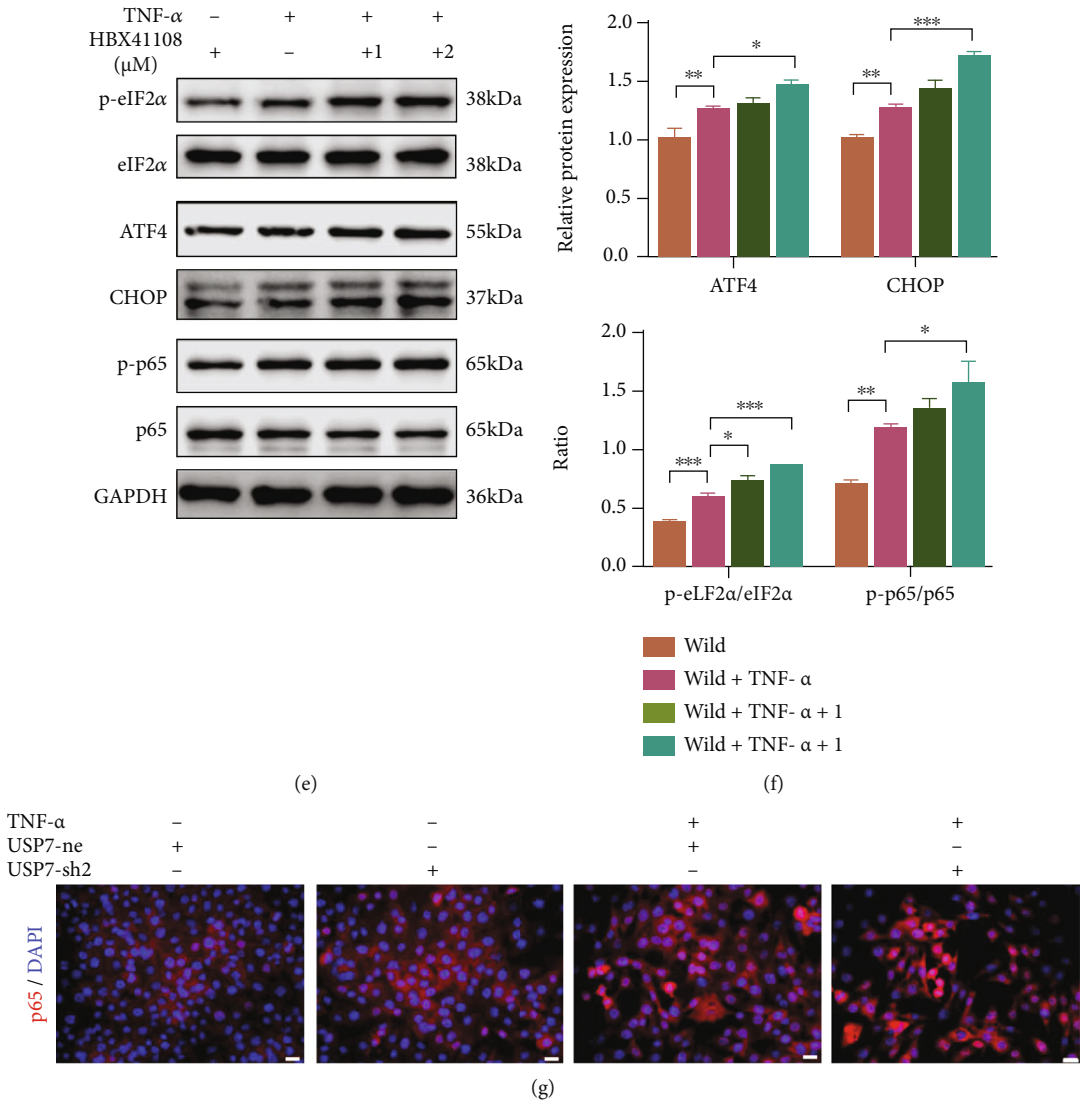

Figure 4: Knocking down and inhibitor HBX41108 of USP7 activate ERS and NF-κB signaling under TNF-α-induced inflammation. (a) Relative *BiP* and *CHOP* mRNA expression of in USP7 knockdown and its control groups under TNF-α-induced inflammation after 48 h chondrogenic induction. (b) p-eIF2α, eIF2α, ATF4, CHOP, p-p65, and p65 protein expression of in USP7 knockdown and its control groups under TNF-α-induced inflammation after 48 h chondrogenic induction. (c) Quantitative measurement of (b). (d) Relative *BiP* and *CHOP* mRNA expression of wild ATDC5 cells under TNF-α-induced inflammation after 48 h chondrogenic induction in HBX41108. (e) p-eIF2α, eIF2α, ATF4, CHOP, p-p65, and p65 protein expression of wild ATDC5 cells under TNF-α-induced inflammation after 48 h chondrogenic induction in HBX41108. (f) Quantitative measurement of (e). (g) Immunofluorescent staining of p65 in USP7 knockdown and its control groups under TNF-α-induced inflammation after 48 h chondrogenic induction. Scale bars = 20 μm. $^{*}p < 0.05$, $^{**}p < 0.01$, $^{***}p < 0.001$, and $^{****}p < 0.0001$.

3.5. USP7 Inhibitor HBX41108 Aggravated Cartilage Destruction of OA Mice. To determine the functions of USP7 in vivo four weeks after ACLT, the USP7 inhibitor HBX41108 was injected intraperitoneally into the OA mice twice a week for four weeks (Figure 3(a)). The HE staining showed that the OA group with HBX41108 had fewer chondrocytes than the OA group without HBX41108 (Figure 3(b)). Safranin O-Fast Green staining also showed decreased cartilage thickness and structural breakage of cartilage tissue in the OA group with HBX41108 (Figures 3(c) and 3(d)). This indicated that the USP7 inhibitor HBX41108 aggravated cartilage destruction in OA mice.

3.6. Knocking Down and Inhibitor HBX41108 of USP7 Activate ERS and NF-κB Signaling under TNF-α-Induced Inflammation. PCR showed that USP7 knockdown increased*BiP* and *CHOP* mRNA under inflammation (Figure 4(a)). Western blot showed that USP7 knockdown upregulated ATF4 and CHOP proteins, and the ratios of p-eIF2α/eIF2α and p-p65/p65 under inflammation (Figures 4(b) and 4(c)). Moreover, HBX41108 displayed the same trends (Figures 4(d)–4(f)). Immunofluorescence staining showed that p65 was primarily expressed in the cytoplasm under noninflammation but partially transferred into the nucleus under TNF-α-induced inflammation, with

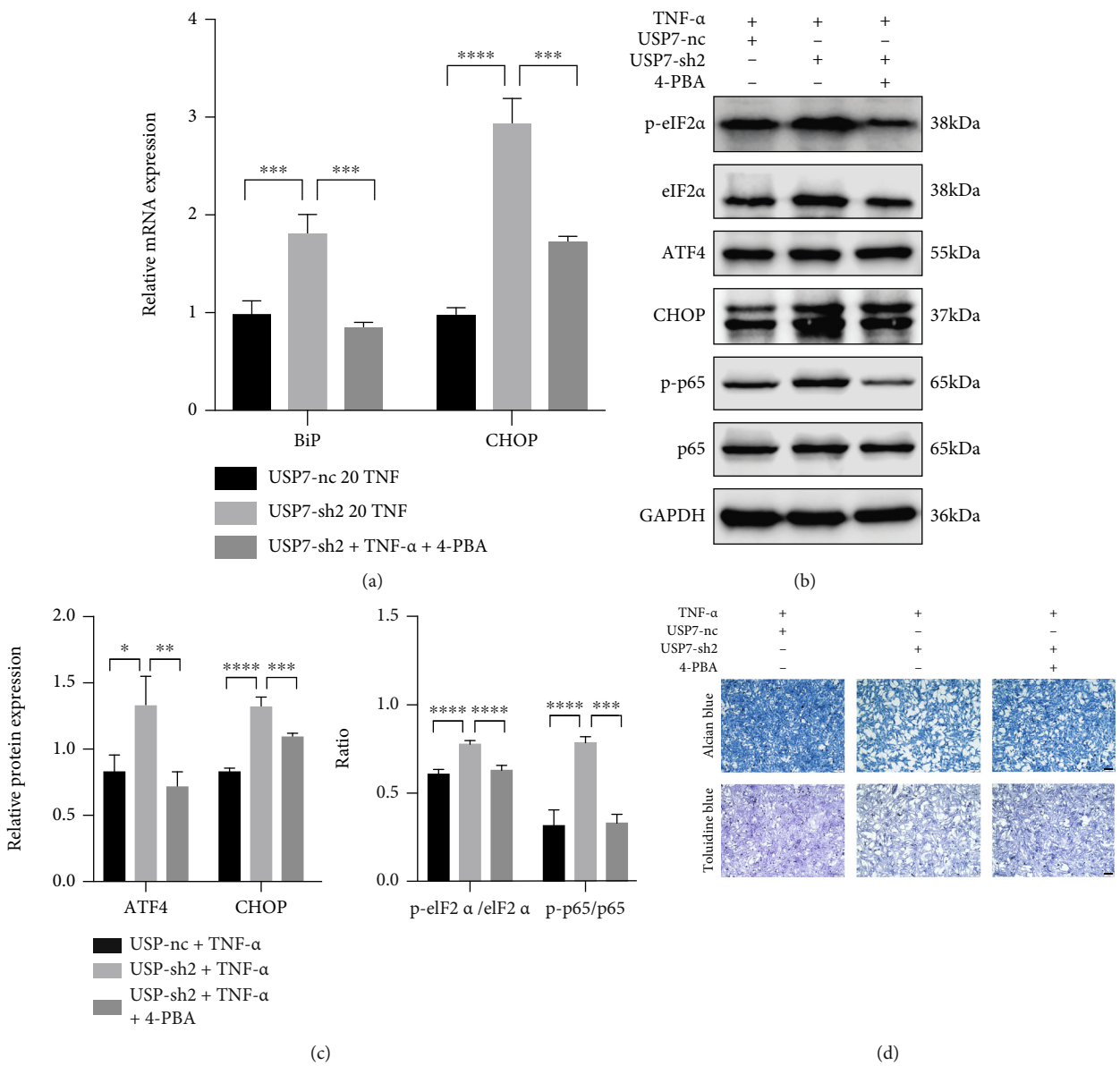

Figure 5: Continued.

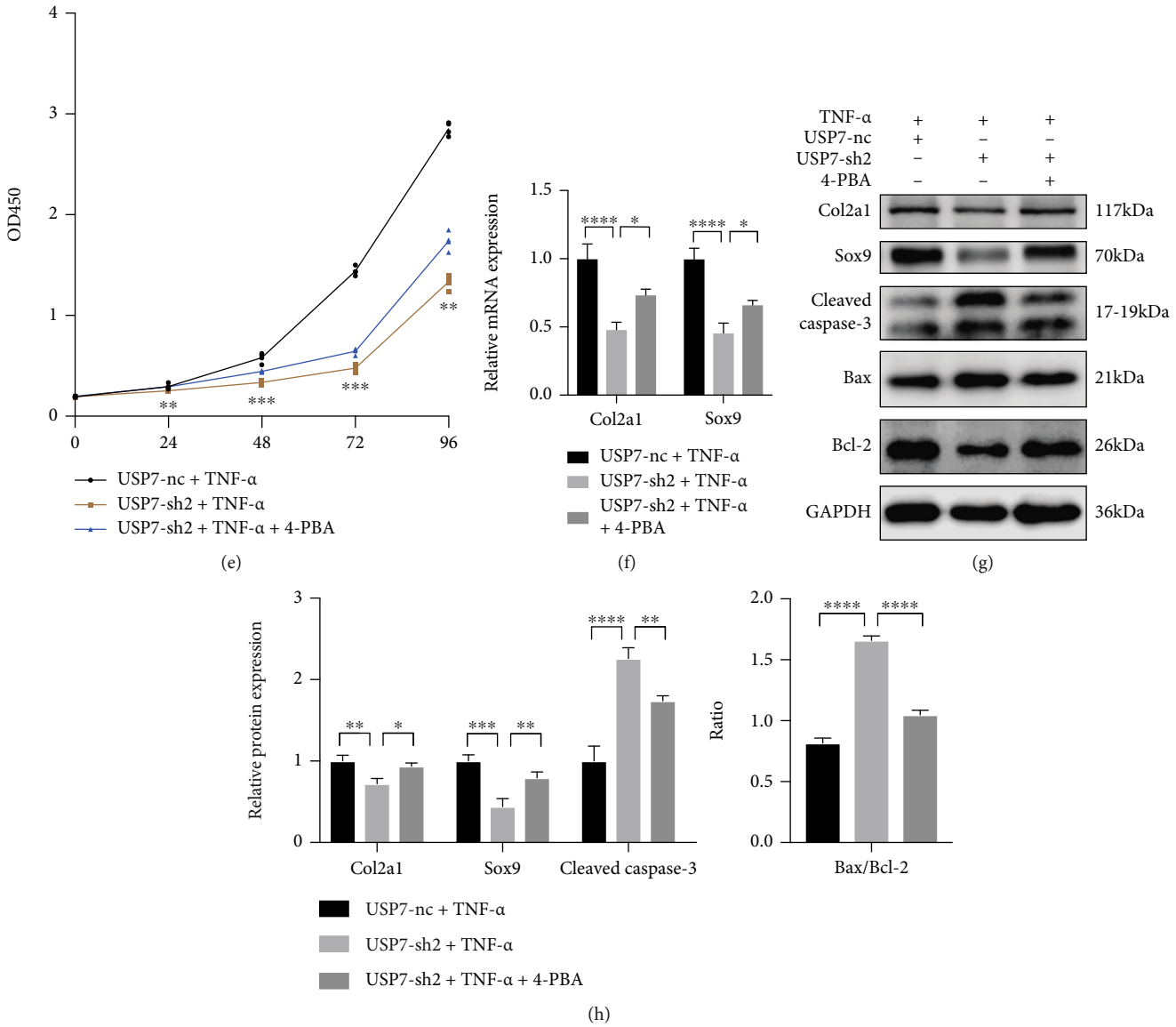

Figure 5: Continued.

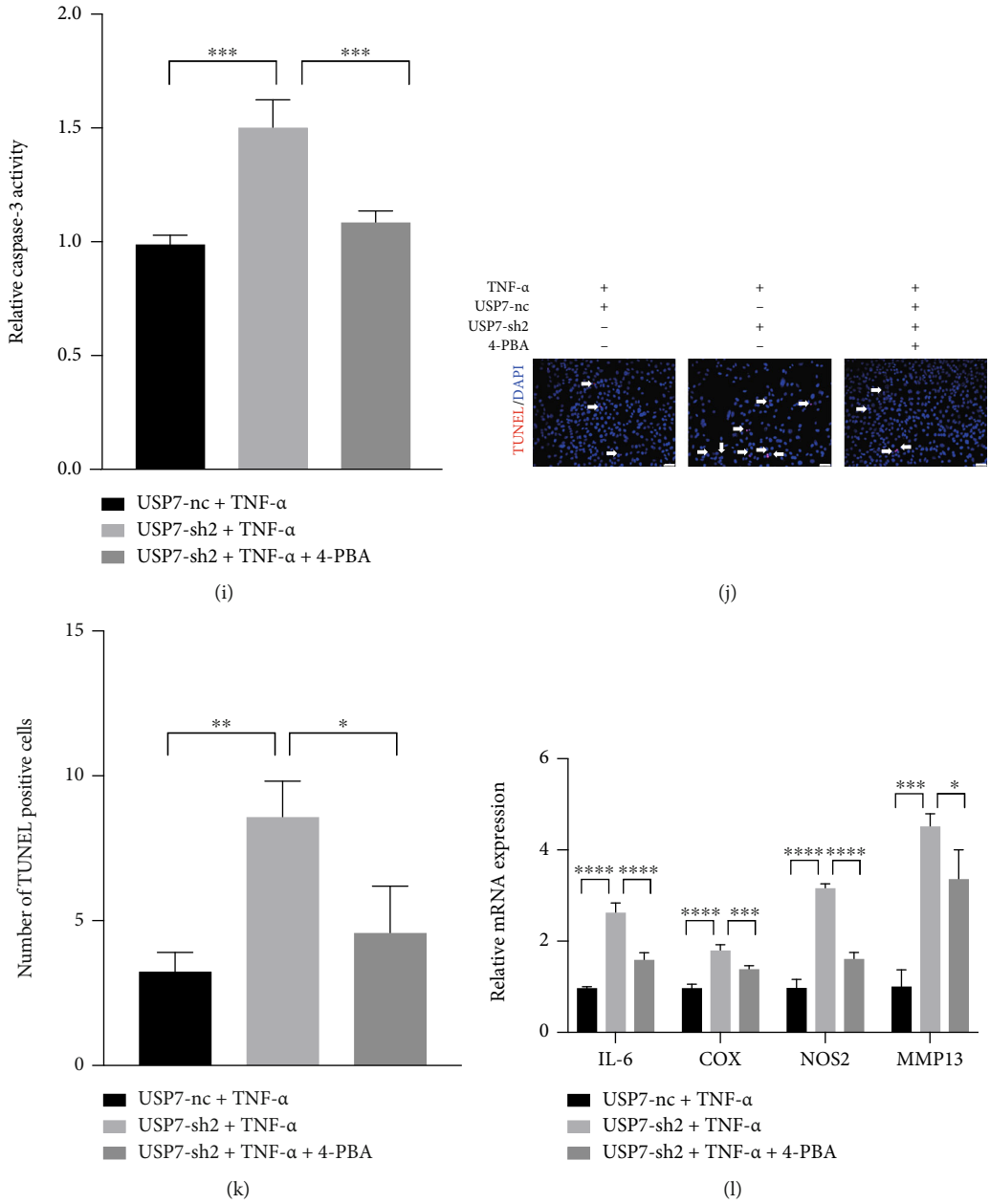

Figure 5: Continued.

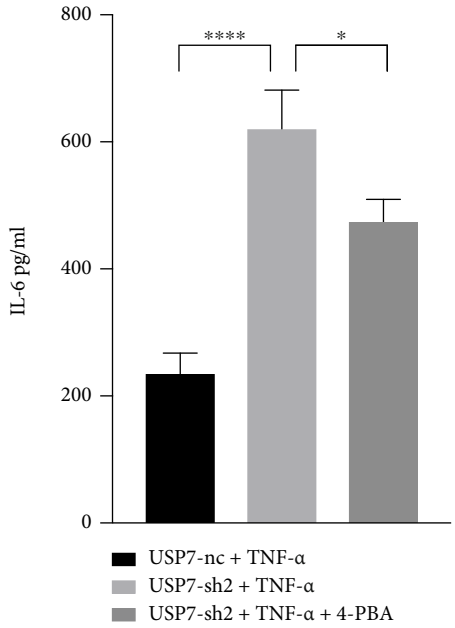

(m)

Figure 5: ERS signaling inhibitor 4-PBA reverses chondrocyte proliferation, apoptosis, and inflammation caused by USP7 knockdown under TNF-α-induced inflammation. (a) Relative *BiP* and *CHOP* mRNA expression in USP7 knockdown and its control groups under TNF-α-induced inflammation after 48 h chondrogenic induction, with and without 4-PBA. (b) p-eIF2α, eIF2α, ATF4, CHOP, p-p65, and p65 protein expression in USP7 knockdown and its control groups under TNF-α-induced inflammation after 48 h chondrogenic induction, with and without 4-PBA. (c) Quantitative measurement of (b). (d) Alcian blue and toluidine blue staining in USP7 knockdown and its control groups under TNF-α-induced inflammation after 48 h chondrogenic induction, with and without 4-PBA. Scale bars = 100 μm. (e) Growth curves in USP7 knockdown and its control groups under TNF-α-induced inflammation after 48 h chondrogenic induction, with and without 4-PBA, measured by CCK8-assay. (f) Relative *Col2a1* and *Sox9* mRNA expression in USP7 knockdown and its control groups under TNF-α-induced inflammation after 48 h chondrogenic induction, with and without 4-PBA. (g) Col2a1, Sox9, Cleaved Caspase-3, Bax, and Bcl-2 protein expression in USP7 knockdown and its control groups under TNF-α-induced inflammation after 48 h chondrogenic induction, with and without 4-PBA. (h) Quantitative measurement of (g). (i) Relative Caspase-3 activity in USP7 knockdown and its control groups under TNF-α-induced inflammation after 48 h chondrogenic induction, with and without 4-PBA. (j) TUNEL staining in USP7 knockdown and its control groups under TNF-α-induced inflammation after 48 h chondrogenic induction, with and without 4-PBA. White arrows indicate TUNEL-positive cells. Scale bars = 50 μm. (k) Quantitative measurement of (j). (l) Relative *IL-6*, *COX*, *NOS2*, and *MMP13* mRNA expression of in USP7 knockdown and its control groups under TNF-α-induced inflammation after 48 h chondrogenic induction, with and without 4-PBA. (m) IL-6 expression in USP7 knockdown and its control group supernatant under TNF-α-induced inflammation after 48 h chondrogenic induction, with and without 4-PBA. $^{*}p < 0.05$, $^{**}p < 0.01$, $^{***}p < 0.001$, and $^{****}p < 0.0001$.

more nuclear p65 in the USP7-sh2 group (Figure 4(g)). Collectively, it is suggested that USP7 may through ERS and NF-κB signaling regulate chondrocytes under inflammation. To verify this hypothesis, inhibitors of these two signaling and si-CHOP were used in the following experiments under TNF-α-induced inflammation.

3.7. ERS Inhibitor 4-PBA Reverses Chondrocyte Proliferation, Apoptosis, and Inflammatory Response Caused by USP7 Knockdown under TNF-α-Induced Inflammation. 4-PBA is a widely used ERS inhibitor. PCR and western blot revealed that 4-PBA effectively inhibited the activated ERS and NF-κB signaling in the USP7-sh2 group under inflammation (Figures 5(a)–5(c)). 4-PBA increased chondrocyte proliferation (Figures 5(d) and 5(e)) and enhanced the expression of Col2a1 and Sox9 (Figures 5(f)–5(h)). Moreover, 4-PBA downregulated chondrocyte apoptosis under inflammation in the USP7-sh2 group (Figures 5(g)–5(k)). 4-PBA also reduced proinflammatory cytokines (Figures 5(l) and 5(m)). These results suggested that 4-PBA reversed chondrocyte proliferation, apoptosis, and inflammatory response caused by USP7 knockdown under TNF-α-induced inflammation.

3.8. si-CHOP Reverses Chondrocyte Proliferation, Apoptosis, and Inflammatory Response Caused by USP7 Knockdown under TNF-α-Induced Inflammation. PCR and western blot revealed that si-CHOP efficiently decreased the expression of CHOP (Figures (6)–6(c)). si-CHOP inhibited the activated NF-κB/p65 signaling of USP7 knockdown under inflammation (Figures 6(b) and 6(c)). si-CHOP also upregulated the low expression of Col2a1, Sox9, and PCNA in the USP7-sh2 group (Figures 6(d)–6(f)). Moreover, si-CHOP inhibited the increase of chondrocyte apoptosis and proinflammatory cytokines (Figures 6(e)–6(h)). These indicated that si-CHOP reversed chondrocyte proliferation, apoptosis,

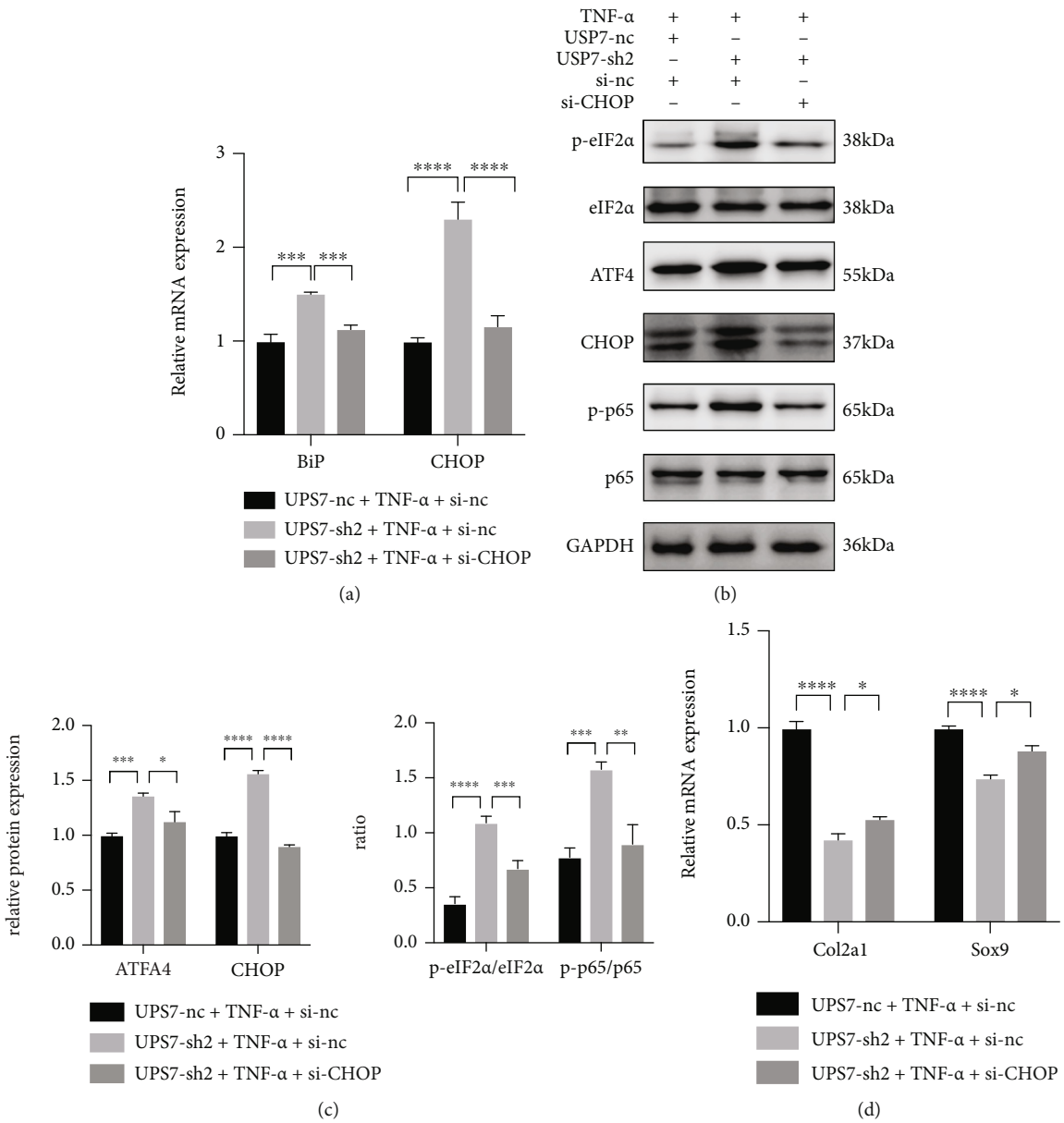

Figure 6: Continued.

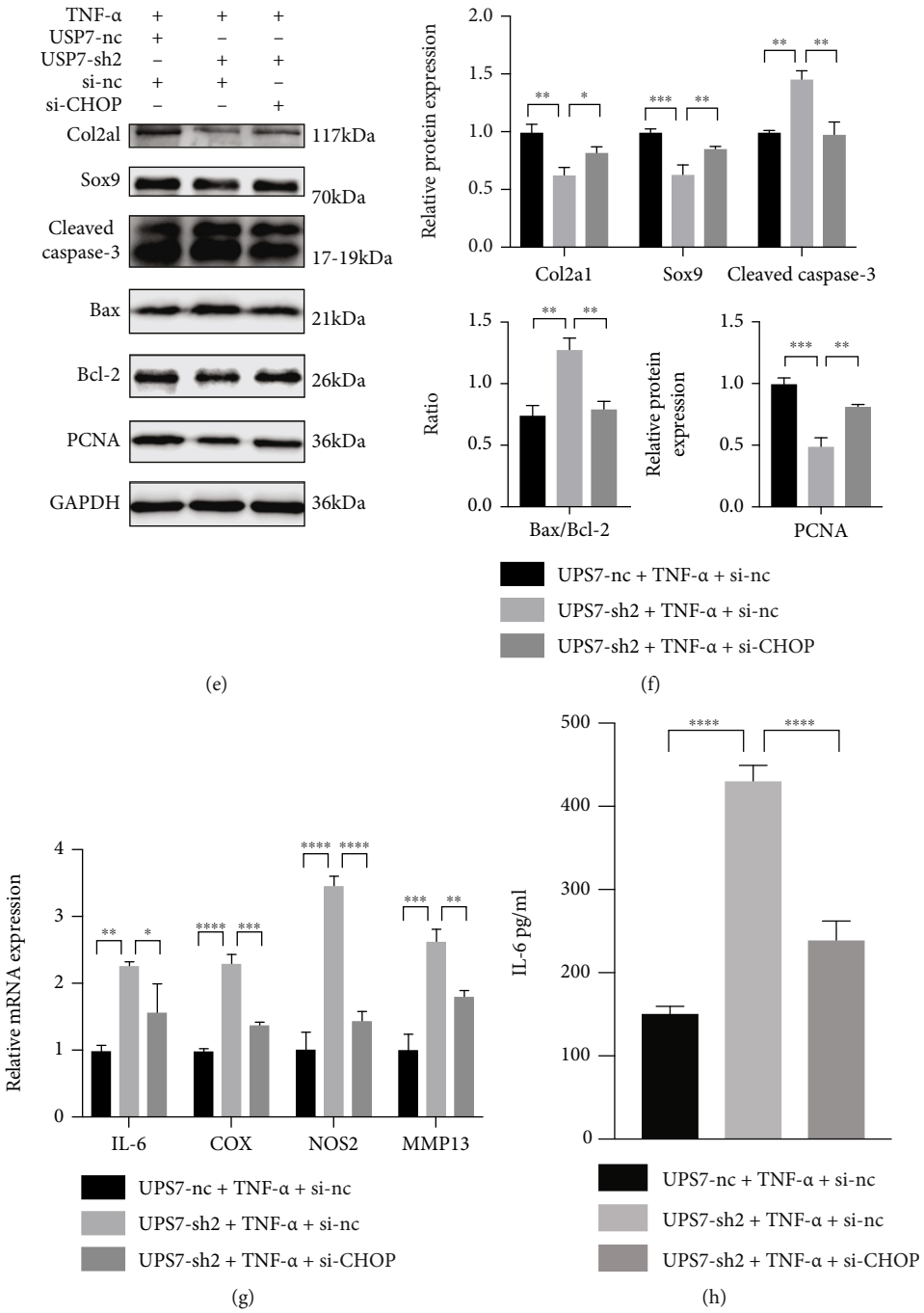

Figure 6: si-CHOP reverses chondrocyte proliferation, apoptosis, and inflammatory response caused by USP7 knockdown under TNF-α-induced inflammation. (a) Relative *BiP* and *CHOP* mRNA expression in USP7 knockdown and its control groups under TNF-α-induced inflammation after 48 h chondrogenic induction, with and without si-CHOP. (b) p-eIF2α, eIF2α, ATF4, CHOP, p-p65, and p65 protein expression of in USP7 knockdown and its control groups under TNF-α-induced inflammation after 48 h chondrogenic induction, with and without si-CHOP. (c) Quantitative measurement of (b). (d) Relative Col2a1 and Sox9 mRNA expression in USP7 knockdown and its control groups under TNF-α-induced inflammation after 48 h chondrogenic induction, with and without si-CHOP. (e) Col2a1, Sox9, Cleaved Caspase-3, Bax, Bcl-2, and PCNA protein expression in USP7 knockdown and its control groups under TNF-α-induced inflammation after 48 h chondrogenic induction, with and without si-CHOP. (f) Quantitative measurement of (e). (g) Relative *IL-6*, *COX*, *NOS2*, and *MMP13* mRNA expression of in USP7 knockdown and its control groups under TNF-α-induced inflammation after 48 h chondrogenic induction, with and without si-CHOP. (h) IL-6 expression in USP7 knockdown and its control group supernatant under TNF-α-induced inflammation after 48 h chondrogenic induction, with and without si-CHOP. $^{*}p < 0.05$, $^{**}p < 0.01$, $^{***}p < 0.001$, and $^{****}p < 0.0001$.

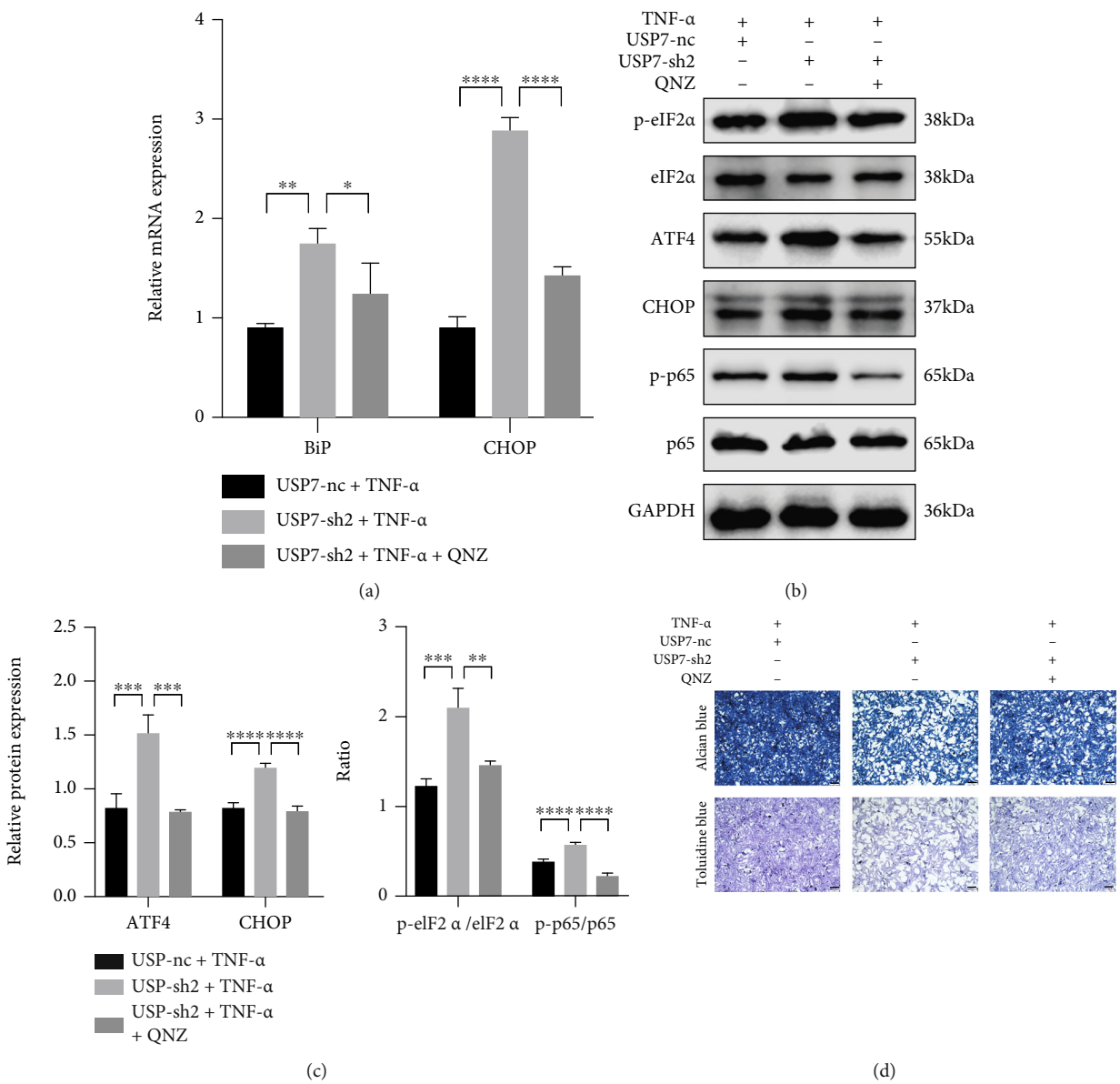

Figure 7: Continued.

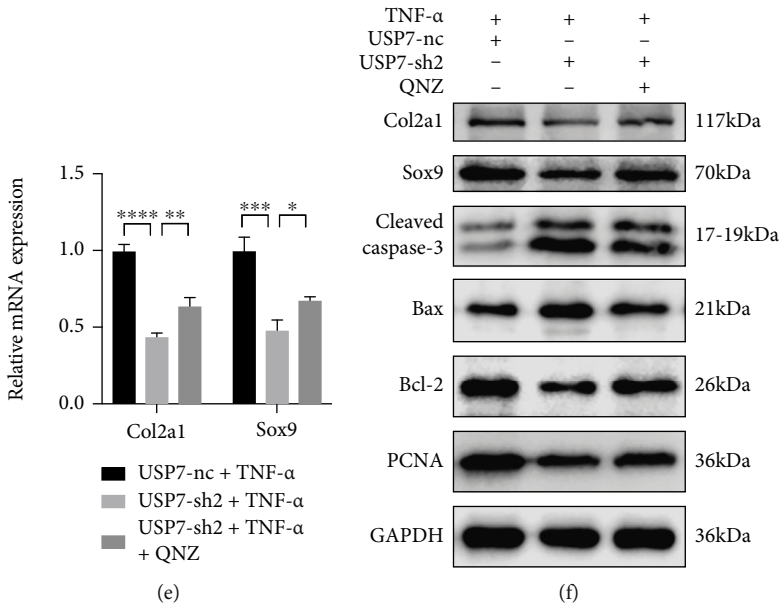

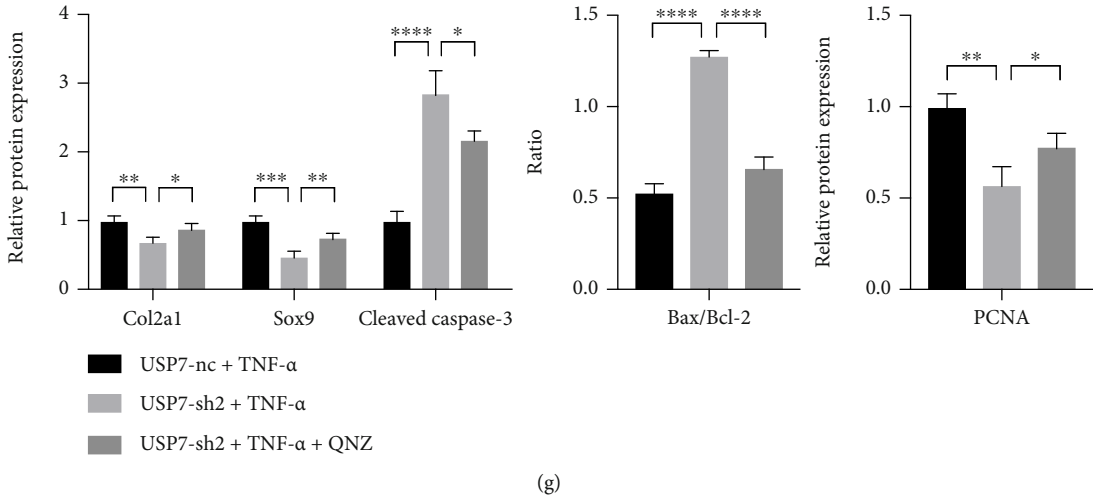

Figure 7: Continued.

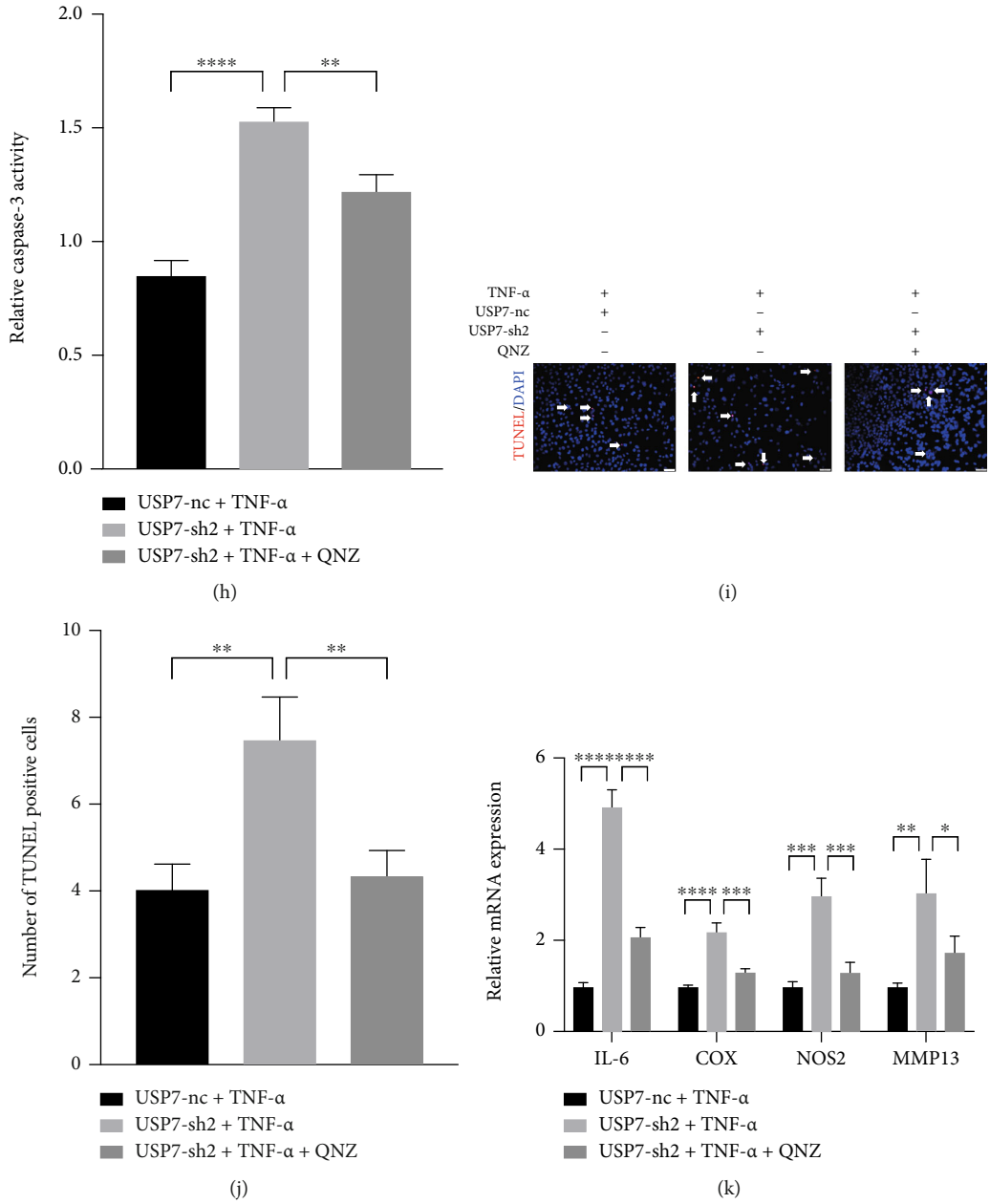

Figure 7: Continued.

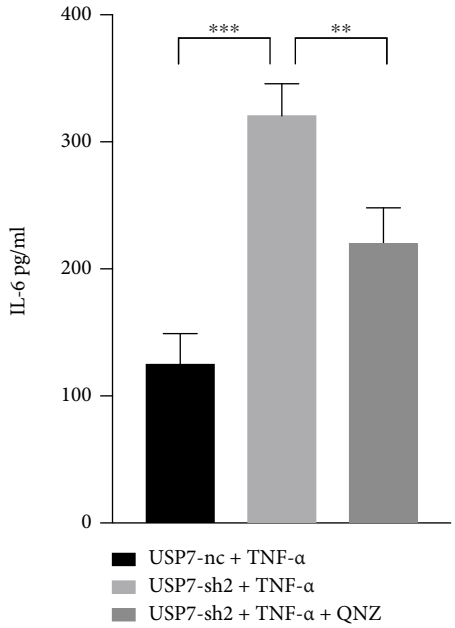

(l)

Figure 7: NF-κB signaling inhibitor QNZ reverses chondrocyte proliferation, apoptosis, and inflammatory response caused by USP7 knockdown under TNF-α-induced inflammation. (a) Relative *BiP* and *CHOP* mRNA expression in USP7 knockdown and its control groups under TNF-α-induced inflammation after 48 h chondrogenic induction, with and without QNZ. (b) p-eIF2α, eIF2α, ATF4, CHOP, p-p65, and p65 protein expression of in USP7 knockdown and its control groups under TNF-α-induced inflammation after 48 h chondrogenic induction, with and without QNZ. (c) Quantitative measurement of B. (d) Alcian blue and toluidine blue staining in USP7 knockdown and its control groups under TNF-α-induced inflammation after 48 h chondrogenic induction, with and without QNZ. Scale bars = 100 μm. (e) Relative *Col2a1* and *Sox9* mRNA expression in USP7 knockdown and its control groups under TNF-α-induced inflammation after 48 h chondrogenic induction, with and without QNZ. (f) Col2a1, Sox9, Cleaved Caspase-3, Bax, Bcl-2, and PCNA protein expression of in USP7 knockdown and its control groups under TNF-α-induced inflammation after 48 h chondrogenic induction, with and without QNZ. (g) Quantitative measurement of F. (h) Relative Caspase-3 activity in USP7 knockdown and its control groups under TNF-α-induced inflammation after 48 h chondrogenic induction, with and without QNZ. (i) TUNEL staining in USP7 knockdown and its control groups under TNF-α-induced inflammation after 48 h chondrogenic induction, with and without QNZ. White arrows indicated TUNEL-positive cells. Scale bars = 50 μm. (j) Quantitative measurement of (i). (k) Relative *IL-6*, *COX*, *NOS2*, and *MMP13* mRNA expression in USP7 knockdown and its control groups under TNF-α-induced inflammation after 48 h chondrogenic induction, with and without QNZ. (l) IL-6 expression in USP7 knockdown and its control group supernatant under TNF-α-induced inflammation after 48 h chondrogenic induction, with and without QNZ. $^{*}p < 0.05$, $^{**}p < 0.01$, $^{***}p < 0.001$, and $^{****}p < 0.0001$.

and inflammatory response caused by USP7 knockdown under inflammation.

3.9. NF-κB Signaling Inhibitor QNZ Reverses Chondrocyte Proliferation, Apoptosis, and Inflammatory Response Caused by USP7 Knockdown under TNF-α-Induced Inflammation after Chondrogenic Induction. The QNZ was a strong inhibitor of NF-κB signaling. QNZ effectively inhibited the activated ERS and NF-κB signaling of USP7 knockdown under TNF-α-induced inflammation (Figures 7(a)–7(c)). Histological stainings showed that QNZ reversed the reduced chondrocytes and extracellular cartilage matrix formation of USP7 knockdown (Figure 7(d)). The expression of Col2a1, Sox9, and PCNA showed the same trend (Figures 7(e)–7(g)). Further, QNZ downregulated the increased chondrocyte apoptosis and proinflammatory cytokines of USP7 knockdown under inflammation (Figures 7(f)–7(l)). These results implied that QNZ reversed chondrocyte proliferation, apoptosis, and inflammatory response of USP7 knockdown under TNF-α-induced inflammation.

4. Discussion

Posttraumatic OA is caused by joint trauma like anterior cruciate ligament (ACL) injury and meniscus tears [27]. Acute ACL injury caused serious local inflammation in the joint, inducing the proteolysis of aggrecan and Col2a1. Although joint trauma leads to OA in only 12% of cases, it mainly troubles young patients and causes long-term implications [28]. Hence, research on reducing cartilage destruction after ACT injury for OA patients has significant implications.

Increasing evidence suggests that deubiquitinases are essential in bone metabolism; however, their roles in cartilage and related diseases are poorly understood. Our previous study demonstrated that USP7 stimulated chondrocyte proliferation and chondrogenic differentiation in vitro and in vivo [26]. In this study, the knee OA model of mice was successfully constructed by ACLT, and USP7 was found to reduce in the knee joint of OA mice. Continuous local TNF-α levels were observed in the injured joint and

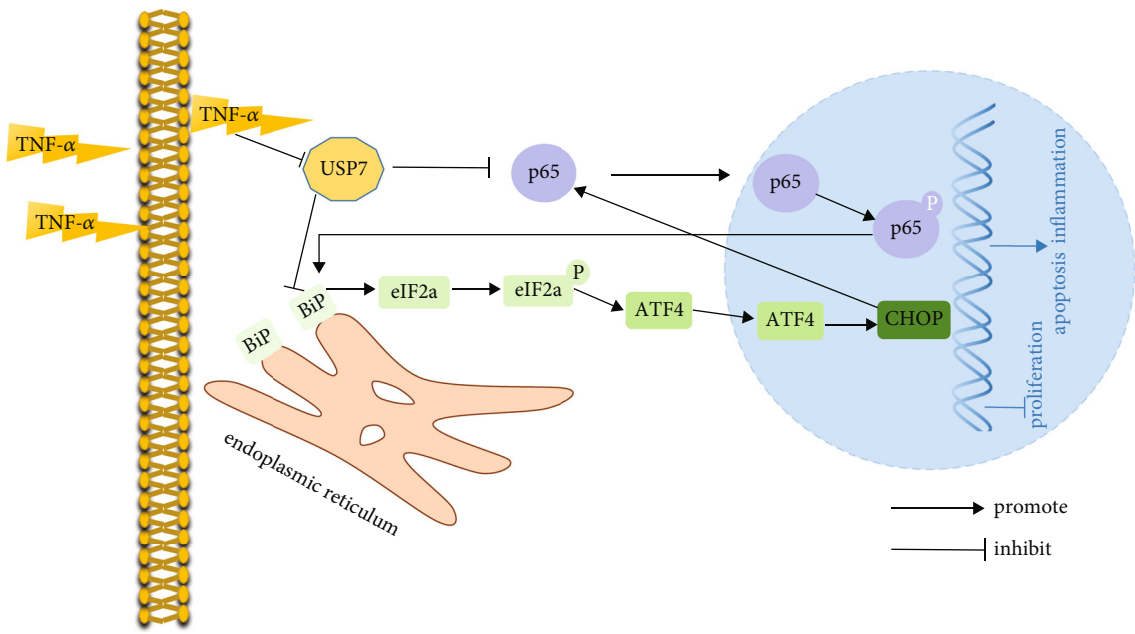

Figure 8: Schematic diagram of the effects and underlying mechanisms of USP7 on chondrocyte proliferation, apoptosis, and inflammatory response under TNF-α-induced inflammation. Under TNF-α-induced inflammation, USP7 promotes chondrocyte proliferation and suppresses chondrocyte apoptosis and inflammatory response, through inhibiting the BiP-eIF2α-ATF4-CHOP signaling of ERS and NF-κB signaling.

provided continued stimulation to the surrounding cells [29]. To further study the influence of USP7 on chondrocytes under inflammation and the underlying mechanisms, TNF-α was supplemented to mimic OA in vitro. The results revealed that under TNF-α-induced inflammation in vitro, inactivation of USP7 inhibited chondrocyte proliferation and accelerated chondrocyte apoptosis and inflammatory response through activation of ERS and NF-κB signaling.

Recent studies confirm that USP7 and its inhibitors regulate cell proliferation and apoptosis, especially in cancers. Inhibition of USP7 reduced cell growth of esophageal squamous cell carcinoma and activated ERS to induce NOXA-mediated apoptosis [30]. In this study, USP7 knockdown activated chondrocyte apoptosis and suppressed chondrocyte proliferation under TNF-α-induced inflammation. Further, the USP7 inhibitor HBX41108 showed the same trend in vitro. However, this result differs from a study that found USP7 inhibition alleviated hydrogen peroxide-induced injury, like reduced proliferation and increased inflammation, by regulating NOX4 ubiquitination in rat chondrocytes [31]. Supplementation of hydrogen peroxide or TNF-α can mimic OA in vitro, but it led to different expressions and functions of USP7, possibly because USP7, as a deubiquitinase, modulates deubiquitination of diverse proteins to exert its functions under various stimulations. Moreover, the simulated conditions in vitro are not the same as those in vivo, given that the USP7 inhibitor HBX41108 was injected intraperitoneally in vivo and resulted in HBX41108 exacerbated cartilage destruction in OA mice. Hence, these results strongly indicate that USP7 protects cartilage and reduces its destruction in posttraumatic OA.

ERS is regarded as necessary in cartilage development. Chondrocytes, the only cell type in cartilage, showed impaired growth and upregulated apoptosis under ERS-induced conditions [32]. In human OA, ERS contributed to enhanced chondrocyte apoptosis and increased CHOP expression in chondrocytes [33]. Our previous study also found that CHOP suppressed ATDC5 cell proliferation and differentiation after chondrogenic induction [34]. However, the current study found that USP7 promoted ATDC5 cell proliferation. Considering that CHOP is the later event of BiP-PERK-eIF2α-ATF4 axis of ERS [35], it is suggested that USP7 may exert its effects through inhibiting BiP-eIF2α-ATF4-CHOP signaling.

The results of this study confirmed the supposition. Firstly, it was found that USP7 knockdown and its inhibitor activated BiP-eIF2α-ATF4-CHOP signaling of ERS. And then, reduction of ERS with its inhibitor, 4-PBA, could partially rescue the inhibition of chondrocyte proliferation, the promotion of chondrocyte apoptosis, and inflammatory response caused by USP7 knockdown. A recent study also found that administration of 4-PBA alleviated ERS, decreasing the chondrocyte apoptosis in mouse knee joints with obesity-linked OA [36]. According to these results, 4-PBA may be used to treat human OA, but this needs to be investigated further. Furthermore, the current study found that si-CHOP had the same effect as 4-PBA. This was consistent with the finding of Uehara et al. that CHOP knockout restrained the chondrocyte apoptosis and cartilage destruction in mice with OA [37]. Such results might be explained by that CHOP directly decreased antiapoptotic Bcl-2 protein but increased proapoptotic Bax protein to induce cell apoptosis [38]. However, since there were three ERS signalings and our study only demonstrated that CHOP knockdown decreased the BiP-eIF2α-ATF4-CHOP signaling, a study of relationship between CHOP knockdown and other ERS

signalings may provide better understanding of ERS in chondrocytes under inflammation. Collectively, USP7 modulates chondrocyte proliferation, apoptosis, and inflammatory response via inhibiting BiP-eIF2α-ATF4-CHOP signaling of ERS under TNF-α-induced inflammation.

On the other hand, inflammation also leads to ERS in the pathogenesis of inflammatory diseases [39, 40]. It was found that ERS could increase proinflammatory cytokines via NF-κB signaling [41]. NF-κB signaling is crucial in OA, and its activation causes cartilage destruction to aggravate the progression of OA [15, 42]. The current study found that USP7 knockdown or its inhibitor activated NF-κB signaling. Moreover, supplementation of this signaling inhibitor QNZ rescued the chondrocyte proliferation, apoptosis, and inflammatory response caused by USP7 knockdown. Other research also reported that QNZ accelerated chondrocyte proliferation and decreased chondrocyte degeneration by promoting glucose uptake [43]. Taken together, this study demonstrates that USP7 suppresses NF-κB/p65 signaling to regulate chondrocyte proliferation, apoptosis, and inflammatory response under TNF-α-induced inflammation.

Additional, small molecule inhibitors of USP7 were considered as potential therapies to delay cancer progression by many researchers [3, 44]. However, the results of this study found that the inhibitor of USP7 aggravated cartilage destruction. Hence, clinical doctors should pay more attention to cartilage if the USP7 inhibitor is used for cancers patients with OA. Besides, 4-PBA and QNZ may be potential drugs to slow cartilage destruction of OA and deserve further investigation.

Anyway, this study was based on the function loss of USP7 since the overexpressed lentivirus plasmid was too large to be successfully transfected into ATDC5 cells. The USP7-overexpressed adenovirus vector might be an alternative to be studied in the future. Another limitation was the lack of in vivo studies to verify the underlying mechanisms of USP7 on OA.

5. Conclusions

In conclusion, this study found that USP7 was reduced at the knee articular cartilage of mice with OA. The knockdown and inhibitor HBX41108 of USP7 hindered chondrocyte proliferation and accelerated chondrocyte apoptosis and inflammatory response under inflammation. USP7 may exert these effects through inhibiting BiP-eIF2α-ATF4-CHOP signaling of ERS and NF-κB signaling (Figure 8). This study shows new sights into the effects of USP7 on chondrocyte functions under inflammation.

Data Availability

This research article data used to support the finding of this study are included within the article.

Conflicts of Interest

All authors confirm that this article has no conflict of interest.

Authors' Contributions

Xiaofei Dong was responsible for the conceptualization, methodology, writing of original draft, and data curation. Chang Yang was responsible for the validation and data curation. Yao Luo was responsible for the methodology and investigation. Wei Dong was responsible for the visualization. Xiaoxiao Xu was responsible for the resources. Yanru Wu was responsible for the formal analysis. Jiawei Wang was responsible for the writing, review, editing, supervision, and project administration.

Acknowledgments

This study was financially supported by the National Natural Science Foundation of China (82170930, 81870744, 81570956, and 31600757).

Supplementary Materials

Fig. S1: ATDC5 cell proliferation decreases, and apoptosis and inflammation increase under increasing TNF-α. (A) Alcian blue and toluidine blue staining of wild ATDC5 cells under increasing TNF-α stimulation after 48 h chondrogenic induction. Scale bars = 100 μm. (B) Growth curves of wild ATDC5 cells under increasing TNF-α stimulation after 48 h chondrogenic induction. (C) Relative *Col2a1* and *Sox9* mRNA expression in wild ATDC5 cells under increasing TNF-α stimulation after 48 h chondrogenic induction. (D) Col2a1 and Cleaved Caspase-3 protein expression in wild ATDC5 cells under increasing TNF-α stimulation after 48 h chondrogenic induction. (E) Quantitative measurement of D. (F) Relative Caspase-3 activity in wild ATDC5 cells under increasing TNF-α stimulation after 48 h chondrogenic induction. (G) Cell apoptosis measured by flow cytometry in wild ATDC5 cells under increasing TNF-α stimulation after 48 h chondrogenic induction. (H) Quantitative measurement of G. (I) Relative mRNA expression of *IL-6*, *COX*, *NOS2*, and *MMP13* in wild ATDC5 cells under increasing TNF-α stimulation after 48 h chondrogenic induction. (J) IL-6 expression in wild ATDC5 cell supernatant under increasing TNF-α stimulation after 48 h chondrogenic induction. Data were analyzed using one-way ANOVAs. $^{*}p < 0.05$, $^{**}p < 0.01$, $^{***}p < 0.001$, and $^{****}p < 0.0001$. Fig. S2: ATDC5 cells in USP7 knockdown and its control groups after lentiviral transfection. Scale bars = 100 μm. Fig. S3: cell apoptosis measured by flow cytometry in USP7 knockdown and its control groups under TNF-α-induced inflammation after 48 h chondrogenic induction. Fig. S4: USP7 inhibitor inhibits ATDC5 cell proliferation and increases apoptosis and inflammatory response under TNF-α-induced inflammation. (A) Alcian blue and toluidine blue staining of wild ATDC5 cells under TNF-α-induced inflammation after 48 h chondrogenic induction in USP7 inhibitor HBX41108. Scale bars = 100 μm. (B) Growth curves of wild ATDC5 cells under TNF-α-induced inflammation after 48 h chondrogenic induction in HBX41108. (C) Cell apoptosis measured by flow cytometry of wild ATDC5 cells under TNF-α-induced inflammation after 48 h chondrogenic induction at

different concentrations of HBX41108. (D) Quantitative measurement of C. (E) Relative Col2a1 and Sox9 mRNA expression of wild ATDC5 cells under TNF-α-induced inflammation after 48 h chondrogenic induction in HBX41108. (F) Col2a1, Sox9, Cleaved Caspase-3, Bax, and Bcl-2 protein expression of wild ATDC5 cells under TNF-α-induced inflammation after 48 h chondrogenic induction in HBX41108. (G) Quantitative measurement of F. (H) Relative Caspase-3 activity of wild ATDC5 cells under TNF-α-induced inflammation after 48 h chondrogenic induction in HBX41108. (I) TUNEL staining of wild ATDC5 cells under TNF-α-induced inflammation after 48 h chondrogenic induction in HBX41108. White arrows indicated TUNEL-positive cells. Scale bars = 50 μm. (J) Quantitative measurement of I. (K) Relative *IL-6*, *COX*, *NOS2*, and *MMP13* mRNA expression of wild ATDC5 cells under TNF-α-induced inflammation after 48 h chondrogenic induction in HBX41108. $^{*}p < 0.05$, $^{**}p < 0.01$, $^{***}p < 0.001$, and $^{****}p < 0.0001$. *(Supplementary Materials)*

References

[1] R. D. Everett, M. Meredith, A. Orr, A. Cross, M. Kathoria, and J. Parkinson, "A novel ubiquitin-specific protease is dynamically associated with the PML nuclear domain and binds to a herpesvirus regulatory protein," *The EMBO Journal*, vol. 16, no. 7, pp. 1519–1530, 1997.

[2] A. Pozhidaeva and I. Bersonova, "USP7: structure, substrate specificity, and inhibition," *DNA Repair*, vol. 76, pp. 30–39, 2019.

[3] Z. Wang, W. Kang, Y. You et al., "USP7: novel drug target in cancer therapy," *Frontiers in Pharmacology*, vol. 10, 2019.

[4] D. J. Hunter and S. Bierma-Zeinstra, "Osteoarthritis," *Lancet*, vol. 393, no. 10182, pp. 1745–1759, 2019.

[5] C. R. Scanzello, "Role of low-grade inflammation in osteoarthritis," *Current Opinion in Rheumatology*, vol. 29, no. 1, pp. 79–85, 2017.

[6] M. B. Goldring and M. Otero, "Inflammation in osteoarthritis," *Current Opinion in Rheumatology*, vol. 23, no. 5, pp. 471–478, 2011.

[7] J. S. Lewis, W. C. Hembree, B. D. Furman et al., "Acute joint pathology and synovial inflammation is associated with increased intra-articular fracture severity in the mouse knee," *Osteoarthritis and Cartilage*, vol. 19, no. 7, pp. 864–873, 2011.

[8] S. Hashimoto, R. L. Ochs, S. Komiya, and M. Lotz, "Linkage of chondrocyte apoptosis and cartilage degradation in human osteoarthritis," *Arthritis and Rheumatism*, vol. 41, no. 9, pp. 1632–1638, 1998.

[9] H. S. Hwang and H. A. Kim, "Chondrocyte apoptosis in the pathogenesis of osteoarthritis," *International Journal of Molecular Sciences*, vol. 16, no. 11, pp. 26035–26054, 2015.

[10] S. L. Hu, C. W. Zhang, L. B. Ni et al., "Stabilization of HIF-1α alleviates osteoarthritis via enhancing mitophagy," *Cell Death & Disease*, vol. 11, no. 6, 2020.

[11] H.-T. Wu, Y.-C. Kuo, J.-J. Hung et al., "K63-polyubiquitinated HAUSP deubiquitinates HIF-1α and dictates H3K56 acetylation promoting hypoxia-induced tumour progression," *Nature Communications*, vol. 7, no. 1, 2016.

[12] P. Palazón-Riquelme, J. D. Worboys, J. Green et al., "USP7 and USP47 deubiquitinases regulate NLRP3 inflammasome activation," *Embo Reports*, vol. 19, no. 10, 2018.

[13] M. Millerand, F. Berenbaum, and C. Jacques, "Danger signals and inflammaging in osteoarthritis," *Clinical and Experimental Rheumatology*, vol. 37 Suppl 120, no. 5, pp. 48–56, 2019.

[14] I. Mitxitorena, D. Somma, J. P. Mitchell et al., "The deubiquitinase USP7 uses a distinct ubiquitin-like domain to deubiquitinate NF-κB subunits," *The Journal of Biological Chemistry*, vol. 295, no. 33, pp. 11754–11763, 2020.

[15] M. C. de Andres, A. Takahashi, and R. O. C. Oreffo, "Demethylation of an NF-κB enhancer element orchestrates iNOS induction in osteoarthritis and is associated with altered chondrocyte cell cycle," *Osteoarthritis and Cartilage*, vol. 24, no. 11, pp. 1951–1960, 2016.

[16] Y. C. Li, W. B. Mu, J. D. Ren et al., "Artesunate alleviates interleukin-1β-induced inflammatory response and apoptosis by inhibiting the NF-κB signaling pathway in chondrocyte-like ATDC5 cells, and delays the progression of osteoarthritis in a mouse model," *International Journal of Molecular Medicine*, vol. 44, no. 4, pp. 1541–1551, 2019.

[17] Z. Q. Ma, T. K. Piao, Y. L. Wang, and J. Y. Liu, "Astragalin inhibits IL-1β-induced inflammatory mediators production in human osteoarthritis chondrocyte by inhibiting NF-κB and MAPK activation," *International Immunopharmacology*, vol. 25, no. 1, pp. 83–87, 2015.

[18] Y. K. Liu, H. Zhu, X. Yan, H. Y. Gu, Z. F. Gu, and F. Liu, "Endoplasmic reticulum stress participates in the progress of senescence and apoptosis of osteoarthritis chondrocytes," *Molecular Cell Biology Research Communications*, vol. 491, no. 2, pp. 368–373, 2017.

[19] A. P. King and J. J. Wilson, "Endoplasmic reticulum stress: an arising target for metal-based anticancer agents," *Chemical Society Reviews*, vol. 49, no. 22, pp. 8113–8136, 2020.

[20] A. Hosseinzadeh, S. K. Kamrava, M. T. Joghataei et al., "Apoptosis signaling pathways in osteoarthritis and possible protective role of melatonin," *Journal of Pineal Research*, vol. 61, no. 4, pp. 411–425, 2016.

[21] K. Feng, Y. W. Ge, Z. X. Chen et al., "Curcumin inhibits the PERK-eIF2α-CHOP pathway through promoting SIRT1 expression in oxidative stress-induced rat chondrocytes and ameliorates osteoarthritis progression in a rat model," *Oxidative Medicine and Cellular Longevity*, vol. 2019, 17 pages, 2019.

[22] X. M. Kang, W. Yang, D. X. Feng et al., "Cartilage-specific autophagy deficiency promotes ER stress and impairs chondrogenesis in PERK-ATF4-CHOP-dependent manner," *Journal of Bone and Mineral Research*, vol. 32, no. 10, pp. 2128–2141, 2017.

[23] X. M. Kang, W. Yang, R. Q. Wang et al., "Sirtuin-1 (SIRT1) stimulates growth-plate chondrogenesis by attenuating the PERK–eIF-2α–CHOP pathway in the unfolded protein response," *The Journal of Biological Chemistry*, vol. 293, no. 22, pp. 8614–8625, 2018.

[24] N. Song, C. Cao, S. Tian, M. Long, and L. Liu, "USP7 deubiquitinates and stabilizes SIRT1," *The Anatomical Record*, vol. 303, no. 5, pp. 1337–1345, 2020.

[25] S. S. Glasson, T. J. Blanchet, and E. A. Morris, "The surgical destabilization of the medial meniscus (DMM) model of osteoarthritis in the 129/SvEv mouse," *Osteoarthritis and Cartilage*, vol. 15, no. 9, pp. 1061–1069, 2007.

[26] X. Dong, X. Xu, C. Yang, Y. Luo, Y. Wu, and J. Wang, "USP7 regulates the proliferation and differentiation of ATDC5 cells through the Sox9-PTHrP-PTH1R axis," *Bone*, vol. 143, p. 115714, 2021.

[27] M. F. Rai, R. H. Brophy, and L. J. Sandell, "Osteoarthritis following meniscus and ligament injury: insights from translational studies and animal models," *Current Opinion in Rheumatology*, vol. 31, no. 1, pp. 70–79, 2019.

[28] T. D. Brown, R. C. Johnston, C. L. Saltzman, J. L. Marsh, and J. A. Buckwalter, "Posttraumatic osteoarthritis: a first estimate of incidence, prevalence, and burden of disease," *Journal of Orthopaedic Trauma*, vol. 20, no. 10, pp. 739–744, 2006.

[29] A. Struglics, S. Larsson, N. Kumahashi, R. Frobell, and L. S. Lohmander, "Changes in cytokines and aggrecan ARGS neoepitope in synovial fluid and serum and in C-terminal crosslinking telopeptide of type II collagen and N-terminal crosslinking telopeptide of type I collagen in urine over five years after anterior cruciate ligament rupture: an exploratory analysis in the knee anterior cruciate ligament, nonsurgical versus surgical treatment trial," *Arthritis & Rheumatology*, vol. 67, no. 7, pp. 1816–1825, 2015.

[30] T. Hu, J. Zhang, B. Sha et al., "Targeting the overexpressed USP7 inhibits esophageal squamous cell carcinoma cell growth by inducing NOXA-mediated apoptosis," *Molecular Carcinogenesis*, vol. 58, no. 1, pp. 42–54, 2019.

[31] G. Liu, Q. B. Liu, B. Yan, Z. Q. Zhu, and Y. Z. Xu, "USP7 inhibition alleviates H_2O_2-induced injury in chondrocytes via inhibiting NOX4/NLRP3 pathway," *Frontiers in Pharmacology*, vol. 11, 2021.

[32] L. Yang, S. G. Carlson, D. McBurney, and W. E. Horton, "Multiple signals induce endoplasmic reticulum stress in both primary and immortalized chondrocytes resulting in loss of differentiation, impaired cell growth, and apoptosis," *The Journal of Biological Chemistry*, vol. 280, no. 35, pp. 31156–31165, 2005.

[33] K. Takada, J. Hirose, K. Senba et al., "Enhanced apoptotic and reduced protective response in chondrocytes following endoplasmic reticulum stress in osteoarthritic cartilage," *International Journal of Experimental Pathology*, vol. 92, no. 4, pp. 232–242, 2011.

[34] M. Yu, S. Q. Yi, Y. R. Wu, H. L. Sun, F. F. Song, and J. W. Wang, "Ddit 3 suppresses the differentiation of mouse chondroprogenitor cells," *The International Journal of Biochemistry & Cell Biology*, vol. 81, Part A, pp. 156–163, 2016.

[35] H. Nishitoh, "CHOP is a multifunctional transcription factor in the ER stress response," *Journal of Biochemistry*, vol. 151, no. 3, pp. 217–219, 2012.

[36] L. Tan, L. Harper, M. A. McNulty, C. S. Carlson, and R. R. Yammani, "High-fat diet induces endoplasmic reticulum stress to promote chondrocyte apoptosis in mouse knee joints," *The FASEB Journal*, vol. 34, no. 4, pp. 5818–5826, 2020.

[37] Y. Uehara, J. Hirose, S. Yamabe et al., "Endoplasmic reticulum stress-induced apoptosis contributes to articular cartilage degeneration via C/EBP homologous protein," *Osteoarthritis and Cartilage*, vol. 22, no. 7, pp. 1007–1017, 2014.

[38] Y. M. Li, Y. S. Guo, J. Tang, J. L. Jiang, and Z. N. Chen, "New insights into the roles of CHOP-induced apoptosis in ER stress," *Acta Biochimica et Biophysica Sinica*, vol. 46, no. 8, pp. 629–640, 2014.

[39] K. Z. Zhang and R. J. Kaufman, "From endoplasmic-reticulum stress to the inflammatory response," *Nature*, vol. 454, no. 7203, pp. 455–462, 2008.

[40] S. Z. Hasnain, R. Lourie, I. Das, A. C. H. Chen, and M. A. McGuckin, "The interplay between endoplasmic reticulum stress and inflammation," *Immunology and Cell Biology*, vol. 90, no. 3, pp. 260–270, 2012.

[41] S. Kim, Y. Joe, Y. J. Surh, and H. T. Chung, "Differential regulation of toll-like receptor-mediated cytokine production by unfolded protein response," *Oxidative Medicine and Cellular Longevity*, vol. 2018, 8 pages, 2018.

[42] T. Saito and S. Tanaka, "Molecular mechanisms underlying osteoarthritis development: Notch and NF-κB," *Arthritis Research & Therapy*, vol. 19, no. 1, p. 94, 2017.

[43] S. B. Zhu, Y. O. Xu, H. Gao, and Y. Deng, "NF-κB inhibitor QNZ protects human chondrocyte degeneration by promoting glucose uptake through Glut4 activation," *European Review for Medical and Pharmacological Sciences*, vol. 24, no. 9, pp. 4642–4651, 2020.

[44] P. Li and H.-M. Liu, "Recent advances in the development of ubiquitin-specific-processing protease 7 (USP7) inhibitors," *European Journal of Medicinal Chemistry*, vol. 191, 2020.

Hindawi
Oxidative Medicine and Cellular Longevity
Volume 2022, Article ID 3955748, 17 pages
https://doi.org/10.1155/2022/3955748

Research Article

Decorin Protects Retinal Pigment Epithelium Cells from Oxidative Stress and Apoptosis via AMPK-mTOR-Regulated Autophagy

Xinyi Xie, Duo Li, Yuqing Cui, Tianhua Xie, Jiping Cai, and Yong Yao

Department of Ophthalmology, Wuxi People's Hospital Affiliated to Nanjing Medical University, Wuxi, Jiangsu, China

Correspondence should be addressed to Yong Yao; yaoyongnjmu@126.com

Received 4 November 2021; Revised 29 January 2022; Accepted 23 February 2022; Published 29 March 2022

Academic Editor: Cristina Cosentino

Age-related macular degeneration (AMD) is the leading cause of irreversible visual loss among the elderly worldwide with unidentified pathogenesis and limited therapeutic options. Oxidative stress-induced damage to the retinal pigment epithelium (RPE) is central in the development and progression of AMD. Decorin (DCN), a small leucine-rich proteoglycan, possesses powerful antifibrotic, anti-inflammatory, and antiangiogenic properties. DCN has also been reported to serve a cytoprotective role in various cell types, but its protective effects against H_2O_2-induced oxidative stress and apoptosis in ARPE-19 cells remain unclear. In this study, we showed that DCN significantly attenuated the increase in cell viability loss, apoptosis rate, and reactive oxygen species (ROS) levels in ARPE-19 cells induced by H_2O_2. Furthermore, DCN activated the AMPK/mTOR pathway to promote autophagy while genetic inhibition of autophagy-related gene 5 (ATG5) hindered autophagic process and diminished the protective role of DCN against oxidative stress in ARPE-19 cells. Collectively, these results suggest that DCN could protect RPE cells from H_2O_2-induced oxidative stress and apoptosis via autophagy promotion, thus providing the therapeutic potential for AMD prevention and treatment.

1. Introduction

Age-related macular degeneration (AMD) is a chronic, progressive neurodegenerative disease that affects older individuals and features loss of central vision. AMD accounts for 8.7% of all blindness worldwide and is the leading cause of irreversible vision disability among older adults in developed countries. By 2040, it is expected that 288 million individuals will be diagnosed with AMD [1]. Broadly, AMD can present in three clinical forms: early nonexudative (dry), late nonexudative (atrophic), and exudative or neovascular (wet). Early AMD is characterized by the presence of drusen in the aging macula without visual loss [2]. The vast majority of AMD patients suffer from dry or atrophic AMD, characterized by the accumulation of drusen, the degeneration of RPE cells and photoreceptors, and geographic atrophy [3]. Choroidal neovascularization is accompanied by an advanced form of wet AMD, leading to exudation and bleeding within the macula. Therapeutic intervention for patients with wet AMD involves repeated administration of intravitreal antivascular endothelial growth factor (VEGF) [4]. However, currently, there is no intervention to slow the progression of the early stages of AMD, and no definitive treatment is available for nonexudative AMD due partly to our incomplete understanding of the underlying pathogenesis of AMD.

AMD is a highly complex neurodegenerative disease that is affected by a combination of aging, genetic, and environmental stressors. The exact pathogenesis of AMD remains unknown [5, 6]. Aging is the primary risk factor associated with AMD, as this irreversible process is accompanied by accumulated oxidative stress, chronic inflammation, and mitochondrial dysfunction [7]. Among these risk factors, numerous studies have shown that the accumulation of oxidative stress may lead to morphological and functional abnormalities in retinal pigment epithelial (RPE) cells, which is the core pathophysiological change in AMD [8, 9]. In physiological processes, normal active retinal metabolism

involves high oxygen levels and promotes the generation of reactive oxygen species (ROS), leading to a highly oxidative environment in which the RPE is exposed [10, 11] Dysfunction of the antioxidant system and other pathological factors during aging contributes to ROS overaccumulation, resulting in oxidative cell damage in RPE cells [12].

Autophagy is particularly important for maintaining the homeostasis of the RPE because these cells are exposed to sustained oxidative stress [13]. Several studies have reported that autophagy plays a vital role in the antioxidative process and promotes the clearance of damaged organelles or misfolded proteins in RPE cells during oxidative stress [14–16]. Autophagy dysfunction has also been associated with pathogenesis of AMD [17]. Numerous studies have demonstrated that autophagy activators such as melatonin and rapamycin showed great potential in AMD treatment [18, 19]. Among these activators, decorin (DCN) has been shown to promote autophagy in various cells including endothelial, nucleus pulposus, and breast carcinoma cells [20–23]. DCN, identified as a class I small leucine-rich proteoglycan (SLRP), localizes to the cornea, skin, and other connective tissue and serves as a regulator of various cellular function by fettering to extracellular matrix molecules or through cell receptors [24]. The biological function of DCN mainly involves cell growth, differentiation, and proliferation through its interaction with various molecules, such as transforming growth factor-beta and insulin-like growth factor receptor 1 [25, 26]. A previous study demonstrated that DCN showed an inhibitory effect on oxidative stress and apoptosis in posttraumatic brain injury in rat cerebrum as depicted by increased activity of superoxide dismutase (SOD) and glutathione peroxidase (GSH) [27, 28]. Moreover, DCN may inhibit glucose-induced oxidative stress and apoptosis of human lens epithelial cells and protect the barrier function of RPE cells under high-glucose conditions [23]. However, the potential protective effects of DCN on AMD have not yet been studied. In this study, we aimed to investigate whether DCN could protect RPE cells from H_2O_2-induced oxidative stress and explore the underlying mechanism.

2. Materials and Methods

2.1. Cell Culture. The ARPE-19 human cell line was purchased from the Cell Bank of the Chinese Academy of Sciences (Shanghai, China). Before the experiment, the cells were seeded at approximately $0.5 \times 10^5/cm^2$ and maintained in culture for two weeks unless otherwise stated to establish a robust oxidative stress model. The cells were cultured in Dulbecco's modified Eagle's/Ham's F-12 medium (DMEM/F12) containing 10% fetal bovine serum (FBS, Gibco, USA) in humidified air with 5% CO_2 at 37°C. The culture medium was changed every two days.

2.2. Cell Viability Assay. The viability of ARPE-19 cells was evaluated using the CCK-8 reagent (Dojindo, Japan) according to the manufacturer's instructions. Briefly, ARPE-19 cells were seeded in 96-well culture plates with 1×10^4 cells per well and treated with H_2O_2 and DCN for the indicated times. Subsequently, the culture medium was replaced with medium containing 10% CCK-8 solution at 37°C for 4 h. The absorbance of each well was determined using microplate spectrophotometer (BioTek, USA) at a wavelength of 450 nm. The OD absorbance was normalized to that of the untreated controls.

2.3. Measurement of SOD, Malondialdehyde, and GSH. For SOD determination, ARPE-19 cells were treated with different conditions, and the SOD activity was determined using Superoxide Dismutase Assay Kit (Beyotime, China) according to the manufacturer's instructions. Briefly, after the indicated treatment, the cells were washed twice with cold PBS. Subsequently, the sample solution was added to the working solution and incubated at 37°C for 30 min. As a result, the absorbance was determined at the wavelength of 450 nm as describe above. In addition, the content of malondialdehyde (MDA) and glutathione was determined using a commercial assay kit (Beyotime, China) and measured at wavelength of 532 nm and 414 nm, respectively, after incubation with the working solution according to the manufacturer's instructions.

2.4. Western Blot. Western blot analysis was conducted as described previously [29]. Briefly, the cells were lysed with buffers containing inhibitor targeting protease and phosphatase. Equal volumes of protein were then subjected to sodium dodecyl sulfate-polyacrylamide gel electrophoresis and transferred to polyvinylidene difluoride membranes (Millipore, USA). Subsequently, the transferred membrane was blocked with bovine serum albumin for 1 h and incubated with the following primary antibodies against ATG5 (60061-1-Ig, PTG, China), LC3 (12741, CST, USA), p62 (5114, CST, USA), BAX (50599-2-Ig, PTG, China), Bcl-2 (12789-1-AP, PTG, China), cleaved-caspase 3 (5A1E, CST, USA), AMPK(5831, CST, USA), p-AMPK(50081, CST, USA), mTOR(2983, CST, USA), p-mTOR(5536, CST, USA), p70S6K(9202, CST, USA), p-p70S6K(97596, CST, USA), and β-actin (4970, CST, USA). The membranes were then washed with Tris-buffered saline with 0.1% Tween 20 (TBST) and incubated with the horseradish peroxidase-conjugated secondary antibodies (7074, CST, USA). The membranes were then washed and visualized using a chemiluminescence system with an ECL reagent (Yeasen, China).

2.5. mRFP-GFP-LC3 Transduction and Analysis. Before DCN treatment, ARPE-19 cells were transduced with Ad-mRFP-GFP-LC3 (HanBio, China) at five multiplicities of infection for 3 h according to the manufacturer's instructions. The autophagosomes and autolysosomes in ARPE-19 cells were visualized using a Leica SP5 confocal laser scanning microscope (CLSM) and quantified using ImageJ software.

2.6. Transmission Electron Microscopy. ARPE-19 cells were cultured in 6 cm dishes and subjected to different treatments. The cells were washed carefully and collected by scrapping. Then, the cells were collected after centrifugation and fixed in 2.5% glutaraldehyde solution for 24 h at 4°C. Subsequently, the ARPE-19 cell pellets were hydrated with acetone

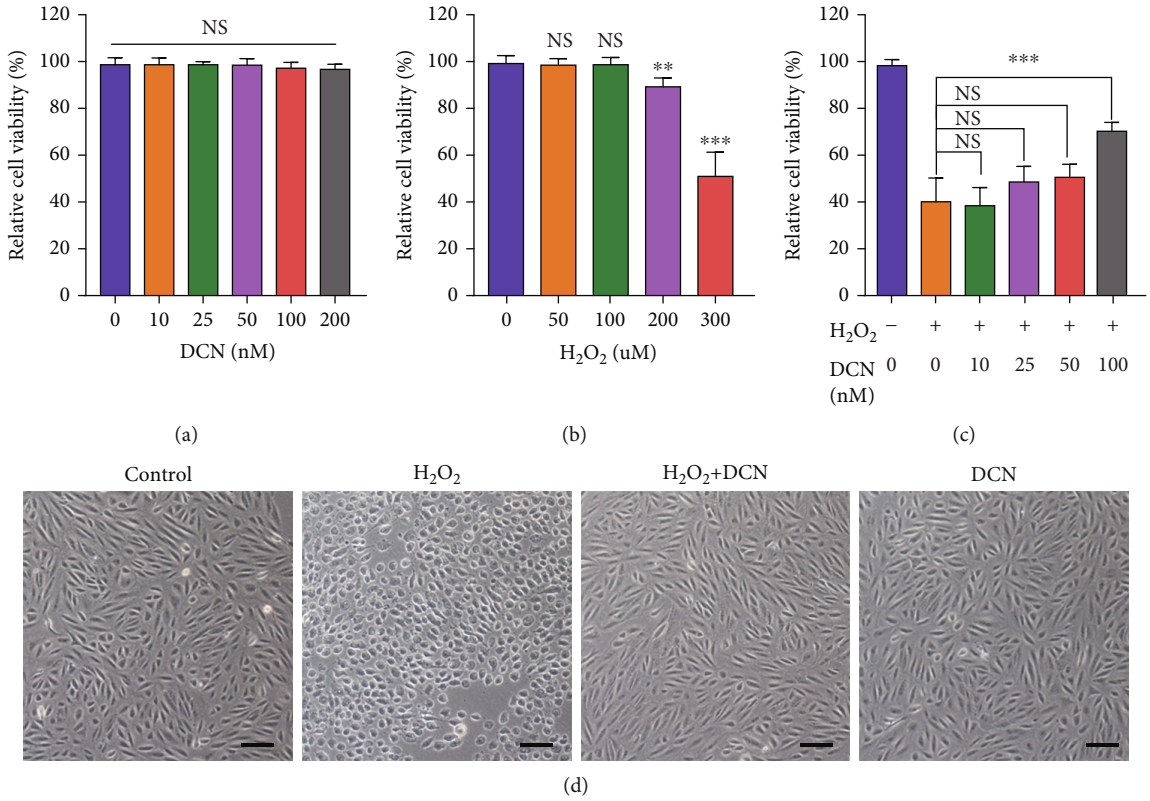

Figure 1: DCN exhibited a protective effect against H_2O_2-induced cell damage. (a and b) ARPE-19 cells were treated with DCN or H_2O_2 for 24 h at different concentrations and the cell viability was assessed using CCK8. (c) ARPE-19 cells were pretreated with DCN for 24 h at various concentrations and incubated with H_2O_2 (300 μM) for another 24 h to determine the cell viability. (d) Morphological changes in ARPE-19 cells following indicated treatment. Data is shown as mean ± SD, $^{**}p < 0.01$, and $^{***}p < 0.001$.

and embedded in Epon. Ultrathin sections were cut and the cellular structure was observed using a transmission electron microscope (Hitachi, Japan).

2.7. Cell Transfection with ATG5 siRNA. ARPE-19 cells were seeded in 6-well plates and transfected with ATG5 siRNA or nontargeting control siRNA at a concentration of 50 nM by Lipofectamine PLUS reagent (Invitrogen, USA) according to the manufacturer's instruction. The transfected ARPE-19 cells were then subjected to different treatments.

2.8. Immunofluorescence Staining. ARPE-19 cells were cultured in a confocal dish. To evaluate intracellular ROS, the cells were incubated with 2′,7′-dichlorodihydrofluorescein diacetate (DCFH-DA, Sigma, USA) probes for 30 min at 37°C according to the manufacturer's instructions. Then, the incubated cells were washed with three times PBS and visualized by CLSM. For terminal deoxynucleotidyl transferase dUTP nick end labeling (TUNEL) staining, the cells were fixed with 4% paraformaldehyde for 15 min and washed with PBS three times. Finally, the cells were incubated with 0.1% Triton X-100 for 5 min and stained with the In Situ Cell Death Detection Kit (Beyotime, China) according to the manufacturer's instructions. Then, the cells were visualized by CLSM.

2.9. Fluorescence-Activated Cell Sorting Analysis (FACS). For quantitative evaluation of intracellular ROS, ARPE-19 cells were stained with DCFH-DA as described above. ARPE-19 cells were collected and analyzed by flow cytometry (BD FACS Aria III, USA). For apoptosis evaluation, the cells exposed to different treatments were washed with cold PBS and incubated with the Annexin V-FITC Apoptosis Detection Kit (BD, USA). Stained cells were washed and then collected by trypsin. Then, the cell pellets were resuspended by cold PBS and analyzed by flow cytometry.

2.10. Statistical Analysis. All data is presented as mean ± standard deviation (SD) from the results obtained from at least three independent experiments. One-way analysis of variance (ANOVA) with Dunnett's multiple comparisons test was used for statistical analysis. Difference with p value less than 0.05 was considered statistically significant. GraphPad Prism 8 was used for the statistical analysis.

3. Results

3.1. DCN Protected ARPE-19 Cells against H_2O_2-Induced Oxidative Cell Death. In this study, H_2O_2 was used to induce oxidative stress, which plays a vital role in the pathology of AMD. As it has been reported that ARPE-19 cells are less vulnerable to oxidative stress with over 1-week longer culture periods, all experiments were conducted after a 2-

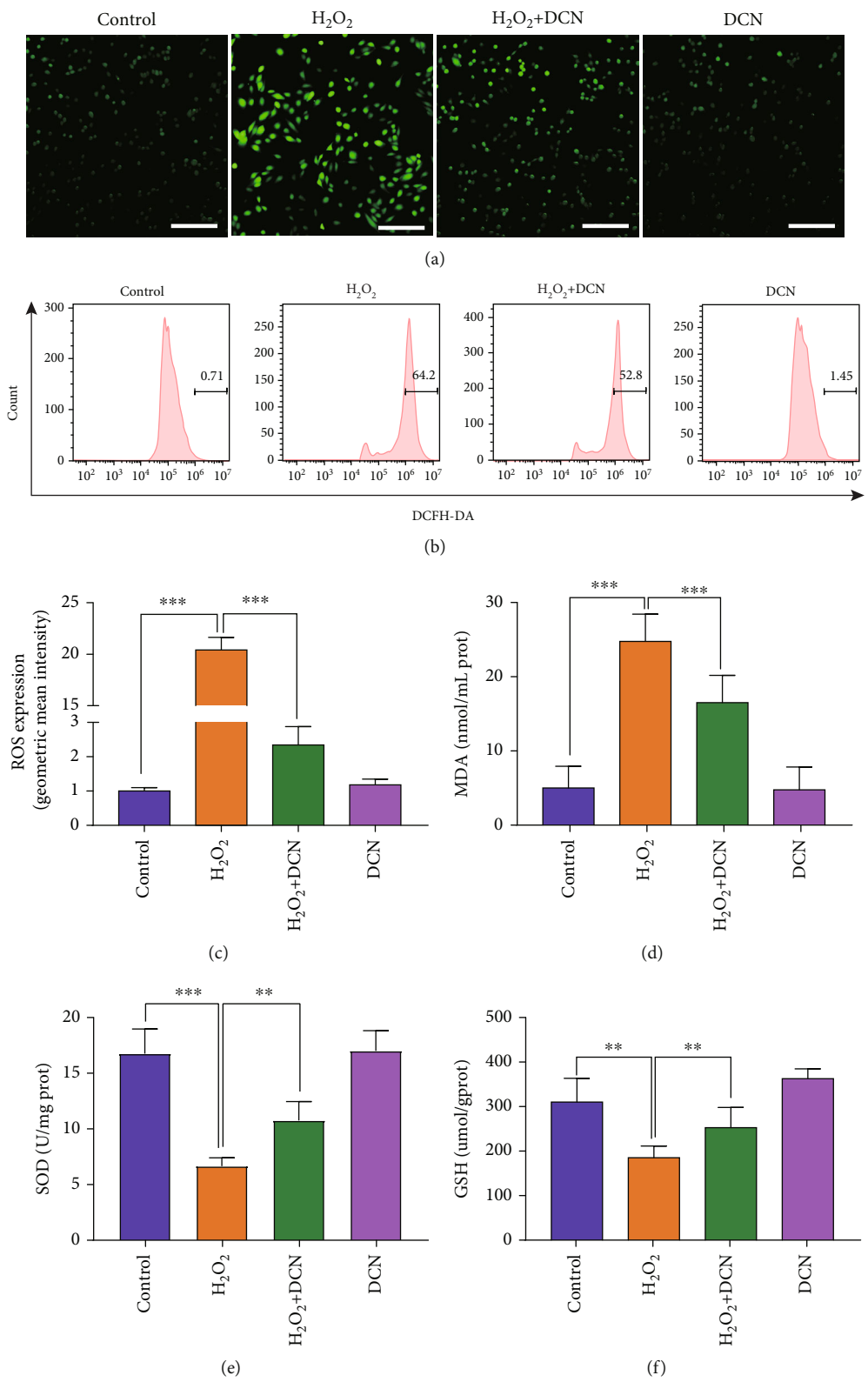

Figure 2: DCN inhibited H_2O_2-induced oxidative stress. (a) CLSM images of ARPE-19 cells using ROS detection probes as indicators. (b and c) ROS analysis with flow cytometry and quantitative analysis of ROS fluorescence intensity. (d–f) DCN treatment reversed the H_2O_2-induced changes in the level of MDA, SOD, and GSH. Data is shown as mean ± SD, $^{**}p < 0.01$, and $^{***}p < 0.001$.

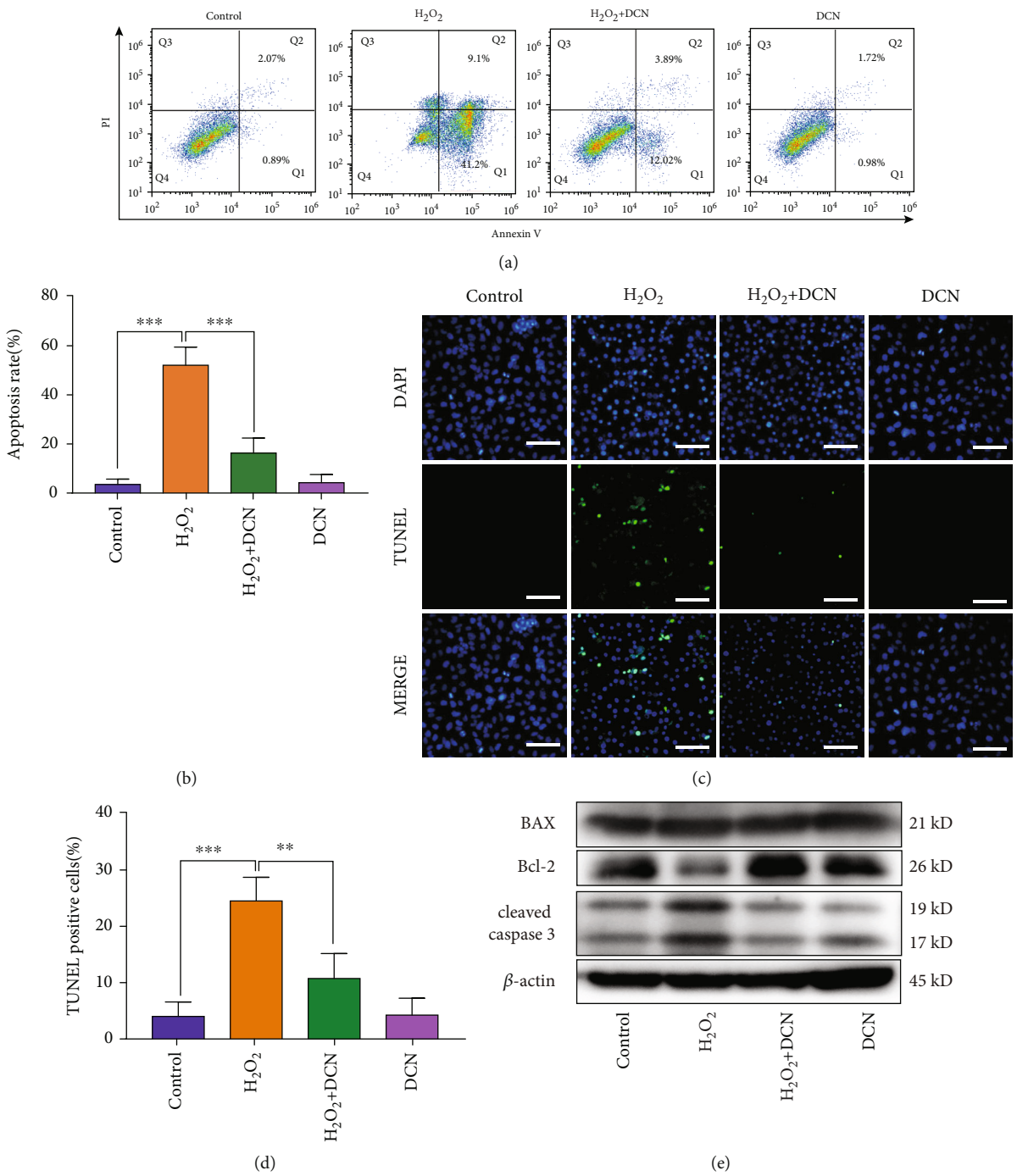

Figure 3: Continued.

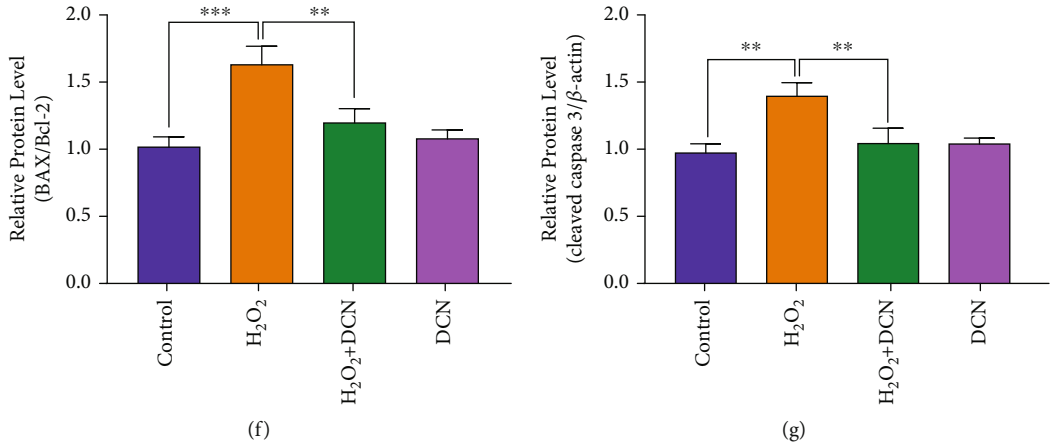

Figure 3: DCN ameliorated the cell apoptosis in oxidative stress. (a) Representative flow cytometry plots using Annexin V-FITC/PI staining for apoptosis in ARPE-19 cells. (b) Quantification of apoptotic cells. (c) TUNEL staining was applied to measure apoptosis levels in ARPE-19 cells. (d) Quantification of TUNEL staining. (e–g) Western blot analysis and quantitative analysis of BAX, BCL2, and Cleaved-Caspase 3 protein level in ARPE-19 cells. Data is shown as mean ± SD, $^{*}p < 0.05$, $^{**}p < 0.01$, and $^{***}p < 0.001$.

week cell culture to establish a vigorous oxidative stress model for significant cell damage and death [30]. First, we examined the potential cytotoxicity of DCN in ARPE-19 cells. No significant changes in cell viability were observed after incubation with DCN for 24 h at concentrations of 10–200 nM (Figure 1(a)). Then, to evaluate the protective effect of DCN, ARPE-19 cells were exposed to different concentrations of H_2O_2 for 24 h. As shown in Figure 1(b), ARPE-19 cells endured H_2O_2 incubation at concentration of 50–100 μM, and the cell viability decreased in a dose-dependent manner at 200 and 300 μM. Furthermore, treatment with 300 μM H_2O_2 inhibited cell viability by approximately 50%. Based on these results, ARPE-19 cells were first subjected to DCN at various concentrations for 24 h and then incubated with H_2O_2 (300 μM) for another 24 h. Dramatically, DCN significantly attenuated H_2O_2-induced cytotoxic effect as demonstrated by 75% increase in the cell viability when ARPE-19 cells were cotreated with DCN at the concentration of 100 nM (Figure 1(c)). Morphological changes in the ARPE-19 cells were also assessed. Incubation with H_2O_2 led to apparent cellular changes such as cellular shrinkage. However, coincubation with DCN diminished these morphological changes induced by H_2O_2 (Figure 1(d)).

3.2. DCN Inhibited H_2O_2-Induced Oxidative Stress in ARPE-19 Cells. To evaluate the effects of DCN on oxidative stress, ROS generation was assessed. As shown in Figure 2(a), H_2O_2 induced a significant increase in ROS expression. Comparatively, cotreatment with DCN remarkably decreased the upregulated level of ROS induced by H_2O_2. Similar trends were observed in the quantitative assessment of ROS by flow cytometry (Figures 2(b) and 2(c)). MDA, a lipid peroxidation product, is a kind of biomarkers for oxidative damage [31]. The MDA level in ARPE-19 cells was significantly increased (-4.95-fold) upon H_2O_2 treatment, but this increase was notably blocked by DCN treatment (Figure 2(d)). Oxidative stress arises due to redox imbalance between oxidant and antioxidant systems of the cells. SOD and GSH are viewed as important parts in a sophisticated antioxidative defense system to prevent cellular damage by scavenging ROS in the cells [32]. We found that the H_2O_2 stimulation decreased the level of both SOD and GSH by 58% and 43%, respectively, compared with the untreated control, while pretreatment with DCN attenuated the reduction induced by H_2O_2 (Figures 2(e) and 2(f)).

3.3. DCN Ameliorated Apoptotic Cell Death in ARPE-19 Cells under Oxidative Stress. To evaluate whether DCN could protect ARPE-19 cells from apoptotic cell death, we determined the apoptosis by flow cytometry, immunofluorescence, and western blot. As shown in Figures 3(a) and 3(b), the population of apoptotic cells was significantly increased by 13.9-fold under oxidative stress conditions. However, treatment with DCN exhibited a significant inhibitory effect on apoptosis of ARPE-19 cells induced by H_2O_2. In addition, we performed TUNEL staining and similar results were observed (Figures 3(c) and 3(d)). The Bcl-2 (B-cell lymphoma-2) family proteins play an important role in regulating the mitochondria-dependent extrinsic and intrinsic cell apoptosis. This family of proteins is mainly divided into various antiapoptotic and proapoptotic categories, among which antiapoptotic Bcl-2 and proapoptotic BAX (Bcl-2 Associated X-protein) play a central role in regulating apoptosis [33]. Subsequently, western blot was applied to evaluate the Bax/Bcl-2 ratio accompanied by the downstream protein cleaved caspase-3. As shown in Figures 3(e)–3(g), western blot results indicated that H_2O_2 significantly increased the Bax/Bcl-2 ratio and the expression level of cleaved caspase-3 by 60% and 43%, respectively. However, DCN intervention could reverse above effects induced by H_2O_2. These results indicated that DCN exerted a protective effect against H_2O_2-induced oxidative cell damage via antiapoptosis.

3.4. DCN Promoted Autophagy in H_2O_2-Treated ARPE-19 Cells. Autophagy is intricately linked to apoptosis in

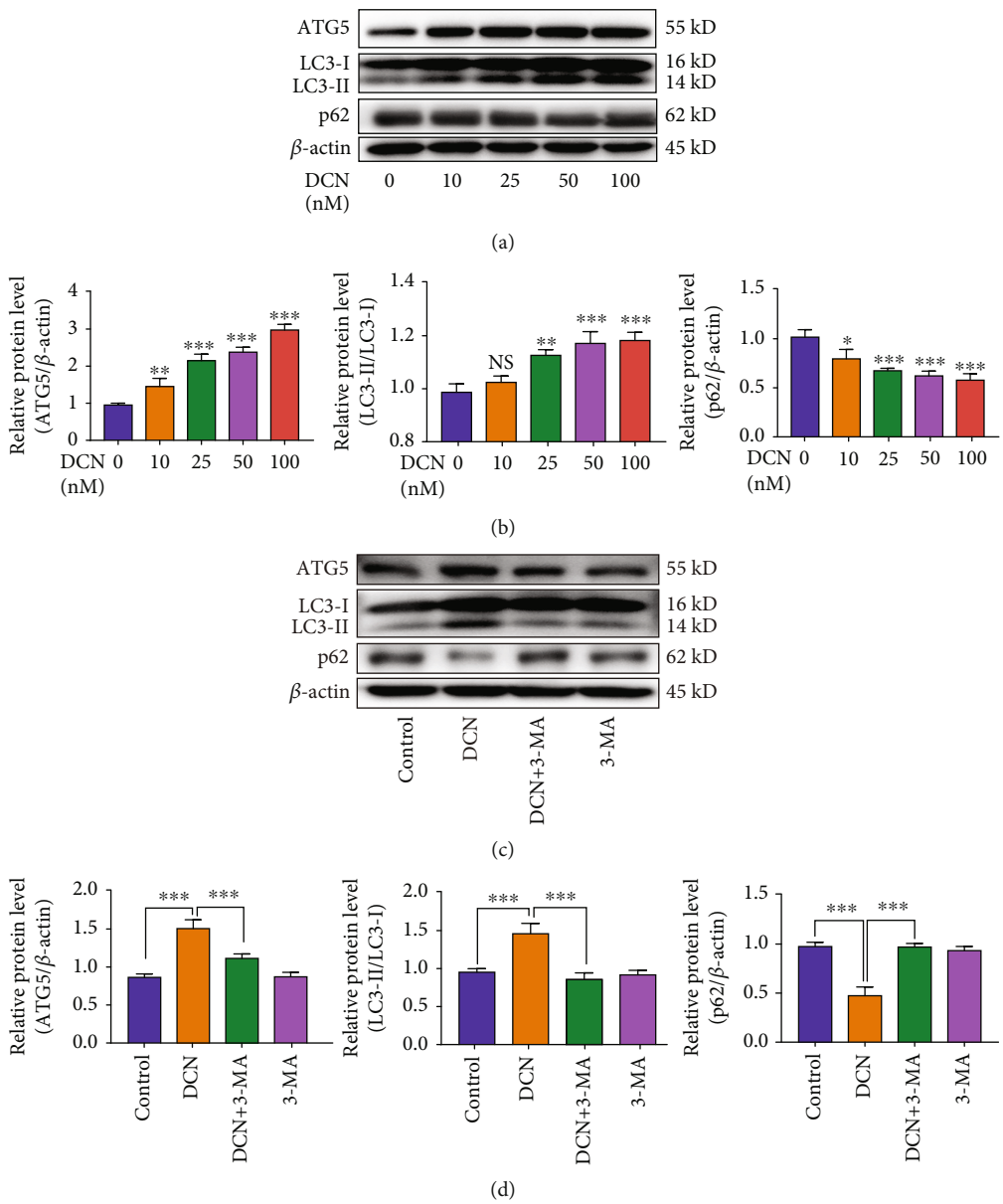

Figure 4: Continued.

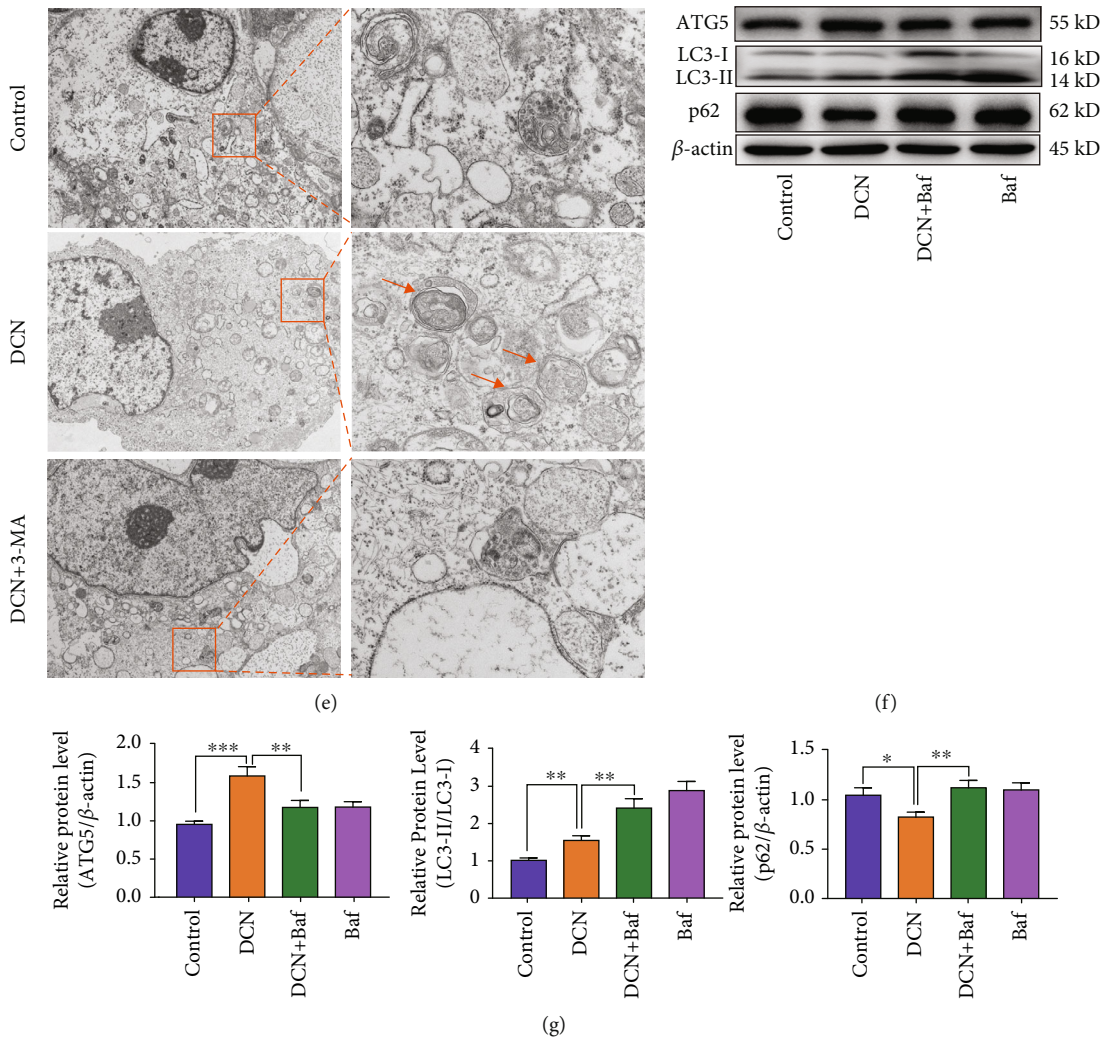

Figure 4: Continued.

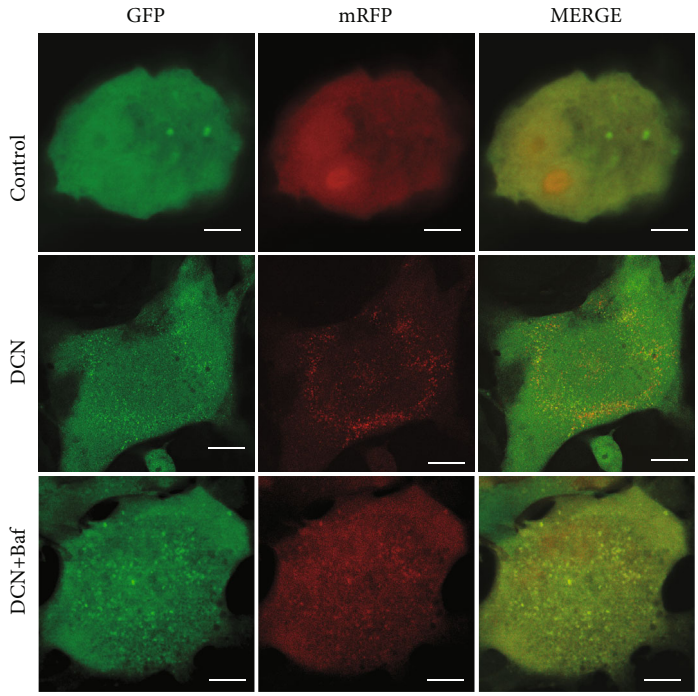

(h)

Figure 4: DCN promoted autophagy in ARPE-19 cells. (a and b) The protein level of ATG5, p62, and LC3 in ARPE-19 cells. ARPE-19 cells were treated with DCN in indicated concentrations for 24 h. The densities of ATG5/β-actin, p62/β-actin, and LC3II/LC3I were analyzed. (c and d) The protein level of ATG5, p62, and LC3 in ARPE-19 cells treated with 100 nM DCN in the presence of 5 mM 3-MA. The densities of ATG5/β-actin, p62/β-actin, and LC3II/LC3I were analyzed. (e) The ultrastructures in ARPE-19 cells were examined by transmission electron microscopy (TEM). The orange arrow indicates autophagosome and autolysosomes in the cytoplasm. (f and g) The protein level of ATG5, p62, and LC3 in ARPE-19 cells treated with 100 nM DCN in the presence of 0.1 μM bafilomycin A1 (Baf). The densities of ATG5/β-actin, p62/β-actin, and LC3-II/LC3-I were analyzed. (h) ARPE-19 cells were transfected with mRFP-GFP-LC3 and subjected to 100 nM DCN treatment. Data is shown as mean ± SD, $^{*}p < 0.05$, $^{**}p < 0.01$, and $^{***}p < 0.001$.

various degenerative diseases. Aberrant autophagy has been reported to be associated with AMD. Several lines of evidence have demonstrated that autophagy acts as a mediator in maintaining ROS balance to protect ARPE-19 cells against oxidative stress [13, 15]. To determine whether DCN could activate autophagy in ARPE-19 cells, we examined autophagy proteins by western blot. The results showed that the ATG5 protein expression and LC3-II/LC3-I ratio were increased, accompanied by decreased P62 expression under DCN stimulation in a dose-dependent manner (Figures 4(a) and 4(b)). To further investigate autophagy promotion by DCN, ARPE-19 cells were treated with the autophagy inhibitor 3-methyladenine (3-MA). Treatment with 3-MA partly diminished the autophagy process induced by DCN, as 3-MA decreased ATG5 expression and the ratio of LC3-II/LC3-I by 26% and 41%, respectively, while increased the accumulation of p62 by 104% compared with the treatment with DCN (Figures 4(c) and 4(d)). To confirm the activation of DCN-induced autophagy, transmission electron microscope (TEM) ultrastructural analysis was performed as golden standard for autophagy detection. TEM images showed that an increased number of autophagic vacuoles were observed in DCN-treated ARPE-19 cells, but not in the control cells, and cotreatment with 3-MA inhibited the formation of autophagosome induced by DCN (Figure 4(e) and S1). To further confirm the autophagic changes and validate the autophagic flux induced by DCN, bafilomycin A1 (Baf), an H+-ATPase inhibitor, was used to inhibit the fusion of autophagosomes with lysosomes during autophagy. As shown in Figures 4(f) and 4(g), Baf significantly increased the ratio of LC3-II/LC3-I by 55% and p62 expression by 36% while downregulated ATG5 expression by 26% in DCN-treated ARPE-19 cells compared to treatment with DCN alone. Moreover, we assessed autophagic flux in ARPE-19 cells using adenovirus-mediated mRFP-GFP-LC3. The autophagosomes in transduced ARPE-19 cells were marked by mRFP-GFP-LC3 and exhibited both red fluorescent protein (RFP) and green fluorescent protein (GFP), displayed as yellow dots. In contrast, only red dots were observed in autolysosomes because the green GFP fluorescence was eliminated in the acidic environment of the lysosomes. DCN significantly increased the number of both autophagosomes and autolysosomes compared with control cells, indicating a high level of autophagy flux. However, the number of red autolysosomes declined in the case that Baf was present to blockage of autophagy flux (Figure 4(h) and S2).

3.5. DCN Inhibited H_2O_2-Induced Oxidative Stress in Autophagy-Dependent Manner. To further investigate whether the protective effect of DCN against oxidative stress was autophagy-dependent in ARPE-19 cells, we next

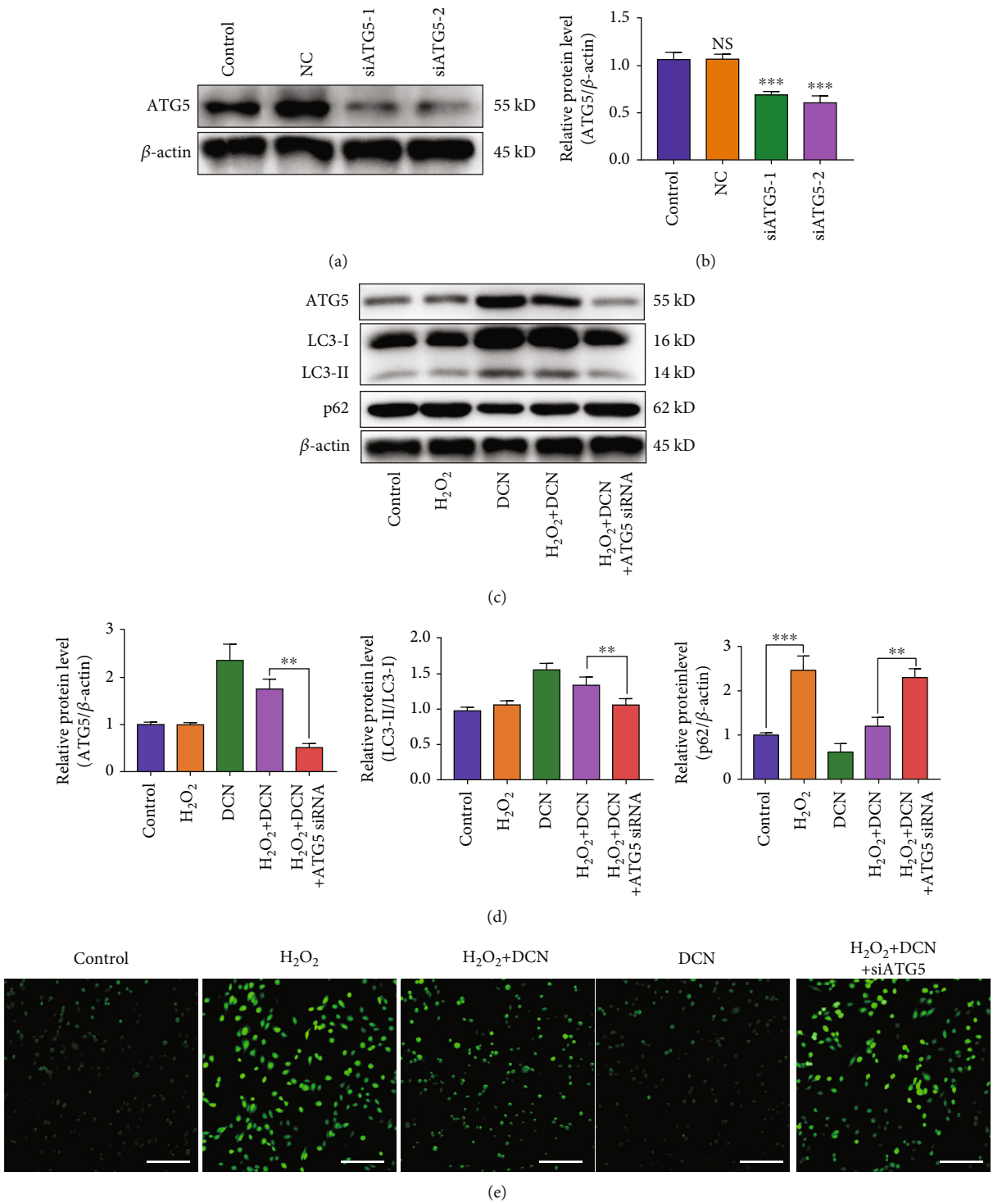

Figure 5: Continued.

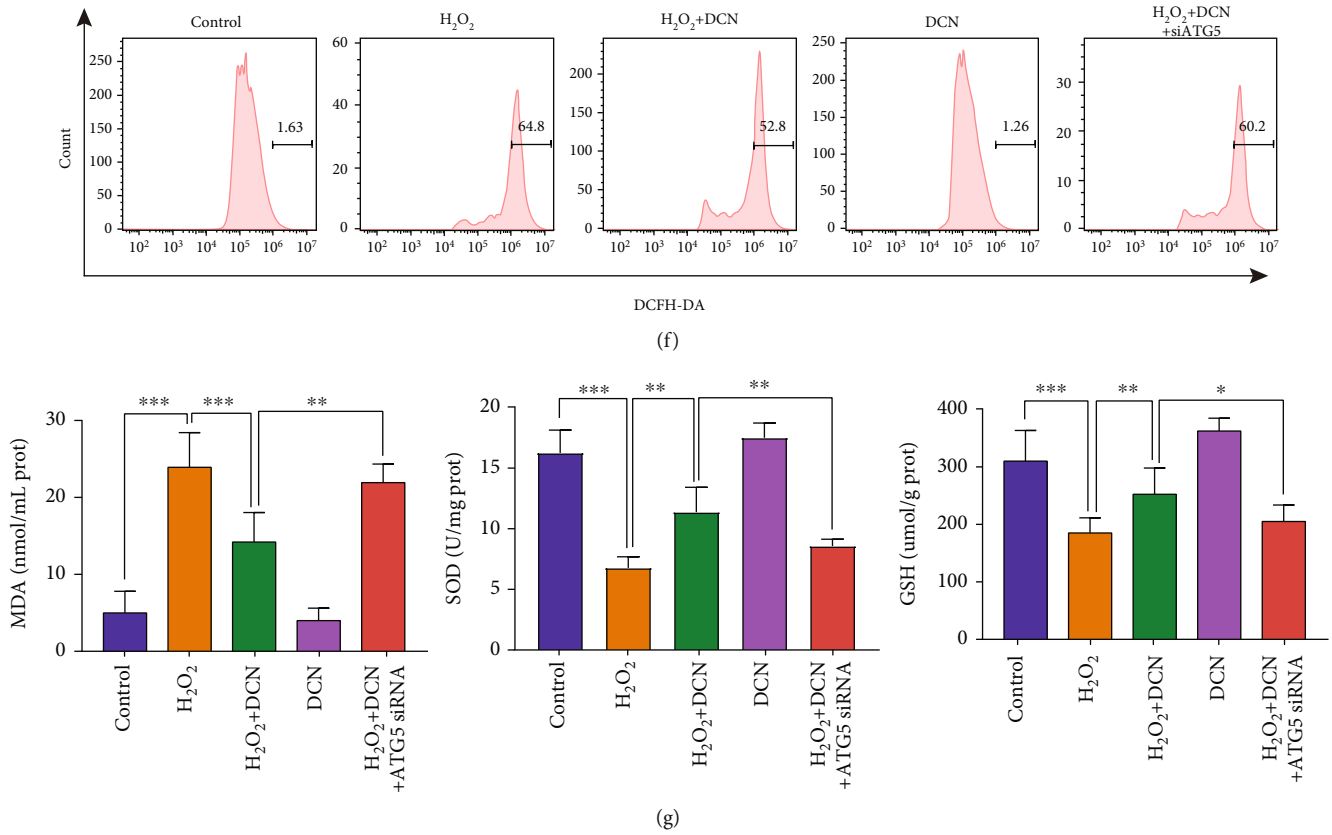

Figure 5: Protective effect of DCN against oxidative stress was dependent on autophagy. ARPE-19 cells were first transfected with ATG5 siRNA and received different treatments. (a and b) The expression level of ATG5 in ARPE-19 cells after ATG5 small interfering RNA (siRNA) transfection. The densities of ATG5/β-actin were analyzed. (c and d) The protein levels of ATG5, p62, and LC3 in ARPE-19 cells in the presence of ATG5 siRNA transfection followed by treatment of DCN under the stimulation of H_2O_2. (e) CLSM images of ARPE-19 cells using ROS detection probes as indicators. (f) ROS analysis with flow cytometry and quantitative analysis of ROS fluorescence intensity. (g) The expression level of MDA, SOD, and GSH following indicated treatment. Data is shown as mean ± SD, $^{*}p < 0.05$, $^{**}p < 0.01$, and $^{***}p < 0.001$.

silenced the expression of autophagy-related protein 5 (ATG5), which is indispensable for autophagy. As shown in Figures 5(a) and 5(b), silencing of ATG5 by siRNA resulted in a significant decrease in ATG5 protein expression level. Oxidative stress induced by H_2O_2 led to the augmented accumulation of p62 but did not alter the ATG5 protein level and LC3-II/LC3-I ratio. As expected, DCN treatment reduced the expression level of p62 while increased ATG5 expression and LC3-II/LC3-I ratio. However, genetic inhibition of ATG5 diminished the autophagy promotion induced by DCN under oxidative stress (Figures 5(c) and 5(d)). Moreover, ATG5 silencing attenuated the protective effect of DCN against oxidative stress as ROS accumulation was augmented by 109% compared with DCN treatment under H_2O_2 stimulation (Figures 5(e) and 5(f) and S3). Similar results were observed for the expression levels of MDA, SOD, and GSH (Figure 5(g)). Also, the antiapoptotic effect of DCN on oxidative stress was prominently impaired by ATG5 knockdown (Figures 6(a)–6(f)).

3.6. DCN Induced Autophagy via AMPK-mTOR Pathway. Autophagy is modulated by a variety of signaling pathways. Among these pathways, AMP-activated protein kinase (AMPK)/mammalian target of rapamycin (mTOR) is involved in the regulation of autophagy under oxidative stress [34]. As shown in Figures 7(a)–7(d), H_2O_2 stimulation decreased the phosphorylation of AMPK by 52% and increased the phosphorylation of mTOR and its downstream target p70S6K by 18% and 13%, respectively. Treatment with DCN under oxidative stress increased the expression level of p-AMPK by 375% while decreased the phosphorylation level of both mTOR and p70S6K by 27% and 24%, respectively (Figures 7(a)–7(d)). To further elucidate the role of AMPK-mTOR in DCN-induced autophagy, ARPE-19 cells were treated with the AMPK inhibitor compound C or mTOR activator MHY1485 prior to DCN treatment. Compound C inhibited the AMPK-mTOR signaling pathway and antagonized the autophagy promotion by DCN under oxidative stress. Likewise, the mTOR activator MHY1485 was applied to activate mTOR signaling, leading to attenuation of DCN-induced autophagy (Figures 7(e)–7(k)). These results above indicate that autophagy induced by DCN in ARPE-19 cells is dependent on the AMPK-mTOR signaling pathway.

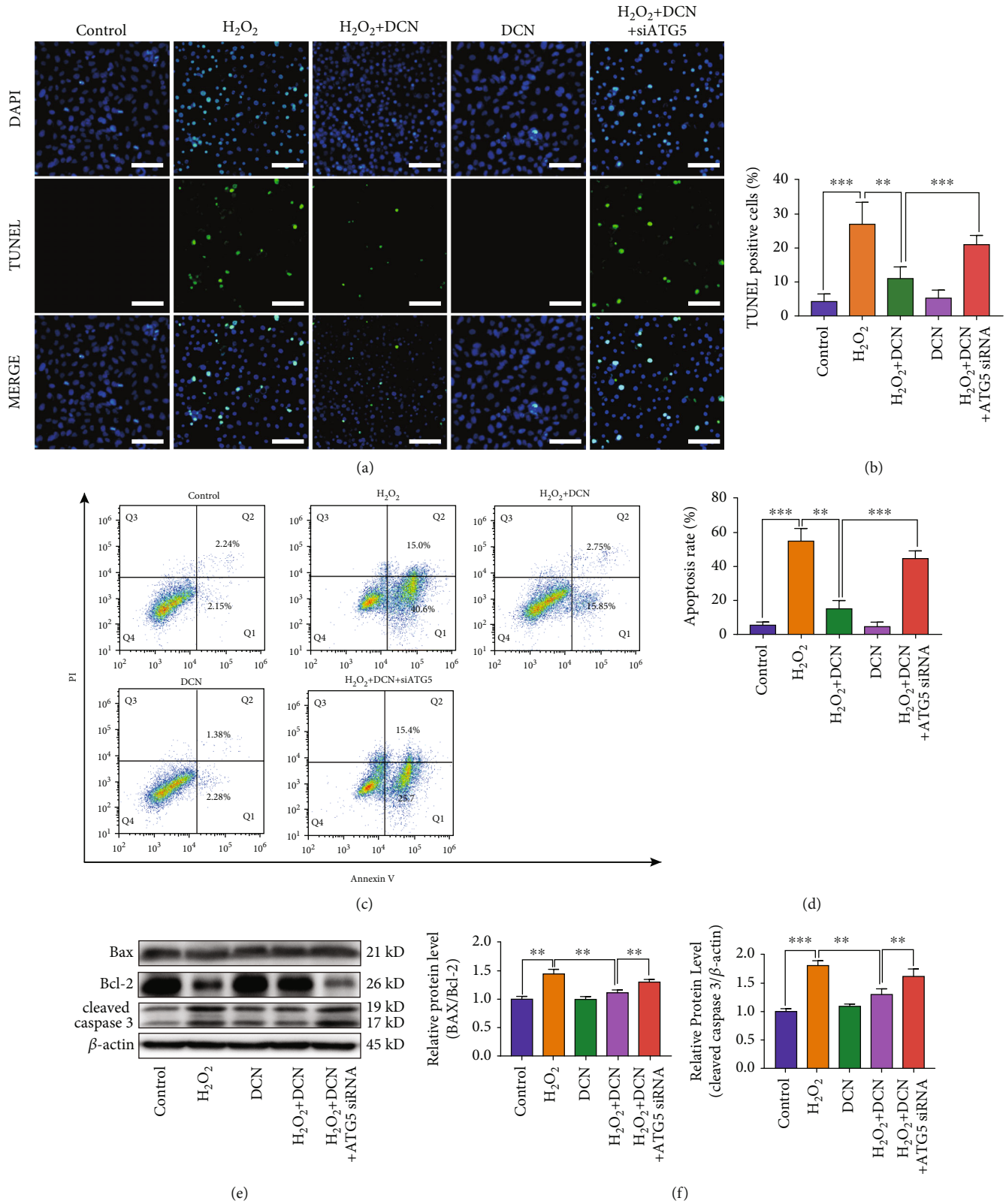

Figure 6: Autophagy inhibition attenuated the protective effect of DCN against cell apoptosis in ARPE-19 cells. (a and b) Microscopic images and quantification of TUNEL-positive ARPE-19 cells. (c) Flow cytometry results with Annexin V-FITC/PI staining. (d) Quantification of apoptotic cells. (e and f) Western blot analysis and quantitative analysis of BAX, BCL2, and Cleaved-Caspase 3 protein level in ARPE-19 cells. Data is shown as mean ± SD, $^{**}p < 0.01$, and $^{***}p < 0.001$.

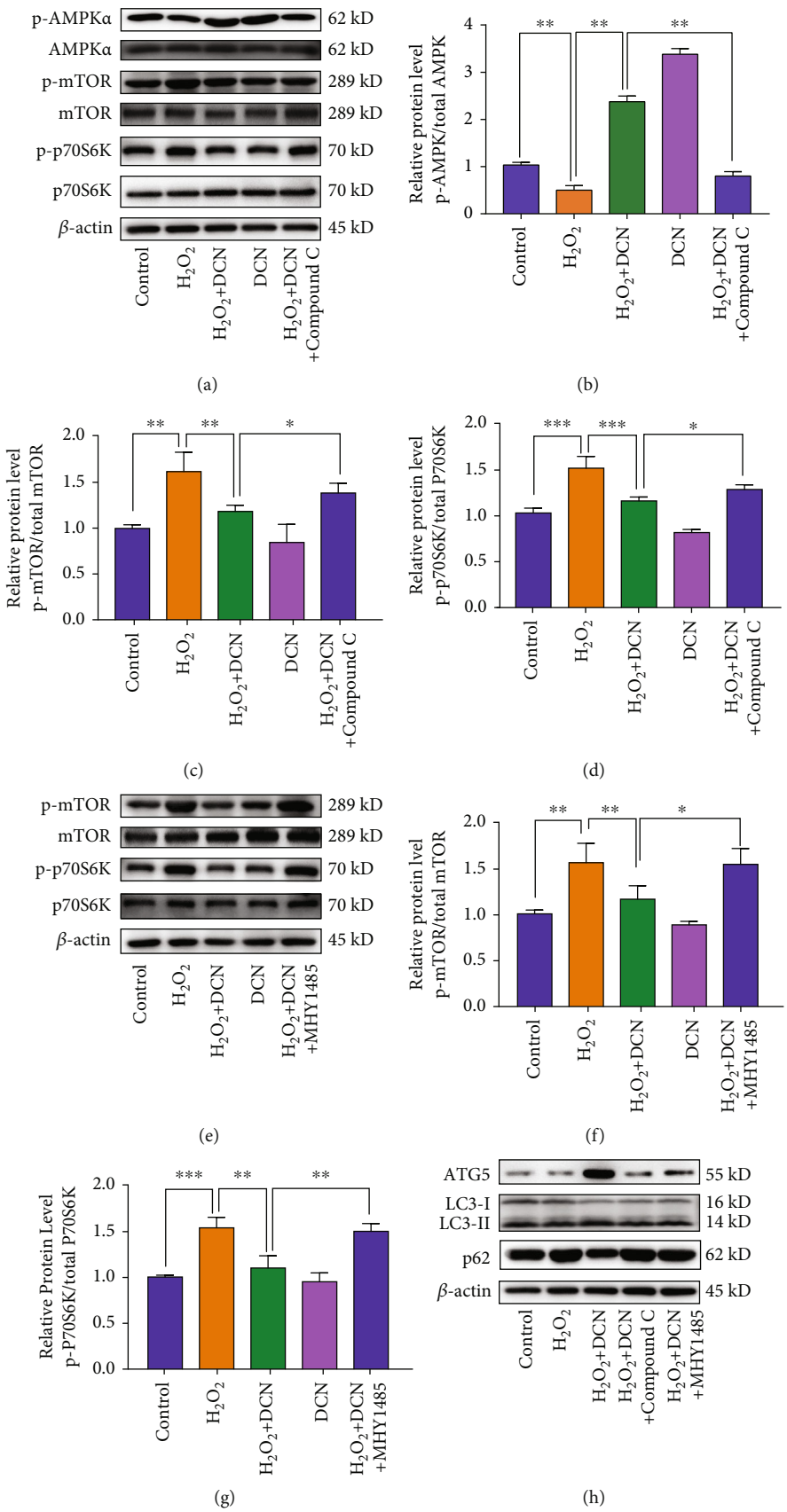

Figure 7: Continued.

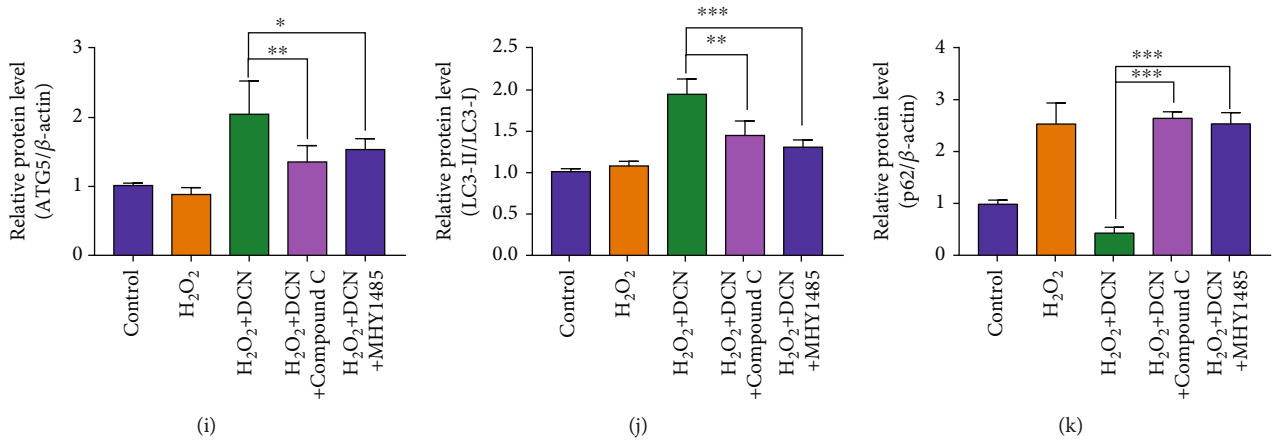

Figure 7: DCN promoted autophagy through AMPK/mTOR signaling pathway. (a–d) The protein levels of p-AMPK, AMPK, p-mTOR, mTOR, p-p70S6K, and p70S6K in ARPE-19 cells. ARPE-19 cells were treated with 5 mM compound C prior to DCN treatment. The densities of p-AMPK/AMPK, p-mTOR/mTOR, and P-p70S6K/p70S6K were analyzed. (e–g) The protein levels of p-AMPK, AMPK, p-mTOR, mTOR, p-p70S6K, and p70S6K in ARPE-19 cells. ARPE-19 cells were treated with 5 μM MHY1485 prior to DCN treatment. The densities of p-mTOR, mTOR, p-p70S6K, and p70S6K were analyzed. (h–k) The protein levels of ATG5, p62, and LC3 in ARPE-19 cells. ARPE-19 cells were treated with 5 mM compound C or 5 μM MHY1485 prior to DCN treatment under oxidative stress. Data is shown as mean ± SD, $^{*}p < 0.05$, and $^{**}p < 0.01$.

4. Discussion

The irreversible visual impairment caused by AMD has become a vital clinical problem, affecting the quality of life among people worldwide [1]. There are two forms of advanced AMD: wet and dry AMD. Currently, the administration of intravitreal anti-VEGF is viewed as a standard therapy with the desired safety and efficacy for wet AMD. Yet there is still no effective therapeutic intervention for dry AMD [6]. Numerous studies have demonstrated that oxidative stress is a key mediator of RPE death or dysfunction in the pathophysiology of AMD [9, 14, 35]. In this manner, approaches aimed at alleviating oxidative stress during AMD progression show promise for treating dry AMD.

In the present study, a reliable *in vitro* cellular model was established, and the protective effect of DCN against oxidative stress was investigated. DCN is a member of the SLRP family and is widely located in various connective tissues, serving as a vital regulator in the physiological processes [21]. Previous study reported that DCN could protect against oxidative stress in glucose-induced lens epithelial cell apoptosis [23]. In the kidney and neuronal tissues, the administration of DCN intraperitoneally ameliorated the MDA level and increased the SOD level [27, 36]. In this study, the viability of ARPE-19 cells decreased by approximately 50% in H_2O_2-induced oxidative stress, while pretreatment with DCN increased cell viability and hindered oxidative damage by H_2O_2 stimulation, as reflected by decreased MDA and intracellular ROS production. DCN treatment also increased the activity of SOD and GSH in ARPE-19 cells, which was similar to a previous report on the anti-oxidative role of DCN against posttraumatic brain injury [27]. H_2O_2-induced oxidative stress also promotes oligomerization of BAX, releases of the apoptosis-related proteins in the cytoplasm, and induced caspase activation, consequently leading to cell apoptosis [37]. In the present study, we found that pretreatment with DCN significantly decreased the expression level of both BAX and cleaved-caspase 3 while increased Bcl-2 expression under oxidative stress. These findings suggest that DCN plays a prominent role in hindering H_2O_2-induced oxidative stress and apoptosis in ARPE-19 cells, demonstrating that DCN show potential as a therapeutic approach for dry AMD in the future.

Autophagy is a key process in cellular metabolism and plays a significant role in adaptation to oxidative stress [15]. Downregulated autophagy in RPE cells is associated with the increased susceptibility to oxidative stress in AMD [38]. Previous studies found that DCN could activate autophagy in different kinds of cells including glioma, human hepatoma HepG2, endothelial, and nucleus pulposus cells [22, 23, 39, 40]. To investigate the underlying protective mechanism of DCN against oxidative stress, autophagic markers were evaluated. In the present study, we found that DCN treatment increased autophagy activity in a dose-dependent manner and enhanced the autophagy protein ATG5. ATG5 is essential for the autophagosome precursor and participates in the formation of autophagosome, and loss of ATG5 inhibits autophagy [41]. To further determine whether autophagy participated in the protective effect of DCN against oxidative stress, ATG5 was silenced in ARPE-19 cells to inhibit autophagy. We observed that DCN significantly promoted autophagic flux and protected ARPE-19 cells from oxidative damage, but this effect was mostly diminished after the silencing of ATG5, indicating that DCN protected ARPE-19 cells in an autophagy-dependent manner.

Intriguingly, we noticed a decreased level of autophagy as shown by elevated expression of p62 in H_2O_2-treated ARPE-19 cells, which varied from some researchers who hold the opinion that oxidative stress could induce autophagy [18]. In fact, it has also been reported that oxidative stress would either increase or decrease the autophagy

activity. In response to transient oxidative stress, autophagy may serve as a self-protective role with increased activity to help rebuild the balance between ROS production and removal. However, oxidative stress in various age-related degenerative diseases, including AMD, tends to be persistent [18, 42]. In this case, autophagy activity was dysregulated, and defective autophagy would finally increase oxidative stress owing to the inability to remove harmful damaged organelles and contribute to AMD progression, which is in line with a previous study on the role of autophagy in osteoarthritis [43].

Furthermore, we investigated the potential molecular mechanisms by which DCN induced autophagy. AMPK-mTOR plays an essential role in regulating autophagy. Autophagy is promoted by AMPK, which is a key energy sensor and an important mediator in maintaining cellular energy homeostasis. Conversely, autophagy is inhibited by mTOR, which plays a key role at the interface of the pathways that coordinately regulate the balance between cell growth and autophagy in response to nutritional status, growth factors, and stress signals [34, 44]. In the process of cellular senescence and aging, such as in RPE cells of AMD patients, decreased phosphorylation of AMPK and overactivated mTOR activity can be observed [45]. To investigate whether AMPK-mTOR signaling was involved in the activation of autophagy following DCN treatment, ARPE-19 cells were first treated with the AMPK inhibitor compound C or mTOR activator MHY1485 prior to DCN treatment. We found that the induction of autophagy by DCN was completely reversed after coincubation with 3-MA or MHY1485. These results indicate that DCN activates AMPK to inhibit mTOR and promotes autophagy in AMPK-dependent manner in ARPE-19 cells, in line with previous studies that observed DCN evoked autophagy by regulating AMPK-mTOR signaling in endothelial, nucleus pulposus, and glioma cells [22, 39, 46].

Emerging evidence indicates that autophagy is a double-edged sword in various physiological and pathophysiological processes [47]. The regulation of autophagy regulation remains complex and has a critical point [48]. In most cases, when the autophagy is mildly activated and the level of autophagy is less than the critical point, autophagy serves as a cytoprotective mechanism by clearing damaged cell components. However, when the autophagy level is above the critical point, overactivation of autophagy may lead to cell death and apoptosis by triggering autophagic cell death pathway and lose cytoprotective function, which is opposite of our goal [47, 48]. To investigate whether prolonged exposure of DCN would exert any cytotoxic effect on ARPE-19 cells, we incubated ARPE-19 cells with DCN for 4 days and found that the treatment of DCN did not exhibit any inhibition on cell proliferation compared with untreated control (Figure S4), which imply that DCN would not induce cytotoxicity after prolonged exposure. The possible mechanism may be related to a negative feedback mechanism termed as autophagic lysosome formation (ALR).

ALR reserves over activated autophagy and restores lysosome homeostasis, coupling the induction and cessation of autophagy [49, 50]. Previous study has demonstrated that ALR requires the activation of mTOR. The reactivation of mTOR initiates ALR to replenish the lysosomal pool for preservation of lysosome homeostasis [50, 51]. In our study, although the activation of mTOR decreased following DCN stimulation for short period, the phosphorylation of mTOR gradually restored to baseline during prolonged DCN treatment (Figure S5), implying that DCN served as an important role in maintaining lysosome homeostasis during long-term incubation by reactivating mTOR. However, more comprehensive studies are needed to clarify the exact role of DCN on the regulation of lysosome biology during autophagy.

5. Conclusions

Taken together, we demonstrated that DCN had protective effects against oxidative stress and apoptosis by promoting autophagy in ARPE-19 cells mediated by AMPK-mTOR signaling. Our study not only provided a new insight into the pharmacological mechanism of DCN against oxidative stress but also supported therapeutic potential of DCN in the prevention and treatment of AMD.

Data Availability

The raw data supporting the conclusions of this article will be made available by the authors upon reasonable request, without undue reservation.

Conflicts of Interest

The authors declare that they have no competing interests.

Acknowledgments

This work was supported by grants from the Wuxi Taihu Lake Talent Plan, Supports for Leading Talents in Medical and Health Profession (no. 2020-THRCTD-1).

Supplementary Materials

Figure S1: quantification of autophagosomes in 20 cells for each condition. Data is shown as mean ± SD and $^{***}p < 0.001$. Figure S2: ARPE-19 cells were transfected with mRFP-GFP-LC3 and treated with DCN. The number of yellow autophagosomes(R+G-) and red autolysosomes(R+G+) was quantified. Data is shown as mean ± SD and $^{**}p < 0.01$. Figure S3: quantitative analysis of ROS fluorescence intensity. Data is shown as mean ± SD and $^{***}p < 0.001$. Figure S4: relative cell viability of ARPE-19 cells after incubation with DCN for indicated times. The cell viability was determined by CCK8. Figure S5: the protein levels of p-mTOR and β-actin in ARPE-19 cells. ARPE-19 cells were treated with DCN for indicated time. The densities of p-mTOR/β-actin were analyzed. Data is shown as mean ± SD, $^{*}p < 0.05$, and $^{***}p < 0.001$. *(Supplementary Materials)*

References

[1] W. L. Wong, X. Su, X. Li et al., "Global prevalence of age-related macular degeneration and disease burden projection

for 2020 and 2040: a systematic review and meta-analysis," *The Lancet Global Health*, vol. 2, no. 2, pp. e106–e116, 2014.

[2] R. D. Jager, W. F. Mieler, and J. W. Miller, "Age-related macular degeneration," *New England Journal of Medicine*, vol. 358, no. 24, pp. 2606–2617, 2008.

[3] F. G. Holz, E. C. Strauss, S. Schmitz-Valckenberg, and M. van Lookeren Campagne, "Geographic atrophy: clinical features and potential therapeutic approaches," *Ophthalmology*, vol. 121, no. 5, pp. 1079–1091, 2014.

[4] J. L. Kovach, S. G. Schwartz, H. W. Flynn, and I. U. Scott, "Anti-VEGF treatment strategies for wet AMD," *Journal of Ophthalmology*, vol. 2012, 7 pages, 2012.

[5] K. M. Gehrs, D. H. Anderson, L. V. Johnson, and G. S. Hageman, "Age-related macular degeneration–emerging pathogenetic and therapeutic concepts," *Annals of Medicine*, vol. 38, no. 7, pp. 450–471, 2006.

[6] M. van Lookeren Campagne, J. LeCouter, B. L. Yaspan, and W. Ye, "Mechanisms of age-related macular degeneration and therapeutic opportunities," *The Journal of Pathology*, vol. 232, no. 2, pp. 151–164, 2014.

[7] A. Kauppinen, "Introduction to the multi-author review on macular degeneration," *Cellular and Molecular Life Sciences*, vol. 77, no. 5, pp. 779-780, 2020.

[8] M. P. Rozing, J. A. Durhuus, M. Krogh Nielsen et al., "Age-related macular degeneration: a two-level model hypothesis," *Progress in Retinal and Eye Research*, vol. 76, article 100825, 2020.

[9] J. G. Hollyfield, V. L. Bonilha, M. E. Rayborn et al., "Oxidative damage-induced inflammation initiates age-related macular degeneration," *Nature Medicine*, vol. 14, no. 2, pp. 194–198, 2008.

[10] S. Datta, M. Cano, K. Ebrahimi, L. Wang, and J. T. Handa, "The impact of oxidative stress and inflammation on RPE degeneration in non-neovascular AMD," *Progress in Retinal and Eye Research*, vol. 60, pp. 201–218, 2017.

[11] J. Cai, K. C. Nelson, M. Wu, P. Sternberg Jr., and D. P. Jones, "Oxidative damage and protection of the RPE," *Progress in Retinal and Eye Research*, vol. 19, no. 2, pp. 205–221, 2000.

[12] J. Hanus, H. Zhang, Z. Wang, Q. Liu, Q. Zhou, and S. Wang, "Induction of necrotic cell death by oxidative stress in retinal pigment epithelial cells," *Cell Death & Disease*, vol. 4, no. 12, pp. e965–e965, 2013.

[13] S. K. Mitter, H. V. Rao, X. Qi et al., "Autophagy in the retina: a potential role in age-related macular degeneration," *Advances in Experimental Medicine and Biology*, vol. 723, pp. 83–90, 2012.

[14] Z. Y. Zhang, X. L. Bao, Y. Y. Cong, B. Fan, and G. Y. Li, "Autophagy in age-related macular degeneration: a regulatory mechanism of oxidative stress," *Oxidative Medicine and Cellular Longevity*, vol. 2020, Article ID 2896036, 2020.

[15] A. Baek, S. Yoon, J. Kim et al., "Autophagy and KRT8/keratin 8 protect degeneration of retinal pigment epithelium under oxidative stress," *Autophagy*, vol. 13, no. 2, pp. 248–263, 2017.

[16] X. Zhao, L. Liu, Y. Jiang, M. Silva, X. Zhen, and W. Zheng, "Protective effect of metformin against hydrogen peroxide-induced oxidative damage in human retinal pigment epithelial (RPE) cells by enhancing autophagy through activation of AMPK pathway," *Oxidative Medicine and Cellular Longevity*, vol. 2020, 14 pages, 2020.

[17] N. Golestaneh, Y. Chu, Y.-Y. Xiao, G. L. Stoleru, and A. C. Theos, "Dysfunctional autophagy in RPE, a contributing factor in age-related macular degeneration," *Cell Death & Disease*, vol. 8, no. 1, pp. e2537–e2537, 2018.

[18] C. C. Chang, T. Y. Huang, H. Y. Chen et al., "Protective effect of melatonin against oxidative stress-induced apoptosis and enhanced autophagy in human retinal pigment epithelium cells," *Oxidative Medicine and Cellular Longevity*, vol. 2018, Article ID 9015765, 2018.

[19] A. Stahl, L. Paschek, G. Martin et al., "Rapamycin reduces VEGF expression in retinal pigment epithelium (RPE) and inhibits RPE-induced sprouting angiogenesis in vitro," *FEBS Letters*, vol. 582, no. 20, pp. 3097–3102, 2008.

[20] X. Hu, E. S. Villodre, R. Larson et al., "Decorin-mediated suppression of tumorigenesis, invasion, and metastasis in inflammatory breast cancer," *Communications biology*, vol. 4, no. 1, p. 72, 2021.

[21] M. A. Gubbiotti, T. Neill, H. Frey, L. Schaefer, and R. V. Iozzo, "Decorin is an autophagy-inducible proteoglycan and is required for proper in vivo autophagy," *Matrix Biology*, vol. 48, pp. 14–25, 2015.

[22] T. W. Zhang, Z. F. Li, W. Ding et al., "Decorin inhibits nucleus pulposus apoptosis by matrix-induced autophagy via the mTOR pathway," *Journal of Orthopaedic Research*, vol. 39, no. 8, pp. 1777–1788, 2021.

[23] S. Du, J. Shao, D. Xie, and F. Zhang, "Decorin inhibits glucose-induced lens epithelial cell apoptosis via suppressing p22phox-p38 MAPK signaling pathway," *PLoS One*, vol. 15, no. 4, article e0224251, 2020.

[24] R. V. Iozzo, S. Goldoni, A. D. Berendsen, and M. F. Young, *Small leucine-rich proteoglycans*, Springer, 2011.

[25] Z. Ferdous, V. M. Wei, R. Iozzo, M. Höök, and K. J. Grande-Allen, "Decorin-transforming growth factor-β interaction regulates matrix organization and mechanical characteristics of three-dimensional collagen matrices," *Journal of Biological Chemistry*, vol. 282, no. 49, pp. 35887–35898, 2007.

[26] Z. Ahmed, D. Bansal, K. Tizzard et al., "Decorin blocks scarring and cystic cavitation in acute and induces scar dissolution in chronic spinal cord wounds," *Neurobiology of Disease*, vol. 64, pp. 163–176, 2014.

[27] R. Özay, E. Türkoğlu, B. Gürer et al., "Does decorin protect neuronal tissue via its antioxidant and antiinflammatory activity from traumatic brain injury? An experimental study," *An experimental study, World neurosurgery*, vol. 97, pp. 407–415, 2017.

[28] J. E. Davies, X. Tang, J. W. Denning, S. J. Archibald, and S. J. Davies, "Decorin suppresses neurocan, brevican, phosphacan and NG2 expression and promotes axon growth across adult rat spinal cord injuries," *The European Journal of Neuroscience*, vol. 19, no. 5, pp. 1226–1242, 2004.

[29] Y. Ge, Y. Li, Z. Wang, L. Li, H. Teng, and Q. Jiang, "Effects of mechanical compression on chondrogenesis of human synovium-derived mesenchymal stem cells in agarose hydrogel," *Frontiers in Bioengineering and Biotechnology*, vol. 9, article 697281, 2021.

[30] P. Karimi, A. Gheisari, S. J. Gasparini et al., "Crocetin prevents RPE cells from oxidative stress through protection of cellular metabolic function and activation of ERK1/2," *International Journal of Molecular Sciences*, vol. 21, no. 8, p. 2949, 2020.

[31] S. Gaweł, M. Wardas, E. Niedworok, and P. Wardas, "Malondialdehyde (MDA) as a lipid peroxidation marker," *Wiadomosci lekarskie*, vol. 57, no. 9-10, pp. 453–455, 2004.

[32] V. M. Di Mambro, M. F. Borin, and M. J. Fonseca, "Topical formulations with superoxide dismutase: influence of formulation composition on physical stability and enzymatic activity," *Journal of Pharmaceutical and Biomedical Analysis*, vol. 32, no. 1, pp. 97–105, 2003.

[33] A. Burlacu, "Regulation of apoptosis by Bcl-2 family proteins," *Journal of Cellular and Molecular Medicine*, vol. 7, no. 3, pp. 249–257, 2003.

[34] J. Kim, M. Kundu, B. Viollet, and K. L. Guan, "AMPK and mTOR regulate autophagy through direct phosphorylation of Ulk1," *Nature Cell Biology*, vol. 13, no. 2, pp. 132–141, 2011.

[35] B. S. Winkler, M. E. Boulton, J. D. Gottsch, and P. Sternberg, "Oxidative damage and age-related macular degeneration," *Molecular Vision*, vol. 5, p. 32, 1999.

[36] C. Alan, H. Kocoglu, R. AltIntas, B. AlIcI, and A. R. Ersay, "Protective effect of decorin on acute ischaemia-reperfusion injury in the rat kidney," *Archives of Medical Science*, vol. 7, no. 2, pp. 211–216, 2011.

[37] K. Kannan and S. K. Jain, "Oxidative stress and apoptosis," *Pathophysiology*, vol. 7, no. 3, pp. 153–163, 2000.

[38] S. K. Mitter, C. Song, X. Qi et al., "Dysregulated autophagy in the RPE is associated with increased susceptibility to oxidative stress and AMD," *Autophagy*, vol. 10, no. 11, pp. 1989–2005, 2014.

[39] T. Yao, C. G. Zhang, M. T. Gong, M. Zhang, L. Wang, and W. Ding, "Decorin-mediated inhibition of the migration of U87 MG glioma cells involves activation of autophagy and suppression of TGF-β signaling," *FEBS Open Bio*, vol. 6, no. 7, pp. 707–719, 2016.

[40] W. Ju, S. Li, Z. Wang, Y. Liu, and D. Wang, "Decorin protects human hepatoma HepG2 cells against oxygen-glucose deprivation via modulating autophagy," *International Journal of Clinical and Experimental Medicine*, vol. 8, no. 8, pp. 13347–13352, 2015.

[41] M. Matsushita, N. N. Suzuki, K. Obara, Y. Fujioka, Y. Ohsumi, and F. Inagaki, "Structure of Atg5.Atg16, a complex essential for autophagy," *The Journal of Biological Chemistry*, vol. 282, no. 9, pp. 6763–6772, 2007.

[42] Z. Du, W. Zhang, S. Wang et al., "Celastrol protects human retinal pigment epithelial cells against hydrogen peroxide mediated oxidative stress, autophagy, and apoptosis through sirtuin 3 signal pathway," *Journal of Cellular Biochemistry*, vol. 120, no. 6, pp. 10413–10420, 2019.

[43] Q. Tang, G. Zheng, Z. Feng et al., "Trehalose ameliorates oxidative stress-mediated mitochondrial dysfunction and ER stress via selective autophagy stimulation and autophagic flux restoration in osteoarthritis development," *Cell Death & Disease*, vol. 8, no. 10, article e3081, 2017.

[44] X. Zhang, Q. Wang, X. Wang et al., "Tanshinone IIA protects against heart failure post-myocardial infarction via AMPKs/mTOR-dependent autophagy pathway," *Biomedicine & Pharmacotherapy*, vol. 112, article 108599, 2019.

[45] M. Zhang, N. Jiang, Y. Chu et al., "Dysregulated metabolic pathways in age-related macular degeneration," *Scientific Reports*, vol. 10, no. 1, p. 2464, 2020.

[46] A. Goyal, T. Neill, R. T. Owens, L. Schaefer, and R. V. Iozzo, "Decorin activates AMPK, an energy sensor kinase, to induce autophagy in endothelial cells," *Matrix Biology*, vol. 34, pp. 46–54, 2014.

[47] G. Filomeni, D. De Zio, and F. Cecconi, "Oxidative stress and autophagy: the clash between damage and metabolic needs," *Cell Death and Differentiation*, vol. 22, no. 3, pp. 377–388, 2015.

[48] R. Kiffin, U. Bandyopadhyay, and A. M. Cuervo, "Oxidative stress and autophagy," *Antioxidants & Redox Signaling*, vol. 8, no. 1-2, p. 152, 2006.

[49] T. Neill, C. Sharpe, R. T. Owens, and R. V. Iozzo, "Decorin-evoked paternally expressed gene 3 (PEG3) is an upstream regulator of the transcription factor EB (TFEB) in endothelial cell autophagy," *The Journal of Biological Chemistry*, vol. 292, no. 39, pp. 16211–16220, 2017.

[50] Y. Rong, C. K. McPhee, S. Deng et al., "Spinster is required for autophagic lysosome reformation and mTOR reactivation following starvation," *Proceedings of the National Academy of Sciences of the United States of America*, vol. 108, no. 19, pp. 7826–7831, 2011.

[51] L. Yu, C. K. McPhee, L. Zheng et al., "Termination of autophagy and reformation of lysosomes regulated by mTOR," *Nature*, vol. 465, no. 7300, pp. 942–946, 2010.

Hindawi
Oxidative Medicine and Cellular Longevity
Volume 2022, Article ID 1744408, 21 pages
https://doi.org/10.1155/2022/1744408

Research Article

Pterostilbene Promotes Mean Lifespan in Both Male and Female *Drosophila Melanogaster* Modulating Different Proteins in the Two Sexes

Daniela Beghelli,[1] Lorenzo Zallocco,[2] Maria Cristina Barbalace,[3] Simona Paglia,[4] Silvia Strocchi,[5] Ilenia Cirilli,[6] Valeria Marzano,[7] Lorenza Putignani,[8] Giulio Lupidi,[6] Silvana Hrelia,[3] Laura Giusti,[6] and Cristina Angeloni[3]

[1]*School of Biosciences and Veterinary Medicine, University of Camerino, Via Gentile III da Varano, 62032 Camerino (MC), Italy*
[2]*Department of Pharmacy, University of Pisa, 56126 Pisa, Italy*
[3]*Department for Life Quality Studies, Alma Mater Studiorum, University of Bologna, Corso d'Augusto 237, 47921 Rimini (RN), Italy*
[4]*Department of Pharmacy and Biotechnology, University of Bologna, Via Selmi 3, 40126 Bologna (BO), Italy*
[5]*Translational Research Lab-Santa Maria Nuova Hospital-IRCCS, Viale Umberto I 50, 42123 Reggio Emilia, Italy*
[6]*School of Pharmacy, University of Camerino, Via Gentile III da Varano, 62032 Camerino (MC), Italy*
[7]*Multimodal Laboratory Medicine Research Area, Unit of Human Microbiome, Bambino Gesù Children's Hospital, IRCCS, Viale di San Paolo 15, 00146 Rome, Italy*
[8]*Department of Diagnostics and Laboratory Medicine, Unit of Microbiomics and Multimodal Laboratory Medicine Research Area, Unit of Human Microbiome, Bambino Gesù Children's Hospital, IRCCS, Viale di San Paolo 15, 00146 Rome, Italy*

Correspondence should be addressed to Cristina Angeloni; cristina.angeloni@unicam.it

Received 5 October 2021; Revised 2 February 2022; Accepted 3 February 2022; Published 16 February 2022

Academic Editor: Cristina Cosentino

Aging is a multifactorial phenomenon characterized by degenerative processes closely connected to oxidative damage and chronic inflammation. Recently, many studies have shown that natural bioactive compounds are useful in delaying the aging process. In this work, we studied the effects of an *in vivo* supplementation of the stilbenoid pterostilbene on lifespan extension in *Drosophila melanogaster*. We found that the average lifespan of flies of both sexes was increased by pterostilbene supplementation with a higher effect in females. The expression of longevity related genes (Sir2, Foxo, and Notch) was increased in both sexes but with different patterns. Pterostilbene counteracted oxidative stress induced by ethanol and paraquat and up-regulated the antioxidant enzymes Ho e Trxr-1 in male but not in female flies. On the other hand, pterostilbene decreased the inflammatory mediators dome and egr only in female flies. Proteomic analysis revealed that pterostilbene modulates 113 proteins in male flies and only 9 in females. Only one of these proteins was modulated by pterostilbene in both sexes: vacuolar H[+] ATPase 68 kDa subunit 2 (Vha68-2) that was strongly down-regulated. These findings suggest a potential role of pterostilbene in increasing lifespan both in male and female flies by mechanisms that seem to be different in the two sexes, highlighting the need to conduct nutraceutical supplementation studies on males and females separately in order to give more reliable results.

1. Introduction

Aging is a natural physiological process triggered by different molecular pathways and biochemical events that are promoted by both environmental and genetic factors. Aging is characterized by a time-dependent decline of functional capabilities and impaired stress resistance, that damage biomolecules compromising cellular homeostasis. The factors involved in aging are commonly referred to as the "hallmarks of aging". Among them, oxidative stress and inflammation have been widely investigated. In 1956 Denham Harman [1] proposed"The Free Radical Theory of Aging"

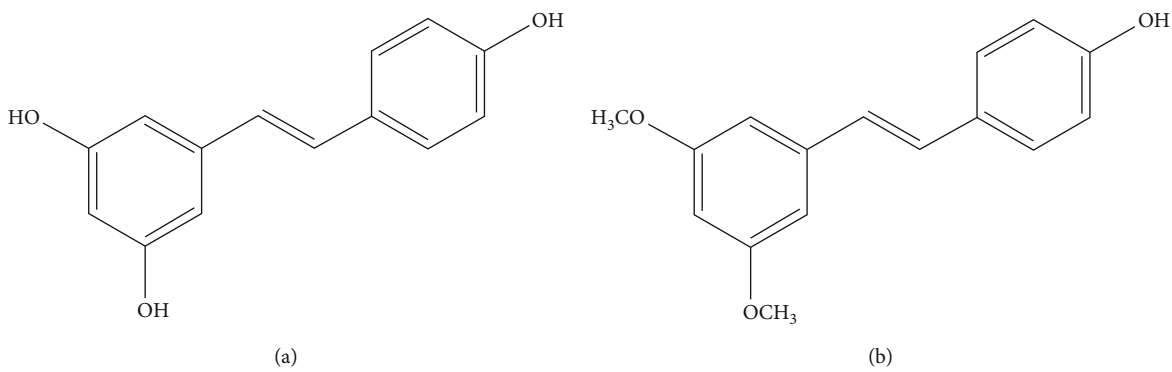

Figure 1: Chemical structure of A) resveratrol and B) pterostilbene.

that has been updated in recent years to include the suggestion of a central role for reactive oxygen species (ROS) produced by mitochondria [2]. On the other hand, the term "inflammaging" has been created to indicate the significant contribution of low-grade, systemic inflammation to normal aging [3].

The findings that the modification of environmental factors, such as diet, can increase lifespan, make natural dietary compounds extraordinary potential tools in the major healthcare challenge of delaying aging. Over the past 20 years, many studies have suggested that dietary polyphenols may exert beneficial effects as anti-aging compounds through the modulation of the hallmarks of aging, including inflammation, oxidative damage, cell senescence and telomere attrition [4–8]. Among the most prominent polyphenols, the stilbene resveratrol (5-[(E)-2-(4-hydroxyphenyl)ethenyl]-benzene-1,3-diol) (Figure 1(a)) has gained widespread attention due to its ability to extend the lifespan of yeast, worms, and flies, and its ability to protect against age-related diseases such as cancer, Alzheimer's disease, and diabetes in mammals [9, 10].

Recently, pterostilbene (PTS) (Figure 1(b)) a dimethoxylated ether resveratrol derivative, has been gaining more and more attention thanks to its greater *in vivo* bioavailability and higher potential in modulating cognition and cellular stress with respect to resveratrol [11]. Both stilbenoids represent a group of natural phenolic compounds present in different types of plants and fruits such as grapes, tree wood, *Pterocarpus marsupium*, heartwood of sandalwood, leaves of *Vitis vinifera* and blueberries [12, 13].

Resveratrol has been more extensively characterized in terms of bioavailability and pharmacokinetics in human and animal studies compared to PTS. [9, 14–17]. What is known about PTS is that its structure, which differs from that of resveratrol by the presence of two methoxy (–OCH_3) instead of two hydoxy (-OH) groups, may overcome the pharmacologic efficacy limitations observed in resveratrol (due to its poor absorption and rapid first-pass metabolism). When PTS is orally administered, it shows higher bioavailability (80% vs 20% of resveratrol), hepatic stability and total plasma levels when compare to resveratrol [18, 19]. Riche et al. [20] showed that PTS in a dose up to 250 mg per day is safe for humans and, thanks to its dimethoxy structure, that creates a favorable lipophilicity, has a higher membrane permeability and biological potency [21]. Furthermore, glucuronidation and sulfation processes are restricted by the methylation of the phenolic hydroxyl in PTS thus providing fewer conjugating sites compared to resveratrol and resulting in better metabolic stability.

In 2003, Howitz and colleagues [22] identified resveratrol as a potent activator of Sir2, the mammalian Sirt1 ortholog, capable of mimicking the effects of caloric restriction (CR) and regulating longevity in lower organisms such as worms and yeasts, while in *Drosophila melanogaster* there are contradictory results [23–25]. Besides NAD^+ dependent histone deacetylase Sir2 [26], that controls enzymes regulating a large number of cellular pathways [27], there are other genes associated with longevity in *Drosophila*. Reduction in the activity of the nutrient-sensing insulin/IGF Signaling (IIS) pathway and the associated Target of Rapamycin (TOR) pathway results in one of the best understood interventions to extend flies lifespan [26]. The IIS pathway, in turn, intersects with a variety of other pathways that impact longevity such as the stress-responsive Jun-N-terminal kinase pathway, or the pathways that promote protein homeostasis and activate the mitochondrial unfolded protein response. Lifespan is also regulated by other mechanisms such as the loss of the mitochondrial co-transporter I'm Not Dead Yet (INDY) and the modulation of the mitochondrial electron transport chain [26].

To the best of our knowledge, there is no evidence that shows a direct effect of PTS on lifespan extension *in vivo*. Therefore, the present work sets out to study the potential role of PTS on longevity, oxidative stress and inflammation in *D. melanogaster* taking into consideration sex differences. We also carried out proteomic analysis on the whole *Drosophila* body, to have a deeper insight in the potential different effects of PTS supplementation on male and female flies.

2. Materials and Methods

2.1. Fly Strain, Rearing and Supplementation. The *Drosophila melanogaster* Canton S strain was a kind gift of Prof. Daniela Grifoni (University of l'Aquila, Italy). Flies were supplied with Formula 4–24 ® media (Carolina Biological, Burlington, NC, USA) and maintained at constant temperature (21°C) and humidity (60%) with a 12/12 h light–dark cycle. The diet contained: oat flour, soy flour, wheat flour,

other starches, dibasic calcium phosphate, calcium carbonate, citric acid, niocinamide, riboflavin, sodium chloride, sodium iron pyrophosphate, sucrose, thiamine, mononitrate, brewer's yeast, emulsifier preservatives, mold inhibitor, food coloring [28]. Yeast pellets (*Saccharomyces cerevisiae*) were added to each tube after diet hydration. After eclosion, males and females were synchronized as reported in [29] and allowed to mate freely for two days before separating them according to sex [30]. PTS (Sigma-Aldrich s.r.l., Milan, Italy) was dissolved in DMSO (0.1%) and 50, 100, and 200 mM stocks were prepared and kept at -20°C until use. For supplementation, PTS was dissolved at different concentrations (50, 100 or 200 μM) in the water used to soak 1.0 g of diet. A total of 20 flies were placed in each vial. The water used to prepare the control food contained 0.1% of DMSO.

2.2. Longevity Assay. Adult flies of both sexes were collected under FlyNap (Carolina Biological) anesthesia. A total of 800 male and 800 female fruit flies were randomly divided into 4 groups: CTR (control), PTS 50 (50 μM PTS), PTS 100 (100 μM PTS), and PTS 200 (200 μM PTS). Every 2–3 days, the flies were transferred into vials containing fresh food and the number of living flies was counted. This was repeated until all flies died. Kaplan–Meier survival curves were generated for lifespan assessment.

2.3. Measurement of Body Weights. Body weights of male and female flies were recorded on days 15, 30, 45 and 60. Briefly, 20 flies in each group were anesthetized by FlyNap (Carolina Biological) and then weighed on a balance. The mean body weights of the flies in each group were calculated.

2.4. CApillary FEeder (CAFE) Assay. Food intake was measured using the capillary feeder method (CAFE) as reported in [31] with minor modifications. Flies were held in shortened culturing vials of 7 cm in length. Cotton balls, soaked with 500 μL of water, were inserted at the bottom of tubes for humidity, the tubes were then parafilmed to reduce evaporation and keep a high level of humidity inside the vials. Microcapillary tubes were inserted into the tubes through a 200 μL pipette tip in the foam plug. Four microcapillary tubes were used per vial and filled with 100 μM PTS (PTS) or 0.1% DMSO diluted in 2.5% sucrose (CTRL). The assay was performed on flies never supplemented (3 days old male and female flies) or on flies supplemented with PTS or 0.1% DMSO for 15 days. At each time point 2 groups for sex were considered: PTS and CTRL. On the day of the experiment, flies were weighted, starved for two hours, and then separated into CAFE vials, with eight flies for vial (40 flies/sex/condition; n =80 flies). To account for evaporation of the liquid food, three vials were set up with feeding capillaries but without flies. Fly consumption was evaluated after four hours measuring the amount of liquid consumed from the microcapillary tube (in mm) as described by Fiocca et al. [32] and data were reported as μL/mg of fly.

2.5. Paraquat Toxicity. Oxidative stress resistance was measured using paraquat (1,1′-dimethyl-4,4′-bi-pyridinium dichloride, Sigma-Aldrich s.r.l.) as stress inducer. Briefly, 15 days-old flies were subjected to starvation for 2 hours then transferred to parafilm-sealed vials (ten flies per vial) containing capillaries filled with 2.5 mM paraquat prepared with 2.5% sucrose solution. For each condition, 50 flies per sex were tested. Mortality was scored every 6 hours until all flies died and expressed as percentage of survival.

2.6. Ethanol Toxicity. Ethanol toxicity was evaluated as reported by Niveditha [33] with some modifications. Briefly, 15 days-old flies (supplemented and CTR) were first subjected to starvation for 2 h then transferred to parafilm-sealed vials (ten flies per vial) containing Whatman filter paper discs (diameter 2 cm) soaked with 2.5% sucrose solution and 17.5%, ethanol (Carlo Erba, Milano, Italy). Mortality was scored every 2 hours until all flies died and expressed as percentage of survival. For each condition, 50 flies per sex were tested.

2.7. DCFH-DA Assay. ROS content was evaluated using 2′-7′-dichlorodihydrofluorescein diacetate (DCFH-DA). Groups of 25 flies were mechanically homogenized in 1 mL of 0.1 M PBS. The homogenate was centrifuged at 6,000 rpm for 10 min and 200 μL of supernatant was incubated with 50 μM DCFH-DA (Sigma-Aldrich s.r.l.) at 37°C. The fluorescence was measured each 10 minutes in a FLUOstar Omega plate reader (BMG Labtech, Ortenberg, Germany) using ex/em wavelength of 485/520 nm. ROS levels were quantified as increase in DCF fluorescence through the time normalized by protein and expressed as increase/min/μg protein. The protein concentration in the homogenate was quantified by Bradford method using bovine serum albumin (Sigma-Aldrich s.r.l) as standard. Each condition was the results of six replicates and was expressed as mean ± SEM.

2.8. Total Antioxidant Capacity. To assess the total antioxidant capacity of flies, the 2, 2′-azino-bis (3-ethylbenzothiazoline-6-sulphonic acid, Sigma-Aldrich s.r.l.) (ABTS) assay, as reported by Re et al. [34] and modified for application to a 96-well microplate, was used.

Flies were mechanically homogenized in 1 mL of 0.1 M PBS on ice. The homogenate was centrifuged at 6,000 rpm for 10 min and the supernatant was used for the assay.

The $ABTS^{\bullet+}$ solution was freshly prepared by the oxidation of ABTS (10 mg) by MnO_2 (0.75 g) in the presence of water (4 mL), followed by 30 min at room temperature. The working solution was obtained by diluting the previous mixture with H_2O to have an absorbance around 1 at 734 nm.

For the assay, 200 μL of the working solution was added to 50 μL aliquot of progressively diluted samples and Trolox as a standard. The absorbance of each well was measured after 15 min incubation at 734 nm.

The protein concentration in the homogenates was quantified by Bradford method using bovine serum albumin as standard. Each condition was the results of six replicates and was expressed as mean ± SEM. The total antioxidant capacity of flies was compared to Trolox used as positive control and expressed as mg of Trolox-equivalent antioxidant capacity for mg of homogenate protein (TEAC).

Table 1: List of primers for real-time PCR.

Gene	5'-Forward-3'	5'-Reverse-3'
Sir2	CATTATGCCGCATTTCGCCA	GAAGGTGTTCACTGAGGCCA
Foxo	AGGCTGACCCACACAGATAAC	GGCTCCACAAAGTTTTCGGG
Notch	CGCTTCCTGCACAAGTGTC	GCGCAGTAGGTTTTGCCATT
Ho	ATGTCAGCGAGCGAAGAAACA	TGGCTTTACGCAACTCCTTTG
Trxr-1	TGGATCTGCGCGACAAGAAAG	GAAGGTCTGGGCGGTGATTG
Dome	GGCAGCTTCTATGTCTACTC	GTTGGACTCCACCTTGATG
Egr	GAAATCACACAGAGCTTCAG	AAGAAGAGATTCACCTTTGC
RPL32	GCCCACCGGATTCAAGAAGT	CTTGCGCTTCTTGGAGGAGA

2.9. RNA Extraction. RNA was extracted from the whole bodies of flies using RNeasy Mini Kit (QIAGEN GmbH, Hilden, Germany). NanoVue Spectrophotometer (GE Healthcare, Milano, Italy) was used to measure the yield and purity of the RNA. Only samples with ratios A260/A280>1.8 were used.

2.10. Analysis of mRNA Levels by Reverse Transcriptase Polymerase Chain Reaction. For each sample, 1 μg of total RNA was reverse transcribed to obtain cDNA using iScript cDNA Synthesis Kit (Bio-Rad Laboratories, Hercules, CA, USA) following the manufacturer's instructions. The subsequent polymerase chain reaction (PCR) was performed in a total volume of 10 μL containing 2 μL of dH_2O RNAsi free, 2.5 μL (12.5 ng) of cDNA, 5 μL SsoAdvanced Universal SYBR Green Supermix (Bio-Rad Laboratories), and 0.5 μL (500 nM) of each primer. The primers used were purchased from Sigma-Aldrich s.r.l. and they are reported in Table 1; RPL32 was used as reference gene.

2.11. Proteomic Analysis. For proteomic analysis, proteins were extracted from total body of male and female flies supplemented with 100 μM PTS for 15 days using 8 M urea, 2 M thiourea, 4% CHAPS and 60 mM dithiothreitol (DTT) extraction solution. Briefly, bodies of flies were resuspended in extraction solution using a microtube pestle and sonicated 1 min for 5 times in an ultrasonic bath. After incubation for 1 h at room temperature, samples were centrifuged at 16,000 x g for 10 min to remove undissolved material. Protein concentration was determined using the Pierce Protein Assay (Thermo Fisher Scientific, Waltham, MA, USA) and bovine serum albumin was used as standard. Two-dimensional gel electrophoresis (2DE) was carried out as previously described [35]. Briefly, 200 μg of proteins were filled up to 350 μL in rehydration solution. Isoelectrofocusing (IEF) was performed using 18 cm Immobiline Dry Strips (GE Health Care Europe, Uppsala, Sweden) with a nonlinear pH 3-10 gradient. IEF was carried on the Ettan IPGphor Cup Loading Manifold (GE Healthcare). After IEF, the strips were equilibrated during two steps of 15 min each in equilibration buffer (0.05 M Tris, 6 M urea, 2% SDS, 20% glycerol) with 1% DTT in the first incubation or 2.5% iodoacetamide in the second one. The subsequent electrophoresis (Sodium Dodecyl Sulphate-Polyacrylamide Gel Electrophoresis; SDS-PAGE) was carried out by transferring the proteins to 12% polyacrylamide, running at 16 mA per gel and 10°C for about 16 h, using the Protean® Plus Dodeca Cell (Bio-Rad). The gels were stained with Ruthenium II tris (bathophenanthroline disulfonate) tetrasodium salt (Cyanagen, Bologna, Italy) (RuBP). ImageQuant LAS4010 (GE Health Care) was used for the acquisition of images. The analysis of images was performed using Same Spot (v4.1, TotalLab, Newcastle Upon Tyne, UK) software.

Gel spots were excised and in-gel digested [36]. Peptides were lyophilized and resuspended in 2% acetonitrile (ACN), 0.1% formic acid (FA) and 97.9% water.

2.12. Mass Spectrometry Analysis. NanoLiquid Chromatography coupled tandem mass spectrometry analysis (nLC-ESI-MS/MS) was achieved on an analytical platform comprising an UltiMate3000 RSLCnano System interfaced with an Orbitrap Fusion Tribrid mass spectrometer through a nanoESI source (EASY-Spray NG) (Thermo Fisher Scientific, Milan, Italy) operating in positive ion mode, as already described [37] with minor modifications. After trapping and desalting on a micro-precolumn, a 15 min linear gradient starting from 95% solution A (0.1% FA in water) to 25% solution B (0.1% FA in ACN) allowed peptides' separation on an EASY-Spray PepMap RSLC C18 column (2 μm particle size, 100 Å pore size, 75 μm i.d. x 25 cm length, Thermo Fisher Scientific) for a total run of 40 min.

Precursor ions were recorded by the Orbitrap detector and fragments (MS/MS) ions by the Ion Trap at rapid scan rate. Twenty most abundant multiple-charged (2^+ – 7^+) precursor ions, detected within the range of 275–1,750 m/z, were subjected to fragmentation by Collision-Induced Dissociation (CID) with dynamic exclusion of 45 s and using 35% normalized collision energy. The signal intensity threshold for MS/MS was set to 5×10^3. Proteome Discoverer software (version 2.4, Thermo Fisher Scientific) was used to process the raw data searching the fruit fly UniProtKB reference proteome (*Drosophila melanogaster* database, ID: UP000000803, release: 2021_01, 22,117 proteins) to which 39 common contaminant sequence entries were appended. Protein identification search parameters were set as follows: chosen enzyme: trypsin with a maximum of 1 missed cleavage per peptide; variable modification: oxidation of methionine and acetylation of lysines at protein N-terminus; static modification: carbamidomethylation of cysteine; mass tolerance of precursor: 10 ppm; fragment

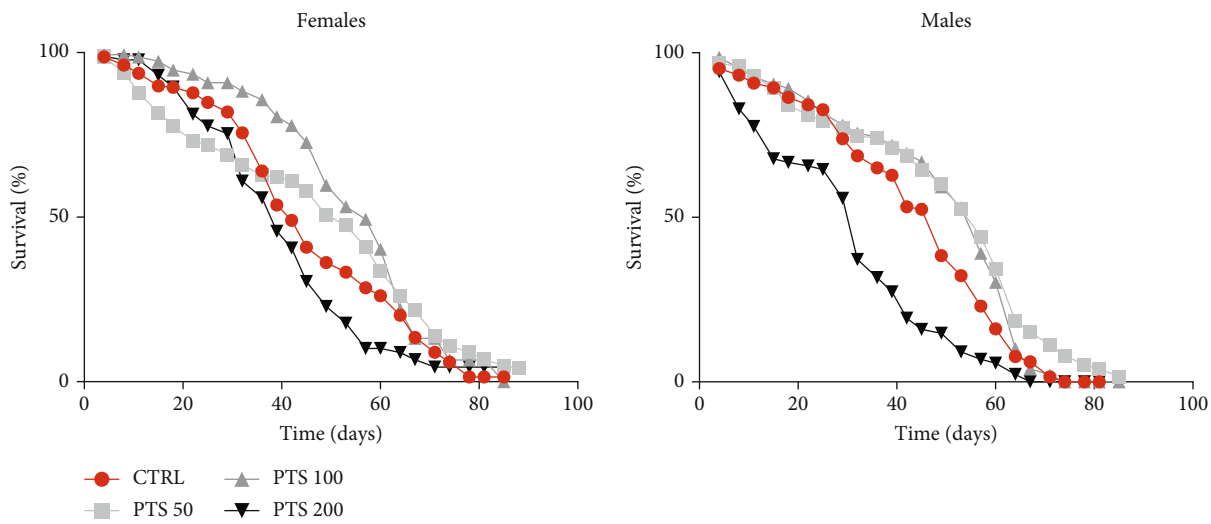

Figure 2: Survival assay of adult female and male flies. Flies were supplemented with 50, 100, and 200 μM PTS lifelong. Data are presented as percentage of survival of flies as function of time (in days). The Kaplan–Meier test was used to detect the significant differences among the fourth groups of flies.

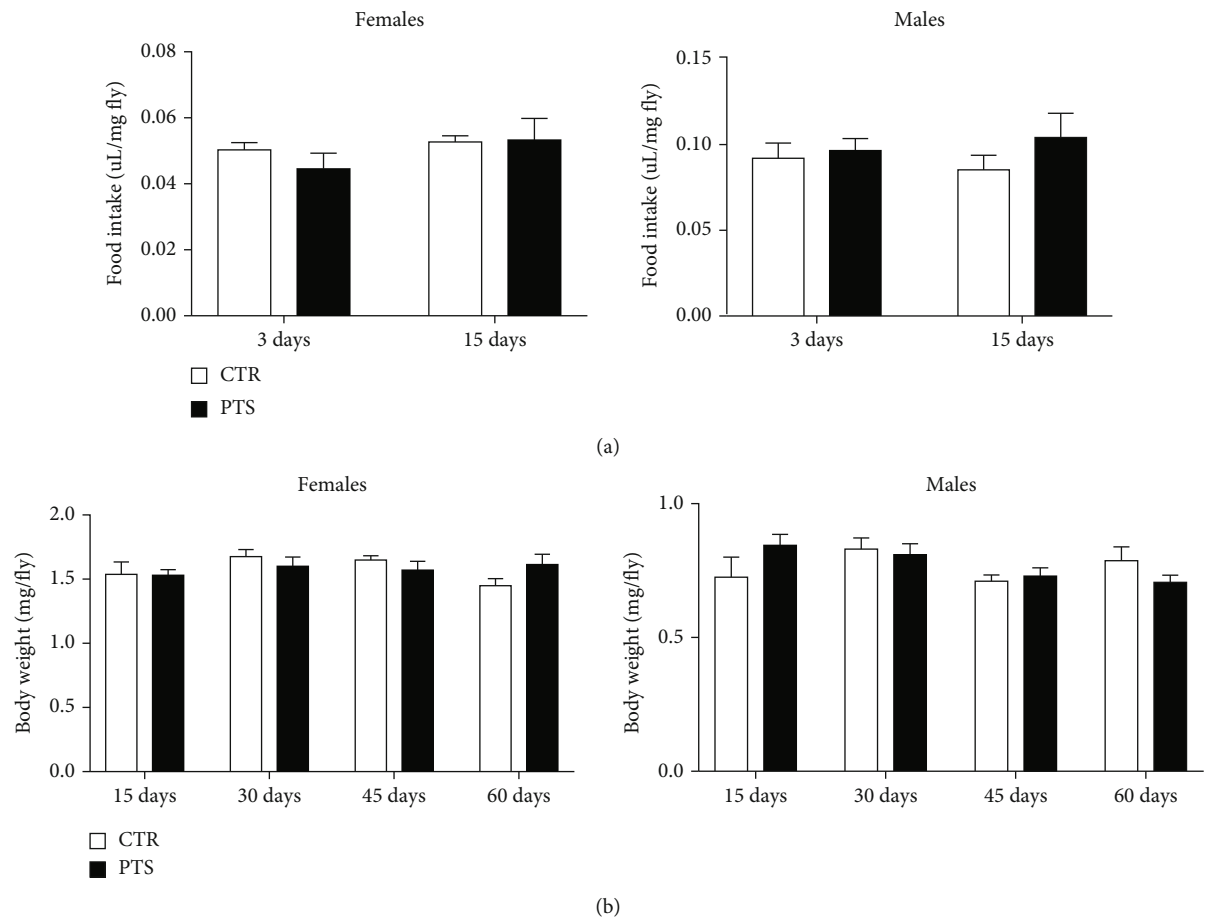

Figure 3: Food intake and body weights of *D. melanogaster* supplemented with PTS. (a). Flies were not supplemented with PTS or supplemented with 100 μM PTS for 15 days before CAFE assay. (b). Flies were supplemented with 100 μM PTS for 15, 30, 45, and 60 days before body weight measurement. Each bar represents the mean ± SEM. Data were analyzed by Student's t-test comparing each supplementation to the corresponding control.

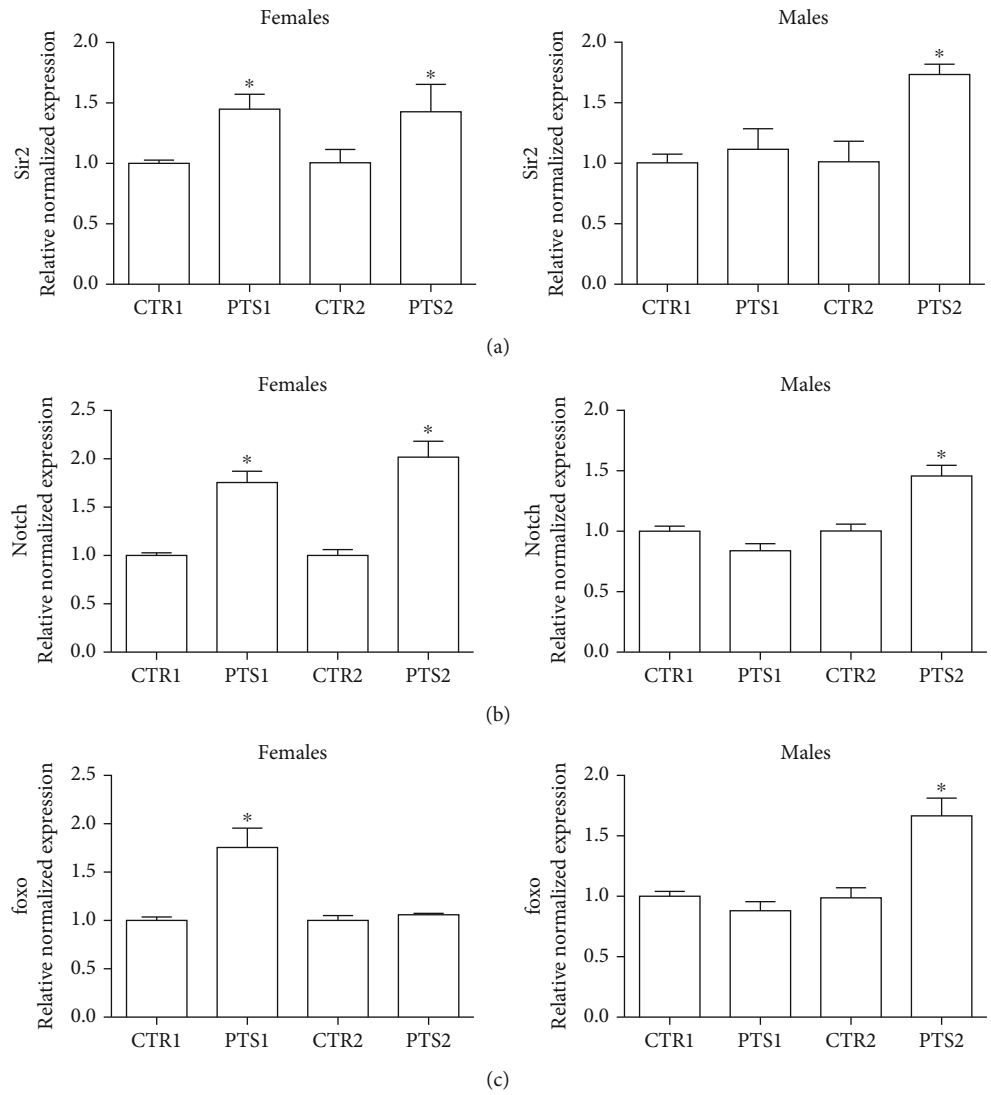

Figure 4: Expression of genes related to longevity in D. melanogaster supplemented with PTS. Flies were supplemented with 100 μM PTS for 15 days (PTS1) or 60 days (PTS2). Total RNA was isolated, and the mRNA levels of A) Sir2, B) Notch, and C) foxo were quantified using RT-PCR normalized to RPL32 reference gene as reported in Materials and Methods. Triplicate reactions were performed for each experiment. Each bar represents the mean ± SEM of three independent experiments. Data relative to 15 days and 60 days were grouped into one graph but analyzed separately by Student's t-test. $*p < 0.05$ with respect to the corresponding controls, CTR1 or CTR2.

mass tolerance: 0.6 Da. A threshold of two peptides with high confidence peptide-spectrum matches was applied for protein identification.

2.13. Statistical Analysis. Each experiment was performed at least three times, and all values are represented as means ± SEM. Student's t-test or one-way ANOVA were used to compare differences among groups followed by Bonferroni's test (Prism 5, GraphPad Software, San Diego, CA). Values of $p < 0.05$ were considered statistically significant. Survival curves were prepared by Kaplan-Meier survival analysis and analyzed using the OASIS2 software [38]. For proteomic experiments, statistical analysis was based on the normalized volume of each spot calculated by the software. Comparison analysis was performed between PTS-treated and control images in both females and males, using One-way ANOVA. Spots that exhibited ratio ≥1.2 or ≤0.83, p-value <0.05 and q value <0.05 were taken into consideration for further protein identification. Bioinformatic analysis was carried out using ShinyGO v.0.66 software to obtain interactive plots showing the relationship between enriched pathways whereas heat map was build using NG-CHM GUI 2.20.2 software [39].

3. Results

3.1. Effect of PTS on Longevity. To examine the pro-longevity effect of PTS, male and female Canton S flies were reared on standard diet supplemented with different concentrations of PTS (50, 100, and 200 μM) lifelong (Figure 2). DMSO vehicle (0.1%) has been added to control groups. DMSO did not influence fly longevity as no significant differences have been observed between control groups reared in the presence or

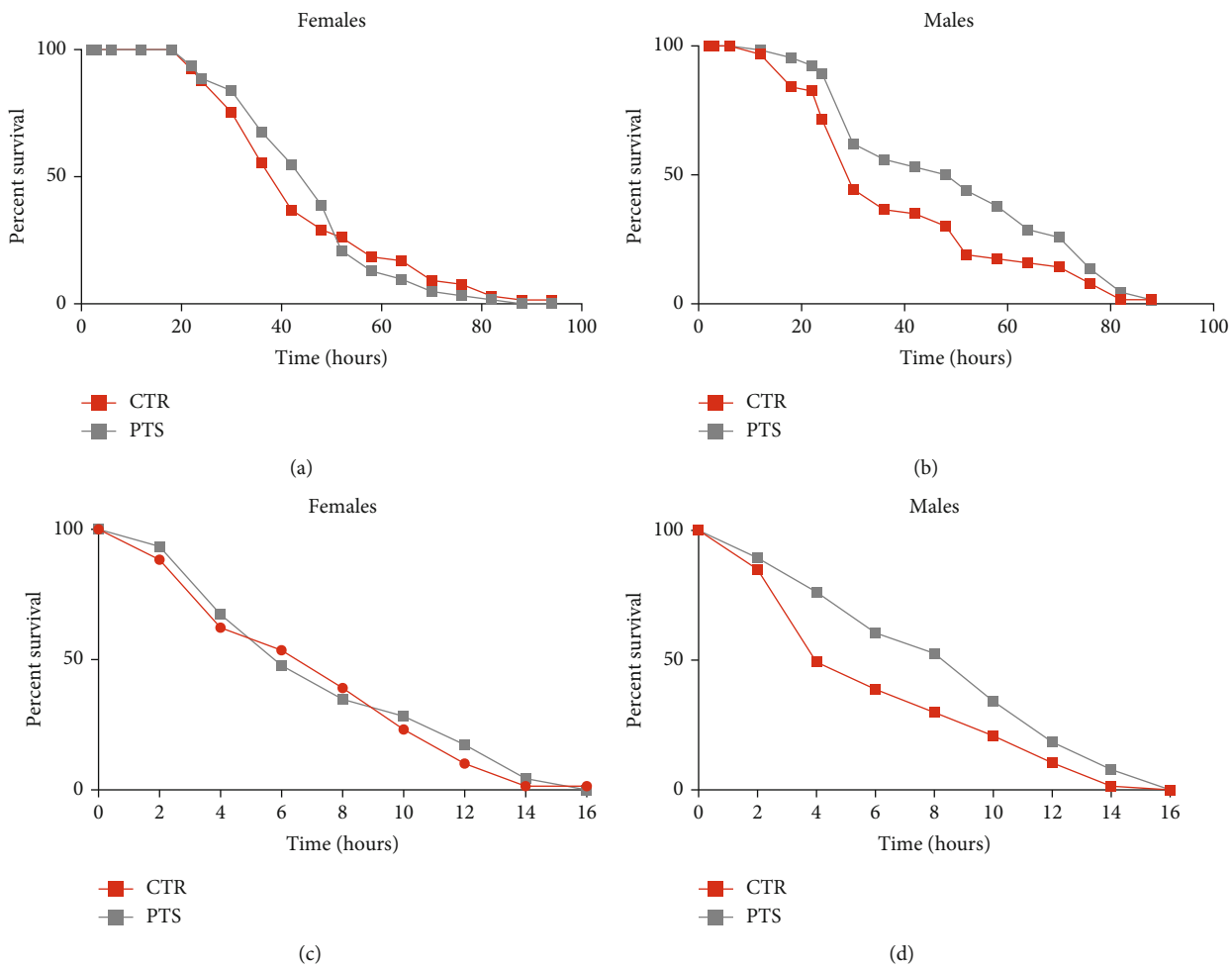

Figure 5: Survival assay of adult female and male flies after oxidative stress induction. Flies were supplemented with 100 μM PTS for 15 days, then were exposed to 2.5 mM Paraquat **(A, B)** or 17.5% ethanol **(C, D)**. Data are presented as percentage survival of flies as function of time (in hours). The Kaplan–Meier test was used to detect the significant differences among the two groups of flies.

absence of 0.1% DMSO both in male and female flies (data not shown). Moreover, this concentration of DMSO has been used by different authors as control vehicle [40–42]. A significant increase in mean lifespan was observed in 50 μM PTS supplemented male flies compared to control flies (14% increase, $p < 0.0034$), while mean lifespan of female flies treated with 50 μM PTS was comparable to that of control flies (Figure 2). 100 μM PTS was effective both in male and female flies leading to a significant increase of mean lifespan of 12% ($p < 0.0196$) and 20% ($p < 0.0072$), respectively. Of note, 200 μM PTS had a negative effect in both sexes as it significantly reduced mean lifespan in respect to control flies.

To verify that the improvement of the mean lifespan was due to PTS supplementation itself and not to CR induced by PTS off-flavor, food intake was evaluated by CAFE assay in flies before supplementation and after 15 days of PTS supplementation (Figure 3(a)). Interestingly, PTS did not influence food intake in female and male flies both before and after PTS supplementation. Of note, male flies had a higher food intake in respect to female flies. In particular, PTS supplemented male flies had a significant higher food intake in respect to female PTS supplemented flies both at 3 days and 15 days ($p < 0.0014$ and $p < 0.0341$, respectively). Body weights of flies supplemented with 100 μM PTS were recorded on days 15, 30, 45 and 60 (Figure 3(b)) to further confirm that PTS did not modify food intake throughout fly life. No differences in body weights were observed both in female and male flies at any time points, suggesting an equal food intake in control and PTS supplemented groups.

To better clarify, at a molecular level, the effect of PTS on the lifespan of male and female flies, the expression of 3 genes related to longevity were investigated. As 100 μM PTS supplementation was effective both in males and females, and in males showed comparable effects to 50 μM PTS, 100 μM PTS supplementation was used in the following experiments. Flies were supplemented with PTS for 15 days (PTS1) or 60 days (PTS2) and the expression of Sir2, foxo, and Notch was evaluated by RT-PCR (Figure 4).

Sir2, a member of the Sirtuin family of protein acylases, deacetylates lysine residues within many proteins and has been implicated in the extension of longevity in *D. melanogaster* [43]. In Figure 4(a) the expression levels of Sir2 are reported. Sir2 was significantly upregulated in female

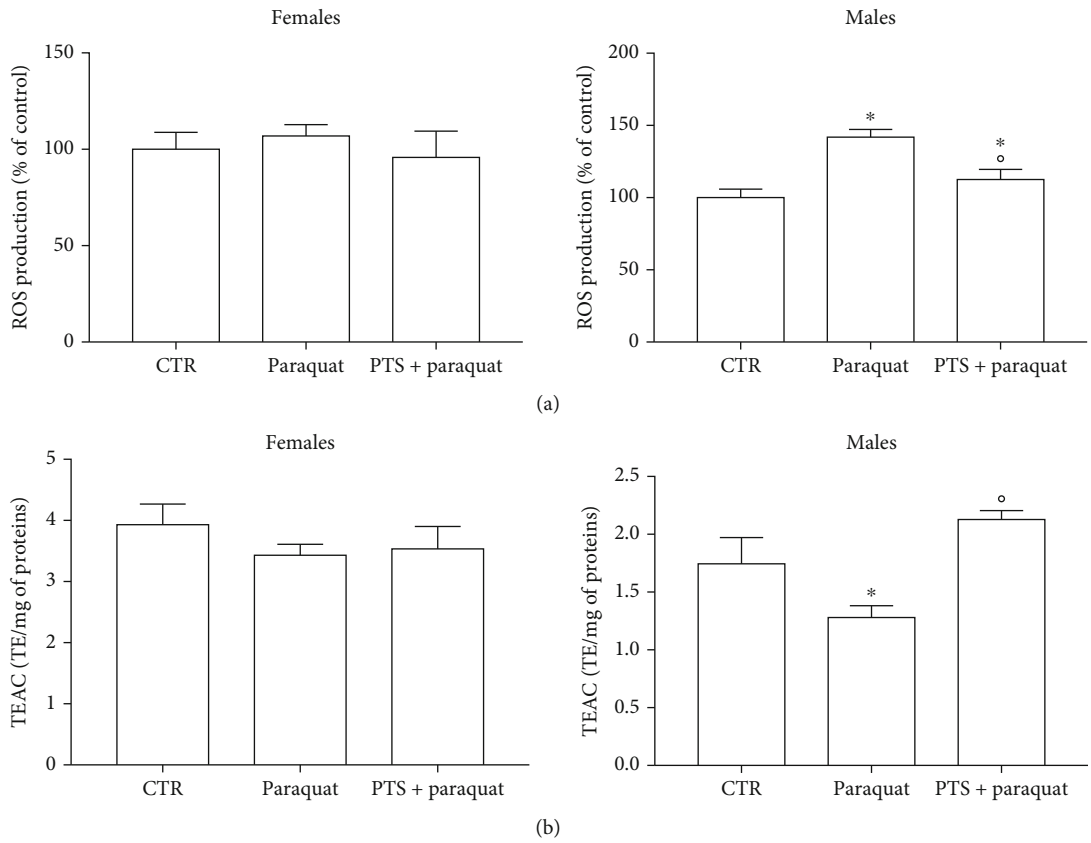

Figure 6: Redox state of flies supplemented with PTS and exposed paraquat. Flies were supplemented with 100 μM PTS for 15 days, then were exposed to 2.5 mM paraquat. A. ROS production was measured with the peroxide-sensitive probe DCFH-DA B. Total radical scavenging capacity was evaluated by ABTS assay. Each value represents mean ± SD. Data were analyzed by One-way ANOVA followed by Bonferroni's test. $*p < 0.05$ with respect to CTR; $^{\circ}p < 0.05$ with respect to Paraquat.

flies both after 15 days and 60 days, meanwhile in male flies the gene was overexpressed only after 2-month supplementation. As it has been recently demonstrated that Sir2 is a positive regulator of the Notch pathway in *Drosophila* [44], we also investigate the effect of a short and long term supplementation of PTS on the expression of Notch in male and female flies (Figure 4(b)). Interestingly, the obtained data were perfectly in agreement with the results on Sir2 expression. In fact, in female flies, both the short- and long-term supplementations with PTS were able to up-regulate Notch expression. In male flies only the 2-month supplementation led to a significant Notch over-expression. In *D. melanogaster*, FOXO, the orthologous of the nematode DAF-16/FoxO and mammalian FOXO3A, has been shown to be a key transcriptional regulator of the insulin pathway that modulates growth and proliferation, and the increase of its activity in certain tissues is sufficient to extend fly lifespan [45]. In our study, PTS triggered a significant foxo up-regulation after 15 days supplementation in female flies and after 2-month supplementation in male flies (Figure 4(c)).

3.2. Antioxidant Effect of PTS. To study the antioxidant effect of PTS, flies were supplemented with 100 μM PTS for 15 days before the induction of oxidative stress. As we mentioned above, we chose this PTS concentration because, it was the most effective in increasing lifespan in both sexes. Oxidative stress was induced by 2.5 mM paraquat or 17.5% ethanol exposure in both male and female flies [33, 46–49]. PTS did not show any protective activity against both paraquat and ethanol-induced damage in female flies since the survival curves of control and PTS supplemented flies were comparable (Figure 5(a)–5(c)). On the contrary, 100 μM PTS significantly increased the percentage of survival in male flies exposed to both paraquat and ethanol ($p < 0.017$ and $p < 0.0284$, respectively). The redox state of flies supplemented with PTS and exposed to paraquat or ethanol was investigated evaluating both the production of ROS and the total radical scavenging capacity (Figures 6 and 7). In male flies paraquat significantly increased ROS production with respect to control, and PTS administration was able to partially counteract this effect significantly reducing ROS production compared to paraquat but maintaining ROS production to levels significantly higher in respect to controls (Figure 6(a)). These data are strengthened by the results on the antioxidant capacity of male flies, as paraquat significantly reduced the total radical scavenging capacity in respect to controls, meanwhile PTS reverted this effect significantly increasing the endogenous antioxidant levels to value comparable to controls (Figure 6(b)). In female flies paraquat did not modify endogenous ROS production

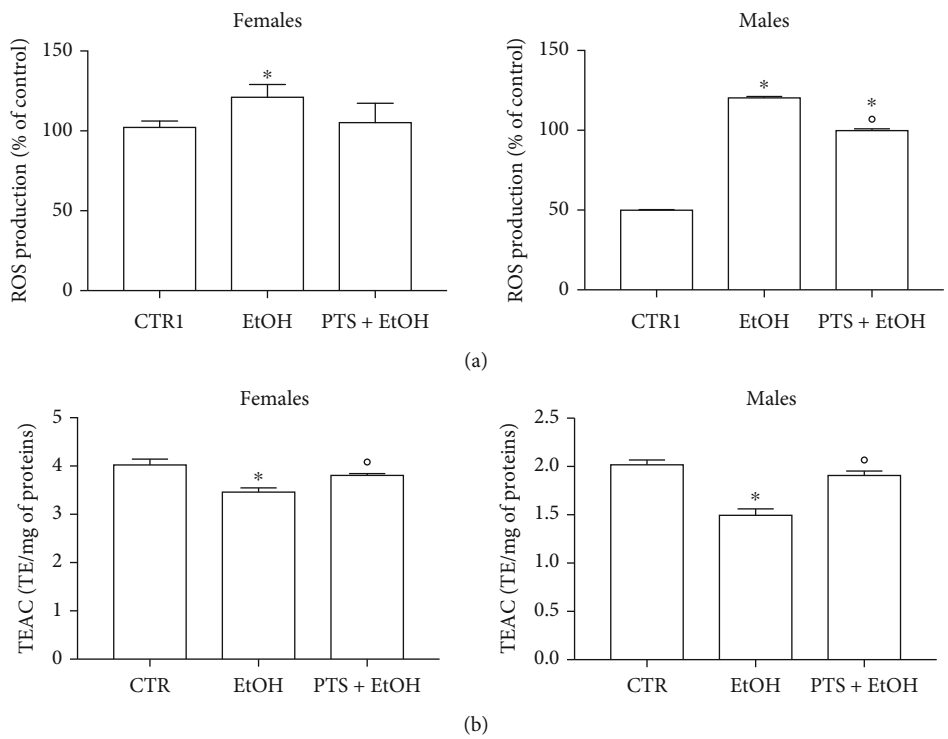

Figure 7: Redox state of flies supplemented with PTS and exposed to ethanol. Flies were supplemented with 100 μM PTS for 15 days, then were exposed to 17.5% ethanol (EtOH) for 4 h. A. ROS production was measured with the peroxide-sensitive probe DCFH-DA B. Total radical scavenging capacity was evaluated by ABTS assay. Each value represents mean ± SD. Data were analyzed by One-way ANOVA followed by Bonferroni's test. $*p < 0.05$ with respect to CTR; $^{\circ}p < 0.05$ with respect to EtOH.

(Figure 6(a)). Slight reduction of the total radical scavenging capacity is observable both in females exposed to paraquat and in those pre-treated with PTS even if these results are not statistically significant (Figure 6(b)).

Ethanol significantly and strongly increased ROS production (Figure 7(b)) and decreased the total radical scavenging capacity (Figure 7(c)) in male flies. PTS supplementation significantly decreased ROS levels and increased the total radical scavenging capacity in respect to male flies exposed to ethanol, but only the total radical scavenging capacity reached levels comparable to control flies. In agreement with the data obtained with paraquat, in female flies, ethanol induced a lower increase of ROS levels in respect to male flies. PTS triggered a slight reduction of ROS levels with intermediate values between control and ethanol stressed flies. Total radical scavenging capacity was significantly reduced by ethanol exposure in female flies and PTS was able to significantly increase this value in respect to ethanol treated flies.

To further investigate the antioxidant activity of PTS, the expression of 2 antioxidant genes, heme oxygenase (Ho) and thioredoxin reductase 1 (Trxr-1), was evaluated. Flies were supplemented with PTS for 15 days (PTS1) or 60 days (PTS2) and the expression of Ho and Trxr-1 was measured by RT-PCR (Figure 8).

In agreement with the previous data on oxidative stress, PTS did not influence the expression of both the enzymes in female flies. On the other hand, in male flies, PTS supplementation significantly up-regulated Trxr-1 at both supplementation times, and triggered Ho over-expression at the second time point.

3.3. Anti-Inflammatory Effect of PTS. One of the most recent theories on aging focuses on the activation of a subclinical, chronic low-grade inflammation that occurs within this process, named "inflammaging" [3]. Even if a lot of studies have demonstrated PTS anti-inflammatory activity in different model systems, no study investigated the anti-inflammatory effect of PTS in *D. melanogaster*. On this basis, female and male flies were supplemented with 100 μM PTS for 15 days (PTS1) or 60 days (PTS2) and the expression of two pro-inflammatory genes, domeless (dome) and eiger (egr), were measured by RT-PCR (Figure 9). In particular, dome is a signal-transducing receptor with most similarities to the IL-6 receptor family [50], whereas egr is the fly ortholog of TNFα [51]. In female flies, PTS significantly reduced the expression of dome at 60 days supplementation and the expression of egr at 15 days supplementation. No effect has been observed in male flies.

3.4. Proteome Changes Induced by PTS Supplementation. To understand why PTS supplementation for 15 days counteracted oxidative stress in male but not in female flies, we decided to look at the proteome changes that may be aroused from this supplementation in the two sexes. Figure 10 shows representative 2DE images of protein extracts of bodies of both female (A) and male (B) flies supplemented with 100 μM PTS for 15 days. Comparative

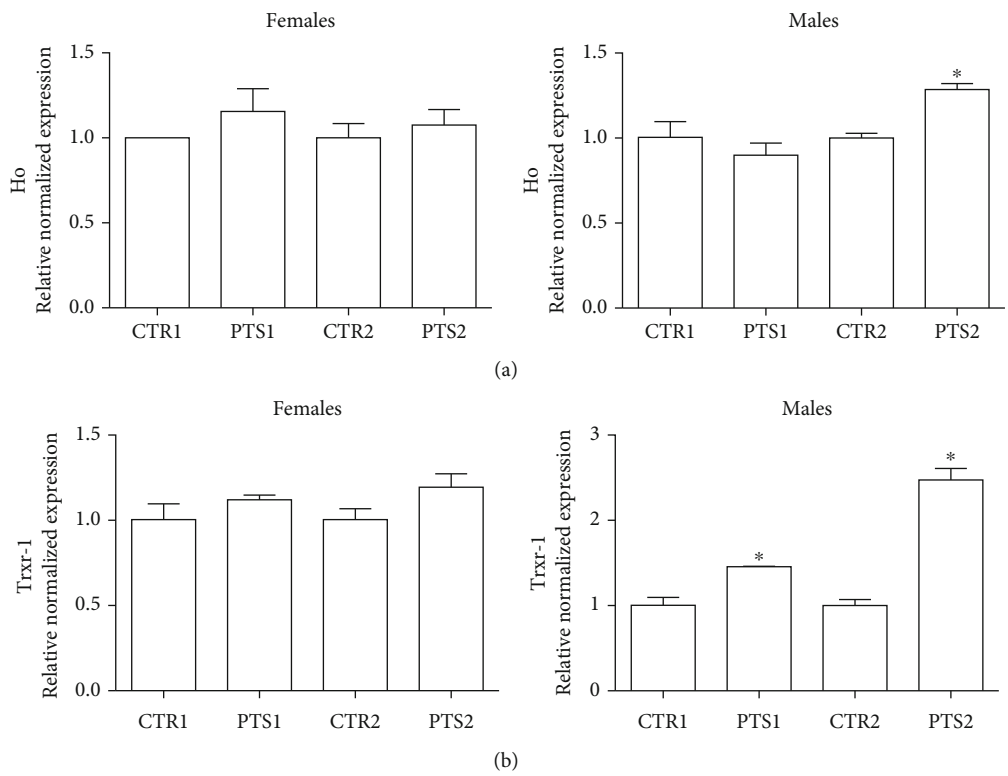

Figure 8: Expression of antioxidants enzymes in *D. melanogaster* supplemented with PTS. Flies were supplemented with 100 μM PTS for 15 days (PTS1) or 60 days (PTS2). Total RNA was isolated, and the mRNA level of A) Ho and B) Trxr-1 was quantified using RT-PCR normalized to RPL32 reference gene as reported in Materials and Methods. Triplicate reactions were performed for each experiment. Each bar represents the mean ± SEM of three independent experiments. Data relative to 15 days and 60 days were grouped into one graph but analyzed separately by Student's t-test. $*p < 0.05$ with respect to controls, CTR1 and CTR2.

analysis was performed to investigate the effects of PTS in respect to control both in female and male groups. One-hundred and thirteen and nine spots were found differentially expressed (ratio ≥1.2 or ≤0.83, $p < 0.05$, q value < 0.05) in male and female flies supplemented with PTS in respect to controls, respectively. For males, only 23 proteins were identified, of which 19 were significantly induced in respect to control flies and 4 were significantly lower than control flies. Venn diagram (Figure 11) illustrates the number of spots differentially expressed which are common and exclusive between the two sexes. Of the nine proteins modulated by PTS in female flies, only two were in common with the proteins differentially expressed in males. Spots of interest were subsequently subjected to nLC-ESI-MS/MS analysis and identified. Table 2 shows the list of identified proteins together with their MW, pI, peptides and coverage values of MS/MS, ratio and p values. Moreover, normalized mean values of optical density of the identified differentially expressed spots were analyzed using Next-Generation Clustered Heat Map to generate a clustered heat map (Figure 12). In the heat map it is possible to appreciate the higher number of up-regulated proteins after PTS treatment in male flies compared to females. In particular, as suggested by gene ontology analysis, the major changes observed in the males involve proteins belonging to metabolic processes (i.e. small molecule metabolic process, carboxylic acid, oxoacid, ATP, and phosphorus metabolic processes) (Figure 13(b)). Very few changes were observed in the females and essentially related to proteins involved in homeostasis processes and to a lesser degree to metabolic processes (Figure 13(a)).

4. Discussion

Recent studies suggest that PTS can be considered a potential candidate as an anti-aging agent thanks to its ability to modulate different hallmarks of aging, including oxidative damage, inflammation, telomere attrition, and cell senescence [52]. The potential health benefits of PTS on lifespan extension are supported by different studies that investigated the effect of blueberry on model organisms. In *Caenorhabditis elegans*, blueberry polyphenols increased lifespan and thermo-tolerance [6] and blueberry extracts contributed to lifespan prolongation of *D. melanogaster* by the up-regulation of the antioxidant enzymes SOD and catalase [53]. These studies hypothesize that PTS plays a role in increasing longevity but, to the best of our knowledge, no author has so far demonstrated a direct effect of PTS on this parameter. Here, we investigated the effect of PTS supplementation on *Drosophila* longevity and its potential mechanisms of action.

Our data show that PTS supplementation increases the mean lifespan of male and female flies at specific concentrations. In particular, 100 μM PTS was effective in both male and female flies, 50 μM increased mean lifespan only in male

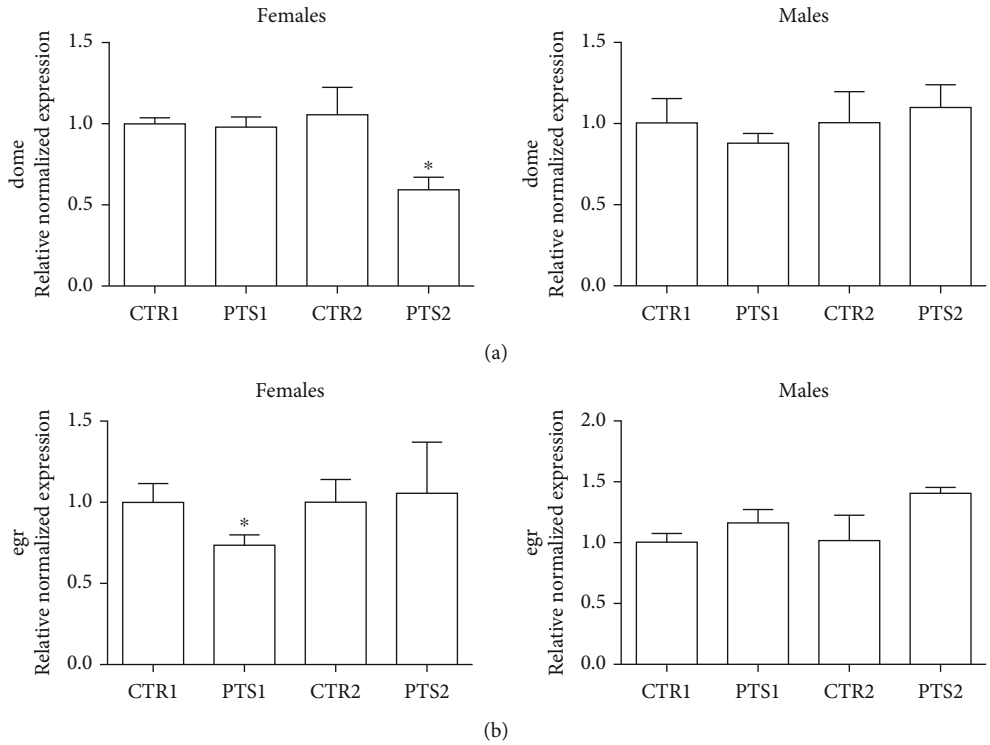

Figure 9: Expression of inflammatory cytokines in *D. melanogaster* supplemented with PTS. Flies were supplemented with100 μM PTS for 15 days (PTS1) or 60 days (PTS2). Total RNA was isolated, and the mRNA level of A) dome and B) egr was quantified using RT-PCR normalized to RPL32 reference gene as reported in Materials and Methods. Triplicate reactions were performed for each experiment. Each bar represents the mean ± SEM of three independent experiments. Data relative to 15 days and 60 days were grouped into one graph but analyzed separately by Student's t-test. $*p < 0.05$ with respect to controls, CTR1 and CTR2.

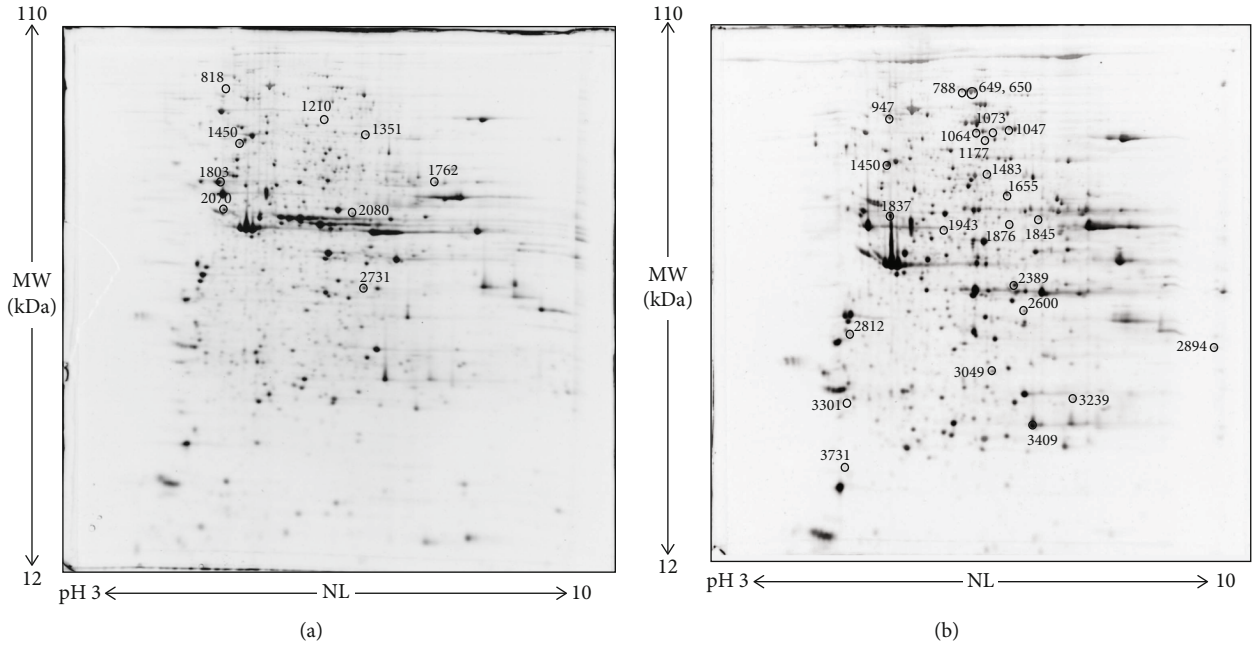

Figure 10: Representative 2DE images of protein extracts of bodies of both female (a) and male (b) flies supplemented with 100 μM PTS for 15 days. Protein extracts were separated in a 3–10 nonlinear gradient. SDS-PAGE was performed using 12% acrylamide. Gels were stained with ruthenium. Spot numbers indicate all the proteins identified by nLC-ESI-MS/MS and refer to the number reported in Table 2.

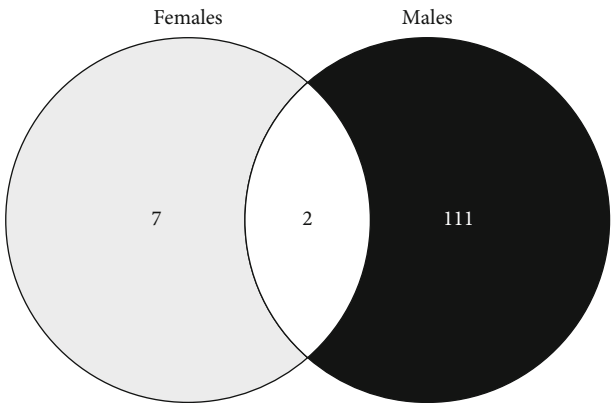

Figure 11: Venn diagram highlighting the distribution of differentially expressed spots in protein extracts obtained by PTS supplemented flies compared to control flies. Both unique and overlapping spots are reported as actual number (Venny 2.0.2).

flies whereas 200 μM PTS evidenced a toxic effect on both sexes. Interestingly, PTS supplementation did not modify the amount of food intake in *Drosophila*, so the observed effect is not due to a potential CR induced by PTS off-flavor. Rather, these results could be related to a hormetic effect, a biphasic dose-response mechanism characterized by a low-dose beneficial effect and a high-dose toxic effect *[54]*. In agreement with our results, different natural products with a pro-longevity effect have been shown to reduce the lifespan of animals when supplemented at high doses *[55]*. PTS is structurally like resveratrol as both are monomeric stilbenes with the only difference that PTS has two methoxy ($-OCH_3$) groups and one hydroxyl (−OH) group, while resveratrol has three −OH groups (Figure 1). Different studies investigated the effect of resveratrol supplementation on D. melanogaster lifespan with apparently contradictory results. Staats et al. [56] did not observe any effect on lifespan after a 500 μM resveratrol supplementation in D. melanogaster, meanwhile Abolaji et al. [57] showed that resveratrol extended lifespan in a dose dependent manner up to a concentration of 60 mg/kg diet. Interestingly, 120 mg/kg diet did not modify lifespan when compared to control flies as observed by Staats et al., suggesting that only specific resveratrol concentrations are effective in prolonging lifespan. These data agree with our observations on the effect of PTS on the mean lifespan of *D. melanogaster* where only one dose in females (100 μM) and two doses in males (50 and 100 μM) where able to increase this parameter. Moreover, we observed a higher food intake in male flies compared to female flies and this could explain why 50 μM PTS supplementation increased mean lifespan of male flies but was not effective on female flies.

As resveratrol has been demonstrated to be effective in increasing lifespan of different model organisms through the up-regulation of Sirt1 [52], we hypothesized that PTS could act on the same molecular target in *Drosophila*. It has been shown that Sirt1, a (NAD+)-dependent deacetylase, has a role in lifespan extension, stress resistance and apoptosis reduction [58, 59]. Sirt1 regulates a great number of downstream molecules, including p53, Foxo1, Foxo3, Foxo4, E2F1, and Notch [44, 60]. Our data demonstrate that PTS supplementation up-regulates the *Drosophila* Sirt1 homolog, Sir2, already after 15 days in females, and in both sexes after 60 days. Of note, to our knowledge, no other study demonstrated that PTS increases Sirt1 in healthy individuals undergoing a physiological aging process. In fact, the research demonstrating PTS ability to increase Sirt1 expression have been carried out in different pathological conditions in which Sirt1 resulted down-regulated in respect to healthy individuals.

To further investigate the effect of PTS on the mean lifespan in *D. melanogaster* we measured the expression of two downstream target of Sir2, Notch and foxo. The Notch signaling pathway is highly conserved among species from *Drosophila* to humans. It has a fundamental role in adult central nervous system for neural plasticity and triggers neural differentiation during development [61]. Notch is a membrane-bound transcription factor that is released to the nucleus by a two-step cleavage mechanism [62]. The second cleavage is carried out by Presenilin and knockout of Presenilin causes the impairment of synaptic plasticity and memory formation in mice [63]. Moreover, it has been observed an impairment in spatial learning and memory of mice carrying a heterozygous mutation of Notch [64]. Presente et al. [61] observed that *D. melanogaster* with a selective loss of Notch function in adulthood show a syndrome that includes loss of flight and premature death from unknown causes. In our study, PTS supplementation triggered a significant up-regulation of Notch with the same regulatory pattern of Sir2, suggesting, as previously underlined, a strong crosstalk between these two proteins.

Foxo is a transcription factor acting as downstream effector of insulin signaling and its activity has been observed to be strictly related with stress resistance and lifespan extension in many organisms including humans [65]. In our model system, PTS led to an increase of foxo expression in female flies only after 15 days supplementation and in male flies only after 2-month supplementation, suggesting a potential role in modulating longevity of both sexes, but indicating that PTS can have different effects in male and female flies.

There are many factors that cause aging, among which oxidative stress and inflammation have been demonstrated to play a fundamental role [66]. Oxidative stress is an imbalance between the production and the removal of reactive oxygen species. According to the oxidative stress theory of aging, the functional impairment typical of elderly is connected to the accumulation of structural alterations due to the oxidative damage to macromolecules by ROS [67]. On these bases, we verified if PTS boosts the *Drosophila* antioxidant system making flies more resistant to oxidative stress. To mimic this condition, we exposed flies to paraquat [48, 49] and ethanol [47, 68]. Interestingly, after exposure to acute ethanol doses, fruit flies show behaviors similar to those observed in humans and mammalian models [69].

A PTS supplementation for 15 days was able to counteract oxidative stress only in male flies, while it was not effective in female flies, evidencing, once again, the different

Table 2: List of differentially expressed proteins identified by nLC-ESI-MS/MS.

Spot n°	Accession (UniProtKB)	Gene symbol	Protein name	Cov [%]	PSMs	Unique peptides	MW [kDa]	Calc. pI	Score	Ratio (PTS/CTR)	p value
	FEMALES										
818	Q24253	AP-1-2beta	AP complex subunit beta	46	68	45	101.1	5.11	227	1.3	0.00087
1210	Q9VA70	CDase	Neutral ceramidase	12	6	6	78.2	6.6	19	0.45	0.00055
1351	Q9VWV6	Tsf1	Transferrin	63	71	42	71.8	7.06	233	1.5	0.00094
1450	A4V0N4	Vha68-2	H(+)-transporting two-sector ATPase	49	38	18	68.3	5.34	142	0.63	0.00074
1762	Q7KW39	CG17896	Probable methylmalonate-semialdehyde dehydrogenase [acylating], mitochondrial	34	21	15	55.9	8.35	85	0.83	0.001
1803	Q24560	betaTub56D	Tubulin beta-1 chain	69	191	11	50.1	4.86	627	1.2	0.00039
2070	M9NH07	Up	Upheld, isoform N	41	35	2	47.2	4.96	102	0.7	0.00068
2080	E1JHR5	Eno	Enolase	42	19	15	46.6	6.55	73	0.48	0.000096
2731	Q7K5K3	Pdhb	Pyruvate dehydrogenase E1 component subunit beta	34	17	12	39.3	7.8	60	0.56	0.00012
	MALES										
649	Q7KN97	PCB	Pyruvate carboxylase	61	92	65	130.8	6.81	312	1.5	0.001
650	Q7KN97	PCB	Pyruvate carboxylase	62	116	70	130.8	6.81	385	1.67	0.005
788	H9XVM8	Dmel\CG1674	Uncharacterized protein, isoform K	37	33	7	96.2	6.7	107	1.62	0.00039
947	Q7KN62	TER94	Transitional endoplasmic reticulum ATPase TER94	72	135	5	88.8	5.35	455	1.58	0.002
1047	Q9VHP0	Bel	ATP-dependent RNA helicase bel	18	13	12	85	7.53	41	1.70	0.004
1064	Q9VNW6	P5CS	Delta-1-pyrroline-5-carboxylate synthase	48	39	31	84	6.73	135	1.56	0.013
1073	Q9VNW6	P5CS	Delta-1-pyrroline-5-carboxylate synthase	54	64	35	84	6.73	230	1.57	0.004
1177	P52034	Pfk	ATP-dependent 6-phosphofructokinase	58	64	42	86.6	6.83	232	1.91	0.002
	Q9VNV3	Ddx1	ATP-dependent RNA helicase Ddx1	11	6	6	80.8	6.87	16		
1450	A4V0N4	Vha68-2	H(+)-transporting two-sector ATPase	49	38	18	68.3	5.34	142	0.68	0.007
1483	Q07327	Rop	Protein ROP	52	50	31	67.8	6.7	193	1.78	0.006
1655	O62619	PyK	Pyruvate kinase	55	31	23	57.4	7.44	115	1.97	0.005
1837	E1JIJ5	Vha55	Vacuolar proton pump subunit B	54	92	25	54.5	5.4	318	1.65	0.014
1845	Q9VBP6	Ssadh	Succinate-semialdehyde dehydrogenase	50	26	22	54.9	8.21	85	1.55	0.00073
	Q9W058	SCOT	Succinyl-CoA:3-ketoacid-coenzyme A transferase, mitochondrial	43	24	16	54.9	8.37	82		
1876	Q9VEP6	AdSL	Adenyluccinate lyase	43	30	20	53.8	7.49	103	1.5	0.013
1943	Q7K4Q9	Hmgs	3-hydroxy-3-methylglutaryl coenzyme A synthase	54	30	19	51.1	6.32	112	1.52	0.022
2389	Q9VSA3	CG12262	Probable medium-chain specific acyl-CoA dehydrogenase, mitochondrial	47	64	24	45.8	7.94	207	1.51	0.015
2600	M9PF46	Prps	Ribe-phphate diphphokinase	58	34	22	40.9	7.91	120	1.57	0.028
2812	P22465	AnxB10	Annexin B10	29	7	7	35.7	4.74	24	0.67	0.018
2894	Q9VEB1	Mdh2	Malate dehydrogenase	54	71	23	35.3	9.11	237	3.46	0.00060

Table 2: Continued.

Spot n°	Accession (UniProtKB)	Gene symbol	Protein name	Cov [%]	PSMs	Unique peptides	MW [kDa]	Calc. pI	Score	Ratio (PTS/CTR)	p value
3049	Q9VM18	21430192	Trehalose 6-phosphate phosphatase	33	10	9	31.2	7.12	29	1.5	0.004
	Q7KN94	Wal	Electron transfer flavoprotein subunit alpha	44	46	13	34.2	8.32	148		
3239	Q0KHZ6	ETFB	Electron transfer flavoprotein subunit beta	79	51	21	27.2	8.05	177	0.73	0.023
	Q7JR58	Echs1	Enoyl-CoA hydratase, short chain 1, isoform A	39	14	10	31.6	8.63	47		
3301	P29310	14-3-3zeta	14-3-3 protein zeta	41	10	9	28.2	4.88	30	0.42	0.015
3409	P00334	Adh	Alcohol dehydrogenase	68	66	12	27.7	7.96	234	1.60	0.013
3731	Q9VGS2	Tctp	Translationally-controlled tumor protein homolog	80	43	17	19.6	4.81	140	0.71	0.004

Cov [%] = coverage [%], the percentage of the sequence covered by identifications (PSMs only) from the included searches; PSMs = the total number of peptide spectrum matches identified from all included searches; Unique Peptides: the total number of distinct peptide sequences unique to the protein group; MW [kDa]: the molecular weight of the protein; calc. pI: the isoelectric point calculated for the protein; Score = Score Sequest HT, the protein score which is calculated by summing the individual scores of each peptide. The higher this score, the higher the individual scores of the peptides, and thus the better the identification. Sequest HT is the name of the employed search engine.

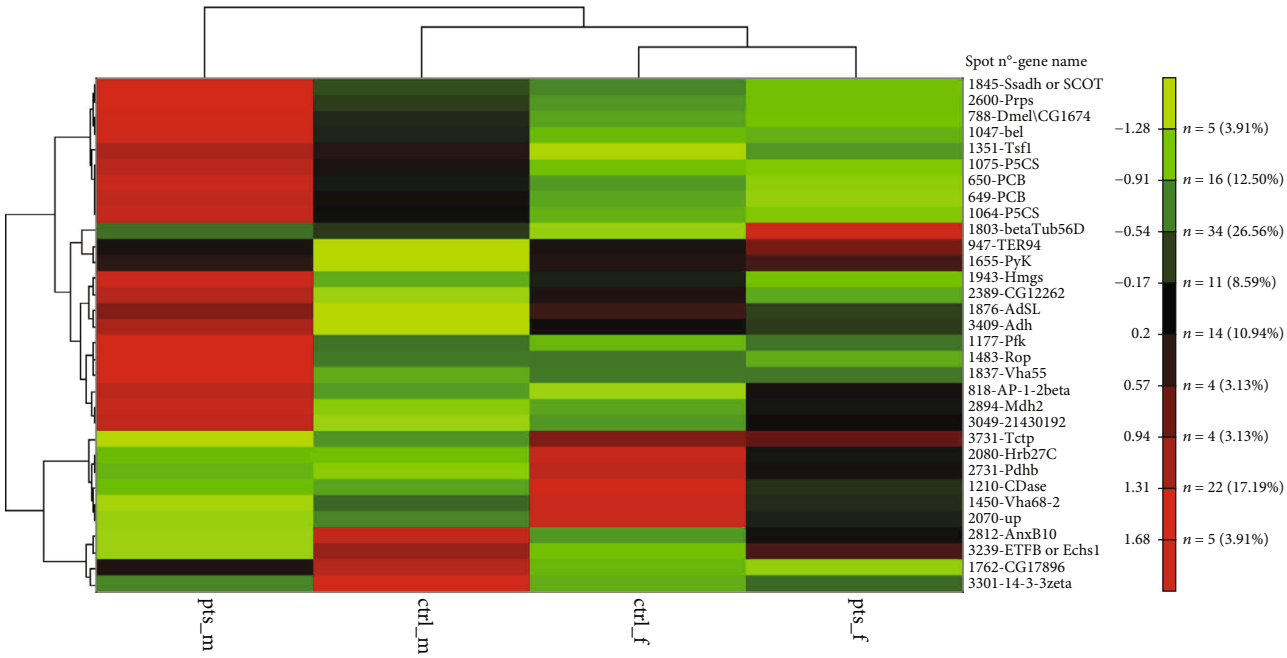

Figure 12: Clustered heat map of differentially expressed proteins after PTS supplementation in female and male samples. Heat map was generated using NG-CHM GUI 2.20.2 software. Z-norm transform was used to normalize the row values (mean of normalized optical densities of spots, n =3) and resulting transform data matrix used to build the heat map. A hierarchical ordering method was applied to clustered rows and columns. Euclidean distance metric was applied to hierarchically clustered rows and columns. Data matrix distribution values range from -1.72 to +1.72. The brighter the color, the more intense the changes are. ctrl_m: male control; ctrl_f: female control; pts_m: males treated with PTS; pts_f: females treated with PTS.

effect of PTS on the two sexes. Interestingly, our data obtained by proteomic analysis indicate that PTS is able to significantly increase alcohol dehydrogenase (ADH) expression only in male flies, supporting the positive PTS activity against ethanol in male flies but not in female flies. In D. melanogaster, ADH metabolizes more than 90% of ethanol and in ADH deficient flies a higher toxicity of ethanol has been observed [70]. Of note, in the first 24 h, paraquat induced a higher mortality in male flies in respect to female flies ($p < 0.0063$). Our results are in agreement with the data of Krůček et al. [71] that observed a higher mortality induced by 25 mM Paraquat in male flies in respect to female flies. This could be ascribed to a different expression of the endogenous antioxidant enzymes in the two sexes. In fact, as demonstrated by Niveditha et al. [33], in female flies the activity of the antioxidant enzymes SOD and catalase is significantly higher in respect to male flies. These data are in agreement with our results that evidenced a higher antioxidant capacity of females flies (~3.9 mg TE/mg protein) in respect to male flies (~1.7 mg TE/mg protein).

To have a better insight on the antioxidant mechanisms of PTS in *Drosophila* we investigated the effect of PTS on the expression of two antioxidants enzymes, Ho and Trxr-1. We decided to investigate these two antioxidant enzymes because Ho has been demonstrated to be upregulated by PTS in both cell cultures and animals [72–76] and many studies observed an up-regulation of Trxr-1 and Trx-1 triggered by resveratrol [77, 78] but no studies investigated PTS effect on Trxr-1. Moreover, Ho and Trxr-1 are classified as vitagenes, a group of genes which are strictly involved in preserving cellular homeostasis during stressful conditions [79]. The vitagene family is composed of the heat shock proteins (Hsp) Hsp32 (also known as HO-1), Hsp70, sirtuins and by the thioredoxin system [70, 80–82]. In agreement with the data on the protection against oxidative stress, PTS up-regulated Ho and Trxr-1 only in male flies. Our hypothesis is that PTS is more effective in inducing the antioxidant system in males in respect to females because the female endogenous antioxidant system is already highly expressed, and maybe PTS is not able to trigger a further increase.

Many studies have associated an anti-inflammatory activity to PTS. It has been described that PTS inhibited mitogen-activated protein kinase (MAPK) phosphorylation and the production of pro-inflammatory cytokines (Interleukin-6 and TNF-α) in mouse microglial cells activated by lipopolysaccharides [83]. Moreover, PTS showed inhibitory effect on inflammatory responses following the interaction of 3 T3-L1 adipocytes with RAW 264.7 macrophages [84]. Our data demonstrated that PTS supplementation reduced the expression of two pro-inflammatory cytokines, in particular dome, that has similarities with the mammalian IL-6 receptor family [9] and egr, the fly orthologue of TNFα [51], in female flies, but had no effect in male flies.

We performed proteomic analyses of male and female flies supplemented for 15 days with PTS to better characterized the mechanisms behind the higher protection of PTS against oxidative stress in males in respect to female flies.

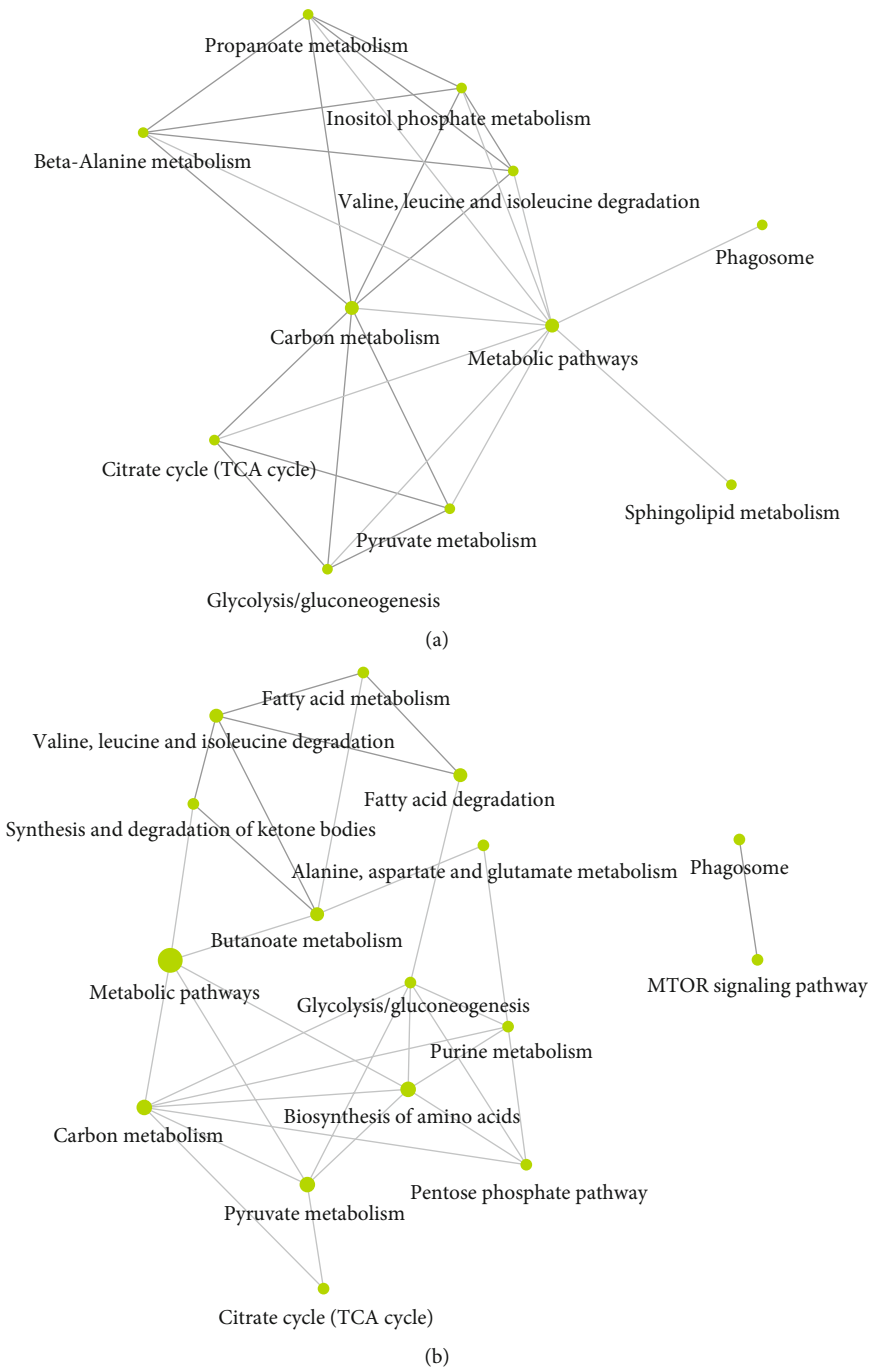

Figure 13: KEGG Pathway analysis of differentially expressed proteins both in females (a) and males (b) *D. melanogaster*. ShinyGO v.0.66 software was used to obtain interactive plots which show the relationship between enriched pathways. Two pathways (nodes) are connected if they share 20% (default) or more genes. Darker nodes are more significantly enriched gene sets. Bigger nodes represent larger gene sets. Thicker edges represent more overlapped genes.

Unlike what we would have expected, the proteomics data did not provide further information useful for understanding the different effect of PTS supplementation on oxidative stress. Nevertheless, several interesting aspects emerged. The results showed that PTS modulates a higher number of proteins in male in respect to female flies (113 and 9, respectively). Among the identified proteins, only one is in common between the two sexes: vacuolar H[+] ATPase 68 kDa subunit 2 (Vha68-2).The strong down-regulation of Vha68-2 by PTS is comparable in the two sexes. This protein is part of the vacuolar proton-translocating ATPase (V-ATPase) that is organized into 2 subcomplexes, namely, the ATP-catalyzing domain (V1) and a proton-translocation domain (V0) and Vha68-2 belongs to V0 domain. V-ATPase is a key regulator of organelle acidification in eukaryotic cells [85, 86] and has been demonstrated to modulate several

cellular processes, like membrane trafficking and protein degradation [86, 87]. In *D. melanogaster* the role of Vha68-2 has been marginally investigated in only one study related to the function of *Drosophila* salivary glands during the early- to mid-prepupal period [88]. However, a role of V-ATPase in longevity has been demonstrated in *C. elegans* where the RNAi downregulation of 2 different subunits of the V-ATPase, vha-3 and vha-12 belonging to V0 and V1, respectively, increased lifespan. The authors suggested that this lifespan extension might be due to Ce.TOR inhibition, because V-ATPase is required for the spatial regulation and subsequent activation of TORC1 [89]. On the other hand, only in male flies, vacuolar proton pump subunit B (Vha55), that corresponds to vha-21 in *C. elegans* [90], is induced by PTS supplementation. These observations suggest that Vha68-2 downregulation by PTS could be involved in the observed increase in both male and female lifespan. Further studies should be carried out to better investigate this point and to verify how this protein is modulated in older flies.

Among the proteins modulated by PTS in female flies, enolase and pyruvate dehydrogenase are particularly interesting as are enzymes related to glucose metabolism, the first one is a glycolytic enzyme, meanwhile the second one transforms the product of glycolysis, pyruvate, in acetyl CoA. Both are strongly downregulated, and this is in agreement with the observations that caloric restriction is characterized by a decreased glucose metabolism [91, 92]. Moreover, Schriner et al. [91], studying the mechanisms behind *Rhodiola rosea* ability to extend life span in *Drosophila*, evidenced that *R. rosea* significantly reduced the expression of enolase in female and not in male flies and associated this effect with lifespan increase. This is supported by our data as we observed the downregulation of this enzyme only in female flies that showed a higher mean lifespan in respect to male flies. The limitation of our results is that they were obtained analyzing relatively young flies (15 days old) and as underlined previously, to draw more reliable conclusions, further studies should be carried out to investigate the proteome of older flies.

Among the proteins modulated by PTS in male flies, malate dehydrogenase 2 (mdh2) shows the highest upregulation (fold >3). Mdh2 is closely related to mitochondrial malate dehydrogenases from multiple animal species, including mouse Mdh2 and yeast Mdh1 and localizes to mitochondria *in vivo* [93]. Its main role is to transform malate to oxalacetate in the tricarboxylic acid cycle and is critical for cellular energy production. This is supported by the observation of Wang et al. [93] that observed significantly lower levels of ATP in Mdh2 *Drosophila* mutants and an accumulation of late-stage citric acid cycle intermediates. Of note, this protein is strongly up-regulated in male and not in female flies and this suggests that this up-regulation triggered by PTS could be linked to the presence of specific male hormones. In general, PTS induces different proteins related to metabolic pathways, among them pyruvate carboxylase and kinase, succinate-semialdehyde dehydrogenase, 3-hydroxy-3-methylglutaryl coenzyme A synthase, and ATP-dependent 6-phosphofructokinase. On the other hand, PTS downregulates few proteins, among them Vha68-2, previously discussed, Annexin B10 (AnxB10), electron transfer flavoprotein subunit beta (ETFB), 14-3-3 protein zeta (14-3-3zeta), and translationally-controlled tumor protein homolog (Tctp). Interestingly, in *D. melanogaster* it has been demonstrated that 14-3-3 genes show strong genetic interaction with Tctp [94], a protein involved in Tor signalling [94–97]. In particular, in *Drosophila*, Tctp is essential for organ growth by promoting Rheb function for Tor signalling as a guanine nucleotide exchange factor [95]. Moreover, Tctp is over-expressed in cancer cells, and its downregulation induces the reversion of tumour phenotypes [98–100]. From this point of view, the reduction of Tcpt triggered by PTS supplementation in male flies could have a role in counteracting tumorigenesis. Further studies should be carried out to better clarify this interesting aspect.

5. Conclusions

In conclusion, our data demonstrate for the first time that PTS increases average lifespan of both male and female flies. Interestingly, the mechanisms behind this effect are different in the two sexes. Protein related to longevity are modulated with different time patterns in the two sexes, moreover PTS was able to increase the expression of two genes (Ho and Trxr-1) involved in the antioxidant defense only in male flies and reduces pro-inflammatory proteins only in female flies. Proteomic analysis suggests a potential involvement of Vha68-2 in the observed increase of lifespan, a reduction of glucose metabolism in female flies and an induction of different metabolic pathways in male flies together with the downregulation of 14-3 3zeta and Tctp suggesting a potential role of PTS in reducing tumorigenesis. These data show that males and females respond differently to treatments, reinforcing the emerging idea that studies on drugs and nutraceuticals should be conducted separately in the two sexes to give more reliable answers. Moreover, these results stressed on the importance of creating personalized treatment, that take into consideration the genetic and biological diversity that arise among different individuals and among the two sexes.

Data Availability

The data used to support the findings of this study are available from the corresponding author upon request.

Conflicts of Interest

The authors declare that no conflict of interest and no competing financial interest exist.

References

[1] D. Harman, "Aging: a theory based on free radicals and radiation chemistry," *Journal of Gerontology*, vol. 11, no. 3, pp. 298–300, 1956.

[2] L. C. D. Pomatto and K. J. A. Davies, "Adaptive homeostasis and the free radical theory of ageing," *Free Radical Biology and Medicine*, vol. 124, pp. 420–430, 2018.

[3] C. Franceschi, M. Bonafè, S. Valensin et al., "Inflamm-aging: An Evolutionary Perspective on Immunosenescence," *Annals of the New York Academy of Sciences*, vol. 908, pp. 244–254, 2000.

[4] C. Peng, H. Y. Chan, Y. Huang, H. Yu, and Z. Y. Chen, "Apple polyphenols extend the mean lifespan of Drosophila melanogaster," *Journal of Agricultural and Food Chemistry*, vol. 59, no. 5, pp. 2097–2106, 2011.

[5] T. E. Lopez, H. M. Pham, B. V. Nguyen et al., "Green tea polyphenols require the mitochondrial iron transporter,mitoferrin, for lifespan extension inDrosophila melanogaster," *Archives of Insect Biochemistry and Physiology*, vol. 93, no. 4, pp. 210–221, 2016.

[6] M. A. Wilson, B. Shukitt-Hale, W. Kalt, D. K. Ingram, J. A. Joseph, and C. A. Wolkow, "Blueberry polyphenols increase lifespan and thermotolerance in Caenorhabditis elegans," *Aging Cell*, vol. 5, no. 1, pp. 59–68, 2006.

[7] L. Valentini, A. Pinto, I. Bourdel-Marchasson et al., "Impact of personalized diet and probiotic supplementation on inflammation, nutritional parameters and intestinal microbiota - The "RISTOMED project": Randomized controlled trial in healthy older people," *Clinical Nutrition*, vol. 34, no. 4, pp. 593–602, 2015.

[8] E. Y. Platonova, M. V. Shaposhnikov, H. Y. Lee, J. H. Lee, K. J. Min, and A. Moskalev, "Black chokeberry (*Aronia melanocarpa*) extracts in terms of geroprotector criteria," *Trends in Food Science & Technology*, vol. 114, pp. 570–584, 2021.

[9] K. S. Bhullar and B. P. Hubbard, "Lifespan and healthspan extension by resveratrol," *Biochimica et Biophysica Acta*, vol. 1852, no. 6, pp. 1209–1218, 2015.

[10] S. Timmers, J. Auwerx, and P. Schrauwen, "The journey of resveratrol from yeast to human," *Aging*, vol. 4, no. 3, pp. 146–158, 2012.

[11] J. Chang, A. Rimando, M. Pallas et al., "Low-dose pterostilbene, but not resveratrol, is a potent neuromodulator in aging and Alzheimer's disease," *Neurobiology of Aging*, vol. 33, no. 9, pp. 2062–2071, 2012.

[12] H. P. Chang, C. C. Lu, J. H. Chiang et al., "Pterostilbene modulates the suppression of multidrug resistance protein 1 and triggers autophagic and apoptotic mechanisms in cisplatin-resistant human oral cancer CAR cells via AKT signaling," *International Journal of Oncology*, vol. 52, no. 5, pp. 1504–1514, 2018.

[13] P. Rodríguez-Bonilla, L. Méndez-Cazorla, J. M. López-Nicolás, and F. García-Carmona, "Kinetic mechanism and product characterization of the enzymatic peroxidation of pterostilbene as model of the detoxification process of stilbene-type phytoalexins," *Phytochemistry*, vol. 72, no. 1, pp. 100–108, 2011.

[14] M. Briguglio, S. Hrelia, M. Malaguti et al., "Food Bioactive Compounds and Their Interference in Drug Pharmacokinetic/Pharmacodynamic Profiles," *Pharmaceutics*, vol. 10, no. 4, p. 277, 2018.

[15] Y. S. Chiou, M. L. Tsai, K. Nagabhushanam et al., "Pterostilbene is more potent than resveratrol in preventing azoxymethane (AOM)-induced colon tumorigenesis via activation of the NF-E2-related factor 2 (Nrf2)-mediated antioxidant signaling Pathway," *Journal of Agricultural and Food Chemistry*, vol. 59, no. 6, pp. 2725–2733, 2011.

[16] W. Nutakul, H. S. Sobers, P. Qiu et al., "Inhibitory effects of resveratrol and pterostilbene on human colon cancer cells: a side-by-side Comparison," *Journal of Agricultural and Food Chemistry*, vol. 59, no. 20, pp. 10964–10970, 2011.

[17] K. Hagiwara, N. Kosaka, Y. Yoshioka, R. U. Takahashi, F. Takeshita, and T. Ochiya, "Stilbene derivatives promote Ago2-dependent tumour-suppressive microRNA activity," *Scientific Reports*, vol. 2, no. 1, p. 314, 2012.

[18] I. M. Kapetanovic, M. Muzzio, Z. Huang, T. N. Thompson, and D. L. McCormick, "Pharmacokinetics, oral bioavailability, and metabolic profile of resveratrol and its dimethylether analog, pterostilbene, in rats," *Cancer Chemotherapy and Pharmacology*, vol. 68, no. 3, pp. 593–601, 2011.

[19] H. S. Lin, B. D. Yue, and P. C. Ho, "Determination of pterostilbene in rat plasma by a simple HPLC-UV method and its application in pre-clinical pharmacokinetic study," *Biomedical Chromatography*, vol. 23, no. 12, pp. 1308–1315, 2009.

[20] D. M. Riche, M. E. CL, K. D. Riche et al., "Analysis of safety from a human clinical trial with pterostilbene," *Journal of Toxicology*, vol. 2013, Article ID 463595, 5 pages, 2013.

[21] P. Wang and S. Sang, "Metabolism and pharmacokinetics of resveratrol and pterostilbene," *BioFactors*, vol. 44, no. 1, pp. 16–25, 2018.

[22] K. T. Howitz, K. J. Bitterman, H. Y. Cohen et al., "Small molecule activators of sirtuins extend *Saccharomyces cerevisiae* lifespan," *Nature*, vol. 425, no. 6954, pp. 191–196, 2003.

[23] B. Agarwal and J. A. Baur, "Resveratrol and life extension," *Annals of the New York Academy of Sciences*, vol. 1215, no. 1, pp. 138–143, 2011.

[24] C. Burnett, S. Valentini, F. Cabreiro et al., "Absence of effects of Sir2 overexpression on lifespan in *C. elegans* and *Drosophila*," *Nature*, vol. 477, no. 7365, pp. 482–485, 2011.

[25] T. M. Bass, D. Weinkove, K. Houthoofd, D. Gems, and L. Partridge, "Effects of resveratrol on lifespan in *Drosophila melanogaster* and *Caenorhabditis elegans*," *Mechanisms of Ageing and Development*, vol. 128, no. 10, pp. 546–552, 2007.

[26] Y. He and H. Jasper, "Studying aging in *Drosophila*," *Methods*, vol. 68, no. 1, pp. 129–133, 2014.

[27] A. Chalkiadaki and L. Guarente, "The multifaceted functions of sirtuins in cancer," *Nature Reviews. Cancer*, vol. 15, no. 10, pp. 608–624, 2015.

[28] K. G. Ormerod, O. K. LePine, P. S. Abbineni et al., "Drosophila development, physiology, behavior, and lifespan are influenced by altered dietary composition," *Fly*, vol. 11, no. 3, pp. 153–170, 2017.

[29] N. J. Linford, C. Bilgir, J. Ro, and S. D. Pletcher, "Measurement of lifespan in Drosophila melanogaster," *Journal of Visualized Experiments*, vol. 71, 2013.

[30] S. Piegholdt, G. Rimbach, and A. E. Wagner, "The phytoestrogen prunetin affects body composition and improves fitness and lifespan in maleDrosophila melanogaster," *The FASEB Journal*, vol. 30, no. 2, pp. 948–958, 2016.

[31] S. Diegelmann, A. Jansen, S. Jois et al., "The CApillary FEeder Assay Measures Food Intake in *Drosophila melanogaster*," *Journal of Visualized Experiments*, vol. 10, no. 121, 2017.

[32] K. Fiocca, M. Barrett, E. A. Waddell et al., "Mannitol ingestion causes concentration-dependent, sex-biased mortality in adults of the fruit fly (Drosophila melanogaster)," *PLoS One*, vol. 14, no. 5, article e0213760, 2019.

[33] S. Niveditha, S. Deepashree, S. R. Ramesh, and T. Shivanandappa, "Sex differences in oxidative stress resistance in relation to longevity in Drosophila melanogaster,"

Journal of Comparative Physiology. B, vol. 187, no. 7, pp. 899–909, 2017.

[34] R. Re, N. Pellegrini, A. Proteggente, A. Pannala, M. Yang, and C. Rice-Evans, "Antioxidant activity applying an improved ABTS radical cation decolorization assay," *Free Radical Biology & Medicine*, vol. 26, no. 9-10, pp. 1231–1237, 1999.

[35] M. C. Barbalace, L. Zallocco, D. Beghelli et al., "Antioxidant and Neuroprotective Activity of Extra Virgin Olive Oil Extracts Obtained from Quercetano Cultivar Trees Grown in Different Areas of the Tuscany Region (Italy),," *Antioxidants*, vol. 10, no. 3, p. 421, 2021.

[36] L. Giusti, C. Angeloni, M. Barbalace et al., "A Proteomic Approach to Uncover Neuroprotective Mechanisms of Oleocanthal against Oxidative Stress," *International Journal Of Molecular Sciences*, vol. 19, no. 8, p. 2329, 2018.

[37] V. Marzano, S. Pane, G. Foglietta et al., "Mass Spectrometry Based-Proteomic Analysis of Anisakis spp.: A Preliminary Study towards a New Diagnostic Tool," *Genes*, vol. 11, no. 6, p. 693, 2020.

[38] J. S. Yang, H. J. Nam, M. Seo et al., "OASIS: online application for the survival analysis of lifespan assays performed in aging Research," *PLoS One*, vol. 6, no. 8, article e23525, 2011.

[39] M. C. Ryan, M. Stucky, C. Wakefield et al., "Interactive clustered heat map builder: an easy web-based tool for creating sophisticated clustered heat maps," *F1000Research*, vol. 8, 2019.

[40] A. G. Vorobyeva, R. Lee, S. Miller et al., "Cyclopamine Modulates γ-Secretase-mediated Cleavage of Amyloid Precursor Protein by Altering Its Subcellular Trafficking and Lysosomal Degradation∗," *The Journal of Biological Chemistry*, vol. 289, no. 48, pp. 33258–33274, 2014.

[41] X. Wang, H. Perumalsamy, H. W. Kwon, Y. E. Na, and Y. J. Ahn, "Effects and possible mechanisms of action of acacetin on the behavior and eye morphology of *Drosophila* models of Alzheimer 's disease," *Scientific Reports*, vol. 5, no. 1, article 16127, 2015.

[42] X. Wang, J. R. Kim, S. B. Lee et al., "Effects of curcuminoids identified in rhizomes of Curcuma longa on BACE-1 inhibitory and behavioral activity and lifespan of Alzheimer's disease drosophila models," *BMC Complementary and Alternative Medicine*, vol. 14, no. 1, p. 88, 2014.

[43] S. Frankel, T. Ziafazeli, and B. Rogina, "dSir2 and longevity in *Drosophila*," *Experimental Gerontology*, vol. 46, no. 5, pp. 391–396, 2011.

[44] M. Horvath, Z. Mihajlovic, V. Slaninova, R. Perez-Gomez, Y. Moshkin, and A. Krejci, "The silent information regulator 1 (Sirt1) is a positive regulator of the Notch pathway in Drosophila," *Biochemical Journal*, vol. 473, no. 22, pp. 4129–4143, 2016.

[45] N. Alic, M. E. Giannakou, I. Papatheodorou et al., "Interplay of dFOXO and two ETS-family transcription factors determines lifespan in Drosophila melanogaster," *PLoS Genetics*, vol. 10, no. 9, article e1004619, 2014.

[46] S. Deepashree, S. Niveditha, T. Shivanandappa, and S. R. Ramesh, "Oxidative stress resistance as a factor in aging: evidence from an extended longevity phenotype of Drosophila melanogaster," *Biogerontology*, vol. 20, no. 4, pp. 497–513, 2019.

[47] M. Comporti, C. Signorini, S. Leoncini et al., "Ethanol-induced oxidative stress: basic knowledge," *Genes & Nutrition*, vol. 5, no. 2, pp. 101–109, 2010.

[48] M. L. Doran, J. M. Knee, N. Wang et al., "Metabolomic analysis of oxidative stress: *Superoxide dismutase* mutation and paraquat induced stress in *Drosophila melanogaster*," *Free Radical Biology and Medicine*, vol. 113, pp. 323–334, 2017.

[49] R. Hosamani and Muralidhara, "Acute exposure of Drosophila melanogaster to paraquat causes oxidative stress and mitochondrial dysfunction," *Archives of Insect Biochemistry and Physiology*, vol. 83, no. 1, pp. 25–40, 2013.

[50] S. Brown, N. Hu, and J. C. Hombría, "Identification of the first invertebrate interleukin JAK/STAT receptor, the *Drosophila* gene *domeless*," *Current Biology*, vol. 11, no. 21, pp. 1700–1705, 2001.

[51] J. A. Sanchez, D. Mesquita, M. C. Ingaramo, F. Ariel, M. Milán, and A. Dekanty, "Eiger/TNFα-mediated Dilp8 and ROS production coordinate intra-organ growth in Drosophila," *PLoS Genetics*, vol. 15, no. 8, article e1008133, 2019.

[52] Y. R. Li, S. Li, and C. C. Lin, "Effect of resveratrol and pterostilbene on aging and longevity," *BioFactors*, vol. 44, no. 1, pp. 69–82, 2018.

[53] C. Peng, Y. Zuo, K. M. Kwan et al., "Blueberry extract prolongs lifespan of *Drosophila melanogaster*," *Experimental Gerontology*, vol. 47, no. 2, pp. 170–178, 2012.

[54] S. I. Rattan, "Hormesis in aging," *Ageing Research Reviews*, vol. 7, no. 1, pp. 63–78, 2008.

[55] S. H. Lee, H. S. An, Y. W. Jung et al., "Korean mistletoe (Viscum album coloratum) extract extends the lifespan of nematodes and fruit flies," *Biogerontology*, vol. 15, no. 2, pp. 153–164, 2014.

[56] S. Staats, A. Wagner, B. Kowalewski et al., "Dietary Resveratrol Does Not Affect Life Span, Body Composition, Stress Response, and Longevity-Related Gene Expression in Drosophila melanogaster," *International Journal of Molecular Sciences*, vol. 19, no. 1, p. 223, 2018.

[57] A. O. Abolaji, A. O. Adedara, M. A. Adie, M. Vicente-Crespo, and E. O. Farombi, "Resveratrol prolongs lifespan and improves 1-methyl-4-phenyl-1,2,3,6-tetrahydropyridine-induced oxidative damage and behavioural deficits in *Drosophila melanogaster*," *Biochemical and Biophysical Research Communications*, vol. 503, no. 2, pp. 1042–1048, 2018.

[58] T. Finkel, C. X. Deng, and R. Mostoslavsky, "Recent progress in the biology and physiology of sirtuins," *Nature*, vol. 460, no. 7255, pp. 587–591, 2009.

[59] J. Li, L. Feng, Y. Xing et al., "Radioprotective and antioxidant effect of resveratrol in hippocampus by activating Sirt1," *International Journal of Molecular Sciences*, vol. 15, no. 4, pp. 5928–5939, 2014.

[60] J. Li, C. X. Zhang, Y. M. Liu, K. L. Chen, and G. Chen, "A comparative study of anti-aging properties and mechanism: resveratrol and caloric restriction," *Oncotarget*, vol. 8, no. 39, pp. 65717–65729, 2017.

[61] A. Presente, A. Andres, and J. S. Nye, "Requirement of notch in adulthood for neurological function and longevity," *Neuroreport*, vol. 12, no. 15, pp. 3321–3325, 2001.

[62] D. Selkoe and R. Kopan, "NOTCH ANDPRESENILIN: regulated intramembrane proteolysis links development and Degeneration," *Annual Review of Neuroscience*, vol. 26, no. 1, pp. 565–597, 2003.

[63] C. A. Saura, S. Y. Choi, V. Beglopoulos et al., "Loss of Presenilin Function Causes Impairments of Memory and Synaptic Plasticity Followed by Age-Dependent Neurodegeneration," *Neuron*, vol. 42, no. 1, pp. 23–36, 2004.

[64] R. M. Costa, T. Honjo, and A. J. Silva, "Learning and Memory Deficits in Notch Mutant Mice," *Current Biology*, vol. 13, no. 15, pp. 1348–1354, 2003.

[65] C. J. Kenyon, "The genetics of ageing," *Nature*, vol. 464, no. 7288, pp. 504–512, 2010.

[66] S. Dodig, I. Čepelak, and I. Pavić, "Hallmarks of senescence and aging," *Biochemia Medica*, vol. 29, no. 3, article 030501, 2019.

[67] K. B. Beckman and B. N. Ames, "The free radical theory of aging Matures," *Physiological Reviews*, vol. 78, no. 2, pp. 547–581, 1998.

[68] T. Logan-Garbisch, A. Bortolazzo, P. Luu et al., "Developmental ethanol exposure leads to dysregulation of lipid metabolism and oxidative stress in drosophila," *G3: Genes, Genomes, Genetics*, vol. 5, no. 1, pp. 49–59, 2014.

[69] F. W. Wolf, A. R. Rodan, L. T. Tsai, and U. Heberlein, "High-Resolution analysis of ethanol-induced locomotor stimulation inDrosophila," *The Journal of Neuroscience*, vol. 22, no. 24, pp. 11035–11044, 2002.

[70] V. Calabrese, D. Boyd-Kimball, G. Scapagnini, and D. A. Butterfield, "Nitric oxide and cellular stress response in brain aging and neurodegenerative disorders: the role of vitagenes," *In Vivo*, vol. 18, no. 3, pp. 245–267, 2004.

[71] T. Krůček, M. Korandová, M. Šerý, R. Frydrychová, and K. Szakosová, "EFFECT of low doses of herbicide paraquat on antioxidant defense INDrosophila," *Archives of Insect Biochemistry and Physiology*, vol. 88, no. 4, pp. 235–248, 2015.

[72] H. Deng, H. Li, Z. Y. Ho et al., "Pterostilbene's protective effects against photodamage caused by UVA/UVB irradiation," *Pharmazie*, vol. 73, no. 11, pp. 651–658, 2018.

[73] X. Fan, L. Wang, J. Huang, H. Lv, X. Deng, and X. Ci, "Pterostilbene reduces acetaminophen-induced liver injury by activating the Nrf2 Antioxidative defense system via the AMPK/Akt/GSK3β Pathway," *Cellular Physiology and Biochemistry*, vol. 49, no. 5, pp. 1943–1958, 2018.

[74] R. Kosuru, V. Kandula, U. Rai, S. Prakash, Z. Xia, and S. Singh, "Pterostilbene Decreases Cardiac Oxidative Stress and Inflammation via Activation of AMPK/Nrf2/HO-1 Pathway in Fructose-Fed Diabetic Rats," *Cardiovascular Drugs and Therapy*, vol. 32, no. 2, pp. 147–163, 2018.

[75] Z. W. Chen, H. F. Miu, H. P. Wang et al., "Pterostilbene protects against uraemia serum-induced endothelial cell damage via activation of Keap1/Nrf2/HO-1 signaling," *International Urology and Nephrology*, vol. 50, no. 3, pp. 559–570, 2018.

[76] Y. Yang, C. Fan, B. Wang et al., "Pterostilbene attenuates high glucose-induced oxidative injury in hippocampal neuronal cells by activating nuclear factor erythroid 2-related factor 2," *BBA: Molecular Basis of Disease*, vol. 1863, no. 4, pp. 827–837, 2017.

[77] R. Lakshmanan, J. Campbell, G. Ukani et al., "Evaluation of dermal tissue regeneration using resveratrol loaded fibrous matrix in a preclinical mouse model of full-thickness ischemic wound," *International Journal of Pharmaceutics*, vol. 558, pp. 177–186, 2019.

[78] D. Xu, Y. Li, B. Zhang et al., "Resveratrol alleviate hypoxic pulmonary hypertension via anti-inflammation and antioxidant pathways in rats," *International Journal of Medical Sciences*, vol. 13, no. 12, pp. 942–954, 2016.

[79] V. Calabrese, C. Cornelius, C. Mancuso et al., "Vitagenes, dietary antioxidants and neuroprotection in neurodegenerative diseases," *Frontiers in Bioscience*, vol. 14, no. 3, pp. 376–397, 2009.

[80] C. Mancuso, G. Scapagini, D. Currò et al., "Mitochondrial dysfunction, free radical generation and cellular stress response in neurodegenerative disorders," *Frontiers in Bioscience*, vol. 12, no. 1, pp. 1107–1123, 2007.

[81] V. Calabrese, E. Guagliano, M. Sapienza et al., "Redox regulation of cellular stress response in aging and neurodegenerative disorders: role of vitagenes," *Neurochemical Research*, vol. 32, no. 4-5, pp. 757–773, 2007.

[82] V. Calabrese, C. Cornelius, C. Mancuso et al., "Cellular stress response: a novel target for chemoprevention and nutritional neuroprotection in aging, neurodegenerative disorders and Longevity," *Neurochemical Research*, vol. 33, no. 12, pp. 2444–2471, 2008.

[83] Y. Hou, G. Xie, F. Miao et al., "Pterostilbene attenuates lipopolysaccharide-induced learning and memory impairment possibly via inhibiting microglia activation and protecting neuronal injury in mice," *Progress in Neuro-Psychopharmacology & Biological Psychiatry*, vol. 54, pp. 92–102, 2014.

[84] C. L. Hsu, Y. J. Lin, C. T. Ho, and G. C. Yen, "The inhibitory effect of pterostilbene on inflammatory responses during the interaction of 3T3-L1 adipocytes and RAW 264.7 macrophages," *Journal of Agricultural and Food Chemistry*, vol. 61, no. 3, pp. 602–610, 2013.

[85] M. Forgac, "Vacuolar ATPases: rotary proton pumps in physiology and pathophysiology," *Nature Reviews. Molecular Cell Biology*, vol. 8, no. 11, pp. 917–929, 2007.

[86] K. Cotter, L. Stransky, C. McGuire, and M. Forgac, "Recent Insights into the Structure, Regulation, and Function of the V-ATPases," *Trends in Biochemical Sciences*, vol. 40, no. 10, pp. 611–622, 2015.

[87] M. E. Maxson and S. Grinstein, "The vacuolar-type H^+-ATPase at a glance - more than a proton pump," *Journal of Cell Science*, vol. 127, Part 23, pp. 4987–4993, 2014.

[88] R. Farkaš, D. Beňová-Liszeková, L. Mentelová et al., "Vacuole dynamics in the salivary glands ofDrosophila melanogasterduring prepupal development," *Growth & Differentiation*, vol. 57, no. 1, pp. 74–96, 2015.

[89] J. Chen, Y. Ou, Y. Li, S. Hu, L. W. Shao, and Y. Liu, "Metformin extends *C. elegans* lifespan through lysosomal pathway," *eLife*, vol. 6, no. 10, p. 13, 2017.

[90] A. K. Allan, J. Du, S. A. Davies, and J. A. Dow, "Genome-wide survey of V-ATPase genes in Drosophila reveals a conserved renal phenotype for lethal alleles," *Physiol Genomics*, vol. 22, no. 2, pp. 128–138, 2005.

[91] S. E. Schriner, K. Lee, S. Truong et al., "Extension of drosophila lifespan by Rhodiola rosea through a mechanism independent from dietary Restriction," *PLoS One*, vol. 8, no. 5, article e63886, 2013.

[92] D. K. Ingram and G. S. Roth, "Glycolytic inhibition: an effective strategy for developing calorie restriction mimetics," *Geroscience*, vol. 43, no. 3, pp. 1159–1169, 2021.

[93] L. Wang, G. Lam, and C. S. Thummel, "Med24andMdh2are required forDrosophilalarval salivary gland cell death," *Developmental Dynamics*, vol. 239, no. 3, pp. 954–964, 2010.

[94] T. P. Le, L. T. Vuong, A. R. Kim, Y. C. Hsu, and K. W. Choi, "14-3-3 proteins regulate Tctp-Rheb interaction for organ growth in *Drosophila*," *Nature Communications*, vol. 7, no. 1, article 11501, 2016.

[95] Y. C. Hsu, J. J. Chern, Y. Cai, M. Liu, and K. W. Choi, "*Drosophila* TCTP is essential for growth and proliferation through regulation of dRheb GTPase," *Nature*, vol. 445, no. 7129, pp. 785–788, 2007.

[96] D. Kobayashi, M. Hirayama, Y. Komohara et al., "Translationally Controlled Tumor Protein Is a Novel Biological Target for Neurofibromatosis Type 1-associated Tumors," *Journal of Biological Chemistry*, vol. 289, no. 38, pp. 26314–26326, 2014.

[97] X. Dong, B. Yang, Y. Li, C. Zhong, and J. Ding, "Molecular Basis of the Acceleration of the GDP-GTP Exchange of Human Ras Homolog Enriched in Brain by Human Translationally Controlled Tumor Protein," *Journal of Biological Chemistry*, vol. 284, no. 35, pp. 23754–23764, 2009.

[98] M. J. Koziol and J. B. Gurdon, "TCTP in development and cancer," *Biochemistry Research International*, vol. 2012, Article ID 105203, 9 pages, 2012.

[99] M. Tuynder, L. Susini, S. Prieur et al., "Biological models and genes of tumor reversion: cellular reprogramming through tpt1/TCTP and SIAH-1," *Proceedings of the National Academy of Sciences of the United States of America*, vol. 99, no. 23, pp. 14976–14981, 2002.

[100] R. Amson, S. Pece, J. C. Marine, P. P. Di Fiore, and A. Telerman, "TPT1/TCTP-regulated pathways in phenotypic reprogramming," *Trends in Cell Biology*, vol. 23, no. 1, pp. 37–46, 2013.

Hindawi
Oxidative Medicine and Cellular Longevity
Volume 2021, Article ID 7064179, 18 pages
https://doi.org/10.1155/2021/7064179

Research Article

Theaflavin 3, 3′-Digallate Delays Ovarian Aging by Improving Oocyte Quality and Regulating Granulosa Cell Function

Jiahuan He,[1,2] **Guidong Yao**,[1,2] **Qina He**,[1,2] **Tongwei Zhang**,[1,2] **Huiying Fan**,[1,2] **Yucheng Bai**,[1,2] **Junya Zhang**,[1,2] **Guang Yang**,[1,2] **Ziwen Xu**,[1,2] **Jingyi Hu**,[1,2] **and Yingpu Sun**[1,2]

[1]*Center for Reproductive Medicine, The First Affiliated Hospital of Zhengzhou University, Zhengzhou, China*
[2]*Henan Key Laboratory of Reproduction and Genetics, The First Affiliated Hospital of Zhengzhou University, Zhengzhou, China*

Correspondence should be addressed to Guidong Yao; ygdzzu@163.com and Yingpu Sun; syp2008@vip.sina.com

Jiahuan He, Guidong Yao, Qina He, and Tongwei Zhang contributed equally to this work.

Received 6 September 2021; Accepted 2 November 2021; Published 8 December 2021

Academic Editor: Cecile Jacovetti

Ovarian aging refers to the gradual decline of ovarian function with increasing physiological age, manifested as decreased ovarian reserve, elevated aging-related markers, and reduced oocyte quality. With a declining female fertility and a growing aging population, it is urgent to delay ovarian aging to maintain fertility and improve the life quality of women. Theaflavin 3, 3′-digallate (TF3) is a naturally bioactive polyphenol compound extracted from black tea, and its antioxidant properties play an important role in maintaining human health and delaying aging; however, the effects of TF3 on female reproduction and ovarian function are not yet clear. Here, we show that TF3 can preserve primordial follicle pool, partially restore the estrous cycle, and increase the offspring number of aged mice. Meanwhile, TF3 gavage increased the number of oocytes retrieved, decreased the level of reactive oxygen species, increased the level of glutathione, and decreased the abnormal rate of oocyte spindle after ovulation induction. Moreover, TF3 inhibited human granulosa cell apoptosis and improved their antioxidative stress ability. High-throughput sequencing and small-molecule-targeted pharmacological prediction show that TF3 affects multiple pathways and gene expression levels, mainly involved in reproductive and developmental processes. It may also affect cellular function by targeting mTOR to regulate the autophagic pathway, thereby delaying the process of ovarian aging. This study shows that TF3 can be used as a potential dietary supplement to protect ovary function from aging and thereby improving the life quality of advanced-age women.

1. Introduction

Ovarian aging is defined as a gradual decline in ovarian function with age. Female fertility generally begins to decline after the age of 30 and declines more significantly after 35. The general postponement of women's childbearing age nowadays makes reproductive aging a common fertility concern [1]. The clinical manifestations of fertility decline include decreased ovarian reserve, female endocrine hormone disorders, and irregular menstrual cycles [2], which are mainly related to a series of ovarian function downregulation indicators such as increased secretion of aging inflammatory substances in the ovarian microenvironment, abnormal granulosa cell number and function, and decreased oocyte quality [3–5].

Accumulation of reactive oxygen species (ROS) is closely associated with organ aging [6]. Studies have reported that oxidative stress damage caused by excessive accumulation of ROS in the ovary leads to impaired granulosa cell function and decreased oocyte quality, which causes reduced follicle number and quality as well as endocrine abnormalities, ultimately leading to ovarian aging [7]. In women undergoing *in vitro* fertilization embryo transfer (IVF-ET), the ROS content in both oocytes and granulosa cells is significantly

higher in older patients than that in younger patients, with reduced antioxidant levels [8]. The high levels of ROS in follicular fluid may be associated with poor embryo quality [9]. This suggests that excessive ROS in the ovaries of older women is an important factor leading to decreased ovarian function and adverse pregnancy outcomes. Reducing ROS levels in the ovary could play a pivotal role in improving female ovarian function and prolonging female fertility.

Tea polyphenols are important natural antioxidant compounds derived from food. Theaflavin extracted from black tea fermentation is an antioxidant class with natural bioactivities, mainly including theaflavin (TF1), theaflavin-3-gallate (TF2A), theaflavin-3′-gallate (TF2B), and theaflavin 3, 3′-digallate (TF3) [10]. Among these four monomers, the proportion of TF3 components is highest and has the greatest antioxidant effect [11]. Previous studies on tea polyphenols have focused on the green tea extract epigallocatechin gallate (EGCG), which is a powerful antioxidant. EGCG supplementation can inhibit the transition from primordial follicle to growing follicle, which is essential for prolonging the follicular growth phase, reducing oocyte apoptosis, and protecting female fertility [12]. However, in recent years, it was discovered that tea polyphenol TF3 in fermented black tea even possesses stronger antioxidant activity than EGCG [13]. TF3 shows antioxidant function by modulating an organism's biological enzyme activity system to eliminate free radicals [11] and preventing hydroxyl radical-induced DNA damage by scavenging ROS [14]. In a mouse model of nonalcoholic fatty liver disease and primary hepatocytes, the theaflavin family attenuated inflammatory responses and reduced hepatocyte apoptosis through antioxidant pathways [15].

In a double-blind, randomized controlled study in humans, oral supplementation with TF3 significantly reduced inflammatory factors and oxidative stress injury due to high-intensity exercise [16]. Others have suggested that TF3 is a noncompetitive adenosine triphosphate (ATP) synthase inhibitor that reduces energy metabolism by directly binding to ATPase without inducing or even decreasing superoxide production [17]. Current research on TF3 in the female reproductive system has focused on a possible antitumor ability, and multiple studies have indicated that TF3 can protect female fertility by selectively inhibiting ovarian cancer cell proliferation [18, 19]. Nevertheless, the functional role of TF3 in the regulation of ovarian aging remains unclear.

In this study, we first investigated the role of TF3 supplementation in improving fertility and ovarian function in aged mice and further studied the effects of TF3 on oocyte quality, embryonic developmental potential, and granulosa cell function. In addition, the potential molecular mechanism of TF3 in regulating granulosa cell function was studied by sequencing analysis and small molecule compound-protein simulation docking. These results demonstrate that TF3 is a therapeutically promising polyphenol compound and plays an important role in protecting ovarian function from aging.

2. Materials and Methods

2.1. Ethical Approval. This study was approved by the Scientific Research and Clinical Trial Ethics Committee of the First Affiliated Hospital of Zhengzhou University.

2.2. Animals and Experiment Design. All CD-1 mice used in this study were purchased from Vital River (Vital River, Beijing, China) and housed in the Henan Animal Experimental Center with a 12 h dark/light cycle and at a room temperature of 22–25°C. Nine-month-old, aged female mice were randomly divided into two groups: old TF3 gavage experimental (O-TF3) and old control (O-Ctrl). The O-TF3 group mice were fed with TF3 (Biopurify, Chengdu, China) at 30 mg/kg every other day, and the O-Ctrl group mice were fed with an equal volume of normal saline every other day; both groups were, respectively, treated for 90 days.

Eight-week-old adult CD-1 female mice served as young controls (Y-Ctrl). For mating tests, 8-week-old adult male mice were cohabited with three groups at a ratio of 1 : 2 and housed separately after 1 week. The number of offspring was statistically analyzed.

2.3. Estrous Cycle Monitoring. At the end of the gavage period, the estrous cycle of mice was examined using the smear method. The vaginal orifice was exposed, and vaginal secretions were collected with a small cotton swab and smeared on a glass slide. The samples were fixed with 95% ethanol for 5 min, dried, stained with hematoxylin for 15 min, and then rinsed with water for 5 min, dehydrated with 95% ethanol for 3 min, and then repeatedly rinsed and stained. The cell morphology was observed under a light microscope. Estrous cycle monitoring was based on a previous study [20]. In the diestrus, there were a few shrunken, nucleated epithelial cells and occasional keratinocytes. During proestrus, epithelial cells were significantly reduced, with more basophilic cells or cells that lost the ability to be stained. In estrus, almost all the enucleated keratinocytes were stained red without white blood cells; during metestrus, nucleated epithelial cells and leukocytosis were present.

2.4. In Vitro Fertilization and Immunofluorescence Staining of Oocytes. At the end of treatment, mice were intraperitoneally injected with 10 IU pregnant mare serum gonadotropin (PMSG; Solarbio, Beijing, China); after 48 h, the mice were intraperitoneally injected with 10 IU human chorionic gonadotropin (hCG; Livzon, Zhuhai, China). Fourteen hours later, the mice were sacrificed by cervical dislocation, and cumulus oocyte complexes (COCs) were obtained at the tubal enlargement and washed in handling medium G-MOPS™ Plus (Vitrolife, Goteborg, Sweden) preheated at 37°C and then transferred to G-IVF™ Plus medium (Vitrolife) for culture prior to insemination. Adult male sperm were obtained 1 h in advance for capacitation in G-IVF™ Plus droplets, and the capacitated sperm were added to droplets containing COCs for insemination. Fertilized oocytes were removed 4 h after insemination and continued to be cultured and observed in G-1™ Plus (Vitrolife). The culture medium was changed to G-2™ Plus (Vitrolife) droplets on the third day after insemination to continue culturing

until blastocyst development. The following formulae were used:

$$\text{Fertilization rate (\%)} = \frac{\text{number of fertilized zygotes}}{\text{recovered oocytes}} \times 100\%,$$

$$\text{Blastocyst formation rate (\%)} = \frac{\text{number of blastocysts}}{\text{cleaved embryos}} \times 100\%. \quad (1)$$

COCs used for immunofluorescence staining were digested with hyaluronidase (Vitrolife) to remove granulosa cells around oocytes, and subsequent experiments were performed after the granulosa cells were decontaminated. ROS (Beyotime, Shanghai, China), JC1 (Beyotime), and Glutathione (GSH) Detection Reagent (Invitrogen, Carlsbad, CA, USA) kits were used for staining according to the manufacturer's protocols. Oocytes were stained for 30 min at 37°C, eluted three times using phosphate-buffered saline (PBS) with 0.1% Triton X-100 (PBST), and then imaged using a confocal laser scanning microscope (Zeiss LSM 700, Oberkochen, Germany).

For spindle staining experiments, oocytes after granulosa cell removal were fixed in 4% paraformaldehyde (PFA) for 1 h at room temperature, after which they were transferred to 0.5% Triton X-100 permeabilization solution formulated using 4% PFA for 30 min at room temperature. At the end of permeabilization, three washes were performed using PBST, blocked using 5% bovine serum albumin (BSA) for 1 h at room temperature, and then incubated with α-tubulin-FITC (1 : 200, Thermo Fisher Scientific, Waltham, MA, USA) and diluted in 5% BSA overnight at 4°C. After incubation, oocytes were transferred to an antifluorescent quencher with 4′,6-diamidino-2-phenylindole (DAPI) dye (Cell Signaling Technology, Danvers, MA, USA) for mounting and photography after three washes in PBST. Blastocysts were stained using DAPI in blastocyst cell counting experiments, imaged under a confocal laser scanning microscope, and counted according to the number of nuclei.

2.5. Serum Hormone Assay. Mouse serum follicle-stimulating hormone (FSH), estradiol (E_2), and progesterone (P4) levels were measured using a chemiluminescence immunoassay kit (Roche Diagnostics, Basel, Switzerland) on a Roche Diagnostics Cobas 6000 analyzer.

2.6. Ovarian Follicle Grading and Counting. After the mice were sacrificed by cervical dislocation, the ovaries were removed and transferred into 4% PFA, embedded in paraffin, and then sectioned serially at a thickness of 5 μm; every fifth slide was stained with hematoxylin and eosin (HE). Follicular grading and counting methods were based on a previous publication [21].

2.7. Immunohistochemical Staining. Mouse ovaries were fixed in 4% PFA, then embedded in paraffin, and sectioned to 5 μm thick section obtained. The sections with the largest cross sections were used for staining. Slides were baked at 65°C for 1 h, deparaffinized in xylene, soaked in distilled water after graded ethanol addition into the water along with antigen retrieval, and incubated in 3% hydrogen peroxide solution for 10 min at room temperature. After that, slides were washed three times with PBS and incubated with 5% BSA for 10 min. After pouring off the liquid, overnight incubation was performed at 4°C with antibodies against mammalian target of rapamycin (mTOR) (1 : 1000, Abcam, Cambridge, UK) or P16 (1 : 1000, Abcam). For negative controls, serum was used instead of primary antibody. After overnight incubation, the primary antibody was discarded, the slides were washed three times with PBS, and horseradish peroxidase secondary antibody (Goat Anti-Rabbit IgG H&L, 1 : 5000, Abcam) was added for 1 h at 37°C. After incubation, the slides were washed in PBS three times, and DAB chromogen was added dropwise. After color development was complete, the slides were washed thrice in PBS and counterstained for 20 s in hematoxylin. The slide was then rinsed with tap water for 3 min, mounted using neutral gum, and imaged under a light microscope.

2.8. Masson's Trichrome Staining. Paraffin-embedded tissue was processed as described above and stained using the Masson Stain Kit (Servicebio, Wuhan, China). Mouse ovary sections were dewaxed in xylene in turn and soaked in distilled water with gradient ethanol addition; then, the sections were washed using distilled water and soaked in Masson A dye solution overnight. After overnight culture, the sections were rinsed with tap water, and then, they were immersed in the dye solution mixed with Masson B and Masson C in equal proportion for 1 min. After that, the sections were rinsed with distilled water for 1 min, soaked in 1% hydrochloric acid alcohol for 1 min, then rinsed with tap water, and then immersed in Masson D dye solution for 6 min followed by a final rinse in tap water. After that, the sections were immersed in Masson E for 1 min, placed in Masson F staining solution for 30 s after turning slightly dry, rinsed with 1% glacial acetic acid for 1 min, dehydrated twice with absolute ethanol, and soaked in fresh absolute ethanol for 5 min. Finally, they were immersed in xylene for transparentizing for 5 min, mounted in neutral gum, and imaged.

2.9. Cell Culture. Human primary granulosa cells (pGCs) were collected from the follicular fluid of patients undergoing IVF-assisted pregnancy at reproductive center of the First Affiliated Hospital of Zhengzhou University, and the specific methods were based on previous publications [22].

2.10. RNA Extraction and Real-Time Polymerase Chain Reaction (PCR). After treatment, the cells were first washed once with precooled PBS, and the cells were lysed by adding the corresponding volume of TRIzol (Invitrogen); 200 μl chloroform was added per 1 ml of TRIzol, and the tube was then vigorously shaken for 15 s, placed at room temperature for 10 min, and then centrifuged the sample at 12,000 rpm for 15 min at low temperature. The upper aqueous phase was harvested, followed by addition of 200 μl

isopropanol, vigorous shaking for 15 s, and allowing to stand at room temperature for 10 min, and then centrifuged the sample at 12,000 rpm for 15 min at low temperature; the supernatant was discarded, followed by washing twice with 75% ethanol and addition of an appropriate amount of RNase-free double-distilled H_2O for dissolution to determine RNA concentration and quality. Qualified RNA was reversely transcribed using the iScript™ cDNA Synthesis Kit (Bio-Rad, Hercules, CA, USA), and reversely transcribed cDNA was detected by fluorescence quantitative PCR using the SYBR® Green Master Mix Kit (Bio-Rad) with a QuantStudio 12K Flex instrument (Applied Biosystems, Foster City, CA, USA). All primer sequences are shown in Supplementary Table S1.

2.11. Western Blotting. Treated granulosa cells were washed using prechilled PBS, and 100 μl radioimmunoprecipitation assay buffer (Solarbio) lysate was added to each well and lysed on ice for 15 min. The lysed cells were transferred to a centrifuge tube and centrifuged at 12,000 rpm for 15 min at 4°C, and then, the supernatant protein was collected for quantification and treated with sodium dodecyl loading buffer at 100°C for 5 min before being stored at -80°C until future use. Electrophoresis was performed using a precast gel (Genscript, Nanjing, China) and transferred to a 0.45 μm PVDF membrane under semidry transfer at 25 mA for 14 min. The membranes were blocked using 5% skimmed milk for 1 h at room temperature, and then, the membranes were incubated overnight at 4°C with primary antibodies. At the end of the primary antibody incubation, the corresponding secondary antibody was added for 1 h at room temperature after elution three times with TBST. At the end of secondary antibody incubation, the membranes were washed in TBST three times, and bands were developed using an enhanced chemiluminescence detection system (Bio-Rad). The primary antibodies used were as follows: Bcl-2 (1 : 1000, Abcam), BAX (1 : 1000, Abcam), Caspase-3 (1 : 1000, Abcam), γH2AX (1 : 1000, Abcam), nuclear factor-(NF-) κB (1 : 1000, Cell Signaling Technology); mTOR (1 : 1000, Abcam); β-actin (1 : 5000, Bioworld, Bloomington, MN, USA); and GAPDH (1 : 5000, Abcam). The mouse and rabbit secondary IgG antibodies (1 : 5000) were both from Abcam. Beta-actin and GAPDH were used as internal controls.

2.12. Apoptosis and ROS Analysis by Flow Cytometry. Granulosa cells were routinely cultured in 6-well plates for 24 h. After starving for 24 h, the cells were cultured with different concentrations of TF3 or controls for another 48 h and then washed thrice with PBS. Apoptosis detection was performed using the Annexin V-FITC/PI Apoptosis Kit (KeyGEN BioTECH, Nanjing, China). A Reactive Oxygen Species Assay Kit (Beyotime) was used to evaluate ROS levels in granulosa cells. The samples were analyzed on a BD C6 Flow Cytometer (BD Biosciences, Franklin Lakes, NJ, USA).

2.13. β-Galactosidase Staining. Senescence staining analysis was performed using the Senescence β-Galactosidase Staining Kit (Beyotime) according to the kit instructions. Briefly, pGCs and KGN cell lines were seeded in 6-well plates at a density of 2×10^5 cells/well and routinely cultured for 24 h. Serum-free culture medium was starved for 24 h, followed by different concentrations of TF3 or control culture for 48 h. At the end of treatment, the cells were washed with PBS three times, fixed in a fixative at room temperature for 15 min, stained with staining solution at 37°C overnight, and then photographed for analysis. For periovarian adipose tissue, the samples were rinsed in PBS three times, fixed in the fixative at room temperature for 15 min, and then stained with the staining solution in the kit at 37°C overnight prior to imaging.

2.14. Immunofluorescence Staining of Cells. The treated granulosa cells were fixed using 4% PFA for 30 min at room temperature and then permeabilized with PBST for 30 min at room temperature. At the end of permeabilization, 5% BSA was used to block for 1 h at room temperature and γH2AX antibody (1 : 1000, Abcam) was added for overnight incubation at 4°C. Rabbit IgG secondary antibody (1 : 5000, Abcam) was added after three PBST washes for a 60 min incubation at room temperature. At the end of secondary antibody incubation, the samples were washed three times in PBST and mounted with antifluorescence quencher containing DAPI. Images were analyzed on a laser scanning confocal microscope.

2.15. Cell Viability Analysis. Cell proliferation viability was detected and analyzed using the cell counting kit-8 (CCK-8; Dojindo, Tokyo, Japan). Briefly, pGCs were routinely cultured in 24-well plates at 1×10^5 seeds per well for 24 h, starved for another 24 h, and then treated with different doses of TF3 for 96 h. After treatment, the culture medium was changed to 300 μl of DMEM containing 10% CCK-8 solution, and the culture was continued for 2 h. The luminosity value at 450 nm was detected on a Varioskan Flash microplate reader (Thermo Fisher Scientific).

2.16. RNA Sequencing and Analysis. Human pGCs were routinely cultured for 24 h and then starved for 24 h. The culture medium was changed to the one containing 10 μM TF3, or the control medium was used for a total of 6 h incubation. At the end of the treatment, cellular RNA was collected, cDNA libraries were constructed, and transcriptome PE150 sequencing was performed using the Illumina NovaSeq platform (Illumina, San Diego, CA, USA). Target prediction and functional analysis were performed on 454 selected differential genes using Metascape Online [23]. The GSEA was performed using the OmicStudio tools at https://www.omicstudio.cn/tool.

2.17. Statistical Analysis. All experiments were performed in triplicate, and results are presented as mean ± SEM. Statistical analyses were performed using t-tests. A value of $p < 0.05$ was considered to indicate statistical significance.

3. Results

3.1. TF3 Improves Ovarian Function and Increases Litter Size in Aged Mice. To explore the effect of TF3 on ovarian

function, aged mice were given gavage administration of TF3 (30 mg/kg) every two days for 90 days, and aged mice in the control group were given the same volume of saline. At the end of treatment, estrous cycles were monitored for 14 consecutive days, and the results revealed that the estrous cycle of the old TF3 group increased compared with that of the old control group, although it was still prolonged compared with the young control group (Figure 1(a)). Serum FSH level in the old control group was significantly higher than that in the young control group ($p < 0.01$) and decreased after TF3 treatment ($p < 0.05$); estradiol and progesterone levels were not significantly different between the groups ($p > 0.05$) (Figure 1(b)).

The ovarian volume of aged mice was significantly increased after TF3 gavage treatment (Figures 1(c) and 1(e)), and the ovarian weight and ovarian/body weight ratio were significantly higher than those of old controls ($p < 0.001$) (Figure 1(d)). Hematoxylin and eosin staining of the treated ovarian sections was performed to analyze the effect of TF3 on follicular development, and the results revealed that more follicles remained on the ovaries in the TF3-treated group than the old control group (Figure 1(e)). The number of primordial follicles was also significantly increased ($p < 0.05$) (Figure 1(f)). More interestingly, the degree of ovarian interstitial fibrosis decreased in TF3-treated aged mice compared with old controls (Figure 1(g)). In addition, the mRNA expression level analysis of ovarian reserve markers showed that the expression levels of AMH, BMP15, and GDF9 in old control mice were significantly lesser than those in the young controls ($p < 0.05$); nonetheless, TF3 treatment restored the expression level of AMH and GDF9 ($p < 0.05$) (Figure 1(h)).

To investigate the effect of TF3 on mouse fertility, we performed natural fertility assays in different groups of mice. The litter size of young control mice was the highest after natural mating, that of old control mice was significantly decreased ($p < 0.01$), and the litter size of mice treated with TF3 gavage was higher than that of the old control group ($p < 0.05$) (Figures 1(i) and 1(j)).

3.2. TF3 Downregulates the Expression Level of Ovarian Aging-Related Genes. The above findings indicate that TF3 can improve ovarian function and increase litter size in aged mice, which seems to indicate that TF3 helps delay ovarian aging. The aging of adipose tissue around the ovary is closely related to ovarian function and aging. In this study, beta-galactosidase staining was first performed on adipose tissue adjacent to the ovary, and the results showed adipose tissue in the aged control group was darker, which became lighter after TF3 treatment, indicating that TF3 treatment reduced the aging level of adipose tissue around the ovary (Figure 2(a)). Hematoxylin and eosin staining analysis of periovarian adipose tissue sections showed that the size of lipid droplets in ovarian adipose tissue of the aged control group was significantly increased compared with that of the young group, and TF3 treatment significantly decreased lipid droplet size ($p < 0.01$) (Figures 2(b) and 2(c)). Immunohistochemical results revealed reduced expression of mTOR and p16 in the ovarian tissue of aged mice treated with TF3 (Figure 2(d)). RNA was extracted from the ovaries of treated mice to analyze mRNA expression levels of inflammatory marker genes interleukin- (IL-) 2, *IL-6*, and tumor necrosis factor-alpha (*TNFα*). TF3 treatment significantly decreased IL-2 mRNA levels ($p < 0.01$), and IL-6 and TNFα tended to decrease after TF3 treatment but not significantly ($p > 0.05$) (Figure 2(e)).

3.3. TF3 Improves Oocyte Quality in Aged Mice. Oocyte quality directly reflects ovarian function. In view of this, mice in each group were subjected to ovulation induction, and the harvested COCs were used in subsequent experiments. Compared with young control mice, the granulosa cells around COCs in aged control mice were relatively loosely arranged and scarce, while the number of granulosa cell layers around COCs was tightly arranged after TF3 treatment (Figure 3(a)). To further assess the effect of TF3 treatment on mouse oocyte quality, granulosa cells were removed from the obtained COCs for immunofluorescence staining. The results showed that the ROS level of oocytes in the aged control group was higher than that in the young control group, and levels of the antioxidant GSH were lower than those in the young control group. After TF3 treatment, the ROS level of oocytes in the aged mice decreased, and GSH expression increased (Figure 3(b)). Analysis of oocytes stained for the mitochondrial membrane potential marker JC1 revealed that young control mice had higher oocyte mitochondrial membrane potential, mostly in the form of JC1 polymers (red fluorescence). Aged control mice had poorer oocyte mitochondrial function and lower membrane potential, mostly in the form of JC1 monomers (green fluorescence), and TF3-treated aged mice had partially recovered mitochondrial function, and more JC1 polymers were present in the cytoplasm (Figure 3(c)). In addition, α-tubulin-stained spindles of mouse oocytes showed that most of the spindle arrangements in the young control group were normal, and the spindle fibers were tightly regulated and continuous, and the nuclear arrangement was tight. Furthermore, the ratio of abnormal spindle of oocytes in the aged control group was significantly increased ($p < 0.05$), which manifested as loose spindle breaks with scattered nuclear morphology. The ratio of abnormal spindles significantly decreased in the aged mice after TF3 treatment ($p < 0.05$) (Figures 3(d) and 3(e)).

To investigate the effects of different treatments on mouse embryo development, mouse oocytes were obtained after ovulation induction for *in vitro* fertilization experiments (Figure 3(f)). The number of oocytes retrieved in TF3-treated aged mice was significantly higher than that in the aged control mice ($p < 0.05$) (Figure 3(g)). In addition, although the fertilization rate and blastocyst formation rate after *in vitro* fertilization in TF3-treated aged mice were slightly increased, they were not significantly different ($p > 0.05$). Furthermore, the numbers of blastocyst cells were not significantly different between the two groups ($p > 0.05$) (Figure 3(g)).

3.4. TF3 Inhibits Apoptosis of Cultured pGCs. Follicular granulosa cells are closely related to ovarian function. To explore

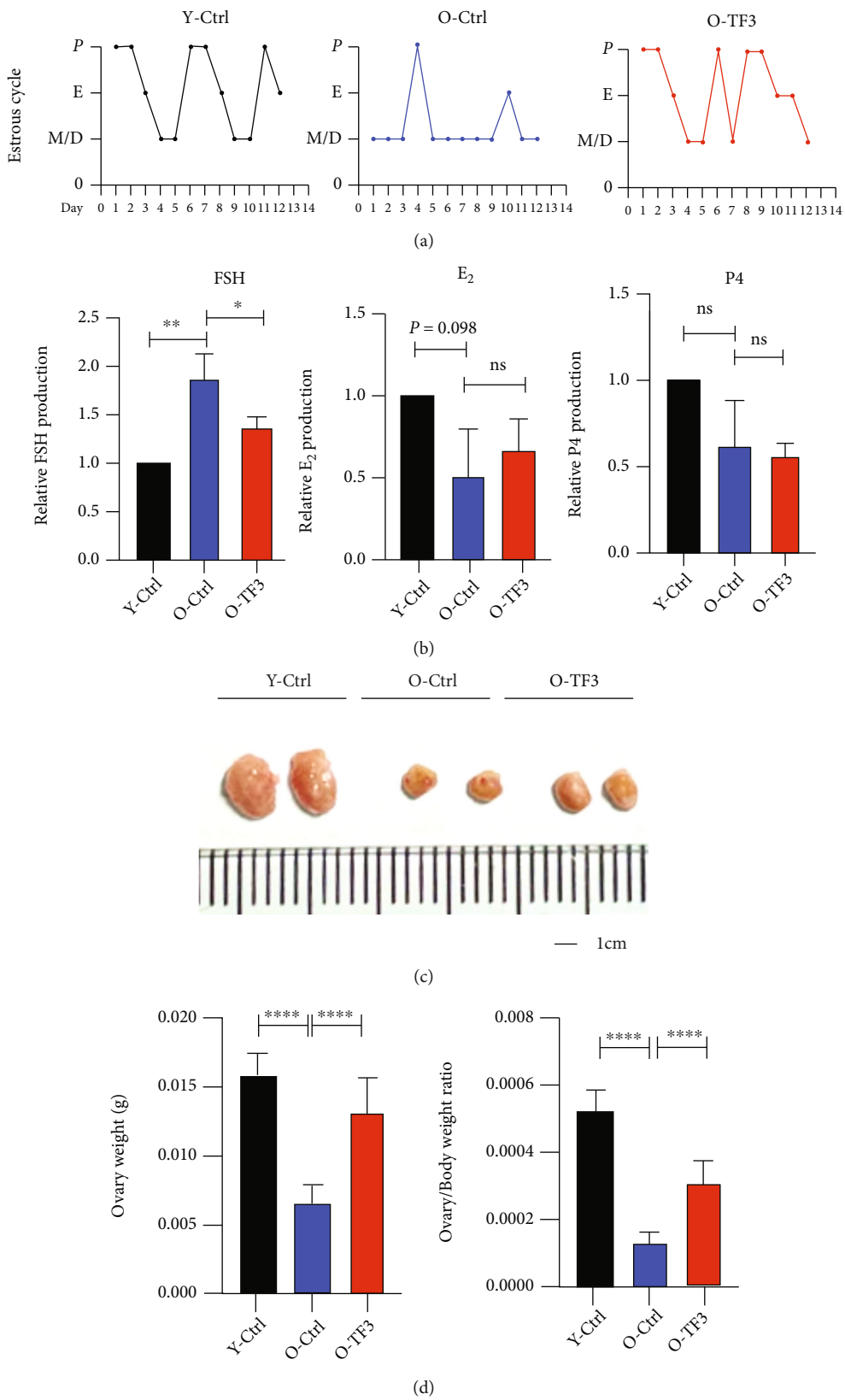

Figure 1: Continued.

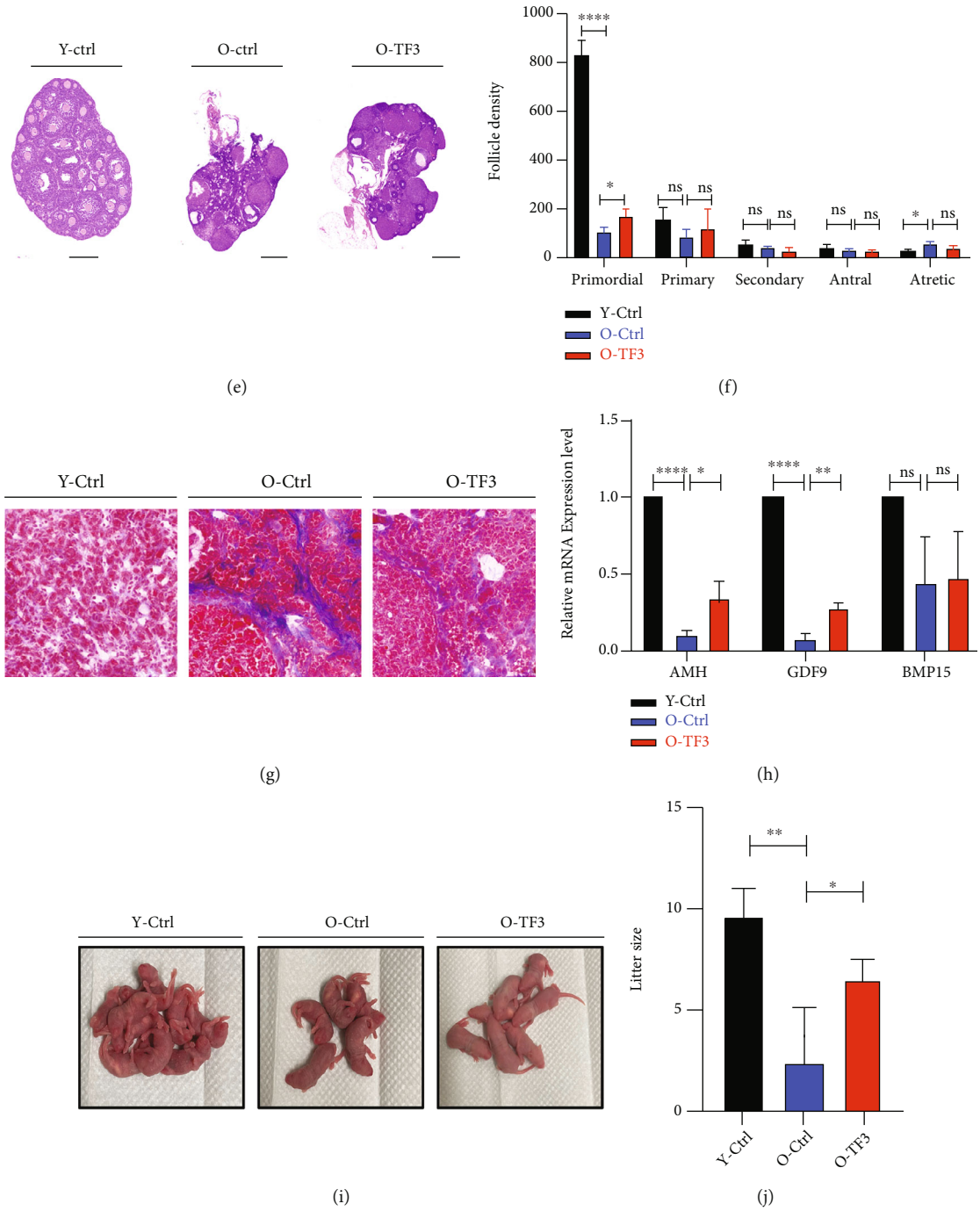

Figure 1: TF3 promotes ovarian function maintenance in aged mice. Vaginal cells were obtained from aged mice treated with intragastric administration (TF3 or control) for 90 days and 8-week-old young control mice without intragastric administration for 14 days. Estrous cycle was monitored and analyzed by HE staining, expressed as a line graph (a). P denotes metestrus, E denotes estrus, and M/D denotes diestrus and proestrus. Serum FSH, E_2, and P4 secretion levels were measured by enzyme-linked immunosorbent assays (b). After gavage administration, the ovaries were photographed to compare the change of ovarian volume (bar = 1 cm) (c). The body and ovary weights of mice in each group after treatment were obtained, and the ovary weight and ovary/body weight ratio (d) of mice in each group were compared and analyzed. HE staining was performed on the largest cross sections to observe and analyze ovarian and follicular development (bar = 500 μm) (e). Follicle count (f) after HE staining of serial ovarian sections and Masson staining of frozen ovarian sections were performed to analyze ovarian fibrosis status (bar = 20 μm) (g). Total RNA was extracted from mouse ovaries, and the expression levels (h) of ovarian reserve markers AMH, GDF9, and BMP15 mRNA were analyzed by real-time PCR. GAPDH was the internal reference gene. At the end of gavage treatment, the mice were naturally mated with adult male mice, and the litter size (i) was recorded. Young Ctrl (Y-Ctrl): 8-week-old CD-1 mice; old Ctrl (O-Ctrl): 9-month-old CD-1 mice treated with saline for 90 days; old+TF3(O-TF3): 9-month-old CD-1 mice treated with 30 mg/kg/day TF3 for 90 days. $^{*}p < 0.05$, $^{**}p < 0.01$, $^{***}p < 0.001$, and $^{****}p < 0.0001$.

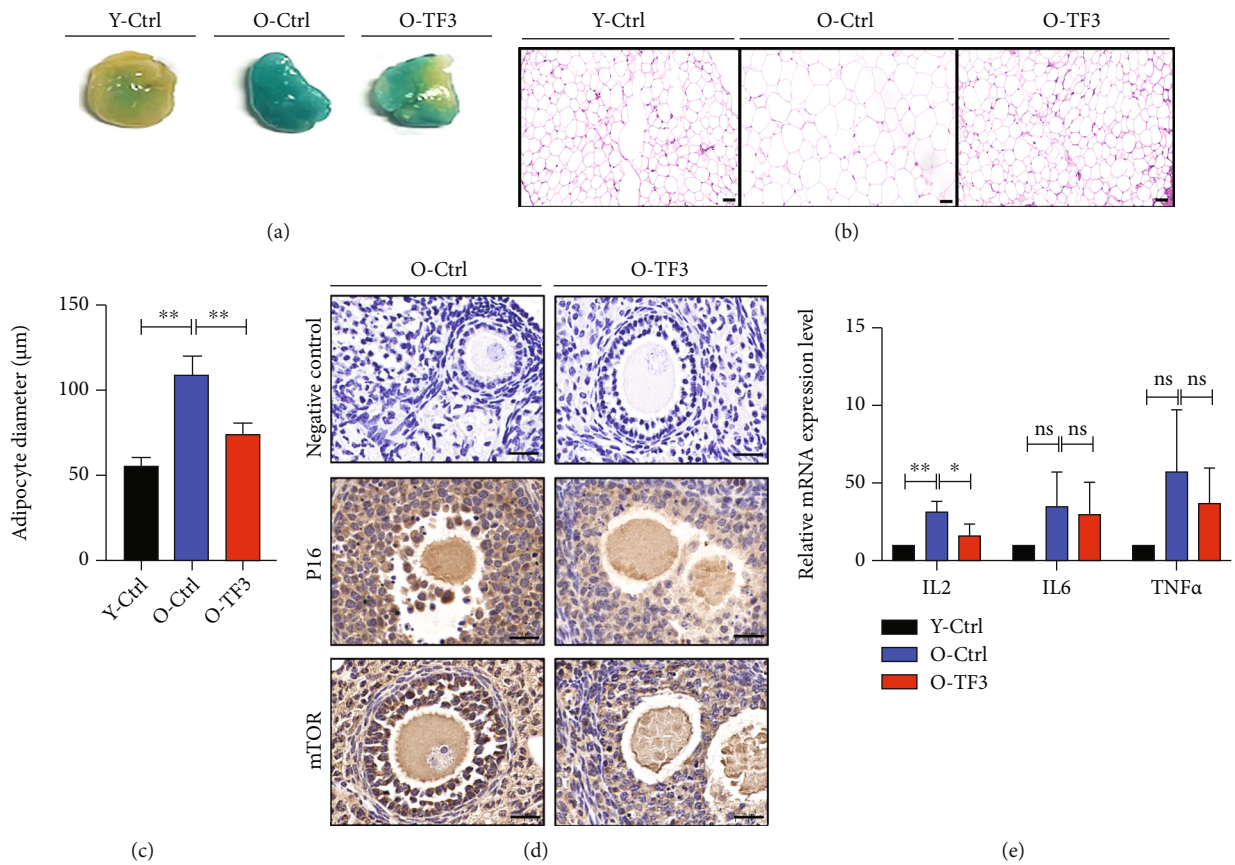

Figure 2: Effect of TF3 on the expression of marker genes of aging in mice. After treatment, adipose tissue around the ovary was stained for the aging marker galactosidase (a) and HE to statistically analyze lipid droplet size (b, c) (bar = 50 μm). Immunohistochemical staining of ovarian tissue sections showed expression of P16 and mTOR protein, with negative control (d) on the left side (bar = 20 μm). Total RNA was extracted from the ovaries and reversely transcribed, and the relative expression levels of *IL-2*, *IL-6*, and *TNFα* were analyzed using real-time PCR, with GAPDH as the internal reference gene (e). $^{*}p < 0.05$, $^{**}p < 0.01$, and $^{****}p < 0.0001$.

the potential regulatory mechanism of TF3 on ovarian function, we investigated the effect of TF3 on granulosa cell apoptosis. In an *in vitro* culture model of human pGCs, the results revealed that TF3 was beneficial to maintain healthy pGC morphology, and the number of adherent cells after 96 h of culture was significantly greater compared with the control group (Figure 4(a)). The CCK-8 cell viability assay analysis also showed that TF3 could significantly resist pGC apoptosis levels (Figure 4(b)). Staining for the aging marker galactosidase after 48 h of culture of pGCs and KGN granulosa cell lines revealed that TF3 treatment could significantly reduce the expression level of beta-galactosidase and delay cellular aging ($p < 0.05$) (Figures 4(c)–4(e)). The flow cytometry results showed that the proportion of pGC apoptosis after 48 h of TF3 treatment was significantly decreased ($p < 0.05$) (Figures 4(f) and 4(g)). Inhibition of apoptosis by TF3 in cultured pGCs may be related to the upregulation of Bcl-2/BAX ratio by TF3 and downregulation of the protein expression levels of BAX, caspase-3, and γH2AX (Figure 4(h)). The quantitative results are shown in supplementary materials (Supplementary Figure S1). The results of fluorescence staining for γH2AX, a marker of DNA damage, also indicated that TF3-treated pGCs had significantly reduced γH2AX fluorescence (Figure 4(i)).

3.5. TF3 Improves the Antioxidative Ability of Granulosa Cells Cultured In Vitro. To further investigate the role of TF3 in granulosa cells, we constructed a H_2O_2-treated pGC oxidative stress model and used flow cytometry to analyze the ability of TF3 to counteract cellular oxidative stress. The results showed that H_2O_2 significantly increased the proportion of apoptosis ($p < 0.001$), which was attenuated by TF3 treatment ($p < 0.001$) (Figures 5(a) and 5(b)). Analysis of intracellular ROS levels revealed that TF3 could also significantly reduce the H_2O_2-induced increase in cellular ROS levels ($p < 0.01$) (Figures 5(c) and 5(d)). The intracellular JC1 mitochondrial membrane potential assay analysis confirmed that TF3 could significantly upregulate the decrease in mitochondrial membrane potential caused by H_2O_2 (Figure 5(e)).

3.6. TF3 May Regulate Ovarian Function by Affecting the Autophagy Pathway. To further explore the potential action pathway of TF3 in regulating granulosa cell function, whole transcriptome sequencing analysis was performed on pGCs after TF3 treatment. A total of 454 genes had significantly altered the expression after TF3 treatment ($p < 0.05$) (Supplementary Table S2). The Gene Ontology (GO) analysis of differentially expressed genes indicated that TF3 in

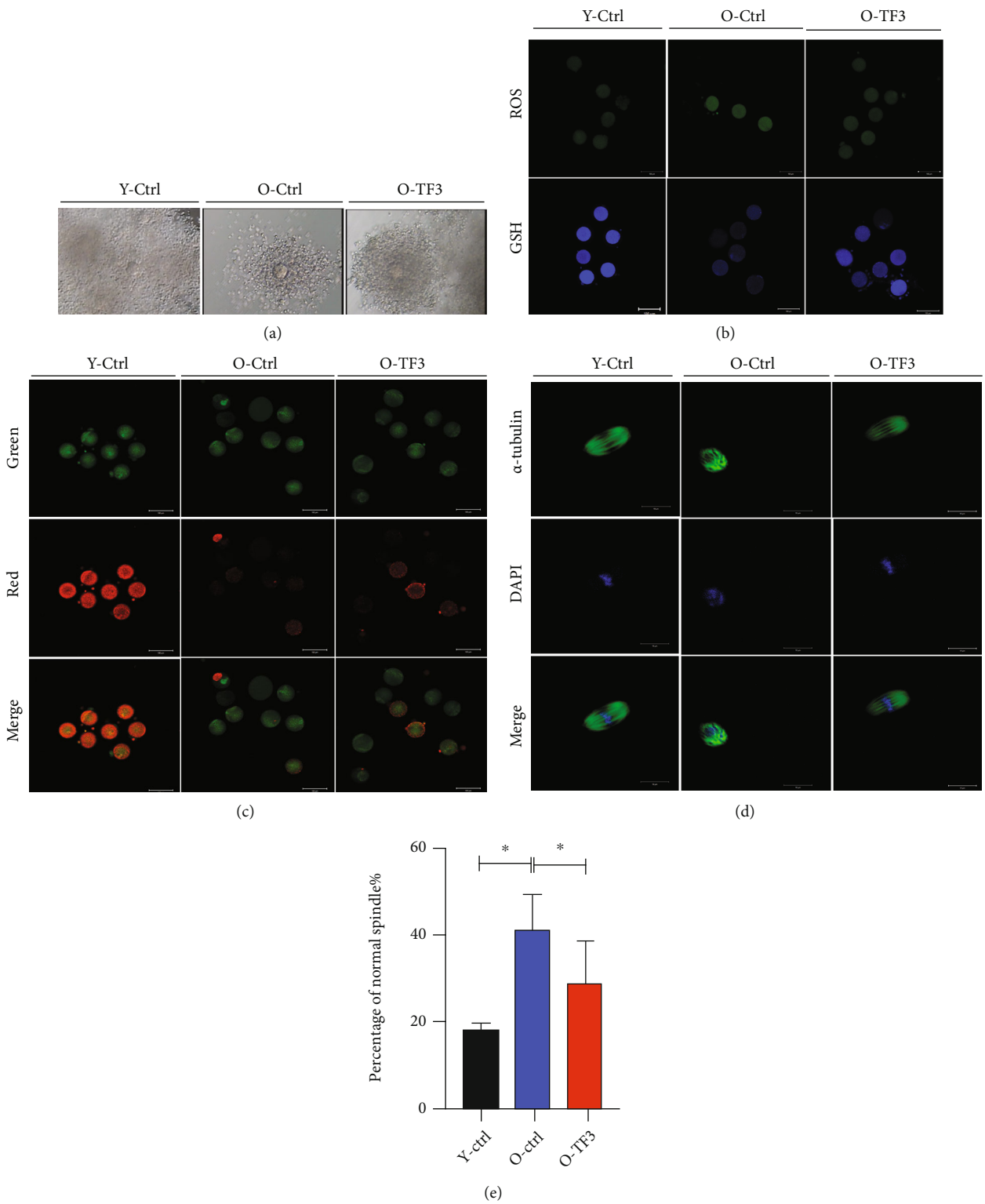

Figure 3: Continued.

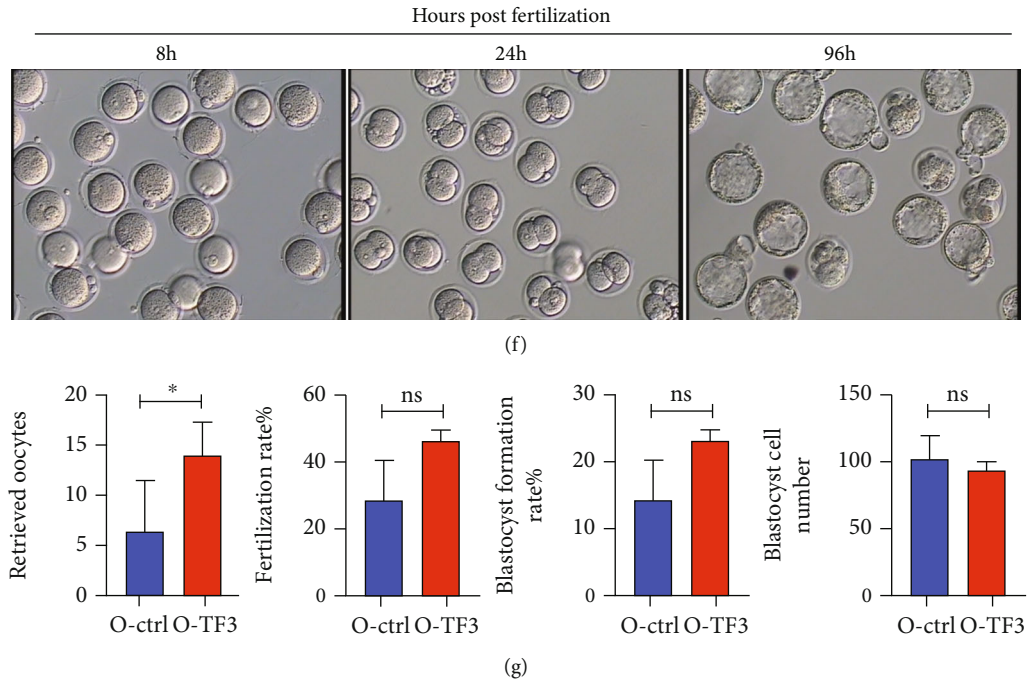

Figure 3: TF3 slows down the age-related decline in mouse oocyte quality. Mice in each treatment group were intraperitoneally injected with 10 IU PMSG and, after 48 h of treatment, injected with 10 IU hCG, and COCs were obtained from the ampulla of the fallopian tube 14 h later to analyze the effect of TF3 on COC morphology (a). The oxidative stress status of oocytes was analyzed by ROS and GSH staining after removing granulosa cells from COCs obtained from each treatment group (b). JC1 staining was performed to analyze oocyte mitochondrial membrane potential; red (polymers) and green (monomers) represent higher and lower oocyte mitochondrial membrane potential, respectively (c). The effect of TF3 on oocyte spindle morphology was analyzed by staining oocytes with α-tubulin antibody (green) and DAPI (blue); the right panel shows statistical analysis of abnormal spindle morphology and the ratio (d, e). COCs obtained by ovarian hyperstimulation were inseminated *in vitro* to analyze the effects of TF3 on oocyte retrieval, fertilization rate, blastocyst formation rate, and blastocyst cell number in aged mice (f, g). $^{*}p < 0.05$.

granulosa cells mainly affected the regulation of reproductive and developmental processes (Figure 6(a)). Analysis of the involved signaling pathways suggested that TF3 might be involved in the regulation of reproductive and developmental processes through the Class A/1(Rhodopsin-like receptors), GPCR ligand binding, Wnt signaling pathway, and PI3K-AKT-mTOR clusters (Figure 6(b)). Based on further analysis of key signaling pathways and significantly differential genes, we hypothesize that the mTOR pathway and its downstream associated molecular regulatory networks may be regulated by TF3. We performed enrichment analysis of the differentially expressed genes involved by using the gene set enrichment analysis (GSEA) algorithm, and the results showed that TF3 treatment could significantly affect autophagy function ($p < 0.05$) (Figure 6(c)). This was validated in granulosa cells and mouse ovaries; the results revealed that expression of the granulosa cell autophagy-related proteins mTOR and NF-κB decreased after TF3 treatment, suggesting that TF3 may scavenge ROS-damaged proteins and damaged mitochondria by activating the autophagy pathway (Figure 6(d)). The quantitative results are shown in supplementary materials (Supplementary Figure S2). NF-κB and mTOR protein expression levels were increased in the ovarian tissue of aged control mice compared with young control mice, while they were decreased in the ovaries of aged mice after TF3 treatment (Figure 6(e)). The quantitative results are shown in supplementary materials (Supplementary Figure S3). Furthermore, we used the AutoDock Vina method to perform semiflexible docking of TF3 to FRB domain of mTOR and selected the optimal conformation of affinity (Figure 6(f)). The affinity binding energy of TF3 to FRB domain of mTOR (5WBH) protein was -7.7 kcal/mol; six hydrogen bonds could be formed with amino acid residues Asp2102, Glu2032, Ser2015, and Tyr2105 of the mTOR protein, and two π–π interactions could be formed with Phe2039. The molecule also formed hydrophobic interactions with amino acid residues Phe2039 and Tyr2105. TF3 was predicted to affect mTOR to form a more stable complex through hydrogen bonding and hydrophobic interactions.

4. Discussion

The natural tea polyphenol TF3 is a small molecule compound that has become increasingly popular as a dietary supplement in clinical practice; such compounds are characterized by multiple targets with naturally low toxicity or even no toxicity [24]. In this study, intragastric administration of TF3 in aged mice significantly delayed ovarian aging, as shown by maintaining ovarian reserve, shortening estrous cycle, and enlarging litter size. Further studies revealed that

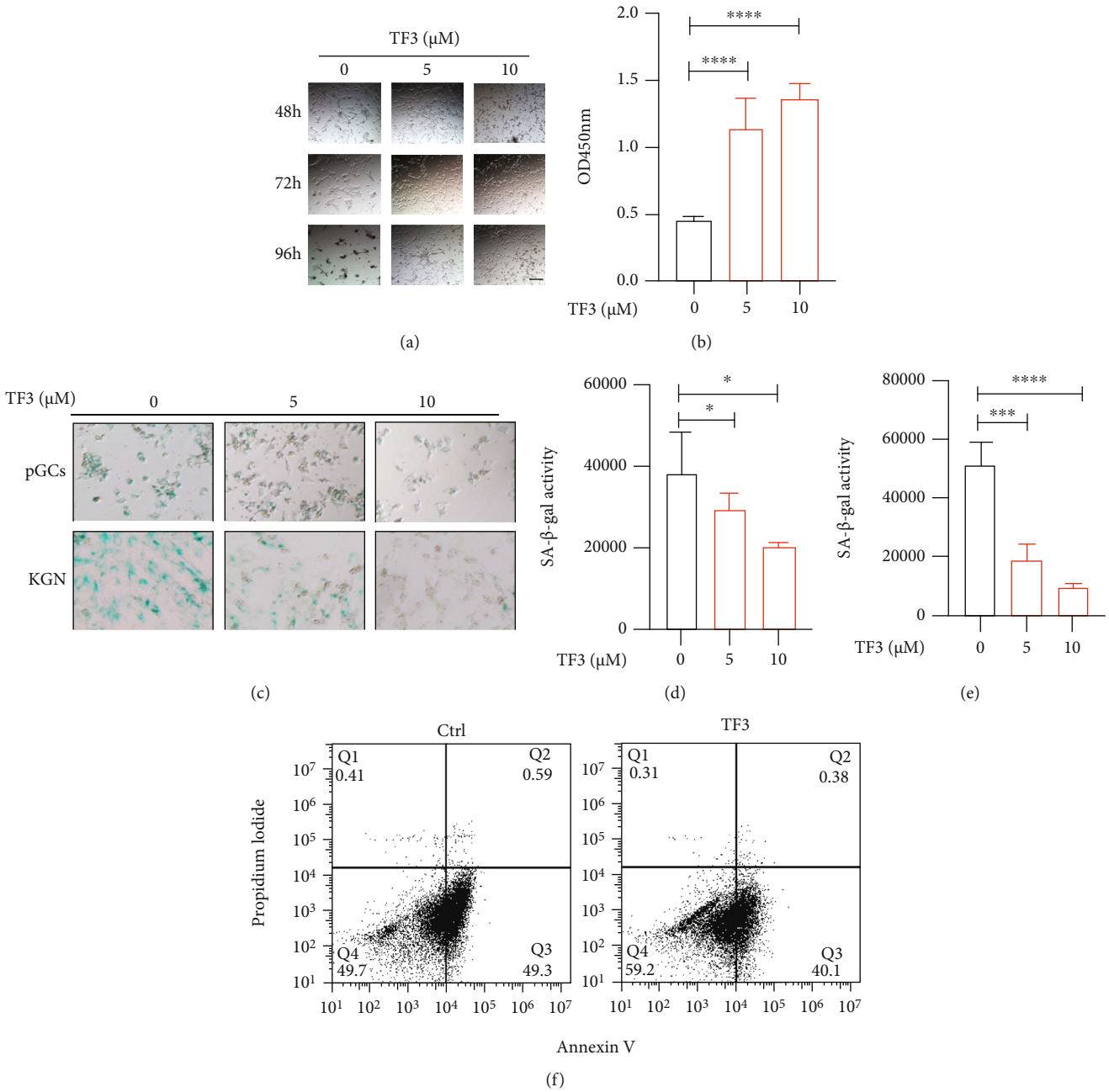

Figure 4: Continued.

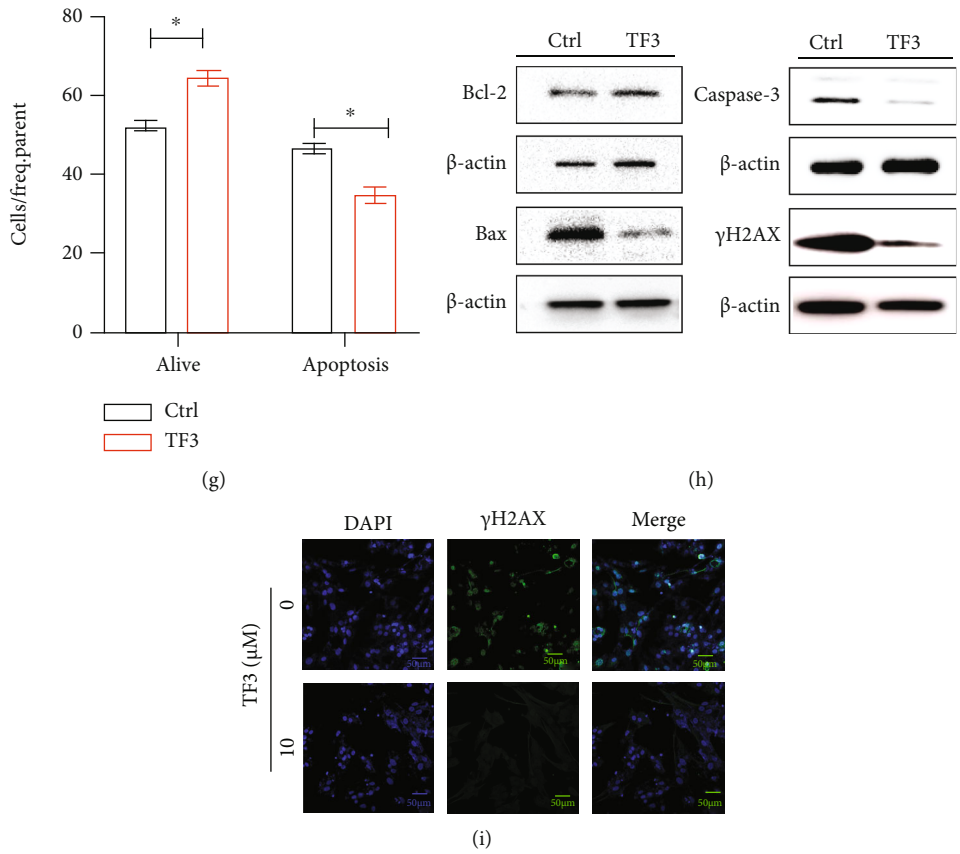

Figure 4: TF3 inhibits apoptosis of granulosa cells cultured *in vitro*. Granulosa cells were routinely cultured and treated with different concentrations of TF3 (0, 5, and 10 μM) with the time to start TF3 addition set at 0 h, bar = 50 μm (a). CCK8 cell viability assay kits were used to detect the effect of TF3 on cell viability after 120 h of culture (b). Human pGCs and KGN granulosa cell lines were cultured to analyze the effect of TF3 on beta-galactosidase expression, bar = 50 μm (c). Quantitative statistical analysis of beta-galactosidase staining in pGCs (d) and KGN (e) cells was performed using ImageJ software. Flow cytometry was performed to analyze the effect of TF3 (10 μM) on pGC apoptosis (f), and the ratios of apoptosis of different types of cells were statistically analyzed (g). Total protein was extracted from pGCs treated with TF3/control, and the expression levels of apoptosis-related proteins Bcl-2, BAX, caspase-3, and γH2AX were analyzed by western blotting (h). Immunofluorescence staining was performed to analyze the expression of the apoptotic marker γH2AX, bar = 50 μm (i). $^{*}p < 0.05$, $^{***}p < 0.001$, and $^{****}p < 0.0001$.

TF3 treatment significantly downregulated oocyte ROS levels and abnormal spindle rates, which in turn improved oocyte quality. Our analyses of ovarian granulosa cells showed that TF3 improved the antioxidative ability of granulosa cells and decreased apoptosis, which may be related to the targeting of TF3 to bind to mTOR FRB domain and regulate the autophagy pathway.

Female reproductive performance decreases with age, manifested as the continuous depletion of follicle pools and irregular menstrual cycles; these changes are accompanied by increased FSH and decreased AMH, and excessive FSH levels will lead to follicular overgrowth, thereby exacerbating follicle pool depletion [25]. The number of primordial follicles in the ovaries of women with regular menstruation is 10 times higher than the primordial follicles in those with irregular menstruation, and the rate of follicular depletion dramatically increases during the final stages of the female reproductive life (perimenopausal period) [26]. In addition, the ability to secrete hormones and the response to pituitary hormones are important manifestations of ovarian function, and excessive FSH levels also indicate poor follicular growth [27]. In this study, we found that aged mice supplemented with TF3 had significantly lower FSH levels than the aged control group, suggesting that TF3 can improve follicular development in aged mice, which is consistent with our ovarian follicle counts. Women with endocrine disorders have reduced quality of life because of hot flashes, night sweats, sleep disorders, osteoporosis, and even depression [28, 29]. Our experiments showed that TF3 gavage treatment of 9-month-old mice was equivalent to intervention in the early perimenopausal period of humans, and the results revealed that TF3 was beneficial to maintain the follicle pool and improve ovarian function. This treatment partially restored the estrous cycle of mice, suggesting that TF3 also has a potential role in improving the quality of life of women.

The condition of periovarian adipose tissue is closely related to ovarian function; moderate adipose tissue plays a protective role, but excessive adipose tissue secretes proinflammatory factors that cause cellular senescence, which in

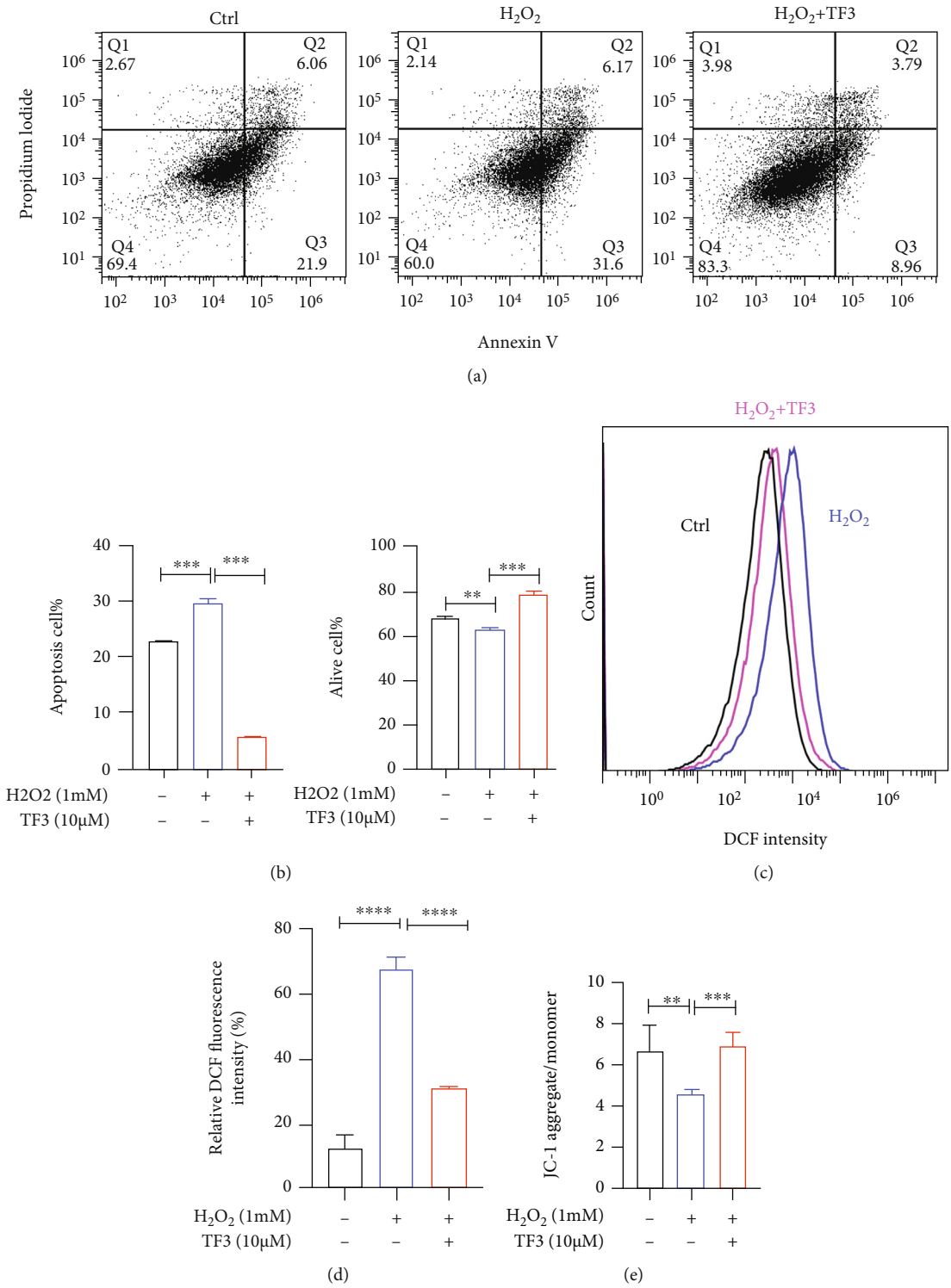

Figure 5: TF3 alleviates the damaging effect of oxidative stress on granulosa cells. pGCs were routinely cultured for 24 h and then starved and cultured in serum-free culture medium for 24 h. Cells were treated with TF3 (10 μM) or control for 24 h and then treated with H_2O_2 (1 mM) or an equal volume of pure water control for another 6 h to generate a pGC oxidative stress injury model. After treatment, apoptosis under anticell stress conditions was analyzed by flow cytometry (a), and the results were statistically analyzed (b). An oxidative stress model was used to analyze the effect of TF3 on ROS levels in granulosa cells (c), and the results were statistically analyzed (d). TF3 resistance to H_2O_2-induced decrease in mitochondrial membrane potential (e) was analyzed by detecting intracellular mitochondrial membrane potential with JC1. $^{*}p < 0.05$, $^{**}p < 0.01$, $^{***}p < 0.001$, and $^{****}p < 0.0001$.

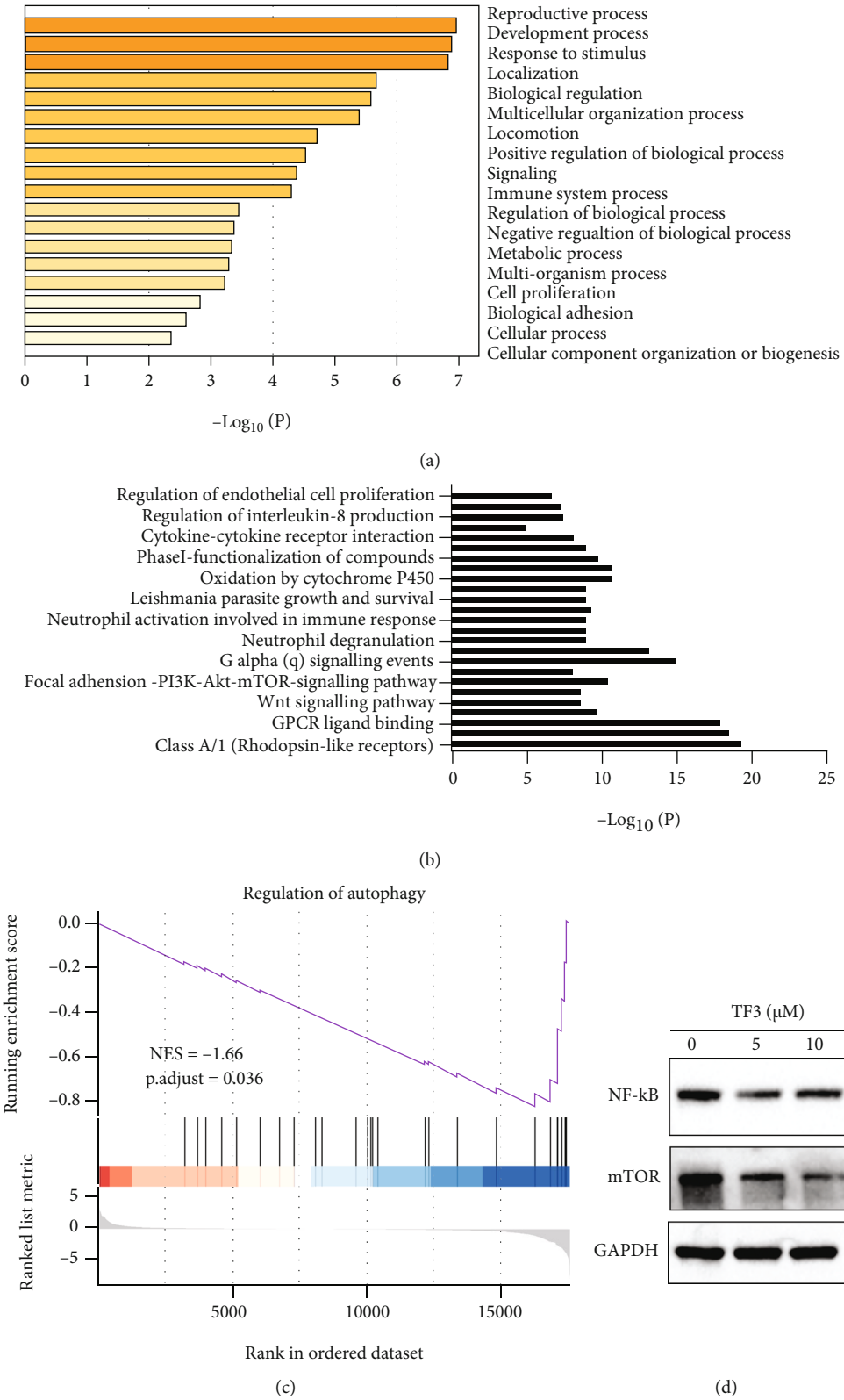

Figure 6: Continued.

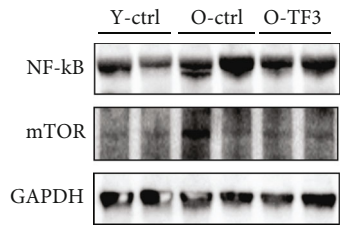

(e)

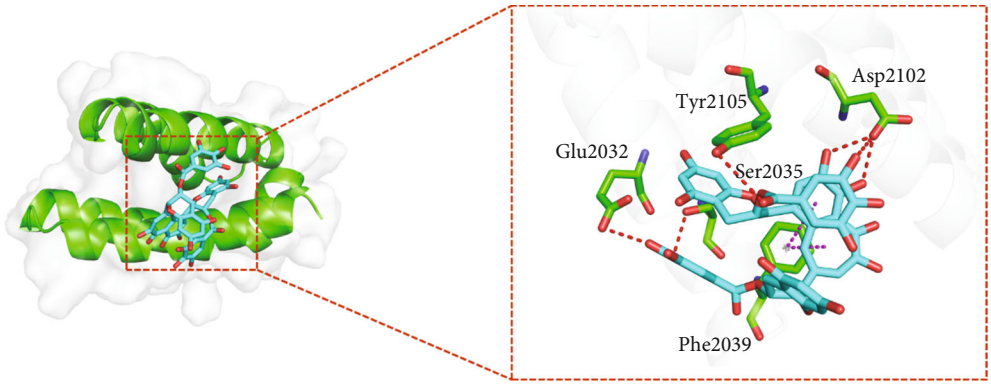

(f)

Figure 6: TF3 may affect granulosa cell function by regulating autophagy through the mTOR pathway. pGCs were routinely cultured for 24 h and then starved in a serum-free culture medium for 24 h. TF3 (10 μM) or control treatment was given for 6 h. Cells were collected for transcriptome sequencing, and differentially expressed genes were subjected to GO analysis related to cell biological processes (a) and MCODE analysis related to signaling pathways (b). GSEA algorithm enrichment of all genes and calculation of enrichment scores were performed to find the key pathways affected by TF3 (c). Granulosa cells after TF3 treatment were collected, proteins were extracted, and the effect of TF3 on related proteins was analyzed by western blotting (d). Ovarian tissues were collected from all three groups, and proteins were extracted to analyze the effects of TF3 on NF-κB and mTOR protein levels (e). GAPDH was the internal reference protein. The molecular docking mode of TF3 to mTOR protein was predicted using AutoDock Vina software to map the action mode of TF3-5WBH, with the blue part indicating TF3 and the red box indicating the docking site (f).

turn leads to decreased quality of oocytes and granulosa cells and accelerates ovarian aging [30]. TF3 downregulates the expression of inflammatory factors secreted by adipose tissue [31], and a human randomized controlled trial showed that oral theaflavin administration for 10 weeks significantly reduced subcutaneous fat content and increased skeletal muscle percentage [32]. Our results showed significantly larger lipid droplet area in the periovarian adipose tissue of aged mice than in the young controls, and TF3 supplementation significantly reduced the lipid droplet area, which was consistent with previous literature reports. Beta-galactosidase staining also showed that TF3 could significantly delay ovarian adipose tissue aging in aged mice.

Overactivation of the primordial follicle pool causes persistent loss of primordial follicles, which leads to the development of premature ovarian failure (POF) [33]. The incidence of POF is approximately 1% in women and represents accelerated aging of the female reproductive system before the age of 40 years [34]. The use of chemotherapeutic drugs such as cisplatin can also lead to POF, thereby decreasing ovarian function [35]. It is important to prevent excessive activation of the follicular pool, thereby maintaining the ovarian reserve and prolonging female reproduction. Administering TF3 to aged mice preserved the primordial follicle pool and increased the litter size. These findings suggest that TF3 slows down excessive activation of the follicle pool, which is important for improving and prolonging female fertility.

The autophagy-lysosomal system is an important method to remove damaged organelles and plays a pivotal role in both targeted degradation therapy for various diseases [36] and the regulation of ovarian aging [37]. Physiologically, the oxidative stress system maintains homeostasis, and when ROS levels are slightly increased, the autophagy system is activated to scavenge them. When age-related ROS accumulation becomes excessive and autophagic activity decreases with age [38], the scavenging ability of ROS also decreases, at which time the damage caused by excessive ROS will lead to aggravated aging and chronic injury. Therefore, increasing the autophagy activity is beneficial to delay the aging processes [39] [40].

In the follicular microenvironment, granulosa cells and oocytes interact to regulate the process of follicular development. Granulosa cells can directly affect oocyte quality through gap junctions, and this can lead to decreased oocyte quality when oxidative stress is exacerbated in the granulosa cells [41]. Normal granulosa cell function is therefore essential for oocyte development [42]. The *in vitro* culture model of pGCs purified from human follicles is widely used in reproductive research [43, 44], but the viability and status of pGCs also gradually decreased with longer culture time;

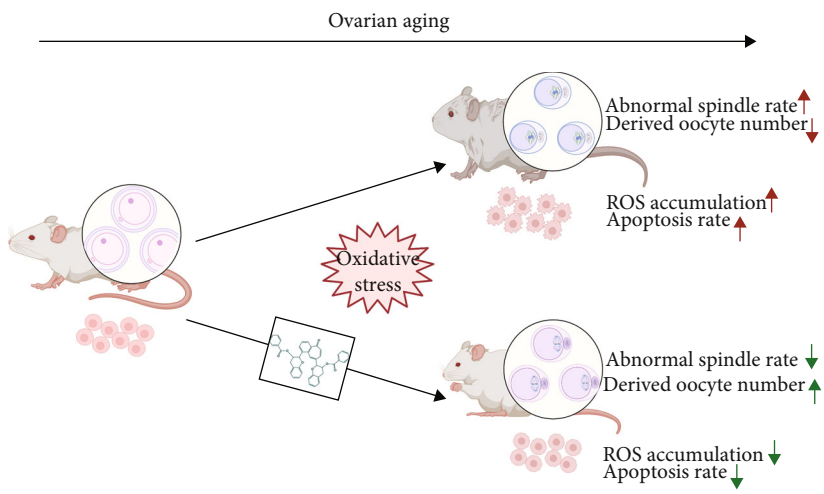

Figure 7: The mechanism model of TF3 working on ovarian function. This chart illustrates a possible mechanism model by which TF3 regulates oocyte quality and granulosa cell function during the process of ovarian aging. This work is created with http://BioRender.com with the permission to publish.

thus, it is a potential aging cell model. We found that TF3 could delay granulosa cell apoptosis *in vitro* and significantly reduce ROS-induced apoptosis and oxidative stress injury in the H_2O_2-induced oxidative stress model. Beta-galactosidase staining was performed on pGCs, KGN cells, and mouse periovarian adipose tissues cultured *in vitro*; the results suggested that TF3 treatment could delay the senescence of granulosa cells and periovarian adipose tissue. This indicates that TF3 can promote lysosomal degradation at the cellular and organism levels to facilitate the removal of senescent cells and harmful substances and effectively slow down the aging process.

Studies on oocytes derived from TF3-treated aged mice revealed that TF3 can reduce ROS levels, increase GSH levels, attenuate the decrease of mitochondrial membrane potential in oocytes, and improve oocyte quality. Presumably, TF3 can reduce damage to the ovary caused by ROS overaccumulation through scavenging ROS and increasing antioxidant enzyme activities. Tea polyphenols have been found to partially restore meiotic abnormalities, DNA damage, and apoptosis in porcine oocytes after cisplatin exposure [45], which is consistent with our findings that TF3 can significantly reduce the ratio of abnormal spindles in oocytes from aged mice. In addition, it was reported that *in vitro* maturation of bovine oocytes and the addition of certain concentrations of tea polyphenols to the *in vitro* culture medium can improve the conception rate [46]. Tea polyphenols such as TF3 seem to have a positive effect on oocyte maturation and embryo development *in vitro*.

Some researchers have found that TF3 can act directly on ATP-binding enzymes, thereby affecting their structural activity and inhibiting ATP turnover and production [17]. Polyphenolic compounds can also regulate the aging processes by targeting mTOR [47]. These studies seem to suggest that TF3 may protect ovarian function by regulating energy metabolism pathways. To clarify the role of TF3 in ovarian follicle development, we performed RNA sequencing of granulosa cells after TF3 treatment and performed deep GSEA of the sequencing results, which showed that TF3 mainly affected reproductive and developmental processes by regulating autophagy and pathways such as PI3K-AKT-mTOR.

Autophagy reduces the death of healthy cells and has an important role in maintaining homeostasis. In addition to its ability to remove potential prototoxins, autophagy improves mitochondrial function and helps recovery from acute cellular injury with damaged mitochondria; in addition, it can help avoid apoptosis or necrosis [48]. During aging, oxidative stress and increased inflammation can cause DNA damage and accumulation of IκB kinases, leading to increased expression of mTOR and NF-κB, thereby inhibiting autophagy and further exacerbating aging [49, 50]. Polyphenolic compounds can mimic caloric restriction to induce autophagy [51], mainly by increasing AMP-activated protein kinase to decrease mTOR and induce autophagy [38]. Our sequencing results confirmed that TF3 mainly regulates granulosa cell function by affecting the autophagy pathway, and further analysis showed that the natural small molecule compound TF3 may act on mTOR FRB domain to exert its regulatory effect.

5. Conclusions

In vitro and *in vivo* mouse model experiments revealed that TF3 can effectively slow down the process of ovarian aging and improve ovarian function in aged mice by improving oocyte quality and granulosa cell function (Figure 7). As a natural polyphenolic compound, TF3 could regulate mTOR to reduce ovarian metabolism to maintain the ovarian reserve, reduce the accumulation of ROS due to ATP overproduction, improve ovarian autophagy to remove aging substances, reduce ROS damage to oocytes and granulosa cells, delay female ovarian aging, and prolong female fertility.

Data Availability

The data will be available in the supplementary materials.

Conflicts of Interest

The authors declare no conflicts of interest.

Authors' Contributions

Jiahuan He was responsible for performing most of the experiment, data interpretation, data analysis, and preparing the manuscript. Guidong Yao was responsible for designing the study, performing the experiment, and analyzing the data. Qina He and Tongwei Zhang were responsible for performing the experiment, data interpretation, data analysis. Huiying Fan, Yucheng Bai, Junya Zhang, Guang Yang, Ziwen Xu, and Jingyi Hu were responsible for collecting samples, data interpretation, and data analysis. Yingpu Sun was responsible for designing and supervising the study. All authors participated in the revision of the manuscript. Jiahuan He, Guidong Yao, Qina He, and Tongwei Zhang contributed equally to this work.

Acknowledgments

This study was supported by the National Natural Science Foundation of China (U1904138 to Guidong Yao) and National Key R&D Program of China (2019YFA0110900 to Yingpu Sun).

Supplementary Materials

Supplementary 1. Supplementary Table S1: primers used in the study.

Supplementary 2. Supplementary Table S2: differentially expressed genes treated by TF3 in primary granulosa cells.

Supplementary 3. Supplementary Figure S1: the statistical analysis of apoptosis protein expression in different groups. Supplementary Figure S2: statistical analysis of NF-κB and mTOR protein expression in different groups. Supplementary Figure S3: statistical analysis of NF-κB and mTOR protein expression in different groups.

References

[1] F. J. Broekmans, E. A. Knauff, E. R. te Velde, N. S. Macklon, and B. C. Fauser, "Female reproductive ageing: current knowledge and future trends," *Trends in Endocrinology & Metabolism*, vol. 18, pp. 58–65, 2007.

[2] F. Broekmans, M. Soules, and B. Fauser, "Ovarian aging: mechanisms and clinical consequences," *Endocrine Reviews*, vol. 30, pp. 465–493, 2009.

[3] E. R. Te Velde and P. L. Pearson, "The variability of female reproductive ageing," *Human Reproduction Update*, vol. 8, pp. 141–154, 2002.

[4] E. A. McGee and A. J. Hsueh, "Initial and cyclic recruitment of ovarian follicles," *Endocrine Reviews*, vol. 21, pp. 200–214, 2000.

[5] C. Tatone, F. Amicarelli, M. C. Carbone et al., "Cellular and molecular aspects of ovarian follicle ageing," *Human Reproduction Update*, vol. 14, no. 2, pp. 131–142, 2008.

[6] E. Verdin, M. D. Hirschey, L. W. Finley, and M. C. Haigis, "Sirtuin regulation of mitochondria: energy production, apoptosis, and signaling," *Trends in Biochemical Sciences*, vol. 35, pp. 669–675, 2010.

[7] J. Lim and U. Luderer, "Oxidative damage increases and antioxidant gene expression decreases with aging in the mouse ovary1," *Biology of Reproduction*, vol. 84, pp. 775–782, 2010.

[8] C. Tatone, M. C. Carbone, S. Falone et al., "Age-dependent changes in the expression of superoxide dismutases and catalase are associated with ultrastructural modifications in human granulosa cells," *Molecular Human Reproduction*, vol. 12, no. 11, pp. 655–660, 2006.

[9] S. Das, R. Chattopadhyay, S. Ghosh et al., "Reactive oxygen species level in follicular fluid—embryo quality marker in IVF?," *Human Reproduction*, vol. 21, no. 9, pp. 2403–2407, 2006.

[10] W. Łuczaj and E. Skrzydlewska, "Antioxidative properties of black tea," *Preventive Medicine*, vol. 40, pp. 910–918, 2005.

[11] L. K. Leung, Y. Su, R. Chen, Z. Zhang, Y. Huang, and Z. Y. Chen, "Theaflavins in black tea and catechins in green tea are equally effective antioxidants," *The Journal of Nutrition*, vol. 131, no. 9, pp. 2248–2251, 2001.

[12] L. Luo, J. Huang, Y. Fu, J. Xu, and Y. Qian, "Effects of tea polyphenols on ovarian development in rats," *Journal of Endocrinological Investigation*, vol. 31, pp. 1110–1118, 2008.

[13] H.-F. He, "Research progress on theaflavins: efficacy, formation, and preparation," *Food & Nutrition Research*, vol. 61, no. 1, article 1344521, 2017.

[14] Y. Y. Wu, W. Li, Y. Xu, E. H. Jin, and Y. Y. Tu, "Evaluation of the antioxidant effects of four main theaflavin derivatives through chemiluminescence and DNA damage analyses," *Journal of Zhejiang University Science B*, vol. 12, pp. 744–751, 2011.

[15] X.-Y. Luo, T. Takahara, J. Hou et al., "Theaflavin attenuates ischemia-reperfusion injury in a mouse fatty liver model," *Biochemical and Biophysical Research Communications*, vol. 417, no. 1, pp. 287–293, 2012.

[16] S. M. Arent, M. Senso, D. L. Golem, and K. H. McKeever, "The effects of theaflavin-enriched black tea extract on muscle soreness, oxidative stress, inflammation, and endocrine responses to acute anaerobic interval training: a randomized, double-blind, crossover study," *Journal of the International Society of Sports Nutrition*, vol. 7, pp. 1–10, 2010.

[17] B. Li, S. B. Vik, and Y. Tu, "Theaflavins inhibit the ATP synthase and the respiratory chain without increasing superoxide production," *The Journal of Nutritional Biochemistry*, vol. 23, pp. 953–960, 2012.

[18] Y. Gao, G. O. Rankin, Y. Tu, and Y. C. Chen, "Theaflavin-3, 3'-digallate decreases human ovarian carcinoma OVCAR-3 cell-induced angiogenesis via Akt and Notch-1 pathways, not via MAPK pathways," *International Journal of Oncology*, vol. 48, pp. 281–292, 2016.

[19] Y. Tu, E. Kim, Y. Gao, G. O. Rankin, B. Li, and Y. C. Chen, "Theaflavin-3, 3'-digallate induces apoptosis and G2 cell cycle arrest through the Akt/MDM2/p53 pathway in cisplatin-resistant ovarian cancer A2780/CP70 cells," *International Journal of Oncology*, vol. 48, no. 6, pp. 2657–2665, 2016.

[20] S. L. Byers, M. V. Wiles, S. L. Dunn, and R. A. Taft, "Mouse estrous cycle identification tool and images," *PLoS One*, vol. 7, article e35538, 2012.

[21] M. Myers, K. L. Britt, N. G. Wreford, F. J. Ebling, and J. B. Kerr, "Methods for quantifying follicular numbers within the mouse ovary," *Reproduction*, vol. 127, pp. 569–580, 2004.

[22] G. Yang, G. Yao, Z. Xu et al., "Expression Level of ADAMTS1 in Granulosa Cells of PCOS Patients Is Related to Granulosa Cell Function, Oocyte Quality, and Embryo Development," *Frontiers in Cell and Developmental Biology*, vol. 9, p. 887, 2021.

[23] Y. Zhou, B. Zhou, L. Pache et al., "Metascape provides a biologist-oriented resource for the analysis of systems-level datasets," *Nature Communications*, vol. 10, no. 1, pp. 1–10, 2019.

[24] P. I. Oteiza, C. G. Fraga, and M. Galleano, "Linking biomarkers of oxidative stress and disease with flavonoid consumption: from experimental models to humans," *Redox Biology*, vol. 42, article 101914, 2021.

[25] A. Allshouse, J. Pavlovic, and N. Santoro, "Menstrual cycle hormone changes associated with reproductive aging and how they may relate to symptoms," *Obstetrics and Gynecology Clinics*, vol. 45, pp. 613–628, 2018.

[26] S. J. Richardson, V. Senikas, and J. F. Nelson, "Follicular depletion during the menopausal transition: evidence for accelerated loss and ultimate exhaustion∗," *The Journal of Clinical Endocrinology & Metabolism*, vol. 65, pp. 1231–1237, 1987.

[27] C. M. Howles, "Role of LH and FSH in ovarian function," *Molecular and Cellular Endocrinology*, vol. 161, pp. 25–30, 2000.

[28] H. Buckler, "The menopause transition: endocrine changes and clinical symptoms," *British Menopause Society Journal*, vol. 11, pp. 61–65, 2005.

[29] D. Bruce and J. Rymer, "Symptoms of the menopause," *Best practice & research Clinical obstetrics & gynaecology*, vol. 23, pp. 25–32, 2009.

[30] C. E. Boots and E. S. Jungheim, "Inflammation and human ovarian follicular dynamics," *Seminars in reproductive medicine*, vol. 33, no. 4, pp. 270–275, 2015.

[31] H.-J. Ko, C.-Y. Lo, B.-J. Wang, R. Y.-Y. Chiou, and S.-M. Lin, "Theaflavin-3, 3′-digallate, a black tea polyphenol, attenuates adipocyte-activated inflammatory response of macrophage associated with the switch of M1/M2-like phenotype," *Journal of Functional Foods*, vol. 11, pp. 36–48, 2014.

[32] T. Aizawa, A. Yamamoto, and T. Ueno, "Effect of oral theaflavin administration on body weight, fat, and muscle in healthy subjects: a randomized pilot study," *Bioscience, Biotechnology, and Biochemistry*, vol. 81, pp. 311–315, 2017.

[33] D. Adhikari, S. Risal, K. Liu, and Y. Shen, "Pharmacological inhibition of mTORC1 prevents over-activation of the primordial follicle pool in response to elevated PI3K signaling," *PLoS One*, vol. 8, article e53810, 2013.

[34] L. Pal and N. Santoro, "Premature ovarian failure (POF): discordance between somatic and reproductive aging," *Ageing Research Reviews*, vol. 1, pp. 413–423, 2002.

[35] H. Jang, O. H. Lee, Y. Lee et al., "Melatonin prevents cisplatin-induced primordial follicle loss via suppression of PTEN/AKT/FOXO3a pathway activation in the mouse ovary," *Journal of Pineal Research*, vol. 60, no. 3, pp. 336–347, 2016.

[36] S. Giordano, V. Darley-Usmar, and J. Zhang, "Autophagy as an essential cellular antioxidant pathway in neurodegenerative disease," *Redox Biology*, vol. 2, pp. 82–90, 2014.

[37] A. E. Peters, B. P. Mihalas, E. G. Bromfield, S. D. Roman, B. Nixon, and J. M. Sutherland, "Autophagy in female fertility: a role in oxidative stress and aging," *Antioxidants & Redox Signaling*, vol. 32, no. 8, pp. 550–568, 2020.

[38] D. C. Rubinsztein, G. Mariño, and G. Kroemer, "Autophagy and aging," *Cell*, vol. 146, pp. 682–695, 2011.

[39] Y. Aman, T. Schmauck-Medina, M. Hansen et al., "Autophagy in healthy aging and disease," *Nature Aging*, vol. 1, no. 8, pp. 634–650, 2021.

[40] L. Luo and Z.-H. Qin, "Autophagy, aging, and longevity," *Autophagy: Biology and Diseases*, vol. 1206, pp. 509–525, 2019.

[41] Q. Lai, W. Xiang, Q. Li et al., "Oxidative stress in granulosa cells contributes to poor oocyte quality and IVF-ET outcomes in women with polycystic ovary syndrome," *Frontiers of medicine*, vol. 12, no. 5, pp. 518–524, 2018.

[42] C. Tatone and F. Amicarelli, "The aging ovary–the poor granulosa cells," *Fertility and Sterility*, vol. 99, pp. 12–17, 2013.

[43] M. Quinn, S. B. McGregor, J. L. Stanton, P. A. Hessian, W. R. Gillett, and D. P. L. Green, "Purification of granulosa cells from human ovarian follicular fluid using granulosa cell aggregates," *Reproduction, Fertility and Development*, vol. 18, no. 5, pp. 501–508, 2006.

[44] R. Chilvers, Y. Bodenburg, L. Denner, and R. Urban, "Development of a novel protocol for isolation and purification of human granulosa cells," *Journal of Assisted Reproduction and Genetics*, vol. 29, pp. 547–556, 2012.

[45] C. Zhou, X. Zhang, X. ShiYang, H. Wang, and B. Xiong, "Tea polyphenol protects against cisplatin-induced meiotic defects in porcine oocytes," *Aging*, vol. 11, p. 4706, 2019.

[46] Z. Wang, C. Fu, and S. Yu, "Green tea polyphenols added to IVM and IVC media affect transcript abundance, apoptosis, and pregnancy rates in bovine embryos," *Theriogenology*, vol. 79, pp. 186–192, 2013.

[47] H. Pazoki-Toroudi, H. Amani, M. Ajami et al., "Targeting mTOR signaling by polyphenols: a new therapeutic target for ageing," *Ageing Research Reviews*, vol. 31, pp. 55–66, 2016.

[48] A. Colell, J. E. Ricci, S. Tait et al., "GAPDH and Autophagy Preserve Survival after Apoptotic Cytochrome _c_ Release in the Absence of Caspase Activation," *Cell*, vol. 129, no. 5, pp. 983–997, 2007.

[49] A. Salminen and K. Kaarniranta, "Regulation of the aging process by autophagy," *Trends in Molecular Medicine*, vol. 15, pp. 217–224, 2009.

[50] A. Salminen, A. Kauppinen, and K. Kaarniranta, "Emerging role of NF-kappaB signaling in the induction of senescence-associated secretory phenotype (SASP)," *Cellular Signalling*, vol. 24, pp. 835–845, 2012.

[51] S. Davinelli, D. De Stefani, I. De Vivo, and G. Scapagnini, "Polyphenols as caloric restriction mimetics regulating mitochondrial biogenesis and mitophagy," *Trends in Endocrinology and Metabolism*, vol. 31, pp. 536–550, 2020.

Hindawi
Oxidative Medicine and Cellular Longevity
Volume 2021, Article ID 7656834, 11 pages
https://doi.org/10.1155/2021/7656834

Research Article

Trigonelline Extends the Lifespan of *C. Elegans* and Delays the Progression of Age-Related Diseases by Activating AMPK, DAF-16, and HSF-1

Wen-Yu Zeng,[1] Lin Tan,[2] Cong Han,[1] Zhuo-Ya Zheng,[2] Gui-Sheng Wu,[2,3] Huai-Rong Luo,[2,3] and Su-Lian Li[1]

[1]*Affiliated Traditional Chinese Medicine Hospital of Southwest Medical University, Luzhou, Sichuan 646000, China*
[2]*Key Laboratory for Aging and Regenerative Medicine, Department of Pharmacology School of Pharmacy, Southwest Medical University, 319 Zhongshan Road, Luzhou, Sichuan 646000, China*
[3]*Central Nervous System Drug Key Laboratory of Sichuan Province, Luzhou, Sichuan 646000, China*

Correspondence should be addressed to Huai-Rong Luo; lhr@swmu.edu.cn and Su-Lian Li; lyzyyhlb@163.com

Received 16 July 2021; Revised 19 August 2021; Accepted 27 August 2021; Published 26 September 2021

Academic Editor: Stefania D'Adamo

Trigonelline is the main alkaloid with bioactivity presented in fenugreek, which was used in traditional medicine in Asian countries for centuries. It is reported that trigonelline has anti-inflammatory, anti-oxidant, and anti-pathogenic effects. We are wondering whether trigonelline have anti-aging effect. We found that 50 μM of trigonelline had the best anti-aging activity and could prolong the lifespan of *Caenorhabditis elegans* (*C. elegans*) by about 17.9%. Trigonelline can enhance the oxidative, heat, and pathogenic stress resistance of *C. elegans*. Trigonelline could also delay the development of neurodegenerative diseases, such as AD, PD, and HD, in models of *C. elegans*. Trigonelline could not prolong the lifespan of long-lived worms with loss-of-function mutations in genes regulating energy and nutrition, such as *clk-1*, *isp-1*, *eat-2*, and *rsks-1*. Trigonelline requires *daf-16*, *hsf-1*, and *aak-2* to extend the lifespan of *C. elegans*. Trigonelline can also up-regulate the expression of *daf-16* and *hsf-1* targeted downstream genes, such as *sod-3*, *gst-4*, *hsp-16.1*, and *hsp-12.6*. Our results can be the basis for developing trigonelline-rich products with health benefits, as well as for further research on the pharmacological usage of trigonelline.

1. Introduction

The percentage of people aged 65 years and older in developed and developing countries has been steadily increasing. Aging is an intrinsic feature of life and is the greatest risk factor for major age-related disorders, such as diabetes, hypertension, cardiovascular disease, cancer, and neurodegenerative disease [1]. The prevalence of the older population has led to a global burden of age-related disorders. For many years, people have been looking for substances to prevent aging. Experimenting on mammals is time-consuming and expensive. Researchers use cultured human cells to test the anti-aging activity of more substances, but aging is a complex process that is difficult to measure at the cellular level. *Caenorhabditis elegans* (*C. elegans*) is the only multicellular model organism whose somatic developmental lineages have been clearly studied. *C. elegans* has a short life cycle and simple structure. *C. elegans* also has clear genetic background and is easy to manipulate. So, it has become an ideal model for aging research, as well as anti-aging drug screening.

Fenugreek (*Trigonella foenum-graecum L.*) is an annual forage legume and a traditional spice crop and has been used in traditional medicine in Asian countries for centuries [2]. Modern pharmacological studies have shown that fenugreek has antidiabetic, anticarcinogenic, hypocholesterolemic, antioxidant, and immunological activities [3]. Trigonelline (TRG) is one of the main alkaloids and components with pharmacological activities in dried fenugreek seeds (Figure 1(a)). Trigonelline has been reported to have neuroprotective [4, 5], anti-apoptotic [6, 7], anti-inflammatory [8, 9], anti-oxidant [10], anti-diabetic [11, 12], antihyperglycemic effects [13], anti-degranulation [14], and anti-

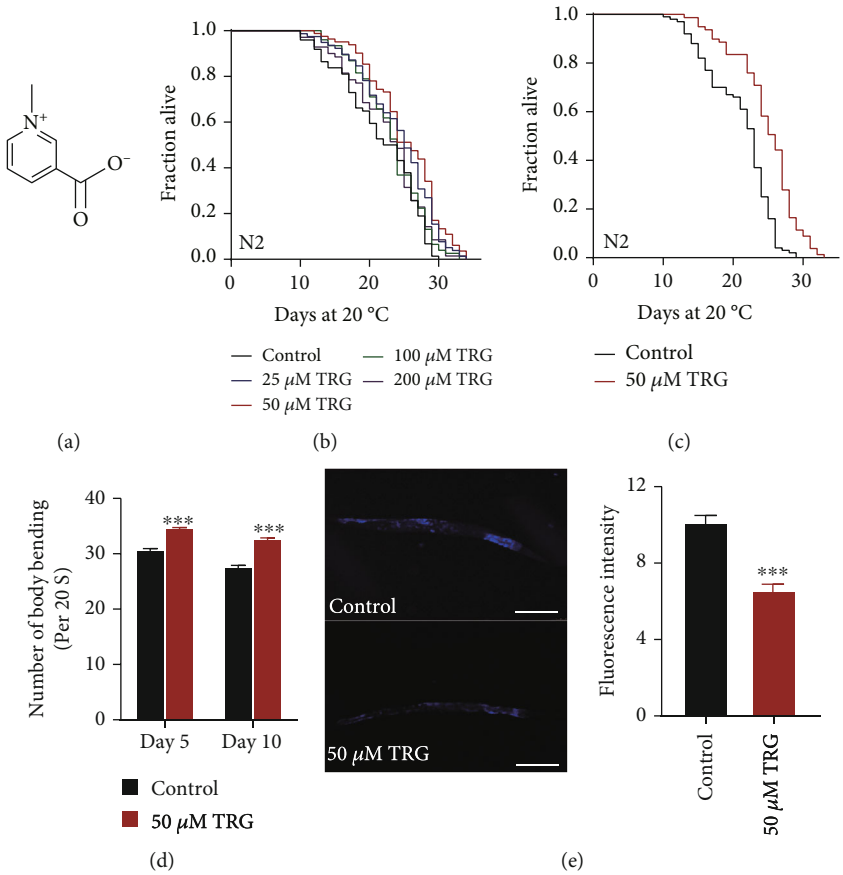

Figure 1: Trigonelline can prolong the lifespan and improve the health of *C. elegans* (a) Chemical structure of trigonelline; (b) Survival curves of wild-type N2 worms raised at 20°C on NGM plates containing either no trigonelline or 25, 50, 100, and 200 μM of trigonelline; (c) Survival curves of wild-type N2 worms treated from hatching and raised at 20°C on NGM plates containing either no trigonelline or 50 μM of trigonelline ($p < 0.001$, log-rank test), Statistical details and repeats of these experiments were summarized in Table S1; (d) Body bending of N2 nematode treated with 50 μM of trigonelline for 5 days and 10 days. Figure shows the mean value of three independent experiments, SEM is represented by error line. $***$ represents $p < 0.001$, calculated by two-tailed t-test. Statistical details and repeats of these experiments were summarized in Table S3; (e) Analysis of lipofuscin in Treatment of N2 nematodes by 50 of μM trigonelline on day 10. Relative Fluorescence Intensity was calculated by Image J. Figure shows the mean value of three independent experiments, SEM is represented by error line. $***$ represents $p < 0.001$, calculated by two-tailed t-test. Statistical details and repeats of these experiments were summarized in Table S2.

carcinogenic effect [15, 16]. Among them, the anti-oxidative activity of trigonelline could explain many of its other activities, such as neuroprotective activity [3]. The antioxidant and neuroprotective effects of trigonelline lead us to speculate that trigonelline may play an important role in anti-aging and treating neurodegenerative diseases.

In this study, we investigated whether trigonelline could extend the lifespan and increase the stress tolerances of *C. elegans*. We also tested whether trigonelline could delay the onset of neurodegenerative disease in models of *C. elegans*, as well as determine its possible mechanisms.

2. Materials and Methods

2.1. Materials. The trigonelline was supplied by Shanghai Yuanye Bio-Technology Ltd (Shanghai,

China, purity ≥95%). Other compounds used in this work were purchased from Sigma-Aldrich (Munich, Germany). Trigonelline was dissolved in ddH_2O. NGM plates with compound were equilibrated overnight before use.

2.2. Worm Strains. All worm strains were provided by the Caenorhabditis Genetic Center (CGC, University of Minnesota, Minneapolis, MN). Except for special cases, worms were cultured in a constant temperature and humidity incubator with a temperature of 20°C and humidity of 60%, on a medium with OP50 *E. coli* food. The nematode strains were as follows: N2 (wild-type), CF1903 *glp-1(e2144) III.*, CF1038 *daf-16 (mu86) I.*, *EU1 skn-1(zu67)IV.*, PS3551 *hsf-1(sy441)I.*, DA1116 *eat-2(ad1116) II.*, MQ887 *isp-1(qm150) IV.*, CB1370 *daf-2(e1370) III.*, RB754 *aak-2(ok524)X.*, RB759 *akt-1(ok525)V.*, VC204 *akt-2(ok393)X.*,VC199 *sir-2.1(ok434)IV.*, CB4876 *clk-1(e2519)III.*, TK22 *mev-1(kn1)III.*, BX165 *nhr-80 (tm1011).*, AA89 *daf-12 (rh274).*, BZ555 *egIs1(dat-1::gfp)*, CF1553 [(pAD76) sod-3::GFP + rol6 (su1006)], CL2166, dvIs19[pAF15(gst-4::GFP::NLS)], SJ4100 (zcIs13[hsp-6::GFP]), SJ4005 zcIs4V (hsp-4::gfp), SJ4058 zcIs9 [hsp-

60::GFP + lin-15(+)], CL4176 [(pAF29)myo-3p::Aβ1-42 + (pRF4) rol-6 (su1006)], CL2006 (dvIs2 [pCL12(unc-54/human Aβ1–42 minigene) + pRF4]), NL5901 [unc54p::alphasynuclein::YFP + unc-119(+)], AM140 (rmIs132[unc-54p::Q35::YFP]).

2.3. Lifespan Assay. All strains were cultured for 2 - 3 generations without starvation on new NGM plates.

The worms were transferred to NGM plates (containing inactivated OP50 (60°C for 35 min)) with or without trigonelline in late L4 or early adult stage. The plates were supplemented with 20 μM of 5-fluoro-2'-deoxyuridine (FUdR) to inhibit oviposition and hatching. The day when *Caenorhabditis elegans* was transferred to the plates was recorded as the 0th day of the experiment [17]. To ensure that trigonelline retained its potency throughout the entire experiment, worms were transferred to fresh plates with or without trigonelline every other day. In the statistics of lifespan test, if nematodes did not move or did not respond to external mechanical stimulation (such as touching them lightly with insect pickers), they would be recorded as dead. The statistical data of experiments were processed by SPSS 20.0 software, and the results were expressed by Kaplan-Meier survival curve. The p value was obtained by log-rank test analysis, while $p < 0.05$ indicates statistical significance. Each group of lifespan experiments included at least three independent repeated experiments, and the number of worms in each group was more than 60.

2.4. Stress Resistance Assay. For the high temperature resistance test, the synchronized larvae were spread on NGM plates, cultured in an incubator at 20°C, and then transferred to NGM plates with or without trigonelline at the late L4 stage or early adult stage. The worms were transferred to 35°C on the 10th day of adult, and the death of the worm was observed and counted every 2 hours.

For anti-oxidative stress test, pretreatment was the same as high temperature test, the adult worms on the 10th day are transferred to NGM plates containing 20 mM of paraquat, and the death of worms is observed and counted every other day.

For the pathogenic stress test, the pre-treatment was the same as high temperature resistance test. On the 10th day of the adulthood, the worms were transferred to the NGM plates covered with bacteria *Pseudomonas aeruginosa* [17]. The death of worms was observed and recorded every 12 hours.

All statistics and analysis methods of stress assays were the same as the lifespan experiment. The sample size of each experiment was at least 60 worms, and each stress assay contains at least three independent repeated experiments.

2.5. Body Bending Behavior Test. The synchronized L1 larva nematodes were spread on NGM plates, cultured in incubator at 20°C. the worms developed to L4 were transferred to experimental plate with or without trigonelline. On the 5th and 10th days of adulthood, the worms were picked up to water droplets and stabilized for 1 minute. Then the bending frequency of the body within 20 seconds were recorded under the microscope, and the back and forth movement of the body was calculated as one bend.

2.6. Determination of Reactive Oxygen Species (ROS). The L1 larvae were spread on NGM plate and cultured in an incubator at 20°C until late L4 or early adulthood. Then, worms were transferred to experimental plates (control group, Trigonelline, NAC, paraquat); After 96 h, the worms were collected and stained with H2DCF-DA probe according to the procedure of ROS detection kit [18]. Then, the nematodes were photographed with fluorescence microscope. The ROS detection experiment includes at least three independent repeated experiments. The sample size of each experiment was at least 30 worms. Image J was used to count the gray value of each nematode. The p value was calculated by two-tailed t-test.

2.7. Determination of Lipofuscin. The preliminary treatment was the same as the lifespan test, the nematodes were collected on the tenth day of the adult and photographed by fluorescence microscope at excitation wavelength of 360-370 nm and emission wavelength of 420-460 nm; The level of lipofuscin in each nematode was quantified by calculating the average pixel intensity of each nematode. Sample size is at least 30 worms.

2.8. Fluorescence Quantification. The preliminary treatment of worms for fluorescence quantification was the same as the lifespan test, then the worms of strains Cl2166 (dvis19 [pgst-4p::GFP::nls]) and CF1553 [(pad76) SOD-3::GFP + rol6 (su1006)] were placed at plates containing 20 mM of paraquat for 30 min on the 6th day of adulthood, anesthetized with 2 mM of tetraimidazole hydrochloride. The expression of GFP in these strains was observed by fluorescence microscope. For Transgenic strains SJ4100 (zcIs13[hsp-6::GFP]), SJ4005 zcIs4V (hsp-4::gfp), and SJ4058zcis9 [HSP-60::GFP + Lin-15 (+)], worms were placed at 35°C for 2 h on the 6th day of adults, and was collected with a 1.5 mL centrifuge tube, washed with ddH_2O for three times to remove OP50, anesthetized with 2 mmol tetraimidazole hydrochloride, and observed the expression of green fluorescent protein with fluorescence microscope.

2.9. Age-Related Neurodegenerative Diseases Related Experiments. For worms of strain CL4176(dvis27 (myo-3/abeta1-42/letutr) + prf4 (rol-6 (su1006)), the synchronized larva were spread on the NGM plates with or without trigonelline, incubated at 15°C for 36 hours, then transferred to 23°C for 24 hours, and then counted and photographed every 12 hours.

For worms of strain CL2006 (dvIs2 [pCL12(unc-54/human Aβ1–42 minigene) + pRF4]), the synchronized larvae were spread on NGM plates until they grow into late L4 or early adult stage. Then, the worms were transferred to NGM plate with or without trigonelline, and counted and photographed every day. Nematodes that remain immobile or move only by the head under external mechanical stimulation (such as touching with an insect picker) were defined as paralyzed. The number of worms per group should be above 60.

For the worms of strain AM40 and NL5901, the late L4 larva or early adulthood worms were transferred to experimental plates with or without trigonelline. AM140 nematodes were collected on the 2nd and 4th day of adulthood, and NL5901 nematodes were collected on the 10th day of adulthood. Then, worms were anesthetized with 2 mM of tetraimidazole hydrochloride. The aggregation of α -synuclein was captured by Leica fluorescence microscope and analyzed by Image J. The experiment was independently repeated at least three times. The number of worms in each group of experiment is at least 30.

For the worms of transgenic strain BZ555, the L3 larva were transferred to a centrifuge tube containing a mixture of 50 mM of 6-OHDA and 10 mM of ascorbic acid and incubated at 20°C for one hour, and gently shaken every 10 minutes to mix. After one hour, the worms were washed three times with M9 and then placed on a culture plate with and without trigonelline for 72 hours. Finally, we washed the worms with M9, took pictures, and calculated statistics. The experiments were repeated independently at least twice. The number of worms in each group of experiment was at least 30.

2.10. Quantitative RT-PCR Assay. About 3,000 synchronized young adult worms were transferred to NGM plates with or without 50 μM of trigonelline and cultured at 20°C for 24 hours. Total RNA was extracted by RNAiso Plus (Takara), converted to cDNA using High Capacity cDNA Reverse Transcription Kit (Applied Biosystems). The quantitative RT-PCR was performed using Power SYBR Green PCR Master Mix (Applied Biosystems) on Quantstudio 6 Flex system. The relative expression levels of genes were calculated by the $2^{-\Delta\Delta Ct}$ and normalized to the expression of gene cdc-42. The p values were calculated using t-test.

3. Results

3.1. Trigonelline Can Prolong the Lifespan of C. Elegans. To investigate whether trigonelline have anti-aging activity, we treated wild-type N2 worms with 0, 25, 50, 100, and 200 μM of trigonelline, respectively. Our results showed that trigonelline can extend the lifespan of *C. elegans* under various concentrations, among which, 50 μM of trigonelline has the best effect on lifespan extension (Figures 1(b)–1(c)). Lipofuscin is a yellow-brown pigment that accumulates with age [19]. Our results showed that trigonelline could decrease the deposition of lipofuscin (Figure 1(e)). The movement of worms declines as age increases. We found that trigonelline treatment could enhance the movement of worms both at day 5 and day 10 of adulthood (Figure 1(d)).

3.2. Trigonelline Can Enhance the Stress Resistance of C. Elegans. Genetic and dietary interference that extend lifespan usually could also enhance the stress resistance of *C. elegans* [20]. So, we investigated if trigonelline could increase the resistance of *C. elegans* to oxidative, heat, and immune stresses. we detected the changes of ROS content in N2 treated with trigonelline. Trigonelline significantly reduced ROS level in nematodes, and the effect was similar to the antioxidant NAC (Figure 2(d)). Moreover, trigonelline increased the survival rate of N2 worms under oxidative stress induced by 20 mM of paraquat (Figure 2(a)). Trigonelline treatment significantly increased the mRNA and protein expression levels of genes encoding superoxide dismutase 3 (SOD-3) and glutathione S-transferase 4 (GST-4) (Figures 2(b)–2(c)). These results suggest that trigonelline had strong antioxidant effects.

Trigonelline can enhance the survival of *C. elegans* under high temperature of 35°C (Figure 3(a)). Our results showed that trigonelline could increase the mRNA levels of heat shock protein encoding genes, such as *hsp-4*, *hsp-60*, and *hsp-6* (Figure 4(g)). trigonelline treatment could also increase the fluorescence intensity of transgenic nematode strains expressing HSP-4::GFP or HSP-6::GFP (Figures 3(b)–3(d)).

Our results also showed that the survival of N2 nematodes in pathogenic bacteria PA14 was prolonged after being treated with trigonelline for 10 days. Trigonelline treatment increased the mRNA expression levels of immune-related genes, such as *T24B8.5*, *F08G5.6*, *F35E12.5*, *F55G11.4* and *irg-1* (Figures 3(e)–3(f)).

3.3. Trigonelline Can Delay the Progression of Age-Related Diseases in C. Elegans Models of AD, PD, and HD. Neurodegenerative diseases are characterized by chronic and progressive decline in neuronal function, which in turn leads to memory deficits, cognitive decline and motor coordination disorder [21]. These diseases include Alzheimer's disease (AD), Parkinson's disease (PD), Huntington's disease (HD), amyotrophy lateral sclerosis (ALS), and spinal muscular atrophy Disease (SMA).

The worm CL4176 expresses the human polypeptide $A_{\beta 1\text{-}42}$ in the body wall muscle cells at the ambient temperature, resulting in paralysis phenotype of AD-like symptoms in worms. Our results show that trigonelline treatment could delay the onset of paralysis in CL4176 worms (Figure 5(c)). The worm CL2006 also expresses human $A_{\beta 1\text{-}42}$ driven by the promotor of gene *unc-54* that encoding actin filament. Adult of CL2006 onset paralysis and egg-laying deficiency when raised at 20C. Our results showed that the survival of the nematode CL2006 under progressive paralysis were prolonged after trigonelline treatment (Figures 5(d)–5(e)).

Parkinson's disease (PD) model of nematode NL5901 expresses a human α-syn protein fused with yellow fluorescent protein (YFP) in muscle cells of body wall. Trigonelline significantly reduced the α-syn aggregation (Figure 5(a)). Worms BZ555 expresses green fluorescent protein (GFP) in the somatic cells and axons of dopamine neurons. Treatment of *Caenorhabditis elegans* with 6-hydroxydopamine (6-OH DA) can selectively induces dopaminergic neuron degeneration. We found that trigonelline can recover neuron injury induced by 6-OH DA, and its activity is like that of the positive drug levodopa (Figure 5(b)).

Huntington's disease (HD) is a fatal autosomal dominant neurodegenerative disease. Its neuropathological features are progressive lesions in basal ganglia, and its clinical manifestations are abnormal movement, cognition, and behavior. AM140 is a transgenic strain expressing

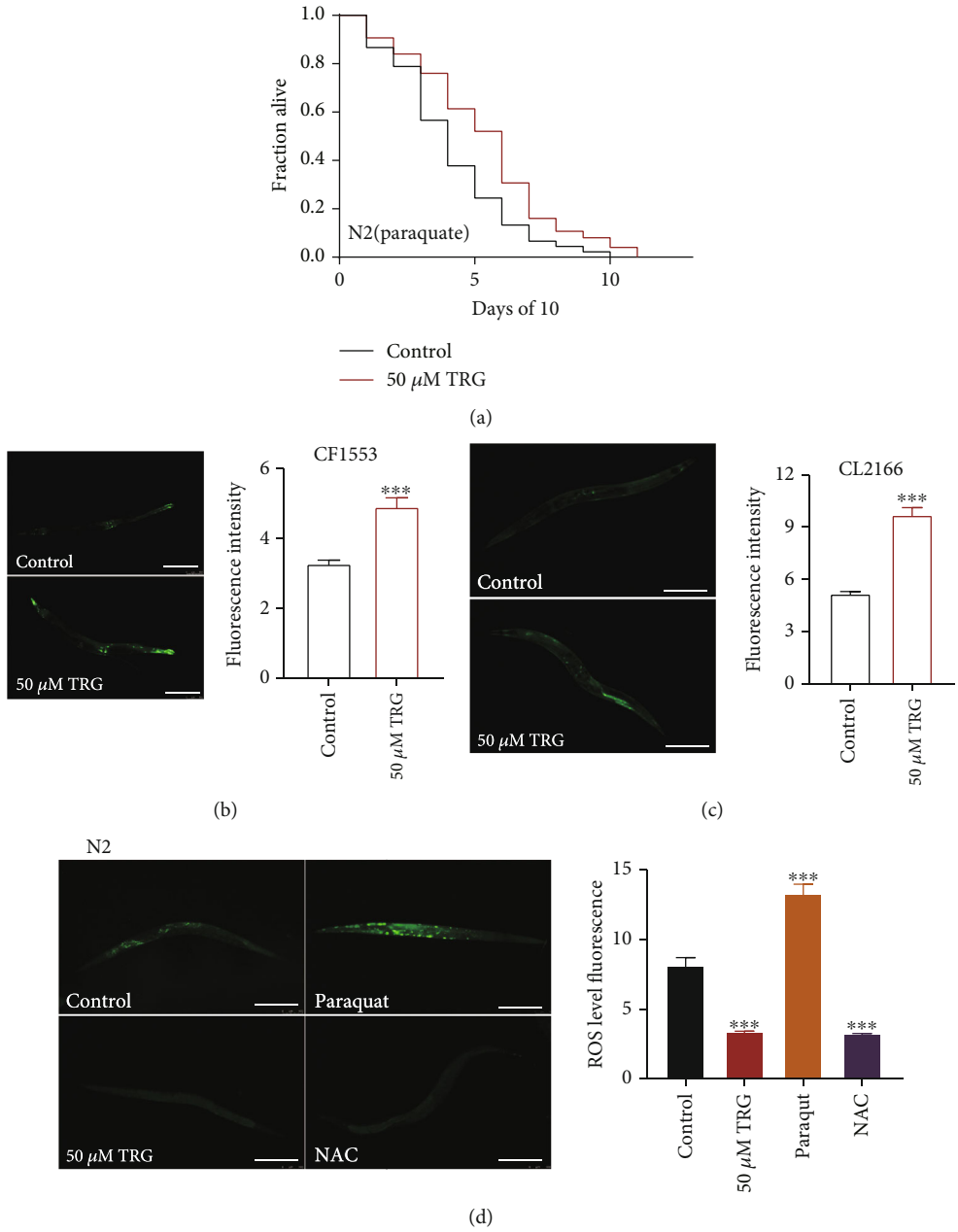

Figure 2: Trigonelline can enhance the oxidative stress resistance of *C. elegans*. The survival percentage of wild-type worms cultured with 20 mM of paraquat under treatment with 50 μM of trigonelline (p <0.001, log-rank test). Statistical details and repeats of these experiments were summarized in Table S6; (B-C) The quantification of fluorescence intensity of SOD-3::GFP in CF1553 and GST-4::GFP in CL2166. Trigonelline significantly increased the expression of SOD-3 and GST-4, Fluorescence intensity was calculated by Image J. The bar chart shows the mean value of three independently repeated experiments, and the error line represents SEM. $***$ represents p <0.001, calculated by two-tailed t-test. Statistical details and repeats of these experiments were summarized in Table S5; (D) ROS content detection of wild type N2 treated with 50 μM of trigonelline, while 10 mM of paraquat and 2 mM of NAC were used as negative control and positive control, respectively. Statistical details and repeats of these experiments were summarized in Table S7.

yellow fluorescent protein (YFP)-labeled polyglutamine (polyQ). We measured the effect of trigonelline on fluorescence intensity and punctate aggregation in AM140. Trigonelline significantly reduced the accumulation of age-related polyQ in body wall muscles on day 2 and day 4 of adults (Figure 5(f)). Above results shows that trigonelline can improve the performance of worms in neurodegenerative diseases models.

3.4. Trigonelline Requires the Transcription Factor DAF-16/FOXO to Extend the Lifespan of C. Elegans. The transcription factor DAF-16/FOXO plays a central role in the regulation of the stress resistance and longevity [22]. So, we examined if trigonelline could extend the lifespan of worms with loss-of-function mutation in *daf-16*. We found that trigonelline could not extend the lifespan of the loss-of-function mutant *daf-16 (mu86) I* (Figure 4(b)).

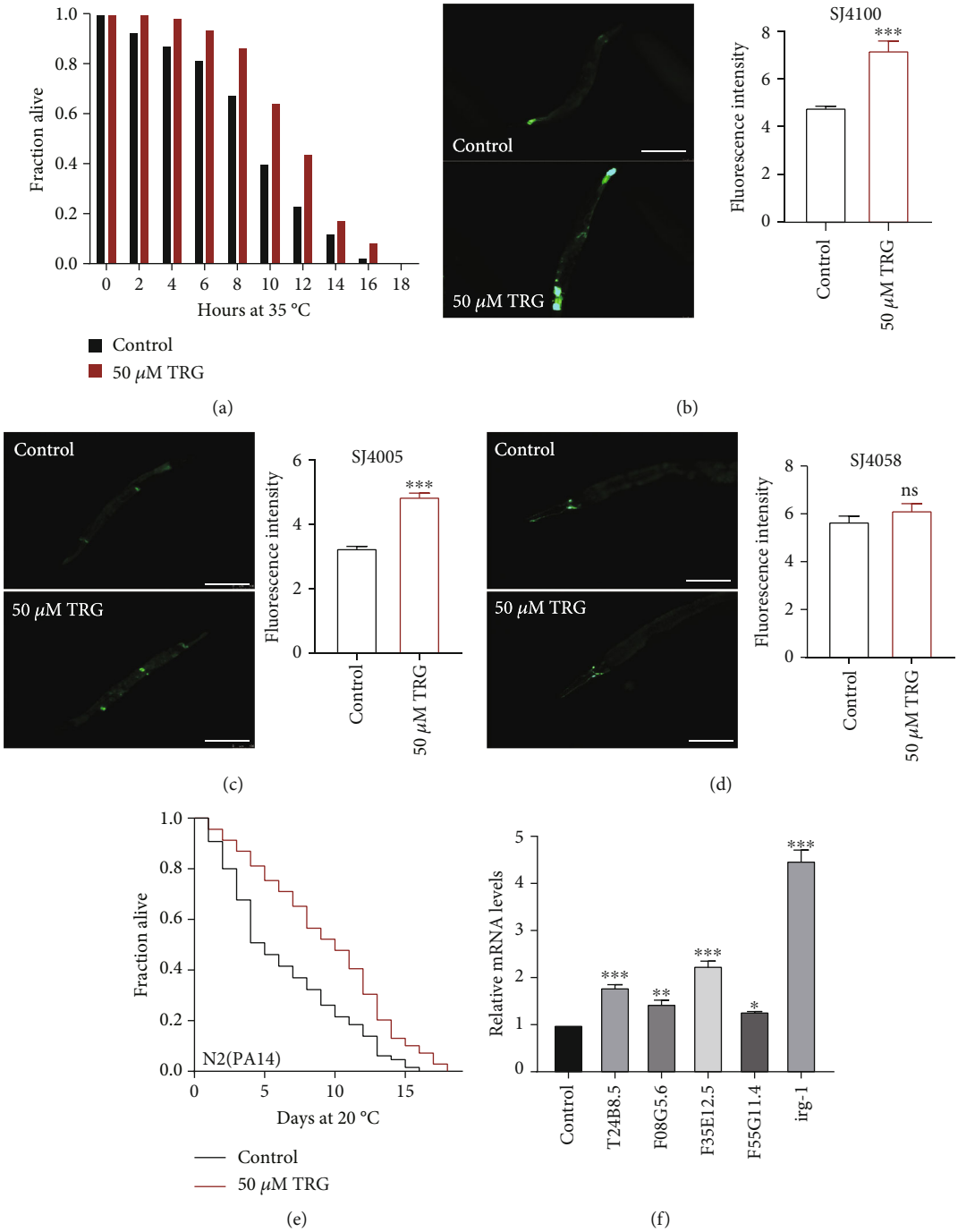

Figure 3: Trigonelline can enhance the ability of nematode to resist heat and pathogenic stresses (a) The survival percentage of wild-type worms treated with or without 50 μM of trigonelline at 35°C ($p < 0.001$), Statistic details and repeats of these experiments were summarized in Table S6; (B-D) The quantification of fluorescence intensity of HSP-6::GFP in SJ4100, HSP-4::GFP in SJ4005,HSP-60::GFP, and in SJ4058. Trigonelline significantly increased the expression of HSP-4 and HSP-6, Fluorescence intensity was calculated by Image J. The bar chart shows the mean value of three independently repeated experiments, and the error line represents SEM. $***$ represents $p < 0.001$, calculated by two-tailed t-test. Statistical details and repeats of these experiments were summarized in Table S5; (E) The survival percentage of wild-type worms cultured with *Pseudomonas aeruginosa* under treatment with 50 μM of trigonelline ($p < 0.001$, log-rank test). Statistical details and repeats of these experiments were summarized in Table S6; (F) Relative Expression of Immune Genes in L4 Wild-type Worm (N2) Treated with 50 μM of trigonelline for 24 h. Statistical details and repeats of these experiments were summarized in Table S9.

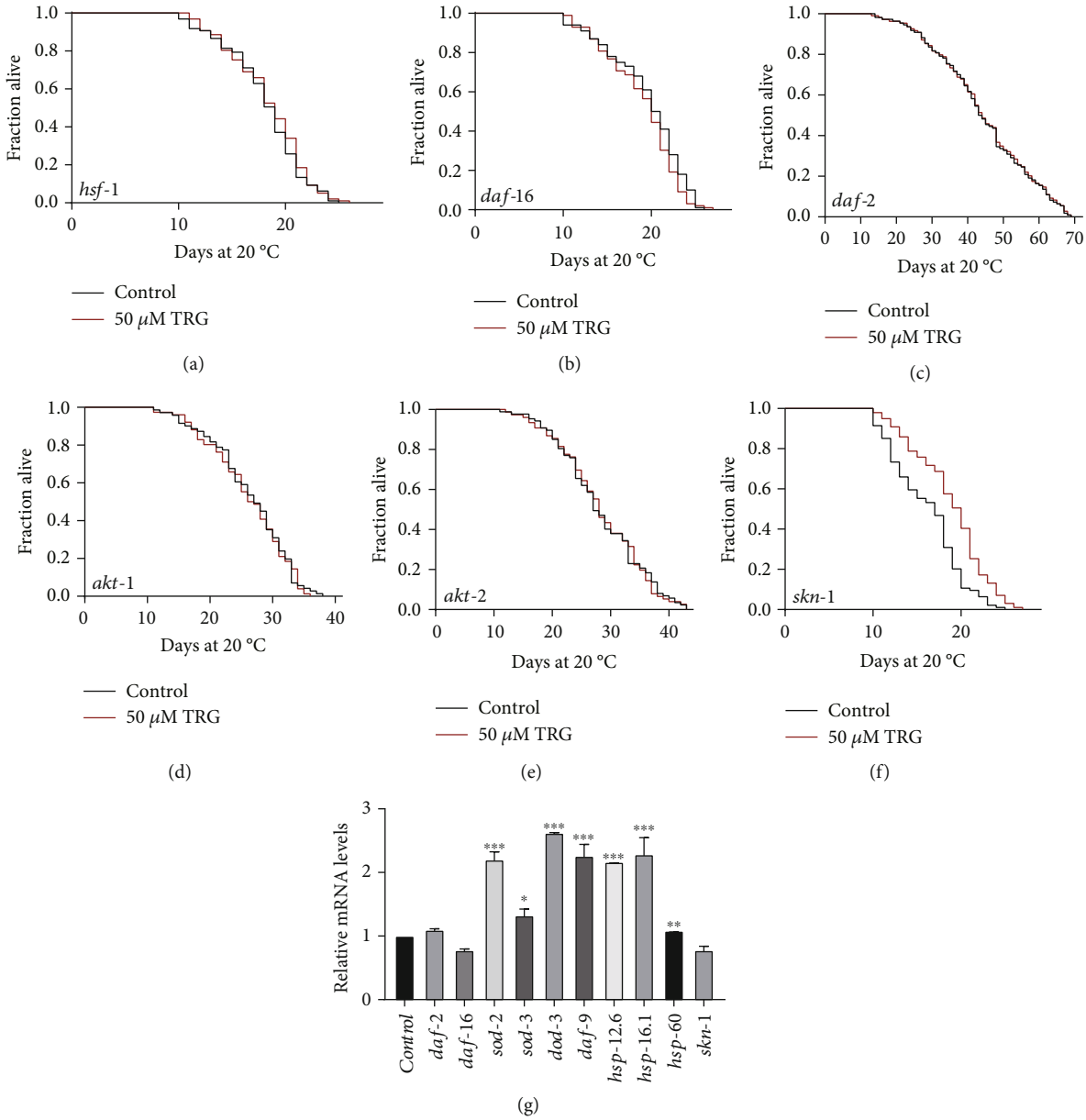

Figure 4: HSF-1 is required for trigonelline to extend nematode lifespan. (A-F) Survival curves of *hsf-1(sy441)I.*, *daf-16(mu86)I.*, *daf-2(e1370)III.*, *akt-1(ok525)V.*, *akt-2(ok393)X.*, and *skn-1(zu67)*, raised at 20°C on NGM plates containing either no trigonelline or 50 μM of trigonelline in lifespan assays ($p > 0.05$). Lifespan was analyzed using Kaplan–Meier analysis and p values were calculated using log-rank test. Statistic details and repeats of these experiments were summarized in Table S4; (G) Relative expression of downstream *daf-2* genes in L4 wild-type worms (N2) treated with 50 μM of trigonelline for 24 h. Statistical details and repeats of these experiments were summarized in Table S9.

The kinases AKT-1 and AKT-2 act at upstream of DAF-16 in the insulin signaling pathway. We found that trigonelline also could not extend the lifespan of worms with loss-of-function mutations in *akt-1* and *akt-2*. (Figures 4(c)–4(e)).

The transcription factor SKN-1 is the homologue of mammalian NF-E2-related factor 2 (Nrf2), plays a central role in the induction of cytoprotective genes in response to oxidative stress [23]. We found that trigonelline could extend the lifespan of worms with a loss-of-function mutation in *skn-1* (Figure 4(f)).

The conserved heat stress transcription factor HSF-1 regulates the expression of cellular chaperone genes to maintain the proteostasis from external environmental stresses and internal age-related damages [24]. We investigated if trigonelline need HSF to extend the lifespan of worms. Our results showed that trigonelline could not extend the lifespan of worms with loss-of-function mutant in *hsf-1* (Figure 4(a)).

3.5. Trigonelline Could Not Further Extend the Lifespan of Worms with Mutations in the Genes Regulating Energy Production and Nutrition Uptake. The decline in

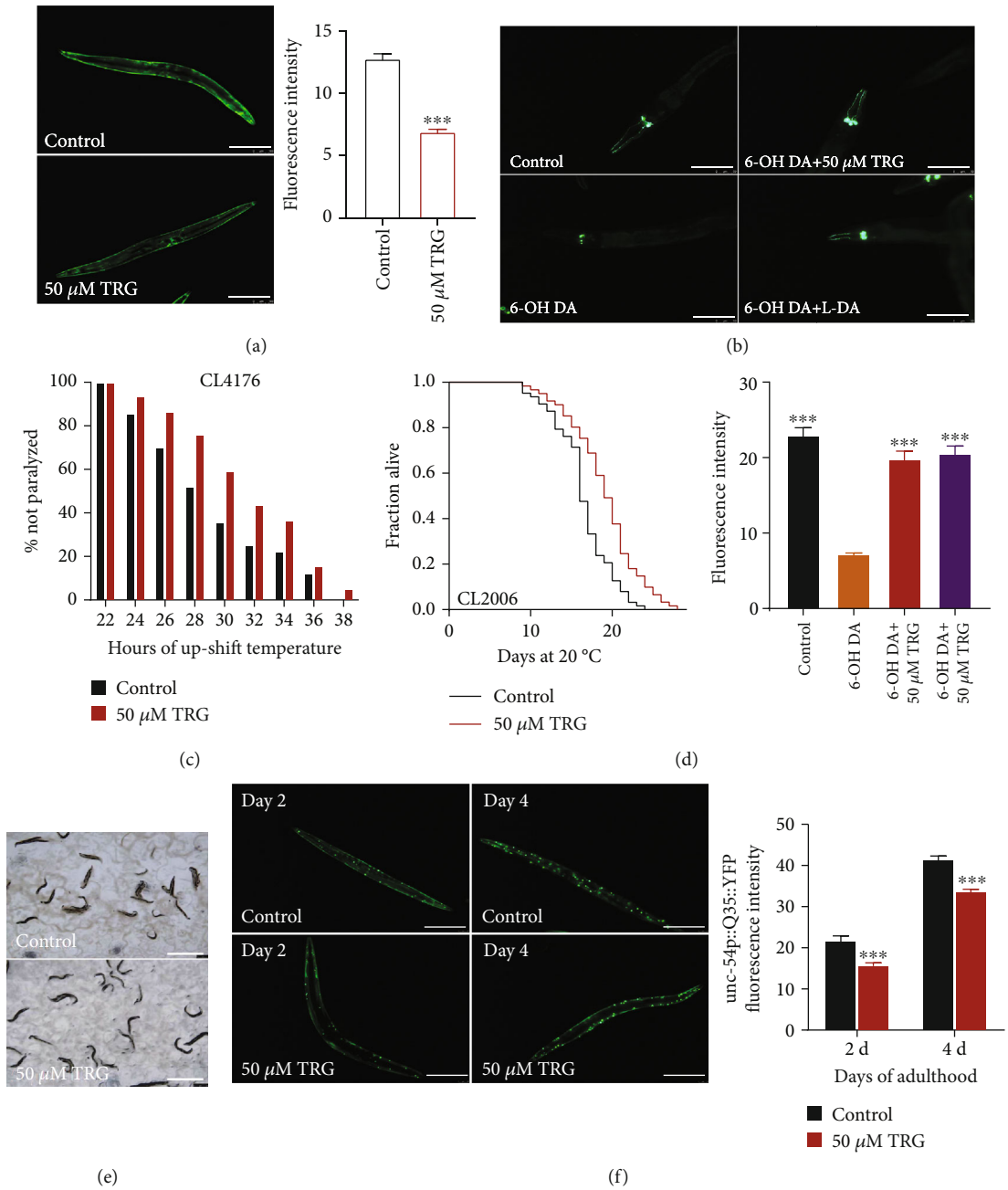

Figure 5: Trigonelline can delay the progression of age-related diseases in *C. elegans* models of AD, PD, and HD Effect of trigonelline on the accumulation of A-synuclein in PD model nematodes; (C-D) Effect of trigonelline on the paralysis rate of AD model in nematode strains CL4176 and CL2006; (E) Effect of trigonelline on the accumulation of Poly-Q in PD model nematodes on day 2 and day 4, Statistical details and repeats of these experiments were summarized in Table S8.

mitochondrial energy production and the damage caused by mitochondrial reactive oxygen species (ROS) are the main causes of aging [25]. The genes involved in mitochondrial electron transport are also the regulators of oxidative stress responses [26]. The gene *clk-1* encodes a mitochondrial enzyme or regulatory molecule in the ubiquinone biosynthetic pathway. The gene *mev-1* encodes a homolog of the C subunit of the human succinate dehydrogenase complex, while *isp-1* encodes the ubiquitin-cytochrome c reductase, the homolog of Rieske iron-sulfur polypeptide 1. We investigated if interruption of these genes would affect the effect of trigonelline on lifespan extension. Our results showed that trigonelline could not extend the lifespan of worms carrying the loss-of-function mutations of the three genes (Figures 6(a)–6(c)).

Dietary restriction can affect a variety of metabolic pathways and stress resistance pathways, including reducing cell damage induced by oxidative stress, improving mitochondrial function, thereby reducing age-related mitochondria function decline [27]. DA1116 *eat-2(ad1116) II.* has slowed pumping rate, mimics dietary restriction phenotypes and presents extended lifespan compared with wild type N2.

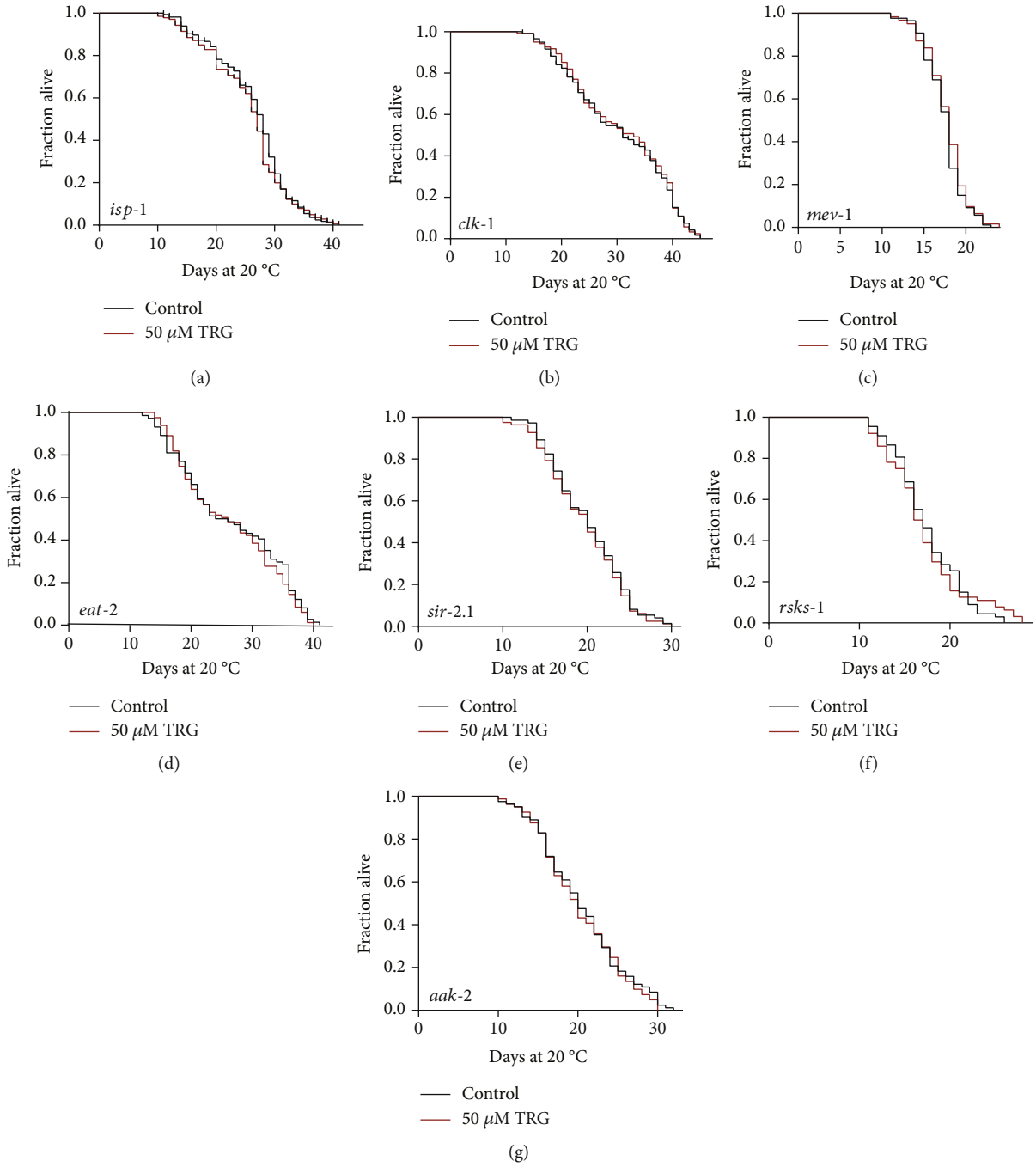

Figure 6: Trigonelline prolongs lifespan through mitochondrial signaling pathways (A-G) Survival curves of *isp-1 (qm150)*, *clk-1(e2519)III.*, and *mev-1(kn1)III.* raised at 20°C on NGM plates containing either no trigonelline or 50 μM trigonelline in lifespan assays ($p > 0.05$). Lifespan was analyzed using Kaplan-Meier analysis and p values were calculated using log-rank test. Statistic details and repeats of these experiments were summarized in Table S4.

We found that trigonelline could not extend the lifespan of DA1116 *eat-2(ad1116) II.*. Dietary restriction regulates the activity of NAD-dependent protein deacetylase SIR-2.1, 5'-AMP-activated protein kinase (AMPK) catalytic subunit 2, and Ribosomal protein S6 kinase beta (encoded by gene *rsks-1*). We found that trigonelline treatment could not extend the lifespan of DA1116 *eat-2(ad1116) II* and worms with loss-of-function mutation in *sir-2*, which encodes NAD-dependent protein deacetylase (Figures 6(d)–6(e)). Gene aak-2 encodes 5'-AMP-activated protein kinase catalytic subunit 2, which plays a role in the regulation of lifespan, dauer larval development and protein secretion. Ribosomal protein S6 kinase beta is a key factor of the target-of-rapamycin (TOR) pathway, regulates nematode lifespan and iron homeostasis. Our experiments show that trigonelline could not extend the lifespan of worms with loss-of-function mutations in genes *aak-2* and *rsks-1* (Figures 6(f)–6(g)).

4. Discussion

Trigonelline, a plant alkaloid, is the main active ingredient of coffee and fenugreek [2, 28]. We found that trigonelline at different concentrations can prolong the lifespan of *C. elegans*. Trigonelline treatment could enhance the locomotor ability of *C. elegans*, reduce the accumulation of lipofuscin in the body. Trigonelline can increase the heat, oxidative, and pathogenic stress resistance of worms. Trigonelline could also delay the progression of age-related diseases in *C. elegans* models of AD, PD, and HD.

The transcription factor DAF-16/FOXO plays a central role in the regulation of the stress resistance and longevity [22]. The kinases AKT-1 and AKT-2 act at upstream of DAF-16 in the insulin signaling pathway [29]. The anti-aging activity of trigonelline requires the transcription factor DAF-16/FOXO. Trigonelline also could not further extend the lifespan of worms with the loss-of-function mutations in *akt-1* and *akt-2*. Since the mutants of *akt-1* and *akt-2* are long-lived, it was uncertain if trigonelline act on the upstream of AKT or the effect of Trigonelline on lifespan extension was not strong enough to show significant difference from the mutants of *akt-1* and *akt-2*. The transcription factor SKN-1plays a central role in the induction of cytoprotective genes in response to oxidative stress [23]. The conserved heat stress transcription factor HSF-1 regulates the expression of cellular chaperone genes to maintain the proteostasis [24]. Both SKN-1 and HSF-1 are the downstream target of DAF-16. Our results showed that trigonelline require HSF-1, but not SKN-1 to extend the lifespan of *C. elegans*, indicating trigonelline might act through stabilizing the proteostasis of *C. elegans*.

We found that trigonelline could not extend the lifespan of the worms with loss-of-function mutations in the genes *clk-1*, *mev-1*, *isp-1*, *eat-2*, *sir-2.1*, *aak-2*, and *rsks-1*. The genes *clk-1*, *mev-1*, and *isp-1* encode mitochondrial proteins regulating energy production, while *eat-2* regulates food uptake. AMPK senses the energy level and passes the information to TOR, which regulates the activity of ribosomal protein S6 kinase beta [27]. TOR is the central energy and nutrition sensor and plays a critical role in growth, metabolism, autophagy, and proteostasis [30]. Above results showed that trigonelline requires *aak-2* and extends the lifespan of *C. elegans* through the energy pathway.

A common etiology of neurodegenerative diseases, such as AD, PD, and HD, is the abnormal deposition of proteins [31]. Our results showed that trigonelline could delay the onset of neurodegenerative diseases in various models of *C. elegans*. Trigonelline could delay the paralysis rate of Alzheimer's disease, reduce the accumulation of α-syn in the worm muscle of Parkinson's model, repair the 6-OH DA-induced neuronal damage, and reduce the accumulation of Poly Q in AM140 worm of Huntington model. These results showed that trigonelline could improve the proteostasis of *C. elegans*. This is consistent with that trigonelline requires HSF-1 and AMPK for anti-aging effects, because both HSF-1 and AMPK could regulate the protein homeostasis of *C. elegans*.

In summary, trigonelline treatment can prolong the healthy lifespan, increase the stress tolerance of *C. elegans*, and delay the development of neurodegenerative diseases in models of nematodes. Finally, trigonelline appear to require transcription factor DAF-16/FOXO, HSF-1 and AMPK to maintain the protein homeostasis and extend the lifespan of *C. elegans*. Our results can be the basis for developing trigonelline-rich products with health benefits, as well as for further research on the pharmacological usage of trigonelline.

Data Availability

All the figures and tables used to support the findings of this study are included within the article and supplementary materials.

Conflicts of Interest

The authors declare that there is no conflict of interest.

Authors' Contributions

Wen-Yu Zeng and Lin Tan have contributed equally to this work.

Acknowledgments

Financial supports were received from the Natural Science Foundation of China (81771516), Central Nervous System Drug Key Laboratory of Sichuan Province (200014-01SZ and 200016-01SZ), Cooperation Project of Luzhou City Hospital of traditional Chinese medicine and Southwest Medical University (2019-LH005), and the Science and Technology Cooperation Project of Luxian and Southwest Medical University (2019LXXNYKD-04).

Supplementary Materials

Table S1. Lifespan of wild-type nematode (N2) treated with TRG in different concentrations. Table S2. Effect of TRG on lipofuscin in wild-type nematode (N2). Table S3. Effect of TRG on body movement in wild-type nematode (N2). Table S4. Effect of TRG on lifespan of mutant nematode. Table S5. Effect of TRG on DAF-16 nuclear localization and expression of HSP-4, HSP-6, HSP-60, GST-4 and SOD-3 in mutant nematode. Table S6. Effect of TRG on resistance to bacteria, high temperature and oxidation in wild-type nematode (N2). Table S7. Effects of TRG on age-related diseases. Table S8. Effect of TRG on gene expression at mRNA level in nematode. Table S9. Primers used for the analysis of mRNA expression levels in nematode. *(Supplementary Materials)*

References

[1] C. López-Otín, M. A. Blasco, L. Partridge, M. Serrano, and G. Kroemer, "The hallmarks of aging," *Cell*, vol. 153, no. 6, pp. 1194–1217, 2013.

[2] S. A. Wani and P. Kumar, "Fenugreek: a review on its nutraceutical properties and utilization in various food products," *Journal of the Saudi Society of Agricultural Sciences*, vol. 17, no. 2, pp. 97–106, 2018.

[3] N. Mohamadi, F. Sharififar, M. Pournamdari, and M. Ansari, "A review on biosynthesis, analytical techniques, and pharmacological activities of trigonelline as a plant alkaloid," *Journal of Dietary Supplements*, vol. 15, no. 2, pp. 207–222, 2018.

[4] K. Pravalika, D. Sarmah, H. Kaur et al., "Trigonelline therapy confers neuroprotection by reduced glutathione mediated myeloperoxidase expression in animal model of ischemic stroke," *Life Sciences*, vol. 216, pp. 49–58, 2019.

[5] Z. Qiu, K. Wang, C. Jiang et al., "Trigonelline protects hippocampal neurons from oxygen-glucose deprivation- induced injury through activating the PI3K/Akt pathway," *Chemico-Biological Interactions*, vol. 317, p. 108946, 2020.

[6] S. Ilavenil, D. H. Kim, Y. I. Jeong et al., "Trigonelline protects the cardiocyte from hydrogen peroxide induced apoptosis in H9c2 cells," *Asian Pacific Journal of Tropical Medicine*, vol. 8, no. 4, pp. 263–268, 2015.

[7] A. N. Lone, A. T. Malik, H. S. Naikoo, R. S. Raghu, and S. A. Tasduq, "Trigonelline, a naturally occurring alkaloidal agent protects ultraviolet-B (UV-B) irradiation induced apoptotic cell death in human skin fibroblasts via attenuation of oxidative stress, restoration of cellular calcium homeostasis and prevention of endoplasmic reticulum (ER) stress," *Journal of Photochemistry and Photobiology. B*, vol. 202, p. 111720, 2020.

[8] H. Omidi-Ardali, Z. Lorigooini, A. Soltani, S. Balali-Dehkordi, and H. Amini-Khoei, "Inflammatory responses bridge comorbid cardiac disorder in experimental model of IBD induced by DSS: protective effect of the trigonelline," *Inflammopharmacology*, vol. 27, no. 6, pp. 1265–1273, 2019.

[9] M. Pournamdari, A. Mandegary, F. Sharififar et al., "Anti-inflammatory subfractions separated from acidified chloroform fraction of Fenugreek Seeds (Trigonella foenum-graecumL.)," *Journal of Dietary Supplements*, vol. 15, no. 1, pp. 98–107, 2018.

[10] M. Khalili, M. Alavi, E. Esmaeil-Jamaat, T. Baluchnejadmojarad, and M. Roghani, "Trigonelline mitigates lipopolysaccharide-induced learning and memory impairment in the rat due to its anti-oxidative and anti-inflammatory effect," *International Immunopharmacology*, vol. 61, pp. 355–362, 2018.

[11] O. Yoshinari, H. Sato, and K. Igarashi, "Anti-diabetic effects of pumpkin and its components, trigonelline and nicotinic acid, on Goto-Kakizaki rats," *Bioscience, Biotechnology, and Biochemistry*, vol. 73, no. 5, pp. 1033–1041, 2009.

[12] A. E. van Dijk, M. R. Olthof, J. C. Meeuse, E. Seebus, R. J. Heine, and R. M. van Dam, "Acute effects of decaffeinated coffee and the major coffee components chlorogenic acid and trigonelline on glucose tolerance," *Diabetes Care*, vol. 32, no. 6, pp. 1023–1025, 2009.

[13] H. V. Kamble and S. L. Bodhankar, "Antihyperglycemic activity of trigonelline and sitagliptin in nicotinamide- streptozotocin induced diabetes in Wistar rats," *Biomed Agiicine andng Pathology*, vol. 3, no. 3, pp. 125–130, 2013.

[14] A. D. Nugrahini, M. Ishida, T. Nakagawa, K. Nishi, and T. Sugahara, "Trigonelline: an alkaloid with anti-degranulation properties," *Molecular Immunology*, vol. 118, pp. 201–209, 2020.

[15] J. C. Liao, K. T. Lee, B. J. You et al., "Raf/ERK/Nrf 2 signaling pathway and MMP-7 expression involvement in the trigonelline-mediated inhibition of hepatocarcinoma cell migration," *Food & Nutrition Research*, vol. 59, no. 1, article e29884, 2015.

[16] A. Arlt, S. Sebens, S. Krebs et al., "Inhibition of the Nrf2 transcription factor by the alkaloid trigonelline renders pancreatic cancer cells more susceptible to apoptosis through decreased proteasomal gene expression and proteasome activity," *Oncogene*, vol. 32, no. 40, pp. 4825–4835, 2013.

[17] M. Lu, L. Tan, X. G. Zhou et al., "Secoisolariciresinol diglucoside delays the progression of aging-related diseases and extends the lifespan of Caenorhabditis elegans via DAF-16 and HSF-1," *Oxidative Medicine and Cellular Longevity*, vol. 2020, Article ID e1293935, 2020.

[18] C. Rety, R. Gilbin, and E. Gomez, "Induction of reactive oxygen species and algal growth inhibition by tritiated water with or without copper," *Environmental Toxicology*, vol. 27, no. 3, pp. 155–165, 2012.

[19] N. Sitte, M. Huber, T. Grune et al., "Proteasome inhibition by lipofuscin/ceroid during postmitotic aging of fibroblasts," *FASEB Journal*, vol. 14, no. 11, pp. 1490–1498, 2000.

[20] D. E. Shore, C. E. Carr, and G. Ruvkun, "Induction of cytoprotective pathways is central to the extension of lifespan conferred by multiple longevity pathways," *PLoS Genetics*, vol. 8, no. 7, article e1002792, 2012.

[21] B. N. Dugger and D. W. Dickson, "Pathology of neurodegenerative diseases," *Cold Spring Harbor Perspectives in Biology*, vol. 9, no. 7, p. a028035, 2017.

[22] G. Murtaza, A. K. Khan, R. Rashid, S. Muneer, S. M. F. Hasan, and J. Chen, "FOXO transcriptional factors and long-term living," *Oxidative Medicine and Cellular Longevity*, vol. 2017, 8 pages, 2017.

[23] J. Tullet, J. W. Green, C. Au et al., "The SKN-1/Nrf2 transcription factor can protect against oxidative stress and increase lifespan inC. elegansby distinct mechanisms," *Aging Cell*, vol. 16, no. 5, pp. 1191–1194, 2017.

[24] W. C. Chiang, T. T. Ching, H. C. Lee, C. Mousigian, and A. L. Hsu, "HSF-1 regulators DDL-1/2 link insulin-like signaling to heat-shock responses and modulation of longevity," *Cell*, vol. 148, no. 1-2, pp. 322–334, 2012.

[25] G. Barja, "Updating the mitochondrial free radical theory of aging: an integrated view, key aspects, and confounding concepts," *Antioxidants & Redox Signaling*, vol. 19, no. 12, pp. 1420–1445, 2013.

[26] S. Yanase, K. Yasuda, and N. Ishii, "Adaptive responses to oxidative damage in three mutants of _Caenorhabditis elegans_ (_age-1_ , _mev-1_ and _daf-16_) that affect life span," *Mechanisms of Ageing & Development*, vol. 123, no. 12, pp. 1579–1587, 2002.

[27] H. J. Weir, P. Yao, F. K. Huynh et al., "Dietary restriction and AMPK increase lifespan via mitochondrial network and peroxisome remodeling," *Cell Metabolism*, vol. 26, no. 6, pp. 884–896.e5, 2017.

[28] J. Zhou, L. Chan, and S. Zhou, "Trigonelline: a plant alkaloid with therapeutic potential for diabetes and central nervous system disease," *Current Medicinal Chemistry*, vol. 56, pp. 333–345, 2012.

[29] C. T. Murphy and P. J. Hu, "Insulin/insulin-like growth factor signaling in *C. elegans*," *Worm Book*, vol. 26, pp. 1–43, 2013.

[30] S. C. Johnson, P. S. Rabinovitch, and M. Kaeberlein, "mTOR is a key modulator of ageing and age-related disease," *Nature*, vol. 493, no. 7432, pp. 338–345, 2013.

[31] A. Kurtishi, B. Rosen, K. S. Patil, G. W. Alves, and S. G. Møller, "Cellular proteostasis in neurodegeneration," *Molecular Neurobiology*, vol. 56, no. 5, pp. 3676–3689, 2019.

Hindawi
Oxidative Medicine and Cellular Longevity
Volume 2021, Article ID 7726058, 15 pages
https://doi.org/10.1155/2021/7726058

Research Article

Peroxisome Deficiency Dysregulates Fatty Acid Oxidization and Exacerbates Lipotoxicity in β Cells

Hongbo Guan, Yanyan Guo, Liangliang Zhu, Yisheng Jiao, and Xiaomei Liu

Key Laboratory of Maternal-Fetal Medicine of Liaoning Province, Department of Obstetrics and Gynecology, Shengjing Hospital of China Medical University, Shenyang 110004, China

Correspondence should be addressed to Yisheng Jiao; shengjing2019@yeah.net and Xiaomei Liu; liuxm@cmu.edu.cn

Received 26 April 2021; Revised 1 August 2021; Accepted 6 August 2021; Published 23 August 2021

Academic Editor: Cecile Jacovetti

An adverse intrauterine environment impairs the development of pancreatic islets in the fetus and leads to insufficient β cell mass and β cell dysfunction. We previously reported that Pex14, a peroxin protein involved in the biogenesis and degradation of peroxisomes, is markedly reduced in the pancreas of an intrauterine growth restriction fetus and last into adulthood. Peroxisomes function in a wide range of metabolic processes including fatty acid oxidization, ROS detoxification, and anti-inflammatory responses. To elucidate the impact of downregulation of the Pex14 gene on β cell, Pex14 was knocked down by siRNA in INS-1 cells. Pex14 knockdown disturbed peroxisomal biogenesis and dysregulated fatty acid metabolism and lipid storage capability, thereby increased ROS level and blunted insulin secretion. Moreover, Pex14 knockdown upregulated inflammation factors and regulators of endoplasmic reticulum stress. The lipotoxicity of fatty acid (including palmitic acid and linoleic acid) in β cells was exacerbated by knockdown of Pex14, as indicated by H_2O_2 accumulation and increased programmed cell death. The present results demonstrate the vital role of Pex14 in maintaining normal peroxisome function and β cell viability and highlight the importance of a functional peroxisomal metabolism for the detoxification of excess FAs in β cells.

1. Introduction

The peroxisome is an organelle with multiple biological functions that is widely present in mammalian cells. Human peroxisomes contain more than 80 proteins that can be divided into two categories. The first is constitutive proteins, called peroxins (PEX), which interact with each other and participate in peroxisome biogenesis, division, and proliferation. The second class comprises metabolic, oxidative, and antioxidant enzymes (around 50 in mammals), which are critical for the maintenance of cellular homeostasis and activity [1, 2]. Peroxisomes are involved in a wide variety of metabolic pathways such as β-oxidization of very-long-chain fatty acids (VLCFAs), α-oxidization and β-oxidization of long branched-chain fatty acids (FAs), phospholipid synthesis, reactive oxygen species (ROS) metabolism, and anti-inflammatory functions [3–5]. PEX gene mutations cause defects in peroxisome production and loss of mature peroxisomes, leading to a group of diseases known as peroxisomal biogenesis disease [2]. The underlying pathological mechanism involves impaired oxidization of VLCFAs, which accumulate in the cytoplasm, affecting cell function and embryo development [6, 7]. In addition, the peroxisome can produce ROS and reactive nitrogen species (RNS), as well as remove ROS/RNS. The imbalance between the two processes causes oxidative stress (OS) [8].

Type 2 diabetes (T2D) is a multifactorial disease caused by genetic and environmental factors. Dysfunction of β cells is one of the main processes involved in the pathogenesis of T2D [9]. One important mechanism underlying β cell dysfunction is glucose and FFA toxic action-induced OS. OS results in glucose intolerance, inhibits insulin secretion and activity, and promotes the onset of T2D [10, 11]. Epidemiological studies show that intrauterine growth restriction (IUGR) increases the susceptibility to adult T2D, owing to the maldevelopment of islets and β cell dysfunction [12, 13]. In a previous study, we used a rat model to demonstrate the aberrant expression of pancreatic peroxisome factors in

the IUGR fetus induced by malnutrition in utero [14]. Pex14, a peroxisome marker protein involved in the biogenesis and degradation of peroxisomes [15], was markedly reduced in the fetal pancreas that persist into adulthood. Another downregulated protein was Pex3, an integral membrane protein involved in peroxisome biogenesis by interacting directly with Pex16 and 19 that contributes to peroxisome membrane protein (PMP) protein import [16]. Acyl-CoA oxidase (Acox) 1 and peroxisomal 17β-hydroxysteroid dehydrogenase type 4 (Hsd17b4), which are rate-limiting enzymes in FA β-oxidation (FAO), were downregulated, and this was accompanied by activation of OS in the IUGR fetus. Therefore, we hypothesized that downregulation of Pex14 impairs peroxisome biogenesis and function, leading to β cell dysfunction.

In this study, using siRNA to knock down the expression of Pex14, we found that downregulation of Pex14 induced β cell death and damaged insulin secretion function by affecting multiple proteins involved in peroxisome biogenesis, FAO, and ROS scavenging, subsequently leading to cell autophagy and apoptosis. These results suggest that the downregulation of Pex14, at least partly, lead to pancreatic dysplasia in IUGR offspring.

2. Materials and Methods

2.1. Cell Culture and Transfection. The rat INS-1 cell line was purchased from the Type Culture Collection Center of Chinese Academy of Science (Shanghai, China). Cells were cultured in 1640 medium containing 10% fetal bovine serum and 100 U/ml penicillin-streptomycin and maintained at 37°C under 5% CO_2. The sequences of siRNAs targeting rat Pex14 and a negative control (NC) are shown in Table S1. siRNAs were transfected into INS-1 cells using the siRNA transfection reagent INTERFERin (Polyplus 409-10), according to the manufacturer's manual. At 24 h after transfection, the cells were incubated with the saturated FA palmitic acid (PA) or the unsaturated FA linoleic acid (LA) at concentrations of 30 μM and 10 μM, respectively, for 24 hours. The cell media were then changed to basal media, and cells were collected for subsequent experiments.

2.2. RNA Isolation and q-PCR. Total RNA was extracted using the TRIzol reagent (Invitrogen) according to the manufacturer's protocol. cDNA was obtained with the Reverse Transcription System (Takara, Dalian, China). q-PCR was performed using a SYBR Green PCR Kit (Vazyme, Q711-02, Nanjing, China) on a 7500 Fast system (Applied Biosystems). Data were analyzed using the relative quantification ($2^{-\Delta\Delta Ct}$) method with β-actin as the endogenous control. Primer sequences are listed in Table S1.

2.3. Western Blot Analysis. INS-1 cells were lysed in SDT buffer (4% sodium dodecyl sulfate (SDS), 1 mM dithiothreitol, 150 mM Tris-HCl, and pH 8.0), and protein content was quantified with the BCA method. Equal amounts of protein were separated by 12% (w/v) SDS–PAGE and transferred to a polyvinylidene difluoride membrane. The membrane was cut into several strips, blocked in TBS-Tween-20 containing 5% (w/v) skimmed milk for 2 h at room temperature, and incubated with the indicated primary antibodies (Table S2) overnight at 4°C. The membrane was then incubated with secondary antibodies and visualized using a commercial enhanced chemiluminescence detection kit (Millipore, USA). Gel-Pro Analyzer software was used for quantification of immunoblots.

2.4. Apoptosis Analysis. After siRNA transfection, cells were collected for apoptosis assays with an Annexin V-FITC Apoptosis Kit (Vazyme, Nanjing, China). Cells were washed with PBS and resuspended in 500 μL of binding buffer. Subsequently, 5 μL of Annexin V-FITC and 5 μL of propidium iodide (PI) were added into the cell suspension and incubated at room temperature for 15 min in the dark. The apoptosis rate of cells in each group was measured using a BD FACSCalibur flow cytometer.

2.5. Cell Counting Kit-8 Assay. Cell viability was measured using the Cell Counting kit-8 (CCK8) assay. Briefly, INS-1 cells (5×10^3 cells/well) were seeded into 96-well plates. At 24 h after transfection, cells were incubated in 10% CCK8 solution (Vazyme) at 37°C for 2 h until visual color conversion occurred. The absorbance at 450 nm was measured using a microplate spectrophotometer (BioTek Instruments, Winooski, VT, USA).

2.6. Autophagy Detection. Autophagic flux was analyzed using the Cyto-ID® Autophagy Detection Kit (Enzo Life Sciences, ENZ-51031-K200) in INS-1 cells. Briefly, after treatment with LA or PA for 2 h, cells (1×10^6 cells/mL) were incubated with Cyto-ID Green Detection Reagent (1 μL/mL) adding in culture medium for 30 min at 37°C and 5% CO_2 in the dark. Images were taken with a Nikon inverted microscope at 200x amplification.

2.7. Cellular ROS Detection. Intracellular ROS were detected with fluorescent probes 5-(and-6)-chloromethyl-2-,7-dichlorofluorescin diacetate (DCFH-DA, indicator of H_2O_2). INS-1 cells were harvested and incubated DCFH-DA (10 μM, 30 min) at 37°C in the dark, according to the manufacturer's protocol. For fluorescence quantitative analysis, the cells were collected and analyzed by flow cytometry. At least 10,000 events were analyzed.

2.8. Immunofluorescence (IF) and Nile Red Staining. INS-1 cells were fixed for 15 min with ice-cold 4.0% paraformaldehyde and then permeabilized with 0.2% Triton X-100 for 30 min. IF staining was performed by incubating cells with the indicated primary antibodies (Table S2) at 4°C overnight, and then labeled with fluorescence conjugated anti-rabbit or anti-mouse IgG (Invitrogen, A11029 and A11036, respectively) at 37°C for 60 min, followed by nuclear staining with DAPI. Images were captured with a laser scanning confocal microscopy at the same magnification, ×400. Intracellular lipid droplets were observed with Nile Red staining (0.1 μmol/mL). Images were acquired with the confocal microscopy with magnification of 200x.

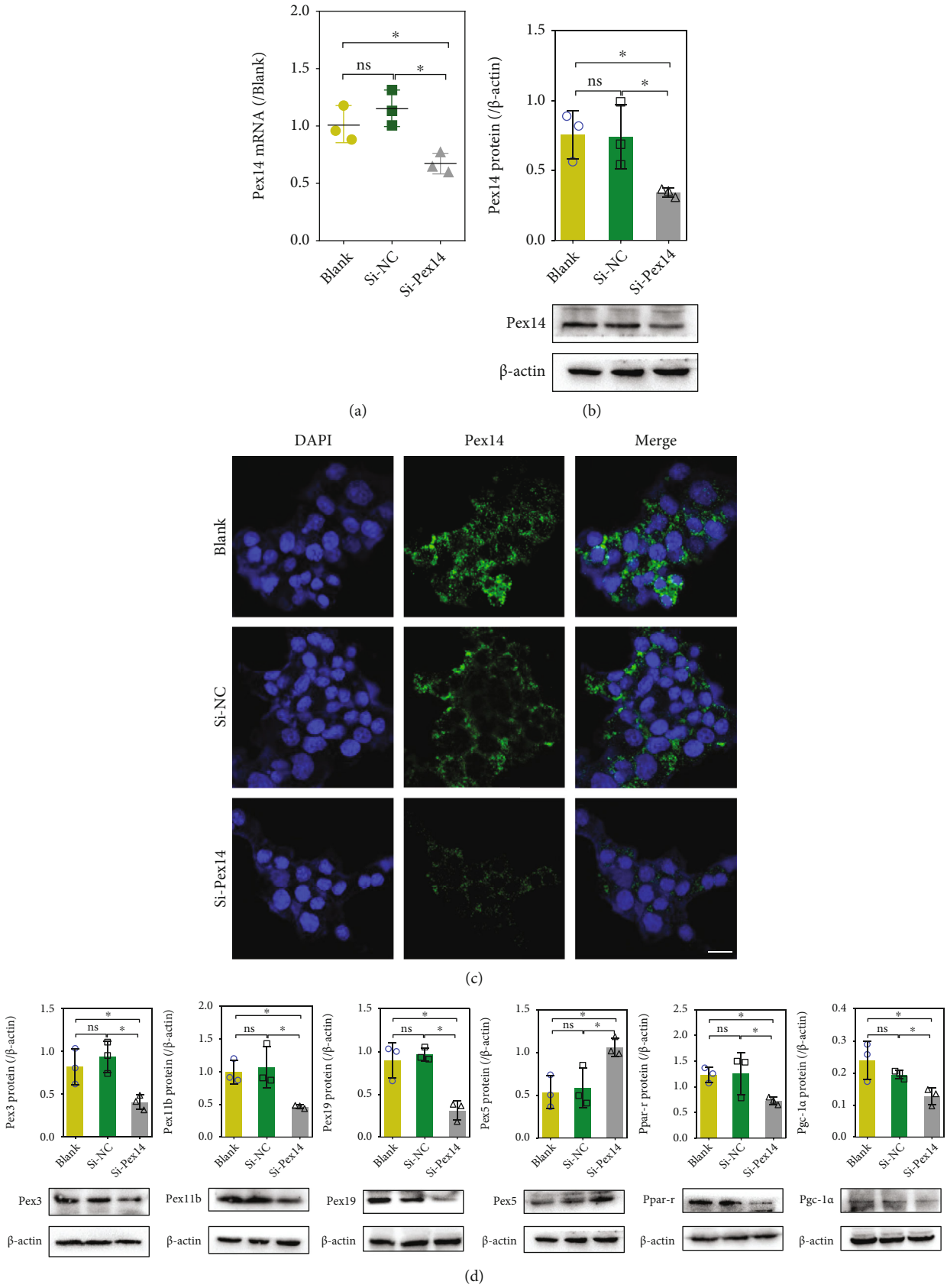

Figure 1: Continued.

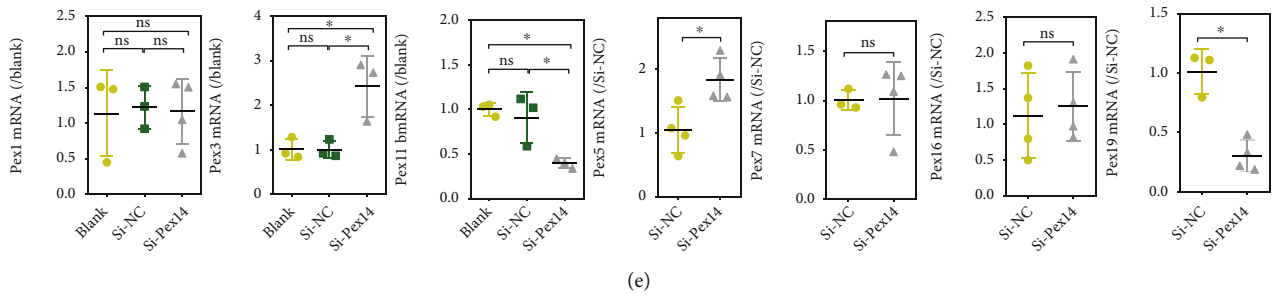

Figure 1: Knockdown (KD) of Pex14 causes defective expression of peroxins implicated in peroxisome biogenesis and degradation. (a, b) Knockdown efficiency of INS-1 cells transfected with si-Pex14 or si-NC was examined by q-PCR (a) and western blotting (b). (c) Representative IF photomicrographs of Pex14 in INS-1 cells (×800 magnification, scale bar 100 μm). (d, e) The expression of peroxins and the transcription factors that regulate peroxins was detected by western blot (d) or q-PCR (e). $n = 3$-4; error bars indicate SD. $^*p < 0.05$, vs. the blank or si-NC group.

2.9. Glucose-Stimulated Insulin Secretion (GSIS) Experiment. INS-1 cells were incubated in Krebs-Ringer buffer (KRB, 4.7 mM KCl, 115 mM NaCl, 1.2 mM $MgSO_4$, 0.5 mM NaH_2PO_4, 1.5 mM $CaCl_2$, 2.5 mM $NaHCO_3$, 0.1% BSA, and pH 7.4) containing 2.5 mmol/L glucose (basal secretion) or KRB buffer containing 20 mmol/L glucose (stimulatory) for 1 h. An aliquot of the medium was collected for assay of insulin with an ELISA kit (CUSABIO, China) according to the manufacturer's protocol.

2.10. Statistical Analysis. Results are presented as the mean ± standard deviation of the mean (SD) from at least three separate experiments. Differences between two groups were analyzed with the unpaired Student two-tailed t-test, and one-way ANOVA was used for comparison of more than two groups. $p < 0.05$ was considered statistically significant.

3. Results

3.1. Pex14 Knockdown Alters Peroxin Expression and Induces Peroxisomal Deficiency in INS-1 Cells. INS-1 cells transfected with siRNA against Pex14 showed up to 55% reduction of Pex14 expression compared with scrambled siRNA-transfected cells (Figures 1(a) and 1(b)). The observation that si-NC did not decrease Pex14 expression confirmed that the silencing was specific. IF staining also confirmed that Pex14 were downregulated in si-Pex14 INS-1 cells (Figure 1(c)). Pex14 KD significantly downregulated the protein expression of Pex3, Pex5, Pex19, and Pex11b (Figure 1(d)). q-PCR assays revealed a decrease in the mRNA level of Pex11b and 19, consistent with the protein data. The mRNA level of Pex1, Pex7, and Pex16 were not affected. In contrast, the mRNA level of Pex3 and Pex5 was upregulated by Pex14 KD which was inconsistent with the protein data (Figure 1(e)). We speculate that the increased mRNA expression might be a feedback response to the decreased protein amount. It is interested to find that the transcription factors that regulate peroxisome proliferation, Ppar-γ and its coactivator Pgc-1α, were both diminished after Pex14 KD (Figure 1(d)).

3.2. Fatty Acid Metabolism in Pex14 KD Cells. q-PCR assay showed that Pex14 KD lead to different variation tendencies in the mRNA level of peroxisome FAO enzymes. Regarding Acox isozymes, Acox1 was downregulated and Acox3 was upregulated, whereas the heterodimer Acox2 was unaffected. The mRNA level of Mfe1 was also unchanged, while 3-ketoacyl-CoA thiolase A (Acaa1a) was decreased (Figure 2(a)). Western blot analysis showed that the protein expression of Hsd17b4 and Abcd3 *was upregulated*, while carnitine palmitoyltransferase-1A (Cpt1a), was decreased in Pex14 KD cells (Figure 2(b)). IF staining demonstrated the enhanced expression of Fasn(Figure 2(c)). Nile Red staining showed that Pex14 KD caused a slight increase in lipid droplets in INS-1 cells compared with the si-NC group. After exposure to PA, Pex14 KD led to much higher predisposition to fat accumulation compared with the si-NC group (Figure 2(d)).

3.3. ROS Detoxification and Proinflammatory Factors in Pex14 KD Cells. Western blot analysis showed a decrease in the protein expression of antioxidant catalase (CAT) and Sod2 and an increase in Sod3 protein level. q-PCR assay also demonstrated a decrease in mRNA level of Sod2 and CAT. Prdx5, an antioxidant localized in peroxisomes and mitochondria, was unchanged in the mRNA level (Figures 3(a)–3(c)). We further investigated ROS levels in Pex14 KD cells with DCFH-DA. As shown in Figure 3(d), Pex14 silencing caused a marginal increase in H_2O_2 in INS-1 cells. Moreover, H_2O_2 was markedly increased upon exposure to LA in Pex14 KD cells, whereas LA exposure showed no significant effect on H_2O_2 in the blank and si-NC cells. Exposure to PA led to a moderate increase in ROS in blank cells compared with the LA exposure groups, whereas in Pex14 KD cells, PA exposure caused a less increase in ROS levels than LA exposure.

ROS play a critical role in the signaling cascade of inflammatory factors and endoplasmic reticulum stress (ERS). Therefore, we examined the OS/inflammatory response in Pex14 KD cells. As shown in Figure 4(a), Tnf-α and IL-6 mRNA level was significantly enhanced in Pex14 KD cultures. Atf6 and spliced-Xbp1 mRNA levels were also increased

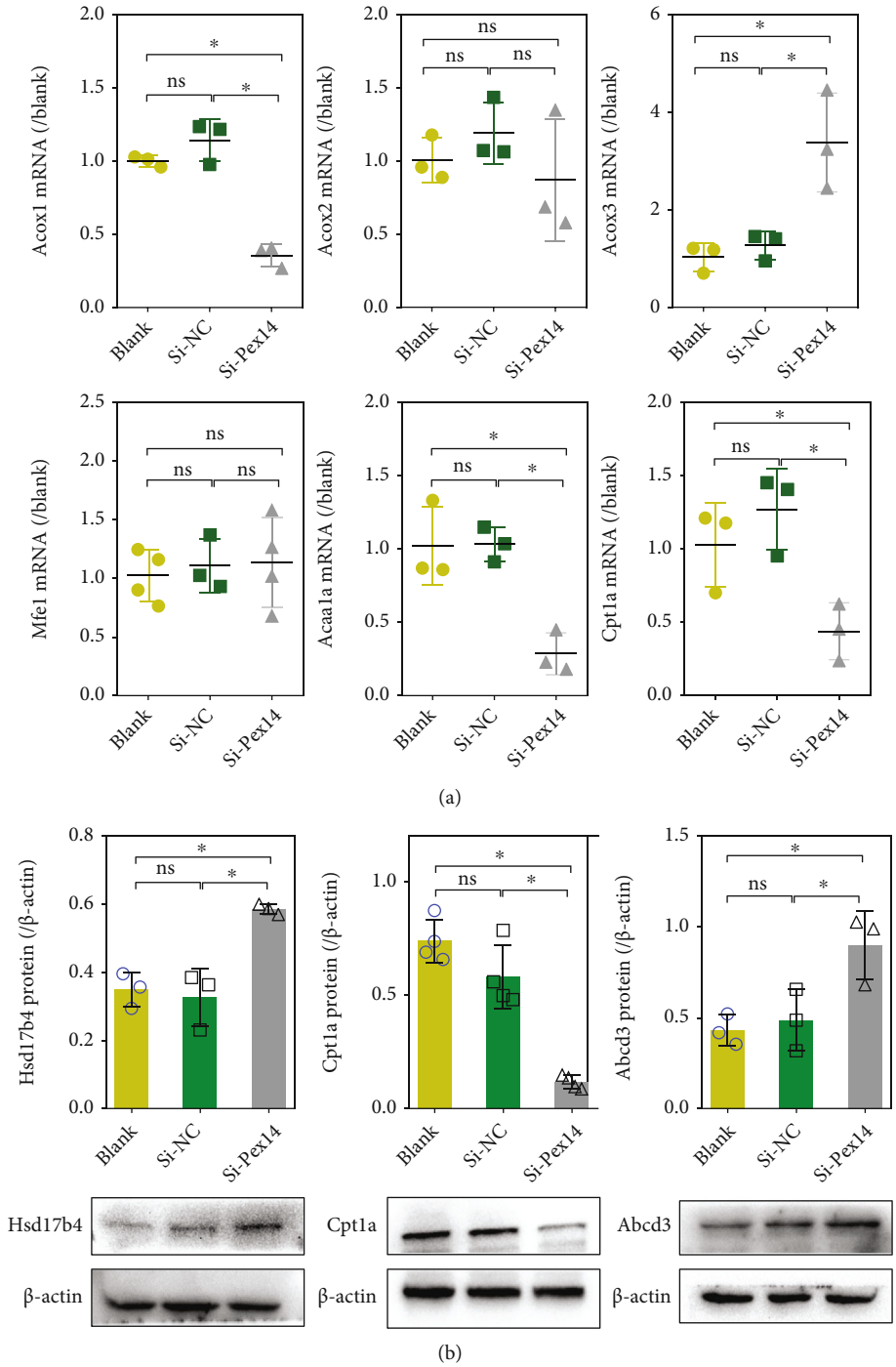

Figure 2: Continued.

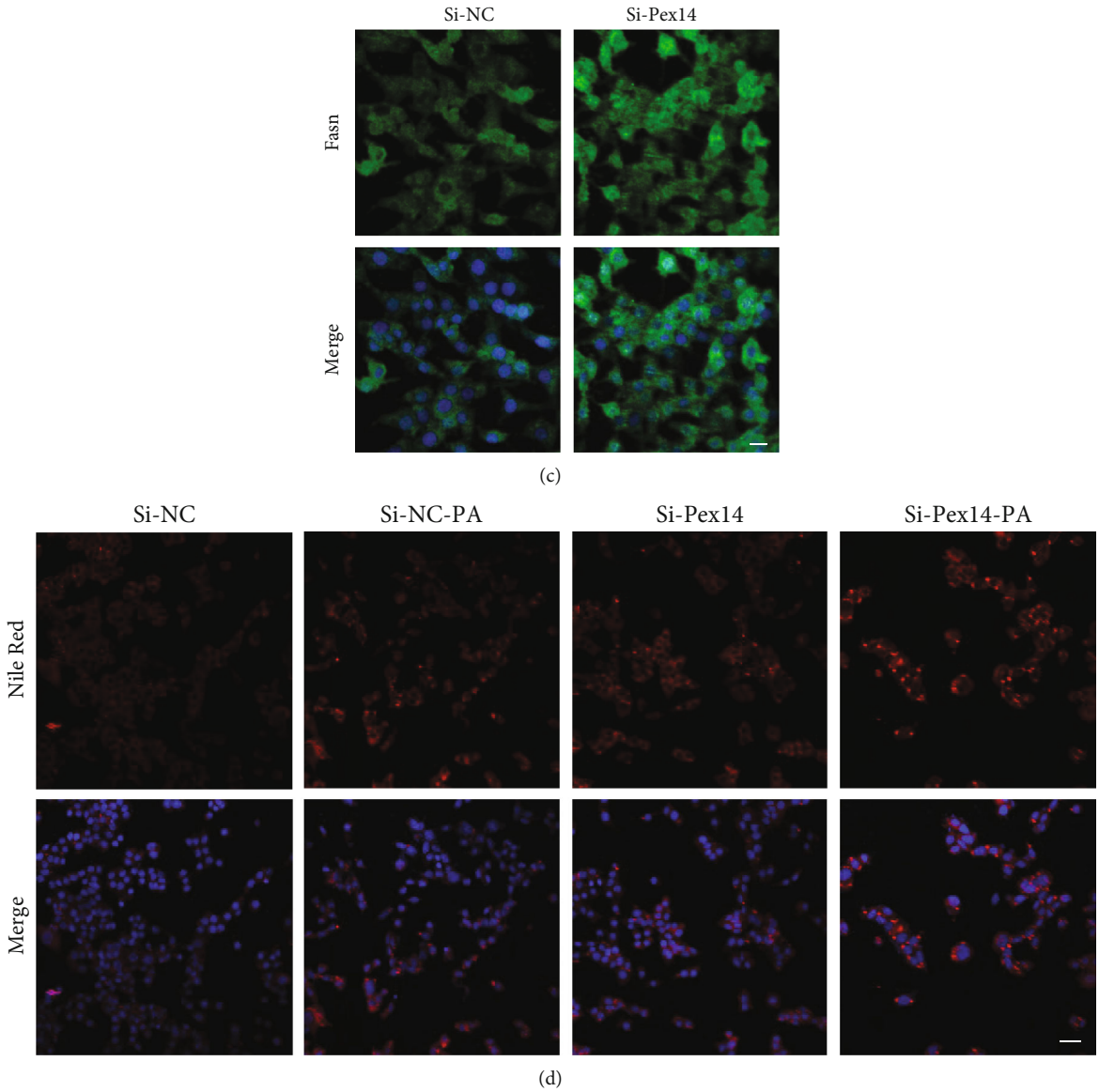

Figure 2: Dysregulated expression of genes implicated in fatty acid metabolism are shown in Pex14 KD INS-1 cells. (a, b) The expression of FAO enzymes and Abcd3 was detected by q-PCR (a) and western blot analysis (b). $^{*}p < 0.05$, vs. the blank or si-NC group. (c) Fasn protein expression was detected by IF staining (×400), scale bar 50 μm. (d) Nile Red staining of INS-1 cells (×200). Scale bar 100 μm.

(Figure 4(b)). These observations indicate that OS caused by deletion of Pex14 leads to the upregulation of the proinflammatory factors and activates ERS.

3.4. Effect of Pex14 KD on INS-1 Cell Viability after Exposure to FA. A CCK8 assay showed that Pex14 KD significantly reduced INS-1 cell viability. This tendency was further strengthened by LA or PA exposure (Figures 5(a) and 5(b)). A dramatic reduction in cell viability was observed after 48 h in blank cells treated with PA, whereas in blank cells exposed to LA, a significant decrease in cell viability was not observed until 72 h. This indicates that the lipotoxicity of PA is greater than that of LA, which is consistent with a previous report [10].

3.5. Effects of Pex14 KD on INS-1 Cell Apoptosis and Autophagy. We examined the impact of Pex14 KD on programmed cell death including apoptosis and autophagy in cells treated with FAs. Pex14 KD caused a slight increase in the number of early apoptosis cells (Q2) and late apoptosis or necrotic cells (Q4) (Figure 5(c)). The rates of cell apoptosis and necrosis were dramatically increased in Pex14 KD cells exposed to LA or PA; especially in PA exposure, the number of apoptotic and necrotic cells increased to 90%. Pex14 KD upregulated the protein expression of the proapoptotic factors cleaved-caspase 3 (Figure 5(d)). The results of the apoptosis assay were consistent with the cell viability assay data, and both indicated that Pex14 KD exacerbated the FA-induced lipotoxicity of β cells, especially in response

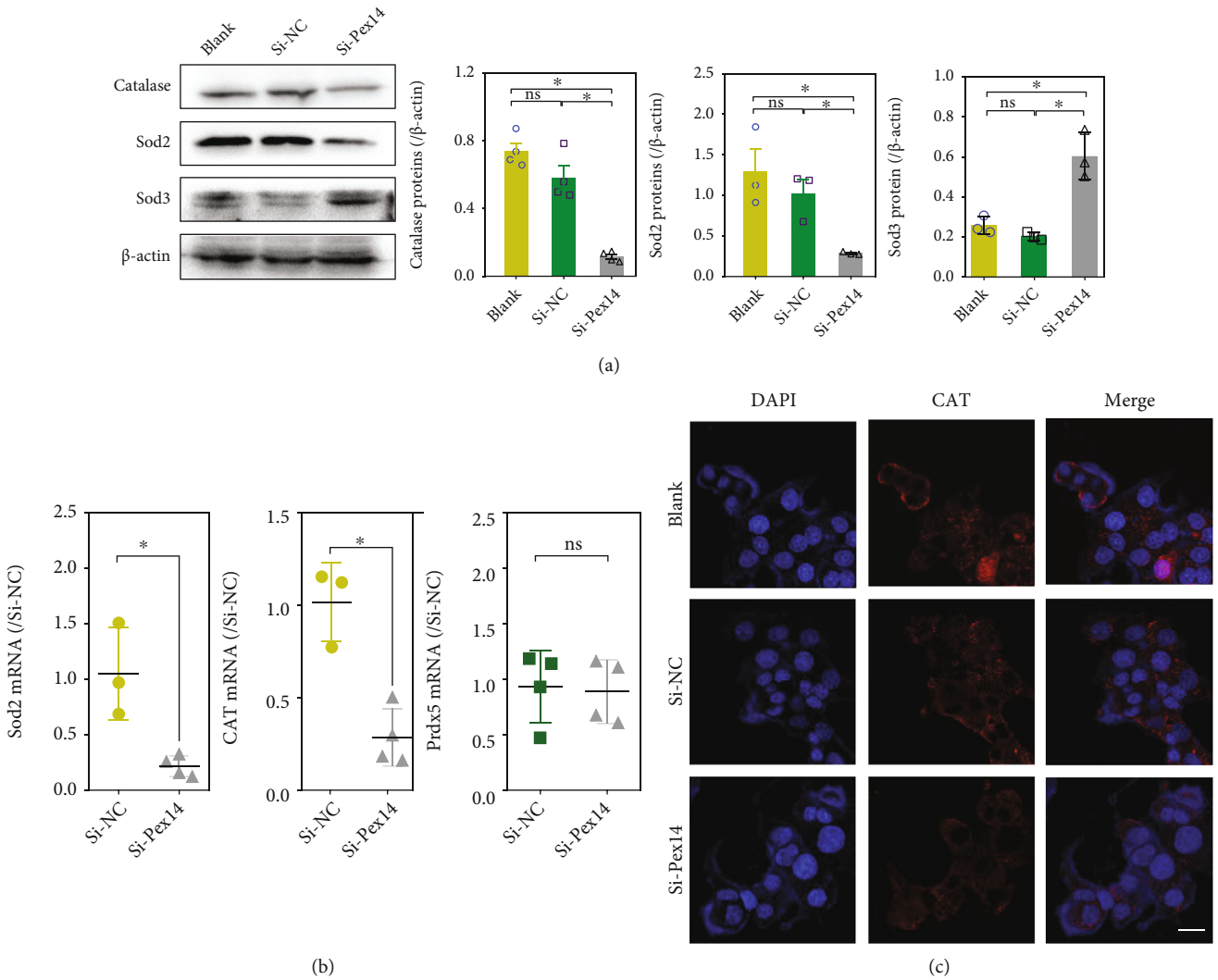

Figure 3: Continued.

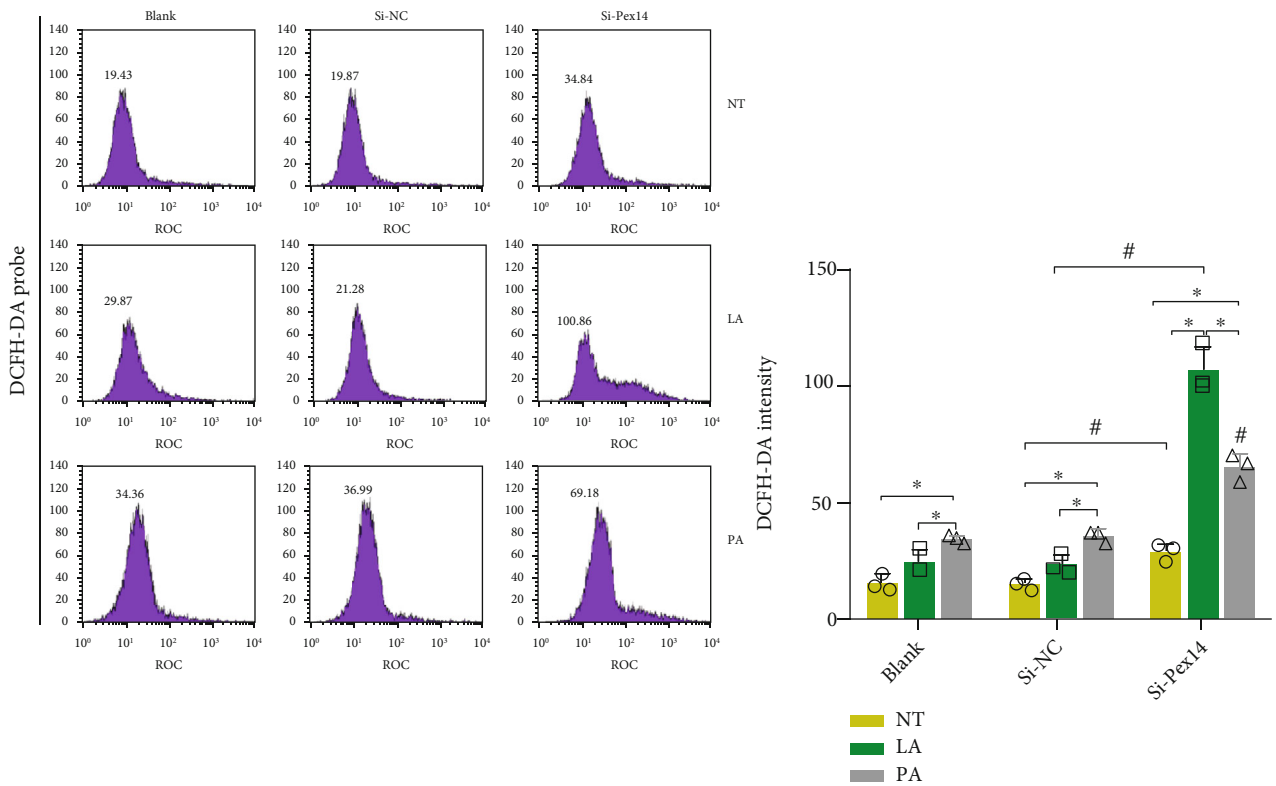

(d)

Figure 3: Knockdown of Pex14 aggravated fatty acid-induced intracellular ROS accumulation. (a, b) Antioxidant factors were detected by immunoblot assay (a) and q-PCR (b); $^{*}p < 0.05$, vs. the blank or si-NC group. (c) IF showed the decreased expression and location of catalase. (d) Intracellular ROS were detected by flow cytometry in INS-1 cells treated with LA or PA using the probes DCFH-DA and the average *G*-mean values were calculated. NT: no treatment. $^{*}p < 0.05$, vs. the NT or LA group. $^{\#}p < 0.05$, vs. the si-NC with or without LA/PA group.

to PA exposure. Consistently, we showed that PA exposure could further reduce Pex14, Abcd3, and Acaa1a expression in INS-1 cells (Figure 5(e)). Moreover, the fact that PA induced more apoptotic cell death in Pex14 KD cells than LA could explain the decrease in detectable ROS levels in PA-exposed cells.

Next, we examined the effect of Pex14 KD on autophagy. Increased LC3b and decreased p62 expressions indicated the activation of autophagy in Pex14 KD cells (Figure 6(a)). Pex14 KD increased the number of autophagy vacuoles detected using the CYTO-ID autophagy detection kit. Moreover, autophagy vacuoles were markedly increased upon treatment of Pex14 KD cells with LA. PA exposure also led to a moderate increase in autophagy vacuoles compared with the blank groups. However, in Pex14 KD cells, the number of detectable autophagy vacuoles decreased after PA exposure (Figures 6(b)–6(e)). These results indicate that Pex14 KD can lead to the simultaneous activation of apoptotic and autophagic cell deaths.

3.6. Pex14 KD Impairs Insulin Secretion. We examined glucose-stimulated insulin secretion in Pex14 KD INS-1 cell. ELISA assay revealed that Pex14 KD caused blunted glucose-stimulated insulin secretion in INS-1 cell. IF staining also showed reduced insulin in Pex14 KD cells (Figures 7(a) and 7(b)). To explore the mechanism underlying impaired insulin secretion, we examined the expression of the PDX1 gene that regulates insulin secretion. However, Pex14 KD showed no effect on the mRNA level of Pdx1 (Figure 7(c)).

4. Discussion

IUGR increases the susceptibility to T2D and impairs glucose tolerance in adults [12, 13]. We previously reported that maternal protein malnutrition leads to aberrant expression of Pex14 and FA metabolic enzymes in the fetal pancreas using an IUGR rat model [14]. Our knockdown assays using Pex14 siRNA support the hypothesis that downregulation of Pex14 lead to programed cell death and reduced resistance to lipotoxicity in the β cell.

Cells regulate the number of peroxisomes through a dynamic interplay between biogenesis and degradation. Pex14, a component of the docking complex on the peroxisomal membrane, functions in the dual processes of peroxisomal biogenesis and degradation in response to environmental changes [17]. Here, we showed that Pex14 KD downregulated the expression of Pex3, Pex5, and Pex19, all functioning in membrane protein insertion, inducing de novo biogenesis of peroxisomes. Previous reports show that depletion of Pex3 or Pex9 leads to complete loss of

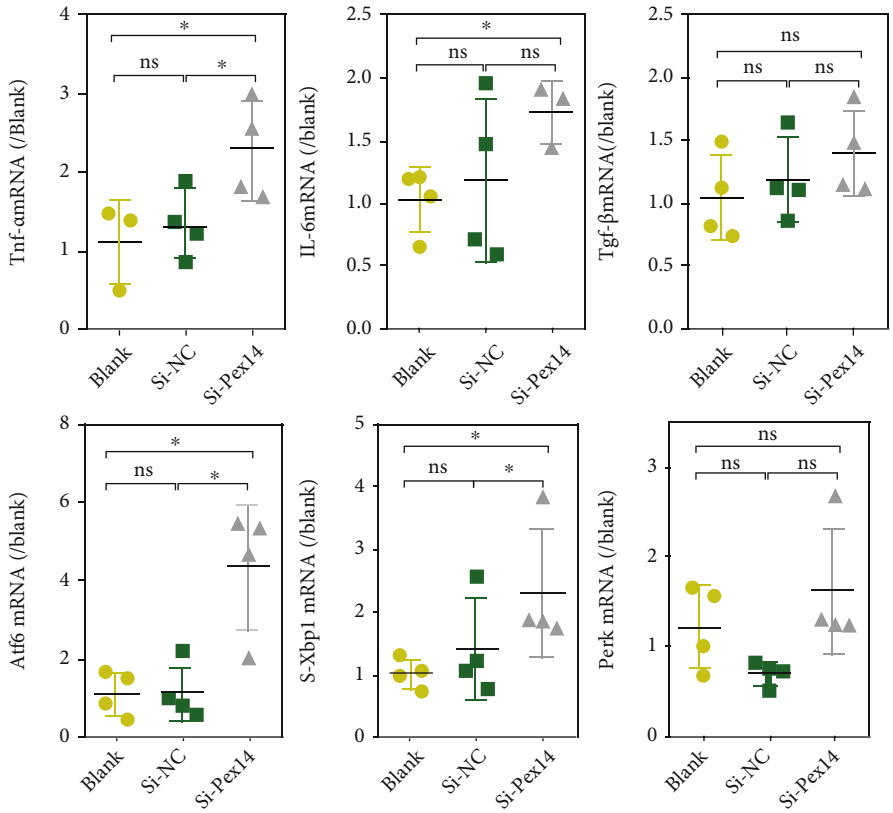

Figure 4: Effects of Pex14 suppression on proinflammation factors and regulators of ERS. The three proinflammation factors and three ERS regulators were detected by q-PCR. $^{*}p < 0.05$, vs. the blank or si-NC group.

peroxisomal function [16, 18, 19]. Pex11b, a cellular protein that induces peroxisome division, [20] was also downregulated upon Pex14 KD. Pex11b gene mutations may cause peroxisome biosynthesis disorders [21, 22], and its overexpression results in increased numbers of peroxisomes [23]. Pex14 KD also upregulated Pex5, a cytosolic receptor for matrix protein docking at Pex14 [24]. Of note, downregulation of the transcription factor Ppar-γ and Pgc-1α, both regulating peroxisome proliferation, may have contributed to the decreased expression of the peroxins. The downregulation of peroxins indicated that defective biogenesis and division was responsible for the reduced number of peroxisomes, although the precise molecular mechanism remains to be defined.

Functional autophagic pathways play a central role in the recycling of peroxisomes. Pexophagy, the selective degradation of peroxisomes via the autophagy machinery, is related to the quantitative regulation of peroxisomes and homeostasis in the metabolism of numerous substrates including lipids [25, 26]. Pex14 directly binds to Pex5 under normal conditions and is involved in peroxisome biogenesis. It interacts with LC3-II, an essential factor for autophagosome formation, under the nutrient starved condition, and is involved in the degradation of peroxisomes [19]. Decreased Pex14 levels in HeLa cells decrease pexophagy [27]. In contrast, Pex14 KD activated autophagy in INS-1 cells. We speculate that accumulation of ROS and subsequent OS led to autophagy activation, which might be a protective response for cells.

Both saturated and unsaturated FAs such as PA and LA trigger autophagy in β cells, although the underlying molecular mechanisms differ [28–30]. Our results showed that LA exposure increased the number of autophagy vacuoles in INS-1 cells. Pex14 KD further markedly increased autophagy induced by LA exposure. By contrast, Pex14 KD reduced the number of detectable autophagy vacuoles in PA exposure cells. A previous study suggested that the autophagy system is activated in PA-treated cells, and the induction of autophagy might play an adaptive and protective role in PA-induced cell death [31]. The fact that PA treatment increased apoptosis in Pex14 KD cells may explain the decrease in invisible autophagy vacuoles in the PA treatment group.

Long-term exposure to FAs and their accumulation induce apoptosis in β cells and contribute to the pathogenesis of T2D [32]. The molecular mechanisms potentially involved in FA-induced β cell apoptosis include ROS production, endoplasmic reticulum stress, trigger of apoptogenic factors, and accumulation of lipid intermediate molecules [2, 3, 33]. The present study also confirmed that exposure to either the saturated or the unsaturated FA (PA/LA) induced β cell apoptosis. Moreover, Pex14 KD reduced INS-1 cell resistance to lipotoxicity and caused more cell apoptosis.

Pex14 KD dysregulated the key enzymes involved in peroxisomal FAO. Acox1/3 is the rate-limiting enzyme of the first step of FAO. Hsd17b4 catalyzes the second step of FAO and leads to the formation of chain-shortened acyl-

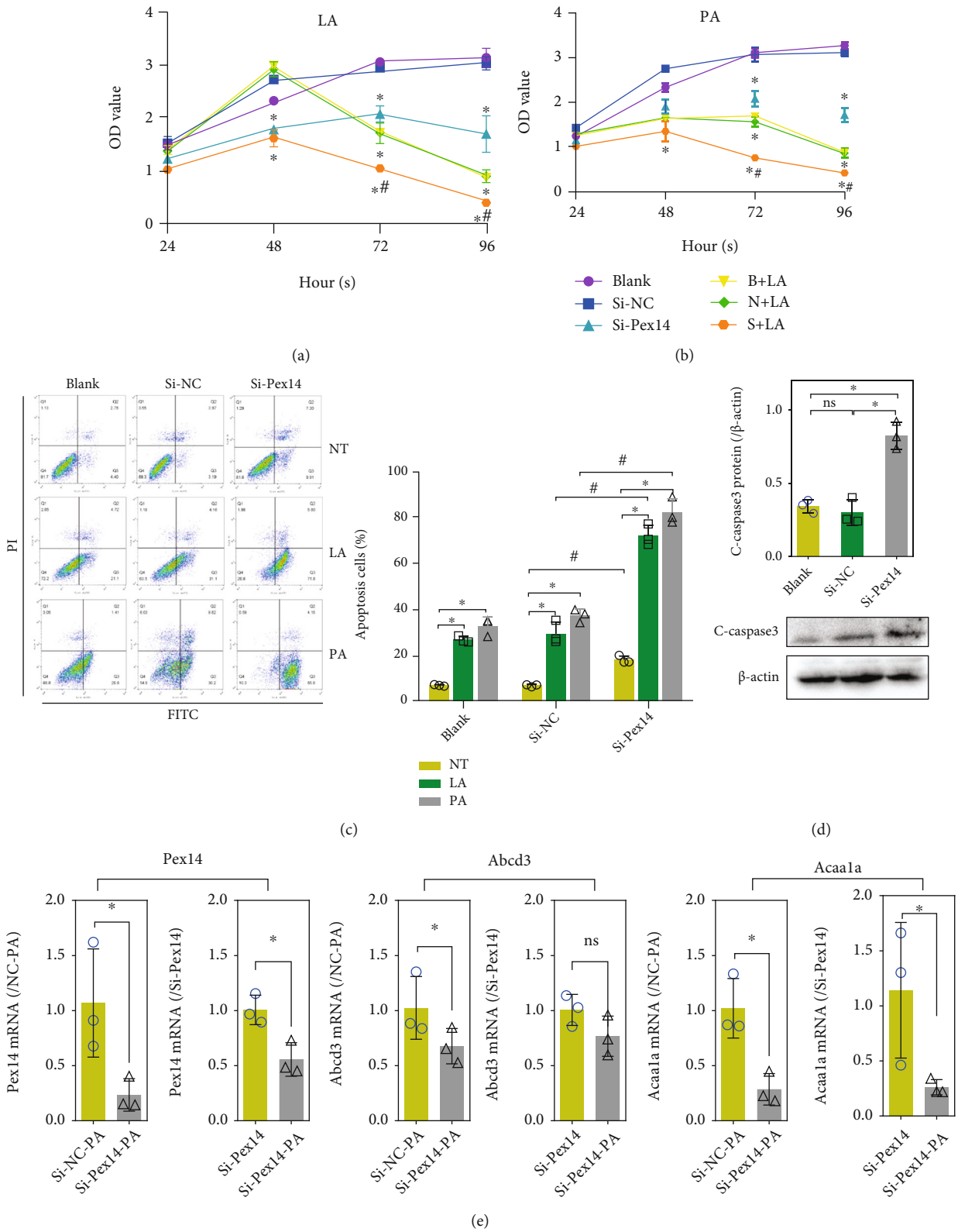

Figure 5: Knockdown of Pex14 aggravated fatty acid-induced apoptosis. (a, b) Cell Counting kit-8 assay was used to evaluate the effect of Pex14 KD on INS-1 cell viability with or without LA (a) or PA (b) treatment. $^{*}p < 0.05$, vs. the time-matched blank or si-NC group. $^{\#}p < 0.05$, vs. the si-NC with or without LA/PA group. (c) Cell apoptosis was assessed by flow cytometry with an Annexin V-PI kit. $^{*}p < 0.05$, vs. the NT or LA group. $^{\#}p < 0.05$, vs. the si-NC with or without LA/PA group. (d) The apoptosis regulators c-caspase3 were detected by immunoblot assay. (e) q-PCR detect the transcription of Pex14, Abcd3, and Acaa1a in Pex14 KD cells with PA treatment. $^{*}p < 0.05$, vs. the blank or si-NC group.

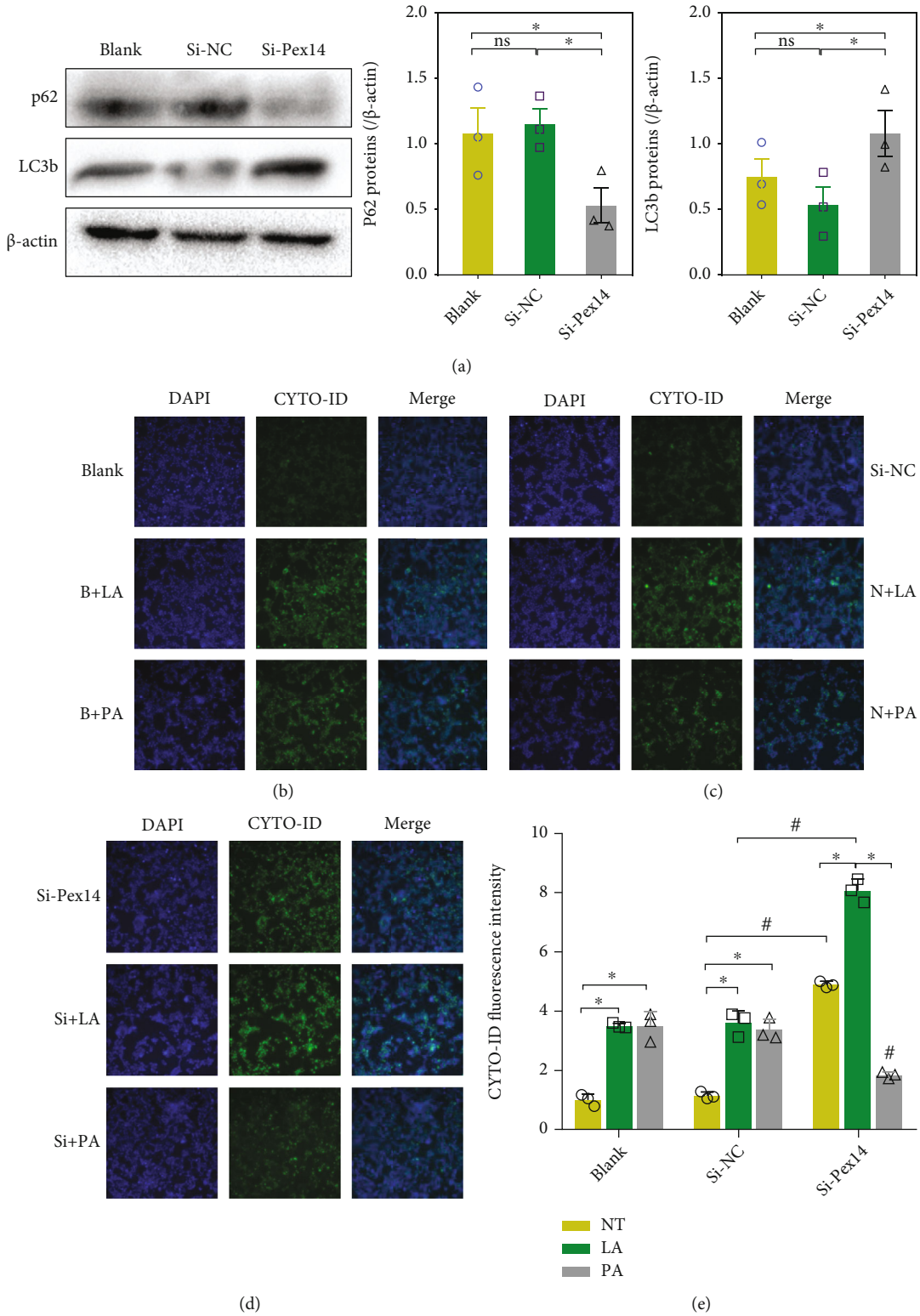

Figure 6: Effect of Pex14 KD on autophagy in INS-1 cells. (a) The autophagy markers were detected by western blotting; $^{*}p < 0.05$, vs. the blank or si-NC. (b–e) Autophagy vacuoles were detected by flow cytometry with Cyto-ID fluorescence dye in blank cells (b), si-NC group (c), and si-Pex14 cells (d) with LA or PA treatment. $^{*}p < 0.05$, vs. the NT or LA group. $^{\#}p < 0.05$, vs. the si-NC with or without LA/PA group.

CoA and acetyl-CoA [34]. Acaa1a catalyzes the final step of the peroxisomal β-oxidation of straight-chain acyl-CoAs [35]. Abcd3 is a peroxisomal membrane protein required for fatty acyl-CoA transport into peroxisomes. Fasn plays a critical role in the de novo synthesis of fatty acid. Pex14 KD downregulated Acox1, Hsd17b4, and Acaa1a,

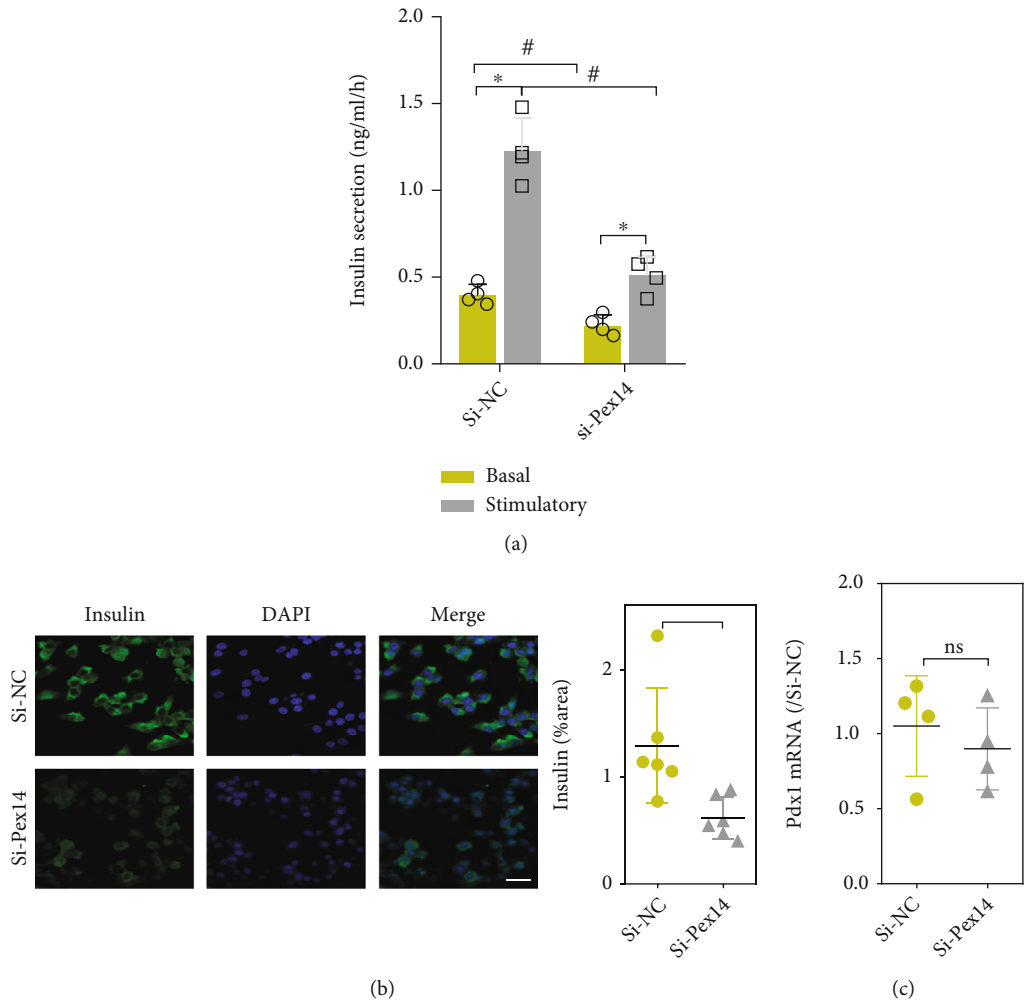

Figure 7: Effect of Pex14 KD on INS-1 cells function. (a) Analysis of insulin secretion in INS-1 cells with Pex14 KD. $^{*}p < 0.05$, vs. basal. $^{\#}p < 0.05$, vs. the si-NC with or without stimulatory. (b) The mRNA level of transcription factors PDX1 was detected by q-PCR. (c) Insulin expression was detected by IF staining. $^{*}p < 0.05$, vs. the si-NC group.

meanwhile it upregulated Acox3, Abcd3, and Fasn. Similar changes were observed in the IUGR pancreas. In addition, Pex14 KD decreased the expression of Cpt1a, a rate-limiting enzyme for long-chain FAO in the mitochondrion, and its deficiency results in a decreased rate of *FAO* [36]. These changes could lead to increased lipid accumulation in INS-1 cells. Given the complexity of FA metabolism, to determine the lipid profile by gas chromatography-mass spectroscopy would help to elucidate the true variation induced by peroxisome dysfunction. Recently, Baboota et al. reports that deletion of Pex5 lead to impairment of peroxisomal FAO and mitochondrial disruptions, thereby increasing β cell apoptosis and decreases insulin secretion in islet [37]. We speculate that downregulation of Pex14 contributes to islet dysplasia in the IUGR fetus, which still needs to be confirmed by in vivo studies.

Peroxisomes play a critical role in maintaining cellular redox homeostasis [38, 39]. Pex14 KD lead to the downregulation of catalase, which may lead to reduced degradation of H_2O_2. Downregulation of Sod2, a key mitochondria antioxidant catalyzing the conversion of superoxide radicals to H_2O_2, can also lead to an increase in superoxide radicals [40]. The present results suggest that the ROS accumulation in Pex14 KD β cells was caused by the absence of functional peroxisomes and subsequent mitochondrial alterations.

ROS are key signaling molecules that have important functions in regulating proinflammatory cytokines, and the two influence each other in a positive feedback loop [41–43]. Tnf-α and IL-6 were upregulated in Pex14 KD cells. In addition, Pex14 KD activated ER stress and proapoptotic factor in INS-1 cells. Prolonged ER stress causes pancreatic β cell apoptosis. Hence, induction of proinflammatory factors, ER stress, and subsequent apoptosis by the downregulation of Pex14 was a plausible explanation for our previous finding that ERS is dysregulated in the pancreas of IUGR models [43].

In general, one important finding of this study was that downregulation of Pex14 plays a fundamental role in INS-1 cell viability and resistance against lipotoxicity by affecting the expression of multiple genes involved in peroxisome

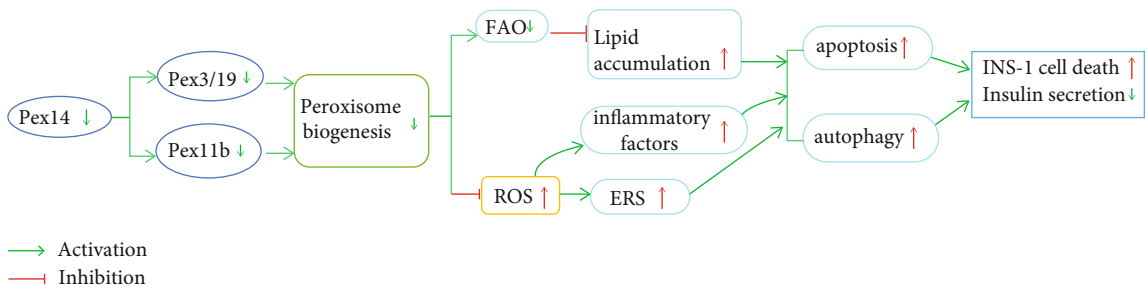

Figure 8: Hypothesis schematic. A unifying hypothesis depicting the cascade of events in response to Pex14 KD that result in oxidative stress and programmed cell death in β cells. We speculate that Pex14 KD inhibits peroxisome biogenesis, which disturbs fatty acid oxidization, thus leading to lipid accumulation. Peroxisome deficiency also causes downregulation of catalase and Sod2, in turn H_2O_2 accumulation. H_2O_2 activates inflammatory factors and ERS, which in turn induces apoptosis and autophagy.

biogenesis, FAO, and ROS detoxification (Figure 8). However, a limit in this study is that as a rat insulinoma cell line, INS-1 cells cannot fully mimic the phenotype of primary β cells in vivo. And the data obtained in INS-1 cells are not fully consistent with the data obtained from investigation of the pancreas in IUGR rats, so the impact of other genetic changes on pancreatic development warrant further research. Another limit of this study is that the mechanism underlying the decrease in insulin secretion in Pex14 KD cells remains to be explored. Nevertheless, the present results suggest that downregulation of Pex14 underlies, at least in part, the pancreatic dysplasia in the IUGR fetus. Further elucidation of the role of peroxisomes in β cell function might contribute to improve our understanding of T2D and prevent this disease in adulthood.

Abbreviations

Acox:	Acyl-CoA oxidase
CoA:	Coenzyme A
Acaa1:	3-Ketoacyl-CoA thiolase
Abcd:	ABC transporter D
CAT:	Catalase
Cpt1:	Carnitine palmitoyltransferase-1
DCFH-DA:	Dichlorodihydrofluorescein diacetate assay
FAO:	Fatty acid beta-oxidation
FBS:	Fetal bovine serum
Fasn:	Fatty acid synthase
Hsd17b4:	Peroxisomal 17β-hydroxysteroid dehydrogenase type 4
H_2O_2:	Hydrogen peroxide
IF:	Immunofluorescence
IUGR:	Intrauterine growth restriction
Pex:	Peroxin
ROS:	Reactive oxygen species
Sod:	Superoxide dismutase
siRNA:	Small interfering RNA
T2D:	Type 2 diabetes
VLCFA:	Very-long-chain fatty acids.

Data Availability

The data used to support the findings of this study are available from the corresponding author upon request.

Conflicts of Interest

No potential conflict of interest was reported by the authors.

Authors' Contributions

Xiaomei Liu and Yisheng Jiao are the guarantors of this work and contributed to the experimental design, obtained funding, and led the writing of the manuscript. Hongbo Guan and Yanyan Guo performed most of the experiments including cell culture, IF, and western blot. Liangliang Zhu contributed to the q-PCR experiments. All authors read and approved the submitted version.

Acknowledgments

We would like to thank International Science Editing (http://www.internationalscienceediting.com) for editing this manuscript. This work was supported by grant from the National Natural Science Foundation of China (No. 81971400), Outstanding Scientific Fund of Shengjing Hospital (No. 201707), Natural Fund Guidance Program Project of Liaoning Province (2019-ZD-0754), and Higher Education Innovative Talent Support Plan of Liaoning Province (LR2019074).

Supplementary Materials

The Supplementary Material for this article can be found online. Table S1: primer sequences of q-PCR and sequence of siRNA. Table S2: antibodies for western blotting and IF. *(Supplementary Materials)*

References

[1] M. Schrader and H. D. Fahimi, "The peroxisome: still a mysterious organelle," *Histochemistry and Cell Biology*, vol. 129, no. 4, pp. 421–440, 2008.

[2] M. Islinger, A. Voelkl, H. D. Fahimi, and M. Schrader, "The peroxisome: an update on mysteries 2.0," *Histochemistry and Cell Biology*, vol. 150, no. 5, pp. 443–471, 2018.

[3] C. Colasante, J. Chen, B. Ahlemeyer, and E. Baumgart-Vogt, "Peroxisomes in cardiomyocytes and the peroxisome / peroxisome proliferator-activated receptor-loop," *Thrombosis and Haemostasis*, vol. 113, no. 3, pp. 452–463, 2015.

[4] R. J. A. Wanders, S. Ferdinandusse, P. Brites, and S. Kemp, "Peroxisomes, lipid metabolism and lipotoxicity," *Biochimica et Biophysica Acta (BBA)-Molecular and Cell Biology of Lipids*, vol. 1801, no. 3, pp. 272–280, 2010.

[5] R. J. Wanders, H. R. Waterham, and S. Ferdinandusse, "Metabolic interplay between peroxisomes and other subcellular organelles including mitochondria and the endoplasmic reticulum," *Frontiers in cell and developmental biology*, vol. 3, 2016.

[6] C. Wiesinger, M. Kunze, G. Regelsberger, S. Forss-Petter, and J. Berger, "Impaired Very Long-chain Acyl-CoA β-Oxidation in Human X-linked Adrenoleukodystrophy Fibroblasts Is a Direct Consequence of ABCD1 Transporter Dysfunction," *Journal of Biological Chemistry*, vol. 288, no. 26, pp. 19269–19279, 2013.

[7] R. J. A. Wanders, F. C. C. Klouwer, and S. Ferdinandusse, *Clinical and laboratory diagnosis of peroxisomal disorders*, M. Schrader, Ed., In Peroxisomes: Methods and Protocols, New York, NY: Springer New York, 2017.

[8] L. A. Del Río and E. López-Huertas, "ROS generation in peroxisomes and its role in cell signaling," *Plant and Cell Physiology*, vol. 57, no. 7, pp. 1364–1376, 2016.

[9] H. Yuan, X. Zhang, X. Huang et al., "NADPH oxidase 2-derived reactive oxygen species mediate FFAs-induced dysfunction and apoptosis of β-cells via JNK, p 38 MAPK and p 53 pathways," *Plo S one*, vol. 5, no. 12, p. e15726, 2010.

[10] Y. Lee, H. Hirose, M. Ohneda, J. H. Johnson, J. D. McGarry, and R. H. Unger, "Beta-cell lipotoxicity in the pathogenesis of non-insulin-dependent diabetes mellitus of obese rats: impairment in adipocyte-beta-cell relationships," *Proceedings of the National Academy of Sciences*, vol. 91, no. 23, pp. 10878–10882, 1994.

[11] M. Cnop, N. Welsh, J.-C. Jonas, A. Jorns, S. Lenzen, and D. L. Eizirik, "Mechanisms of Pancreatic-Cell Death in type 1 and type 2 diabetes: many differences, few similarities," *Diabetes*, vol. 54, Supplement 2, pp. S97–S107, 2005.

[12] T. Harder, E. Rodekamp, K. Schellong, J. W. Dudenhausen, and A. Plagemann, "Birth weight and subsequent risk of type 2 diabetes: a meta-analysis," *American Journal of Epidemiology*, vol. 165, no. 8, pp. 849–857, 2007.

[13] G. Tian, C. Guo, Q. Li et al., "Birth weight and risk of type 2 diabetes mellitus: a dose-response meta-analysis of cohort studies," *Diabetes/metabolism research and reviews*, vol. 35, 2019.

[14] X. Liu, Y. Guo, J. Wang, L. Gao, and C. Liu, "Label-free proteomics of the fetal pancreas identifies deficits in the peroxisome in rats with intrauterine growth restriction," *Oxidative Medicine and Cellular Longevity*, vol. 2019, 15 pages, 2019.

[15] P. Grant, B. Ahlemeyer, S. Karnati et al., "The biogenesis protein PEX14 is an optimal marker for the identification and localization of peroxisomes in different cell types, tissues, and species in morphological studies," *Histochemistry and Cell Biology*, vol. 140, no. 4, pp. 423–442, 2013.

[16] C. Colasante, J. Chen, B. Ahlemeyer, R. Bonilla-Martinez, S. Karnati, and E. Baumgart-Vogt, "New insights into the distribution, protein abundance and subcellular localisation of the endogenous peroxisomal biogenesis proteins PEX3 and PEX19 in different organs and cell types of the adult mouse," *PLoS One*, vol. 12, no. 8, p. e0183150, 2017.

[17] J. Liu, X. Jin, C.-H. Yu, S.-H. Chen, W.-P. Li, and Y.-M. Li, "Endoplasmic reticulum stress involved in the course of lipogenesis in fatty acids-induced hepatic steatosis," *Journal of Gastroenterology and Hepatology*, vol. 25, no. 3, pp. 613–618, 2010.

[18] K. Ghaedi, M. Honsho, N. Shimozawa, Y. Suzuki, N. Kondo, and Y. Fujiki, "_PEX3_ Is the Causal Gene Responsible for Peroxisome Membrane Assembly -Defective Zellweger Syndrome of Complementation Group G," *American Journal of Human Genetics*, vol. 67, no. 4, pp. 976–981, 2000.

[19] S. Hara-Kuge and Y. Fujiki, "The peroxin Pex14p is involved in LC3-dependent degradation of mammalian peroxisomes," *Experimental Cell Research*, vol. 314, no. 19, pp. 3531–3541, 2008.

[20] C. M. Kassmann, S. Quintes, J. Rietdorf et al., "A role for myelin-associated peroxisomes in maintaining paranodal loops and axonal integrity," *FEBS Letters*, vol. 585, no. 14, pp. 2205–2211, 2011.

[21] M. S. Ebberink, J. Koster, G. Visser et al., "A novel defect of peroxisome division due to a homozygous non-sense mutation in the PEX11β gene," *Journal of Medical Genetics*, vol. 49, no. 5, pp. 307–313, 2012.

[22] Y. Tian, L. Zhang, Y. Li et al., "Variant analysis of PEX11B gene from a family with peroxisome biogenesis disorder 14B by whole exome sequencing," *Molecular Genetics & Genomic Medicine*, vol. 8, no. 1, 2020.

[23] C. P. Wong, Z. Xu, and S. Hou, "Interplay between Zika virus and peroxisomes during infection," *Cell*, vol. 8, 2019.

[24] M. Meinecke, C. Cizmowski, W. Schliebs et al., "The peroxisomal importomer constitutes a large and highly dynamic pore," *Nature Cell Biology*, vol. 12, no. 3, pp. 273–277, 2010.

[25] R. Vasko, B. B. Ratliff, S. Bohr et al., "Endothelial peroxisomal dysfunction and impaired pexophagy promotes oxidative damage in lipopolysaccharide-induced acute kidney injury," *Antioxidants & Redox Signaling*, vol. 19, no. 3, pp. 211–230, 2013.

[26] Y. S-i and Y. Fujiki, *Assessing pexophagy in mammalian cells*, M. Schrader, Ed., In Peroxisomes: Methods and Protocols, New York, NY: Springer New York, 2017.

[27] E. Deosaran, K. B. Larsen, R. Hua et al., "NBR1 acts as an autophagy receptor for peroxisomes," *Journal of Cell Science*, vol. 126, Part 4, pp. 939–952, 2013.

[28] M. Niso-Santano, S. A. Malik, F. Pietrocola et al., "Unsaturated fatty acids induce non-canonical autophagy," *The EMBO Journal*, vol. 34, no. 8, pp. 1025–1041, 2015.

[29] M. M. K. Shahzad, M. Felder, K. Ludwig et al., "Trans10,cis12 conjugated linoleic acid inhibits proliferation and migration of ovarian cancer cells by inducing ER stress, autophagy, and modulation of Src," *PLoS One*, vol. 13, no. 1, p. e0189524, 2018.

[30] K. Eitel, H. Staiger, M. D. Brendel et al., "Different role of saturated and unsaturated fatty acids in β-cell apoptosis," *Biochemical and Biophysical Research Communications*, vol. 299, no. 5, pp. 853–856, 2002.

[31] S.-E. Choi, S.-M. Lee, Y.-J. Lee et al., "Protective role of autophagy in palmitate-induced INS-1 β-cell death," *Endocrinology*, vol. 150, no. 1, pp. 126–134, 2009.

[32] M. Shimabukuro, Y.-T. Zhou, M. Levi, and R. H. Unger, "Fatty acid-induced cell apoptosis: a link between obesity and diabetes," *Proceedings of the National Academy of Sciences*, vol. 95, no. 5, pp. 2498–2502, 1998.

[33] M. Morita and T. Imanaka, "Peroxisomal ABC transporters: structure, function and role in disease," *Biochimica et Biophysica Acta (BBA)-Molecular Basis of Disease*, vol. 1822, no. 9, pp. 1387–1396, 2012.

[34] S. Violante, N. Achetib, C. W. T. Roermund et al., "Peroxisomes can oxidize medium- and long-chain fatty acids

through a pathway involving ABCD3 and HSD17B4," *The FASEB Journal*, vol. 33, no. 3, pp. 4355–4364, 2019.

[35] P. P. Van Veldhoven, "Biochemistry and genetics of inherited disorders of peroxisomal fatty acid metabolism," *Journal of Lipid Research*, vol. 51, no. 10, pp. 2863–2895, 2010.

[36] J. D. McGarry and N. F. Brown, "The mitochondrial carnitine palmitoyltransferase system — from concept to molecular analysis," *European Journal of Biochemistry*, vol. 244, no. 1, pp. 1–14, 1997.

[37] R. K. Baboota, A. B. Shinde, K. Lemaire et al., "Functional peroxisomes are required for β-cell integrity in mice," *Molecular Metabolism*, vol. 22, pp. 71–83, 2019.

[38] B. Ahlemeyer, M. Gottwald, and E. Baumgart-Vogt, "Deletion of a single allele of the Pex11β gene is sufficient to cause oxidative stress, delayed differentiation and neuronal death in mouse brain," *Disease Models & Mechanisms*, vol. 5, no. 1, pp. 125–140, 2012.

[39] M. Fidaleo, "Peroxisomes and peroxisomal disorders: the main facts," *Experimental and Toxicologic Pathology*, vol. 62, no. 6, pp. 615–625, 2010.

[40] M. Schrader and H. D. Fahimi, "Peroxisomes and oxidative stress," *Biochimica et Biophysica Acta (BBA)-Molecular Cell Research*, vol. 1763, no. 12, pp. 1755–1766, 2006.

[41] H. Blaser, C. Dostert, T. W. Mak, and D. Brenner, "TNF and ROS crosstalk in inflammation," *Trends in Cell Biology*, vol. 26, no. 4, pp. 249–261, 2016.

[42] M. Mittal, M. R. Siddiqui, K. Tran, S. P. Reddy, and A. B. Malik, "Reactive oxygen species in inflammation and tissue injury," *Antioxidants & Redox Signaling*, vol. 20, pp. 1126–1167, 2013.

[43] T. Nishikawa and E. Araki, "Impact of mitochondrial ROS production in the pathogenesis of diabetes mellitus and its complications," *Antioxidants & Redox Signaling*, vol. 9, no. 3, pp. 343–353, 2007.

Hindawi
Oxidative Medicine and Cellular Longevity
Volume 2021, Article ID 9711176, 22 pages
https://doi.org/10.1155/2021/9711176

Research Article

The Antioxidative Role of Natural Compounds from a Green Coconut Mesocarp Undeniably Contributes to Control Diabetic Complications as Evidenced by the Associated Genes and Biochemical Indexes

Rickta Rani Das,[1] Md. Atiar Rahman,[1] Salahuddin Qader Al-Araby,[1] Md. Shahidul Islam,[1] Md. Mamunur Rashid,[1] Nouf Abubakr Babteen,[2] Afnan M. Alnajeebi,[2] Hend Faisal H. Alharbi,[3] Philippe Jeandet,[4] Md. Khalid Juhani Rafi,[1] Tanvir Ahmed Siddique,[1] Md. Nazim Uddin,[5] and Zainul Amiruddin Zakaria[6]

[1]*Department of Biochemistry and Molecular Biology, University of Chittagong, Chittagong 4331, Bangladesh*
[2]*Department of Biochemistry, Collage of Science, University of Jeddah, Jeddah 80203, Saudi Arabia*
[3]*Department of Food Science and Human Human Nutrition, Collage of Agriculture and Veterinary Medicine, Qassim University, Buraydah, Saudi Arabia*
[4]*Department of Biology and Biochemistry, Faculty of Sciences, University of Reims, PO Box 1039, Reims, France*
[5]*Institute of Food Science and Technology, Bangladesh Council of Scientific and Industrial Research, Dhaka 1205, Bangladesh*
[6]*Department of Biomedical Science, Faculty of Medicine and Health Sciences, Universiti Putra Malaysia (UPM), Serdang, 43400 Selangor, Malaysia*

Correspondence should be addressed to Md. Atiar Rahman; atiar@cu.ac.bd and Zainul Amiruddin Zakaria; zaz@upm.edu.my

Received 26 May 2021; Accepted 5 July 2021; Published 28 July 2021

Academic Editor: Cristina Cosentino

The purpose of this study was to look into the effects of green coconut mesocarp juice extract (CMJE) on diabetes-related problems in streptozotocin- (STZ-) induced type 2 diabetes, as well as the antioxidative functions of its natural compounds in regulating the associated genes and biochemical markers. CMJE's antioxidative properties were evaluated by the standard antioxidant assays of 1,1-diphenyl-2-picrylhydrazyl (DPPH), superoxide radical, nitric oxide, and ferrous ions along with the total phenolic and flavonoids content. The α-amylase inhibitory effect was measured by an established method. The antidiabetic effect of CMJE was assayed by fructose-fed STZ-induced diabetic models in albino rats. The obtained results were verified by bioinformatics-based network pharmacological tools: STITCH, STRING, GSEA, and Cytoscape plugin cytoHubba bioinformatics tools. The results showed that GC-MS-characterized compounds from CMJE displayed a very promising antioxidative potential. In an animal model study, CMJE significantly ($P < 0.05$) decreased blood glucose, serum alanine aminotransferase (ALT), aspartate aminotransferase (AST), creatinine, uric acid, and lipid levels and increased glucose tolerance as well as glucose homeostasis (HOMA-IR and HOMA-b scores). The animal's body weights and relative organ weights were found to be partially restored. Tissue architectures of the pancreas and the kidney were remarkably improved by low doses of CMJE. Compound-protein interactions showed that thymine, catechol, and 5-hydroxymethylfurfural of CMJE interacted with 84 target proteins. Of the top 15 proteins found by Cytoscape 3.6.1, 8, *CAT* and *OGG1* (downregulated) and *CASP3*, *COMT*, *CYP1B1*, *DPYD*, *NQO1*, and *PTGS1* (upregulated), were dysregulated in diabetes-related kidney disease. The data demonstrate the highly prospective use of CMJE in the regulation of tubulointerstitial tissues of patients with diabetic nephropathy.

1. Introduction

Diabetes mellitus (DM), a metabolic disorder characterized by hyperglycemia induced by insulin secretion deficiency and/or resistance to its action, affects more than millions of people across the world [1]. DM impairs several nonenzymatic and enzymatic antioxidative defense mechanisms that lead to cause oxidative stress as well as tissue damage in DM-associated comorbidities such as cataracts, neuropathy, nephropathy, and retinopathy [2]. Until now, no single effective treatment for DM has been developed in medicine, and the current therapeutic supports such as biguanides, sulfonylureas, meglitinides, thiazolidinediones, dipeptidyl peptidase IV inhibitors, and α-glucosidase inhibitors and their analogs have many side effects, such as weight gain, hypoglycemia, gastrointestinal disorders, liver and kidney damage, and hypersensitivity reactions [2, 3].

The above-mentioned side effects suggest that further development of new, safer, and more powerful oral antihyperglycemic agents, particularly in long-term therapy, is needed. In this context, medicinal plants have emerged as promising adjuvants to treat chronic, oxidative stress-mediated disorders [3]. Several medicinal plants recommended for the treatment of DM have been shown to protect β-cells, increase insulin secretion and glucose absorption by the adipose tissue, and decrease glucose absorption in the intestines [2, 4]. Some experiments have shown in recent years that most plants produce carotenoids, flavonoids, terpenoids, alkaloids, glycosides, and anthocyanin that exert a significant impact on diabetes and other chronic diseases as well as minimize oxidative stress [5]. Treatments which involve the use of medicinal plants provoking antioxidative actions are therefore highly recommended [6, 7].

Different parts of coconut have long been used as one of the most popular edible foods in almost every part of the world. Nutritional and medicinal values of coconuts have been investigated, and especially, their antibacterial, antihypertensive, oral microflora inhibitory, antiviral, antifungal, antidermatophytic, antiparasitic, hypoglycemic, immunostimulant, and hepatoprotective properties are reported by many scientists [8–10]. Microminerals and nutrients of coconut water are essentially important for human health while the endocarp part is cited to contain high contents of phenolic and flavonoids. Coconut milk has also been shown effective in the management of diabetes [10]. Interestingly, the mesocarp part of coconut has not yet been studied, and we tried here to investigate the antioxidative effect of coconut mesocarp juice which eventually and undeniably contributes to the management of diabetes and renal diabetic complications using a fructose-fed streptozotocin-induced diabetic rat model. The observed effect has been verified and networked with the genes linked in reducing oxidative stress in the biological system and through bioinformatics-based network pharmacological approach in a computational model.

2. Materials and Methods

2.1. Collection of Coconut Mesocarp. Green coconut mesocarps were collected from the local green coconut seller around the University of Chittagong. The mesocarp juice was extracted using a mechanical sugarcane juicer machine (detailed in the extraction section) with the aid of a local sugarcane juice seller. The mesocarp part of coconut has been keenly identified with the help of a plant scientist Dr. Sheikh Bokhtear Uddin, Professor, Department of Botany, University of Chittagong. A sample specimen of collected mesocarp has been preserved in the institutional herbarium with an identification number (MPSS2017/02).

2.2. Chemicals and Reagents. All the chemicals and reagents used in this study were of analytical grade unless specified. ABTS (2,2′-azino-bis(3-ethylbenzthiazoline-6-sulfonic acid)), dinitrosalicylic acid, Folin-Ciocalteu reagent, dimethyl sulfoxide (DMSO), 1,1-diphenyl-2-picrylhydrazyl (DPPH), nitro blue tetrazolium (NBT), potassium ferric cyanide, sodium hydroxide, trichloroacetic acid (TCA), nitroprusside, N-(1-naphthyl) ethylene diamine dihydrochloride, *O*-phenanthroline, and α-amylase were procured from Sigma-Aldrich Co., St. Louis, USA. Butanol, n-hexane, methanol (absolute), ethanol (99.99%), and acetone were purchased from Sigma-Aldrich.

2.3. Preparation of Coconut Mesocarp Juice Extract (CMJE). Coconut mesocarp juice extract was prepared as previously described by Rahman et al. [11]. Briefly, the green coconut's mesocarp, which is also known as coir, is situated just beneath the exocarp or outer skin of the fruit. The exocarp part was plucked, and the mesocarp was removed. The liquid sap of the mesocarp (coir) was then mechanically collected. The collected sap was filtered by using filter paper (Whatman filter paper #1) and a funnel. The filtered sap was then evaporated by an electromantle at 45-50°C for several days. The sample collected from the electromantle was further evaporated through a rotary evaporator (RE 200, Bibby Sterilin Ltd., UK) at 55-60°C, and the final extract was collected and stored in the refrigerator.

2.4. Screening for Phytochemical Content of CMJE

2.4.1. Total Flavonoid Content (TFC) and Total Phenolic Content (TPC) Determinations. The total flavonoid content (TFC) of CMJE was determined according to the method established by Kumaran and Karunakaran [12]. The total phenolic content (TPC) of the CMJE was measured according to a method described by Singleton and Rossi [13].

2.4.2. Gas Chromatography-Mass Spectroscopy (GC-MS) Analysis of CMJE. The crude CMJE was analyzed by GC-MS using electron impact ionization (EI) with a gas chromatograph (GC-17A, Shimadzu Corporation, Kyoto, Japan) coupled to a mass spectrometer (GC-MS TQ 8040, Shimadzu Corporation, Kyoto, Japan). A fused silica capillary column (Rxi-5ms; 0.25 m film thickness) is coated with DB-1 (J&W). The inlet temperature of the capillary was set at 260°C, and the oven temperature was set at 70°C (0 min), 10°C and 150°C (5 min), 12°C and 200°C (15 min), and 12°C and 220°C (5 min). The column flow rate was 0.6 mL/min of helium gas at a constant pressure of 90 kPa. The auxiliary (GC to MS interface) temperature was set at 280°C. The MS was set in scan mode with a scanning range of 40-350 amu. The mass range

was set in the range of 50-550 m/z. The prepared sample was then run for GC-MS analysis. The total GC-MS running time was 35 minutes. All peak areas were compared with the database in the GC-MS library version NIST 08-S.

2.4.3. Estimation of Beta-Carotene and Lycopene Contents of CMJE. Beta-carotene and lycopene contents of CMJE were estimated using a slightly modified method of that described by Kumari et al. [14]. Briefly, 100 mg of the extract was mixed with 10 mL of the acetone-hexane mixture (4 : 6) for 1 minute and filtered. The absorbance was measured at three different wavelengths (453, 505, and 663 nm).

The beta-carotene and lycopene contents were calculated as follows:

Beta-carotene: $(\text{mg}/100\,\text{mL}) = (0.216 \times A_{663}) - (0.304 \times A_{505}) + (0.452 \times A_{453})$

Lycopene: $(\text{mg}/100\text{mL}) = -(0.0458 \times A_{663}) + (0.372 \times A_{505}) - (0.0806 \times A_{453})$.

2.4.4. Determination of the DPPH Free Radical Scavenging Activity of CMJE. The DPPH free radical scavenging effect was measured according to the method of Shen et al. [15] supplemented with the established protocol described by Brand-Williams et al. [16]. Ascorbic acid was used as a reference antioxidant agent in this experiment. The required amount (0.96 mg) of ascorbic acid and CMJE sample was individually dissolved in 12 mL methanol to prepare stock solution. The stock solution of both CMJE and ascorbic acid was diluted to the concentrations of 40, 20, 10, and 5 μg/mL. Two milliliters of both CMJE solution and ascorbic acid solution of different concentrations was taken as triplicate into test tubes where 2 mL of the freshly prepared DPPH solution was added. The reaction mixture was incubated in the dark for 30 min at room temperature, and the absorbance of the reaction mixture was measured at 517 nm by using a visible spectrophotometer. Control was prepared in similar manner excluding sample.

The percentage of inhibition was calculated by the following equation:

$$\%\text{Inhibition} = \left\{\frac{A_0 - A_1}{A_0}\right\} \times 100 \quad (1)$$

where A_0 is the absorbance of control (freshly prepared DPPH solution) and A_1 is the absorbance of extract/Std. Then, the percentage of scavenging activity or inhibition was plotted against the concentration, and IC_{50} was calculated by the linear regression analysis from the graph.

2.4.5. Determination of ABTS Radical Scavenging Activity of CMJE. The ABTS free radical scavenging activity of CMJE was measured by using the ABTS (2,2′-azino-bis(3-ethylbenzthiazoline-6-sulfonic acid)) radical cation decolorization assay [17]. ABTS•+ was generated by reacting 7 mM ABTS aqueous solution with 2.45 mM potassium persulfate in the dark for 12-16 h at room temperature. At the beginning of the assay, this solution was diluted in ethanol (about 1 : 49, *v*/*v*) and equilibrated at 30 ± 2°C to give an absorbance of 0.7 ± 0.02 at 734 nm. The stock solution of the CMJE extract was diluted to yield a concentration range of 50-8000 μg/mL. The final concentration (0-15 μM) was obtained by the addition of 1 mL of the diluted ABTS•+ solution to 62 μL of CMJE sample in ethanol. After 40 minutes of mixing, absorbance was estimated at 25°C. Trolox and ethanol were used as a positive control and blank, respectively. At each dilution of the standard and sample, triplicate determinations were made, and absorption was measured at 734 nm in the UV-Vis spectrophotometer (UV-1200S UV-VIS 1200, Shimadzu Corporation, Japan). The ABTS•+ scavenging capability of the extract was compared with that of Trolox. The percentage inhibition calculated as follows:

$$\text{ABTS radical scavenging activity}(\%) = \left[\frac{(\text{Absorbance of control} - \text{Absorbance of the sample})}{\text{Absorbance of control}}\right] \times 100 \quad (2)$$

2.4.6. Determination of Superoxide Scavenging Activity of CMJE. The superoxide radical scavenging power of CMJE was assessed by an updated protocol of Rana et al. [18]. Using alkaline dimethyl sulfoxide (DMSO), the superoxide radical was formed by dissolving 250 μL of 1 M NaOH in double-distilled water to 49.750 μL of DMSO. With a NaOH concentration of 5 mM and a volume of 50 mL, air bubbled through the mixture for 1 h and 30 minutes. The solution of NBT (nitro blue tetrazolium) was prepared by dissolving 12 mg of NBT in 12 mL of double-distilled water (pH 7.4), with a final concentration of NBT of 1 mg/mL. The sample was diluted, and each test tube received a volume of 43 μL of each sample, where the sample concentration ranged from 25 to 800 μg/mL. Furthermore, 143 μL of alkaline DMSO and 14 μL of NBT (1 mg/mL) were added to each test tube, incubated for 20 minutes and read at 560 nm for absorbance. DMSO and ascorbic acid were used as negative and positive controls, respectively. Triplicates were confirmed for each experiment. The percentage inhibition calculated as follows:

$$\text{Superoxide radical scavenging activity}(\%) = \left[\frac{\text{sample Absorbance} - \text{control Absorbance}}{\text{sample Absorbance}}\right] \times 100 \quad (3)$$

2.4.7. Estimation of Nitric Oxide Scavenging Activity of CMJE. The nitric oxide scavenging effect was estimated based on the principle of the analysis of nitrite ions which are generated from sodium nitroprusside through nitric oxide in an aqueous solution at a physiological pH [19]. Nitric oxide scavengers compete with oxygen, resulting in decreased nitrite ion production. For the experiment, 1.5 mL of sodium nitroprusside (10 mM) in phosphate-buffered saline (pH 7.4) was combined with various 100 μL volumes of water-dissolved CMJE extracts and incubated for 150 min at room temperature. Without CMJE, the same reaction mixture, but an equal amount of water, served as control. 1.5 mL of the Griess reagent, 1% sulfanilamide, 2 percent H_3PO_4, and 0.1 percent N-(1-naphthyl) ethylene diamine dihydrochloride, was added after the incubation time. At 546 nm against the blank, the absorbance of the chromophore formed was read. Ascorbic acid was used as a positive control. The nitric oxide radical scavenging power was calculated by the following formula:

$$\text{Scavenging activity of nitric oxide radical}\,(\%) = \left[\frac{\text{Control OD} - \text{Sample OD}}{\text{Control OD}}\right] \times 100 \quad (4)$$

2.4.8. Determination of the Iron-Chelating Activity of CMJE. The iron-chelating activity of CMJE was measured using the method of Benzie and Strain [20]. The theory is based on the formation of, and destruction of, the *O*-phenanthroline-Fe^{2+} complex in the presence of chelating agents. A reaction mixture containing 1 mL of 0.05% *O*-phenanthroline in methanol, 2 mL of fresh ferrous chloride (200 μM), and 2 mL of different CMJE concentrations was incubated at room temperature for 10 min, and absorbance was measured at 510 nm. Experiments were performed in triplicate, and the operation was correlated with the usual positive control, ascorbic acid.

$$\text{Inhibition of Iron radical}\,(\%) = [A_0 - A_1]/A_0 \times 100 \quad (5)$$

where A_0 is the test absorbance and A_1 is the control absorbance.

2.5. Determination of the α-Amylase Inhibition Capacity of CMJE. The α-amylase inhibitory action of CMJE was determined by a modified procedure of McCue et al. [21, 22]. Briefly, 4 mg CMJE was dissolved in 5 mL water to prepare a stock solution of 800 μg/mL, which was diluted to 50, 100, 200, and 400 μg/mL. Four milligrams of acarbose (standard) was dissolved in 5 mL water to prepare similar concentrations of standard solutions as was done for CMJE sample. 250 μL of CMJE was mixed in a tube with 250 μL of 0.02 M sodium phosphate buffer (pH 6.9) containing the α-amylase solution (0.5 mg/mL). This solution was preincubated at 25°C for 10 min, after which 250 μL of 1% starch solution in 0.02 M sodium phosphate buffer (pH 6.9) was added at timed intervals and then further incubated at 25°C for 10 min. Termination of the reaction was ensured by adding 500 μL of the dinitrosalicylic acid (DNS) reagent. The assay mixtures were then incubated for 5 min in boiling water and cooled to room temperature. The reaction mixture was diluted with 5 mL distilled water, and the absorbance was measured at 540 nm using a spectrophotometer (UV-1280, UV-Vis spectrophotometer, Shimadzu Corporation, Japan). A control was prepared using the same procedure replacing the extract with distilled water. The α-amylase inhibitory activity was calculated as percentage inhibition:

$$\%\text{Inhibition} = (\text{Abs}_{\text{control}} - \text{Abs}_{\text{extract}})/\text{Abs}_{\text{control}} \times 100 \quad (6)$$

2.6. Experimental Animals and their Maintenance. Twenty-five adult male (body weight 150-200 g, age 6-7 weeks) Wistar albino rats were purchased from BCSIR, Chittagong. The animals were randomly grouped into normal control (NC, animals received no treatment), diabetic control (DC, streptozotocin-induced and received no treatment), and treatment group (CMJE50, CMJE100, and CMJE200 mg/kg bw). The animals were individually housed in a polycarbonated cage bedded with wood husk at a temperature around 22 ± 2°C and humidity 55-60% with a 12 h light-dark cycle. All animals were supplied with a commercial pellet diet for the entire intervention period. All animal experimentations were carried out according to the guideline of the Institutional Animal Ethics Committee (EACUBS2018-4).

2.6.1. Acute Oral Toxicity Test. The acute oral toxicity test was performed using standard laboratory conditions according to the "Organization for Environmental Control Development" guidelines (OECD: Guidelines 420; fixed-dose method). The allocated animals ($n = 6$) were administered a single oral dose (500 to 2000 mg/kg, body weight) of the test extract (CMJE). Before the administration of the extract, rats were fasted overnight, and food was also delayed between 3 and 4 h. After administration, food was withheld for the next 3-4 h. Experimental animals were observed individually during the first 30 minutes after dosing, periodically for the first 24 minutes (special attention for the first 4 h), with particular monitoring for possible unusual responses including allergic syndromes (itching, swelling, skin, and rash), behavioral changes, and mortality over the next 72 h. The median therapeutic effective dose was intervened as one-tenth of the median lethal dose ($LD_{50} > 5.0$ g/kg) [23].

2.6.2. Induction of Diabetes Using Streptozotocin. Diabetes induction was accomplished with slightly modifying of protocol addressed by Al-Araby et al. [22]. Briefly, the animals

were randomly divided into control and treatment groups comprising of 5 animals in each group. The normal control group (NC) received vehicle only. Diabetic control (DC) was left untreated, and the treatment groups were administered with three different doses (CMJE50, CMJE100, and CMJE200 mg/kg bw) of coconut mesocarp juice extracts. All animals except those of normal control (NC) were fed with 10% fructose solutions before one week of intraperitoneal injection of streptozotocin (50 mg/kg bw dissolved in 0.1 M citrate buffer, pH 4.5) [24] to induce diabetes which is confirmed with the fasting blood glucose level ≥ 16 mmol/L after one week of injection (measured by glucometer, Accu-Chek, USA). Once the animals were confirmed diabetic after STZ injection, each animal of CMJE50 group has been treated by the CMJE extract at the dose of 50 mg/kg bw once daily; each animal of the CMJE100 group has been treated with the CMJE extract at the dose of 100 mg/kg bw once daily, and each animal of CMJE200 group has been treated with CMJE extract at the dose of 200 mg/kg bw once daily. The treatment was continued for three weeks.

2.6.3. Determination of Body Weight, Blood Glucose, and Oral Glucose Tolerance (OGT). Weekly body weights and blood glucose levels of animals were measured and recorded. Blood glucose was measured by tail prick method using a glucometer as stated above. The glucose tolerance capacity of each animal was measured by the oral glucose tolerance test (OGTT) at the 3rd week of the intervention. Animals were administered a single dose of oral glucose solution (2 g/kg body weight) and blood glucose levels were measured at 0 (just before glucose ingestion), 30, 60, 90, and 120 min after the glucose dose.

2.6.4. Animal's Blood and Organ Collection. After 4 weeks of intervention, animals were sacrificed, their blood being collected in heparinized test tubes as well as their kidney and pancreas. Blood samples were centrifuged at 3000 rpm for 15 min at 25-37°C to separate serum which was further analyzed for hepatic enzymes (alanine aminotransferase, aspartate aminotransferase), insulin, lipid profile, uric acid, and creatinine. The serum glucose level (mmol/L) was determined using the glucose test kit based on the glucose oxidase method as described [25]. The pancreas and livers were washed with 0.9% NaCl solution, wiped with tissue paper, and weighed to be preserved in 10% buffered formalin. The kidney and the pancreas were used for histopathological investigations. The homeostatic model assessment (HOMA-IR and HOMA-b) was estimated using serum insulin levels measured at the end of the experiment using the following expression:

$$\text{HOMA-IR} = \frac{\text{Serum insulin (U/L)} \times \text{Blood glucose(mg/dL)}}{22.5},$$
$$\text{HOMA} - \beta - \text{cell function} = \frac{20 \times \text{Serum insulin in U/L}}{\text{Blood glucose in mg/dL} - 3.5}. \quad (7)$$

2.6.5. Histopathological Analyses. The pancreas and the kidney tissues were fixed with a buffered formalin solution for 48 h, dehydrated by passing through graded series of alcohol, and embedded in paraffin blocks [22]. The embedded tissues were sectioned at 5 μm using a semiautomated rotator microtome (Biobase Bk-2258, Laboratory Manual Microtome, China). The tissue sections were then mounted on glass slides using an incubator at 60-70°C for 30 min. Afterwards, the tissue sections were deparafinized with xylene and rehydrated by using different graded ethanol dilutions (100%, 90%, and 70%). The sections were stained with hematoxylin and eosin (H&E). All slides of kidney and pancreas were examined under the Olympus BX51 Microscope (Olympus Corporation, Tokyo, Japan), and the histopathological images were taken with the help of the Olympus DP20 system under a magnification of ×200.

2.7. Pharmacology-Based Analysis of Thymine, Catechol, and 5-Hydroxymethylfurfural: Antidiabetic Nephropathy Ingredients

2.7.1. Bioactive Compound-Target Protein Network Construction. On the basis of the network pharmacology-based prediction, STITCH 5 (http://stitch.embl.de/, ver.5.0) was used to identify target proteins related to the identified bioactive phytochemicals [25]. The software calculates a score for each pair of proteins-phytochemicals interactions. The SMILES structure of bioactive compounds (thymine, catechol, 5-hydroxymethylfurfural, 2,3-dihydro-3,5-dihydroxy-6-methyl-4H-pyran-4-one, 2H-pyran-2-methanol, 2-hydroxy-4-methyl-benzaldehyde, and 2-methylbutanoic anhydride) was put into STITCH 5 singly to match their potential targets, with the organism selected as "Homo sapiens," the medium required interaction score being ≥0.4. We predicted a total of 84 target proteins with a medium confidence score for thymine, catechol, and 5-hydroxymethylfurfural, which were identified. The compound targets having no relationship with the compound-proteins interactions were not considered for further analysis.

2.7.2. Construction of the Protein-Protein Interaction (PPI) Network of the Predicted Genes. A PPI network of the predicted genes was constructed by a search tool for the retrieval of interacting genes (STRING) database (https://string-db.org/cgi/input.pl; STRING-DB v11.0) [26]. The rank of the target proteins based on the degree of interactions in the PPI network was identified using the Cytoscape plugin cytoHubba [27]. The obtained protein interaction data of 84 target proteins were imported into the Cytoscape 3.6.1 software to construct a PPI network [28].

2.7.3. Pathway Enrichment Analyses of the Target Proteins by Gene Ontology (GO) and Kyoto Encyclopedia of Genes and Genomes (KEGG). To investigate the role of target proteins which interact with the selected phytoconstituents in gene function and signaling pathway, the Database for Annotation, Visualization, and Integrated Discovery (DAVID, https://david.ncifcrf.gov/) v6.8 was employed [29]. The KEGG [30] pathways significantly associated with the predicted genes were identified. We analyzed the Gene Ontology (GO) function and KEGG pathway enrichment of proteins (for 75 target proteins) involved in the PPI network. A brief description was made for target proteins involved in the

cellular components (CC), molecular function (MF), biological process (BP), and the KEGG pathways. The adjusted P value < 0.05, calculated by the Benjamini–Hochberg method [31], was considered significant.

2.7.4. Differential Expression of Hub Targets in the Diabetic Nephropathy Cohort. The gene expression profiling dataset GSE30122 (https://www.ncbi.nlm.nih.gov/geo/query/acc.cgi?acc=GSE30122) for diabetic nephropathy was downloaded from the NCBI gene expression omnibus (GEO) database (https://www.ncbi.nlm.nih.gov/geo/) [32]. This dataset contains tubules of 10 patients and 24 controls. An interactive web tool GEO2R (http://www.ncbi.nlm.nih.gov/geo/geo2r) was applied to screen the differential expression. The GEO2R tool used the GEOquery and limma R packages from the Bioconductor project (http://www.bioconductor.org/). To find out significant levels, the thresholds of P value < 0.05 and |FC| (fold change) > 0.50 were ensured.

2.8. Statistical Analysis. All the data are presented as a mean ± SD. The data were analyzed by one-way ANOVA (analysis of variance) using the SPSS (Statistical Package for Social Science) software (version 20.0, IBM Corporation, NY) followed by Tukey's post hoc tests. The values at $P < 0.05$ were considered significantly different.

3. Results

3.1. Total Flavonoid (TFC), Total Phenolic (TPC), Lycopene, and Beta-Carotene Contents of CMJE. TFC was estimated by the standard rutin curve ($y = 2.497x + 0.307$, $R^2 = 0.979$) and expressed as rutin equivalents per gram of the plant extract. The TFC of the sample was found to be 80.0 mg rutin/g while the total phenolic content using the Folin-Ciocalteu reagent method was found to be 102.0 mg GAE/g. The beta-carotene content of the extract was found to be 0.057056 mg/g, and the lycopene content was 0.0300688 mg/g. The data are presented in Table 1.

3.2. Antioxidative Capacity and α-Amylase Inhibitory Action of CMJE. Antioxidative capacities were measured by the DPPH scavenging method, the superoxide scavenging method, the nitric oxide scavenging method, and the iron-chelating method. The reduction of DPPH in the scavenging assay was reflected through the decrease of absorbance. The IC_{90} values of the sample (CMJE) and the standard (ascorbic acid) were found to be 123.02 ± 6.42 and 16.21 ± 2.34 μg/mL, respectively. The CMJE displayed the IC_{50} value 27.85 ± 1.32 μg/mL in the superoxide scavenging assay and 284.40 ± 5.05 μg/mL in the nitric oxide scavenging assays. The iron-chelating capacity in terms of IC_{50} was found to be 245.47 ± 4.34 μg/mL. ABTS assays showed a dose-dependent radical scavenging capacity of CMJE. The results showed the inhibition concentrations (IC_{50}) 386.36 ± 1.22 μg/mL for CMJE and 92.07 ± 3.21 μg/mL for the standard Trolox. The comparative scavenging effect data are presented in Figure 1, and IC_{50} values are summarized in Table 2.

The α-amylase inhibitory effect of CMJE is presented in Figure 2. Acarbose, an antidiabetic α-amylase inhibitory drug, was used as a reference standard for this assay. The α-amylase inhibitory activity of CMJE was significantly ($P < 0.05$) lower at each concentration of acarbose. The highest inhibition for CMJE was achieved at the concentration of 100 μg/mL.

Table 1: Total phenolic, total flavonoid, lycopene, and carotenoid contents of CMJE.

Phytochemical index	Quantity
Total flavonoid	80.0 mg rutin/g
Total phenolic content	102.0 mg GAE/g
Lycopene	0.031 mg/g
Total carotenoids	0.058 mg/g

3.3. Effects of CMJE on Blood Glucose, Glucose Tolerance, and Glucose Homeostasis. CMJE was found nontoxic in the acute toxicity study. Data regarding the effect of CMJE on animals' body weight and blood glucose levels are displayed in Figure 3. The body weight of the animals was not found to vary statistically among the treatment groups, but the weight of the CMJE50 group was close to that of the normal control (NC). Data reflected that the CMJE50 group has the best glucose-lowering effect, which was statistically significant ($P < 0.05$) with the DC group.

Glucose tolerances were assessed by the oral glucose tolerance test (OGTT) at the third week of the treatment period. Acquired data are presented in Figure 4. The glucose tolerance of the DC group was significantly ($P < 0.05$) lower than that of the other groups. However, the CMJE50 group showed the highest tolerance of glucose load than the other group, which is consistent with the other parameters achieved by this group. Effects of CMJE extracts on the glucose homeostatic status are summarized in Table 3.

3.4. Effects of CMJE on Pancreas and Kidney Weights. Weights of the pancreas and kidney of treated animals are listed in Table 4. Among the doses, CMJE100 in case of pancreatic recovery and CMJE50 in case of kidney recovery were found to be effective. The weight of kidneys was found to be remarkably recovered by CMJE50 while the weight of the pancreas was found to be better ameliorated by CMJE100.

3.5. Effects of CMJE on ALT, AST, Uric Acid, and Creatinine. Changes in ALT, AST, uric acid, and creatinine levels at the end of the intervention are presented in Table 5. The ALT levels of the different groups were not found to significantly ($P < 0.05$) differ from the NC group although the ALT level of the DC group was somehow lower than that of all other groups as well as that of the NC group. The AST level of CMJE50 and CMJE100 group is lower than that of the DC group. The uric acid level of all treated groups is almost similar to that of the NC group. Lower creatinine levels for all the treatments than DC were marked in the result.

3.6. Effects of CMJE on Serum Total Cholesterol and Triglyceride Levels. Both serum total cholesterol and triglyceride levels for the treatment groups were consistently lower than those of the DC group while CMJE100 was found to reduce the total cholesterol more than other doses and

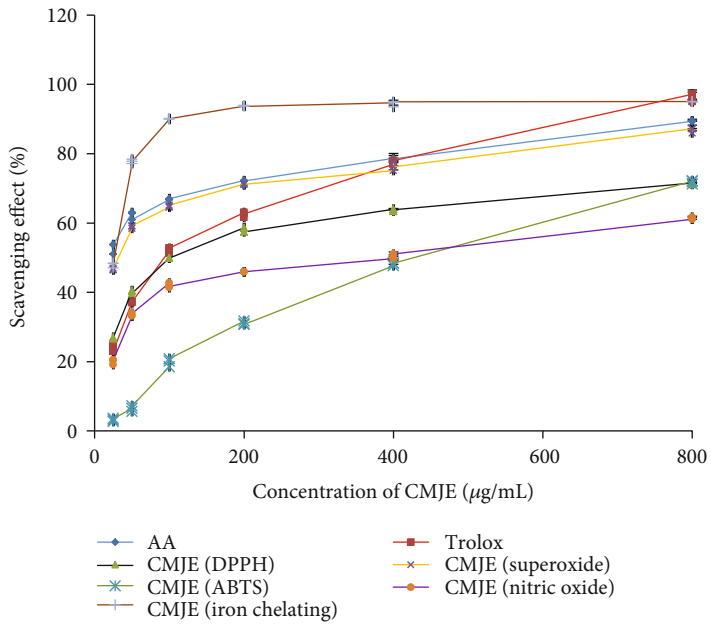

Figure 1: Effect of CMJE on scavenging capacities in DPPH (2,2-diphenyl 1-picrylhydrazyl) radical scavenging, SO (superoxide) scavenging, ABTS (2,2′-azino-bis(3-ethylbenzothiazoline-6-sulfonic acid)) radical scavenging, NO (nitric oxide) scavenging, and IC (iron-chelating) assays. All values were presented as means ± SD (triplicate). Data were analyzed by one-way ANOVA (analysis of variance) using the SPSS (Statistical Package for Social Science) software followed by Tukey's post hoc test.

Table 2: Comparative IC_{50} values achieved by CMJE in different antioxidative models.

Antioxidative models	Test sample	Reference standard	Inhibition concentration (IC_{50}, μg/mL)	
			CMJE	Reference standard
DPPH scavenging assay	CMJE	Ascorbic acid	123.02 ± 6.42	
Superoxide scavenging assay	CMJE	Ascorbic acid	27.85 ± 1.32	16.21 ± 2.34
Nitric oxide assay	CMJE	Ascorbic acid	284.40 ± 5.05	
Iron-chelating assay	CMJE	Ascorbic acid	245.47 ± 4.34	
ABTS assay	CMJE	Trolox	386.36 ± 1.22	92.07 ± 3.21

CMJE200 showed better effects than other doses to normalize triglyceride levels. Effects of CMJE extracts on serum total cholesterol and triglyceride are shown in Figure 5.

3.7. Effects of CMJE on Tissue Architecture. A summary of the changes observed in the different CMJE-treatment groups is presented in Table 6. The pancreas and the kidney tissue architectures of the treated animals are presented in Figure 6. STZ induction was reflected through the decreased size of the islets of Langerhans and tissue degeneration in the pancreas of the DC group (Figure 6(a)). On the contrary, the other animal tissues were less degenerated resembling the animals' NC group. The kidney cells were remarkably recovered by CMJE50 (Figure 6(b)) while the two other treatments failed to display the same action.

3.8. GC-MS Compound Characterization from the CMJE. The GC-MS spectra of the CMJE extracts are shown in Figure 7. Catechol, thymine, 2,3-dihydro-3,5-dihydroxy-6-methyl-4H-pyran-4-one, 5-hydroxymethylfurfural, and 3-(methylthio)-propanoic acid ethyl ester are noted as the constituents displaying the highest occurrence. The peak areas and occurrence of the compounds are summarized in Table 7.

3.9. Analyses of the Interactions between Active Ingredients of the Extracts and Target Proteins. To evaluate the antidiabetic activities of the constituents of the extracts, it is essential to scrutinize the target proteins on which these compounds act. We found that only thymine, catechol, and 5-hydroxymethylfurfural interacted with 84 target proteins. Based on the compound-protein targets relationships, our results indicate that these three compounds play substantial biological and physiological activities.

3.10. Construction and Analysis of the Target Proteins PPI Network. The PPI network analysis plays a substantial role in studying molecular processes, and abnormal PPI is at the basis of many pathological processes [33]. Using the STRING2 database, all target proteins (84) were mapped into the PPI network. Interestingly, we found that 75 target

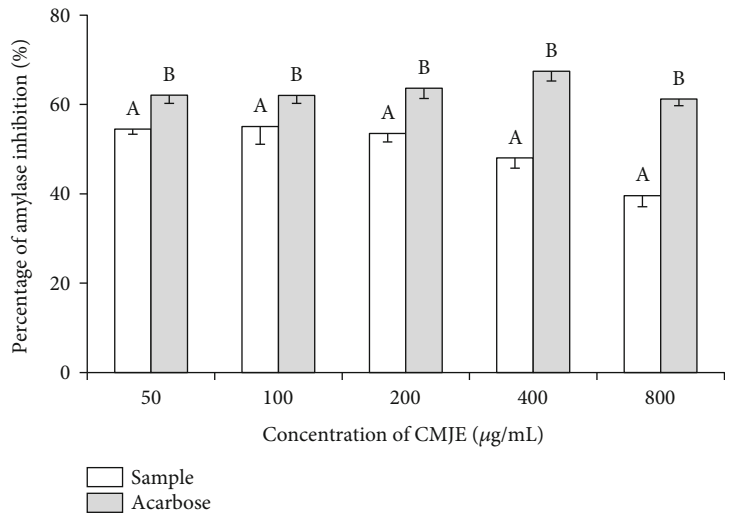

Figure 2: Effects of CMJE on the α-amylase inhibitory activity. Acarbose was used as the reference standard. Data are presented as means ± SD (triplicate). All data were analyzed by one-way ANOVA (analysis of variance) using the statistical software SPSS (Statistical Package for Social Science, version 20.0) followed by Tukey's post hoc test. Superscript letters (a, b) over the graphical bars indicate the statistical difference between inhibitory effect of CMJE and acarbose.

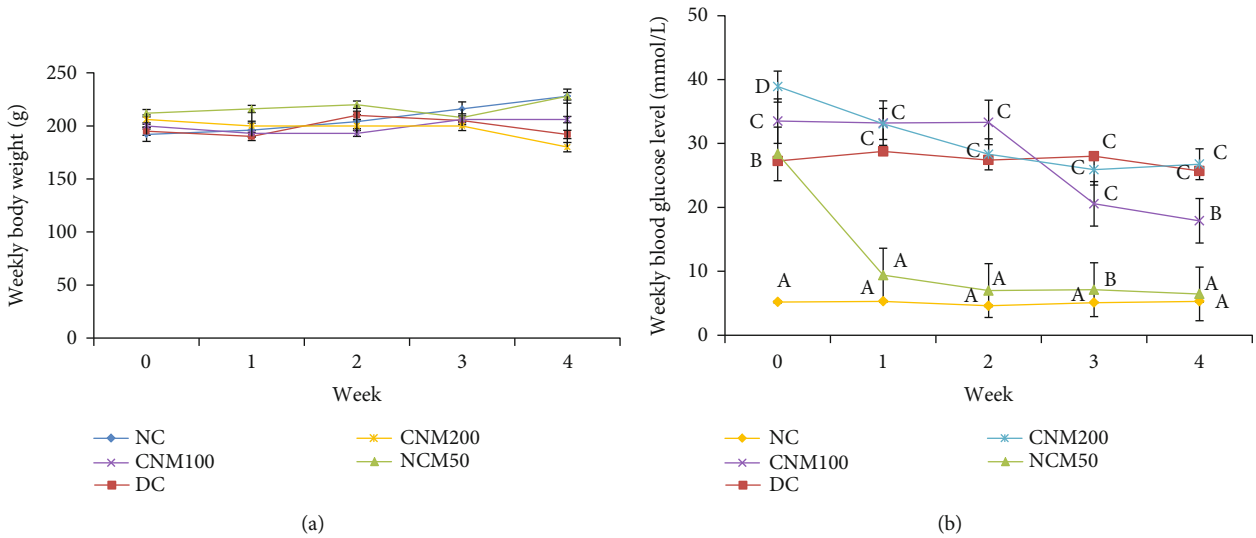

Figure 3: Effects of CMJE extracts on body weight (a) and weekly blood glucose levels (b) of treated animals. Data are expressed as means ± SD ($n = 6$). All data were analyzed by one-way ANOVA (analysis of variance). Significance was confirmed at $P < 0.05$. Alphabets (a–c) over the line graphs indicate the statistical differences among the groups.

proteins were involved in PPI which have 235 edges, and an average node degree 5.88 with a PPI enrichment P value of less than 1.0×10^{-16}. In this PPI network, the larger the node degree, the stronger relationship between the proteins corresponding to the node, suggesting that the target proteins plays a key role in the whole interaction network. Only nine target proteins were not included in PPI. We only got one subnetwork in PPI and this subnetwork included 75 target proteins. All target proteins with interactions with other proteins are illustrated in Figure 8. Cytoscape 3.6.1 was used to analyze the interactions among the top 15 hub target proteins (degree of interaction with no less than 10). The hub target proteins are TP53, CASP3, COMT, CYP1B1, DPYD, NQO1, PTGS1, PTGS2, CAT, OGG1, GSTP1, MLH1, CYP1A1, TYMS, and TH.

3.11. Gene Ontology Analyses of the Interacting Target Proteins. The GO enrichment analysis of the interacting target proteins (total 75 involved in PPI) which act with compounds of the CMJE extracts was performed by DAVID (https://david.ncifcrf.gov/). The significantly enriched terms in CC, BP, and MF categories were selected according to the Benjamini–Hochberg-corrected P value < 0.05. A total of 43 significant BP was listed in Table 8. In addition, two significant CC were also identified, as illustrated in Table 8.

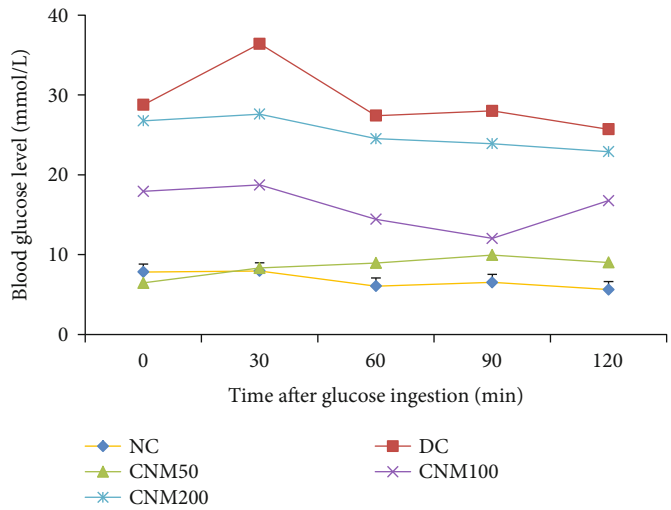

Figure 4: Effects of CMJE on oral glucose tolerance (OGT) at the third week of intervention. Data are expressed as means ± SD ($n = 6$). All data were analyzed by one-way ANOVA (analysis of variance) using the statistical software SPSS (Statistical Package for Social Science, version 20.0) followed by Tukey's post hoc test. Data significance was confirmed at $P \leq 0.05$.

Table 3: Effects of CMJE on the glucose homeostatic status (HOMA-IR and HOMA-β).

Treatment groups	HOMA-IR (mIU/L)	HOMA-β (%)
NC	0.017	0.460
DC	0.116	0.036
CMJE50	0.052	0.240
CMJE100	0.155	0.045
CMJE200	0.111	0.082

HOMA-IR stands for homeostatic model assessment for insulin resistance, and HOMA-β represents the pancreatic beta cell function (%).

Table 4: Effects of CMJE on the relative weight of the pancreas and kidney of treated animals.

Tissue weight	Pancreas weight (g)	Kidney weight (g)
NC	0.569 ± 0.105^{a}	1.794 ± 0.106^{a}
DC	0.304 ± 0.047^{b}	1.738 ± 0.093^{a}
CMJE50	0.215 ± 0.044^{c}	1.772 ± 0.127^{a}
CMJE100	0.320 ± 0.050^{b}	1.690 ± 0.031^{a}
CMJE200	0.215 ± 0.035^{c}	1.663 ± 0.199^{a}

Data are expressed as means ± SD ($n = 6$). All data were analyzed by one-way ANOVA (analysis of variance) using the statistical software SPSS (Statistical Package for Social Science, version 20.0) followed by Tukey's post hoc test. Data significance was confirmed at $P \leq 0.05$. The superscript alphabets (a–c) in the table denote the reciprocal significance between and among the groups.

3.12. Target Proteins Are Associated with the Enrichment of the KEGG Pathways. To further elucidate the relationship between target proteins and pathways, we identified 20 KEGG pathways significantly associated with the target proteins (Table 9), and they were found to be involved in secretion (pancreatic secretion), metabolism, and cellular signaling.

3.13. Validation of Hub Target Proteins in Diabetic Nephropathy Cohort (GSE30122). We screened all 15 hub proteins in independent tubulointerstitial tissues of diabetic kidney disease. Interestingly, we found that 8 targets are dysregulated in this cohort. Among them, CAT and OGG1 are downregulated, and CASP3, COMT, CYP1B1, DPYD, NQO1, and PTGS1 are upregulated in diabetic kidney disease (DKD) tubuli (Figure 9).

4. Discussion

Coconut mesocarp juice extract (CMJE) was comprehensively studied for its antidiabetic effects which have been evaluated in the light of CMJE's phytoconstituent status and antioxidative potential. It is believed that oxidative stress plays an important role in the development of vascular complications in diabetes particularly type 2 diabetes [34]. Free radical formation in diabetes by nonenzymatic glycation of proteins, glucose oxidation, and increased lipid peroxidation leads to damage of enzymes and cellular machinery and increases insulin resistance [35]. Free radicals, therefore, through their aforesaid abilities play a major role in damaging lipids, proteins, and DNA [36] in the onset of diabetic complication. Additionally, the elevation of reactive oxygen species (ROS) decreases the production of biological antioxidative enzymes such as catalase, superoxide dismutase (SOD), and glutathione peroxidase (GSH-Px) [37]. Variations in the levels of these enzymes render the tissues susceptible to oxidative stress leading to the development of diabetic complications [38]. Our data are strongly supportive for the antidiabetic action of CMJE extracts because of their high total phenolic content, total flavonoid content, and carotenoid and lycopene contents. Similar researches on the antidiabetic actions of plant phenolics especially flavonoids, triterpenoids, and saponins have been published recently [39, 40]. Phenolic compounds have attracted tremendous interest due to their outstanding free radical scavenging

Table 5: Effects of CMJE on serum ALT, AST, uric acid and creatinine levels.

Treatment groups	ALT (U/L)	AST (U/L)	Uric acid (mg/dL)	Creatinine (mg/dL)
NC	71.60 ± 2.40^{a}	4.80 ± 1.76^{a}	6.60 ± 2.40^{a}	0.49
DC	33.75 ± 2.50^{b}	7.62 ± 2.00^{b}	12.00 ± 2.80^{b}	1.23
CMJE50	$73.5\,0 \pm 7.20^{a}$	$6.00 \pm 1.2\,0^{c}$	6.30 ± 0.72^{a}	0.71
CMJE100	80.00 ± 8.00^{a}	5.17 ± 1.04^{c}	6.59 ± 0.82^{a}	0.77
CMJE200	79.00 ± 8.10^{a}	6.50 ± 0.85^{b}	7.18 ± 0.71^{c}	0.68

Data are expressed as means ± SD ($n = 6$). All data were analyzed by one-way ANOVA (analysis of variance) using the statistical software SPSS (IBM Corporation, NY, version 20.0) followed by Tukey's post hoc test for significance at $P \leq 0.05$. The significant differences among and between the groups at least in the experimental condition are represented through the superscript letters (a–c) in the table.

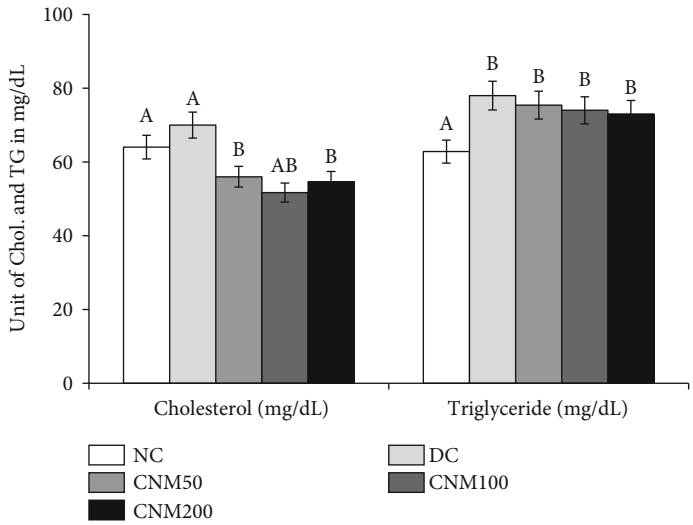

Figure 5: Effects of CMJE on serum cholesterol and triglyceride levels of treated animals. Data are expressed as means ± SD ($n = 6$). All data were analyzed by one-way ANOVA (analysis of variance) using the statistical software SPSS (Statistical Package for Social Science, version 20.0) followed by Tukey's post hoc test for significance at $P \leq 0.05$. Superscript letters (a, b) on the bar graph represent the values that are significantly different compared to each other at least at the intervention period.

Table 6: Effect of CMJE on the tissue architectures of the pancreas and kidney.

Name of the tissues and parameters	Group				
	NC	DC	CMJE50	CMJE100	CMJE200
Pancreas					
Degenerated cells	-	+++	++	+	+
Necrotic cells	-	+++	+	+	++
Kidney					
Atrophic glomerulus and tubules	-	++	-	-	-
Eosinophilic secretion in the tubules lumen	-	-	-	-	-
Tubular epithelial cell degeneration	-	+++	-	++	++
Increased fibrous tissue	-	++	+	+	+
Hyperemic vessels in the interstitium	-	+++	+	+	+

Histopathological assessments are graded as follows: (i) (-) indicates "no abnormality." (ii) (+) indicates "mild injury." (iii) (++) indicates "moderate injury." (iv) (+ + +) indicates "severe injury".

capacity which is measured by both in vivo and in vitro methods; some of in vitro methods, such as DPPH, ABTS, superoxide, NO, iron-chelating assays, were opted for our CMJE samples. Promising free radical scavenging effects of CMJE noted with our extracts imply their potential to be reflected in cellular systems for reducing oxidative stress [41, 42], a pivotal factor for diabetes and diabetes-related diseases, leading to attenuate diabetic complications [43]. The use of CMJE extracts, therefore, might have a highly prospective use as antioxidative food supplements in diabetes treatment [44].

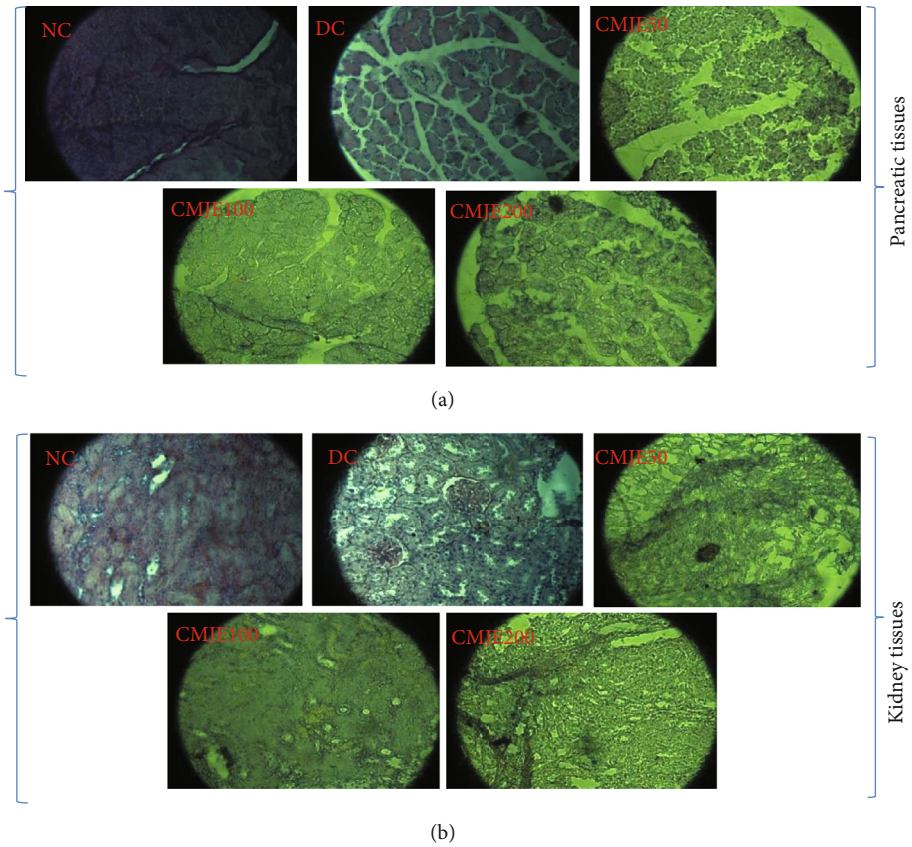

Figure 6: Histopathological examination by hematoxylin and eosin staining of pancreatic (a) and kidney (b) tissues after the intervention (microscopic resolution: 10×40). Light microscopies of pancreatic sections stained with PAS and counterstained with hematoxylin are shown. NC, DC, CMJE50, CMJE100, and CMJE200 stand for normal control (diabetic control, coconut mesocarp juice extract 50 mg/kg bw, coconut mesocarp juice extract 100 mg/kg bw, and coconut mesocarp juice extract 200 mg/kg bw).

One of the methods used to treat diabetes mellitus is the inhibition of carbohydrate-digesting enzymes such as α-amylase and α-glucosidase upon gastrointestinal glucose absorption [21]. In this study, the effect of the mesocarp part of coconut fruit was evaluated on the activity of α-amylase, which could constitute a basis for searching alternative drugs from CMJE extracts. This finding is in line with previous reports which showed that promising inhibition of pancreatic α-amylase could lead to the fermentation of undigested carbohydrates by bacteria in an irregular way in the colon, such that a mild activity of α-amylase inhibition is desirable [44]. This suggests that the three interactive components characterized here in the CMJE extracts may compete with the substrate for binding to the active site of the enzyme thereby preventing the breaking down of oligosaccharides to disaccharides.

In a study using the animals, body weights were found to be higher than that in the diabetic control, which is literally the sign of ameliorating the trend of diabetes. Weekly blood glucose and oral glucose tolerance have tremendously been favored by the lowest dose of CMJE50, which is seemingly a very remarkable and promising feature for the further use of CMJE extracts as drug molecules. Probably, the recovery of the pancreas in the STZ-induced rats was the highest with the administration of the coconut aqueous extract, as a consequence of the restoration of glucose levels reflected by the higher pancreatic weights of CMJE-treated groups compared to diabetic rats. The pancreas weight loss observed in the DC group could be related to both the destruction and the disappearance of pancreatic islet cells as well as the selective disruption of insulin-producing cells [45].

The increase in aminotransferase levels recorded in our study may be linked to cellular damage in the liver caused by STZ-induced diabetes. Lowering of total cholesterol and triglycerides could be ascribed as an effective role of CMJE extracts in controlling diabetic dyslipidemia, a harbinger of future diabetes, characterized by increased triglycerides, and postprandial lipemia [46]. Improvement of the tissue architecture of the pancreas and the kidney could be ascertained through the absence of tubular epithelial cell necrosis and the presence of degenerated cells, although the lowest CMJE dose was more effective than the others. This could be explained by the receptor occupancy of respective cells with the lower CMJE doses. Additionally, low CMJE doses proportionally cause smaller digestive disturbance and are responsible for higher drug absorption. Low digestive disturbance thus leads to higher insulin sensitivity to control the blood glucose level to a higher extent [47]. The Hormesis effect may be attributed to trigger the receptors with lower doses of treatment.

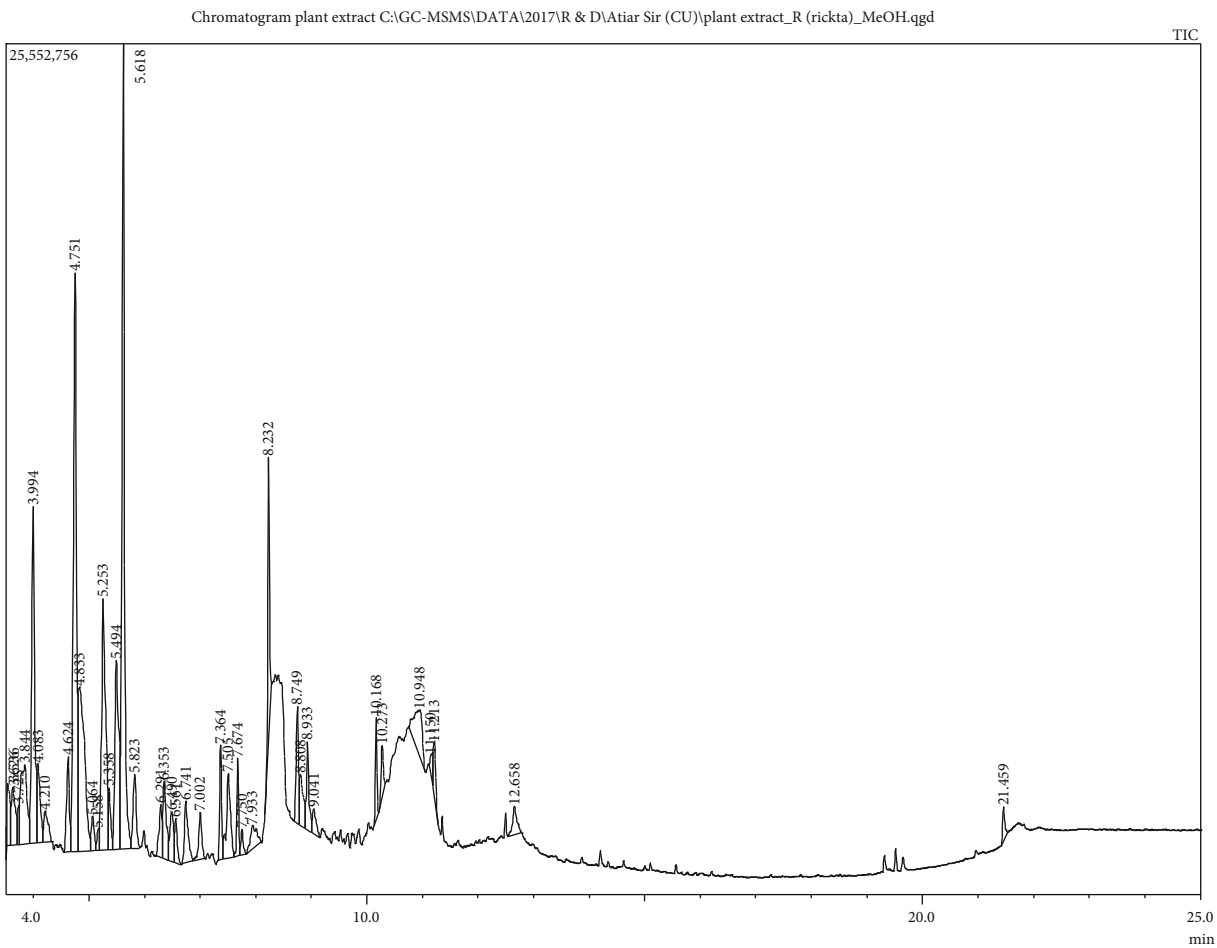

Instrument Name: GC-MS/MS

Model: GCMS-TQ8040

Column: Rxi-5ms

(a)

Figure 7: Continued.

Most probable compounds:

S/N	Ret. time	Compound name
1	3.533	3-trans-methoxy-2-cis-methyl-1R-cyclohexanol
2	3.625	2,4 (1H,3H)-pyrimidinedione, dihydro-
3	3.725	Butanoic acid, 2-(hydroxymethyl)-, ethyl ester, (R)-
4	3.842	2-methylbutanoic anhydride
5	3.992	Thymine
6	4.083	Methyl 2-furoate
7	4.208	Trimethylaluminum
8	4.625	Ethanamine, N-ethyl-N-nitroso-
9	4.75	4H-pyran-4-one, 2,3-dihydro-3,5-dihydroxy-6-methyl-
10	4.833	3-(methylthio) propanoic acid ethyl ester
11	5.067	(S)-5-hydroxymethyl-2[5H]-furanone
12	5.158	4H-pyran-4-one, 3,5-dihydroxy-2-methyl-
13	5.25	Catechol
14	5.358	Butanedioic acid, 2-hydroxy-2-methyl-, dimethyl ester, (2R)-
15	5.492	2H-pyran-2-methanol, tetrahydro-
16	5.617	5-hydroxymethylfurfural
17	5.825	Butanedioic acid, hydroxy-, dimethyl ester
18	6.292	Undecenyl tiglate, 10-
19	6.35	1-(methylthio)-3-pentanone
20	6.492	3,4-hexanediol, 2,5-dimethyl-
21	6.558	Fumaric acid, monoamide, N,N-dimethyl-, 2-ethylhexyl ester
22	6.742	Heptyl caprylate
23	7	Butanedioic acid, 2-hydroxy-2-methyl-, (S)-
24	7.367	Phenol, 4-propyl-
25	7.508	1,2,3-benzenetriol

(b)

Figure 7: Continued.

26	7.675	Tetradecane
27	7.75	Benzene, 1-chloro-4-methoxy-
28	7.933	Butanamide, 2-hydroxy-N, 2,3,3-tetramethyl-
29	8.233	Benzaldehyde, 2-hydroxy-4-methyl-
30	8.75	Benzoic acid, 3-hydroxy-
31	8.808	(Z), (Z)-2, 5-Dimethyl-2, 4-hexadienedioic acid
32	8.933	Pentadecane
33	9.042	Benzoic acid, 4-hydroxy-
34	10.167	Hexadecane
35	10.275	1,3-benzenediol, 4-propyl-
36	10.95	3-deoxy-d-mannoic lactone
37	11.15	Butanoic acid, 2-methyl-, hexyl ester
38	11.217	3-deoxy-d-mannonic acid
39	12.658	2-hydroxy-5-methylisophthalaldehyde

(c)

Peak report TIC

Peak#	R.time	Area%	Name
1	3.536	1.27	3-trans-methoxy-2-cis-methyl-1R-cyclohexanol
2	3.626	1.58	2, 4 (1H, 3H)-pyrimidinedione, dihydro-
3	3.725	0.52	Butanoic acid, 2-(hydroxymethyl)-, ethyl ester, (R)-
4	3.844	3.61	2-methylbutanoic anhydride
5	3.994	7.15	Thymine
6	4.083	1.73	Methyl 2-furoate
7	4.210	0.96	Trimethylaluminum
8	4.624	1.91	Ethanamine, N-ethyl-N-nitroso-
9	4.751	12.94	4H-pyran-4-one, 2,3-dihydro-3,5-dihydroxy-6-methyl-
10	4.833	7.24	3-(methylthio) propanoic acid ethyl ester
11	5.064	0.71	(S)-5-Hydroxymethyl-2[5H]-furanone
12	5.158	0.34	4H-pyran-4-one, 3,5-dihydroxy-2-methyl-
13	5.253	7.20	Catechol
14	5.358	1.00	Butanedioic acid, 2-hydroxy-2-methyl-, dimethyl ester, (2R)-
15	5.494	5.20	2H-pyran-2-methanol, tetrahydro-
16	5.618	14.41	5-Hydroxymethylfurfural
17	5.823	1.71	Butanedioic acid, hydroxy-, dimethyl ester
18	6.291	1.07	Undecenyl tiglate, 10-
19	6.353	1.86	1-(methylthio)-3-pentanone
20	6.490	1.26	3,4-hexanediol, 2,5-dimethyl-
21	6.561	0.78	Fumaric acid, monoamide, N, N-dimethyl-, 2-ethylhexyl ester
22	6.741	1.57	Heptyl caprylate
23	7.002	1.08	Butanedioic acid, 2-hydroxy-2-methyl-, (S)-
24	7.364	1.58	Phenol, 4-propyl-
25	7.505	2.44	1,2,3-benzenetriol
26	7.674	1.20	Tetradecane
27	7.750	0.42	Benzene, 1-chloro-4-methoxy-
28	7.933	1.04	Butanamide, 2-hydroxy-N,2,3,3-tetramethyl-
29	8.232	3.70	Benzaldehyde, 2-hydroxy-4-methyl-
30	8.749	2.01	Benzoic acid, 3-hydroxy-
31	8.808	1.34	(Z),(Z)-2,5-Dimethyl-2,4-hexadienedioic acid
32	8.933	1.50	Pentadecane
33	9.041	0.62	Benzoic acid, 4-hydroxy-
34	10.168	1.04	Hexadecane
35	10.273	0.81	1, 3-Benzenediol, 4-propyl-
36	10.948	2.49	3-Deoxy-d-mannoic lactone
37	11.150	0.40	Butanoic acid, 2-methyl-, hexyl ester
38	11.213	0.95	3-Deoxy-d-mannonic acid
39	12.658	0.87	2-Hydroxy-5-methylisophthalaldehyde
40	21.459	0.48	13-Docosenamide, (Z)-
		100.00	

(d)

Figure 7: GC-MS spectra of CMJE obtained from the mass spectrometer-electron impact ionization (EI) method (GC-MS TQ 8040, Shimadzu Corporation, Kyoto, Japan) coupled with a gas chromatograph (GC-17A, Shimadzu Corporation, Kyoto, Japan). A fused silica capillary column with inlet temperature 260°C and oven temperature 70°C (0 min) was programmed. The mass range was set in the range of 50-550 m/z.

Table 7: Compounds obtained from GC-MS analyses of the CMJE.

SL No.	Compound name	RT	Peak area (%)
1	3-Trans-methoxy-2-cis-methyl-1R-cyclohexanol	3.53	1.27
2	2,4(1H, 3H)-Pyrimidinedione, dihydro	3.625	1.58
3	Butanoic acid, 2-(hydroxymethyl)-ethyl ester (R)-	3.72	0.52
4	2-Methylbutanoic anhydride	3.844	3.61
5	Thymine	3.994	7.1
6	Methyl 2-furoate	4.083	1.73
7	Trimethylaluminum	4.210	0.96
8	Ethanamine, N-ethyl-N-nitroso-	4.624	1.91
9	2,3-Dihydro-3,5-dihydroxy-6-methyl-4H-pyran-4-one	4.751	12.94
10	3-(Methylthio)propanoic acid ethyl ester	4.833	7.24
11	(S)-5-Hydroxymethyl-2[5H]-furanone	5.064	0.71
12	3,5-Dihydroxy-2-methyl-4H-pyran-4-one	5.158	0.34
13	Catechol	5.253	7.20
14	Butanedioic acid, 2-hydroxy-2-methyl-, dimethyl ester, (2R)-	5.358	1.00
15	2H-pyran-2-methanol, tetrahydro-	5.494	5.20
16.	5-Hydroxymethylfurfural	5.618	14.41
17	Butanedioic acid, hydroxy-, dimethyl ester	5.82	1.71
18	Undecenyl tiglate, 10-	6.291	1.07
19	1-(Methylthio)-3-pentanone	6.353	1.86
20	3,4-Hexanediol, 2,5-dimethyl-	6.49	1.26
21	Fumaric acid, monoamide, N,N-dimethyl-, 2-ethylhexyl ester	6.561	0.78
22	Heptyl caprylate	6.741	1.57
23	Butanedioic acid, 2-hydroxy-2-methyl-, (S)-	7.002	1.08
24	Phenol, 4-propyl-	7.364	1.58
25	1,2,3-Benzenetriol	7.505	2.44
26	Tetradecane	7.674	1.20
27	Benzene, 1-chloro-4-methoxy-	7.75	0.42
28	Butanamide, 2-hydroxy-N,2,3,3-tetramethyl-	7.933	1.04
29	2-hydroxy-4-methyl-benzaldehyde	8.23	3.70
30	(Z),(Z)-2,5-Dimethyl-2,4-hexadienedioic acid	8.808	1.34
31	Pentadecane	8.933	1.50
32	Hexadecane	10.168	1.04
33	1,3-Benzenediol, 4-propyl-	10.273	0.81
34	3-Deoxy-d-mannoic lactone	10.948	2.49
35	Butanoic acid, 2-methyl-, hexyl ester	11.150	0.40
36	3-Deoxy-d-mannonic acid	11.213	0.95
37	2-Hydroxy-5-methylisophthalaldehyde	12.658	0.87

The effects of CMJE extracts described above could be linked with the presence of a few polyphenolic compounds characterized by GC-MS, such as catechol, 4-hydroxybenzoic acid, 1-chloro-4-methoxy-benzene, methyl 2-furoate, thymine, 4-propyl-phenol, 2,3-dihydro-3,5-dihydroxy-6-methyl-4H-pyran-4-one, 5-hydroxymethylfurfural, and 2-hydroxy-5-methylisophthalaldehyde, which are well known as antioxidant and antidiabetic constituents. The aforesaid statement has been confirmed by network pharmacological bioinformatics tools using the PPI network and gene ontology analyses.

The PPI network plays substantial roles in studying molecular processes, and abnormal PPI is at the basis of many pathological processes [48]. From the PPI of targeted proteins, we identified hub nodes which are markedly associated with diabetes. For example, ABCA1 protein with 10 degrees of interaction plays an inevitable role in regulating lipid metabolism, and defect in this gene disrupts lipid transport of HDL-cholesterol associated with the development of T2DM [49]. TNF-alpha concentration is also linked with peripheral insulin resistance and elevated plasma glucose as well as insulin levels before the onset of type 2 diabetes

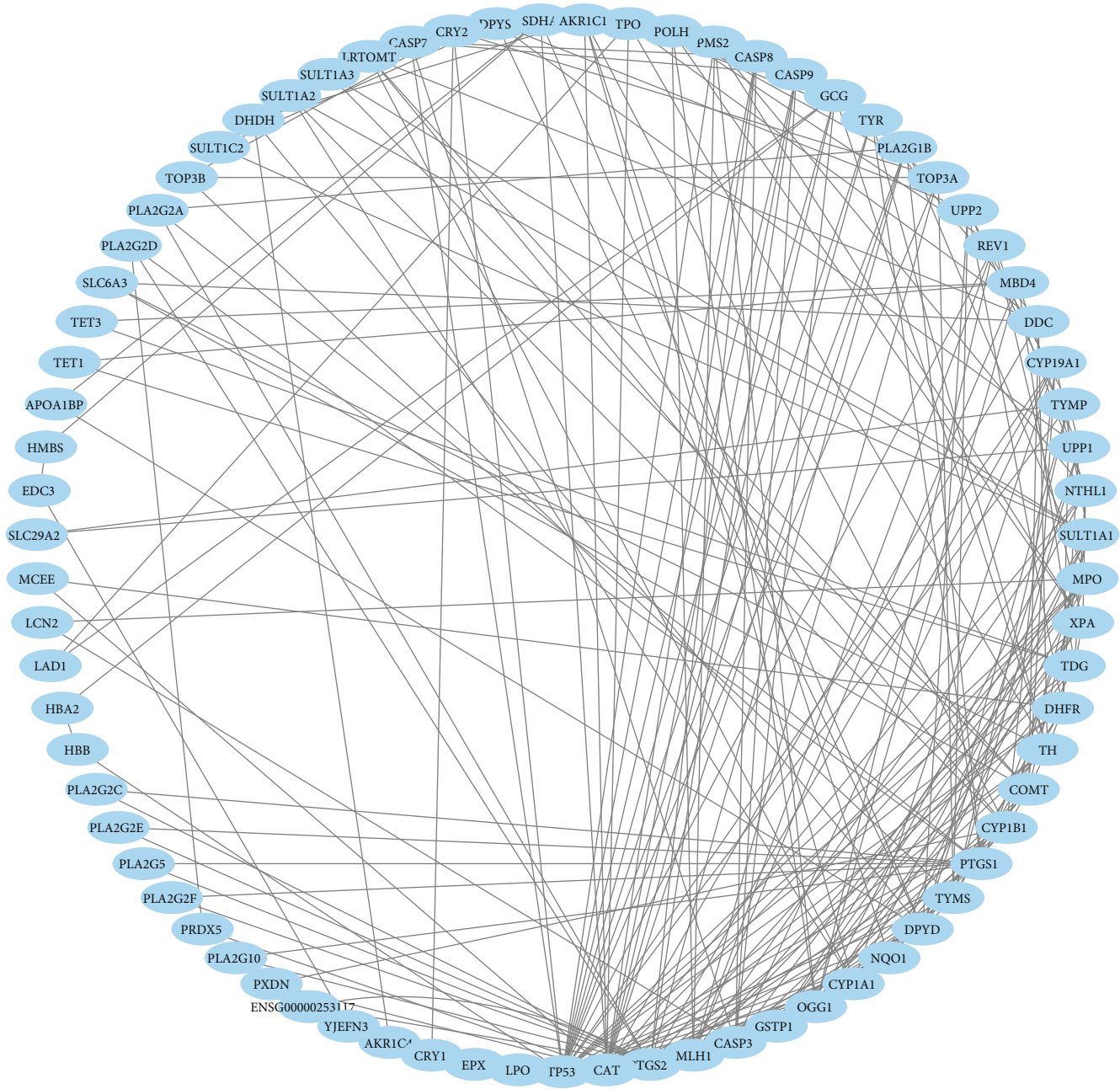

Figure 8: The protein-protein interaction (PPI) network of the 75 target proteins.

[50]. It was observed that a CXCL8 antagonist ameliorates diabetic nephropathy in diabetic male mice and attenuates high glucose-induced mesangial injury [51]. Caspase-3 promotes diabetic kidney disease [52]. The *HMGCR* gene, in population studies, was also found to be associated with bodyweight gain and a higher risk of type 2 diabetes [53]. Interleukin-10 (IL10), an anti-inflammatory cytokine, is supposed to play a type 2 diabetes (T2D) protective role [54]. Figure 9 shows that the immunological target proteins including IL10, CXCL8, and TNF are located in the PPI networks with a top degree of interaction, indicating that this PPI network is associated with immunological activities. It was stated that humans' chemokines have been associated with, or implicated in, the pathogenesis of type 1 diabetes [55]. Altogether, these compound-proteins interactions may be associated with the regulation of diabetes pathophysiology.

In addition, we identified the GO and pathway enrichment of target proteins. The GO analysis indicated that the target proteins may bind with plasma membranes, chromosomes, chromatin, regulatory regions of nucleic acids, or/and cellular receptors of cells for mediating metabolic, immunological processes, signaling, and/or other activities, so as to exert signaling and antidiabetic potentials [56]. Pathway analysis revealed some pathways being also associated with diabetes. Retinol metabolism is the most significantly

Table 8: Gene Ontology (GO) enrichment analysis of the interacting target proteins; 43 biological processes, 15 molecular functions, and 2 cellular components.

Category	Term	Benjamini-corrected *P* value
BP	GO:0042744, hydrogen peroxide catabolic process	$5.78E-12$
	GO:0098869, cellular oxidant detoxification	$1.08E-10$
	GO:0055114, oxidation-reduction process	$6.90E-10$
	GO:0050482, arachidonic acid secretion	$1.03E-09$
	GO:0036149, phosphatidylinositol acyl-chain remodeling	$5.02E-09$
	GO:0036148, phosphatidylglycerol acyl-chain remodeling	$9.64E-09$
	GO:0036150, phosphatidylserine acyl-chain remodeling	$9.64E-09$
	GO:0032355, response to estradiol	$1.53E-08$
	GO:0036152, phosphatidylethanolamine acyl-chain remodeling	$5.14E-08$
	GO:0006979, response to oxidative stress	$6.62E-08$
	GO:0036151, phosphatidylcholine acyl-chain remodeling	$8.95E-08$
	GO:0006654, phosphatidic acid biosynthetic process	$4.34E-07$
	GO:0006805, xenobiotic metabolic process	$2.18E-06$
	GO:0016042, lipid catabolic process	$3.67E-06$
	GO:0046135, pyrimidine nucleoside catabolic process	$4.76E-06$
	GO:0006644, phospholipid metabolic process	$4.76E-06$
	GO:0045471, response to ethanol	$1.29E-05$
	GO:0007568, aging	$1.91E-05$
	GO:0008202, steroid metabolic process	$3.89E-05$
	GO:0045008, depyrimidination	$1.48E-04$
	GO:0042493, response to drug	$1.82E-04$
	GO:0032496, response to lipopolysaccharide	$1.97E-04$
	GO:0006584, catecholamine metabolic process	$1.91E-04$
	GO:0046677, response to antibiotic	$2.95E-04$
	GO:0051923, sulfation	$3.42E-04$
	GO:0006284, base-excision repair	$3.92E-04$
	GO:0050427, 3′-phosphoadenosine 5′-phosphosulfate metabolic process	$8.60E-04$
	GO:0032025, response to cobalt ion	$6.80E-03$
	GO:0009635, response to herbicide	$9.14E-03$
	GO:0009636, response to toxic substance	$1.11E-02$
	GO:0009308, amine metabolic process	$1.13E-02$
	GO:0009812, flavonoid metabolic process	$1.13E-02$
	GO:0008635, activation of cysteine-type endopeptidase activity involved in apoptotic process by cytochrome c	$1.40E-02$
	GO:0043066, negative regulation of apoptotic process	$1.42E-02$
	GO:0042416, dopamine biosynthetic process	$1.64E-02$
	GO:0043525, positive regulation of neuron apoptotic process	$1.63E-02$
	GO:0008210, estrogen metabolic process	$1.89E-02$
	GO:0043097, pyrimidine nucleoside salvage	$2.19E-02$
	GO:0042542, response to hydrogen peroxide	$2.45E-02$
	GO:0071407, cellular response to organic cyclic compound	$3.62E-02$
	GO:0097194, execution phase of apoptosis	$3.61E-02$

Table 8: Continued.

Category	Term	Benjamini-corrected *P* value
CC	GO:0080111, DNA demethylation	3.61*E* – 02
	GO:0033189, response to vitamin A	4.45*E* – 02
	GO:0005829, cytosol	4.25*E* – 06
	GO:0005739, mitochondrion	1.18*E* – 04
MF	GO:0004601, peroxidase activity	5.24*E* – 12
	GO:0020037, heme binding	5.97*E* – 11
	GO:0004623, phospholipase A2 activity	3.61*E* – 09
	GO:0003684, damaged DNA binding	1.60*E* – 05
	GO:0005506, iron ion binding	1.30*E* – 05
	GO:0019825, oxygen binding	6.41*E* – 05
	GO:0004062, aryl sulfotransferase activity	5.34*E* – 04
	GO:0097153, cysteine-type endopeptidase activity involved in apoptotic process	6.06*E* – 04
	GO:0008146, sulfotransferase activity	1.35*E* – 02
	GO:0047498, calcium-dependent phospholipase A2 activity	1.48*E* – 02
	GO:0019104, DNA N-glycosylase activity	1.67*E* – 02
	GO:0030983, mismatched DNA binding	1.87*E* – 02
	GO:0016712, oxidoreductase activity, acting on paired donors, with incorporation or reduction of molecular oxygen, reduced flavin or flavoprotein as one donor, and incorporation of one atom of oxygen	3.23*E* – 02
	GO:0004497, monooxygenase activity	3.21*E* – 02
	GO:0004197, cysteine-type endopeptidase activity	3.46*E* – 02

Table 9: Enriched KEGG pathways significantly associated with target proteins in this study.

KEGG pathway	Benjamini-corrected *P* value
hsa00592: alpha-linolenic acid metabolism	1.96*E* – 07
hsa00590: arachidonic acid metabolism	1.81*E* – 07
hsa00591: linoleic acid metabolism	2.06*E* – 07
hsa04975: fat digestion and absorption	1.42*E* – 06
hsa00565: ether lipid metabolism	3.21*E* – 06
hsa01100: metabolic pathways	5.47*E* – 05
hsa04972: pancreatic secretion	3.39*E* – 04
hsa00564: glycerophospholipid metabolism	3.42*E* – 04
hsa05204: chemical carcinogenesis	1.10*E* – 03
hsa04270: vascular smooth muscle contraction	1.05*E* – 03
hsa03460: fanconi anemia pathway	1.23*E* – 03
hsa00140: steroid hormone biosynthesis	1.74*E* – 03
hsa00350: tyrosine metabolism	2.51*E* – 03
hsa00980: metabolism of xenobiotics by cytochrome P450	4.69*E* – 03
hsa00983: drug metabolism—other enzymes	6.29*E* – 03
hsa00240: pyrimidine metabolism	1.66*E* – 02
hsa04210: apoptosis	1.69*E* – 02
hsa03410: base-excision repair	2.19*E* – 02
hsa04014: ras signaling pathway	2.74*E* – 02
hsa00380: tryptophan metabolism	3.39*E* – 02

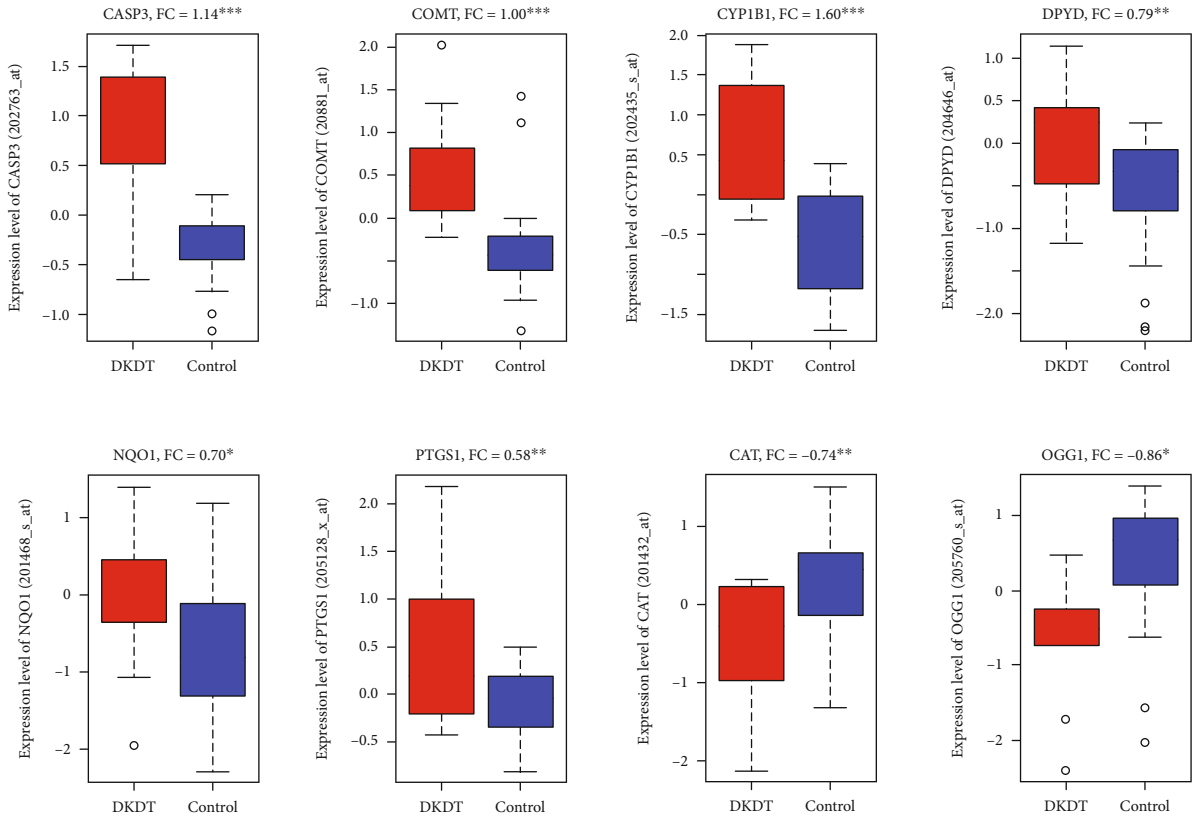

Figure 9: Dysregulation of hub targets (mRNA expression levels) in diabetic human kidney tubuli, when compared with control tubuli. FC: fold change, DKDT: diabetic kidney disease tubuli, control: control tubuli, $^{*}P < 0.05$, $^{**}P < 0.01$, and $^{***}P < 0.001$.

enriched pathway (FDR $< 8.6 \times 10^{-6}$). Retinoids and retinoid-related proteins are associated with signaling molecules linking obesity with the development of type 2 diabetes and in the pancreatic β-cell biology/insulin secretion [57]. Additionally, *CAT* and *SOD1* genes/proteins are assumed to highly influence the control of the PPI network because these are also known as antioxidative enzymes having a very potent role in diabetes and diabetes-related complications including diabetic nephropathy [57]. Apart from these observations, the 15 hub genes are targeted in independent diabetic kidney disease (DKD). Interestingly, dysregulation of eight of those genes in this cohort complies with the fact that *CAT* and *OGG1* are downregulated and *CASP3*, *COMT*, *CYP1B1*, *DPYD*, *NQO1*, and *PTGS1* are upregulated in DKD, suggesting that the target compounds are clearly interacting with potential genes associated with diabetic nephropathy [58]. Moreover, metabolic, oxidative, oxidant detoxification, and inflammatory stresses are common features in diabetic nephropathy [59]. In streptozotocin-induced diabetic rats, modulation of xenobiotic metabolism and oxidative stress in various tissues may be related to altered metabolism [60]. Peroxidase activity, a top molecular function, is increased in advanced diabetic nephropathy [61]. Phospholipase A2 activity is a risk factor in diabetic nephropathy [62]. Altogether, these GO are clearly associated with the dysregulation of diabetic kidney disease (DKD).

The KEGG pathways were mainly involved in secretion (pancreatic secretion), metabolism, and cellular signaling. In type 2 diabetes, alpha-linolenic acid has effects on the control of the glycemic index [63]. Yan et al. revealed that antidiabetic agents are associated with arachidonic acid metabolism, glycerophospholipid metabolism, tryptophan metabolism, and tyrosine metabolism [64]. Another pathway, apoptosis, is also critically associated with diabetes [65]. Collectively, these enriched pathways are associated with the DKD. In a diabetic nephropathy cohort study, *CAT* is a downregulated gene which may be associated with the regulation of kidney functions in diabetes [66]. The gene *CASP3* promotes the DKD through secondary necrosis [53]. Another upregulated gene, *CYP1B1*, is also associated with the damage and dysfunction of renal functions in mice. Increased expression levels of *PTGS1* are associated with the progression of diabetic nephropathy [67] suggesting that these are the potential genes, interacting with our target compounds, which are dysregulated in diabetic kidney diseases.

5. Conclusions

Our investigations revealed that the CMJE partially restored biochemical markers especially ALT, AST, creatinine, uric acid, and lipid profiles and improved glucose homeostasis as well as tissue architecture. The target compounds of CMJE downregulated *CAT* and *OGG1* genes and upregulated *CASP3*, *COMT*, *CYP1B1*, *DPYD*, *NQO1*, and *PTGS1* genes implying to potentiate their antioxidative actions to protect the dysregulation of the pancreas and the kidney of STZ-

diabetic animals. Therefore, the coconut mesocarp juice extract is suggested to produce antidiabetic actions in induced animal models. A further study of in vivo antioxidative effects both in enzymatic and nonenzymatic systems might confirm the use of CMJE as alternative therapeutic in diabetic complications.

Abbreviations

CMJE:	Coconut mesocarp juice extract
TFC:	Total flavonoid content
TPC:	Total phenolic content
SO:	Superoxide scavenging effect
DPPH-1:	1-Diphenyl, 2-picrylhydrazyl free radical scavenging assay
NO:	Nitric oxide scavenging effect
IrC:	Iron-chelating effect
ABTS:	(2,2′-azino-bis(3-ethylbenzothiazoline-6-sulfonic acid)
ALT:	Alanine aminotransferase
AST:	Aspartate aminotransferase
HOMA-IR:	Glucose homeostasis
SPSS:	Statistical Package for Social Science
TCh:	Total cholesterol
TG:	Triglyceride
PPI:	Protein-protein interaction
GO:	Gene Ontology
KEGG:	Kyoto Encyclopedia of Genes and Genomes
BP:	Biological process
MF:	Molecular function
CC:	Cellular component groups.

Data Availability

The data used to support the findings of this study are available from the corresponding authors upon request.

Additional Points

Institutional Review Board Statement. Animal handling and care were ensured through the ethical guideline formed in accord with the Helsinki protocol. All animal experimentations were carried out according to the guideline of Institutional Animal Ethics Committee (EACUBS2018-4).

Disclosure

This research was submitted to Oxidative Medicine and Cellular Longevity.

Conflicts of Interest

The authors declare no conflict of interest.

Authors' Contributions

MAR has designed the research, planned for research conduction, arranged the funding for research, and introduced the way of data collection. RRD, SQA, MMR, MSI, and MKJR have collected sample, set the bench works, produced and analyzed the data, and paid effort in manuscript preparation. MKJR and TAS particularly assessed the antioxidative effects. NAB, AMA, and HFHA along with MAR and PJ have assisted in interpreting the data and made necessary steps to harmonize the data. MNU has accomplished the network pharmacological analyses. ZAZ has facilitated the funding for this research.

Acknowledgments

This research was funded by the Malaysia Ministry of Higher Education under the Fundamental Research Grant Scheme (FRGS; reference no: 04-01-18-1984FR). The APC was funded by the Universiti Putra Malaysia (UPM), Malaysia. The funders had no role in the design of the study; in the collection, analyses, or interpretation of data; in the writing of the manuscript; or in the decision to publish the results. The authors wish to thank Dr. Sheikh Bokhtear Uddin for showing the strategy to minutely separate the coconut mesocarp.

Supplementary Materials

Table S1: list of compounds-targets identification. Table S2: list of targets involved in PPI with degree of interactions. Table S3: ontology (GO) enrichment analysis of the interacted target proteins. Table S4: the enriched KEGG pathways which are significantly associated with target proteins. Figure S1: a comprehensive approach to display the effect of coconut mesocarp juice extract on the streptozotocin-induced diabetes and diabetes-related complications using in vitro, in vivo and computational models. *(Supplementary Materials)*

References

[1] F. G. Lupascu, S. E. Giusca, I. D. Caruntu, A. Anton, C. E. Lupușoru, and L. Profire, "The safety profile of new antidiabetic xanthine derivatives and their chitosan based formulations," *Europian Journal of Pharmaceutical Sciences*, vol. 127, pp. 71–78, 2019.

[2] C. H. Lin, Z. Z. Shih, Y. H. Kuo, G. J. Huang, P. C. Tu, and C. C. Shih, "Antidiabetic and antihyperlipidemic effects of the flower extract of *Eriobotrya japonica* in streptozotocin-induced diabetic mice and the potential bioactive constituents *in vitro*," *Journal of Functional Foods*, vol. 49, no. 11, pp. 122–136, 2018.

[3] A. M. Al-Attar and F. A. Alsalmi, "Effect of *Olea europaea* leaves extract on streptozotocin induced diabetes in male albino rats," *Saudi Journal of Biological Sciences*, vol. 26, no. 1, pp. 118–128, 2019.

[4] H. Choudhury, M. Pandey, C. K. Hua et al., "An update on natural compounds in the remedy of diabetes mellitus: a systematic review," *Journal of Traditional and Complementary Medicine*, vol. 8, no. 3, pp. 361–376, 2018.

[5] C. Forni, F. Facchiano, M. Bartoli et al., "Beneficial role of phytochemicals on oxidative stress and age-related diseases," *BioMed Research International*, vol. 2019, Article ID 8748253, 16 pages, 2019.

[6] W. Kooti, M. T. Moradi, and S. Ali-Akbari, "Therapeutic and pharmacological potential of Foeniculum vulgare Mill: a

review," *Journal of HerbMed Pharmacology*, vol. 4, no. 1, pp. 1–9, 2015.

[7] R. Afrisham, M. Aberomand, M. A. Ghaffari, A. Siahpoosh, and M. Jamalan, "Inhibitory Effect of Heracleum persicum and Ziziphus jujuba on Activity of Alpha-Amylase," *Journal of Botany*, vol. 2015, Article ID 824683, 8 pages, 2015.

[8] Royal Botanic Gardens, "Cocos nucifera L," in *World Checklist of Selected Plant Families [Royal Botanic Gardens]*, Kew: Royal Botanic Gardens, 2014.

[9] A. I. Airaodion, E. O. Ogbuagu, J. A. Ekenjoku, and U. Ogbuagu, "Antidiabetic effect of ethanolic extract of carica papaya leaves in alloxan-induced diabetic rats," *American Journal of Biomedical Science and Research*, vol. 5, no. 3, pp. 227–234, 2019.

[10] B. O. Joshua and A. Muyiwa, "Effects of alkaloids of Cocos nucifera husk fibre on cardiovascular disease indices in albino mice," *Journal of Cardiac Pharmacology*, vol. 8, 2019.

[11] M. A. Rahman, T. . Imran, and S. Islam, "Antioxidative, antimicrobial and cytotoxic effects of the phenolics of *Leea indica* leaf extract," *Saudi Journal of Biological Sciences*, vol. 20, no. 3, pp. 213–225, 2013.

[12] A. Kumaran and R. Joel Karunakaran, "In vitro antioxidant activities of methanol extracts of five *Phyllanthus* species from India," *LWT-Food Science and Technology*, vol. 40, no. 2, pp. 344–352, 2007.

[13] V. L. Singleton and J. A. Rossi, "Colorimetry of total phenolics with phosphomolybdic-phosphotungstic acid reagents," *American Journal of Enology and Viticulture*, vol. 16, no. 3, pp. 144–158, 1965.

[14] R. Kumari, A. Meyyappan, P. Selvamani, J. Mukherjee, and P. Jaisankar, "Lipoxygenase inhibitory activity of crude bark extracts and isolated compounds from *Commiphora berryi*," *Journal of Ethnopharmacolgy*, vol. 138, no. 1, pp. 256–259, 2011.

[15] Q. Shen, B. Zhang, R. Xu, Y. Wang, X. Ding, and P. Li, "Antioxidant activity in vitro of the selenium-contained protein from the Se- enriched *Bifidobacterium animalis* 01," *Anaerobe*, vol. 16, no. 4, pp. 380–386, 2010.

[16] W. Brand-Williams, M. E. Cuvelier, and C. L. W. T. Berset, "Use of a free radical method to evaluate antioxidant activity," *LWT-Food Science and Technology*, vol. 28, no. 1, pp. 25–30, 1995.

[17] R. Re, N. Pellegrini, A. Proteggente, A. Pannala, M. Yang, and C. Rice-Evans, "Antioxidant activity applying an improved ABTS radical cation decolorization assay," *Free Radical Biology & Medicine*, vol. 26, no. 9-10, pp. 1231–1237, 1999.

[18] M. G. Rana, R. V. Katbamna, and A. A. Padhya, "In vitro antioxidant and free radical scavenging studies of alcoholic extract of Medicago sativa L," *Romanian Journal of Biology-Plant Biology*, vol. 55, no. 1, pp. 15–22, 2010.

[19] Sreejayan and M. N. A. Rao, "Nitric oxide scavenging by curcuminoids," *Journal of Pharmacy and Pharmacology*, vol. 49, no. 1, pp. 105–107, 2011.

[20] I. F. Benzie and J. J. Strain, "The Ferric Reducing Ability of Plasma (FRAP) as a Measure of "Antioxidant Power": The FRAP Assay," *Annals of Biochemistry*, vol. 239, no. 1, pp. 70–76, 1996.

[21] P. Mccue, Y. I. KWON, and K. Shetty, "Anti-amylase, anti-glucosidase and anti-angiotensin I-converting enzyme potential of selected foods," *Journal of Food Biochemistry*, vol. 29, no. 3, pp. 278–294, 2005.

[22] S. Q. al-Araby, M. A. Rahman, M. A. H. Chowdhury et al., "*Padina tenuis* (marine alga) attenuates oxidative stress and streptozotocin- induced type 2 diabetic indices in Wistar albino rats," *South African Journal of Botany*, vol. 128, pp. 87–100, 2020.

[23] A. Zaoui, Y. Cherrah, N. Mahassini, K. Alaoui, H. Amarouch, and M. Hassar, "Acute and chronic toxicity of *Nigella sativa* fixed oil," *Phytomedicine*, vol. 9, no. 1, pp. 69–74, 2002.

[24] S. K. Mitra, S. Gopumadhavan, T. S. Muralidhar, S. D. Anturlikar, and M. B. Sujatha, "Effect of a herbomineral preparation D-400 in streptozotocin-induced diabetic rats," *Journal of Ethnopharmacology*, vol. 54, no. 1, pp. 41–46, 1996.

[25] D. Szklarczyk, A. Santos, and C. V. Mering, "STITCH 5: augmenting protein-chemical interaction networks with tissue and affinity data," *Nucleic Acids Research*, vol. 44, no. D1, pp. D380–D384, 2016.

[26] D. Szklarczyk, A. L. Gable, D. Lyon et al., "STRING v11: protein–protein association networks with increased coverage, supporting functional discovery in genome-wide experimental datasets," *Nucleic Acids Research*, vol. 47, no. D1, pp. D607–D613, 2019.

[27] C. H. Chin, S. H. Chen, H. H. Wu, C. W. Ho, M. T. Ko, and C. Y. Lin, "cytoHubba: identifying hub objects and sub-networks from complex interactome," *BMC Systemic Biology*, vol. 8, no. s4, p. S11, 2014.

[28] P. Shannon, A. Markiel, O. Ozier et al., "Cytoscape: a software environment for integrated models of biomolecular interaction networks," *Genome Research*, vol. 13, no. 11, pp. 2498–2504, 2003.

[29] D. W. Huang, B. T. Sherman, and R. A. Lempicki, "Bioinformatics enrichment tools: paths toward the comprehensive functional analysis of large gene lists," *Nucleic Acids Research*, vol. 37, no. 1, pp. 1–13, 2009.

[30] M. Kanehisa, M. Furumichi, M. Tanabe, Y. Sato, and K. Morishima, "KEGG: new perspectives on genomes, pathways, diseases and drugs," *Nucleic Acids Research*, vol. 45, no. D1, pp. D353–D361, 2017.

[31] Y. Benjamini and Y. Hochberg, "Controlling the false discovery rate: a practical and powerful approach to multiple testing," *Journal of the Royal Statistical Society Series B, Statistical methodology*, vol. 57, no. 1, pp. 289–300, 1995.

[32] K. I. Woroniecka, A. S. D. Park, D. Mohtat, D. B. Thomas, J. M. Pullman, and K. Susztak, "Transcriptome analysis of human diabetic kidney disease," *Diabetes*, vol. 60, no. 9, pp. 2354–2369, 2011.

[33] F. H. Wong, C. Y. F. Huang, L. J. Su et al., "Combination of microarray profiling and protein-protein interaction databases delineates the minimal discriminators as a metastasis network for esophageal squamous cell carcinoma," *International Journal of Oncology*, vol. 34, no. 1, pp. 117–128, 2009.

[34] R. Nasrallah, A. Landry, S. Singh, M. Sklepowicz, and R. L. Hébert, "Increased expression of cyclooxygenase-1 and -2 in the diabetic rat renal medulla," *American Journal of Physiology and Renal Physiology*, vol. 285, no. 6, pp. F1068–F1077, 2003.

[35] L. A. Pham-Huy, H. He, and C. Pham-Huy, "Free radicals, antioxidants in disease and health," *International Journal of Biomedical Sciences*, vol. 4, no. 2, pp. 89–96, 2008.

[36] A. C. Maritim, R. A. Sanders, and J. B. Watkins, "Diabetes, oxidative stress, and antioxidants: a review," *Journal of Biochemical and Molecular Toxicology*, vol. 17, no. 1, pp. 24–38, 2003.

[37] J. M. Matés, "Effects of antioxidant enzymes in the molecular control of reactive oxygen species toxicology," *Toxicology*, vol. 153, no. 1-3, pp. 83–104, 2000.

[38] O. R. Ayepola, N. L. Brooks, and O. O. Oguntibeju, "Oxidative stress and diabetic complications: the role of antioxidant vitamins and flavonoids," in *In: Antioxidant-Antidiabeetic Agents and Human Health, Oluwafemi Oguntibeju*, pp. 25–58, Intech Open, 2014.

[39] P. Mehta and V. Dhapte, "A comprehensive review on pharmacokinetic profile of some traditional chinese medicines," *New Journal of Science*, vol. 2016, Article ID 7830367, 31 pages, 2016.

[40] P. Mehta, R. Shah, S. Lohidasan, and K. R. Mahadik, "Pharmacokinetic profile of phytoconstituent(s) isolated from medicinal plants –a comprehensive review," *Journal of Traditional and Complementary Medicine*, vol. 5, no. 4, pp. 207–227, 2015.

[41] M. N. Sarian, Q. U. Ahmed, S. Z. Mat So'ad et al., "Antioxidant and antidiabetic effects of flavonoids: a structure-activity relationship based study," *Biomed Research International*, vol. 2017, Article ID 8386065, 14 pages, 2017.

[42] P. Trinder, "Determination of blood glucose using an oxidase-peroxidase system with a non-carcinogenic chromogen," *Journal of Clinical Pathology*, vol. 22, no. 2, pp. 158–161, 1969.

[43] B. Lipinski, "Pathophysiology of oxidative stress in diabetes mellitus," *The Journal of Diabetic Complications*, vol. 15, no. 4, pp. 203–210, 2001.

[44] S. Golbidi, M. Badran, and I. Laher, "Antioxidant and anti-inflammatory effects of exercise in diabetic patients," *Experimental Diabetes Research*, vol. 2012, Article ID 941868, 16 pages, 2012.

[45] F. A. Matough, S. Budin, Z. Hamid, S. Louis, N. Alwahaibi, and J. Mohamed, "Palm vitamin E reduces oxidative stress, and physical and morphological alterations of erythrocyte membranes in streptozotocin-induced diabetic rats," *Oxidants and Antioxidants in Medical Sciences*, vol. 1, no. 1, pp. 59–68, 2012.

[46] K. Yajima, A. Shimada, H. Hirose, A. Kasuga, and T. Saruta, ""Low dose" metformin improves hyperglycemia better than acarbose in type 2 diabetics," *The Review of Diabetes Studies*, vol. 1, no. 2, pp. 89–94, 2004.

[47] E. Apostolidis, Y. I. Kwon, and K. Shetty, "Inhibitory potential of herb, fruit, and fungal-enriched cheese against key enzymes linked to type 2 diabetes and hypertension," *Innovative Food Sciences and Emerging Technology*, vol. 8, no. 1, pp. 46–54, 2007.

[48] H. S. Jung, K. W. Chung, J. Won Kim et al., "Loss of autophagy diminishes pancreatic β cell mass and function with resultant hyperglycemia," *Cell Metabolism*, vol. 8, no. 4, pp. 318–324, 2008.

[49] I. J. Goldberg, "Diabetic dyslipidemia: causes and consequences," *Journal of Clinical Endocrinology and Metabolism*, vol. 86, no. 3, pp. 965–971, 2001.

[50] B. S. Haerian, M. S. Haerian, A. Roohi, and H. Mehrad-Majd, "ABCA1 genetic polymorphisms and type 2 diabetes mellitus and its complications," *Meta Gene*, vol. 13, pp. 104–114, 2017.

[51] Y. Miyazaki, R. Pipek, L. J. Mandarino, and R. A. DeFronzo, "Tumor necrosis factor α and insulin resistance in obese type 2 diabetic patients," *International Journal of Obesity*, vol. 27, no. 1, pp. 88–94, 2003.

[52] S. Cui, Y. Zhu, J. du et al., "CXCL8 antagonist improves diabetic nephropathy in male mice with diabetes and attenuates high glucose-induced mesangial injury," *Endocrinology*, vol. 158, no. 6, pp. 1671–1684, 2017.

[53] S. Wen, Z. H. Wang, C. X. Zhang, Y. Yang, and Q. L. Fan, "Caspase-3 promotes diabetic kidney disease through gasdermin E-mediated progression to secondary necrosis during apoptosis," *Diabetes Metabolic Syndrome and Obesity*, vol. - Volume 13, pp. 313–323, 2020.

[54] D. I. Swerdlow, D. Preiss, K. B. Kuchenbaecker et al., "HMG-coenzyme A reductase inhibition, type 2 diabetes, and bodyweight: evidence from genetic analysis and randomised trials," *The Lancet*, vol. 385, no. 9965, pp. 351–361, 2015.

[55] J. C. Barry, S. Shakibakho, C. Durrer et al., "Hyporesponsiveness to the anti-inflammatory action of interleukin-10 in type 2 diabetes," *Scientific Reports*, vol. 6, no. 1, 2016.

[56] S. A. Sarkar, C. E. Lee, F. Victorino et al., "Expression and regulation of chemokines in murine and human type 1 diabetes," *Diabetes*, vol. 61, no. 2, pp. 436–446, 2012.

[57] P. J. Brun, K. J. Z. Yang, S. A. Lee, J. J. Yuen, and W. S. Blaner, "Retinoids: potent regulators of metabolism," *Biofactors*, vol. 39, no. 2, pp. 151–163, 2013.

[58] J. Mawa, M. A. Rahman, M. A. Hashem, and M. Juwel Hosen, "*Leea macrophylla* root extract upregulates the mRNA expression for antioxidative enzymes and repairs the necrosis of pancreatic β-cell and kidney tissues in fructose-fed Type 2 diabetic rats," *Biomedicine & Pharmacotherapy*, vol. 110, pp. 74–84, 2019.

[59] G. Manda, A. I. Checherita, M. V. Comanescu, and M. E. Hinescu, "Redox signaling in diabetic nephropathy: hypertrophy versus death choices in mesangial cells and podocytes," *Mediators of Inflammation*, vol. 2015, 604213 pages, 2015.

[60] H. Raza, I. Ahmed, A. John, and A. K. Sharma, "Modulation of xenobiotic metabolism and oxidative stress in chronic streptozotocin-induced diabetic rats fed with Momordica charantia fruit extract," *Journal of Biochemistry and Molecular Toxicology*, vol. 14, no. 3, pp. 131–139, 2000.

[61] E. Lee and H. S. Lee, "Peroxidase expression is decreased by palmitate in cultured podocytes but increased in podocytes of advanced diabetic nephropathy," *Journal of cellular and comparative physiology*, vol. 233, no. 12, pp. 9060–9069, 2018.

[62] Y. Hu, T. T. Li, W. Zhou et al., "Lipoprotein-associated phospholipase A2 is a risk factor for diabetic kidney disease," *Diabetes Research and Clinical Practice*, vol. 150, pp. 194–201, 2019.

[63] E. Jovanovski, D. Li, H. V. Thanh Ho et al., "The effect of alpha-linolenic acid on glycemic control in individuals with type 2 diabetes: a systematic review and meta-analysis of randomized controlled clinical trials," *Medicine*, vol. 96, no. 21, p. e6531, 2017.

[64] Z. Yan, H. Wu, H. Zhou et al., "Integrated metabolomics and gut microbiome to the effects and mechanisms of naoxintong capsule on type 2 diabetes in rats," *Scientific Report*, vol. 10, no. 1, p. 10829, 2020.

[65] P. A. J. Krijnen, S. Simsek, and H. W. M. Niessen, "Apoptosis in diabetes," *Apoptosis*, vol. 14, no. 12, pp. 1387-1388, 2009.

[66] B. I. Freedman, M. Bostrom, P. Daeihagh, and D. W. Bowden, "Genetic factors in diabetic nephropathy," *Clinical Journal of the American Society of Nephrology*, vol. 2, no. 6, pp. 1306–1316, 2007.

[67] V. Vallon and R. Komers, "Pathophysiology of the diabetic kidney," *Comprehensive Physiology*, vol. 1, no. 3, pp. 1175–1232, 2011.

Hindawi
Oxidative Medicine and Cellular Longevity
Volume 2021, Article ID 7501424, 7 pages
https://doi.org/10.1155/2021/7501424

Review Article

Trends in Natural Nutrients for Oxidative Stress and Cell Senescence

Navid Omidifar,[1,2] **Mohsen moghadami**,[3] **Seyyed Mojtaba Mousavi**,[4] **Seyyed Alireza Hashemi**,[5] **Ahmad Gholami**,[6] **Mansoureh Shokripour**,[2] **and Zahra Sohrabi**[7,8]

[1]*Clinical Education Research Center, Shiraz University of Medical Sciences, Shiraz, Iran*
[2]*Department of Pathology, Medical School, Shiraz University of Medical Sciences, Shiraz, Iran*
[3]*Health Policy Research Center, Health Institute, Shiraz University of Medical Sciences, Shiraz, Iran*
[4]*Department Chemical Engineering, National Taiwan University of Science and Technology, Taiwan*
[5]*Nanomaterials and Polymer Nanocomposites Laboratory, School of Engineering, University of British Columbia, Kelowna, BC, Canada V1V 1V7*
[6]*Biotechnology Research Center, Shiraz University of Medical Sciences, Shiraz, Iran*
[7]*Nutrition Research Center, Shiraz University of Medical Sciences, Shiraz, Iran*
[8]*Department of Community Nutrition, School of Nutrition and Food Sciences, Shiraz University of Medical Sciences, Shiraz, Iran*

Correspondence should be addressed to Zahra Sohrabi; zahra_2043@yahoo.com

Received 26 April 2021; Revised 12 June 2021; Accepted 15 June 2021; Published 2 July 2021

Academic Editor: Cristina Cosentino

Due to the increase in the aged population and increased life expectancy, the underlying mechanisms involved in the aging process and cell senescence and the ways for modulating these processes in age-related diseases become important. One of the main mechanisms involved in aging and cell senescence, especially in the diseases related to aging, is the oxidative stress process and the following inflammation. Hence, the effects of antioxidants are highlighted in the literature due to their beneficial impacts on inhibiting telomere shortening or DNA damage and other processes related to aging and cell senescence in age-related diseases. Dietary components, foods, and dietary patterns rich in antioxidants can modulate the aging process and delay the progression of some chronic diseases such as cardiovascular diseases, diabetes, and Alzheimer's disease. Foods high in polyphenols, vitamin C, or carotenoids, olive oil, seeds, nuts, legumes, dietary supplements such as CoQ10, and some other dietary factors are the most important nutritional sources that have high antioxidant contents which can positively affect cell senescence and disease progression. Plant dietary patterns including Mediterranean diets can also inhibit telomere shortening following oxidative damages, and this can delay cell aging and senescence in age-related diseases. Further, olive oil can inhibit protein aggregation in Alzheimer's disease. It can be concluded that nutrition can delay the process of cell senescence in age-related diseases via inhibiting oxidative and inflammatory pathways. However, more studies are needed to better clarify the underlying mechanisms of nutrition and dietary components on cell senescence, aging, and disease progression, especially those related to age.

1. Introduction

According to the growth in aged population and increased life expectancy in different countries [1], more attention is paid to the mechanisms of aging especially at the cellular level [2].

Among the theories of aging, the theory concerning the free radicals explains the underlying mechanism of aging process in age-related diseases including diabetes, osteoporosis, dementia, atherosclerosis, and cardiovascular diseases [3, 4]. Different factors can affect cell senescence and the progression of age-related diseases (Figure 1). Oxidative stress

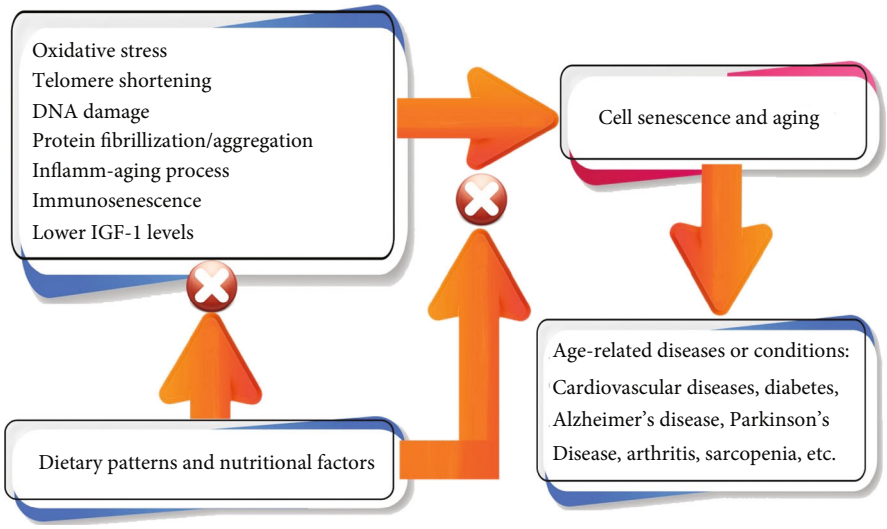

Figure 1: Factors affecting cell senescence and age-related diseases.

is one of the key factors involved in cell damage or injury [5, 6]. Endogenous or exogenous agents could induce tissue or organ damage via oxidative stress [7]. One of the important mechanisms related to aging is about lower immunity toward pathogens and infections which can be defined as immunosenescence [8]. One of the main reasons regarding immune deficiency and aging involves the oxidative pathways. At the time of high levels of oxidative stress, products of peroxidation or lipid membranes including malondialdehyde (MDA) can activate nuclear transcription factors that are all associated with cell senescence and longevity [9]. These nuclear transcription factors include tumor protein p53, nuclear factor kappa-light-chain-enhancer of activated B cells (NF-κB), and transcriptional protein AP-1 [10].

One of the major epigenetic factors related to aging is considered to be oxidative stress, and it can also cause low-grade inflammation. This proinflammatory condition can increase the level of inflammatory cytokines and markers including interleukin-6 and tumor necrosis factor alpha (TNF-α), which can all activate the NF-KB pathway and induce mitochondrial superoxide and oxygen reactive species (ROS) production [2, 10]. ROS accumulation can be damaging for various biologic molecules such as nucleic acids, proteins, and lipids which can result in mutations of nucleic acids, protein deactivation or damage, and peroxidation of lipids [7, 11–13] that can all be important in disease progression via cell senescence. Also, the DNA damage caused by ROS is closely related to the cellular senescence [14] that can be damaging in age-related diseases.

The process called inflamm-aging is an important basis for frailty, aging process, and cell senescence in humans especially in age-related diseases [15]. On the other hand, inflammation can induce oxidative stress in a vicious cycle [16] that can affect the aging process and disease progression.

The antioxidant defense system including the enzymes such as catalase, glutathione peroxidase (GSH), and superoxide dismutase (SOD) decreases substantially during the aging process and nutrition can regulate cell senescence and aging in the related diseases [17].

Further, according to other mechanisms related to oxidative stress and age-related diseases, it can be mentioned that unfolded proteins in the endoplasmic reticulum (ER) can trigger unfolded protein response and this can in turn induce lower protein translation and higher levels of oxidative stress. The oxidative stress can cause ER stress-induced apoptosis and increase the risk of age-related macular diseases such as retinitis [18] (Figure 2).

2. Age-Related Diseases and Nutrition

It is demonstrated that nutrition is an important role modulator of aging process especially through the inflamm-aging process in age-related diseases [19–21]. Some dietary approaches or components were defined to affect aging in disease models [22].

Effects of antioxidant nutrients on modulation of aging have been reported previously [23]. Other strategies affecting aging and cell senescence in diseases related to aging including cardiovascular diseases were also mentioned including calorie restriction without malnutrition [24], Mediterranean diet with olive oil (OO), and the like [25]. Mostly, the aforementioned dietary components could affect the inflamm-aging process and modulate the oxidative pathways [22, 26]. Dietary factors or patterns related to cell senescence are described here in details (Figure 3).

3. Plant-Rich Dietary Patterns

From the theories of aging and cell senescence, one of them is related to the telomere shortening. There is a high correlation between oxidative stress and telomere shortening which can accelerate aging and increase the risk of diseases such as cancer and cardiovascular diseases. It is reported that foods high in antioxidants (mostly plant foods) have beneficial effects against telomere shortening via inhibiting the oxidative damages [27, 28]. Effects of various plant foods including walnut [29], seeds, legumes, nuts [27], and olive oil [22], or plant dietary components such as polyphenols [30] and dietary

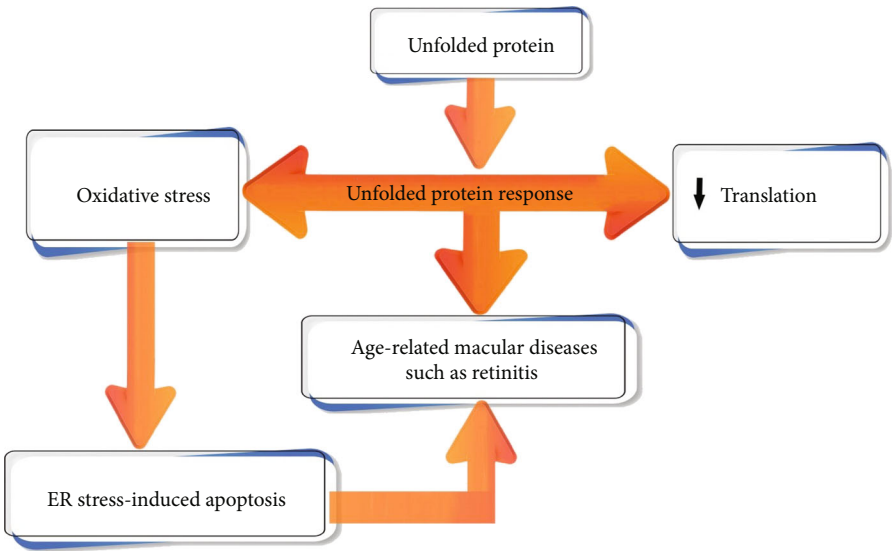

Figure 2: Unfolded protein response, oxidative stress, and age-related macular diseases. ER: endoplasmic reticulum.

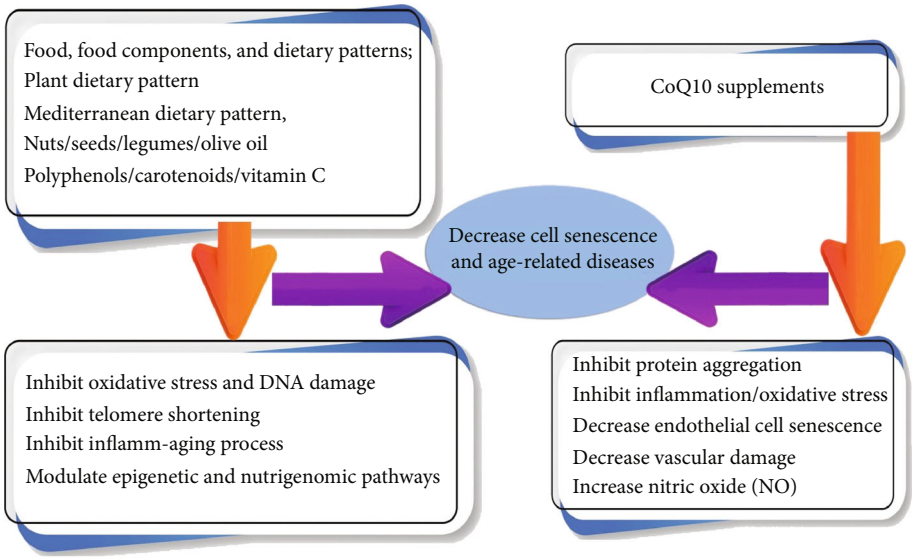

Figure 3: Dietary factors and their underlying mechanism affecting cell senescence and age-related diseases.

carotenoids [5, 27], or plant-based dietary patters such as the Mediterranean dietary pattern [27] on inhibiting telomere shortening and delaying cell aging and age-related diseases were reported. Plant dietary patterns including most edible plants can synergistically modulate various processes such as oxidative stress, inflammation, telomere activity, and DNA methylation that are all associated with telomere attrition [31]. One of the major reasons for telomere shortening is related to oxidative stress damages due to the high content of guanines (5′-TTAGGG-3′) in telomeric DNA repeats [32]. Hence, it seems that plant foods high in antioxidants, especially nuts and seeds, can protect telomeres from oxidative damages and shortening [27]. In a clinical trial in healthy older adults, consumption of walnut for two years showed preventive effects on telomere attrition compared to the control group [29].

4. Polyphenols

Evidence showed that foods high in polyphenols can affect the aging process and cause protection against some age-related diseases including cataract, atherosclerosis, Alzheimer's disease, hypertension, arthritis, and diabetes. From these polyphenols, resveratrol and pterostilbene that are found in grape and blueberries can demonstrate antiaging properties through various mechanisms. These mechanisms include inhibiting oxidative pathways and inflammation and modulating cell senescence and telomere attrition [30]. It is demonstrated that resveratrol, as a potent polyphenol with antioxidant properties, could possibly increase the regulatory protein AROS expression (active regulator of Sirt1) and HuR (Hu antigen R). On the other hand, it could decrease DBC1 (deleted in breast cancer 1) and p53. These

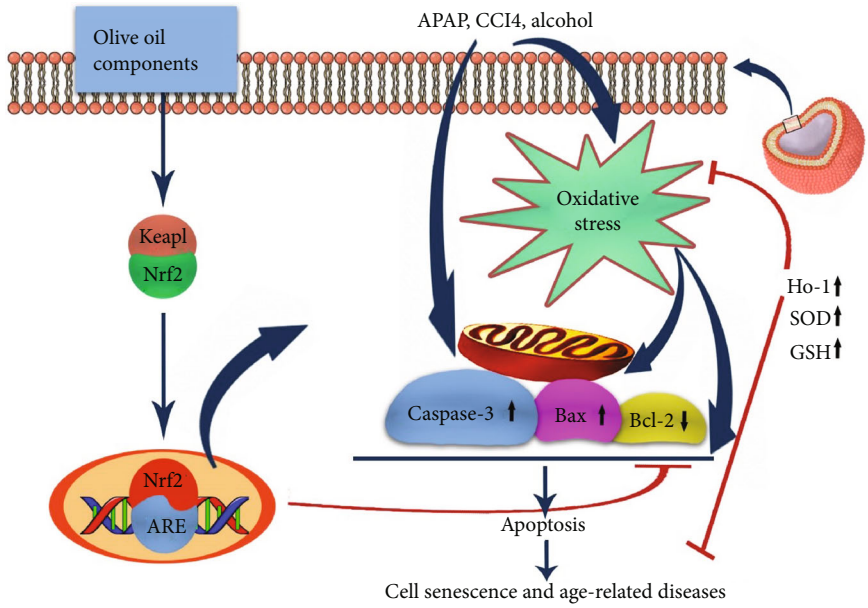

Figure 4: Olive oil effect on cell senescence and age-related diseases through the Nrf2 pathway.

changes can show the antiaging effects of resveratrol as an important polyphenol via Sirt1 induction [33]. Sirt1 can affect autophagy as one of the mechanisms related to longevity [34]. In a study about a model of Alzheimer's disease, in the SAMP8 (senescence-accelerated mouse prone 8) mice, ingestion of resveratrol supplements for long term (1 g/kg) showed beneficial effects by activating the AMPK pathway and Sirt1 and this could affect cell survival and longevity. Further, resveratrol neuroprotective effects were reported while assessing the hallmarks related to Alzheimer's disease as an age-related disease [35]. In a study in the animal model, ingestion of various doses of resveratrol (30 and 100 mg/kg/day) in mice with premature aging of the ovaries, the protective effects of resveratrol against aging were observed and it could improve stem cell renewal due to its antioxidant properties through the activation of Nrf2 [30].

5. Vitamin C

One of the antioxidant nutrients that can modulate the process of inflamm-aging is vitamin C [36, 37]. Any deficiency in vitamin C can affect the demethylation of DNA and histones. This deficiency is present in the aging process. Vitamin C can have beneficial effects on delaying the aging process and age-related diseases [38].

Ascorbic acid or vitamin C is related to various molecular mechanisms associated with aging. This vitamin can modulate the free radical theory and inflamm-aging process by scavenging the free radicals and intercepting immunosenescence. It can also affect cell senescence via modulating nutrigenomic and epigenetic pathways that can be so important for the prevention of age-related diseases such as Alzheimer's disease, insulin resistance, atherosclerosis, and neurodegeneration [39]. In the epigenetic changes of DNA and histones, there are some enzymes including dioxygenase Fe^{2+} and 2-oxoglutarate (2OG-dependent) that need vitamin C for their activity. Hence, vitamin C can affect the epigenome and especially those changes concerned with the age-related diseases through modulating these enzyme activities. One of the major determinants of genome stability is related to the methylation of DNA, and vitamin C availability can affect this process. This can show the effects of vitamin C on aging process through epigenetic pathways [40, 41].

In an in vivo model, it was proposed that vitamin C supplementation can positively affect the aging process and life expectancy and it can reverse the abnormalities related to aging in various organs or tissues including liver and fat mass and those related to genomic stability. In addition to the improvement of inflammatory status following vitamin C use, normalization of AKT kinase phosphorylation, NF-kappa B at the transcriptional level, protein kinase delta (PKC delta), hypoxia-inducible factor-1 alpha (HIF1-alpha), and peroxisome proliferator-activated receptor alpha (PPAR-alpha) were reported that are all related to aging [42].

6. Coenzyme Q10

Coenzyme Q10 (CoQ10) can potentially increase cyclic adenosine monophosphate (cAMP) in the cells, and it can also enhance the antioxidant capacity in the mitochondria through the activation of SIRT1 and PGC-1α. As a result, this can modulate the cell senescence in the vascular endothelial cells [43]. SIRT1 is defined as an essential deacetylase that can increase nitric oxide (NO), and this can inhibit endothelial senescence [44, 45]. Further, it was reported that in an animal model supplemented with CoQ10, the mice had a higher metabolic rate related to fat via inhibiting the signaling pathway of CaMKII-MEK1/2-ERK1/2 and increasing cAMP levels [46]. In vitro studies claimed that CoQ10 bears anti-inflammatory functions in addition to its antioxidant properties in endothelial cells and it can delay the process of senescence by affecting miR-146a expression [47]. The

findings regarding the effects of CoQ10 on the inhibition of cell senescence mostly focus on the dietary supplements and especially in the endothelial cells which can be important for the prevention of age-related diseases related to vascular aging [48].

7. Olive Oil

Olive oil can induce DNA protection against damage due to its phenolic components. Other compounds including tyrosol, oleuropein aglycone, caffeic acid, and oleuropein could show beneficial effects of olive oil due to scavenging free radicals and modulating the oxidative pathways [49] and this can demonstrate the beneficial effects of olive oil on reducing the risk of cancer, cardiovascular diseases, Parkinson's disease, Alzheimer's disease, and other age-related diseases [22]. Olive oil components including oleuropein and oleuropein aglycone can inhibit fibrillization of a protein called Tau that is one of the events happening in Alzheimer's disease (AD) pathogenesis [50]. On the other hand, olive oil phenolic compounds can inhibit DNA damage through protecting APEX1, a repair gene for DNA that is so essential for decreasing the vulnerability to age-related diseases [51].

As it was mentioned, telomere shortening is so important in the aging process, especially in the development of age-related diseases [52]. On the other hand, the activity of telomerase can be negatively affected by inflammation and oxidative stress [53]. However, in the diets rich in monounsaturated fats (MUFAs) such as the Mediterranean diet containing olive oil, lower rates of telomere shortening were reported and this was closely correlated with the lower levels of ROS in the cells and lower rates of apoptosis due to the direct effects of olive oil [54]. In particular, the oleuropein content of olive can decrease oxidative stress, which can directly affect cell senescence [22]. Moreover, olive oil can increase the catalase content in cells during aging that can be protective against oxidative stress during cell senescence [22] and it can cause protection against disease progression.

Further, two components of olive oil named oleuropein and oleacein can also affect cell senescence [55]. These components can positively affect the cells, not only due to their antioxidant effects but also due to the stimulatory effects on the transcription factor Nrf2 and increased the expression of heme oxygenase-1 (HO-1). Nrf2 is an important transcription factor in the intracellular antioxidant defense system that can induce protection against cell apoptosis and cell senescence. HO-1 can also demonstrate antioxidant, anti-inflammatory, and antiapoptotic properties [56, 57] (Figure 4). All of the aforementioned effects can confirm the protective effects of olive oil against cell senescence via modulating oxidative stress [22].

Decreased levels of insulin-like growth factor-1 (IGF-1) were reported in age-related conditions such as sarcopenia [58, 59], diabetes, cardiovascular diseases, frailty, and the like [60, 61] (117, 121 of 4). Activation of the receptors for IGF-1 can upregulate the PI3K/AKT pathway, and this can promote cell survival and decrease cell senescence [62]. IGF-1 can beneficially affect the endothelial and cardiovascular system by increasing nitrite oxide (NO) availability, enhancing the antioxidant system, decreasing inflammation, decreasing cell death, and the like. Through these effects, IGF-1 can decrease the plaque size and the risk of cardiovascular diseases as one of the age-related diseases [63]. Research groups tried to affect aging through consumption of natural foods including olive oil which contains antioxidants that can modulate cell senescence and aging in age-related diseases or conditions [22]. It was reported that olive oil could possibly increase the levels of IGF-1 which can beneficially affect cell survival [64].

8. Conclusion

Because of the growth in aged population and age-related diseases including diabetes, arthritis, cardiovascular diseases, and Alzheimer's disease in various countries, modulating the aging process and cell senescence seems essential. Theory of free radicals and oxidative pathways for aging should be taken into account. Oxidative stress is highly intercorrelated with inflammation, and the process called inflamm-aging is an important basis for frailty, aging process, and cell senescence in humans, especially in the development of age-related diseases. It is obvious that dietary patterns and foods or food components or dietary supplements can modulate cell senescence via inhibiting oxidative stress, inflammation, or telomere shortening and DNA damage and prevent age-related diseases. This would be due to the phenolic compounds and antioxidants present in dietary components. From these nutrients or foods, foods including nuts, seeds, legumes, and olive oil and dietary components such as polyphenols, vitamin C, and carotenoids are of great importance to delay cell senescence in age-related diseases. Moreover, plant dietary patterns such as Mediterranean diet can positively affect telomere length or cell senescence and aging process and prevent the diseases related to aging. According to the dietary supplements, CoQ10 dietary supplements can also delay cell senescence via inhibiting oxidative stress and inflammation and inhibit vascular disease progression. However, more randomized clinical trials (RCTs) or in vitro studies are warranted to better elucidate the exact effects or mechanisms of action regarding the relationship between nutrition, oxidative stress, and cell senescence in age-related diseases.

Conflicts of Interest

The authors declare that they have no conflicts of interest.

References

[1] D. E. Bloom, "7 billion and counting," *Science*, vol. 333, no. 6042, pp. 562–569, 2011.

[2] E. S. Cannizzo, C. C. Clement, R. Sahu, C. Follo, and L. Santambrogio, "Oxidative stress, inflamm-aging and immunosenescence," *Journal of Proteomics*, vol. 74, no. 11, pp. 2313–2323, 2011.

[3] S. Vasto, G. Candore, C. R. Balistreri et al., "Inflammatory networks in ageing, age-related diseases and longevity," *Mechanisms of ageing and development*, vol. 128, no. 1, pp. 83–91, 2007.

[4] C. Franceschi and J. Campisi, "Chronic inflammation (inflammaging) and its potential contribution to age-associated diseases," *Journals of Gerontology Series A: Biomedical Sciences and Medical Sciences*, vol. 69, Supplement 1, pp. S4–S9, 2014.

[5] A. Gholami, S. Ataei, D. Ahmadimoghaddam, N. Omidifar, and A. Nili-Ahmadabadi, "Pentoxifylline attenuates arsenic trioxide-induced cardiac oxidative damage in mice," *Oxidative Medicine and Cellular Longevity*, vol. 2021, Article ID 6406318, 10 pages, 2021.

[6] I. Gheitasi, A. Azizi, N. Omidifar, and A. H. Doustimotlagh, "Renoprotective effects of Origanum majorana methanolic L and carvacrol on ischemia/reperfusion-induced kidney injury in male rats," *Evidence-Based Complementary and Alternative Medicine*, vol. 2020, Article ID 9785932, 9 pages, 2020.

[7] A. Gholami, F. Emadi, A. Amini, M. Shokripour, M. Chashmpoosh, and N. Omidifar, "Functionalization of graphene oxide nanosheets can reduce their cytotoxicity to dental pulp stem cells," *Journal of Nanomaterials*, vol. 2020, Article ID 6942707, 14 pages, 2020.

[8] E. Cevenini, D. Monti, and C. Franceschi, "Inflamm-ageing," *Current Opinion in Clinical Nutrition & Metabolic Care*, vol. 16, no. 1, pp. 14–20, 2013.

[9] A. Gholami, F. Mohammadi, Y. Ghasemi, N. Omidifar, and A. Ebrahiminezhad, "Antibacterial activity of SPIONs versus ferrous and ferric ions under aerobic and anaerobic conditions: a preliminary mechanism study," *IET nanobiotechnology*, vol. 14, no. 2, pp. 155–160, 2020.

[10] M. Michaud, L. Balardy, G. Moulis et al., "Proinflammatory cytokines, aging, and age-related diseases," *Journal of the American Medical Directors Association*, vol. 14, no. 12, pp. 877–882, 2013.

[11] Y. Yuan, G. Hilliard, T. Ferguson, and D. E. Millhorn, "Cobalt inhibits the interaction between hypoxia-inducible factor-α and von Hippel-Lindau protein by direct binding to hypoxia-inducible factor-α," *Journal of Biological Chemistry*, vol. 278, no. 18, pp. 15911–15916, 2003.

[12] X. Wang, I. Yokoi, J. Liu, and A. Mori, "Cobalt(II) and Nickel(II) Ions as Promoters of Free Radicals _in Vivo:_ Detected Directly Using Electron Spin Resonance Spectrometry in Circulating Blood in Rats," *Archives of biochemistry and biophysics*, vol. 306, no. 2, pp. 402–406, 1993.

[13] T. Sakagami, K. Satoh, M. Ishihara et al., "Effect of cobalt ion on radical intensity and cytotoxic activity of antioxidants," *Anticancer Research*, vol. 20, no. 5A, pp. 3143–3150, 2000.

[14] D. Muñoz-Espín and M. Serrano, "Cellular senescence: from physiology to pathology," *Nature reviews Molecular cell biology*, vol. 15, no. 7, pp. 482–496, 2014.

[15] C. Franceschi, M. Bonafè, S. Valensin et al., "Inflamm-aging: an evolutionary perspective on immunosenescence," *Annals of the new York Academy of Sciences*, vol. 908, no. 1, pp. 244–254, 2000.

[16] Z. Sohrabi, M. H. Eftekhari, M. H. Eskandari, A. Rezaianzadeh, and M. M. Sagheb, "Intradialytic oral protein supplementation and nutritional and inflammation outcomes in hemodialysis: a randomized controlled trial," *American Journal of Kidney Diseases*, vol. 68, no. 1, pp. 122–130, 2016.

[17] K. S. vel Szic, K. Declerck, M. Vidaković, and W. vanden Berghe, "From inflammaging to healthy aging by dietary lifestyle choices: is epigenetics the key to personalized nutrition?," *Clinical Epigenetics*, vol. 7, no. 1, pp. 1–18, 2015.

[18] M. Haeri and B. E. Knox, "Endoplasmic reticulum stress and unfolded protein response pathways: potential for treating age-related retinal degeneration," *Journal of ophthalmic & vision research*, vol. 7, no. 1, pp. 45–59, 2012.

[19] A. Santoro, E. Pini, M. Scurti et al., "Combating inflammaging through a Mediterranean whole diet approach: The NU-AGE project's conceptual framework and design," *Mechanisms of ageing and development*, vol. 136-137, pp. 3–13, 2014.

[20] A. Berendsen, A. Santoro, E. Pini et al., "A parallel randomized trial on the effect of a healthful diet on inflammageing and its consequences in European elderly people: design of the NU-AGE dietary intervention study," *Mechanisms of ageing and development*, vol. 134, no. 11-12, pp. 523–530, 2013.

[21] L. Neufcourt, K. Assmann, L. Fezeu et al., "Prospective association between the dietary inflammatory index and metabolic syndrome: findings from the SU.VI.MAX study," *Nutrition, Metabolism and Cardiovascular Diseases*, vol. 25, no. 11, pp. 988–996, 2015.

[22] L. Fernández del Río, E. Gutiérrez-Casado, A. Varela-López, and J. Villalba, "Olive oil and the hallmarks of aging," *Molecules*, vol. 21, no. 2, p. 163, 2016.

[23] A. Mitsui, J. Hamuro, H. Nakamura et al., "Overexpression of human thioredoxin in transgenic mice controls oxidative stress and life span," *Antioxidants and Redox Signaling*, vol. 4, no. 4, pp. 693–696, 2002.

[24] R. S. Sohal and R. Weindruch, "Oxidative stress, caloric restriction, and aging," *Science*, vol. 273, no. 5271, pp. 59–63, 1996.

[25] J. López-Miranda, F. Pérez-Jiménez, E. Ros et al., "Olive oil and health: summary of the II international conference on olive oil and health consensus report, Jaen and Cordoba (Spain) 2008," *Nutrition, metabolism and cardiovascular diseases*, vol. 20, no. 4, pp. 284–294, 2010.

[26] S. M. Mousavi, S. A. Hashemi, M. Zarei et al., "Recent progress in chemical composition, production, and pharmaceutical effects of kombucha beverage: a complementary and alternative medicine," *Evidence-Based Complementary and Alternative Medicine*, vol. 2020, Article ID 4397543, 14 pages, 2020.

[27] M. Crous-Bou, J.-L. Molinuevo, and A. Sala-Vila, "Plant-rich dietary patterns, plant foods and nutrients, and telomere length.," *Advances in Nutrition*, vol. 10, Supplement_4, pp. S296–S303, 2019.

[28] N. Omidifar, A. Nili-Ahmadabadi, A. Gholami, D. Dastan, D. Ahmadimoghaddam, and H. Nili-Ahmadabadi, "Biochemical and histological evidence on the protective effects of *allium hirtifolium boiss* (Persian shallot) as an herbal supplement in cadmium-induced hepatotoxicity," *Evidence-based complementary and alternative medicine*, vol. 2020, Article ID 7457504, 8 pages, 2020.

[29] T.-M. Freitas-Simoes, M. Cofán, M. A. Blasco et al., "Walnut consumption for two years and leukocyte telomere attrition in Mediterranean elders: results of a randomized controlled trial," *Nutrients*, vol. 10, no. 12, p. 1907, 2018.

[30] Y. R. Li, S. Li, and C. C. Lin, "Effect of resveratrol and pterostilbene on aging and longevity," *BioFactors*, vol. 44, no. 1, pp. 69–82, 2018.

[31] L. Paul, "Diet, nutrition and telomere length," *The Journal of nutritional biochemistry*, vol. 22, no. 10, pp. 895–901, 2011.

[32] R. P. Barnes, E. Fouquerel, and P. L. Opresko, "The impact of oxidative DNA damage and stress on telomere homeostasis," *Mechanisms of ageing and development*, vol. 177, pp. 37–45, 2019.

[33] J. Li, C.-X. Zhang, Y.-M. Liu, K.-L. Chen, and G. Chen, "A comparative study of anti-aging properties and mechanism: resveratrol and caloric restriction," *Oncotarget*, vol. 8, no. 39, pp. 65717–65729, 2017.

[34] E. Morselli, M. Maiuri, M. Markaki et al., "Caloric restriction and resveratrol promote longevity through the Sirtuin-1-dependent induction of autophagy," *Cell death & disease*, vol. 1, no. 1, p. e10, 2010.

[35] D. Porquet, G. Casadesús, S. Bayod et al., "Dietary resveratrol prevents Alzheimer's markers and increases life span in SAMP8," *Age*, vol. 35, no. 5, pp. 1851–1865, 2013.

[36] S. J. Padayatty, A. Katz, Y. Wang et al., "Vitamin C as an antioxidant: evaluation of its role in disease prevention," *Journal of the American college of Nutrition*, vol. 22, no. 1, pp. 18–35, 2003.

[37] K. A. Naidu, "Vitamin C in human health and disease is still a mystery? An overview," *Nutrition journal*, vol. 2, no. 1, pp. 1–10, 2003.

[38] L. E. Cahill and A. El-Sohemy, "Vitamin C transporter gene polymorphisms, dietary vitamin C and serum ascorbic acid," *Lifestyle Genomics*, vol. 2, no. 6, pp. 292–301, 2009.

[39] F. Monacelli, E. Acquarone, C. Giannotti, R. Borghi, and A. Nencioni, "Vitamin C, aging and Alzheimer's disease," *Nutrients*, vol. 9, no. 7, p. 670, 2017.

[40] J. I. Young, S. Züchner, and G. Wang, "Regulation of the epigenome by vitamin C," *Annual review of nutrition*, vol. 35, no. 1, pp. 545–564, 2015.

[41] R. Yin, S.-Q. Mao, B. Zhao et al., "Ascorbic acid enhances Tet-mediated 5-methylcytosine oxidation and promotes DNA demethylation in mammals," *Journal of the American Chemical Society*, vol. 135, no. 28, pp. 10396–10403, 2013.

[42] B.-Y. Chen, X. Wang, L.-W. Chen, and Z.-J. Luo, "Molecular targeting regulation of proliferation and differentiation of the bone marrow-derived mesenchymal stem cells or mesenchymal stromal cells," *Current drug targets*, vol. 13, no. 4, pp. 561–571, 2012.

[43] G. Tian, J. Sawashita, H. Kubo et al., "Ubiquinol-10 supplementation activates mitochondria functions to decelerate senescence in senescence-accelerated mice," *Antioxidants & Redox Signaling*, vol. 20, no. 16, pp. 2606–2620, 2014.

[44] M. J. Zarzuelo, R. López-Sepúlveda, M. Sánchez et al., "SIRT1 inhibits NADPH oxidase activation and protects endothelial function in the rat aorta: implications for vascular aging," *Biochemical Pharmacology*, vol. 85, no. 9, pp. 1288–1296, 2013.

[45] G. Arunachalam, H. Yao, I. K. Sundar, S. Caito, and I. Rahman, "SIRT1 regulates oxidant- and cigarette smoke-induced eNOS acetylation in endothelial cells: role of resveratrol," *Biochemical and biophysical research communications*, vol. 393, no. 1, pp. 66–72, 2010.

[46] Z. Xu, J. Huo, X. Ding et al., "Coenzyme Q10 improves lipid metabolism and ameliorates obesity by regulating CaMKII-mediated PDE4 inhibition," *Scientific Reports*, vol. 7, no. 1, article 8899, pp. 1–12, 2017.

[47] F. Olivieri, R. Lazzarini, L. Babini et al., "Anti-inflammatory effect of ubiquinol-10 on young and senescent endothelial cells via miR-146a modulation," *Free Radical Biology and Medicine*, vol. 63, pp. 410–420, 2013.

[48] J. Huo, Z. Xu, K. Hosoe et al., "Coenzyme Q10 prevents senescence and dysfunction caused by oxidative stress in vascular endothelial cells," *Oxidative medicine and cellular longevity*, vol. 2018, Article ID 3181759, 15 pages, 2018.

[49] R. Fabiani, P. Rosignoli, A. de Bartolomeo et al., "Oxidative DNA damage is prevented by extracts of olive oil, hydroxytyrosol, and other olive phenolic compounds in human blood mononuclear cells and HL60 cells," *The Journal of Nutrition*, vol. 138, no. 8, pp. 1411–1416, 2008.

[50] A. Daccache, C. Lion, N. Sibille et al., "Oleuropein and derivatives from olives as Tau aggregation inhibitors," *Neurochemistry International*, vol. 58, no. 6, pp. 700–707, 2011.

[51] Ö. Erol, N. Arda, and G. Erdem, "Phenols of virgin olive oil protects nuclear DNA against oxidative damage in HeLa cells," *Food and chemical toxicology*, vol. 50, no. 10, pp. 3475–3479, 2012.

[52] J. M. de Vos-Houben, N. R. Ottenheim, A. Kafatos et al., "Telomere length, oxidative stress, and antioxidant status in elderly men in Zutphen and Crete," *Mechanisms of ageing and development*, vol. 133, no. 6, pp. 373–377, 2012.

[53] V. Boccardi, A. Esposito, M. R. Rizzo, R. Marfella, M. Barbieri, and G. Paolisso, "Mediterranean diet, telomere maintenance and health status among elderly," *PloS one*, vol. 8, no. 4, article e62781, 2013.

[54] C. Marin, J. Delgado-Lista, R. Ramirez et al., "Mediterranean diet reduces senescence-associated stress in endothelial cells," *Age*, vol. 34, no. 6, pp. 1309–1316, 2012.

[55] A. Parzonko, M. E. Czerwińska, A. K. Kiss, and M. Naruszewicz, "Oleuropein and oleacein may restore biological functions of endothelial progenitor cells impaired by angiotensin II via activation of Nrf2/heme oxygenase-1 pathway," *Phytomedicine*, vol. 20, no. 12, pp. 1088–1094, 2013.

[56] A.-L. Levonen, M. Inkala, T. Heikura et al., "Nrf 2 gene transfer induces antioxidant enzymes and suppresses smooth muscle cell growth in vitro and reduces oxidative stress in rabbit aorta in vivo," *Arteriosclerosis, thrombosis, and vascular biology*, vol. 27, no. 4, pp. 741–747, 2007.

[57] J. Dulak, A. Loboda, and A. Jozkowicz, "Effect of heme oxygenase-1 on vascular function and disease," *Current opinion in lipidology*, vol. 19, no. 5, pp. 505–512, 2008.

[58] N. Nasimi, M. H. Dabbaghmanesh, and Z. Sohrabi, "Nutritional status and body fat mass: determinants of sarcopenia in community- dwelling older adults," *Experimental gerontology*, vol. 122, pp. 67–73, 2019.

[59] N. Nasimi, Z. Sohrabi, M. H. Dabbaghmanesh et al., "A novel fortified dairy product and sarcopenia measures in sarcopenic older adults: a double-blind randomized controlled trial," *Journal of the American Medical Directors Association*, vol. 22, no. 4, pp. 809–815, 2021.

[60] N. Barzilai, D. M. Huffman, R. H. Muzumdar, and A. Bartke, "The critical role of metabolic pathways in aging," *Diabetes*, vol. 61, no. 6, pp. 1315–1322, 2012.

[61] M. Rincon, E. Rudin, and N. Barzilai, "The insulin/IGF-1 signaling in mammals and its relevance to human longevity," *Experimental gerontology*, vol. 40, no. 11, pp. 873–877, 2005.

[62] P. Blume-Jensen and T. Hunter, "Oncogenic kinase signalling," *Nature*, vol. 411, no. 6835, pp. 355–365, 2001.

[63] Y. Higashi, H. C. Quevedo, S. Tiwari et al., "Interaction between insulin-like growth factor-1 and atherosclerosis and vascular aging," *Cardiovascular Issues in Endocrinology*, vol. 43, pp. 107–124, 2014.

[64] OliClinomel N4 Study Group, Z. Y. Jia, J. Yang et al., "Safety and efficacy of an olive oil-based triple-chamber bag for parenteral nutrition: a prospective, randomized, multi-center clinical trial in China," *Nutrition journal*, vol. 14, no. 1, pp. 1–15, 2015.

Hindawi
Oxidative Medicine and Cellular Longevity
Volume 2021, Article ID 5523516, 15 pages
https://doi.org/10.1155/2021/5523516

Review Article

Protective Effects of Estrogen on Cardiovascular Disease Mediated by Oxidative Stress

Du Xiang, Yang Liu, Shujun Zhou, Encheng Zhou, and Yanfeng Wang

Zhongnan Hospital of Wuhan University, Institute of Hepatobiliary Diseases of Wuhan University, Transplant Center of Wuhan University, Wuhan 430071, China

Correspondence should be addressed to Yanfeng Wang; yanfengwang@whu.edu.cn

Received 25 January 2021; Revised 16 May 2021; Accepted 22 May 2021; Published 29 June 2021

Academic Editor: Stefania D'Adamo

Perimenopause is an important stage of female senescence. Epidemiological investigation has shown that the incidence of cardiovascular disease in premenopausal women is lower than that in men, and the incidence of cardiovascular disease in postmenopausal women is significantly higher than that in men. This phenomenon reveals that estrogen has a definite protective effect on the cardiovascular system. In the cardiovascular system, oxidative stress is considered important in the pathogenesis of atherosclerosis, myocardial dysfunction, cardiac hypertrophy, heart failure, and myocardial ischemia. From the perspective of oxidative stress, estrogen plays a regulatory role in the cardiovascular system through the estrogen receptor, providing strategies for the treatment of menopausal women with cardiovascular diseases.

1. Introduction

Cardiovascular disease (CVD) has the highest mortality in the world [1]. With the aging of the population and the increasing incidence of obesity and diabetes, the cost of treatment for CVD will significantly increase worldwide [2]. The incidence of CVD is related to gender, and premenopausal women have a lower incidence of hypertension, atherosclerosis, myocardial dysfunction, ventricular hypertrophy, heart failure, and myocardial ischemia than age-matched men [3]. However, the advantage in women gradually disappears after menopause, which leads to a higher risk of CVD in postmenopausal women than men of the same age. This trend is largely attributed to the role of female estrogen in this process [4]. During the transitional period of menopause, women suffer from blood vessel aging, decreased diastolic ability, insulin sensitivity, and increased blood pressure due to decreased ovarian function and changes in hormone secretion, which increase the risk of CVD development [5]. Several studies have shown that certain functions mediated by estrogen in the cardiovascular system are related to the reduction in local oxidative stress (OS), which can reduce reactive oxygen species (ROS) by regulating the production of ROS enzymes and can enhance ROS clearance [6].

Estrogen has a wide range of critical physiological effects and exerts crucial effects on the growth and maturation of the endocrine, cardiovascular, skeletal, and metabolic systems [7]. With the extension of the human life span, the population of China is gradually aging; so, women will live nearly one-third of their lives without estrogen protection [8]. The decline in the ovarian function and the reduction in estrogen during menopause usually result in physical and psychological changes in females and lead to a series of autonomic dysfunction symptoms (sweating, irritability, insomnia, hot flashes, etc.) [9]. In addition, heart and brain vascular diseases, osteoporosis, and low immunity, which are related to menopause, have become the main risk factors affecting women's quality of life and life span [10].

Cells are involved in a variety of oxidation reactions in physiological processes, which inevitably leads to the release of ROS and reactive nitrogen species (RNS) [11]. If the balance between ROS and the antioxidant defense mechanism is broken, the accumulated ROS thereby destroy cell macromolecules, cause cell dysfunction, and ultimately kill cells

[12]. In the cardiovascular system, excessive ROS production is considered one of the pathogenic mechanisms of atherosclerosis, myocardial dysfunction, myocardial hypertrophy, heart failure, and myocardial ischemia [13]. Reducing the accumulation of ROS in cells, therefore, is a potential strategy to prevent and treat CVD [14]. Estrogen and the body's antioxidant ability decreases as menopausal women grow older, while the body's nicotinamide adenine dinucleotide phosphate (NADPH) and other oxidase activities increase, which results in an inability to clear ROS in time [15]. The accumulated ROS then induce OS, leading to osteoporosis and CVD [16]. Nevertheless, the specific mechanism of how estrogen alleviates CVD remains unclear. This article mainly summarizes the protective effects of estrogen on the cardiovascular system and its mechanism from the perspective of OS, laying the foundation for the treatment of cardiovascular disease in menopausal women.

2. Estrogen

Estrogen is a fat-soluble steroid hormone and plays an essential role in the development and physiology of many organ systems, including the breasts, uterus, bone, and cardiovascular system [17]. Estrogen is mainly produced by cholesterol in the ovaries, corpus luteum, and placenta in premenopausal women, with a small amount of estrogen produced by nonovarian organs, such as the liver, heart, skin, and brain [18]. There are three types of estrogen that have been found in the human body: estrone (E_1), 17β-estradiol (E_2), and estriol (E_3) [19]. Among these types, E_2 has the strongest biological activity [20]. E_1 is synthesized by adrenal dehydroepiandrosterone in the adipose tissue and is more important after menopause; E_2, the main product of the entire biosynthesis process, is the most effective estrogen before menopause; E_3, which is produced by E_1 formed by 16a-hydroxylation, is the weakest estrogen and plays a significant role during pregnancy [21]. In prepubertal women and postmenopausal women, estrogen produced by extragonadal tissues acts locally by paracrine or endocrine means to maintain tissue-specific functions [18]. Estrogen produced by follicles is synthesized by the granulosa cells and inner membrane cells of the follicle under the synergistic effects of follicle-stimulating hormone (FSH) and luteinizing hormone (LH) [18]. Androstenedione and testosterone produced by the inner membrane cells of the follicle under the action of LH diffuse into the granular cells through the basement membrane [22]. Aromatase activity is enhanced under the effects of FSH [23]. Then, androstenedione is converted into estrone, and testosterone is converted into estradiol, which is known as the two-cell-two gonadotropin theory of estrogen synthesis [24]. A small part of the synthesized estrogen enters the follicular cavity, and the majority enter the blood, regulating the differentiation and growth of target cells, such as the endometrium and breasts.

Estrogen inactivation can occur through metabolism, including conversion of E_2 to less active E_1 or E_3 and sulfation by estrogen sulfatase from E_2 to 17β-estradiol-1,3,5-triene-3,17-diol 3-sulfate, so that it no longer interacts with estrogen receptors [25]. In addition, the lack of a new adipose-derived cytokine lipocalin-2 in female mice can limit E_2 production by downregulating aromatase in the adipose tissue [26]. Therefore, the aromatase that controls the production of estrogen in the body can maintain a dynamic balance between estrogen synthesis and inactivation [27].

3. Estrogen Receptor (ER)

The ER is the core target of estrogen to exert its regulatory function and affects diseases in many organ systems including the cardiovascular system and skeletal system [28]. Most human estrogen receptors (ERs) are ligand-dependent transcription factors that belong to the steroid family. Two ERs have been discovered so far: the classic nuclear estrogen receptor (nER) and the membrane estrogen receptor (mER) [29]. The nER has two subtypes: ERα and ERβ [30]. ERα, which was discovered by Elwood Jenson in 1958, is widely distributed and has high mRNA expression in the uterus, testes, ovaries, prostate, skeletal muscle, kidneys, skin, etc. [31] In 1996, Kuiper et al. [32] isolated the second nuclear estrogen receptor, ERβ, which has higher mRNA expression in the ovaries, colon, brain tissue, kidneys, and male reproductive system. With further indepth study of nER, it was found that some target cells can quickly respond to estrogen without ER [33]. Therefore, in addition to the classical nER-mediated slow pathway, there are also fast membrane receptor-mediated estrogen effects that are mediated by G protein-coupled estrogen receptors (GPERs), including G-protein coupled receptor 30 (GPR30) and ER-X [34]. GPR30 is expressed in many brain regions (the hypothalamus, hippocampus, cortex, etc.), the adrenal medulla, renal pelvis, and ovaries [35]. The expression of ER-X is strictly regulated during development, and it is expressed in the brain of fetal baboons and the cerebral cortex, uterus, and lungs of rodents after birth. In adults, ER-X is rarely expressed but is expressed after ischemic injury [36].

4. Action Mode of Estrogen

The ER structure is mainly divided into five domains: transcription activation region-1 (AF-1), the DNA-binding domain, the ligand-binding domain (LBD), the hinge region, and transcription activation region-2 (AF-2) [37]. Each domain has its specific function, and the LBD is the key area where the ligand recognizes and binds the receptor and then triggers its effects [38]. Most signal pathways mediated by estrogen are regulated by ERs, which can be divided into genomic and nongenomic effects according to whether they are transcriptionally regulated [39]. The classic mode of estrogen action is the genomic effect mechanism in which estrogen enters the nucleus and combines with nuclear ERs to form a dimer, and then the estrogen-receptor complex binds to estrogen response elements and further regulates the gene expression and corresponding proteins, which triggers a series of cascade reaction events [40]. The nongenomic effect does not depend on the gene expression regulation mechanism, and its mode of action is that estrogen binds to the estrogen receptor on the cell membrane and activates the corresponding signal transduction, causing related

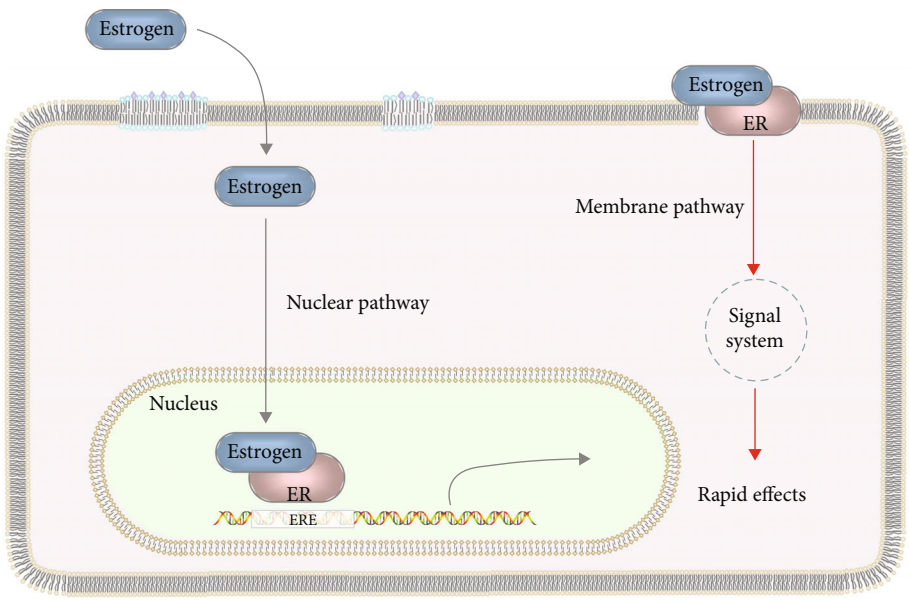

Figure 1: The genomic effect mediated by nuclear ERs and the nongenomic effect mediated by membrane ERs.

responses to exert the effects of estrogen [41]. The genomic effect generally works slowly, as it takes several hours to several days to occur, while the nongenomic effect typically only takes a few seconds to a few minutes, which is relatively fast [42]. The nongenomic effect mainly relies on the G protein-coupled estrogen receptor (GPER/GPR30), which was discovered in recent years. GPER, a member of the G protein-coupled receptor superfamily, is composed of 375 amino acids with a molecular weight of about 40 000 [43]. GPER is distributed in various organs and tissues, including breast, ovary, uterus, cardiovascular system, and lung and bone tissue, and is widely involved in the occurrence and development of estrogen-related diseases such as malignant tumors, inflammatory reactions, CVD, and obesity [44, 45]. The combination of E2 and GPER promotes the dissociation of the G protein trimer structure into α, β, and γ subunits [46]. The α subunit catalyzes cyclic adenosine monophosphate (cAMP) by activating adenylate cyclase on the cell membrane, and cAMP activates protein kinase A (PKA), thereby rapidly regulating cellular function changes [47–49]. In addition, β and γ subunits promote the release of heparin binding epidermal growth factor like growth factor (HBEGF) and the binding to epidermal growth factor receptor (EGFR), leading to the activation of multiple signal factors including mitogen activated protein kinase (MAPKs), phosphatidylinositol 3 kinase (PI3K), protein kinase B (PKB/Akt), and extracellular signal-regulated kinase (ERK1/2), which indirectly regulates the transcriptional activity of related genes and exerts various biological effects in the cell [47, 50–52] (Figure 1).

5. Oxidative Stress

The human body constantly produces oxygen free radicals during normal daily metabolic processes and approximately 95% of which are ROS, including superoxide anions (O_2^-), hydrogen peroxide (H_2O_2), hydroxyl free radicals (-OH), and peroxynitrite ($ONOO^-$) [53]. Normally, the body's oxidation system and the antioxidant defense system maintain a dynamic balance. When the antioxidant and oxidative effects are out of balance, pathological damage occurs. This process is called OS [6]. The main sources of intracellular ROS include xanthine oxidase, lipoxygenases, cyclooxygenases, peroxidases, uncoupled nitric oxide (NO) synthases, NADPH, the mitochondrial respiratory chain, and heme-containing proteins, and among these, an abnormal mitochondrial respiratory chain is the main source of ROS [54]. When the mitochondria cannot undergo normal oxidative phosphorylation, many ROS are produced [55, 56]. The generated ROS damage organelles, such as the mitochondria and plasma membrane and the DNA, proteins, and lipids of the organelle components, which eventually leads to cell death, aggravate the production of mitochondrial ROS and form a vicious circle [57, 58]. Finally, tissue cell dysfunction, such as endothelial cell dysfunction, vasculitis, and the accumulation of low-density lipoprotein in the arterial wall, is triggered. In addition, ROS are not only potentially harmful products of metabolism [59]. They can also act as second messengers to regulate cell growth and apoptosis [60]. The intracellular antioxidant defense system includes superoxide dismutases (SOD), catalase (CAT), glutathione peroxidases (GPx), and other nonenzymatic antioxidants, such as reduced glutathione (GSH), vitamin C, vitamin E, β-carotene, ubiquinone, lipoic acid, and flavonoids, which can inhibit the formation of ROS or reduce the damage caused by ROS [61–63]. Therefore, new treatments involve not only eliminating ROS but also inhibiting the activity of ROS-generating enzymes.

There is an important relationship between sex and OS. Studies have demonstrated that male rats have a higher degree of OS than female rats [64]. Another in vivo study showed that young men have higher OS biochemical markers than women of the same age [3]. In addition, clinical and experimental data show that women have greater antioxidant

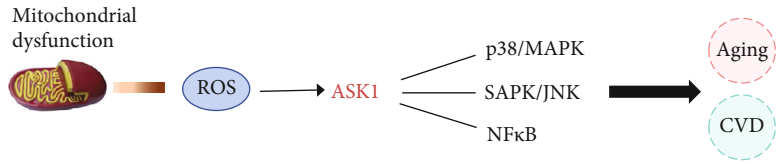

Figure 2: ROS promoted aging and cardiovascular disease by regulating ASK1.

potential than men [65]. In summary, there is a critical relationship between gender and OS [65, 66]. Women are not susceptible to OS and have stronger antioxidative stress capabilities than men, which further demonstrate that there is a strong connection between female estrogen and antioxidants [3].

6. Cardiovascular Diseases Mediated by OS after Menopause

After menopause, due to the exhaustion of ovarian follicles, the production of estrogen is greatly reduced, and the production of extraovarian estrogen becomes dominant [67]. During this period, the main plasma estrogen is estrone, which is less effective than E_2 [68]. Premenopausal women have higher levels of NO, which protects the heart and inhibits smooth muscle proliferation in heart disease [38]. After menopause, due to the decrease in estradiol antioxidants, postmenopausal women are more likely to undergo OS than women of reproductive age, and the incidence of CVD increases [69]. Moreover, the significant reduction in estrogen increases the level of free fatty acids, which makes postmenopausal women more likely to develop metabolic syndrome and insulin resistance, which are considered risk factors for CVD [70, 71].

OS is the main cause of many age-related cardiovascular pathologies, including ischemia/reperfusion (IR), hypertensive heart disease, and heart failure [72]. Under physiological conditions, low levels of ROS produced by mitochondria play an important role in vascular endothelial cells, which are involved in the production of NO, regulation of cell apoptosis, and signal transduction [73]. Some signaling pathways that promote aging, mainly including ASK1-p38-MAPK, ASK1-SAPK/JNK, and ASK1-NFkB, are involved in menopause [74]. These signaling pathways are also involved in oxidative stress-mediated CVD. The ASK1 signal body is a high-molecular weight protein complex composed of ROS-sensitive inhibitor protein and activator protein [74]. Its molecular weight is approximately 1500 kDa, which regulates the response to ROS and the signaling networks that promote aging and age-associated diseases of OS [74, 75]. The ROS related to aging mainly originate from mitochondrial dysfunction [76]. The generated ROS can activate the p38-MAPK and SAPK/JNK pathways, thereby mediating the occurrence of CVD [74]. In an aging mouse model, the inhibition of OS delayed aging through the p38-MAPK pathway, which means these signaling pathways have a certain relationship with aging, OS, and CVD [77] (Figure 2). The mechanism by which ROS mediate CVD is introduced below.

6.1. Oxidative Stress and Hypertrophic Cardiomyopathy (HCM). HCM is characterized by left ventricular hypertrophy, a reduced ventricular cavity and limited ventricular filling [78, 79]. In HCM, Ca^{2+} in myocardial cells in combination with myofilaments can reduce the concentration of Ca^{2+} in the mitochondria, the activity of mitochondrial tricarboxylic acid cycle enzymes, and the level of reduced coenzyme I/II, thereby triggering OS [80]. In addition, excessive production of mitochondrial ROS leads to activation of Ca^{2+} channels and transporters in cardiomyocytes, which activates transcription factors related to cardiomyocyte hypertrophy [79]. Cardiomyocyte hypertrophy can lead to excessive production of mitochondrial ROS, and excessive ROS can cause cardiomyocyte hypertrophy, thus forming a vicious circle [81]. A previous study confirmed that E_2 reduced myocardial OS and improved myocardial diastolic function, prevented myocardial energy dysregulation, thereby improving HCM [82].

6.2. Oxidative Stress and Atherosclerosis. Atherosclerosis is the leading cause of CVD [83]. Increasing evidence showed that the activation of proinflammatory signals, the expression of cytokines/chemokines, and OS are important factors leading to the occurrence of atherosclerosis [84]. Harmful stimuli (such as dyslipidemia, hypertension and smoking) can cause endothelial cell dysfunction, promote the expression of adhesion factors and chemotactic molecules, and increase the permeability of macromolecules [85]. This activity facilitates LDL entry into the arterial wall, resulting in apolipoprotein B100 and extracellular matrix (ECM) proteoglycan binding and retention [85]. In addition, oxidized low-density lipoprotein (OxLDL) activates endothelial cells to release phospholipids [86]. NOX2 is a specific subtype of NADPH oxidases (NOXs) and has been identified to play a key role in atherosclerosis formation [87]. NOX2 deficiency has little effect on blood lipids, but it can reduce the formation of aortic superoxide, increase the bioavailability of NO, and reduce the formation of atherosclerotic plaques [88]. Judkins et al. [89] found that in knockout apolipoprotein E (Apo E -/-) mice, the expression of NOX2 in mouse aortic endothelial cells and macrophages increases before atherosclerosis, and these changes are consistent with the increase in aortic superoxide production. Therefore, this study clearly showed that NOX2 plays a key role in superoxide generation, NO bioavailability reduction, and atherosclerotic plaque formation [90]. In conclusion, OS plays an important role in the progression of atherosclerosis. There is increasing evidence suggested that age is an important risk factor for atherosclerosis, which is promoted by cellular senescence [91]. E2 retarded oxidized low-density lipoprotein-induced premature senescence,

thereby inhibiting arterial aging and the development of atherosclerosis [92].

6.3. Oxidative Stress and Heart Failure (HF). HF is the terminal stage of heart disease. Many experiments and clinical studies have shown that ROS production is related to the pathogenesis of HF [93, 94]. By activating transcription factors and G-protein coupled receptors (GPCRs), ROS can stimulate myocardial cell growth and matrix remodeling and accelerate cell dysfunction [95]. The effects of H_2O_2 on adult rat ventricular myocytes are concentration-dependent [96, 97]. Low H_2O_2 concentrations can cause cardiomyocyte hypertrophy by activating ERK1/2, while high H_2O_2 concentrations can activate JNK and cause cardiomyocyte apoptosis [98]. ROS can also affect the extracellular matrix, stimulate the proliferation of cardiac fibroblasts, and activate matrix metalloproteinases (MMPs), which are the basic effects leading to fibrosis and matrix remodeling [99]. MMPs play an important role in the process of normal tissue remodeling, such as cell migration, invasion, proliferation, and apoptosis and have been shown to be elevated in HF [100]. MMPs are usually secreted in an inactive form and are activated by ROS after translation [100]. Hayashidani et al. [101] have shown that the survival rate of MMP-2 knockout mice after myocardial infarction (MI) is significantly improved because knocking out MMP-2 reduces the incidence of early heart rupture and left ventricular remodeling and failure. Kinugawa et al. [102] explored the role of OS in left ventricular remodeling and failure after myocardial infarction in mice and whether the -OH scavenger dimethylthiourea can alleviate these changes, and compared with untreated mice, mice who received dimethylthiourea demonstrated inhibition of MMP-2 activation, significantly improved left ventricular contractility, and reduced left ventricular hypertrophy. These findings indicate that OS products can stimulate the activation of myocardial MMP, and MMP plays a decisive role in left ventricular remodeling, thereby participating in the development of heart failure [103].

In recent years, OS markers, such as 8-OHdG, which has attracted much attention, have increasingly been used to assist in the diagnosis of heart failure [104]. These markers cause oxidative damage to DNA and serve as biomarkers of endogenous and exogenous factors [105]. The interaction between advanced glycation end products (AGEs) and their receptors (RAGE) initiates a series of signal cascade reactions, activating the transcription factor NF-κB and leading to the release of inflammatory cytokines, such as tumor necrosis factor-α (TNF), and eventually inducing OS; so, AGEs and RAGE are considered OS markers [106]. Another marker, neopterin, is mainly produced by macrophages after γ-interferon stimulation [107]. The higher the neopterin concentration, the higher the NYHA heart function classification, and the higher the probability of CVD. In addition, neopterin is related to the formation of ROS. In summary, biomarkers of OS can be used as reliable indicators for the diagnosis of heart failure [95]. The development of HF is characterized by increased OS in cardiomyocytes. The increased production of ROS correlates with the progression of HF [108]. E2 treatment improves HF by antioxidative mechanisms, and E2 may be an effective adjunctive therapy for patients with HF [109].

6.4. Oxidative Stress and Hypertension. Hypertension is the most common chronic disease, and it is a major risk factor for CVD. OS is a contributing factor in the pathogenesis of hypertension [65]. Excessive OS and a weakened ability to scavenge free radicals can lead to hypertension. Although the sources of intracellular ROS are diverse, the activity of NOXs is the main source of ROS [110]. There are five subtypes of NOXs: NOX1, NOX2, NOX3, NOX4, and NOX5 [111]. In the vasculature, different cells and blood vessels express different NOX subtypes, and there is no specific NOX subtype. NOX4 is mainly expressed in endothelial cells and vascular smooth muscle cells [112]. NOX1 is mainly expressed in large blood vessels, while NOX2 is mainly expressed in resistance blood vessels [103]. In the vasculature, ROS is mainly produced by vascular endothelial cells, adventitia cells, and smooth muscle cells, and it is mainly the NADPH enzyme that produces O_2- under the stimulation of angiotensin II (Ang II) and endothelin-1 [113]. The generated ROS can act as second messengers in the cell, increasing the intracellular concentration of Ca^{2+}, causing vasoconstriction, thereby promoting the development of hypertension [114].

The endothelium is a type of highly active monolayer that plays an important role in regulating vascular wall tension, cell adhesion, thrombosis, smooth muscle cell proliferation, and vascular inflammation [115]. All of these roles are achieved by releasing endothelium-derived relaxing factors, such as prostaglandins, nitric oxide, endothelium-derived hyperpolarizing factors, and endothelium-derived contractile factors [1]. The generated vasodilating factor NO is rapidly degraded by the oxygen free radical O_2-, and the superoxide anion produced by NOX reacts with NO to create peroxynitrite, which reduces the bioavailability of NO and causes vasoconstriction [103]. Therefore, hypertension is related to a decrease in NO and an increase in OS. Ang II is the main bioactive peptide of the renin-angiotensin system (RAS), which plays an important role in vasoconstriction, hypertrophy, fibrosis, inflammation, and aging [116]. Ang II activates the Ang II type 1 (AT_1R) and type 2 (AT_2R) receptors and drives OS through membrane-bound NADPH to increase the production of O_2^- [117]. The mechanisms by which Ang II mediates its physiological and pathophysiological vascular effects are complex [116, 118]. Previous studies have shown that ROS production and activation of reduction-oxidation dependent signaling cascades play key roles in Ang II-induced actions [119]. ROS is produced by various types of vascular cells, including endothelial cells, smooth muscle cells, outer membrane fibroblasts, and resident macrophages [120]. The main source of ROS in vascular cells is nonphagocytic NADPH oxidase, which is regulated by vasoactive agents (including Ang II) [121]. Rajagopalan et al. [122] found that long-term infusion of Ang II increases the oxidase activity of NADPH so that hypertension can be reduced. Some common antihypertensive drugs, such as angiotensin-converting enzyme (ACE) inhibitors and

angiotensin receptor inhibitors, can reduce blood pressure by inhibiting NOXs and reducing the production of ROS [120]. Hypertension susceptibility in women increases at the transition to menopause, and altered estrogen signaling is implicated in the increased hypertension incidence associated with menopause [123]. ER-β signaling plays an important role in blood pressure regulation. The inhibition of increased NMDA receptor signaling and ROS production in ER-β neurons in the paraventricular nucleus of the hypothalamus can reduce the susceptibility to hypertension [124].

6.5. Oxidative Stress and Atrial Fibrillation (AF). AF is the most common arrhythmia in clinical settings. Many experiments have confirmed the role of OS in the pathogenesis of AF [125, 126]. By inducing cardiomyocyte hypertrophy and apoptosis, ROS have a destructive effect on calcium transport channels in cardiomyocytes, leading to arrhythmias and enhancing cardiac remodeling [127]. The atrial type 2 ryanodine receptor (RyR2) has been shown to be a target of OS and is involved in the pathogenesis of AF [128]. The abnormality of intracellular Ca2+ plays an important role in the occurrence of AF [128]. RyR2 is the main calcium release channel in atrial myocytes, and it can become dysfunctional due to OS [129]. The increased RyR2-dependent Ca2+ leakage due to enhanced CaMKII activity can increase the susceptibility of AF [128]. Thus, changing intracellular Ca^{2+} homeostasis is related to the pathogenesis of AF. Studies have shown that reducing the production of ROS can decrease the release of atrial Ca^{2+} during diastole, which hinders the development of AF [130]. Due to the low efficiency of DNA proofreading and repair, human mitochondrial DNA is prone to oxidative damage and mutation during replication. Lin et al. [131] speculated that increased OS and mitochondrial DNA mutation may be related to AF. Polymerase chain reaction (PCR) analysis showed that the probability of mitochondrial DNA deletion in the atrial muscle of patients with AF was 3.75 times higher than that of patients without AF, and the level of oxidative damage to DNA in patients with AF was also higher than that in patients without AF [131]. Dudley et al. [132] used a swine model of AF to further confirm that OS is related to the pathogenesis of AF. In addition, Bretler et al. [133] indicated that E_2 therapy was associated with a decreased risk of new-onset AF especially among women ≥ 80 years old. E_2 therapy can reduce the risk of AF by 9-37 percent, the first year after myocardial infarction.

6.6. Oxidative Stress and Ischemic Cardiomyopathy (ICM). ICM refers to the clinical syndrome of chronic myocardial ischemia caused by coronary atherosclerosis, leading to diffuse fibrosis of myocardium and loss of myocardial function [134]. It is one of the most common causes of end-stage heart failure. Previous studies have shown that OS is closely related to the occurrence and development of ICM [135, 136]. During the pathogenesis of ICM, ischemia and hypoxia trigger a series of physiological and pathological processes, which make ROS accumulate in cells and promote OS [135]. The excessive production of ROS or the reduction of ROS clearance can damage the cell structure, destroy the cell membrane through lipid peroxidation, impair the function of enzymes through the oxidation of proteins, and cause chromosome damage through nucleic acid base modification and chain rupture, thus causing cell dysfunction [137]. In the process of ICM, ROS can destroy the cell membrane during the ICM process, promote calcium overload, cell apoptosis and the production of inflammatory mediators, and damage the function of endothelial cells and platelets, thereby promoting the occurrence and development of ICM [135, 138–141].

7. Estrogen Inhibits Oxidative Stress

OS is associated with a variety of diseases, including heart failure, hypertension, and atherosclerosis. Therefore, OS is an important mechanism of CVD, and any gender differences related to OS may affect the pathogenesis of CVD [3]. Estrogen may not be the only cause of gender differences between men and women but further research is needed to determine the protective effects of estrogen and the mechanisms involved. Jeanes et al. [142] found that E_2 and ERα-specific agonists decreased the infarct size by reducing myocardial lipid peroxidation during I/R in rats. In a hypoxia and reoxygenation model of rat cardiomyocytes in vitro, E_2 reduced cardiomyocyte apoptosis and ROS production by decreasing MAPK activity [143]. Estrogen decreases the risk of CVD by downregulating inflammatory markers, such as chemokines and cell adhesion molecules, to fight atherosclerosis [144]. In addition, it can stabilize atherosclerotic plaques by reducing the expression of matrix metalloproteinases and the production of plasminogen activator inhibitor-1 (PAI-1) [145]. Moreover, high concentrations of estrogen promote vasodilation by producing prostacyclin, inhibiting endothelin synthesis and blocking calcium channels [1]. In addition to its benefits to the cardiovascular system, estrogen also has an effect on biomarkers of vascular activity [146]. For example, a study concerning normal postmenopausal women revealed that taking estrogen for one year significantly reduced catecholamine levels, mean blood pressure, and low-density lipoprotein (LDL), while increasing nitrite and nitrate levels [147–149]. Other studies on the effects of estrogen on OS have shown that serum lipid peroxides decrease, and the overall antioxidant status is upregulated [150]. Estrogen increases binding proteins produced by the liver, such as sex hormone binding globulin, water maintenance, and sodium balance in the body, and it distributes lipids by increasing high-density lipoprotein (HDL) and reducing LDL [151]. It is clear that there is a definite relationship between estrogen and OS (as shown in Table 1).

Some studies have shown that estrogen inhibits OS in cardiac vessels and the myocardium by reducing local ROS production and increasing ROS clearance [143]. In addition, the removal of ROS in the blood vessel wall and heart is essential to ensure the structural and functional integrity of the cardiovascular system. NOXs is the main source of ROS [152]. Estrogen regulates the expression of NOXs subunits in different models, which has a protective effect on the cardiovascular system [153]. NOXs is an oxidase complex composed of NOX1-5, dual oxidase, and regulatory subunits

Table 1: The mechanisms of estrogen inhibiting oxidative stress.

Mechanisms	The changes in oxidative stress	References
E_2 decreased MAPK activity	The cardiomyocyte apoptosis and ROS production were reduced	[74, 77, 143, 180]
Estrogen decreased serum lipid peroxides	Overall antioxidant status was upregulated	[92, 150, 173, 181]
E_2 inhibited NOX subunit p47phox	The reduction of superoxide anion production was inhibited	[155, 160]
E_2 decreased NOX subunits $gp91^{phox}$, $p22^{phox}$, and $p67^{phox}$ induced by Ang II	ROS production was reduced	[143, 158, 182, 183]
E_2 upregulated the expression and activity of SOD induced by Ang II	ROS production wad reduced	[167, 184–190]
Estrogen restored antioxidant enzymes GPX1 and GPX4 expression levels	Oxidative stress balance was maintained	[158, 181, 189]
Estrogen increased the expression of the glutathione rate-limiting enzyme γ-glutamylcysteine synthetase	Oxidative stress balance was maintained	[168, 190, 191]
Estrogen maintained the bioavailability of NO by increasing the expression of eNOS mRNA and protein	The production of NO increased and oxidative stress was reduced	[84, 192–195]
ERα activated eNOS through the PI3/AKT signal pathway	The production of NO increased and oxidative stress was reduced	[175, 189, 195]
Estrogen increased the intracellular availability of the eNOS cofactor BH4 and prevented the uncoupling of eNOS	The production of eNOS-dependent ROS was reduced	[177, 178]

$p22^{phox}$, $p47^{phox}$, $p67^{phox}$, $p40^{phox}$, and Racl [111, 154]. Supplementation of E_2 in ovariectomized rats inhibited the reduction of superoxide anion production by the NOX subunit $p47^{phox}$ [155]. This finding suggested that estrogen changes the production of superoxide anions by regulating the expression or activity of NOXs in vascular smooth muscle cells [156]. Ang II can increase the expression of Rac1 protein in vascular smooth muscle cells, while E_2 can restore it to normal levels [157]. Zhang et al. [158] found that the expression of $p22^{phox}$ increased in salt-sensitive ovariectomized rats that were fed a high-sodium diet, which was reversed by injection of estrogen. Estrogen can also reduce the expression of the NOXs subunit NOX2 in endothelial cells in a time- and concentration-dependent manner, and this effect can be blocked by ER antagonists [159]. To summarize, both estrogen deficiency and estrogen supplementation change the expression and activity of NOXs, thus changing the production of O_2^- [160]. However, due to the different regulation of NOXs subunits in different animals and cells, it is not completely clear how estrogen affects the activity of NOXs through complex mechanisms (as shown in Table 1).

The renin-angiotensin-aldosterone system (RAAS) is an important humoral regulatory system composed of some peptide hormones and corresponding enzymes, which mainly maintain and regulate the balance of blood pressure, water, and electrolytes and maintain human homeostasis [161]. In vivo and in vitro studies have demonstrated that the RAAS plays a key role in the pathogenesis of CVD [162]. Ang II activates the AT_1R and mediates most of the biological effects of Ang II, such as vasoconstriction, aldosterone release, sodium and water maintenance, and cell growth. AT_1R-related NOXs produce many highly active O_2^- molecules, which are the main source of RAAS-induced ROS production, in monocytes, macrophages, endothelial cells, and vascular smooth muscle cells [163]. In addition, estrogen deficiency can also increase the expression of the angiotensin converting enzyme (ACE), thus promoting the production of Ang II [164]. Nickenig et al. [165] found that estrogen deficiency can upregulate AT_1R in isolated vascular smooth muscle, while estrogen supplementation can reverse this phenomenon. The expression of NOXs subunits $gp91^{phox}$, $p22^{phox}$, and $p67^{phox}$ induced by Ang II are decreased by E_2 [143] (as shown in Table 1).

SOD, which converts O_2^- into H_2O_2, is a cellular antioxidant defense mechanism and has been shown to be regulated by steroids [166]. Strehlow et al. [167] found that E_2 upregulated the expression and activity of SOD in vascular smooth muscle cells induced by Ang II, thus inhibiting the production of ROS induced by angiotensin converting enzyme II. In ovariectomized rats, the expression of antioxidant enzymes GPX1 and GPX4 significantly decreased, but estrogen returned expression to normal values [158]. Estrogen can also increase the expression of the glutathione rate-limiting enzyme γ-glutamylcysteine synthetase, which is consistent with the activation of glutathione reductase promoter activity by ERβ-specific *cis*-acting elements [168] (as shown in Table 1).

Nitric oxide synthase (eNOS) produced by endothelial cells can produce the vasodilator NO, and NO spreads to vascular smooth muscle cells, activates guanylate cyclase, and increases cyclic guanosine monophosphate (cGMP) [84]. NO plays a direct role in tissue oxygen balance, organ perfusion, vascular remodeling, and metabolic requirements by regulating vascular tension and diameter [169]. Kauser et al. [170] first found that there were gender differences in the production and release of NO, and the release of NO in the aorta of female rats was higher than that of males. Estrogen maintains the bioavailability of NO by increasing the expression of eNOS mRNA and protein, thus increasing the production of NO in endothelial cells and vascular smooth

muscle cells [171]. Wassmann et al. [172] demonstrated that raloxifene, a selective estrogen receptor modulator, increases the bioavailability of NO by upregulating eNOS mRNA and activity in the aorta of spontaneously hypertensive rats. Estrogen deficiency can increase blood pressure, produce OS, and decrease NO production. Similarly, estrogen supplementation increased NO production and decreased the amount of lipid peroxidation in ovariectomized rats [173]. However, Barbacanne et al. [174] believe that the antioxidant effects of estrogen are not achieved by affecting the activity or expression of eNOS but by directly decreasing the production of O_2^-. In vivo and in vitro experiments demonstrated that estrogen produces NO through nongenomic effects, and the specific mechanism is that ERα activates eNOS through the PI3/AKT signal pathway to produce NO. [175] Wong et al. [176] confirmed that raloxifene can increase the phosphorylation of eNOS and Akt in rat aortae and protect endocrine cells from OS. Estrogen can also increase the intracellular availability of the eNOS cofactor BH4 and prevent the uncoupling of eNOS, thus preventing the production of eNOS-dependent ROS [177] (as shown in Table 1). To summarize, estrogen can be used as a potential mechanism of antioxidation by increasing the production of NO, reducing O_2^-, and increasing the utilization of cofactor BH4 [178]. To support this hypothesis, postmenopausal women taking BH4 can improve endothelial dysfunction and reduce the incidence of atherosclerosis [179].

8. Conclusion

The incidence of CVD is lower in premenopausal women than in men of the same age, but it significantly increases after menopause. This phenomenon shows that estrogen has a protective effect on the cardiovascular system, which is undeniable. OS is an important mechanism of cardiovascular disease. This article mainly indicates the protection of estrogen in cardiovascular disease from the perspective of OS. When postmenopausal women are treated with estrogen, a comprehensive assessment should be performed according to the patient's symptoms, CVD and breast cancer risk, etc. to determine the route of administration, dosage, and frequency, and the risks and benefits should be regularly assessed to obtain minimal risk and maximal benefit through individualized treatment.

Conflicts of Interest

The authors declare that they have no conflicts of interest.

Authors' Contributions

Du Xiang and Yang Liu are contributed equally and share first authorship. Du Xiang and Yang Liu and Yanfeng Wang designed, searched, and wrote the paper. Shujun Zhou and Encheng Zhou revised the paper. Yanfeng Wang is responsible for the critical revision and final approval.

Acknowledgments

The manuscript is supported by the Science and Technology Innovation Incubation Fund of Zhongnan Hospital of Wuhan University (ZNJC201923).

References

[1] Y. B. Somani, J. A. Pawelczyk, M. J. de Souza, P. M. Kris-Etherton, and D. N. Proctor, "Aging women and their endothelium: probing the relative role of estrogen on vasodilator function," *American Journal of Physiology Heart and Circulatory Physiology*, vol. 317, no. 2, pp. H395–H404, 2019.

[2] D. Lin, L. Wang, S. Yan, Q. Zhang, J. H. Zhang, and A. Shao, "The role of oxidative stress in common risk factors and mechanisms of cardio- cerebrovascular ischemia and depression," *Oxidative Medicine and Cellular Longevity*, vol. 2019, Article ID 2491927, 13 pages, 2019.

[3] M. C. Kander, Y. Cui, and Z. Liu, "Gender difference in oxidative stress: a new look at the mechanisms for cardiovascular diseases," *Journal of Cellular and Molecular Medicine*, vol. 21, no. 5, pp. 1024–1032, 2017.

[4] L. Newson, "Menopause and cardiovascular disease," *Post Reproductive Health*, vol. 24, no. 1, pp. 44–49, 2018.

[5] S. Patel, A. Homaei, A. B. Raju, and B. R. Meher, "Estrogen: the necessary evil for human health, and ways to tame it," *Biomedicine & Pharmacotherapy*, vol. 102, pp. 403–411, 2018.

[6] P. Pignatelli, D. Menichelli, D. Pastori, and F. Violi, "Oxidative stress and cardiovascular disease: new insights," *Kardiologia Polska*, vol. 76, no. 4, pp. 713–722, 2018.

[7] E. Morselli, R. S. Santos, A. Criollo, M. D. Nelson, B. F. Palmer, and D. J. Clegg, "The effects of oestrogens and their receptors on cardiometabolic health," *Nature Reviews Endocrinology*, vol. 13, no. 6, pp. 352–364, 2017.

[8] T. Laisk, O. Tšuiko, T. Jatsenko et al., "Demographic and evolutionary trends in ovarian function and aging," *Human Reproduction Update*, vol. 25, no. 1, pp. 34–50, 2019.

[9] P. Monteleone, G. Mascagni, A. Giannini, A. R. Genazzani, and T. Simoncini, "Symptoms of menopause – global prevalence, physiology and implications," *Nature Reviews. Endocrinology*, vol. 14, no. 4, pp. 199–215, 2018.

[10] S. D. Sullivan, P. M. Sarrel, and L. M. Nelson, "Hormone replacement therapy in young women with primary ovarian insufficiency and early menopause," *Fertility and Sterility*, vol. 106, no. 7, pp. 1588–1599, 2016.

[11] E. Niki, "Oxidant-specific biomarkers of oxidative stress. Association with atherosclerosis and implication for antioxidant effects," *Free Radical Biology & Medicine*, vol. 120, pp. 425–440, 2018.

[12] J. Luo, K. Mills, S. le Cessie, R. Noordam, and D. van Heemst, "Ageing, age-related diseases and oxidative stress: what to do next?," *Ageing Research Reviews*, vol. 57, article 100982, 2020.

[13] A. Manea, A. Fortuno, and J. L. Martin-Ventura, "Oxidative stress in cardiovascular pathologies: genetics, cellular, and molecular mechanisms and future antioxidant therapies," *Oxidative Medicine and Cellular Longevity*, vol. 2012, Article ID 373450, 3 pages, 2012.

[14] Y. Zhang, P. Murugesan, K. Huang, and H. Cai, "NADPH oxidases and oxidase crosstalk in cardiovascular diseases:

novel therapeutic targets," *Nature Reviews Cardiology*, vol. 17, no. 3, pp. 170–194, 2020.

[15] N. T. Moldogazieva, I. M. Mokhosoev, T. I. Mel'nikova, Y. B. Porozov, and A. A. Terentiev, "Oxidative stress and advanced lipoxidation and glycation end products (ALEs and AGEs) in aging and age-related diseases," *Oxidative Medicine and Cellular Longevity*, vol. 2019, Article ID 3085756, 14 pages, 2019.

[16] N. N. Wu, Y. Zhang, and J. Ren, "Mitophagy, mitochondrial dynamics, and homeostasis in cardiovascular aging," *Oxidative Medicine and Cellular Longevity*, vol. 2019, Article ID 9825061, 15 pages, 2019.

[17] C. L. Faltas, K. A. Lebron, and M. K. Holz, "Unconventional estrogen signaling in health and disease," *Endocrinology*, vol. 161, no. 4, 2020.

[18] R. Barakat, O. Oakley, H. Kim, J. Jin, and C. M. J. Ko, "Extragonadal sites of estrogen biosynthesis and function," *BMB Reports*, vol. 49, no. 9, pp. 488–496, 2016.

[19] J. Cui, Y. Shen, and R. Li, "Estrogen synthesis and signaling pathways during aging: from periphery to brain," *Trends in Molecular Medicine*, vol. 19, no. 3, pp. 197–209, 2013.

[20] L. Medzikovic, L. Aryan, and M. Eghbali, "Connecting sex differences, estrogen signaling, and microRNAs in cardiac fibrosis," *Journal of Molecular Medicine*, vol. 97, no. 10, pp. 1385–1398, 2019.

[21] C. Lee, J. Kim, and Y. Jung, "Potential therapeutic application of estrogen in gender disparity of nonalcoholic fatty liver disease/nonalcoholic steatohepatitis," *Cell*, vol. 8, no. 10, p. 1259, 2019.

[22] A. Biegon, N. Alia-Klein, D. L. Alexoff et al., "Relationship of estrogen synthesis capacity in the brain with obesity and self-control in men and women," *Proceedings of the National Academy of Sciences of the United States of America*, vol. 117, no. 37, pp. 22962–22966, 2020.

[23] P. Cooke, M. K. Nanjappa, C. M. Ko, G. S. Prins, and R. A. Hess, "Estrogens in male physiology," *Physiological Reviews*, vol. 97, no. 3, pp. 995–1043, 2017.

[24] Z. Shoham and M. Schachter, "Estrogen biosynthesis–regulation, action, remote effects, and value of monitoring in ovarian stimulation cycles," *Fertility and Sterility*, vol. 65, no. 4, pp. 687–701, 1996.

[25] Y. L. Chen, H. Y. Fu, T. H. Lee et al., "Estrogen degraders and estrogen degradation pathway identified in an activated sludge," *Applied and Environmental Microbiology*, vol. 84, no. 10, 2018.

[26] P. Kamble, M. J. Pereira, K. Almby, and J. W. Eriksson, "Estrogen interacts with glucocorticoids in the regulation of lipocalin 2 expression in human adipose tissue. Reciprocal roles of estrogen receptor α and β in insulin resistance?," *Molecular and Cellular Endocrinology*, vol. 490, pp. 28–36, 2019.

[27] M. Khan, R. Ullah, S. U. Rehman et al., "17β-estradiol modulates SIRT1 and halts oxidative stress-mediated cognitive impairment in a male aging mouse model," *Cell*, vol. 8, no. 8, p. 928, 2019.

[28] T. Luo and J. K. Kim, "The role of estrogen and estrogen receptors on cardiomyocytes: an overview," *Canadian Journal of Cardiology*, vol. 32, no. 8, pp. 1017–1025, 2016.

[29] L. Jiao, J. O.'. Machuki, Q. Wu et al., "Estrogen and calcium handling proteins: new discoveries and mechanisms in cardiovascular diseases," *American Journal of Physiology-Heart and Circulatory Physiology*, vol. 318, no. 4, pp. H820–H829, 2020.

[30] S. Novella, D. Pérez-Cremades, A. Mompeón, and C. Hermenegildo, "Mechanisms underlying the influence of oestrogen on cardiovascular physiology in women," *The Journal of Physiology*, vol. 597, no. 19, pp. 4873–4886, 2019.

[31] J. Russell, C. K. Jones, and P. A. Newhouse, "The role of estrogen in brain and cognitive aging," *Neurotherapeutics*, vol. 16, no. 3, pp. 649–665, 2019.

[32] G. Kuiper, E. Enmark, M. Pelto-Huikko, S. Nilsson, and J. A. Gustafsson, "Cloning of a novel receptor expressed in rat prostate and ovary," *Proceedings of the National Academy of Sciences of the United States of America*, vol. 93, no. 12, pp. 5925–5930, 1996.

[33] C. Thomas and J. A. Gustafsson, "The different roles of ER subtypes in cancer biology and therapy," *Nature Reviews Cancer*, vol. 11, no. 8, pp. 597–608, 2011.

[34] A. Knowlton and A. R. Lee, "Estrogen and the cardiovascular system," *Pharmacology & Therapeutics*, vol. 135, no. 1, pp. 54–70, 2012.

[35] J. Xiang, X. Liu, J. Ren et al., "How does estrogen work on autophagy?," *Autophagy*, vol. 15, no. 2, pp. 197–211, 2019.

[36] R. Kiyama and Y. Wada-Kiyama, "Estrogenic endocrine disruptors: molecular mechanisms of action," *Environment International*, vol. 83, pp. 11–40, 2015.

[37] E. Tunc, A. A. Eve, and Z. Madak-Erdogan, "Coronary microvascular dysfunction and estrogen receptor signaling," *Trends in Endocrinology & Metabolism*, vol. 31, no. 3, pp. 228–238, 2020.

[38] P. Gourdy, M. Guillaume, C. Fontaine et al., "Estrogen receptor subcellular localization and cardiometabolism," *Molecular Metabolism*, vol. 15, pp. 56–69, 2018.

[39] K. Ueda, Y. Adachi, P. Liu, N. Fukuma, and E. Takimoto, "Regulatory actions of estrogen receptor signaling in the cardiovascular system," *Frontiers in Endocrinology*, vol. 10, 2020.

[40] A. Iorga, C. M. Cunningham, S. Moazeni, G. Ruffenach, S. Umar, and M. Eghbali, "The protective role of estrogen and estrogen receptors in cardiovascular disease and the controversial use of estrogen therapy," *Biology of Sex Differences*, vol. 8, no. 1, p. 33, 2017.

[41] N. Fuentes and P. Silveyra, "Estrogen receptor signaling mechanisms," *Advances in Protein Chemistry and Structural Biology*, vol. 116, pp. 135–170, 2019.

[42] S. Hewitt, "Estrogen receptors: new directions in the new millennium," *Endocrine Reviews*, vol. 39, no. 5, pp. 664–675, 2018.

[43] D. Rosenbaum, S. G. F. Rasmussen, and B. K. Kobilka, "The structure and function of G-protein-coupled receptors," *Nature*, vol. 459, no. 7245, pp. 356–363, 2009.

[44] M. S. Alavi, A. Shamsizadeh, H. Azhdari-Zarmehri, and A. Roohbakhsh, "Orphan G protein-coupled receptors: the role in CNS disorders," *Biomedicine & Pharmacotherapy*, vol. 98, pp. 222–232, 2018.

[45] M. Barton, "Not lost in translation: emerging clinical importance of the G protein-coupled estrogen receptor GPER," *Steroids*, vol. 111, pp. 37–45, 2016.

[46] W. Weis and B. K. Kobilka, "The molecular basis of G protein-coupled receptor activation," *Annual Review of Biochemistry*, vol. 87, no. 1, pp. 897–919, 2018.

[47] E. J. Filardo, "Epidermal growth factor receptor (EGFR) transactivation by estrogen via the G-protein-coupled

receptor, GPR30: a novel signaling pathway with potential significance for breast cancer," *The Journal of Steroid Biochemistry and Molecular Biology*, vol. 80, no. 2, pp. 231–238, 2002.

[48] J. K. Tan, C. McKenzie, E. Mariño, L. Macia, and C. R. Mackay, "Metabolite-sensing G protein-coupled receptors-facilitators of diet-related immune regulation," *Annual Review of Immunology*, vol. 35, no. 1, pp. 371–402, 2017.

[49] E. Filardo, J. A. Quinn, A. R. Frackelton Jr., and K. I. Bland, "Estrogen action via the G protein-coupled receptor, GPR30: stimulation of adenylyl cyclase and cAMP-mediated attenuation of the epidermal growth factor receptor-to-MAPK signaling axis," *Molecular Endocrinology*, vol. 16, no. 1, pp. 70–84, 2002.

[50] D. Wootten, A. Christopoulos, M. Marti-Solano, M. M. Babu, and P. M. Sexton, "Mechanisms of signalling and biased agonism in G protein-coupled receptors," *Nature reviews Molecular Cell Biology*, vol. 19, no. 10, pp. 638–653, 2018.

[51] J. Bopassa, M. Eghbali, L. Toro, and E. Stefani, "A novel estrogen receptor GPER inhibits mitochondria permeability transition pore opening and protects the heart against ischemia-reperfusion injury," *American Journal of Physiology. Heart and Circulatory Physiology*, vol. 298, no. 1, pp. H16–H23, 2010.

[52] A. Trenti, S. Tedesco, C. Boscaro, L. Trevisi, C. Bolego, and A. Cignarella, "Estrogen, angiogenesis, immunity and cell metabolism: solving the puzzle," *International Journal of Molecular Sciences*, vol. 19, no. 3, p. 859, 2018.

[53] D. Galaris, A. Barbouti, and K. Pantopoulos, "Iron homeostasis and oxidative stress: an intimate relationship," *Biochimica et Biophysica Acta (BBA) - Molecular Cell Research*, vol. 1866, no. 12, article 118535, 2019.

[54] J. Peoples, A. Saraf, N. Ghazal, T. T. Pham, and J. Q. Kwong, "Mitochondrial dysfunction and oxidative stress in heart disease," *Experimental & Molecular Medicine*, vol. 51, no. 12, pp. 1–13, 2019.

[55] D. Arauna, M. Furrianca, Y. Espinosa-Parrilla, E. Fuentes, M. Alarcón, and I. Palomo, "Natural bioactive compounds as protectors of mitochondrial dysfunction in cardiovascular diseases and aging," *Molecules*, vol. 24, no. 23, p. 4259, 2019.

[56] I. Lejri, A. Grimm, and A. Eckert, "Mitochondria, estrogen and female brain aging," *Frontiers in Aging Neuroscience*, vol. 10, p. 124, 2018.

[57] C. Cadeddu Dessalvi, A. Pepe, C. Penna et al., "Sex differences in anthracycline-induced cardiotoxicity: the benefits of estrogens," *Heart Failure Reviews*, vol. 24, no. 6, pp. 915–925, 2019.

[58] T. Liu, N. Li, Y. Q. Yan et al., "Recent advances in the anti-aging effects of phytoestrogens on collagen, water content, and oxidative stress," *Phytotherapy Research*, vol. 34, no. 3, pp. 435–447, 2020.

[59] M. Vernier, C. R. Dufour, S. McGuirk et al., "Estrogen-related receptors are targetable ROS sensors," *Genes & Development*, vol. 34, no. 7-8, pp. 544–559, 2020.

[60] B. Zhou, J. Y. Zhang, X. S. Liu et al., "Tom20 senses iron-activated ROS signaling to promote melanoma cell pyroptosis," *Cell Research*, vol. 28, no. 12, pp. 1171–1185, 2018.

[61] S. B. Doshi and A. Agarwal, "The role of oxidative stress in menopause," *Journal of Mid-life Health*, vol. 4, no. 3, pp. 140–146, 2013.

[62] E. Barati, H. Nikzad, and M. Karimian, "Oxidative stress and male infertility: current knowledge of pathophysiology and role of antioxidant therapy in disease management," *Cellular and Molecular Life Sciences*, vol. 77, no. 1, pp. 93–113, 2020.

[63] M. Maciejczyk, A. Zalewska, and J. R. Ładny, "Salivary antioxidant barrier, redox status, and oxidative damage to proteins and lipids in healthy children, adults, and the elderly," *Oxidative Medicine and Cellular Longevity*, vol. 2019, Article ID 4393460, 12 pages, 2019.

[64] J. Barp, A. S. R. Araújo, T. R. G. Fernandes et al., "Myocardial antioxidant and oxidative stress changes due to sex hormones," *Brazilian Journal of Medical and Biological Research*, vol. 35, no. 9, pp. 1075–1081, 2002.

[65] J. Reckelhoff, D. G. Romero, and L. L. Yanes Cardozo, "Sex, oxidative stress, and hypertension: insights from animal models," *Physiology*, vol. 34, no. 3, pp. 178–188, 2019.

[66] I. Pinchuk, D. Weber, B. Kochlik et al., "Gender- and age-dependencies of oxidative stress, as detected based on the steady state concentrations of different biomarkers in the MARK-AGE study," *Redox Biology*, vol. 24, article 101204, 2019.

[67] P. May-Panloup, L. Boucret, J. M. Chao de la Barca et al., "Ovarian ageing: the role of mitochondria in oocytes and follicles," *Human Reproduction Update*, vol. 22, no. 6, pp. 725–743, 2016.

[68] R. Qureshi, M. Picon-Ruiz, I. Aurrekoetxea-Rodriguez et al., "The major pre- and postmenopausal estrogens play opposing roles in obesity- driven mammary inflammation and Breast cancer development," *Cell Metabolism*, vol. 31, no. 6, pp. 1154–1172.e9, 2020.

[69] A. Díaz, R. López-Grueso, J. Gambini et al., "Sex differences in age-associated type 2 diabetes in rats—role of estrogens and oxidative stress," *Oxidative Medicine and Cellular Longevity*, vol. 2019, Article ID 6734836, 13 pages, 2019.

[70] C. Keck and M. Taylor, "Emerging research on the implications of hormone replacement therapy on coronary heart disease," *Current Atherosclerosis Reports*, vol. 20, no. 12, 2018.

[71] S. R. El Khoudary, "HDL and the menopause," *Current Opinion in Lipidology*, vol. 28, no. 4, pp. 328–336, 2017.

[72] T. Xu, W. Ding, X. Ji et al., "Oxidative stress in cell death and cardiovascular diseases," *Oxidative Medicine and Cellular Longevity*, vol. 2019, Article ID 9030563, 11 pages, 2019.

[73] T. Nakamura, I. Naguro, and H. Ichijo, "Iron homeostasis and iron-regulated ROS in cell death, senescence and human diseases," *Biochimica et Biophysica Acta - General Subjects*, vol. 1863, no. 9, pp. 1398–1409, 2019.

[74] J. Papaconstantinou, "The role of signaling pathways of inflammation and oxidative stress in development of senescence and aging phenotypes in cardiovascular disease," *Cell*, vol. 8, no. 11, p. 1383, 2019.

[75] C. Morales Betanzos, J. D. Federspiel, A. M. Palubinsky, B. A. McLaughlin, and D. C. Liebler, "Dynamic phosphorylation of apoptosis signal regulating kinase 1 (ASK1) in response to oxidative and electrophilic stress," *Chemical Research in Toxicology*, vol. 29, no. 12, pp. 2175–2183, 2016.

[76] T. Finkel and N. J. Holbrook, "Oxidants, oxidative stress and the biology of ageing," *Nature*, vol. 408, no. 6809, pp. 239–247, 2000.

[77] C. Hsieh, J. I. Rosenblatt, and J. Papaconstantinou, "Age-associated changes in SAPK/JNK and p38 MAPK signaling in response to the generation of ROS by 3-nitropropionic

acid," *Mechanisms of Ageing and Development*, vol. 124, no. 6, pp. 733–746, 2003.

[78] E. Rowin, A. Hausvater, M. S. Link et al., "Clinical profile and consequences of atrial fibrillation in hypertrophic cardiomyopathy," *Circulation*, vol. 136, no. 25, pp. 2420–2436, 2017.

[79] P. Wijnker, V. Sequeira, D. W. D. Kuster, and J. Velden, "Hypertrophic cardiomyopathy: a vicious cycle triggered by sarcomere mutations and secondary disease hits," *Antioxidants & Redox Signaling*, vol. 31, no. 4, pp. 318–358, 2019.

[80] J. Gilda and A. V. Gomes, "Proteasome dysfunction in cardiomyopathies," *The Journal of Physiology*, vol. 595, no. 12, pp. 4051–4071, 2017.

[81] D. Zhang, Y. Li, D. Heims-Waldron et al., "Mitochondrial cardiomyopathy caused by elevated reactive oxygen species and impaired cardiomyocyte proliferation," *Circulation Research*, vol. 122, no. 1, pp. 74–87, 2018.

[82] Y. Chen, Z. Zhang, F. Hu et al., "17β-estradiol prevents cardiac diastolic dysfunction by stimulating mitochondrial function: a preclinical study in a mouse model of a human hypertrophic cardiomyopathy mutation," *The Journal of Steroid Biochemistry and Molecular Biology*, vol. 147, pp. 92–102, 2015.

[83] E. Sanchez-Rodriguez, A. Egea-Zorrilla, J. Plaza-Díaz et al., "The gut microbiota and its implication in the development of atherosclerosis and related cardiovascular diseases," *Nutrients*, vol. 12, no. 3, p. 605, 2020.

[84] U. Förstermann, N. Xia, and H. Li, "Roles of vascular oxidative stress and nitric oxide in the pathogenesis of atherosclerosis," *Circulation Research*, vol. 120, no. 4, pp. 713–735, 2017.

[85] A. M. Giudetti, M. Salzet, and T. Cassano, "Oxidative stress in aging brain: nutritional and pharmacological interventions for neurodegenerative disorders," *Oxidative Medicine and Cellular Longevity*, vol. 2018, Article ID 3416028, 2 pages, 2018.

[86] P. Marchio, S. Guerra-Ojeda, J. M. Vila, M. Aldasoro, V. M. Victor, and M. D. Mauricio, "Targeting early atherosclerosis: a focus on oxidative stress and inflammation," *Oxidative Medicine and Cellular Longevity*, vol. 2019, Article ID 8563845, 32 pages, 2019.

[87] A. J. Kattoor, N. V. K. Pothineni, D. Palagiri, and J. L. Mehta, "Oxidative stress in atherosclerosis," *Current Atherosclerosis Reports*, vol. 19, no. 11, 2017.

[88] A. Maqbool, N. T. Watt, N. Haywood et al., "Divergent effects of genetic and pharmacological inhibition of Nox2 NADPH oxidase on insulin resistance-related vascular damage," *American Journal of Physiology. Cell Physiology*, vol. 319, no. 1, pp. C64–C74, 2020.

[89] C. Judkins, H. Diep, B. R. S. Broughton et al., "Direct evidence of a role for Nox2 in superoxide production, reduced nitric oxide bioavailability, and early atherosclerotic plaque formation in ApoE-/- mice," *American Journal of Physiology. Heart and Circulatory Physiology*, vol. 298, no. 1, pp. H24–H32, 2010.

[90] P. P. Sfyri, N. Y. Yuldasheva, A. Tzimou et al., "Attenuation of oxidative stress-induced lesions in skeletal muscle in a mouse model of obesity-independent hyperlipidaemia and atherosclerosis through the inhibition of Nox2 activity," *Free Radical Biology & Medicine*, vol. 129, pp. 504–519, 2018.

[91] J. Wang and M. Bennett, "Aging and atherosclerosis: mechanisms, functional consequences, and potential therapeutics for cellular senescence," *Circulation Research*, vol. 111, no. 2, pp. 245–259, 2012.

[92] Y. Sasaki, Y. Ikeda, T. Miyauchi, Y. Uchikado, Y. Akasaki, and M. Ohishi, "Estrogen-SIRT1 Axis plays a pivotal role in protecting arteries against menopause-induced senescence and atherosclerosis," *Journal of Atherosclerosis and Thrombosis*, vol. 27, no. 1, pp. 47–59, 2020.

[93] L. A. Kiyuna, R. P. Albuquerque, C. H. Chen, D. Mochly-Rosen, and J. C. B. Ferreira, "Targeting mitochondrial dysfunction and oxidative stress in heart failure: challenges and opportunities," *Free Radical Biology and Medicine*, vol. 129, pp. 155–168, 2018.

[94] M. S. Ali Sheikh, U. Salma, B. Zhang, J. Chen, J. Zhuang, and Z. Ping, "Diagnostic, prognostic, and therapeutic value of circulating miRNAs in heart failure patients associated with oxidative stress," *Oxidative Medicine and Cellular Longevity*, vol. 2016, 13 pages, 2016.

[95] A. van der Pol, W. van Gilst, A. A. Voors, and P. van der Meer, "Treating oxidative stress in heart failure: past, present and future," *European Journal of Heart Failure*, vol. 21, no. 4, pp. 425–435, 2019.

[96] Y. Li, J. Xia, N. Jiang et al., "Corin protects H_2O_2-induced apoptosis through PI3K/AKT and NF-κB pathway in cardiomyocytes," *Biomedicine & Pharmacotherapy*, vol. 97, pp. 594–599, 2018.

[97] B. Liu, N. Jia, H. L. Wei, M. Lan, J. M. Liu, and Y. Z. Xue, "Knockdown of p66ShcA activates Nrf2 pathway to protect cardiomyocytes from oxidative stress and inflammation induced by H2O2," *European Review for Medical and Pharmacological Sciences*, vol. 24, no. 12, pp. 6994–7001, 2020.

[98] S. Kwon, D. R. Pimentel, A. Remondino, D. B. Sawyer, and W. S. Colucci, "H_2O_2 regulates cardiac myocyte phenotype via concentration-dependent activation of distinct kinase pathways," *Journal of Molecular and Cellular Cardiology*, vol. 35, no. 6, pp. 615–621, 2003.

[99] K. Ayoub, N. V. K. Pothineni, J. Rutland, Z. Ding, and J. L. Mehta, "Immunity, inflammation, and oxidative stress in heart failure: emerging molecular targets," *Cardiovascular Drugs and Therapy*, vol. 31, no. 5-6, pp. 593–608, 2017.

[100] D. Siwik and W. S. Colucci, "Regulation of matrix metalloproteinases by cytokines and reactive oxygen/nitrogen species in the myocardium," *Heart Failure Reviews*, vol. 9, no. 1, pp. 43–51, 2004.

[101] S. Hayashidani, H. Tsutsui, M. Ikeuchi et al., "Targeted deletion of MMP-2 attenuates early LV rupture and late remodeling after experimental myocardial infarction," *American Journal of Physiology-Heart and Circulatory Physiology*, vol. 285, no. 3, pp. H1229–H1235, 2003.

[102] S. Kinugawa, H. Tsutsui, S. Hayashidani et al., "Treatment with dimethylthiourea prevents left ventricular remodeling and failure after experimental myocardial infarction in mice: role of oxidative stress," *Circulation Research*, vol. 87, no. 5, pp. 392–398, 2000.

[103] T. Senoner and W. Dichtl, "Oxidative stress in cardiovascular diseases: still a therapeutic target?," *Nutrients*, vol. 11, no. 9, p. 2090, 2019.

[104] M. A. Sánchez-Rodríguez and V. M. Mendoza-Núñez, "Oxidative stress indexes for diagnosis of health or disease in humans," *Oxidative Medicine and Cellular Longevity*, vol. 2019, Article ID 4128152, 32 pages, 2019.

[105] M. Graille, P. Wild, J. J. Sauvain, M. Hemmendinger, I. Guseva Canu, and N. B. Hopf, "Urinary 8-OHdG as a biomarker for oxidative stress: a systematic literature review and meta-analysis," *International Journal of Molecular Sciences*, vol. 21, no. 11, p. 3743, 2020.

[106] A. Bierhaus, P. M. Humpert, M. Morcos et al., "Understanding RAGE, the receptor for advanced glycation end products," *Journal of Molecular Medicine*, vol. 83, no. 11, pp. 876–886, 2005.

[107] J. Razumovitch, G. N. Semenkova, D. Fuchs, and S. N. Cherenkevich, "Influence of neopterin on the generation of reactive oxygen species in human neutrophils," *FEBS Letters*, vol. 549, no. 1-3, pp. 83–86, 2003.

[108] A. Sabbatini and G. Kararigas, "Menopause-related estrogen decrease and the pathogenesis of HFpEF:," *Journal of the American College of Cardiology*, vol. 75, no. 9, pp. 1074–1082, 2020.

[109] M. Satoh, C. M. Matter, H. Ogita et al., "Inhibition of apoptosis-regulated signaling kinase-1 and prevention of congestive heart failure by estrogen," *Circulation*, vol. 115, no. 25, pp. 3197–3204, 2007.

[110] H. Y. Small, S. Migliarino, M. Czesnikiewicz-Guzik, and T. J. Guzik, "Hypertension: focus on autoimmunity and oxidative stress," *Free Radical Biology & Medicine*, vol. 125, pp. 104–115, 2018.

[111] G. A. Knock, "NADPH oxidase in the vasculature: expression, regulation and signalling pathways; role in normal cardiovascular physiology and its dysregulation in hypertension," *Free Radical Biology and Medicine*, vol. 145, pp. 385–427, 2019.

[112] K. Bedard and K. H. Krause, "The NOX family of ROS-generating NADPH oxidases: physiology and pathophysiology," *Physiological Reviews*, vol. 87, no. 1, pp. 245–313, 2007.

[113] C. S. Wilcox, C. Wang, and D. Wang, "Endothelin-1-induced microvascular ROS and contractility in angiotensin-II-infused mice depend on COX and TP receptors," *Antioxidants*, vol. 8, no. 6, p. 193, 2019.

[114] R. Brito, G. Castillo, J. González, N. Valls, and R. Rodrigo, "Oxidative stress in hypertension: mechanisms and therapeutic opportunities," *Experimental and Clinical Endocrinology & Diabetes*, vol. 123, no. 6, pp. 325–335, 2015.

[115] P. Thakore and S. Earley, "Transient receptor potential channels and endothelial cell calcium signaling," *Comprehensive Physiology*, vol. 9, no. 3, pp. 1249–1277, 2019.

[116] S. Forrester, G. W. Booz, C. D. Sigmund et al., "Angiotensin II signal transduction: an update on mechanisms of physiology and pathophysiology," *Physiological Reviews*, vol. 98, no. 3, pp. 1627–1738, 2018.

[117] A. Nguyen Dinh Cat, A. C. Montezano, D. Burger, and R. M. Touyz, "Angiotensin II, NADPH oxidase, and redox signaling in the vasculature," *Antioxidants & Redox Signaling*, vol. 19, no. 10, pp. 1110–1120, 2013.

[118] S. Das, E. Zhang, P. Senapati et al., "A novel angiotensin II-induced long noncoding RNA giver regulates oxidative stress, inflammation, and proliferation in vascular smooth muscle cells," *Circulation Research*, vol. 123, no. 12, pp. 1298–1312, 2018.

[119] K. Griendling, D. Sorescu, and M. Ushio-Fukai, "NAD(P)H oxidase: role in cardiovascular biology and disease," *Circulation Research*, vol. 86, no. 5, pp. 494–501, 2000.

[120] R. Touyz, "Reactive oxygen species and angiotensin II signaling in vascular cells: implications in cardiovascular disease," *Brazilian Journal of Medical and Biological Research*, vol. 37, no. 8, pp. 1263–1273, 2004.

[121] A. C. Montezano and R. M. Touyz, "Oxidative stress, Noxs, and hypertension: experimental evidence and clinical controversies," *Ann Med*, vol. 44, no. sup1, pp. S2–S16, 2012.

[122] S. Rajagopalan, S. Kurz, T. Münzel et al., "Angiotensin II-mediated hypertension in the rat increases vascular superoxide production via membrane NADH/NADPH oxidase activation. Contribution to alterations of vasomotor tone," *The Journal of Clinical Investigation*, vol. 97, no. 8, pp. 1916–1923, 1996.

[123] K. Srivaratharajah and B. L. Abramson, "Hypertension in menopausal women: the effect and role of estrogen," *Menopause*, vol. 26, no. 4, pp. 428–430, 2019.

[124] J. Marques-Lopes, E. Tesfaye, S. Israilov et al., "Redistribution of NMDA receptors in estrogen-receptor-β-containing paraventricular hypothalamic neurons following slow-pressor angiotensin II hypertension in female mice with accelerated ovarian failure," *Neuroendocrinology*, vol. 104, no. 3, pp. 239–256, 2017.

[125] A. Samman Tahhan, P. B. Sandesara, S. S. Hayek et al., "Association between oxidative stress and atrial fibrillation," *Heart Rhythm*, vol. 14, no. 12, pp. 1849–1855, 2017.

[126] L. Emelyanova, Z. Ashary, M. Cosic et al., "Selective downregulation of mitochondrial electron transport chain activity and increased oxidative stress in human atrial fibrillation," *American Journal of Physiology. Heart and Circulatory Physiology*, vol. 311, no. 1, pp. H54–H63, 2016.

[127] X. Liu, S. Wang, X. Guo et al., "Increased reactive oxygen species–mediated Ca2+/calmodulin-dependent protein kinase II activation contributes to calcium handling abnormalities and impaired contraction in Barth syndrome," *Circulation*, vol. 143, no. 19, pp. 1894–1911, 2021.

[128] M. Chelu, S. Sarma, S. Sood et al., "Calmodulin kinase II-mediated sarcoplasmic reticulum Ca^{2+} leak promotes atrial fibrillation in mice," *The Journal of Clinical Investigation*, vol. 119, no. 7, pp. 1940–1951, 2009.

[129] M. G. Chelu, S. Sarma, S. Sood et al., "Calmodulin kinase II–mediated sarcoplasmic reticulum Ca^{2+} leak promotes atrial fibrillation in mice," *Journal of Clinical Investigation*, 2009.

[130] W. Xie, G. Santulli, S. R. Reiken et al., "Mitochondrial oxidative stress promotes atrial fibrillation," *Scientific Reports*, vol. 5, no. 1, article 11427, 2015.

[131] P. Lin, S. H. Lee, C. P. Su, and Y. H. Wei, "Oxidative damage to mitochondrial DNA in atrial muscle of patients with atrial fibrillation," *Free Radical Biology & Medicine*, vol. 35, no. 10, pp. 1310–1318, 2003.

[132] S. Dudley, N. E. Hoch, L. A. McCann et al., "Atrial fibrillation increases production of superoxide by the left atrium and left atrial appendage: role of the NADPH and xanthine oxidases," *Circulation*, vol. 112, no. 9, pp. 1266–1273, 2005.

[133] D. M. Bretler, P. R. Hansen, J. Lindhardsen et al., "Hormone replacement therapy and risk of new-onset atrial fibrillation after myocardial infarction–a nationwide cohort study," *PLoS One*, vol. 7, no. 12, article e51580, 2012.

[134] M. Mahmoudi, M. Yu, V. Serpooshan et al., "Multiscale technologies for treatment of ischemic cardiomyopathy," *Nature Nanotechnology*, vol. 12, no. 9, pp. 845–855, 2017.

[135] S. Neidhardt, J. Garbade, F. Emrich et al., "Ischemic cardiomyopathy affects the thioredoxin system in the human myocardium," *Journal of Cardiac Failure*, vol. 25, no. 3, pp. 204–212, 2019.

[136] I. Muthuramu, R. Amin, A. Postnov et al., "Cholesterol-lowering gene therapy counteracts the development of non-ischemic cardiomyopathy in mice," *Molecular Therapy*, vol. 25, no. 11, pp. 2513–2525, 2017.

[137] D. Tan and T. Suda, "Reactive oxygen species and mitochondrial homeostasis as regulators of stem cell fate and function," *Antioxidants & Redox Signaling*, vol. 29, no. 2, pp. 149–168, 2018.

[138] S. Garcia, D. Grotto, R. P. Bulcão et al., "Evaluation of lipid damage related to pathological and physiological conditions," *Drug and Chemical Toxicology*, vol. 36, no. 3, pp. 306–312, 2013.

[139] Y. W. Wang, J. H. Zhang, Y. Yu, J. Yu, and L. Huang, "Inhibition of store-operated calcium entry protects endothelial progenitor cells from H2O2-induced apoptosis," *Biomolecules & Therapeutics*, vol. 24, no. 4, pp. 371–379, 2016.

[140] D. E. le, M. Pascotto, H. Leong-Poi, I. Sari, A. Micari, and S. Kaul, "Anti-inflammatory and pro-angiogenic effects of beta blockers in a canine model of chronic ischemic cardiomyopathy: comparison between carvedilol and metoprolol," *Basic Research in Cardiology*, vol. 108, no. 6, p. 384, 2013.

[141] D. Pietraforte, R. Vona, A. Marchesi et al., "Redox control of platelet functions in physiology and pathophysiology," *Antioxidants & Redox Signaling*, vol. 21, no. 1, pp. 177–193, 2014.

[142] H. Jeanes, C. Tabor, D. Black, A. Ederveen, and G. A. Gray, "Oestrogen-mediated cardioprotection following ischaemia and reperfusion is mimicked by an oestrogen receptor (ER)α agonist and unaffected by an ERβ antagonist," *The Journal of Endocrinology*, vol. 197, no. 3, pp. 493–501, 2008.

[143] P. Arias-Loza, M. Muehlfelder, and T. Pelzer, "Estrogen and estrogen receptors in cardiovascular oxidative stress," *Pflügers Archiv - European Journal of Physiology*, vol. 465, no. 5, pp. 739–746, 2013.

[144] V. Pelekanou, M. Kampa, F. Kiagiadaki et al., "Estrogen anti-inflammatory activity on human monocytes is mediated through cross-talk between estrogen receptor ERα36 and GPR30/GPER1," *Journal of Leukocyte Biology*, vol. 99, no. 2, pp. 333–347, 2016.

[145] S.-l. Liu, A. Bajpai, E. A. Hawthorne et al., "Cardiovascular protection in females linked to estrogen-dependent inhibition of arterial stiffening and macrophage MMP12," *JCI Insight*, vol. 4, no. 1, 2019.

[146] J. Arnal, F. Lenfant, R. Metivier et al., "Membrane and nuclear estrogen receptor alpha actions: from tissue specificity to medical implications," *Physiological Reviews*, vol. 97, no. 3, pp. 1045–1087, 2017.

[147] P. Anagnostis, J. Bitzer, A. Cano et al., "Menopause symptom management in women with dyslipidemias: an EMAS clinical guide," *Maturitas*, vol. 135, pp. 82–88, 2020.

[148] S. Nii, K. Shinohara, H. Matsushita, Y. Noguchi, K. Watanabe, and A. Wakatsuki, "Hepatic effects of estrogen on plasma distribution of small dense low-density lipoprotein and free radical production in postmenopausal women," *Journal of Atherosclerosis and Thrombosis*, vol. 23, no. 7, pp. 810–818, 2016.

[149] N. Hemati, M. Asis, S. Moradi et al., "Effects of genistein on blood pressure: a systematic review and meta-analysis," *Food Research International*, vol. 128, article 108764, 2020.

[150] B. T. Palmisano, L. Zhu, R. H. Eckel, and J. M. Stafford, "Sex differences in lipid and lipoprotein metabolism," *Molecular Metabolism*, vol. 15, pp. 45–55, 2018.

[151] S. H. Ko and H. S. Kim, "Menopause-associated lipid metabolic disorders and foods beneficial for postmenopausal women," *Nutrients*, vol. 12, no. 1, p. 202, 2020.

[152] C. A. Meza, J. D. la Favor, D. H. Kim, and R. C. Hickner, "Endothelial dysfunction: is there a hyperglycemia-induced imbalance of NOX and NOS?," *International Journal of Molecular Sciences*, vol. 20, no. 15, p. 3775, 2019.

[153] F. Magnani and A. Mattevi, "Structure and mechanisms of ROS generation by NADPH oxidases," *Current Opinion in Structural Biology*, vol. 59, pp. 91–97, 2019.

[154] A. Tarafdar and G. Pula, "The role of NADPH oxidases and oxidative stress in neurodegenerative disorders," *International Journal of Molecular Sciences*, vol. 19, no. 12, p. 3824, 2018.

[155] M. Florian, A. Freiman, and S. Magder, "Treatment with 17-β-estradiol reduces superoxide production in aorta of ovariectomized rats," *Steroids*, vol. 69, no. 13-14, pp. 779–787, 2004.

[156] P. Zhang, Y. Fu, J. Ju et al., "Estradiol inhibits fMLP-induced neutrophil migration and superoxide production by upregulating MKP-2 and dephosphorylating ERK," *International Immunopharmacology*, vol. 75, article 105787, 2019.

[157] U. Laufs, O. Adam, K. Strehlow et al., "Down-regulation of Rac-1 GTPase by estrogen," *Journal of Biological Chemistry*, vol. 278, no. 8, pp. 5956–5962, 2003.

[158] L. Zhang, S. Fujii, and H. Kosaka, "Effect of oestrogen on reactive oxygen species production in the aortas of ovariectomized dahl salt-sensitive rats," *Journal of Hypertension*, vol. 25, no. 2, pp. 407–414, 2007.

[159] A. Wagner, M. R. Schroeter, and M. Hecker, "17β-Estradiol inhibition of NADPH oxidase expression in human endothelial cells," *FASEB Journal*, vol. 15, no. 12, pp. 2121–2130, 2001.

[160] M. J. Ronis, M. L. Blackburn, K. Shankar, M. Ferguson, M. A. Cleves, and T. M. Badger, "Estradiol and NADPH oxidase crosstalk regulates responses to high fat feeding in female mice," *Experimental Biology and Medicine*, vol. 244, no. 10, pp. 834–845, 2019.

[161] N. Muñoz-Durango, C. Fuentes, A. Castillo et al., "Role of the renin-angiotensin-aldosterone system beyond blood pressure regulation: molecular and cellular mechanisms involved in end-organ damage during arterial hypertension," *International Journal of Molecular Sciences*, vol. 17, no. 7, p. 797, 2016.

[162] T. von Lueder, D. Atar, and H. Krum, "Current role of neprilysin inhibitors in hypertension and heart failure," *Pharmacology & Therapeutics*, vol. 144, no. 1, pp. 41–49, 2014.

[163] T. M. Paravicini and R. M. Touyz, "NADPH oxidases, reactive oxygen species, and hypertension: clinical implications and therapeutic possibilities," *Diabetes Care*, vol. 31, Supplement 2, pp. S170–S180, 2008.

[164] Z. Zhao, H. Wang, J. A. Jessup, S. H. Lindsey, M. C. Chappell, and L. Groban, "Role of estrogen in diastolic dysfunction," *American Journal of Physiology Heart and Circulatory Physiology*, vol. 306, no. 5, pp. H628–H640, 2014.

[165] G. Nickenig, A. T. Bäumer, C. Grohè et al., "Estrogen modulates AT1Receptor gene expression *in vitro* and *in vivo*," *Circulation*, vol. 97, no. 22, pp. 2197–2201, 1998.

[166] L. Juergens, H. Worth, and U. R. Juergens, "New perspectives for mucolytic, anti-inflammatory and adjunctive therapy with 1,8-cineole in COPD and asthma: review on the new

therapeutic approach," *Advances in Therapy*, vol. 37, no. 5, pp. 1737–1753, 2020.

[167] K. Strehlow, S. Rotter, S. Wassmann et al., "Modulation of antioxidant enzyme expression and function by estrogen," *Circulation Research*, vol. 93, no. 2, pp. 170–177, 2003.

[168] Y. Urata, Y. Ihara, H. Murata et al., "17β-estradiol protects against oxidative stress-induced cell death through the glutathione/glutaredoxin-dependent redox regulation of Akt in myocardiac H9c2 cells," *Journal of Biological Chemistry*, vol. 281, no. 19, pp. 13092–13102, 2006.

[169] A. Ally, I. Powell, M. M. Ally, K. Chaitoff, and S. M. Nauli, "Role of neuronal nitric oxide synthase on cardiovascular functions in physiological and pathophysiological states," *Nitric Oxide*, vol. 102, pp. 52–73, 2020.

[170] K. Kauser and G. M. Rubanyi, "Gender difference in bioassayable endothelium-derived nitric oxide from isolated rat aortae," *The American Journal of Physiology*, vol. 267, 6, Part 2, pp. H2311–H2317, 1994.

[171] C. Stirone, Y. Chu, L. Sunday, S. P. Duckles, and D. N. Krause, "17β-Estradiol increases endothelial nitric oxide synthase mRNA copy number in cerebral blood vessels: quantification by real-time polymerase chain reaction," *European Journal of Pharmacology*, vol. 478, no. 1, pp. 35–38, 2003.

[172] S. Wassmann, U. Laufs, D. Stamenkovic et al., "Raloxifene improves endothelial dysfunction in hypertension by reduced oxidative stress and enhanced nitric oxide production," *Circulation*, vol. 105, no. 17, pp. 2083–2091, 2002.

[173] B. Yazğan, Y. Yazğan, İ. S. Övey, and M. Nazıroğlu, "Raloxifene and tamoxifen reduce PARP activity, cytokine and oxidative stress levels in the brain and blood of ovariectomized rats," *Journal of Molecular Neuroscience*, vol. 60, no. 2, pp. 214–222, 2016.

[174] M. Barbacanne, J. Rami, J. B. Michel et al., "Estradiol increases rat aorta endothelium-derived relaxing factor (EDRF) activity without changes in endothelial NO synthase gene expression: possible role of decreased endothelium-derived superoxide anion production," *Cardiovascular Research*, vol. 41, no. 3, pp. 672–681, 1999.

[175] L. Li, K. Hisamoto, K. H. Kim et al., "Variant Estrogen receptor-c-Src molecular interdependence and c-Src structural requirements for endothelial NO synthase activation," *Proceedings of the National Academy of Sciences*, vol. 104, no. 42, pp. 16468–16473, 2007.

[176] C. Wong, L. M. Yung, F. P. Leung et al., "Raloxifene protects endothelial cell function against oxidative stress," *British Journal of Pharmacology*, vol. 155, no. 3, pp. 326–334, 2008.

[177] K. Lam, Y. M. Lee, G. Hsiao, S. Y. Chen, and M. H. Yen, "Estrogen therapy replenishes vascular tetrahydrobiopterin and reduces oxidative stress in ovariectomized rats," *Menopause*, vol. 13, no. 2, pp. 294–302, 2006.

[178] Y. Shah, L. Bass, G. W. Davison et al., "BH4 improves postprandial endothelial function after a high-fat meal in men and postmenopausal women," *Menopause*, vol. 24, no. 5, pp. 555–562, 2017.

[179] G. Douglas, A. B. Hale, J. Patel et al., "Roles for endothelial cell and macrophage Gch1 and tetrahydrobiopterin in atherosclerosis progression," *Cardiovascular Research*, vol. 114, no. 10, pp. 1385–1399, 2018.

[180] J. Kim, A. Pedram, M. Razandi, and E. R. Levin, "Estrogen prevents cardiomyocyte apoptosis through inhibition of reactive oxygen species and differential regulation of p38 kinase isoforms," *Journal of Biological Chemistry*, vol. 281, no. 10, pp. 6760–6767, 2006.

[181] J. R. Muñoz-Castañeda, I. Túnez, M. C. Muñoz, I. Bujalance, J. Muntané, and P. Montilla, "Effect of catecholestrogen administration during adriamycin-induced cardiomyopathy in ovariectomized rat," *Free Radical Research*, vol. 39, no. 9, pp. 943–948, 2005.

[182] Q. Yang, C. Wang, Y. Jin et al., "Disocin prevents postmenopausal atherosclerosis in ovariectomized LDLR-/- mice through a PGC-1α/ERα pathway leading to promotion of autophagy and inhibition of oxidative stress, inflammation and apoptosis," *Pharmacological Research*, vol. 148, article 104414, 2019.

[183] A. Debortoli, W. D. N. Rouver, N. T. B. Delgado et al., "GPER modulates tone and coronary vascular reactivity in male and female rats," *Journal of Molecular Endocrinology*, vol. 59, no. 2, pp. 171–180, 2017.

[184] S. Laouafa, A. Ribon-Demars, F. Marcouiller et al., "Estradiol protects against cardiorespiratory dysfunctions and oxidative stress in intermittent hypoxia," *Sleep*, vol. 40, no. 8, 2017.

[185] S. A. de Almeida, E. R. G. Claudio, V. Mengal et al., "Estrogen therapy worsens cardiac function and remodeling and reverses the effects of exercise training after myocardial infarction in ovariectomized female rats.," *Frontiers in Physiology*, vol. 9, article 1242, 2018.

[186] R. J. Steagall, F. Yao, S. R. Shaikh, and A. A. Abdel-Rahman, "Estrogen receptor α activation enhances its cell surface localization and improves myocardial redox status in ovariectomized rats," *Life Sciences*, vol. 182, pp. 41–49, 2017.

[187] E. Nozik-Grayck, C. Woods, J. M. Taylor et al., "Selective depletion of vascular EC-SOD augments chronic hypoxic pulmonary hypertension," *American Journal of Physiology Lung Cellular and Molecular Physiology*, vol. 307, no. 11, pp. L868–L876, 2014.

[188] J. Yu, Y. Zhao, B. Li, L. Sun, and H. Huo, "17β-Estradiol regulates the expression of antioxidant enzymes in myocardial cells by increasing Nrf2 translocation," *Journal of Biochemical and Molecular Toxicology*, vol. 26, no. 7, pp. 264–269, 2012.

[189] H. Priyanka, H. C. Krishnan, R. V. Singh, L. Hima, and S. ThyagaRajan, "Estrogen modulates *in vitro* T cell responses in a concentration- and receptor-dependent manner: effects on intracellular molecular targets and antioxidant enzymes," *Molecular Immunology*, vol. 56, no. 4, pp. 328–339, 2013.

[190] C. Campos, K. R. Casali, D. Baraldi et al., "Efficacy of a low dose of estrogen on antioxidant defenses and heart rate variability," *Oxidative Medicine and Cellular Longevity*, vol. 2014, Article ID 218749, 7 pages, 2014.

[191] X. Zhu, Z. Tang, B. Cong et al., "Estrogens increase cystathionine-γ-lyase expression and decrease inflammation and oxidative stress in the myocardium of ovariectomized rats," *Menopause*, vol. 20, no. 10, pp. 1084–1091, 2013.

[192] A. Ribon-Demars, V. Pialoux, A. Boreau et al., "Protective roles of estradiol against vascular oxidative stress in ovariectomized female rats exposed to normoxia or intermittent hypoxia," *Acta Physiologica*, vol. 225, no. 2, article e13159, 2019.

[193] M. R. Meyer and M. Barton, "GPER blockers as Nox downregulators: a new drug class to target chronic non- communicable diseases," *The Journal of Steroid Biochemistry and Molecular Biology*, vol. 176, pp. 82–87, 2018.

[194] O. Lekontseva, Y. Jiang, C. Schleppe, and S. T. Davidge, "Altered neuronal nitric oxide synthase in the aging vascular system: implications for estrogens therapy," *Endocrinology*, vol. 153, no. 8, pp. 3940–3948, 2012.

[195] Pooja, M. Sharma, K. Singh et al., "Estrogen receptor (*ESR1* and *ESR2*)-mediated activation of eNOS-NO-cGMP pathway facilitates high altitude acclimatization," *Nitric Oxide*, vol. 102, pp. 12–20, 2020.

Hindawi
Oxidative Medicine and Cellular Longevity
Volume 2021, Article ID 9980444, 17 pages
https://doi.org/10.1155/2021/9980444

Research Article

PIN1 Protects Hair Cells and Auditory HEI-OC1 Cells against Senescence by Inhibiting the PI3K/Akt/mTOR Pathway

Yanzhuo Zhang,[1] **Zhe Lv**,[1] **Yudong Liu**,[1,2] **Huan Cao**,[1] **Jianwang Yang**,[1] **and Baoshan Wang**[1]

[1]*Department of Otorhinolaryngology, The Second Hospital of Hebei Medical University, No. 215 West Heping Road, Shijiazhuang 050000, China*
[2]*Department of Otorhinolaryngology, Hebei General Hospital, Shijiazhuang 050051, China*

Correspondence should be addressed to Baoshan Wang; hebwangbs@163.com

Received 28 March 2021; Accepted 14 May 2021; Published 2 June 2021

Academic Editor: Cristina Cosentino

A growing amount of evidence has confirmed the crucial role of the prolyl isomerase PIN1 in aging and age-related diseases. However, the mechanism of PIN1 in age-related hearing loss (ARHL) remains unclear. Pathologically, ARHL is primarily due to the loss and dysfunction of hair cells (HCs) and spiral ganglion cells (SGCs) in the cochlea. Therefore, in this study, we aimed to investigate the role of PIN1 in protecting hair cells and auditory HEI-OC1 cells from senescence. Enzyme-linked immunosorbent assays, immunohistochemistry, and immunofluorescence were used to detect the PIN1 protein level in the serum of ARHL patients and C57BL/6 mice in different groups, and in the SGCs and HCs of young and aged C57BL/6 mice. In addition, a model of HEI-OC1 cell senescence induced by H_2O_2 was used. Adult C57BL/6 mice were treated with juglone, or juglone and NAC, for 4 weeks. Interestingly, we found that the PIN1 protein expression decreased in the serum of patients with ARHL, in senescent HEI-OC1 cells, and in the cochlea of aged mice. Moreover, under H_2O_2 and juglone treatment, a large amount of ROS was produced, and phosphorylation of p53 was induced. Importantly, PIN1 expression was significantly increased by treatment with the p53 inhibitor pifithrin-α. Overexpression of PIN1 reversed the increased level of p-p53 and rescued HEI-OC1 cells from senescence. Furthermore, PIN1 mediated cellular senescence by the PI3K/Akt/mTOR signaling pathway. In vivo data from C57BL/6 mice showed that treatment with juglone led to hearing loss. Taken together, these findings demonstrated that PIN1 may act as a vital modulator in hair cell and HEI-OC1 cell senescence.

1. Introduction

Age-related hearing loss (ARHL) or presbycusis is a prevalent disease in aging people [1, 2]. Hearing loss occurs in most people as they age. Approximately one-third of people over 65 years old are affected by hearing loss according to the World Health Organization. With the aging of the population worldwide, more than 500 million people suffer ARHL [3]. This condition significantly affects the daily communication of older people, and has been shown to be associated with predisposing cognitive impairment and dementia. ARHL is characterized by an age-dependent decline in auditory function. Pathologically, this condition is primarily due to the loss of hair cells and spiral ganglion cells (SGCs) in the cochlea [4]. However, the exact mechanisms of ARHL remain largely unknown.

Peptidyl-prolyl *cis*/*trans* isomerase (PIN1) is a novel post-phosphorylation signaling regulator. PIN1 regulates proteins by controlling the structure of phosphoproteins by mediating the isomerization of specific phosphorylated Ser/Thr-Pro motifs. As a molecular timer, PIN1 not only controls cell cycle progression and cell division but also regulates cellular senescence [5–8]. Loss of PIN1 in cultured cells induced senescence [8]. PIN1 knock-out mice showed a senescent phenotype [9]. PIN1 expression declined in the myocardium with aging [10]. All these results indicate that PIN1 is an important anti-aging molecule. However, the role of this critical regulatory molecule in hair cells has not been previously examined.

Many previous studies have shown that the PI3K/Akt/mTOR pathway is an important pathway in regulating autophagy and apoptosis in the inner ear cochlea [11–14]. Liu et al. [11] demonstrated that the antioxidant enzyme PRDX1 triggers autophagy in spiral ganglion neurons through activation of the PTEN-Akt signaling pathway. Rapamycin alleviated cisplatin-induced ototoxicity by promoting autophagy [11, 15]. In Fus1 KO mice, researchers found dysregulation of Akt and activation of mTOR in cochleae [16]. Although the PI3K/Akt/mTOR pathways are associated with sensory hair cell survival, the mechanisms through which PI3K/Akt/mTOR regulate hair cell senescence are not fully defined.

HEI-OC1 cells are a hair-cell-like cell line that maintain hair cell characteristics and have been extensively used in many previous studies to investigate the protective mechanism of hair cells [17–21]. Therefore, in this study, we used aging C57BL/6 mice and H_2O_2-treated HEI-OC1 cells to determine the role and mechanism of PIN1 in the senescence of hair cells and HEI-OC1 cells.

2. Materials and Methods

2.1. Participants. The participants were selected from the Second Hospital of Hebei Medical University. Participants aged 30 to 80 years old without hearing loss were included in the control group (27 people aged 30-60 years old; 25 people aged 65-80 years old). In the study, 20 patients who were clinically determined to have age-related SNHL were included as the study group. The exclusion criteria were severe diseases, such as cancer, dementia, and psychiatric disorders.

2.2. Pure Tone Audiometry. Procedures were conducted in a soundproof booth. Sounds were delivered via earphone (TDH-50P). Six frequencies (250 Hz to 8000 Hz) were tested in routine pure tone audiometric examination (OB922 Audiometer, Madsen, Ltd., Denmark). The mean threshold of each frequency was calculated in both ears for each subject individually. The mean individual subject thresholds of 250, 500, and 1000 Hz were averaged to obtain the average pure tone hearing level of low frequencies (PTA) and that of 2000, 4000, and 8000 Hz as the average pure tone hearing level of high frequencies (PTA). HL was defined as PTA > 30 dB.

2.3. Animals. C57BL/6 mice were purchased from the Laboratory Animal Center, Charles River (Beijing China). Mice were divided into two groups: the young group (2 months old) and the old group (12 months old). Two-month-old mice were randomly divided into the control group, the juglone group, the juglone + NAC group, and the DMSO group. There were 6 mice per group. All experiments were performed according to protocols approved by the Animal Research Center, Hebei Medical University.

2.4. Enzyme-Linked Immunosorbent Assay (ELISA). After centrifugation, serum samples were immediately frozen at -80°C for further analysis. Human PIN1 ELISA kits (Cat# ZC-32747), human ROS ELISA kits (Cat# ZC-33336), mouse PIN1 ELISA kits (Cat# ZC-54798), and mouse ROS ELISA kits (Cat# ZC-38260) were from Shanghai ZCIBIO. Then, the concentrations were measured according to the manufacturer's instructions. The absorbance at 450 nm was measured using a Synergy2 Automated Enzyme-Linked Immunosorbent Assay (Thermo Fisher Scientific, Inc., USA).

2.5. Cell Culture and Cell Transfection. HEI-OC1 cells (the House Ear Institute-Organ of Corti 1 cell line) were grown under permissive conditions (33°C, 10% CO_2) in high-glucose Dulbecco's modified Eagle's medium (DMEM; Gibco USA) containing 10% fetal bovine serum (FBS; Gibco BRL) without antibiotics.

HEI-OC1 cells were cultured in 6-well plates and transfected when the cell fusion degree was 70-90%. The Lipofectamine 3000 Reagent was diluted with serum-free DMEM. A master mix of DNA was prepared by diluting DNA with serum-free DMEM medium, then adding the P3000 Reagent, and mixing. The diluted DNA and Lipofectamine 3000 Reagent were mixed (1 : 1) and incubated for 15 minutes at room temperature. DNA-lipid complexes were added to the cell supernatant and incubated for 2 days at 33°C.

2.6. Auditory Brainstem Response. All mice were anesthetized with an intraperitoneal injection (a mixture of ketamine-xylazine: 100 mg/kg ketamine and 10 mg/kg xylazine). Then, platinum needle electrodes were inserted at the vertex (reference electrode), behind the right ear (active electrode), and at the back (ground electrode) of the mice. Auditory brainstem responses (ABR) were measured in response to tone pips of 8, 12, 16, 20, 24, 28, and 32 kHz. ABR recordings were performed with a Tucker Davis Technologies (TDT) System III workstation running in a BioSigRP Soundbooth (IAC Acoustics). The hearing threshold was defined as the lowest intensity to generate a reproducible ABR waveform.

2.7. Immunohistochemistry. C57BL/6 mice were decapitated after the ABR tests. The temporal bones were dissected, and the cochleae were obtained and fixed with 4% paraformaldehyde at 4°C overnight and decalcified in 4% sodium ethylenediaminetetraacetic acid for 3 days at 4°C.

The cochleae were then dehydrated, processed, and embedded in paraffin. Paraffin-embedded specimens were cut to a thickness of 4 μm. We selected morphologically intact slices to conduct immunohistochemistry staining. The selected 4 μm sections were deparaffinized and rehydrated. Antigen recovery was performed by a microwave. Next, the sections were incubated with a primary antibody against PIN1 (10495-1-AP, Proteintech, USA) overnight at 4°C. The following day, after sequential incubation with a biotinylated secondary antibody and horseradish peroxidase conjugated streptavidin for 30 min at 37°C, the sections were stained with 3,3-diaminobenzidine (DAB). The slides were finally dehydrated, cleared, and mounted with coverslips. The negative controls were prepared by replacing the primary antibody with phosphate-buffered saline.

2.8. Immunofluorescence. After decalcification with 4% sodium EDTA solution for 3 days at 4°C, the cochleae were microdissected into three turns (apex, middle, and base). HEI-OC1 cells were fixed with 4% paraformaldehyde. The

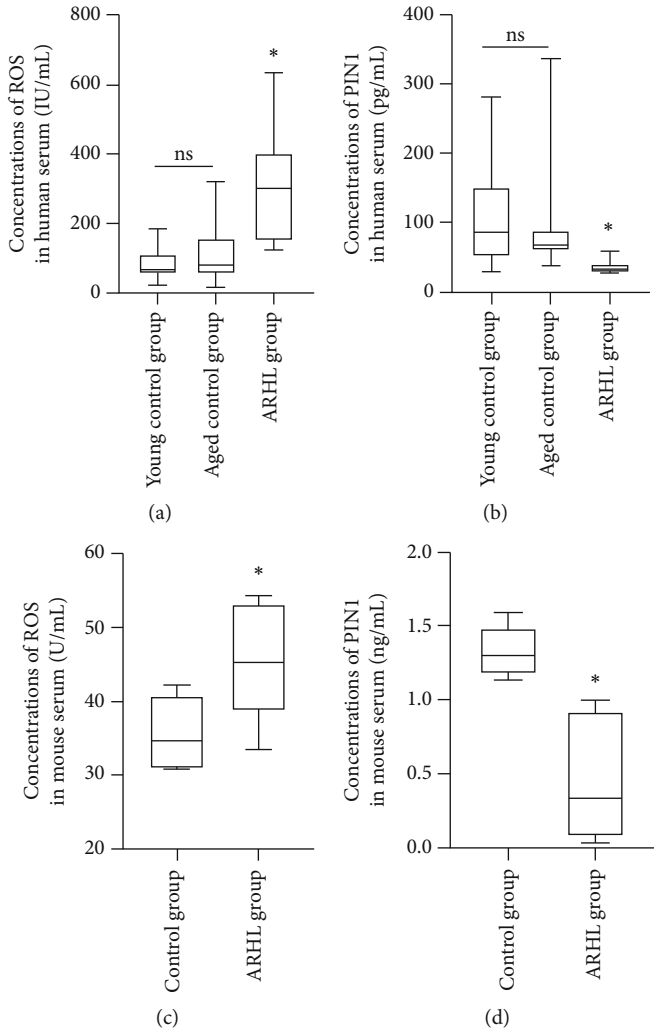

Figure 1: PIN1 and ROS concentrations in human and mouse sera. (a, c) ROS expression levels were increased in the patients of the ARHL group and old C57BL/6 mice ($^*P < 0.05$). (b, d) PIN1 expression levels were decreased in the patients and old C57BL/6 mice with ARHL ($^*P < 0.05$).

tissue and cell specimens were first permeabilized in Triton X-100 solution and then blocked with 10% normal goat serum for 30 min at room temperature. After incubation with primary anti-PIN1 (10495-1-AP, Proteintech, USA) antibody overnight at 4°C, the samples were then washed three times with PBS and incubated with secondary fluorescent antibody for 1 h at 37°C in the dark to detect the primary antibody, followed by incubation with Alexa Fluor 488-phalloidin for 1 h at room temperature in the dark.

2.9. Reagent Treatment. HEI-OC1 cells were seeded in six-well plates for each experiment for 24 h. Before H_2O_2 stimulation, the cells were pretreated with the PI3K inhibitor LY294002 (25 μM, HY-10108/CS-0150, MCE, USA), the Akt activator SC79 (4 μg/mL, B5663, APExBIO, USA) and the ROS scavenger NAC (2 mM, G1902071, Aladdin, China) for 1 h; the p53 inhibitor pifithrin-α (10 μM, A4206, APExBIO, USA) was used for 24 h. The PIN1 inhibitor juglone (1, 5, and 10 μM, STBH9858, Sigma-Aldrich, USA) was used for 45 min.

2.10. Senescence-Associated β-Galactosidase Stain. Cellular senescence-associated β-galactosidase (SA-β-Gal) staining was conducted using a senescence β-galactosidase staining kit (Beyotime Institute of Biotechnology, Shanghai, China) following the manufacturer's instructions. Before staining, cells were gently washed with PBS and fixed with fixing solution. After washing three times with PBS, 1 mL of staining solution was added to each well, sealed with parafilm, and incubated at 37°C without CO_2 overnight.

2.11. Protein Extraction and Western Blotting. The cells were collected and lysed on ice with RIPA buffer and PMSF for 30 min. Detection of phosphorylated proteins requires the addition of phosphorylase inhibitors (04906845001, Roche Switzerland). The supernatant was centrifuged at 12,000 rpm for 20 min at 4°C. The BCA Protein Assay (PC0020, Solarbio, China) was used to determine the protein concentration. The protein extracts from the cells were separated by sodium dodecyl sulfate polyacrylamide gel electrophoresis and then transferred to polyvinylidene fluoride

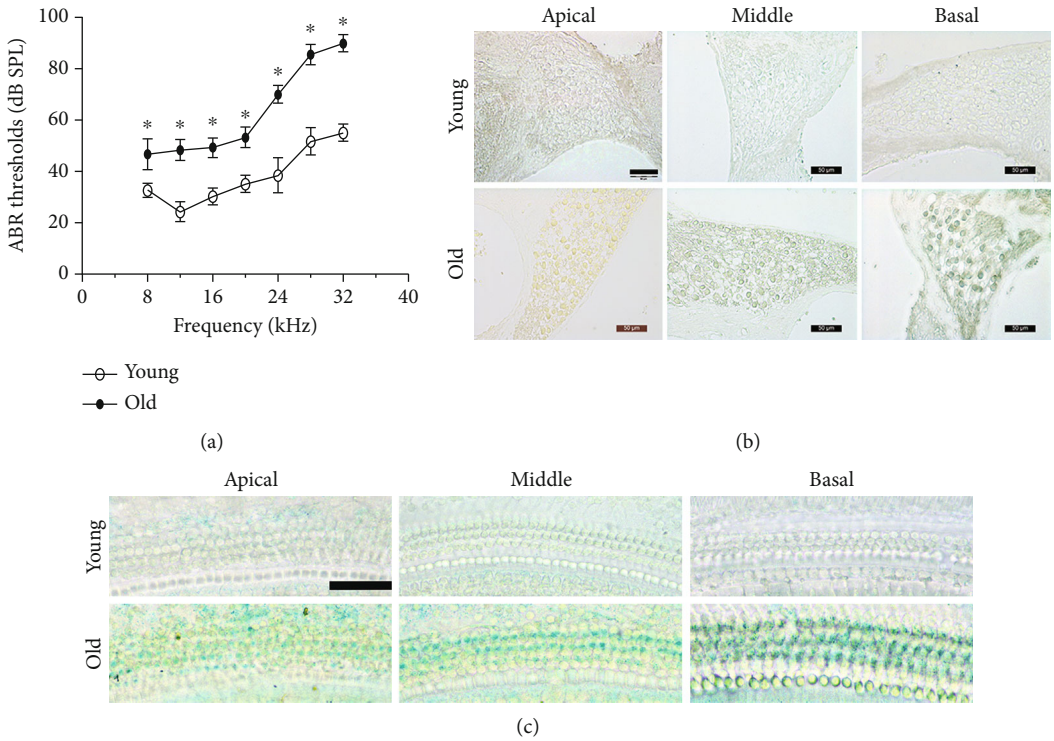

Figure 2: Hearing impairment in old mice at all frequencies and β-gal staining of the cochleae. (a) Compared with young mice, old mice showed significantly increased ABR thresholds at all frequencies ($^{*}P < 0.05$). (b) Representative senescence-associated β-galactosidase (SA-β-gal) staining of SGCs. (c) Representative senescence-associated β-galactosidase (SA-β-gal) staining of HCs. Scale bar = 50 μm.

membranes. The membranes were blocked with 5% nonfat milk for 2 h at 37°C and then incubated overnight at 4°C with anti-PIN1 (dilution, 1 : 1000; 10495-1-AP, Proteintech, USA), p53 (dilution, 1 : 1000; 21891-1-AP, Proteintech, USA), p-p53 (dilution, 1 : 1000; 9284, Cell Signaling Technology, USA), p21 (1 : 1000, dilution, 1 : 1000; 27296-1-AP, Proteintech, USA), p-16 (1 : 1000, 10883-1-AP, Proteintech, USA), Akt (1 : 1000, ab8805, Abcam, USA), p-Akt (1 : 1000, ab81283, Abcam, USA), mTOR (1 : 1000, 2983, Cell Signaling Technology, USA), p-mTOR (1 : 1000, 5536, Cell Signaling Technology, USA), and GAPDH (1 : 2000 Proteintech, USA) antibodies. ImageJ software was used to quantify the band intensity. The intensity value of each target band was normalized to that of GAPDH.

2.12. Statistical Analysis. All experiments were independently repeated at least three times. Data are presented as the mean ± SD and were analyzed with SPSS. Student's t-test and one-way ANOVA were used for statistical analysis. Values with $P < 0.05$ were considered significant.

3. Results

3.1. PIN1 and ROS Concentrations in Human and C57BL/6 Mouse Serum. The serum concentrations of PIN1 and ROS were measured in all participants and C57BL/6 mice. ELISAs revealed that ROS expression levels were increased in the patients in the ARHL group and the old C57BL/6 mice (Figures 1(a) and 1(c)). PIN1 expression levels were decreased in the patients and in the old C57BL/6 mice with ARHL (Figures 1(b) and 1(d)).

3.2. Elevated Auditory Brainstem Response Threshold and Cell Senescence in the Cochleae of the Aged C57BL/6 Mice. We examined the auditory function in young and old mice by measuring ABR. As shown in Figure 2(a), not only was the ABR threshold at a high frequency of the old mice significantly higher than that of the young mice but also that at middle and low frequencies was significantly higher in the old mice than the young mice, which indicated a decline in auditory function in the old mice. In addition, the results showed that senescence-associated β-galactosidase- (SA-β-gal-) positive cells in the aged mice were more abundant than those in the young mice in spiral ganglion cells (SGCs) (Figure 2(b)) and hair cells (HCs) (Figure 2(c)).

3.3. The Expression of PIN1 Is Downregulated in the Cochleae of the Aged C57BL/6 Mice. We examined PIN1 expression in the cochlea of the young and old mice. IF and IHC analysis showed that the PIN1 protein was expressed in the cytoplasm and nucleus of HCs (Figures 3(a) and 3(b)) and SGCs (Figure 3(c)). PIN1 expression was markedly decreased in the old mice compared to the young mice (Figures 3(a)–3(e)). Linear analysis showed that the expression of PIN1 in the cochlea was negatively correlated with hearing threshold (Figures 3(f)–3(h)). Taken together, the results showed that PIN1 might be involved in ARHL.

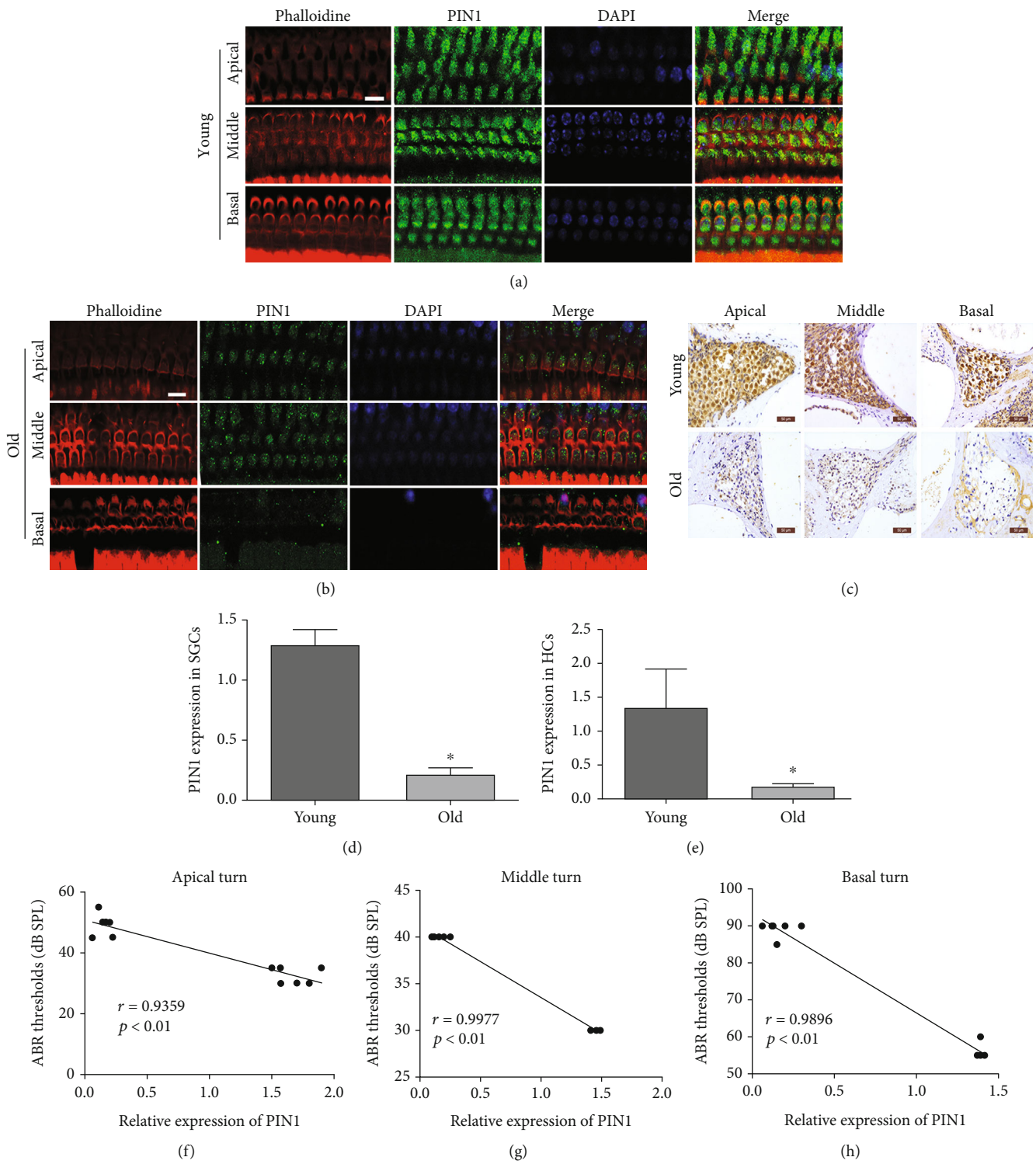

Figure 3: The expression of PIN1 is downregulated in the cochleae of aged C57BL/6 mice. (a, b, and e) Representative images of immunofluorescence staining of PIN1 in HCs from young and old animals (scale bar = 10 μm). (c and d) Immunohistochemistry staining for PIN1 in the SGCs of young and old mice (scale bar = 50 μm). (f–h) Linear analysis showed that the expression of PIN1 in the cochlea was negatively correlated with hearing threshold ($^*P < 0.05$).

3.4. Downregulation of PIN1 Expression in HEI-OC1 Cells Induced by H_2O_2. The different concentrations of H_2O_2 on cell viability were detected by the MTS method. After 2 h of stimulation by H_2O_2, the relative cell survival rate was observed and IC50 = 1.17 mM was calculated (Supplementary Figure 1). Therefore, HEI-OC1 cells were exposed to H_2O_2 (1 mM for 2 h) to induce cellular senescence. Thereafter, senescence-associated SA-β-Gal staining was

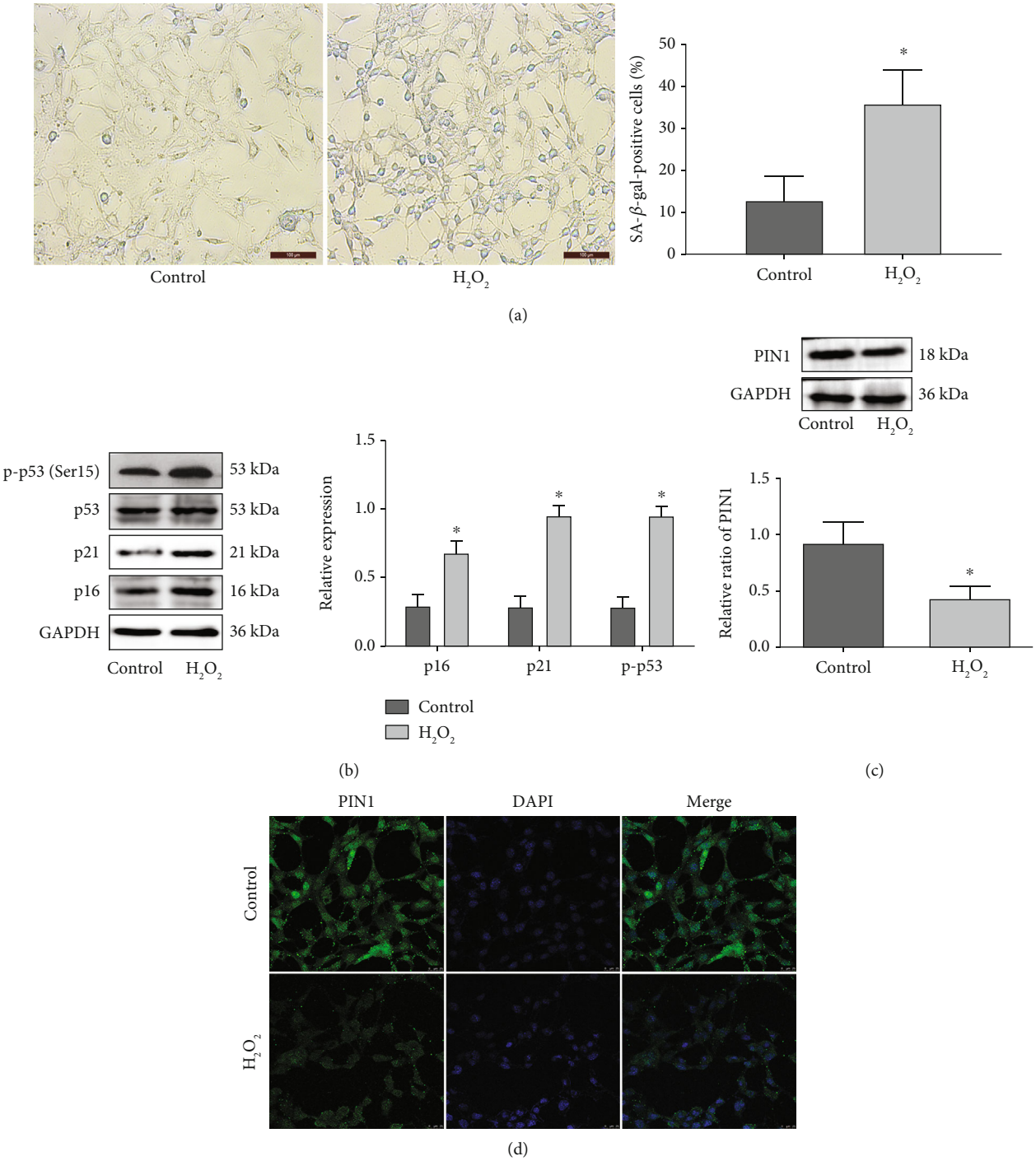

Figure 4: H_2O_2 induces premature senescence and decreases PIN1 expression in HEI-OC1 cells in vitro. (a) Representative senescence-associated β-galactosidase (SA-β-gal) staining of HEI-OC1 cells (scale bar = 100 μm). (b) Western blots for the expression of p53, p-p53, p21, and p16. (c) Western blot for the expression of PIN1 in HEI-OC1 cells. (d) Immunofluorescence staining for PIN1 in HEI-OC1 cells (scale bar = 25 μm) ($^*P < 0.05$).

applied to detect senescent HEI-OC1 cells. As shown in Figure 4(a), the percentage of cells positive for SA-β-Gal was increased in the HEI-OC1 cells treated with H_2O_2. Additionally, H_2O_2 significantly elevated the expression of p-p53, p21, and p16 compared with that in the control group (Figure 4(b)). However, PIN1 protein expression, detected by Western blotting (Figure 4(c)) or immunofluorescence (Figure 4(d)), was significantly decreased in the HEI-OC1 cells treated with H_2O_2.

3.5. PIN1 Modulates HEI-OC1 Cell Senescence. To better understand the role of PIN1 in the cellular senescence of HEI-OC1 cells, we transfected the HA-PIN1 overexpression plasmid into HEI-OC1 cells or treated HEI-OC1 cells with

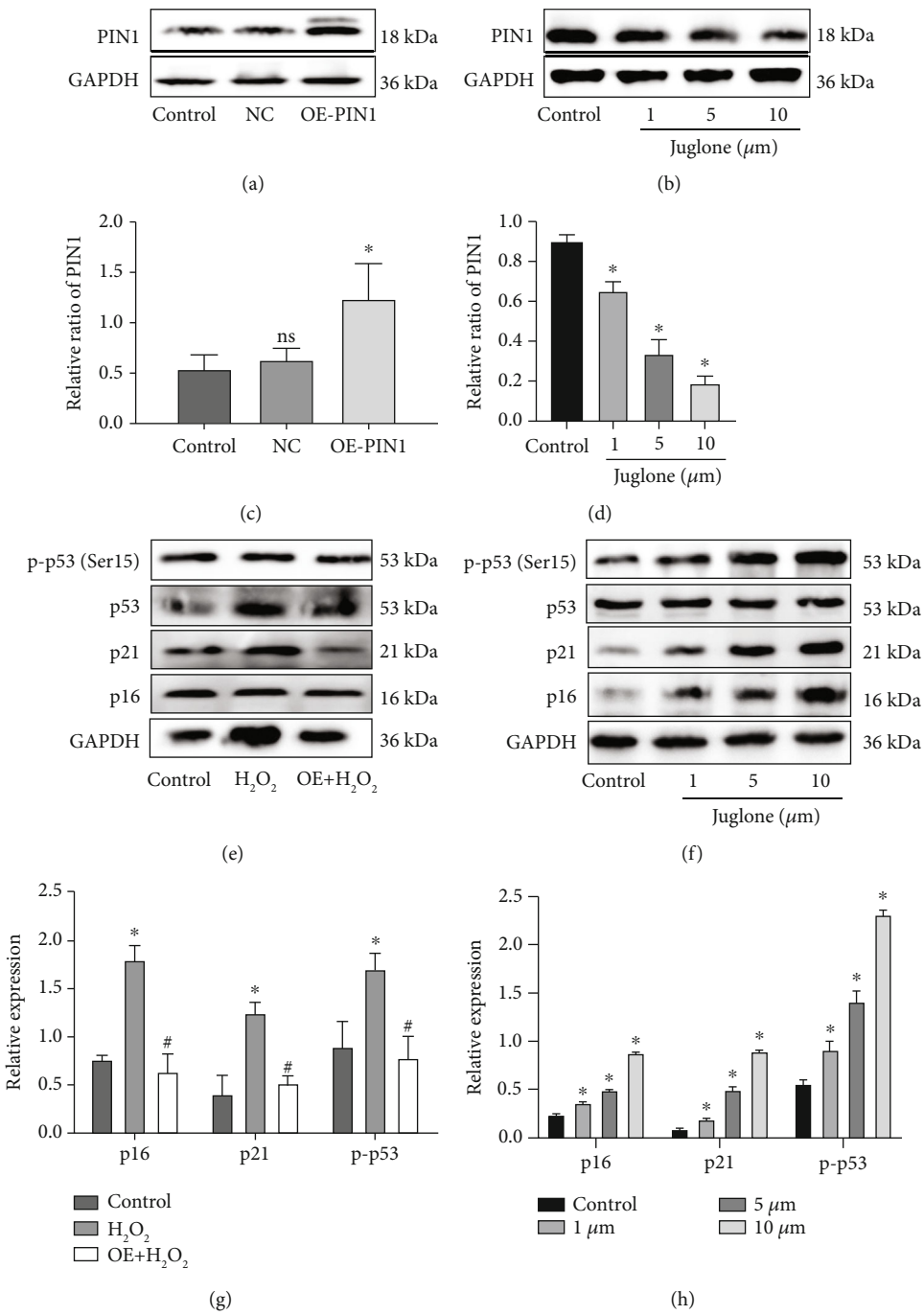

Figure 5: Continued.

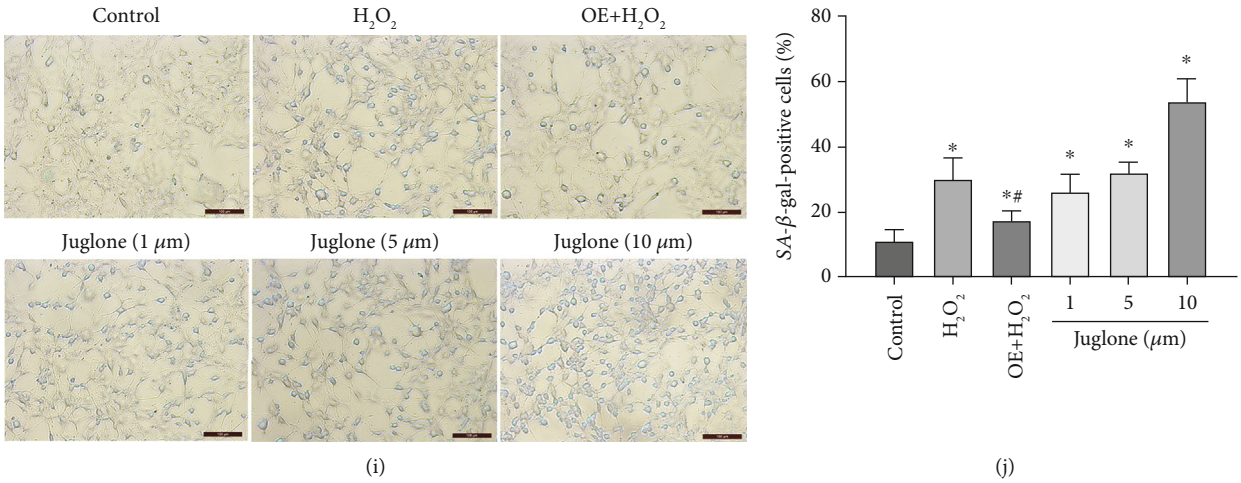

Figure 5: PIN1 modulates HEI-OC1 senescence. (a, c) HEI-OC1 cells were transfected with the HA-PIN1 plasmid. (b, d) HEI-OC1 cells were treated by juglone. (e–h) Western blots for the expression of p53, p-p53, p21, and p16 in HEI-OC1 cells. (i, j) SA-β-gal staining was used to detect the senescent state of HEI-OC1 cells (OE: overexpression-PIN1; $^{*}P < 0.05$ vs. control group, $^{\#}P < 0.05$ vs. H_2O_2 group. Scale bar = 100 μm).

juglone, a PIN1 inhibitor [22]. The transfection effect is shown in Figures 5(a) and 5(c). As illustrated in Figures 5(e) and 5(g), PIN1 overexpression caused a significant reduction in the expression of p-p53, p21, and p16. The percentage of SA-β-gal-positive cells was also reduced in the PIN1 overexpression group (Figures 5(i) and 5(j)). In contrast, juglone inhibited PIN1 in a concentration-dependent manner (Figures 5(b) and 5(g)) and accelerated senescence in HEI-OC1 cells in a concentration-dependent manner (Figures 5(f), 5(h), 5(i), and 5(j)). However, these changes were not found in the different doses of solvent control group (Supplementary Figures 2(A) and 2(B)).

3.6. PIN1 Mediates HEI-OC1 Cell Senescence by Affecting the PI3K/Akt/mTOR Signaling Pathway. Western blotting results showed that PIN1 overexpression rescued the H_2O_2-induced upregulation of p-Akt and p-mTOR expression in HEI-OC1 cells (Figure 6(a)). However, PIN1 inhibition induced upregulation of p-Akt and p-mTOR expression (Figures 7(a) and 7(b)), and the expression of p-Akt and p-mTOR did not change in the different doses of the solvent control group (Supplementary Figures 2(C) and 2(D)). Then, to further study the role of the PI3K/Akt/mTOR signaling pathway in HEI-OC1 cell senescence, we pretreated HEI-OC1 cells with SC79 (Akt activator) or LY294002 (Akt inhibitor) before H_2O_2 stimulation. The results showed that neither SC79 nor LY294002 changed the PIN1 protein levels (Figures 6(b) and 6(d)). SC79 upregulated the expression of p-p53, p16, and p21 (Figure 6(c)) and increased the number of SA-β-gal-positive cells (Figure 6(f)). However, LY294002 had an opposite effect compared with SC79 (Figures 6(e) and 6(f)). These results indicated that the protective role of PIN1 could be mediated by inhibiting the PI3K/Akt/mTOR pathway in senescent HEI-OC1 cells.

3.7. H_2O_2 Affects the Expression of PIN1 through p53, which In Turn Affects Senescence. To further investigate the regulatory mechanism of PIN1 in ARHL, we used the p53 inhibitor pifithrin-α (PFT-α) to evaluate whether H_2O_2 affects the expression of PIN1 through p53. When HEI-OC1 cells were incubated with PFT-α, the p-p53 protein level was decreased, but the PIN1 protein level significantly increased (Figures 7(c) and 7(d)). In addition, we investigated the expression of senescence-associated proteins. The results showed that pretreatment of the cells with PFT-α caused a significant decrease in the expression of p21 and p16 (Figures 7(c) and 7(e)), and the percentage of SA-β-gal-positive cells was also reduced (Figures 7(f) and 7(g)). The results suggested that H_2O_2 inhibited the expression of PIN1 by upregulating p53 expression, which in turn affected senescence.

3.8. H_2O_2 Affects the Expression and Activity of p53 through ROS and Then Affects Senescence. In the model of senescence and in the juglone treatment group, high levels of ROS were produced (Figures 8(a) and 8(b)). To detect whether ROS affect the expression and activity of p53, we used the ROS inhibitor N-acetyl-L-cysteine (NAC). The results showed that the production of ROS almost recovered to the level of the control group after NAC treatment (Figures 8(a) and 8(b)). NAC led to a restoration of p-p53 levels (Figures 8(c)–8(f)). In addition, when cells were pretreated with NAC, the expression level of PIN1 was increased (Figures 8(c) and 8(e)), and the expression levels of p21 and p16 were decreased (Figures 8(c)–8(f)). The percentage of SA-β-gal-positive cells was also reduced by NAC treatment (Figures 8(g) and 8(h)).

3.9. Juglone Treatment Results in C57BL/6 Mouse Hearing Loss. To further study whether the reduction in PIN1 expression could induce hair cell senescence, we treated the mice with juglone, or juglone and NAC at the same time. Intraperitoneal injection of juglone (1 mg/kg, three times a week for 4 weeks) and/or NAC (1.5 g/kg/d, oral, for 4 weeks) was

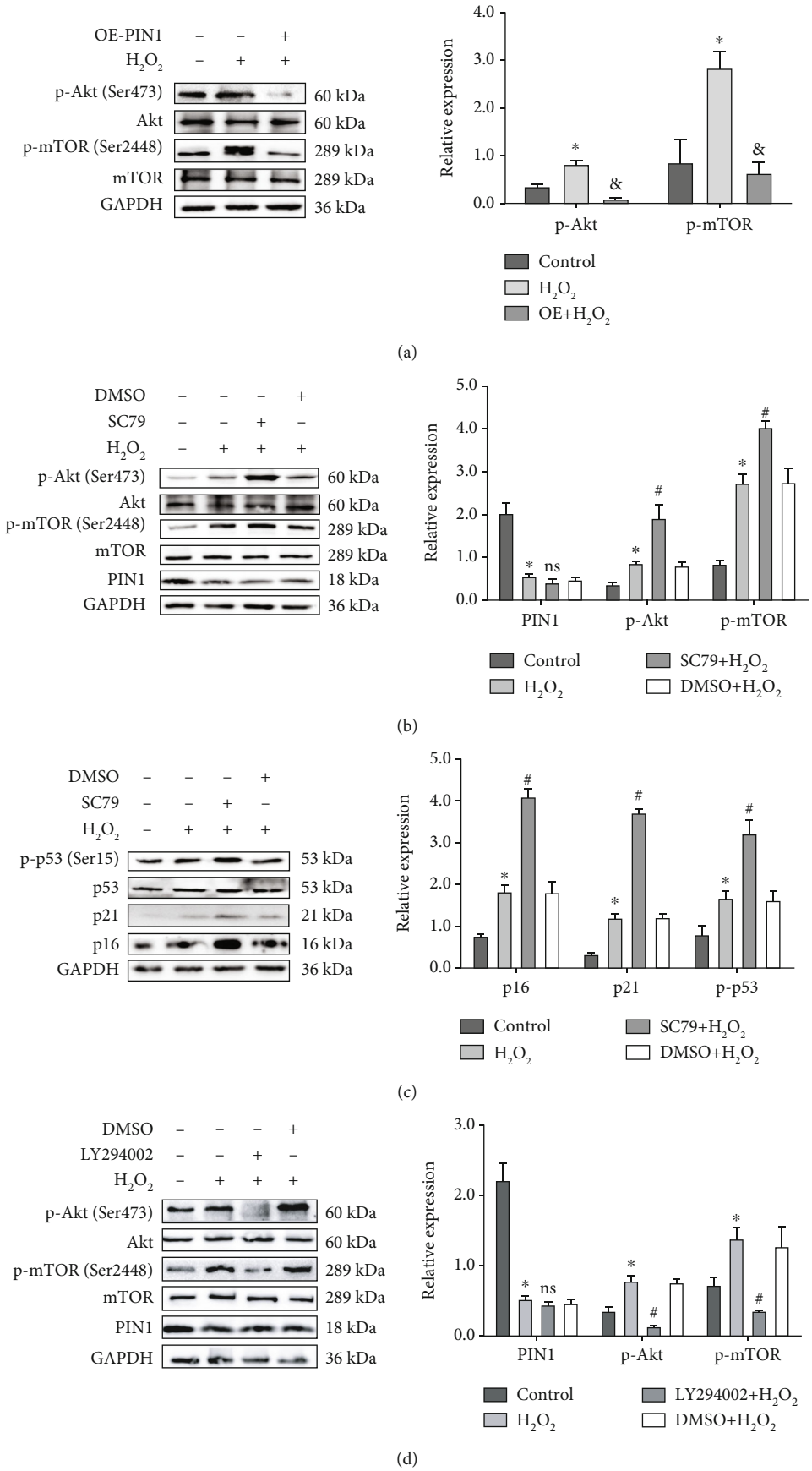

Figure 6: Continued.

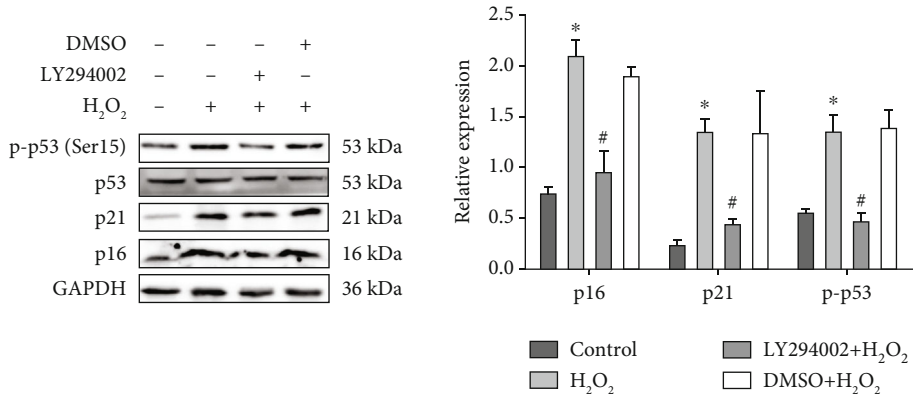

(e)

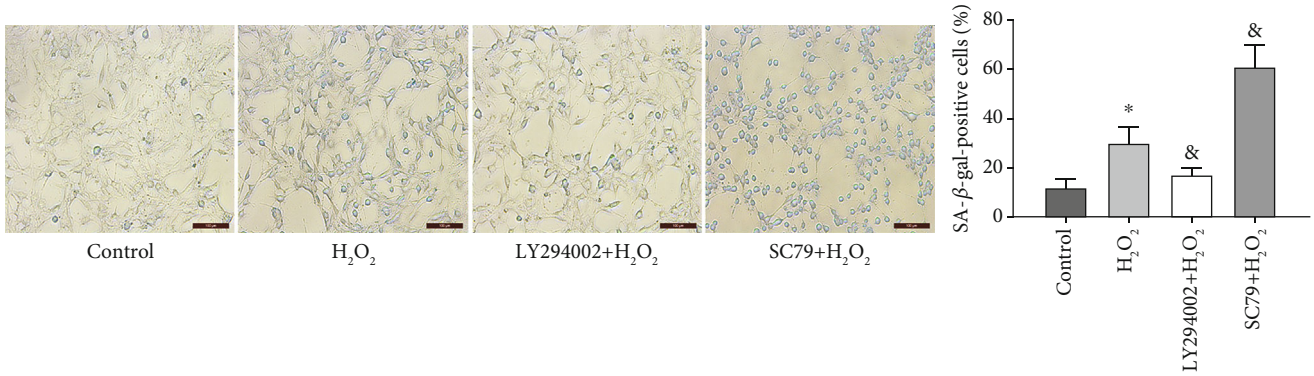

(f)

Figure 6: PIN1 mediates HEI-OC1 cell senescence by affecting the PI3K/Akt/mTOR signaling pathway. (a) Western blots for the expression of p-Akt, Akt, p-mTOR, and mTOR in HEI-OC1 cells after transfection with the HA-PIN1 plasmid. (b) Western blots for the expression of p-Akt, Akt, p-mTOR, mTOR, and PIN1 in HEI-OC1 cells after pretreatment with SC79 (Akt activator). (c) Western blots for the expression of p53, p-p53, p21, and p16 after pretreatment with SC79. (d) Western blots for the expression of p-Akt, Akt, p-mTOR, mTOR, and PIN1 in HEI-OC1 cells after pretreatment with LY294002 (an inhibitor of PI3K/Akt). (e) Western blots for the expression of p53, p-p53, p21, and p16 after pretreatment with LY294002. (f) SA-β-gal staining for HEI-OC1 cells ($^{*}P < 0.05$ vs. control group, $^{\#}P < 0.05$ vs. DMSO+H_2O_2 group, $^{\&}P < 0.05$ vs. H_2O_2 group. Scale bar = 100 μm).

performed. As shown in Figures 9(a) and 9(b), in the juglone-treated group, the ROS level expression increased in the serum compared with the control group and the juglone + NAC group. In the juglone + NAC treatment group, the PIN1 level expression increased in the serum compared with the juglone group. Moreover, in the juglone-treated group, ABR thresholds at all frequencies were increased, especially at high frequency. Compared with the juglone-treated group, the juglone + NAC group had significantly decreased ABR thresholds at high frequencies (Figure 9(c)). In the basal turn hair cells, there were more SA-β-gal-positive cells in the juglone-treated group than in the other groups (Figure 9(d)).

4. Discussion

Sensorineural hearing loss is caused by many factors that impair hair cell and spiral ganglion neuron function [23–28], including ototoxic drugs, genetic factors, aging, noise exposure, and chronic cochlear infections [29–33]. A growing amount of evidence has demonstrated that PIN1 plays critical roles in aging-associated diseases [34–39]. PIN1-deficient mice displayed signs of premature senility, such as rapid telomere shortening and loss of motor coordination and behavioral defects and neuronal loss [7]. It has been reported that overexpression of PIN1 rescues cellular senescence of atherosclerotic VSMCs and downregulates the expression of p53 and p21 [40]. Toko et al. [10] reported that knockdown of PIN1 led to cellular senescence, but overexpression of PIN1 inhibited senescence of cardiac progenitor cells. However, the role of PIN1 in ARHL has not been previously reported. For this research, PIN1 protein expression was markedly reduced in the serum of patients with ARHL, SGCs, and HCs of old mice and senescent HEI-OC1 cells. The expression of PIN1 in the cochlea was negatively correlated with the hearing threshold. In vitro, the overexpression of PIN1 inhibited the senescence of HEI-OC1 cells. Inhibited PIN1 accelerated senescence in HEI-OC1 cells. In vivo, we found that treatment with juglone led to hearing loss in C57BL/6 mice, especially at high frequencies. All of these results support our hypothesis that PIN1 modulates HEI-OC1 and hair cell senescence.

Astle et al. reported that the activation of the PI3K/Akt signaling pathway induces cell senescence, and mTOR is a related mediator [41]. In this signaling pathway, mTOR is a

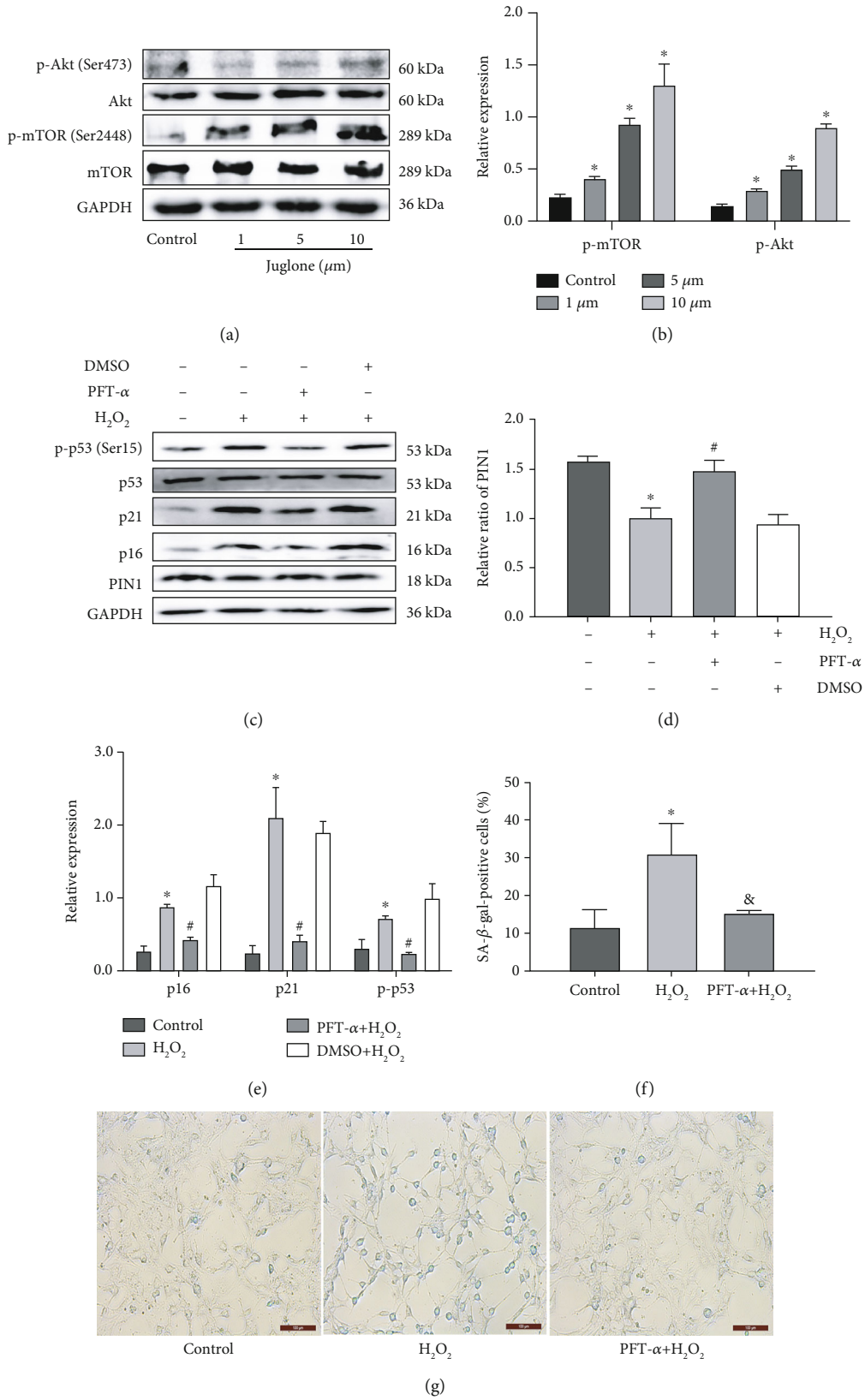

FIGURE 7: H_2O_2 affects the expression of PIN1 through p53, which in turn affects senescence. (a, b) Western blots for the expression of p-Akt, Akt, p-mTOR, and mTOR in HEI-OC1 cells after treatment with juglone. (c–e) Western blots for the expression of p53, p-p53, p21, p16, and PIN1 after pretreatment with the p53 inhibitor pifithrin-α (PFT-α). (f, g) SA-β-gal staining for HEI-OC1 cells ($^{*}P < 0.05$ vs. control group, $^{\#}P < 0.05$ vs. DMSO+H_2O_2 group, $^{\&}P < 0.05$ vs. H_2O_2 group. Scale bar = 100 μm).

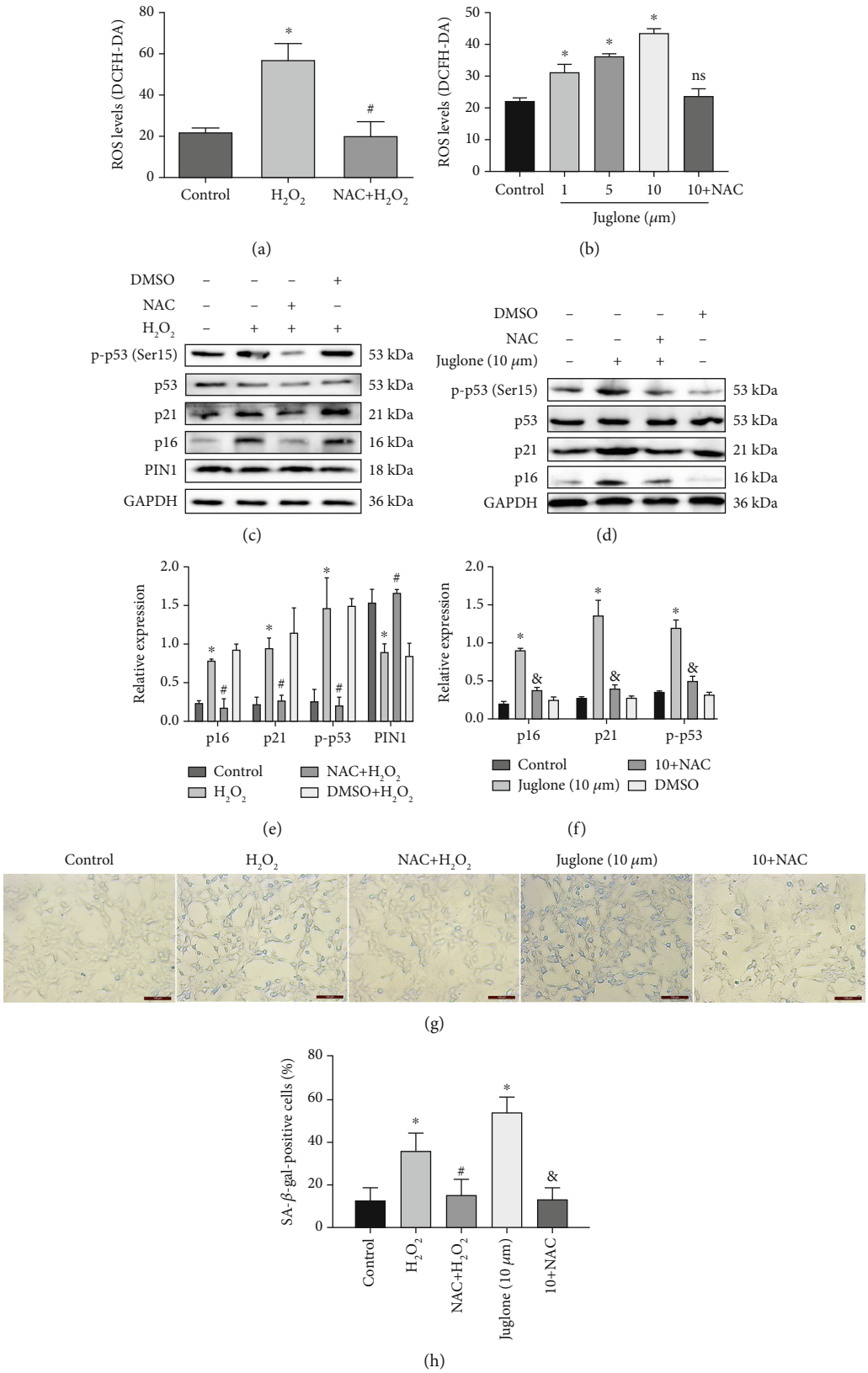

Figure 8: H_2O_2 affects the expression and activity of p53 through ROS and then affects senescence. (a, b) Intracellular ROS levels were measured by DCFH-DA in HEI-OC1 cells (ns: nonsignificant; $^{*}P < 0.05$ vs. control group, $^{\#}P < 0.05$ vs. H_2O_2 group). (c–f) Western blots for the expression of p53, p-p53, p21, p16, and PIN1 after pretreatment with the ROS inhibitor N-acetyl-L-cysteine (NAC) ($^{*}P < 0.05$ vs. the DMSO group, $^{\#}P < 0.05$ vs. H_2O_2 group, $^{\&}P < 0.05$ vs. the juglone group). (g, h) SA-β-gal staining for HEI-OC1 cells ($^{*}P < 0.05$ vs. the control group, $^{\#}P < 0.05$ vs. the H_2O_2 group, $^{\&}P < 0.05$ vs. the juglone group. Scale bars = 100 μm).

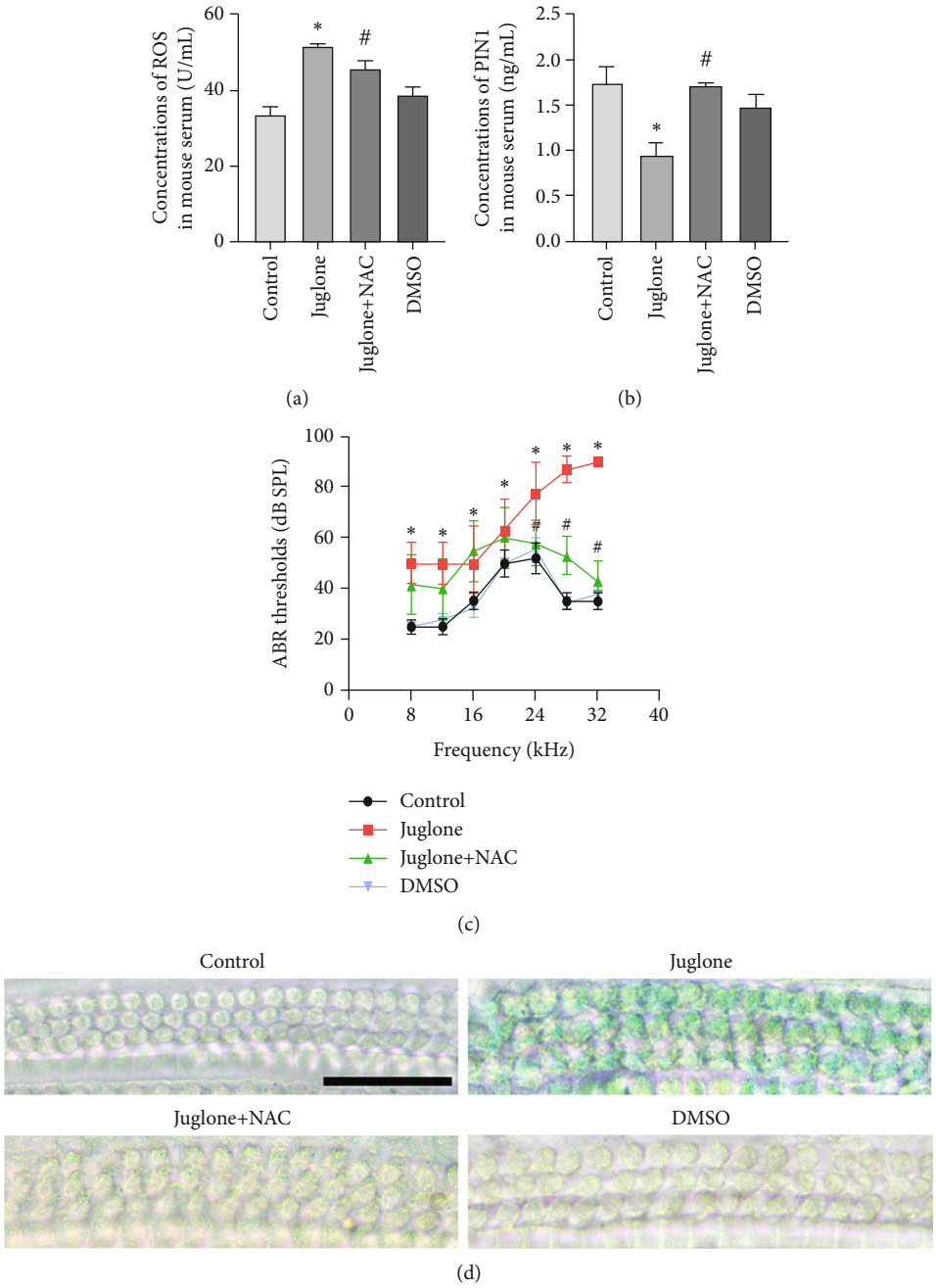

Figure 9: Juglone treatment induces C57BL/6 mouse hearing loss. (a) ROS level in the C57BL/6 mice serum. (b) PIN1 levels in the C57BL/6 mice serum. (c) Compared with the other groups, the juglone-treated group had significantly increased ABR thresholds at all frequencies, especially at high frequencies. Compared with the juglone-treated group, the juglone + NAC group had significantly decreased ABR thresholds at high frequencies. (d) In the basal turn hair cells, SA-β-gal-positive cells in the juglone-treated group were greater than those in the other groups ($^{*}P < 0.05$ vs. the DMSO group; $^{\#}P < 0.05$ vs. the juglone group. Scale bars = 50 μm).

downstream target of the PI3K/Akt signaling pathway, and Akt is a positive regulator of mTOR [42]. Studies have shown that topical application of the mTOR inhibitor rapamycin can reduce p16 protein expression and cell aging in skin tissue [43]. Hu et al. [44] demonstrated that Akt/mTOR activity was increased upon aging in zebrafish retinas, and increased Akt/mTOR activity is a major player in age-related retinal neuropathy in zebrafish. It was also demonstrated that gentamicin resulted in the activation of Akt in the organ of Corti and in spiral ganglion cells [45]. The mTOR inhibitor rapamycin protected sensory hair cells against gentamicin. Furthermore, rapamycin attenuates noise-induced hair cell loss by reducing oxidative stress [46]. Nevertheless, other studies suggest that PI3K/Akt signaling is a protective mechanism of the inner ear. It was reported that PI3K/Akt is an endogenous protective mechanism of the inner ear. The activation of PI3K/Akt protects mice from cochlear injury and hearing damage induced by gentamicin and noise [47, 48]. Inhibition

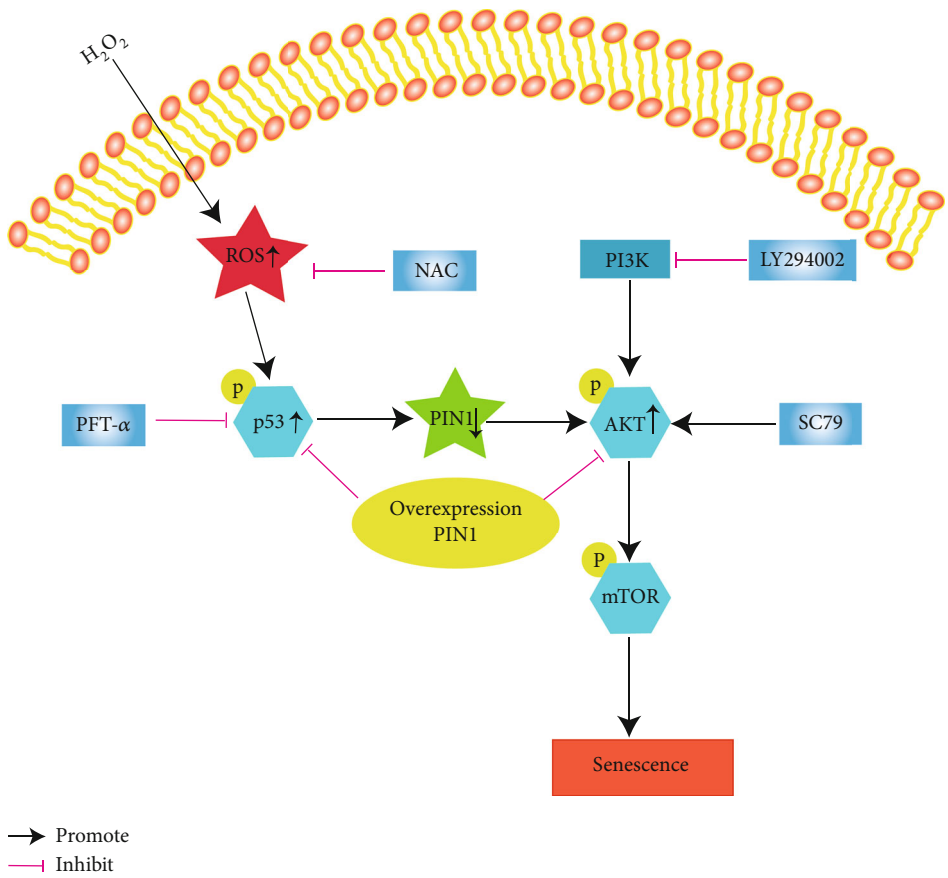

Figure 10: Schematic diagram of the observed effects and the antisenescence mechanism of PIN1 in the present study. H_2O_2 treatment resulted in oxidative damage, upregulated p-p53 expression, and activation of the PI3K/Akt/mTOR pathway. p-p53 negatively regulates PIN1 expression. Overexpression of PIN1 reversed the increase in p-p53 and inhibited the activation of the PI3K/Akt/mTOR pathway.

of mTOR results in auditory hair cell damage and decreased spiral ganglion neuron outgrowth [49]. Inhibition of the PI3K/Akt pathway can induce senescence and directly increase the expression of p21 [50, 51]. In this article, we showed that the expression of p-Akt and p-mTOR in HEI-OC1 cells treated with H_2O_2 and juglone substantially increased. Inhibition of the PI3K/Akt/mTOR pathway significantly alleviated H_2O_2-induced senescence in HEI-OC1 cells. These results suggest that the activation of Akt aggravated senescence in HEI-OC1 cells.

In multiple cancer types, many studies have shown that the expression levels of PIN1 and levels of Akt phosphorylation are strongly correlated. However, experiments have shown that in mouse periodontal tissues, PIN1 siRNA enhanced mTOR and Akt activation, which was attenuated by PIN1 overexpression [52]. In the present study, PIN1 overexpression caused a reduction in the expression of p-Akt. The inhibition of PIN1 caused upregulation of p-Akt and p-mTOR expression. Furthermore, the activation of Akt aggravated H_2O_2-induced senescence in HEI-OC1 cells. All of these results suggested that PIN1 protects HEI-OC1 cells from senescence by inhibiting the PI3K/Akt/mTOR signaling pathway.

p53 plays a crucial role in the process of cellular senescence. p53 initiates various stress responses, including cell cycle arrest and aging [53]. The overexpression of p53 promotes aging. Our data showed that the expression of p-p53 was significantly higher in the H_2O_2-induced HEI-OC1 cells than in the control cells. Jeong et al. [54] reported that endoplasmic reticulum (ER) stress decreased PIN1 expression through p53 activation, and overexpression of p53 observably decreased PIN1 expression in HCT116 cells. However, the regulators of PIN1 expression during aging are still not fully understood, especially in ARHL. In our study, when the cells were treated with the p53 inhibitor pifithrin-α, PIN1 expression was significantly increased, so we hypothesized that H_2O_2 might regulate PIN1 expression through p53. p-p53 expression was significantly decreased by PIN1 overexpression. These findings suggest that PIN1 and p53 regulate each other. However, the exact mechanism remains to be determined.

The gradual accumulation of ROS is a key mediator during the aging process. In the present study, H_2O_2 and juglone treatment resulted in an increase in ROS activity, indicating that H_2O_2 induced senescence via the production of ROS, and inhibition of PIN1 caused increased ROS production also. The ROS scavenger NAC could reduce ROS production, reverse changes in aging-related biomarkers, protect cells from ROS-induced cellular senescence, and indirectly inhibit mTOR [55–57]. In this study, we also found that NAC

reduced the ROS production and reversed changes in aging-related biomarkers. In PDAC cells, silencing PIN1 significantly increased intracellular ROS [58]. In this study, we speculate that significantly decreased PIN1 expression may increase ROS production.

Collectively, under H_2O_2 treatment (or PIN1 inhibition), a large amount of ROS was produced, and the generation of ROS upregulated p-p53 expression. Then, p-p53 negatively regulated PIN1 expression, and overexpression of PIN1 reversed the increase in p-p53. More importantly, PIN1 mediated cellular senescence by affecting the PI3K/Akt/mTOR signaling pathway (Figure 10).

Above all, our findings, for the first time, demonstrated that PIN1 expression is downregulated in the serum of patients with ARHL, in the cochleae of aged C57BL/6 mice, and in senescent HEI-OC1 cells. The in vivo data showed that PIN1 inhibition led to hearing loss. However, only animal and cellular experiments were conducted, and clinical data and conclusions are lacking. These limitations need to be addressed in the future.

Data Availability

Data can be found in the manuscript and supplementary information files.

Conflicts of Interest

All authors declare that they have no conflicts of financial interest.

Supplementary Materials

Supplementary 1. Supplementary Figure 1: the different concentrations of H_2O_2 on cell viability were detected by the MTS method. After stimulation by H_2O_2 for 2 h, we observed the relative cell survival rate and calculated IC50 = 1.17 mM.

Supplementary 2. Supplementary Figure 2: (A, B) Western blot for the expression of p53, p-p53, p21, and p16 in HEI-OC1 cells after treatment with DMSO (0.1, 0.5, and 1 μL); (C, D) Western blot for the expression of p-Akt, Akt, p-mTOR, and mTOR in HEI-OC1 cells after treatment with DMSO (0.1, 0.5, and 1 μL).

References

[1] Z. H. He, S. Y. Zou, M. Li et al., "The nuclear transcription factor FoxG1 affects the sensitivity of mimetic aging hair cells to inflammation by regulating autophagy pathways," *Redox Biology*, vol. 28, article 101364, 2020.

[2] X. Fu, X. Sun, L. Zhang et al., "Tuberous sclerosis complex-mediated mTORC1 overactivation promotes age-related hearing loss," *Journal of Clinical Investigation*, vol. 128, no. 11, pp. 4938–4955, 2018.

[3] WHO, *Addressing the Rising Prevalence of Hearing Loss*, World Health Organization, Geneva, Switzerland, 2018.

[4] S. H. Sha, A. Kanicki, G. Dootz et al., "Age-related auditory pathology in the CBA/J mouse," *Hearing Research*, vol. 243, no. 1–2, pp. 87–94, 2008.

[5] R. La Montagna, I. Caligiuri, A. Giordano, and F. Rizzolio, "Pin1 and nuclear receptors: a new language?," *Journal of Cellular Physiology*, vol. 228, no. 9, pp. 1799–1801, 2013.

[6] H. Toko, N. Hariharan, M. H. Konstandin et al., "Differential Regulation of Cellular Senescence and Differentiation by Prolyl Isomerase Pin1 in Cardiac Progenitor Cells," *The Journal of Biological Chemistry*, vol. 289, no. 9, pp. 5348–5356, 2014.

[7] T. H. Lee, L. Pastorino, and K. P. Lu, "Peptidyl-prolyl cis-trans isomerase Pin1 in ageing, cancer and Alzheimer disease," *Expert Reviews in Molecular Medicine*, vol. 13, article e21, 2011.

[8] K. Wheaton, J. Muir, W. Ma, and S. Benchimol, "BTG2 antagonizes Pin1 in response to mitogens and telomere disruption during replicative senescence," *Aging Cell*, vol. 9, no. 5, pp. 747–760, 2010.

[9] T. H. Lee, A. Tun-Kyi, R. Shi et al., "Essential role of Pin1 in the regulation of TRF1 stability and telomere maintenance," *Nature Cell Biology*, vol. 11, no. 1, pp. 97–105, 2009.

[10] H. Toko, M. H. Konstandin, S. Doroudgar et al., "Regulation of cardiac hypertrophic signaling by prolyl isomerase Pin1," *Circulation Research*, vol. 112, no. 9, pp. 1244–1252, 2013.

[11] W. Liu, L. Xu, X. Wang et al., "PRDX1 activates autophagy via the PTEN-AKT signaling pathway to protect against cisplatin-induced spiral ganglion neuron damage," *Autophagy*, vol. 12, pp. 1–23, 2021.

[12] S. Zhang, Y. Zhang, Y. Dong et al., "Knock-down of *Foxg1* in supporting cells increases the trans-differentiation of supporting cells into hair cells in the neonatal mouse cochlea," *Cellular and Molecular Life Sciences*, vol. 77, no. 7, article 3291, pp. 1401–1419, 2020.

[13] H. Zhou, X. Qian, N. Xu et al., "Disruption of Atg7-dependent autophagy causes electromotility disturbances, outer hair cell loss, and deafness in mice," *Cell Death & Disease*, vol. 11, no. 10, article 3110, p. 913, 2020.

[14] Z. He, L. Guo, Y. Shu et al., "Autophagy protects auditory hair cells against neomycin-induced damage," *Autophagy*, vol. 13, no. 11, pp. 1884–1904, 2017.

[15] B. Fang and H. Xiao, "Rapamycin alleviates cisplatin-induced ototoxicity in vivo," *Biochemical and Biophysical Research Communications*, vol. 448, no. 4, pp. 443–447, 2014.

[16] W. J. T. Tan, L. Song, M. Graham et al., "Novel role of the mitochondrial protein Fus1 in protection from premature hearing loss via regulation of oxidative stress and nutrient and energy sensing pathways in the inner ear," *Antioxidants & Redox Signaling*, vol. 27, no. 8, pp. 489–509, 2017.

[17] Z. Zhong, X. Fu, H. Li et al., "Citicoline protects auditory hair cells against neomycin-induced damage," *Frontiers in Cell and Developmental Biology*, vol. 8, p. 712, 2020.

[18] S. Gao, C. Cheng, M. Wang et al., "Blebbistatin inhibits neomycin-induced apoptosis in hair cell-like HEI-OC-1 cells and in cochlear hair cells," *Frontiers in Cellular Neuroscience*, vol. 13, p. 590, 2020.

[19] Z. H. He, M. Li, Q. J. Fang et al., "FOXG1 promotes aging inner ear hair cell survival through activation of the autophagy pathway," *Autophagy*, vol. 19, pp. 1–22, 2021.

[20] Y. Zhang, W. Li, Z. He et al., "Pre-treatment with Fasudil prevents neomycin-induced hair cell damage by reducing the accumulation of reactive oxygen species," *Frontiers in Molecular Neuroscience*, vol. 12, p. 264, 2019.

[21] A. Li, D. You, W. Li et al., "Novel compounds protect auditory hair cells against gentamycin-induced apoptosis by maintaining

the expression level of H3K4me2," *Drug Delivery*, vol. 25, no. 1, pp. 1033–1043, 2018.

[22] A. A. Mesalam, M. el-Sheikh, M. D. Joo et al., "Induction of oxidative stress and mitochondrial dysfunction by juglone affects the development of bovine oocytes," *International Journal of Molecular Sciences*, vol. 22, no. 1, pp. 168–214, 2020.

[23] W. Liu, X. Xu, Z. Fan et al., "Wnt signaling activates TP53-Induced Glycolysis and Apoptosis Regulator and protects against cisplatin-induced spiral ganglion neuron damage in the mouse cochlea," *Antioxidants & Redox Signaling*, vol. 30, no. 11, pp. 1389–1410, 2019.

[24] J. Qi, Y. Liu, C. Chu et al., "A cytoskeleton structure revealed by super-resolution fluorescence imaging in inner ear hair cells," *Cell Discovery*, vol. 5, no. 1, p. 12, 2019.

[25] C. Cheng, Y. Wang, L. Guo et al., "Age-related transcriptome changes in Sox2+ supporting cells in the mouse cochlea," *Stem Cell Research & Therapy*, vol. 10, no. 1, article 1437, p. 365, 2019.

[26] L. Liu, Y. Chen, J. Qi et al., "Wnt activation protects against neomycin-induced hair cell damage in the mouse cochlea," *Cell Death & Disease*, vol. 7, no. 3, article e2136, 2016.

[27] R. Guo, M. Xiao, W. Zhao et al., "2D $Ti_3C_2T_x$MXene couples electrical stimulation to promote proliferation and neural differentiation of neural stem cells," *Acta Biomaterialia*, vol. -S1742-7061, no. 20, pp. 30749–30752, 2020.

[28] R. Guo, S. Zhang, M. Xiao et al., "Accelerating bioelectric functional development of neural stem cells by graphene coupling: implications for neural interfacing with conductive materials," *Biomaterials*, vol. 106, pp. 193–204, 2016.

[29] F. Tan, C. Chu, J. Qi et al., "AAV-ie enables safe and efficient gene transfer to inner ear cells," *Nature Communications*, vol. 10, no. 1, article 11687, p. 3733, 2019.

[30] Y. Liu, J. Qi, X. Chen et al., "Critical role of spectrin in hearing development and deafness," *Science Advances*, vol. 5, no. 4, article eaav7803, 2019.

[31] J. Lv, X. Fu, Y. Li et al., "Deletion of *Kcnj16* in mice does not alter auditory function," *Frontiers in Cell and Developmental Biology*, vol. 9, article 630361, 2021.

[32] F. Qian, X. Wang, Z. Yin et al., "The *slc4a2b* gene is required for hair cell development in zebrafish," *Aging*, vol. 12, no. 19, article 103840, pp. 18804–18821, 2020.

[33] Z. He, Q. Fang, H. Li et al., "The role of FOXG1 in the postnatal development and survival of mouse cochlear hair cells," *Neuropharmacology*, vol. 144, pp. 43–57, 2019.

[34] K. P. Lu and X. Z. Zhou, "The prolyl isomerase PIN1: a pivotal new twist in phosphorylation signalling and disease," *Nature Reviews. Molecular Cell Biology*, vol. 8, no. 11, pp. 904–916, 2007.

[35] F. Fagiani, S. Govoni, M. Racchi, and C. Lanni, "The peptidyl-prolyl isomerase Pin1 in neuronal signaling: from neurodevelopment to neurodegeneration," *Molecular Neurobiology*, vol. 58, no. 3, article 2179, pp. 1062–1073, 2021.

[36] Y. C. Liou, A. Ryo, H. K. Huang et al., "Loss of Pin1 function in the mouse causes phenotypes resembling cyclin D1-null phenotypes," *Proceedings of the National Academy of Sciences*, vol. 99, no. 3, pp. 1335–1340, 2002.

[37] L. Pastorino, A. Sun, P. J. Lu et al., "The prolyl isomerase Pin1 regulates amyloid precursor protein processing and amyloid-β production," *Nature*, vol. 440, no. 7083, pp. 528–534, 2006.

[38] J. A. Driver, X. Z. Zhou, and K. P. Lu, "Pin1 dysregulation helps to explain the inverse association between cancer and Alzheimer's disease," *Biochimica et Biophysica Acta*, vol. 1850, no. 10, pp. 2069–2076, 2015.

[39] F. W. Atchison, B. Capel, and A. R. Means, "Pin1 regulates the timing of mammalian primordial germ cell proliferation," *Development*, vol. 130, no. 15, pp. 3579–3586, 2003.

[40] L. Lv, M. Ye, R. Duan et al., "Downregulation of Pin1 in human atherosclerosis and its association with vascular smooth muscle cell senescence," *Journal of Vascular Surgery*, vol. 68, no. 3, pp. 873–883.e5, 2018.

[41] M. V. Astle, K. M. Hannan, P. Y. Ng et al., "AKT induces senescence in human cells via mTORC1 and p53 in the absence of DNA damage: implications for targeting mTOR during malignancy," *Oncogene*, vol. 31, no. 15, pp. 1949–1962, 2012.

[42] N. Hay and N. Sonenberg, "Upstream and downstream of mTOR," *Genes & Development*, vol. 18, no. 16, pp. 1926–1945, 2004.

[43] C. L. Chung, I. Lawrence, M. Hoffman et al., "Topical rapamycin reduces markers of senescence and aging in human skin: an exploratory, prospective, randomized trial," *Geroscience*, vol. 41, no. 6, pp. 861–869, 2019.

[44] N. Wang, Z. Luo, M. Jin et al., "Exploration of age-related mitochondrial dysfunction and the anti-aging effects of resveratrol in zebrafish retina," *Aging (Albany NY)*, vol. 11, no. 10, article 101966, pp. 3117–3137, 2019.

[45] U. R. Heinrich, S. Strieth, I. Schmidtmann, K. Helling, and H. Li, "Gentamicin alters Akt-expression and its activation in the guinea pig cochlea," *Neuroscience*, vol. 311, pp. 490–498, 2015.

[46] E. Ebnoether, A. Ramseier, M. Cortada, S. Levano-Huaman, and D. Bodmer, "Sesn2 gene ablation enhances susceptibility to gentamicin-induced hair cell death via modulation of AMPK/mTOR signaling," *Cell Death Discovery*, vol. 3, no. 1, article 17024, 2017.

[47] J. Chen, H. Yuan, A. E. Talaska, S. H. Sha, and K. Hill, "Increased sensitivity to noise-induced hearing loss by blockade of endogenous PI3K/Akt signaling," *Journal of the Association for Research in Otolaryngology*, vol. 16, no. 3, pp. 347–356, 2015.

[48] W. Y. Zhu, X. Jin, Y. C. Ma, and Z. B. Liu, "MIF protects against oxygen-glucose deprivation-induced ototoxicity in HEI-OC1 cochlear cells by enhancement of Akt-Nrf2-HO-1 pathway," *Biochemical and Biophysical Research Communications*, vol. 503, no. 2, pp. 665–670, 2018.

[49] K. Leitmeyer, A. Glutz, V. Radojevic et al., "Inhibition of mTOR by rapamycin results in auditory hair cell damage and decreased spiral ganglion neuron outgrowth and neurite formation in vitro," *BioMed research international*, vol. 2015, Article ID 925890, 10 pages, 2015.

[50] K. Breitschopf, A. M. Zeiher, and S. Dimmeler, "Pro-atherogenic factors induce telomerase inactivation in endothelial cells through an Akt-dependent mechanism," *FEBS Letters*, vol. 493, no. 1, pp. 21–25, 2001.

[51] S. Courtois-Cox, S. M. Genther Williams, B. W. Johnson et al., "A negative feedback signaling network underlies oncogene-induced senescence," *Cancer Cell*, vol. 10, no. 6, pp. 459–472, 2006.

[52] K. H. Park, E. H. Cho, W. J. Bae et al., "Role of PIN1 on in vivo periodontal tissue and in vitro cells," *Journal of Periodontal Research*, vol. 52, no. 3, pp. 617–627, 2017.

[53] Ö. Demir, E. P. Barros, T. L. Offutt, R. E. Amaro, and M. Rosenfeld, "An integrated view of p53 dynamics, function,

and reactivation," *Current Opinion in Structural Biology*, vol. 67, pp. 187–194, 2021.

[54] K. Jeong, S. J. Kim, Y. Oh et al., "p53 negatively regulates Pin1 expression under ER stress," *Biochemical and Biophysical Research Communications*, vol. 454, no. 4, pp. 518–523, 2014.

[55] S. Saxena, H. Vekaria, P. G. Sullivan, and A. W. Seifert, "Connective tissue fibroblasts from highly regenerative mammals are refractory to ROS-induced cellular senescence," *Nature Communications*, vol. 10, no. 1, article 12398, p. 4400, 2019.

[56] M. C. Marazita, A. Dugour, M. D. Marquioni-Ramella, A. M. Suburo, and J. M. Figueroa, "Oxidative stress-induced premature senescence dysregulates VEGF and CFH expression in retinal pigment epithelial cells: implications for age-related macular degeneration," *Redox Biology*, vol. 7, pp. 78–87, 2016.

[57] D. F. Xue, S. T. Pan, G. Huang, and J. X. Qiu, "ROS enhances the cytotoxicity of cisplatin by inducing apoptosis and autophagy in tongue squamous cell carcinoma cells," *The International Journal of Biochemistry & Cell Biology*, vol. 122, article 105732, 2020.

[58] C. Liang, S. Shi, M. Liu et al., "PIN1 maintains redox balance via the c-Myc/NRF2 axis to counteract Kras-induced mitochondrial respiratory injury in pancreatic cancer cells," *Cancer research*, vol. 79, no. 1, pp. 133–145, 2019.

Hindawi
Oxidative Medicine and Cellular Longevity
Volume 2021, Article ID 5533793, 15 pages
https://doi.org/10.1155/2021/5533793

Research Article

Phenolic Compounds of Red Wine *Aglianico del Vulture* Modulate the Functional Activity of Macrophages via Inhibition of *NF-κB* and the Citrate Pathway

Anna Santarsiero,[1] Paolo Convertini,[1] Antonio Vassallo,[1] Valentina Santoro,[2] Simona Todisco,[1] Dominga Iacobazzi,[3] Yvonne Fondufe-Mittendorf,[4] Giuseppe Martelli,[1] Marcos R. de Oliveira,[5] Rosangela Montanaro,[1] Vincenzo Brancaleone,[1] Johannes Stöckl,[6] and Vittoria Infantino[1]

[1]*Department of Science, University of Basilicata, Viale dell'Ateneo Lucano 10, 85100 Potenza, Italy*
[2]*Department of Pharmacy, University of Salerno, Via Giovanni Paolo II 132, 84084 Salerno, Italy*
[3]*Bristol Heart Institute, Bristol Medical School, University of Bristol, Bristol BS2 8HW, UK*
[4]*Department of Molecular and Cellular Biochemistry, University of Kentucky, Lexington, KY 40536, USA*
[5]*Departamento de Bioquímica Rua Ramiro Barcelos, Universidade Federal do Rio Grande do Sul (UFRGS), 2600 Anexo Santa Cecília, Porto Alegre, RS, Brazil*
[6]*Institute of Immunology, Center for Pathophysiology, Infectiology and Immunology, Medical University of Vienna, 1090 Vienna, Austria*

Correspondence should be addressed to Vittoria Infantino; vittoria.infantino@unibas.it

Received 25 February 2021; Revised 30 April 2021; Accepted 8 May 2021; Published 26 May 2021

Academic Editor: Cecile Jacovetti

Phenolic compounds of red wine powder (RWP) extracted from the Italian red wine *Aglianico del Vulture* have been investigated for the potential immunomodulatory and anti-inflammatory capacity on human macrophages. These compounds reduce the secretion of IL-1β, IL-6, and TNF-α proinflammatory cytokines and increase the release of IL-10 anti-inflammatory cytokine induced by lipopolysaccharide (LPS). In addition, RWP restores Annexin A1 levels, thus involving activation of proresolutive pathways. Noteworthy, RWP lowers NF-κB protein levels, promoter activity, and nuclear translocation. As a consequence of NF-κB inhibition, reduced promoter activities of *SLC25A1*—encoding the mitochondrial citrate carrier (CIC)—and *ATP citrate lyase* (*ACLY*) metabolic genes have been observed. CIC, ACLY, and citrate are components of the citrate pathway: in LPS-activated macrophages, the mitochondrial citrate is exported by CIC into the cytosol where it is cleaved by ACLY in oxaloacetate and acetyl-CoA, precursors for ROS, $NO^{\cdot}$, and PGE_2 inflammatory mediators. We identify the citrate pathway as a RWP target in carrying out its anti-inflammatory activity since RWP reduces CIC and ACLY protein levels, ACLY enzymatic activity, the cytosolic citrate concentration, and in turn ROS, $NO^{\cdot}$, PGE_2, and histone acetylation levels. Overall findings suggest that RWP potentially restores macrophage homeostasis by suppressing inflammatory pathways and activating proresolutive processes.

1. Introduction

Immunomodulators are heterogeneous compounds capable to interact with the immune system to upregulate or downregulate specific biological aspects of the host response. For example, phenolic compounds scavenge free radicals, prevent lipid peroxidation, modulate inflammatory pathway, and block the secretion of proinflammatory cytokines [1]. Resveratrol counteracts the production of proinflammatory cytokines, while anthocyanidins downregulate the expression of cyclooxygenase 2 (COX2) in macrophages exposed to lipopolysaccharide (LPS) [2]. Interestingly, resveratrol is able to

dampen inflammation and induce apoptosis in immune cells by triggering proresolutive mediator Annexin A1 (AnxA1) pathway [3, 4].

In addition, cyanidin-3-O-glucoside, petunidin-3-O-glucoside, and delphinidin-3-O-glucoside inhibit the master regulator of the immune function in mammalian cells, the transcription factor NF-κB, in a mitogen-activated protein kinase- (MAPK-) dependent manner [5, 6]. Certain anthocyanidins can suppress the generation of reactive oxygen species (ROS) [7, 8]. For example, cyanidin-3-O-glucoside has great oxygen radical absorbance capacity (ORAC) *in vitro* [9] and delphinidin is one of the most active scavenger against superoxide anion [10]. Compounds found in red wine can also upregulate the transcription factor of the expression of antioxidant and detoxifying enzymes in mammalian cells, improving the cytoprotection against several types of stress [10].

In inflammatory processes, metabolic changes occur to meet the new energetic demands of cells. The result is the production of metabolites, which both can act as immune signaling molecules and supply substrates necessary for the biosynthesis of proinflammatory mediators [11, 12]. Activated dendritic cells and macrophages switch rapidly from a resting to an activated state characterized by a different metabolic profile. In particular, LPS or classically activated macrophages—also known as M1 macrophages—have high rates of glycolysis and pentose phosphate pathway while the Krebs cycle is broken at two points and fatty acid oxidation and oxidative phosphorylation are downregulated [11, 12]. The two breakpoints of Krebs cycle are at succinate dehydrogenase and isocitrate dehydrogenase, with consequent withdrawals of succinate and citrate from the cycle. Most of the citrate is channelled into the citrate pathway, made of the mitochondrial transporter citrate carrier (CIC) and the enzyme ATP citrate lyase (ACLY) [13–16]. CIC exports citrate from the mitochondria in exchange for malate. In the cytosol, ACLY cleaves it into oxaloacetate (OAA) and acetyl-coenzyme A (acetyl-CoA). OAA is converted to malate by cytosolic malate dehydrogenase 1 (MDH1) and to pyruvate by malic enzyme 1 (ME1) with consequent production of nicotinamide adenine dinucleotide phosphate (NADPH). Of note, both NADPH oxidase and inducible nitric oxide synthase (iNOS) need NADPH for ROS and nitric oxide ($NO^{\cdot}$) synthesis, respectively [13, 15]. Acetyl-CoA is processed into malonyl-coenzyme A (malonyl-CoA) by acetyl-coA carboxylase (ACC). Malonyl-CoA is a substrate for cholesterol or fatty acid synthesis. Therefore, it could be used for the production of arachidonic acid, a precursor for prostaglandin E_2 (PGE_2), a key modulator of inflammation with a crucial role in inflammatory diseases [13, 15]. Acetyl-CoA is also a substrate for protein and histone acetylation [17]. Moreover, citrate is implied in itaconate synthesis that modulates the production of different inflammatory mediators, acting as a negative regulator of inflammation [18]. The citrate pathway has a key role also in diseases such as Down syndrome and Behçet syndrome [19, 20].

The red wines have become popular in recent years due to their content of phenolic compounds with antioxidant activity as well as hypolipidemic and anti-inflammatory effects. Although different studies have been performed on the red wine compounds, most of them are aimed at investigating the chemical composition, the biodiversity, the genetic diversity, the pedigree reconstitution, and the general antioxidant properties. In this study, we investigated on the beneficial immunomodulatory effect of a powder rich in phenolic compounds from the red wine *Aglianico del Vulture*. It is one of the best Italian red wines that has never been studied. We have focused on the secretion of proinflammatory and anti-inflammatory cytokines, NF-κB expression, the citrate pathway, and epigenetic modifications in LPS-activated human macrophages. Such studies will help to identify the targets for RWP and the development of potential therapeutics in the prevention and treatment of inflammatory chronic diseases.

2. Material and Methods

2.1. Wine Samples. Red wine (*Vitis vinifera L.*, Aglianico cultivar) was provided by Cantine del Notaio (Rionero, Italy). Grapes were harvested in September 2018, samples were collected after grape pressing, and the wine fermentation was completed (no residual sugar was present into the wine). The samples were frozen and stored at -20°C before freeze drying. The wine samples (500 mL) in a glass cylinder were connected to a freeze drying apparatus and freeze-dried under vacuum using a Stellar Millrock ST8S5-l lyophilizer (Millrock Technology, Kingston, NY, USA).

2.2. LC–MS and LC–MS/MS Analyses. Part of whole and dealcoholized wine sample was dissolved in 100 μL of 40% MeOH with 0.1% (*v*/*v*) formic acid at a concentration of 10 mg/mL and centrifuged (5 min, 13,000 rpm), and 1 μL aliquots were injected in a UPLC–ESI–Qtrap system. Mass spectrometry-based analyses were carried out to evaluate the amount of specialized metabolites (delphinidin, cyanidin, and malvidin, all glucoside, caffeic and coumaric acids, resveratrol, and quercetin). Quali-quantitative analysis was carried out using an API6500 Q-Trap spectrometer (AB Sciex, Foster City, CA, USA) coupled with a Nexerax2 UHPLC apparatus (Shimadzu, Kyoto, Japan), working in both positive and negative MRM modes.

The instrumental parameters were optimized directly injecting solutions containing pure compounds. A Kinetex column (Phenomenex) (C18 100 Å, 50 mm × 2.6 μm × 2.1 mm) was adopted for chromatographic analyses, and compounds were separated using a linear gradient from 5% to 50% of acetonitrile (eluent B) and water containing 0.1% formic acid (eluent A) over 5 minutes followed by a faster gradient until to 95% of B. The flow rate was 0.35 mL/min, and the injection volume was 1 μL. To perform accurate quantitative analyses, 8 points (in the range 0.010–10 μg/mL) calibration curves were built for all the standard compounds. The mean values ± standard deviation from at least three experiments were reported. All data were processed using Analyst software (ABSciex), and identification of compounds was based on retention times, accurate mass measurements, MS/MS data, exploration of specific spectral libraries and public

repositories for MS-based metabolomic analysis [21], and comparison with data reported in the literature [7, 22–25].

2.3. Isolation of Human Monocytes from Whole Blood. Primary human monocytes were isolated from healthy donors after obtaining written informed consent. The study was performed in agreement with the Declaration of Helsinki and in accordance with the Committee on Human Research approved procedures. Venous blood was collected into K2 EDTA-coated BD vacutainer tubes (Becton, Dickinson and Company, Franklin Lakes, NJ, USA). Peripheral blood mononuclear cells (PBMCs) were separated by Histopaque-1077 (Sigma-Aldrich, St Louis, MO) density gradient centrifugation: whole blood was mixed with Hanks' Balanced Salt solution (HBSS, Sigma-Aldrich) at a ratio of 1 : 2 (v/v), layered on the top of Histopaque-1077 (Sigma-Aldrich) and centrifuged at 1000 x g for 15 minutes. The layer of mononuclear cells (PBMCs) at the interphase was recovered and washed twice in HBSS. PBMCs were incubated with CD14 antibody conjugated to magnetic beads (MACS®, Miltenyi Biotec GmbH, Bergisch Gladbach, Germany) for 15 minutes at 4°C. After washing, cells were loaded onto MACS® column (Miltenyi Biotec GmbH) placed in a magnetic field, and CD14- positive ($CD14^+$) and CD14-negative ($CD14^-$) populations were divided. The $CD14^+$ monocytes were differentiated to macrophages by using 100 ng/mL human M-CSF in Roswell Park Memorial Institute (RPMI) 1640 medium (Thermo Fisher Scientific, San Jose, CA, USA) supplemented with 10% fetal bovine serum, 2 mM L-glutamine, 100 U/mL penicillin, and 100 μg/mL streptomycin at 37°C in a humidified atmosphere of 5% CO_2.

2.4. Cell Culture and Treatments. Human embryonic kidney 293 cells (HEK293, Sigma-Aldrich) were grown in Dulbecco's Modified Eagle Medium (DMEM, Thermo Fisher Scientific) supplemented with 10% fetal bovine serum, 2 mM L-glutamine, 100 U/mL penicillin, and 100 μg/mL streptomycin in a humidified chamber with 5% CO_2 at 37°C. To evaluate the immunomodulatory and anti-inflammatory properties of *Aglianico del Vulture* red wine, primary human monocytes and HEK293 cells were treated with RWP 20 or 200 μg/mL for 1 hour. Then, inflammation was induced by 1 μg/mL of lipopolysaccharide isolated and purified from *E. coli* strain EH100 (AdipoGen Life Sciences, Inc., San Diego, USA). Except for cytokines and PGE_2 quantification, cells were washed twice with PBS at the end of LPS treatment before proceeding with subsequent analyses, as detailed further in the sections below.

2.5. Cell Count. $CD14^+$ monocytes were seeded into a 96-well plate (2×10^4 cells/well) and treated with a wide range of RWP concentrations: 2.5, 5, 10, 20, 50, 100, 200, 400, 800, 1600, and 3200 μg/mL. After 72 hours, cell count was carried out by using the automated handheld Scepter 2.0 Cell Counter (Merck Millipore, Switzerland).

2.6. Quantification of Cytokines. $CD14^+$ monocytes (5×10^5 cells) were pretreated in 24-well plates with RWP 20 or 200 μg/mL for 1 hour and then stimulated with 1 μg/mL of LPS. Twenty-four hours later, cell-free supernatants were collected and assayed for the concentration of interleukins 1β, 6, and 10 (IL-1β, IL-6, and IL-10) and tumor necrosis factor α (TNF-α) by Luminex100 System (R&D Systems, Inc., Minneapolis, MN, USA) using specific matched-pair antibodies and recombinant cytokines as standards following the manufacturer's recommendations.

2.7. Western Blotting. Cellular pellet was resuspended in Laemmli buffer and boiled for 5 minutes at 100°C. Thirty micrograms of proteins were subjected to SDS-PAGE and then electroblotted onto nitrocellulose membranes. The membranes were blocked for 1 hour in a tris-buffered saline (TBS) solution containing 5% nonfat dry milk and 0.5% Tween 20 and then immunostained at 4°C overnight with anti-NF-κB/p65 (ab7970, Abcam, Cambridge, MA), anti-CIC [26, 27], anti-ATP citrate lyase (ab157098, Abcam), anti-acetylated H3 (ab47915, Abcam), anti-total H3 (ab1791, Abcam), anti-AnxA1 (GTX101070, GeneTex), and anti-FPR2 or anti-β-actin (ab8227, Abcam) antibodies. Following 1-hour incubation with HRP Goat anti-Rabbit IgG secondary antibody (Santa Cruz Biotechnology, Santa Cruz, CA, USA), the immunoreactions were detected by using the horseradish peroxidase substrate WesternBright™ ECL (Advansta, Menlo Park, CA, USA) at Chemidoc™ XRS detection system equipped with Image Lab Software for image acquisition and densitometric analysis (Bio-Rad Laboratories, Hercules, CA, USA).

2.8. Transient Transfection. For monitoring the activity of the NF-κB signaling pathway, HEK293 cells were transiently transfected with a NF-κB reporter plasmid containing a firefly luciferase gene driven by five copies of NF-κB response element (5′-GGGACTTTCC-3′) located upstream of the minimal TATA box promoter (pGL3–5xNF-κB). To measure SLC25A1 gene promoter activity, HEK293 cells were transfected as previously described [28] using pGL3 basic-LUC vector (Promega, Madison, WI, USA) containing the −1785/−20 bp region of the SLC25A1 gene promoter (SLC25A1pGL3) upstream of the luciferase reporter gene [29]. For ACLY gene promoter activity, in pGL3, basic-LUC vector was cloned the −3116/−20 bp region of the ACLY gene promoter (called "3000") or a deletion fragment of this region (called "1000") [30]. To normalize the extent of transfection, cells were transfected with 10 ng of pRL-CMV (Promega). Twenty-four hours after transfection, HEK293 cells were triggered with LPS in the presence or absence of RWP 20 or 200 μg/mL. The day after, cells were lysed and assayed for LUC activity by using the Dual-Luciferase® Reporter Assay System (Promega), according to the manufacturer's protocol.

2.9. Immunocytochemistry. Cells were induced with LPS for 1 or 3 hours in the presence or not of RWP 20 or 200 μg/mL, then were washed in PBS and fixed by cross-linking with 3% paraformaldehyde solution. Following permeabilization with PBS +0.25% Triton X-100 (PBST) and blocking with PBST +1% BSA (bovine serum albumin), cells were incubated with anti-NF-κB/p65 (ab7970, Abcam) primary antibody at 4°C overnight. The day after, Alexa Fluor 488

(Thermo Fisher Scientific) was used as a secondary antibody while Fluoroshield Mounting Medium with DAPI (ab104139, Abcam) was employed to preserve fluorescence and as a counterstain for DNA. The images were obtained with a fluorescence microscope (EVOS FLoid Cell Imaging Station, Thermo Fisher Scientific).

2.10. Quantification of Citrate. The amount of citrate was quantified in macrophages treated with LPS in the presence or not of RWP 20 or 200 μg/mL by a fluorometric method using the Citrate Colorimetric/Fluorometric Assay Kit (BioVision, Milpitas, CA, USA) as per the manufacturer's instructions.

2.11. ACLY Activity. Primary monocytes were pretreated with RWP 20 or 200 μg/mL for 1 hour and then activated to macrophages with LPS. At the end of treatments, cells were washed twice in ice-cold PBS. The cell pellet was resuspended in ice-cold 0.1% NP40 in PBS, and three freeze-melt cycles (-80°C for 8 minutes/40°C for 4 minutes) were performed. After centrifugation, supernatant was collected and protein concentration was determined by Bradford assay. ACLY activity was assessed by the coupled malic dehydrogenase method [31, 32], as previously described [30]. The specific ACLY activity was expressed as a percentage of the control after normalization to the protein concentration.

2.12. ROS, $NO^{\cdot}$, and PGE_2 Detection. To evaluate ROS and $NO^{\cdot}$ levels, $CD14^+$ monocytes were triggered by LPS in the presence or not of RWP 20 or 200 μg/mL. Where indicated, cells were treated also with 5 mM sodium malate (Sigma-Aldrich) or 500 μM NADPH (Sigma-Aldrich). Following 24 hours, ROS and $NO^{\cdot}$ concentrations were measured by using 6-Carboxy-2′,7′-Dichlorodihydrofluorescein Diacetate (DCF-DA, Thermo Fisher Scientific) and 4-Amino-5-Methylamino-2′,7′-Difluorofluorescein Diacetate (DAF-FM Diacetate, Thermo Fisher Scientific), respectively, as previously reported [33].

For PGE_2 quantification, cells were exposed to RWP 20 or 200 μg/mL for 1 hour and, where indicated, cotreated with 5 mM sodium acetate (Sigma-Aldrich); then inflammation was induced by LPS. At the end of 48 hours LPS treatment; PGE_2 was measured by using DetectX® Prostaglandin E2 High Sensitivity Immunoassay Kit (Arbor Assays, Ann Arbor, MI, USA) as previously described [33].

2.13. Statistical Analysis. Results are shown as the means ± SD of, at least, three independent experiments. Statistical significance of differences was determined by using *one-way ANOVA* followed by *Dunnett's* or *Tukey's* tests for multiple comparisons. The statistical methods used for each experiment are detailed in figure legends. Asterisks in figures denote statistical significance: $^{*}p < 0.05$, $^{**}p < 0.01$, and $^{***}p < 0.001$. When *Tukey's* post hoc test was performed, different letters indicate significant differences between treatments at $p < 0.05$.

3. Results

3.1. Composition and Identification of the Red Wine Powder Components. The red wine powder from *Aglianico del Vulture* was freeze-dried under vacuum. Quali-quantitative analysis of RWP was performed by LC-ESI-QTrap-MS/MS and LC-ESI-QTrap-MS analyses. The use of the Kinetex column and LC-ESI-MS/MS (alternating positive and negative ionization modes) allowed for the simultaneous separation and identification of all compounds. Compounds identified showed very good results in the optimized chromatographic column with retention times that ranged from 1.21 to 2.51 min. Extracted ion chromatograms for each compound are presented in Figure S1. Individual components were identified by comparison of their *m/z* values in the total ion current (TIC) profile with those of the selected compounds described in the literature. In particular, seven compounds were identified in RWP (Table 1) belonging to a wide variety of structurally different metabolic classes: phenolic acids (caffeic acid and p-coumaric acid); stilbenes (resveratrol); anthocyanidins (delphinidin-3-O-glucoside, cyanidin-3-O-glucoside, and malvidin 3-O-glucoside); and flavonols (quercetin).

The tested *Aglianico del Vulture* red wine powder contained significant amounts of anthocyanidins. In particular malvidin-3-*O*-glucoside was the most abundant (14.00 ± 0.23 mg/100 mL), followed by cyanidin-3-*O*-glucoside (1.30 ± 0.218 mg/100 mL) and delphinidin-3-*O*-glucoside (0.072 ± 0.003 mg/100 mL) (Table 1). Our results are in accordance with the typical anthocyanin profiling of *Aglianico* wine, in which malvidin 3-*O*-glucoside represents about 60% of total anthocyanidins while contents of cyanidin-3-*O*-glucoside and delphinidin-3-*O*-glucoside are very low (around 5%) [34]. The content of resveratrol in *Aglianico del Vulture* was 0.053 ± 0.01 mg/100 mL, similar to other Italian red wines [26, 35, 36]. Concentrations of caffeic acid and *p*-coumaric acid were 0.218 ± 0.047 mg/100 mL and 0.078 ± 0.002 mg/100 mL, respectively. Quercetin was determined equal to 0.785 ± 0.02 mg/100 mL as listed on Table 1.

3.2. Evaluation of RWP Toxicity on Primary Human Monocytes. We next investigated the RWP toxicity. Primary human monocytes, isolated from peripheral blood of healthy donors, were treated with increasing concentrations of RWP, ranging from 2.5 to 3200 μg/mL. After 72 hours, cell counts were performed. As shown in Figure 1, RWP did not affect the cell number until at a dose of 800 μg/mL. A slight cytotoxicity was observed at the highest tested concentrations of 1600 and 3200 μg/mL, where reductions in the cell number compared with untreated cells (0) were about 20% and 40%, respectively ($^{***}p < 0.001$, *Dunnett's multiple comparisons test*).

3.3. Effect of RWP on the Secretion of IL-1β, IL-6, TNF-α, and IL-10 Cytokines. To begin to understand the impact of this RWP on the human body, we analyzed its pro- and anti-inflammatory properties. We treated primary human monocytes with LPS, a component of the outer membrane of Gram-negative bacteria that induces inflammatory cascade

Table 1: Composition of the red wine powder (RWP) obtained from Aglianico del Vulture (harvest 2018). Mass spectrometry-based analyses were carried out to evaluate the amount of specialized metabolites in RWP. The mean values ± standard deviation (SD) from at least three independent experiments, each in triplicate, are reported.

	mg/100 mL ± SD
Phenolic acids	
Caffeic acid	0.218 ± 0.047
Coumaric acid	0.078 ± 0.002
Stilbenes	
Resveratrol	0.053 ± 0.01
Anthocyanidins	
Delphinidin-3-O-glucoside	0.072 ± 0.003
Cyanidin-3-O-glucoside	1.30 ± 0.18
Malvidin-3-O-glucoside	14.00 ± 0.23
Flavonols	
Quercetin	0.785 ± 0.02

through the toll-like receptor 4 (TLR4) [27]. LPS leads to the rapid activation of proinflammatory cytokines IL-1β, IL-6, and TNF-α [37] and the production of IL-10, a potent anti-inflammatory cytokine.

We therefore assessed the release of IL-1β, IL-6, TNF-α, and IL-10 cytokines after 24 hours of stimulation of monocytes with LPS in the presence or absence of RWP. We observed marked and significant increases in the levels of all the cytokines analyzed after the induction with LPS (Figures 2(a)–2(d): unstimulated cells *vs.* LPS, $p < 0.001$, *Tukey's test*). RWP lowered IL-1β, IL-6, and TNF-α secretion in a dose-dependent manner (Figures 2(a)–2(c)). Specifically, at a dose of 200 μg/mL, RWP reduced significantly by half the levels of all the proinflammatory cytokines released after stimulation with LPS, whereas RWP at a dose of 20 μg/mL decreased levels of IL-1β, IL-6, and TNF-α (Figures 2(a)–2(c): LPS *vs.* LPS + RWP 20 μg/mL, $p < 0.001$, *Tukey's test*) by about 35%. On the other hand, IL-10 levels increased significantly in a concentration-dependent manner when monocytes were treated with RWP compared to being triggered only with LPS (Figure 2(d): LPS *vs.* LPS + RWP 20 μg/mL–200 μg/mL, $p < 0.001$, *Tukey's test*).

3.4. Aglianico del Vulture Red Wine Powder Modulates Expression of Proresolutive Protein AnxA1 in Inflammatory Conditions. We next focused on the role of the AnxA1/FPR2 axis in LPS-induced inflammation *in vitro*. AnxA1 is a proresolutive protein induced and activated during inflammation, aimed at limiting tissue damage and restoring homeostasis through activation of Formyl Peptide Receptor 2 (FPR2) [3]. LPS treatment reduced total AnxA1 expression, while pretreatment with RWP, at both concentration used (20 or 200 μg/mL), was able to restore its physiological amount, thus preventing cells to undergo excessive inflammation (Figure 3(a)). In addition, expression of FPR2 receptor was downregulated by LPS administration (Figure 3(b)). Although not significantly, RWP slightly increased FPR2 expression, only causing a positive trend (Figure 3(b)).

3.5. Effect on Expression, Promoter Activity and Nuclear Translocation of NF-κB. When LPS binds to TLR4 on the surface of macrophages, a signal transduction cascade leading to transcription of specific enzymes, such as COX2, matrix metalloproteinase-9, and inflammatory cytokines TNF-α, IL-1, IL-6, IL-8, and chemokines [38]. The NF-κB pathway plays a central role for the protective properties of a moderate wine consumption [39]. Therefore, we evaluated if the red wine powder from *Aglianico del Vulture* will affect the NF-κB pathway. We focused on the expression of NF-κB, its promoter activity, and its cellular localization.

For this, primary human monocytes were treated with LPS in the presence or absence of RWP. LPS induced a marked overexpression of subunit p65 of NF-κB (Figure 4(a)). RWP, used as both 20 μg/mL and 200 μg/mL, reduced p65/NF-κB protein levels to about 40% (Figure 4(a)). Likewise, even if significant (*Tukey's test*), no strong differences were found in the ability to inhibit NF-κB promoter activity between RWP 20 μg/mL and RWP 200 μg/mL (Figure 4(b)). To monitor the effect of RWP on the NF-κB signal transduction pathway, HEK293 cells were transiently transfected with a NF-κB reporter plasmid containing a firefly luciferase gene driven by five copies of NF-κB response element located upstream of the minimal TATA box promoter. After activation by proinflammatory stimuli, endogenous NF-κB binds to the DNA response elements, inducing transcription of the luciferase reporter gene. When cells were treated with LPS, we observed a significant increase in luciferase activity, when compared to untreated cells (Figure 4(b) C *vs.* LPS, $p < 0.001$, *Tukey's test*); RWP reported the levels of luciferase activity in LPS-triggered cells at values similar to those of control. Next, we analyzed the cellular localization of p65, the subunit of NF-κB. After 1 hour (Figure 4(c)) and 3 hours (Figure 4(d)) of treatment with LPS, we observed the translocation of subunit p65 of NF-κB from the cytosol to the nucleus. In cells cotreated with RWP, the main NF-κB localization was cytosolic (Figures 4(c) and 4(d)). Altogether, these data suggest that RWP plays a role in inhibiting the NF-κB pathway.

3.6. Effect on the Citrate Export Pathway: Focus on CIC and Citrate. Among the proinflammatory genes activated by NF-κB is *SLC25A1*, which encodes the mitochondrial citrate carrier (CIC). It is the component of the citrate pathway responsible for the export of the citrate withdrawn from the Krebs cycle to the cytosol after LPS stimulation [13, 14].

The human *SLC25A1* promoter contains two NF-κB response elements at positions −414/−405 bp and −1314/−1305 bp. To verify if RWP induced alterations in the transcription rate of the *SLC25A1* promoter, we transfected HEK293 cells with the previously described SLC25A1pGL3—a vector with *SLC25A1*—promoter encompassing the −1785/−20 bp region of the *SLC25A1* gene cloned upstream of the luciferase reporter gene [29]. Next, we treated with LPS, in the presence or absence of RWP. We observed that RWP significantly reduced luciferase activity

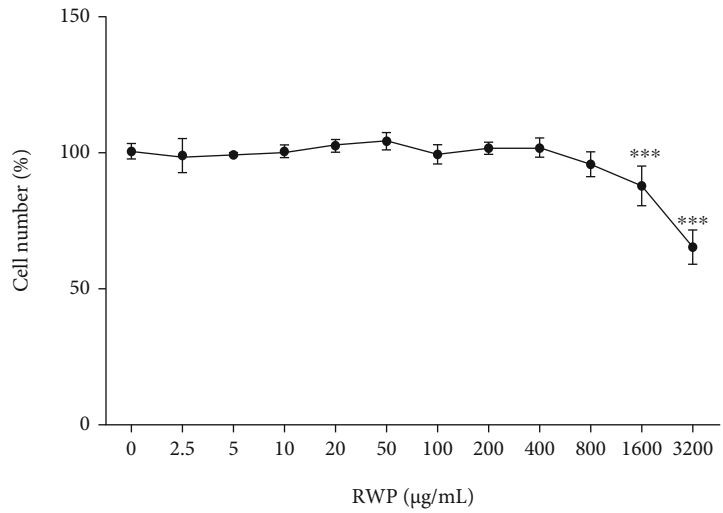

Figure 1: Effect of RWP on primary human monocyte cell number. Primary human monocytes were treated with increasing concentrations of RWP, ranging from 2.5 to 3200 μg/mL, and cell viability was assessed by cell count after 72-hour exposure. The mean values ± SD of three independent experiments with four replicates in each are shown. Differences were significant ($p < 0.001$) according to *one-way ANOVA*. *Dunnett's multiple comparisons test* was run as *post hoc* test to compare treatment groups with the control group (0, set at 100%); where indicated, differences were statistically significant ($^{***}p < 0.001$).

in a dose-dependent manner by 50% (RWP 20 μg/mL) and 60% (RWP 200 μg/mL) in cells upon LPS stimulation (*Tukey's test*, Figure 5(a)). We also measured the protein levels of CIC and confirmed a downregulation at the protein level (Figure 5(b)). However, we did not observe a dose-dependent effect at the protein level. LPS induced a threefold overexpression of CIC with respect to untreated cells (Figure 5(b)), and RWP, as both 20 μg/mL and 200 μg/mL, reported CIC levels to values similar to control cells (Figure 5(b)). A correspondent lowering in cytosolic citrate levels was detected: RWP either as 20 μg/mL or as 200 μg/mL reduced cytosolic citrate by around 40% with respect to LPS-triggered cells (Figure 5(c)).

3.7. Effect on the Citrate Export Pathway: Focus on ATP Citrate Lyase. ACLY is upregulated very early in macrophages activated by LPS or by TNF-α and/or interferon γ (IFNγ) as well as in inflammatory conditions [15, 19, 20]. To determine whether RWP affected NF-κB binding to ACLY, we analyzed the promoter region of the human *ACLY* gene. Since it contains an active NF-κB response element localized at −2048/−2038 bp [15], cells were transiently transfected with pGL3 basic-LUC vectors containing the −3116/−20 bp full-length region of the *ACLY* gene promoter (called "3000," Figure 6(a)), including the NF-κB response element. As a control, we also transfected cells with a mutant version, containing a truncated version of this region (called "1000," Figure 6(a)), without the NF-κB response element. Both plasmids were then used to test the effect of RWP on luciferase activity. The absence of the binding site for NF-κB was responsible for the lower *ACLY* gene promoter activity in cells transfected with 1000 than 3000 (Figure 6(a)). Following 24 hours of LPS treatment, the strongest promoter activity was registered in 3000 transfected cells (3000 + LPS, Figure 6(a)). The luciferase gene reporter activity was significantly reduced to levels similar to unstimulated cells (3000, Figure 6(a)) by RWP 20 μg/mL and to even lower levels by RWP 200 μg/mL (Figure 6(a)). RWP induced a parallel decrease in ACLY protein levels and enzymatic activity in LPS-triggered macrophages (Figures 6(b) and 6(c)). More in detail, LPS induced a twofold increase in ACLY expression levels (Figure 6(b)) and a 35% rise in ACLY activity (Figure 6(c)). No significant differences were observed between RWP 20 μg/mL and 200 μg/mL in bringing ACLY protein levels (Figure 6(b)) and activity (Figure 6(c)) down. These results, together with CIC and cytosolic citrate depletion, define a crucial role of RWP in immunometabolism.

Moreover, it has been recently demonstrated that rapid metabolic changes in LPS-induced macrophages are important to increase ACLY-derived acetyl-CoA that in turn leads to histone acetylation [40, 41], critical in regulating global chromatin accessibility and gene transcription. Transcriptional regulation of genes involved in macrophage activation and inactivation or determination of their polarization state occurs through histone modifications [42]. Therefore, changes in histone acetylation have a great impact in inflammation. We show that after LPS stimulation the levels of ACLY went up, with consequences in increased H3 histone acetylation (Figure 6(d)). On the other hand, treatment of cells with RWP lowered acetylated H3 in a dose-dependent manner (Figure 6(d)), suggesting an epigenetic activity of RWP.

3.8. Effect on the Levels of Inflammatory Mediators Downstream the Citrate Pathway: ROS and NO$^{\cdot}$. Since RWP downregulated CIC and ACLY, we analyzed its role in regulating the citrate pathway in LPS-activated macrophages. Citrate cleavage made by ACLY supplies intermediaries for the biosynthesis of three inflammatory mediators: ROS, NO$^{\cdot}$, and prostaglandin E_2 [16]. In LPS-triggered

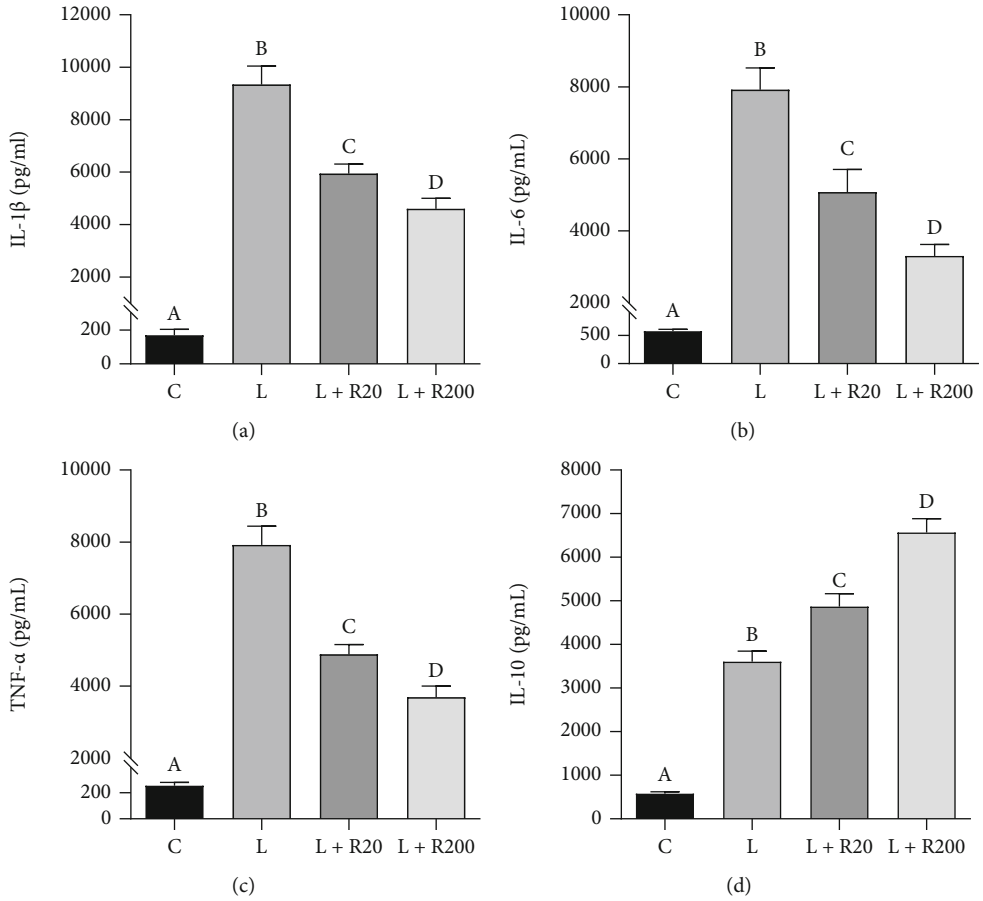

Figure 2: RWP affected the secretion of IL-1β, IL-6, TNF-α, and IL-10 cytokines. Primary human monocytes were incubated with RWP and activated to macrophages with 1 μg/mL LPS. Twenty-four hours later, the concentrations of the proinflammatory IL-1β (a), IL-6 (b), and TNF-α (c) and anti-inflammatory IL-10 (d) cytokines in cell culture supernatants were measured. Values represent the means ± SD of three independent experiments with four replicates in each. According to *one-way ANOVA*, differences in IL-1β (a), IL-6 (b), TNF-α (c), and IL-10 (d) levels were significant ($p < 0.001$). Therefore, *Tukey's post hoc test* was performed, and different letters indicate significant differences between treatments at $p < 0.05$. C: control; L: LPS; R20: RWP 20 μg/mL; R200: RWP 200 μg/mL.

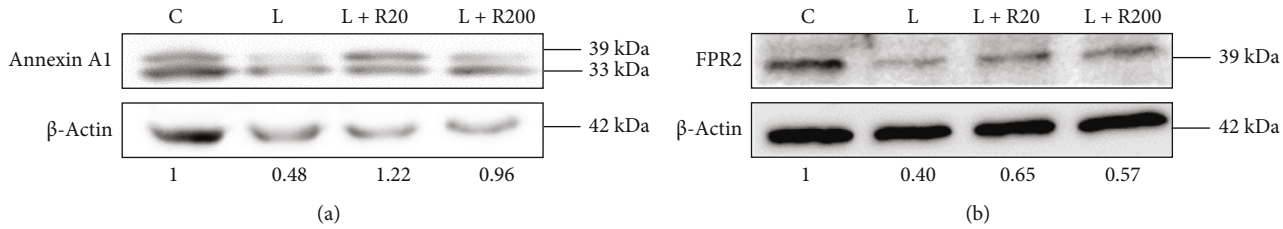

Figure 3: RWP significantly restored expression of AnxA1 in LPS-induced inflammation. Primary human monocytes were incubated with RWP 20 μg/mL or RWP 200 μg/mL and activated with 1 μg/mL LPS. Expression of AnxA1 (a) and FPR2 (b) was assessed following 24 h treatment with LPS. Protein expression was quantified by using optical density (O.D.) ratio for AnxA1 or FPR2 versus β-actin; normalized values obtained are reported under western blot images. C: control; L: LPS; R20: RWP 20 μg/mL; R200: RWP 200 μg/mL.

macrophages, the accumulated citrate is exported by CIC from the mitochondria to the cytosol and converted by ACLY into oxaloacetate and acetyl-CoA. OAA is converted to pyruvate with consequent production of NADPH [43], used for ROS and $NO^{\cdot}$ synthesis. Our analysis showed enhanced and significant releases of ROS and $NO^{\cdot}$ when human primary monocytes were treated with LPS (Figures 7(a) and 7(b)). RWP, on the other hand, reduced the levels of reactive oxygen species and nitric oxide in a dose-dependent manner (Figures 7(a) and 7(b)). In particular, RWP 20 μg/mL decreased by 10 and 15% the levels of ROS and $NO^{\cdot}$, respectively, with respect to cells treated only with LPS; reductions induced by RWP 200 μg/mL were about 20 and 35% (Figures 7(a) and 7(b)).

Malate and NADPH are two metabolites downstream the citrate pathway: in particular, malate is produced in the

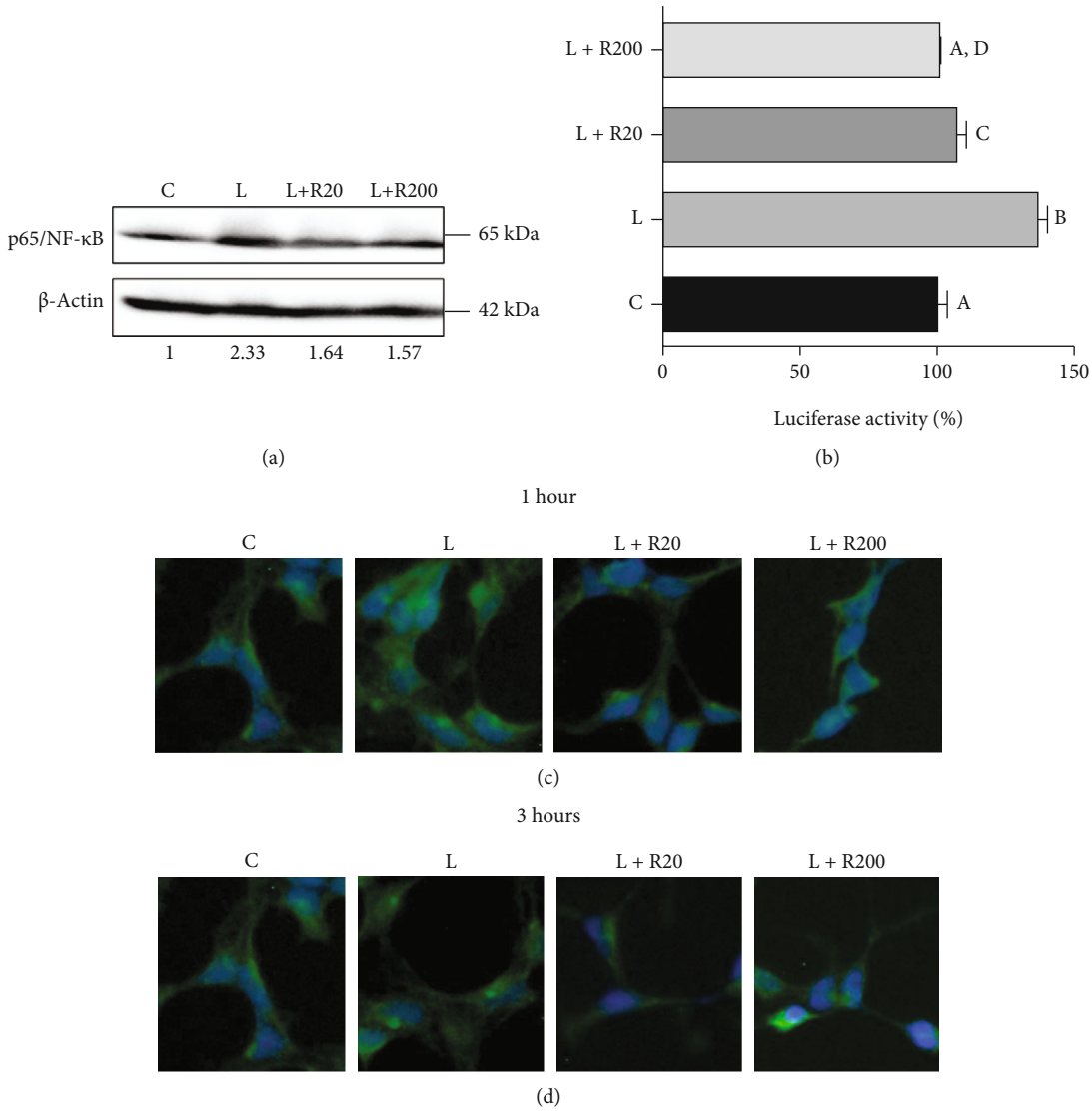

Figure 4: RWP inhibited NF-κB transcription factor. (a) Primary human monocytes were incubated with RWP 20 μg/mL or RWP 200 μg/mL and activated to macrophages with 1 μg/mL LPS. Specific antibodies detected the expression levels of subunit p65 of NF-κB and β-actin. The intensities of immunolabeled protein bands were measured by a quantitative software and normalized to β-actin; values obtained are reported under western blot images. Protein expression levels in control sample were taken as 1, and other samples were expressed in proportion to the control. (b) HEK293 cells were transfected with NF-κB luciferase reporter plasmid and treated with LPS in the presence or not of RWP 20 μg/mL or RWP 200 μg/mL. Bar chart reports the mean values ± SD of three independent experiments, each in triplicate. According to *one-way ANOVA*, differences were significant ($p < 0.001$). Therefore, *Tukey's post hoc test* was performed, and different letters indicate significant differences between treatments at $p < 0.05$. (c-d) Immunocytochemistry experiments were performed to identify the cellular localization of subunit p65 of NF-κB, recognized by a specific antibody. Cells were treated with RWP 20 μg/mL or RWP 200 μg/mL and activated with LPS. C: control; L: LPS; R20: RWP 20 μg/mL; R200: RWP 200 μg/mL.

reaction catalyzed by MDH1, while NADPH derived from the ME1 cleavage of malate in pyruvate. Exogenous malate used alone or in combination with NADPH reverts ACLY inhibition phenotype leading to a huge increase of both ROS and $NO^{\cdot}$ inflammatory mediators. As shown in Figures 6(a) and 6(b), the addition of malate alone or in combination with NADPH was sufficient to increase ROS as well as $NO^{\cdot}$ levels in LPS-triggered cells treated with RWP. Therefore, the effect of RWP on ROS and $NO^{\cdot}$ levels could occur through the citrate pathway suppression together with a direct inhibition of NF-κB, which controls the expression of ACLY, but also the expression of *NADPH oxidase* and *iNOS* genes [44, 45].

3.9. Inhibition of COX2 and Reduction of PGE_2 Level: Involvement of the Citrate Pathway. Finally, the focus was set on the other inflammatory mediator downstream the citrate pathway, PGE_2, and on the enzyme COX2 responsible for its synthesis. It is well known that wine polyphenols inhibit COX2 in inflammation induced by LPS. *Aglianico del Vulture* red wine powder at 20 μg/mL as well as 200 μg/mL reduced COX2 expression levels almost the half

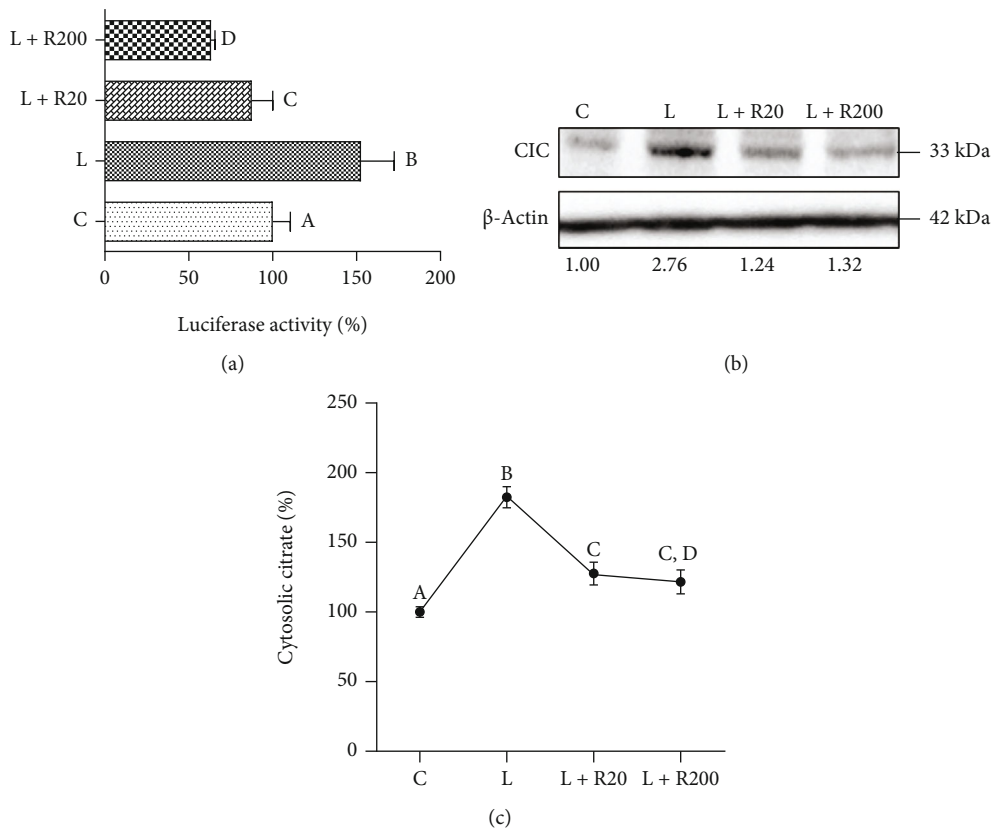

Figure 5: Effect of RWP on CIC and cytosolic citrate. (a) HEK293 cells were transiently transfected with SLC25A1pGL3, the pGL3 basic-LUC vector encompassing the −1785/−20 bp region of the *SLC25A1* gene cloned upstream of the luciferase reporter gene. Then, cells were triggered with LPS in the absence (LPS) or in the presence of RWP 20 μg/mL or RWP 200 μg/mL. Unstimulated cells (c) were used as a negative control. The luciferase gene reporter activity was assessed after 24 hours. (b) Primary human monocytes, preincubated for 1 hour with RWP 20 μg/mL or RWP 200 μg/mL, were activated to macrophages with LPS, and CIC protein levels were evaluated. CIC and β-actin proteins were immunodecorated with specific antibodies. The intensities of immunolabeled protein bands were measured by using a quantitative software and normalized to β-actin: values obtained are reported under western blot images. Protein expression levels in control sample were taken as 1, and other samples were expressed in proportion of the control. (c) In cells treated as in (b), cytosolic citrate levels were quantified. In (a) and (c), values represent means ± SD of three experiments with three replicates in each. Statistical analysis was performed by *one-way ANOVA* followed by *Tukey's test* for multiple comparisons. Different letters indicate significant differences at $p < 0.05$. C: control; L: LPS; R20: RWP 20 μg/mL; R200: RWP 200 μg/mL.

with respect to macrophages activated only with LPS (Figure 8(a)). The strongest reduction was observed with the lowest tested concentration of RWP (Figure 8(a)). Interestingly, acetate, a metabolite downstream of the citrate pathway, reverted the inhibition of COX2 induced by RWP (Figure 8(b)). A similar trend was observed when PGE_2 levels were measured in cell culture supernatants after 48 hours of incubation with LPS (Figure 8(c)). In details, RWP-stimulated cells showed PGE_2 levels similar to unstimulated cells. We observed a 40% decrease in PGE_2 levels when compared to LPS-triggered cells. On the other hand, the addition of acetate brought PGE_2 levels up (Figure 8(c)). This decreased PGE_2 level is most likely because of a decrease in PGE_2 production, due to a reduced availability of precursors for PGE_2 synthesis: as acetate can be converted to acetyl-CoA by acetyl-CoA synthase (ACSS), adding exogenous acetate rescues the effect of ACLY inhibition on PGE_2 production. These data, with the previous regarding the effect of RWP on ROS and $NO^{\cdot}$, strengthened and confirmed our hypothesis that the citrate pathway is a target of RWP in carrying out its anti-inflammatory activity.

4. Discussion

In this study, for the first time, we have investigated the biological properties of *Aglianico del Vulture* red wine and we have shown that it exerts potential health benefits thanks to its content in polyphenols well known to act as immunomodulators and anti-inflammatory molecules [1, 2, 5, 6, 9, 10, 46–49].

Malvidin 3-*O*-glucoside and cyanidin-3-*O*-glucoside are the most abundant phenolic compounds we have found, in accordance with the typical anthocyanin profiling of *Aglianico* wine, in which malvidin 3-*O*-glucoside represents about 60% while cyanidin-3-*O*-glucoside and delphinidin-3-*O*-glucoside are around 5% of total anthocyanidins [34]. These compounds were present in higher concentration with respect to another DOC red wine *Carignano del Sulcis*,

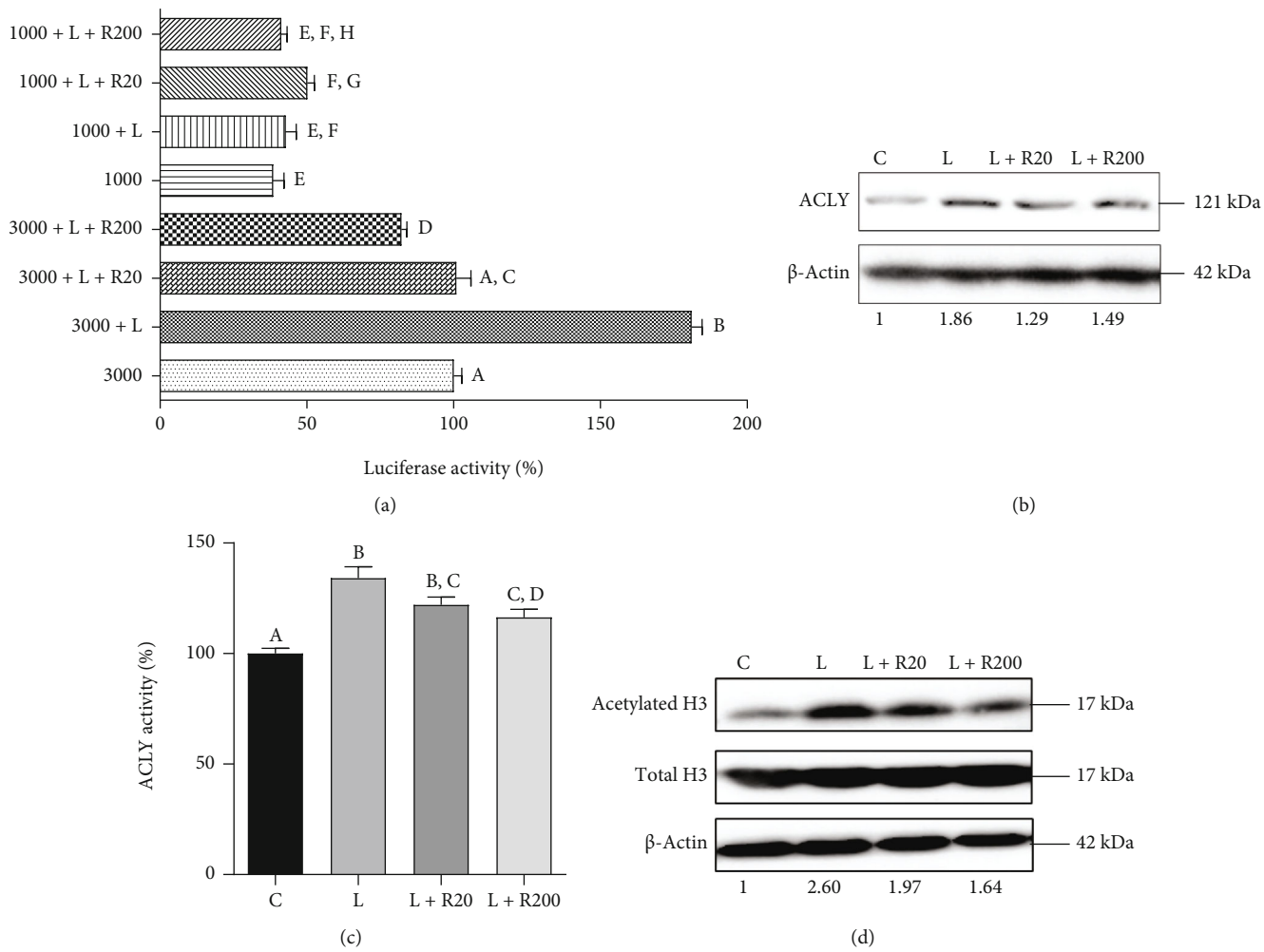

Figure 6: Effect of RWP on ACLY. (a) HEK293 cells were transiently transfected with pGL3 basic-LUC vectors containing the −3116/−20 bp full-length region of the *ACLY* gene promoter (3000) or a truncated version of this region (1000). Then, cells were triggered with LPS in the absence (LPS) or in the presence of RWP 20 μg/mL or RWP 200 μg/mL. Unstimulated cells were used as a negative control. The luciferase gene reporter activity was assessed after 24 hours. Primary human monocytes, preincubated for 1 hour with RWP, were activated to macrophages with LPS, and protein levels of ACLY (b) and acetylated H3 and total H3 (d) were evaluated. In (b, d) ACLY, acetylated H3, total H3, and β-actin proteins were immunodecorated with specific antibodies. The intensities of immunolabeled protein bands were measured by using a quantitative software and normalized to β-actin: values obtained are reported under western blot images. Protein expression levels in control sample were taken as 1, and other samples were expressed in the proportion of the control. (c) In cells treated as in (b, d) ACLY enzymatic activity was quantified. In (a) and (c), values represent means ± SD of three experiments with three replicates in each. Statistical analysis was performed by o*ne-way ANOVA* followed by *Tukey's test* for multiple comparisons. Different letters indicate significant differences at $p < 0.05$. C: control; L: LPS; R20: RWP 20 μg/mL; R200: RWP 200 μg/mL.

cultivated in the southwestern region of Sardinia (Italy) [24]. In our sample, the concentration of the stilbene resveratrol was lower (0.053 ± 0.01 mg/100 mL) than that of red wines from Veneto region (Italy), in which resveratrol averaged 0.083 mg/100 mL [50], and Campania region (Italy) [26]. On the other hand, the flavonol quercetin was more abundant in *Aglianico del Vulture* red wine, compared to the last red wines from Campania, in particular with respect to *Aglianico del Benevento* [26]. Finally, among the phenolic acids, a higher rate of caffeic acid was found in our sample in comparison with wines counted among the best wines for anti-inflammatory properties for their abundance in phenolic compounds, such as Cabernet Sauvignon, Merlot, Syrah, and Carménère [47].

Human primary monocytes have been used for our investigations. Cells were treated with LPS, which triggers innate immune responses leading to the secretion of cytokines IL-1β, IL-6, and TNF-α and proinflammatory mediators blocked by *Aglianico del Vulture* powder. On the other hand, RWP induced an increased release of IL-10, necessary to initiate host defence against microbial invasion [37]. However, excessive secretion of proinflammatory cytokines could be deleterious for the host since they cause systemic metabolic and hemodynamic disturbances. For that reason, macrophages produce IL-10, a potent anti-inflammatory cytokine produced by macrophages as a negative-feedback mechanism to dampen excessive inflammation during infection.

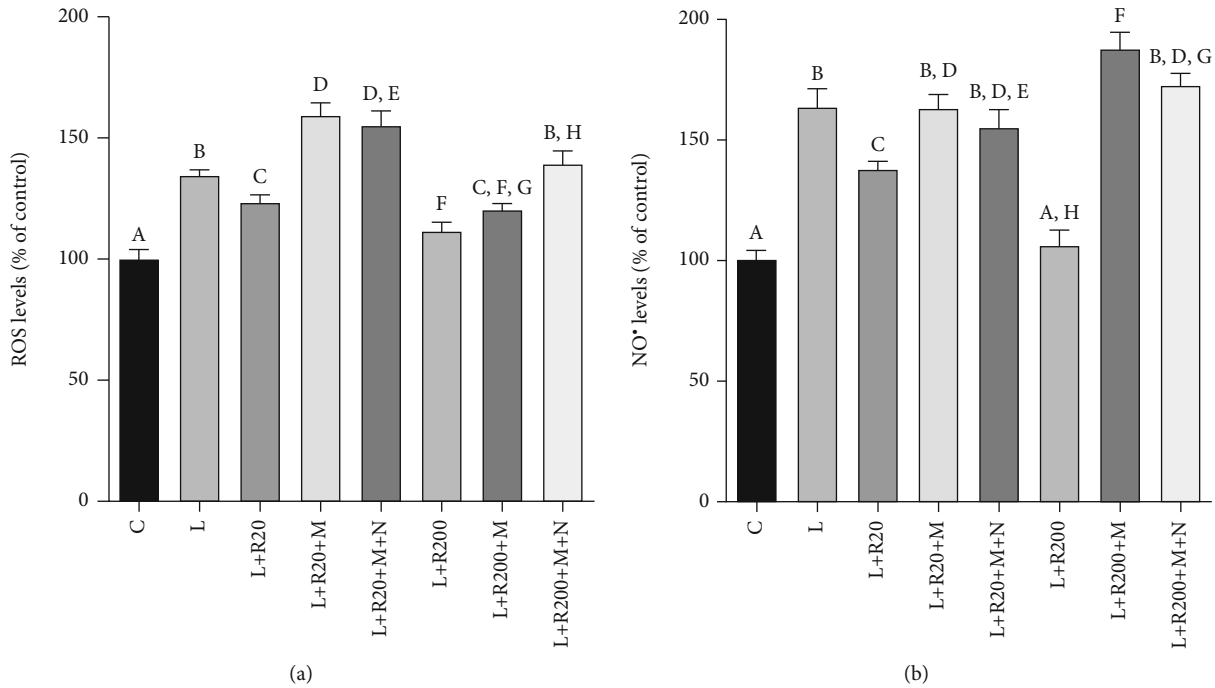

Figure 7: RWP lowered ROS and NO$^{\cdot}$ levels, restored by addition of exogenous malate and NADPH. Primary human monocytes were treated with LPS (L) in absence or in presence of RWP alone or plus malate and NADPH. Following 24 hours, ROS (a) and NO$^{\cdot}$ (b) levels were evaluated and expressed as the percentage of unstimulated cells (set at 100%). Mean values ± SD of three replicate independent experiments with five replicates in each are shown. According to *one-way* ANOVA, differences in ROS (a) and NO$^{\cdot}$ (b) levels were significant ($p < 0.001$). Therefore, *Tukey's post hoc test* was performed, and different letters indicate significant differences between treatments at $p < 0.05$. C: control; L: LPS; R20: RWP 20 μg/mL; R200: RWP 200 μg/mL; M: malate; N: NADPH.

These data are in line with the rescuing effect exerted by RWP on AnxA1 levels, which were decreased upon LPS activation. This impairment could lead to uncontrolled inflammation resulting in chronic disease following unbalance between inflammation and resolution [51]. Thus, RWP could modulate inflammatory response with an alternate mechanism, which controls the resolution pathway associated to the AnxA1/FPR2 axis.

In vitro and in vivo studies reported that polyphenols contained in red grapes and red wines are able to abrogate the LPS-mediated activation of NF-κB with consequent attenuation of the storm of proinflammatory cytokines released by monocytes [52], so that the NF-κB pathway has been identified as a critical target for the protective properties of a moderate wine consumption. Therefore, our attention was directed to evaluate the effect of RWP on an NF-κB transcription factor. As was to be expected, RWP reduced the expression of p65 subunit of NF-κB, promoter activity, and nuclear translocation of NF-κB. As a consequence of NF-κB inhibition, *SLC25A1* and *ACLY* gene promoter activities lowered with consequent reduction in CIC and ACLY protein levels; a parallel decrease in cytosolic citrate concentration and inflammatory mediators linked to the citrate pathway (ROS, NO$^{\cdot}$, and PGE_2) was observed. Obviously, the effect of the tested powder on ROS, NO$^{\cdot}$, and PGE_2 could also be a consequence of the direct inhibition of NF-κB since under its transcriptional controls are genes encoding for iNOS and COX2. However, the inhibition of the citrate pathway has a central role. In fact, treatments with metabolites downstream the citrate pathway removed RWP inhibitory effects on proinflammatory mediators: exogenous malate alone or in combination with NADPH reverted the reduction of ROS and NO$^{\cdot}$ levels; acetate did the same on PGE_2 concentration and COX2 expression levels. Analogous involvement of the citrate pathway was found in Down syndrome, where hydroxycitrate—a natural ACLY inhibitor—reduced the typical prooxidant status, but the addition of malate or NADPH abolished its antioxidant effect [19]. Similarly, *Pistacia lentiscus* hydrosol exhibited its anti-inflammatory activity acting through the citrate pathway [30].

Interestingly, RWP exerts its effect also at the epigenetic level, as shown by reduction of the acetylation of H3 histone. Acetyl-CoA, a product of the citrate pathway needed for histone acetylation [17], represents a key node in metabolism due to its intersection with many metabolic pathways and transformations, influencing the regulation of numerous life processes.

In addition to the effect on the citrate pathway, it cannot be ruled out that the RWP compounds contained in this wine might have other beneficial effect. In fact, it is known that increasing of cytokines IL-1β and TNF-α, with subsequent increased expression of adhesion molecules, contributes to lipid accumulation within the atheroma and dysregulated activity of vascular smooth muscle cells [53]. Thus, reduction of proinflammatory cytokines by RWP might also positively affect the cardiovascular system. Furthermore, since inflammation and ROS may induce the increase/decrease of several miRNAs, including oxidative stress-responsive miRNAs

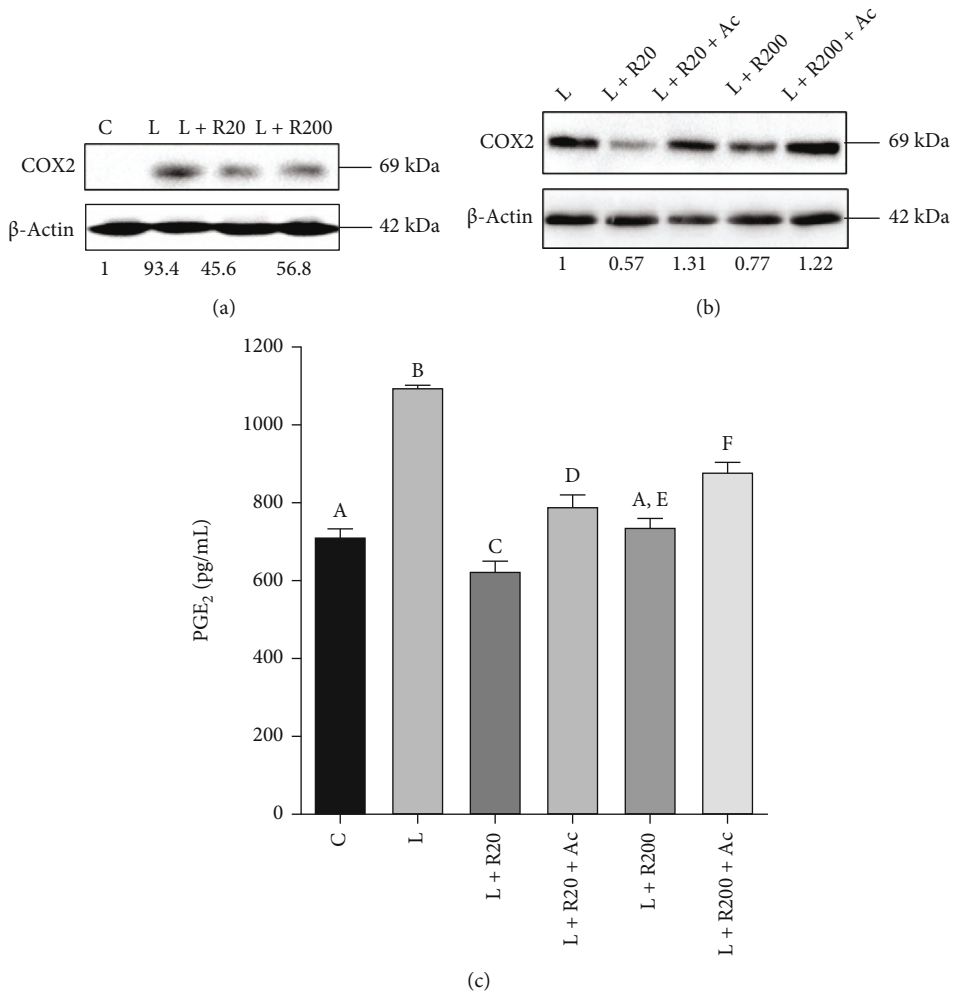

Figure 8: RWP lowered COX2 and PGE_2 levels. Primary human monocytes were activated to macrophages with LPS (LPS) in the absence or in the presence of RWP alone or plus acetate and COX2 (a, b), and PGE_2 levels were quantified. In (a) and (b), COX2 and β-actin proteins were immunodecorated with specific antibodies. The intensities of immunolabeled protein bands were measured by using a quantitative software and normalized to β-actin; values obtained are reported under western blot images. Protein expression levels in control sample were taken as 1, and other samples were expressed in proportion to the control. (c) Following 48 hours, PGE_2 levels were evaluated and expressed as the percentage of the levels in untreated cells (set at 100%). Mean values ± SD of three replicate independent experiments with three replicates in each are shown. According to *one-way* ANOVA, differences were significant ($p < 0.001$). Therefore, *Tukey's post hoc test* was performed, and different letters indicate significant differences between treatments at $p < 0.05$. C: control; L: LPS; R20: RWP 20 μg/mL; R200: RWP 200 μg/mL; Ac: acetate.

[54], it could also be hypothesized that these phytochemicals may also control the expression of some target miRNAs in both normal and pathological conditions [55]. For example, the phytochemical epigallocatechin gallate may act as an epigenetic modulator of DNA methylation and chromatin remodeling, leading to the alteration of gene expression and modification of miRNA activities [56]. Other beneficial effects, such as glucose homeostasis, mitochondrial function, energy metabolism, and stress responses, have been ascribed to phenolic compounds [57]. However, further investigations are needed to elucidate these and other potential beneficial effects of RWP.

In conclusion, our study highlights for the first time the contribution of red wine *Aglianico del Vulture* phenols in modulation of inflammatory response. Notably, our findings suggest a specific signature of this red wine showing its own phenolic profile. The underlying mechanism is associated to different pathways, including the suppression of inflammatory mediators and the inhibition of NF-κB and the citrate pathway. Bioactive compounds from red wines such as malvidin 3-*O*-glucoside and cyanidin-3-*O*-glucoside, quercetin and resveratrol, have been shown to inhibit inflammatory mediators via NF-κB [46, 48, 49]. The involvement of the citrate pathway is the strongest novelty, since this has never been investigated so far as a possible mechanism of action for any wine compounds. Here, we demonstrate that this pathway mediates several anti-inflammatory effects of the red wine *Aglianico del Vulture* phenols. In the recent years, the activation of ACLY and CIC—constituents of the citrate pathway—has been linked to the presence of inflammatory conditions [46, 48, 49]. Therefore, the citrate pathway seems a new hopeful target of inflammation. In this context, its

inhibition by red wine *Aglianico del Vulture* phenols—as a molecular mechanism underlying the regulation of macrophage function—could reveal very interesting applications in the prevention and treatment of inflammatory chronic diseases simply through bioactive food compounds.

5. Conclusions

For the first time, this study investigates the immunomodulatory and anti-inflammatory potential of red wine powder (RWP) extracted from the Italian red wine *Aglianico del Vulture.* RWP reduces IL-1β, IL-6, and TNF-α proinflammatory while increasing IL-10 anti-inflammatory cytokine secretion and inhibiting NF-κB promoter activity in macrophages induced by LPS. In addition, RWP activates proresolutive pathways by restoring Annexin A1 levels. Beyond the classical targets of macrophage function, we also identify the citrate pathway as a RWP target in carrying out its anti-inflammatory activity since, by reducing CIC and ACLY protein levels, ACLY enzymatic activity, RWP lowers ROS, $NO^{\cdot}$, PGE_2, and histone acetylation levels. Overall findings evidence that *Aglianico del Vulture* powder suppresses inflammatory pathways and activates proresolutive processes hinting the potential value of RWP in the prevention and treatment of inflammatory conditions as well as inflammatory chronic diseases.

Data Availability

The data used to support the findings of this study are available from the corresponding author upon request.

Conflicts of Interest

The authors declare no conflict of interest.

Acknowledgments

This research was supported by FSC European funds (grant number C31G19000020002) and Ministry of Education, University and Research (MIUR) PRIN (grant number 2017NKB2N4_004).

Supplementary Materials

Figure S1: MRM data in both positive and negative ions of a mix standard solution. *(Supplementary Materials)*

References

[1] N. Yahfoufi, N. Alsadi, M. Jambi, and C. Matar, "The immunomodulatory and anti-inflammatory role of polyphenols," *Nutrients*, vol. 10, no. 11, p. 1618, 2018.

[2] D. X. Hou, T. Yanagita, T. Uto, S. Masuzaki, and M. Fujii, "Anthocyanidins inhibit cyclooxygenase-2 expression in LPS-evoked macrophages: structure-activity relationship and molecular mechanisms involved," *Biochemical Pharmacology*, vol. 70, no. 3, pp. 417–425, 2005.

[3] M. Perretti and F. D'Acquisto, "Annexin A1 and glucocorticoids as effectors of the resolution of inflammation," *Nature Reviews. Immunology*, vol. 9, no. 1, pp. 62–70, 2009.

[4] G. Li, S. He, L. Chang et al., "GADD45α and annexin A1 are involved in the apoptosis of HL-60 induced by resveratrol," *Phytomedicine*, vol. 18, no. 8-9, pp. 704–709, 2011.

[5] J. W. Jeong, W. Lee, S. Shin, G. Y. Kim, B. Choi, and Y. Choi, "Anthocyanins downregulate lipopolysaccharide-induced inflammatory responses in BV2 microglial cells by suppressing the NF-κB and Akt/MAPKs signaling pathways," *International Journal of Molecular Sciences*, vol. 14, no. 1, pp. 1502–1515, 2013.

[6] S. Vendrame and D. Klimis-Zacas, "Anti-inflammatory effect of anthocyanins via modulation of nuclear factor- B and mitogen-activated protein kinase signaling cascades," *Nutrition Reviews*, vol. 73, no. 6, pp. 348–358, 2015.

[7] C. Caddeo, A. Nacher, A. Vassallo et al., "Effect of quercetin and resveratrol co-incorporated in liposomes against inflammatory/oxidative response associated with skin cancer," *International Journal of Pharmaceutics*, vol. 513, no. 1-2, pp. 153–163, 2016.

[8] T. Liang, R. Guan, Z. Quan, Q. Tao, Z. Liu, and Q. Hu, "Cyanidin-3-o-glucoside liposome: preparation via a green method and antioxidant activity in GES-1 cells," *Food Research International*, vol. 125, p. 108648, 2019.

[9] H. Wang, G. Cao, and R. L. Prior, "Oxygen radical absorbing capacity of anthocyanins," *Journal of Agricultural and Food Chemistry*, vol. 45, no. 2, pp. 304–309, 1997.

[10] T. Tsuda, K. Shiga, K. Ohshima, S. Kawakishi, and T. Osawa, "Inhibition of lipid peroxidation and the active oxygen radical scavenging effect of anthocyanin pigments isolated from *Phaseolus vulgaris* L," *Biochemical Pharmacology*, vol. 52, no. 7, pp. 1033–1039, 1996.

[11] L. A. J. O'Neill, R. J. Kishton, and J. Rathmell, "A guide to immunometabolism for immunologists," *Nature Reviews. Immunology*, vol. 16, no. 9, pp. 553–565, 2016.

[12] L. A. J. O'Neill and E. J. Pearce, "Immunometabolism governs dendritic cell and macrophage function," *The Journal of Experimental Medicine*, vol. 213, no. 1, pp. 15–23, 2016.

[13] V. Infantino, P. Convertini, L. Cucci et al., "The mitochondrial citrate carrier: a new player in inflammation," *The Biochemical Journal*, vol. 438, no. 3, pp. 433–436, 2011.

[14] V. Infantino, V. Iacobazzi, A. Menga, M. L. Avantaggiati, and F. Palmieri, "A key role of the mitochondrial citrate carrier (*SLC25A1*) in TNFα\- and IFNγ-triggered inflammation," *Biochimica et Biophysica Acta*, vol. 1839, no. 11, pp. 1217–1225, 2014.

[15] V. Infantino, V. Iacobazzi, F. Palmieri, and A. Menga, "ATP-citrate lyase is essential for macrophage inflammatory response," *Biochemical and Biophysical Research Communications*, vol. 440, no. 1, pp. 105–111, 2013.

[16] V. Infantino, C. L. Pierri, and V. Iacobazzi, "Metabolic routes in inflammation: the citrate pathway and its potential as therapeutic target," *Current Medicinal Chemistry*, vol. 26, no. 40, pp. 7104–7116, 2019.

[17] L. Shi and B. P. Tu, "Acetyl-CoA and the regulation of metabolism: mechanisms and consequences," *Current Opinion in Cell Biology*, vol. 33, pp. 125–131, 2015.

[18] N. C. Williams and L. A. J. O'Neill, "A role for the Krebs cycle intermediate citrate in metabolic reprogramming in innate immunity and inflammation," *Frontiers in Immunology*, vol. 9, p. 141, 2018.

[19] P. Convertini, A. Menga, G. Andria et al., "The contribution of the citrate pathway to oxidative stress in Down syndrome," *Immunology*, vol. 149, no. 4, pp. 423–431, 2016.

[20] A. Santarsiero, P. Leccese, P. Convertini et al., "New insights into Behçet's syndrome metabolic reprogramming: citrate pathway dysregulation," *Mediators of Inflammation*, vol. 2018, Article ID 1419352, 8 pages, 2018.

[21] H. Horai, M. Arita, S. Kanaya et al., "MassBank: a public repository for sharing mass spectral data for life sciences," *Journal of Mass Spectrometry*, vol. 45, no. 7, pp. 703–714, 2010.

[22] R. Aversano, F. Contaldi, M. G. Adelfi et al., "Comparative metabolite and genome analysis of tuber-bearing potato species," *Phytochemistry*, vol. 137, pp. 42–51, 2017.

[23] C. Chirollo, A. Vassallo, F. Dal Piaz et al., "Investigation of the persistence of penicillin G and dihydrostreptomycin residues in milk of lactating buffaloes (Bubalus bubalis) using ultra-high-performance liquid chromatography and tandem mass spectrometry," *Journal of Agricultural and Food Chemistry*, vol. 66, no. 25, pp. 6388–6393, 2018.

[24] C. I. G. Tuberoso, G. Serreli, F. Congiu, P. Montoro, and M. A. Fenu, "Characterization, phenolic profile, nitrogen compounds and antioxidant activity of Carignano wines," *Journal of Food Composition and Analysis*, vol. 58, pp. 60–68, 2017.

[25] C. I. G. Tuberoso, G. Serreli, P. Montoro, G. D'Urso, F. Congiu, and A. Kowalczyk, "Biogenic amines and other polar compounds in long aged oxidized Vernaccia di Oristano white wines," *Food Research International*, vol. 111, pp. 97–103, 2018.

[26] A. Gambuti, D. Strollo, M. Ugliano, L. Lecce, and L. Moio, "trans-Resveratrol, quercetin, (+)-catechin, and (-)-epicatechin content in south Italian monovarietal wines: relationship with maceration time and marc pressing during winemaking," *Journal of Agricultural and Food Chemistry*, vol. 52, no. 18, pp. 5747–5751, 2004.

[27] R. Medzhitov, "Inflammation 2010: new adventures of an old flame," *Cell*, vol. 140, no. 6, pp. 771–776, 2010.

[28] P. Convertini, V. Infantino, F. Bisaccia, F. Palmieri, and V. Iacobazzi, "Role of FOXA and Sp1 in mitochondrial acylcarnitine carrier gene expression in different cell lines," *Biochemical and Biophysical Research Communications*, vol. 404, no. 1, pp. 376–381, 2011.

[29] V. Infantino, V. Iacobazzi, F. D. Santis, M. Mastrapasqua, and F. Palmieri, "Transcription of the mitochondrial citrate carrier gene: role of SREBP-1, upregulation by insulin and downregulation by PUFA," *Biochemical and Biophysical Research Communications*, vol. 356, no. 1, pp. 249–254, 2007.

[30] A. Santarsiero, A. Onzo, R. Pascale et al., "Pistacia lentiscus Hydrosol: Untargeted Metabolomic Analysis and Anti-Inflammatory Activity Mediated by NF-κB and the Citrate Pathway," *Oxidative Medicine and Cellular Longevity*, vol. 2020, Article ID 4264815, 14 pages, 2020.

[31] T. C. Linn and P. A. Srere, "Identification of ATP citrate lyase as a phosphoprotein.," *The Journal of Biological Chemistry*, vol. 254, no. 5, pp. 1691–1698, 1979.

[32] T. Migita, T. Narita, K. Nomura et al., "ATP citrate lyase: activation and therapeutic implications in non-small cell lung cancer," *Cancer Research*, vol. 68, no. 20, pp. 8547–8554, 2008.

[33] A. Vassallo, V. Santoro, I. Pappalardo et al., "Liposome-mediated inhibition of inflammation by hydroxycitrate," *Nanomaterials (Basel)*, vol. 10, no. 10, p. 2080, 2020.

[34] S. Suriano, L. Tarricone, M. Savino, and M. R. Rossi, "Caratterizzazione fenolica di Uve di Aglianico e Uva di Troia coltivate nel nord barese," *Enologo Milano*, vol. 41, p. 71, 2005.

[35] E. Celotti, R. Ferrarini, R. Zironi, and L. S. Conte, "Resveratrol content of some wines obtained from dried Valpolicella grapes: Recioto and Amarone," *Journal of Chromatography A*, vol. 730, no. 1-2, pp. 47–52, 1996.

[36] F. Galgano, M. Caruso, G. Perretti, and F. Favati, "Authentication of Italian red wines on the basis of the polyphenols and biogenic amines," *European Food Research and Technology*, vol. 232, no. 5, pp. 889–897, 2011.

[37] R. Medzhitov, "Origin and physiological roles of inflammation," *Nature*, vol. 454, no. 7203, pp. 428–435, 2008.

[38] S. Ghosh and M. S. Hayden, "New regulators of NF-κB in inflammation," *Nature Reviews. Immunology*, vol. 8, no. 11, pp. 837–848, 2008.

[39] C. Di Lorenzo, C. Stockley, F. Colombo et al., "The role of wine in modulating inflammatory processes: a review," *Beverages*, vol. 4, no. 4, p. 88, 2018.

[40] N. C. Williams and L. A. O'Neill, "ACLY-matizing macrophages to histone modification during immunometabolic reprogramming," *Trends in Immunology*, vol. 41, no. 2, pp. 93-94, 2020.

[41] M. A. Lauterbach, J. E. Hanke, M. Serefidou et al., "Toll-like receptor signaling rewires macrophage metabolism and promotes histone acetylation via ATP-citrate lyase," *Immunity*, vol. 51, no. 6, pp. 997–1011.e7, 2019.

[42] M. G. Daskalaki, C. Tsatsanis, and S. C. Kampranis, "Histone methylation and acetylation in macrophages as a mechanism for regulation of inflammatory responses," *Journal of Cellular Physiology*, vol. 233, no. 9, pp. 6495–6507, 2018.

[43] S. Todisco, P. Convertini, V. Iacobazzi, and V. Infantino, "TCA cycle rewiring as emerging metabolic signature of hepatocellular carcinoma," *Cancers (Basel)*, vol. 12, no. 1, p. 68, 2020.

[44] F. Aktan, "iNOS-mediated nitric oxide production and its regulation," *Life Sciences*, vol. 75, no. 6, pp. 639–653, 2004.

[45] J. Anrather, G. Racchumi, and C. Iadecola, "NF-κB regulates phagocytic NADPH oxidase by inducing the expression of gp91," *The Journal of Biological Chemistry*, vol. 281, no. 9, pp. 5657–5667, 2006.

[46] A. Decendit, M. Mamani-Matsuda, V. Aumont et al., "Malvidin-3-O-β glucoside, major grape anthocyanin, inhibits human macrophage- derived inflammatory mediators and decreases clinical scores in arthritic rats," *Biochemical Pharmacology*, vol. 86, no. 10, pp. 1461–1467, 2013.

[47] I. Kekelidze, N. Ebelashvili, M. Japaridze, B. Chankvetadze, and L. Chankvetadze, "Phenolic antioxidants in red dessert wine produced with innovative technology," *Annals of Agrarian Science*, vol. 16, no. 1, pp. 34–38, 2018.

[48] M. M. Ma, Y. Li, X. Y. Liu et al., "Cyanidin-3-O-glucoside ameliorates lipopolysaccharide-induced injury both in vivo and in vitro suppression of NF-κB and MAPK pathways," *Inflammation*, vol. 38, no. 4, pp. 1669–1682, 2015.

[49] M. M. Poulsen, K. Fjeldborg, M. J. Ornstrup, T. N. Kjær, M. K. Nøhr, and S. B. Pedersen, "Resveratrol and inflammation: challenges in translating pre-clinical findings to improved patient outcomes," *Biochimica et Biophysica Acta*, vol. 1852, no. 6, pp. 1124–1136, 2015.

[50] G. J. Soleas, D. M. Goldberg, E. Ng, A. Karumanchiri, E. Tsang, and E. P. Diamandis, "Comparative evaluation of four

methods for assay of cis- and trans-resveratrol," *American Journal of Enology and Viticulture*, vol. 48, pp. 169–176, 1997.

[51] G. Schett and M. F. Neurath, "Resolution of chronic inflammatory disease: universal and tissue-specific concepts," *Nature Communications*, vol. 9, no. 1, p. 3261, 2018.

[52] T. Magrone and E. Jirillo, "Polyphenols from red wine are potent modulators of innate and adaptive immune responsiveness," *The Proceedings of the Nutrition Society*, vol. 69, no. 3, pp. 279–285, 2010.

[53] B. J. von Scholten, H. Reinhard, T. W. Hansen et al., "Markers of inflammation and endothelial dysfunction are associated with incident cardiovascular disease, all-cause mortality, and progression of coronary calcification in type 2 diabetic patients with microalbuminuria," *Journal of Diabetes and its Complications*, vol. 30, no. 2, pp. 248–255, 2016.

[54] R. Otton, A. P. Bolin, L. T. Ferreira, M. P. Marinovic, A. L. S. Rocha, and M. A. Mori, "Polyphenol-rich green tea extract improves adipose tissue metabolism by down- regulating miR-335 expression and mitigating insulin resistance and inflammation," *The Journal of Nutritional Biochemistry*, vol. 57, pp. 170–179, 2018.

[55] M. A. Potenza, D. Iacobazzi, L. Sgarra, and M. Montagnani, "The intrinsic virtues of EGCG, an extremely good cell guardian, on prevention and treatment of diabesity complications," *Molecules*, vol. 25, no. 13, p. 3061, 2020.

[56] M. Z. Fang, Y. Wang, N. Ai et al., "Tea polyphenol (-)-epigallocatechin-3-gallate inhibits DNA methyltransferase and reactivates methylation-silenced genes in cancer cell lines," *Cancer Research*, vol. 63, no. 22, pp. 7563–7570, 2003.

[57] Q. Meng, C. N. Velalar, and R. Ruan, "Regulating the age-related oxidative damage, mitochondrial integrity, and antioxidative enzyme activity in Fischer 344 rats by supplementation of the antioxidant epigallocatechin-3-gallate," *Rejuvenation Research*, vol. 11, no. 3, pp. 649–660, 2008.

Hindawi
Oxidative Medicine and Cellular Longevity
Volume 2021, Article ID 5543025, 12 pages
https://doi.org/10.1155/2021/5543025

Research Article

Walnut Supplementation Restores the SIRT1-FoxO3a-MnSOD/Catalase Axis in the Heart, Promotes an Anti-Inflammatory Fatty Acid Profile in Plasma, and Lowers Blood Pressure on Fructose-Rich Diet

Maja Bošković,[1] Maja Živković,[1] Goran Korićanac,[2] Jelena Stanišić,[2] Manja Zec,[3] Irena Krga,[3] and Aleksandra Stanković[1]

[1]*VINČA Institute of Nuclear Sciences, National Institute of the Republic of Serbia, Laboratory for Radiobiology and Molecular Genetics, University of Belgrade, Belgrade, Serbia*
[2]*VINČA Institute of Nuclear Sciences, National Institute of the Republic of Serbia, Laboratory for Molecular Biology and Endocrinology, University of Belgrade, Belgrade, Serbia*
[3]*Center of Research Excellence in Nutrition and Metabolism, Institute for Medical Research, National Institute of the Republic of Serbia, University of Belgrade, Belgrade 11000, Serbia*

Correspondence should be addressed to Aleksandra Stanković; alexas@vinca.rs

Received 25 January 2021; Revised 1 April 2021; Accepted 8 April 2021; Published 22 April 2021

Academic Editor: Stefania D'Adamo

The benefits of walnut (*Juglans regia*) consumption for metabolic health are known, but the molecular background underlying their putative antioxidant and anti-inflammatory/immunomodulatory effects is underexplored. We assessed that walnut supplementation (6 weeks) reverted unfavorable changes of the SIRT1/FoxO3a/MnSOD/catalase axis in the heart induced by fructose-rich diet (FRD). Intriguingly, Nox4 was increased by both FRD and walnut supplementation. FRD increased the cytosolic fraction and decreased the nuclear fraction of the uniquely elucidated ChREBP in the heart. The ChREBP nuclear fraction was decreased in control rats subjected to walnuts. In addition, walnut consumption was associated with a reduction in systolic BP in FRD and a decrease in fatty acid AA/EPA and AA/DHA ratios in plasma. In summary, the protective effect of walnut supplementation was detected in male rats following the fructose-induced decrease in antioxidative/anti-inflammatory capacity of cardiac tissue and increase in plasma predictors of low-grade inflammation. The current results provide a novel insight into the relationship between nutrients, cellular energy homeostasis, and the modulators of inflammatory/immune response in metabolic syndrome, emphasizing the heart and highlighting a track for translation into nutrition and dietary therapeutic approaches against metabolic disease.

1. Introduction

An increase in total fructose consumption over the past several decades has been correlated with metabolic syndrome (MetS) [1] and chronic inflammation [2]. The state of chronic inflammation in MetS can be described as a tissue-level stress response named "parainflammation" characterized by low-grade chronic activation of the immune system [3]. Maladaptive immune and inflammatory responses lead to systemic and cardiovascular insulin resistance [4], which are linked with MetS, cardiovascular disease (CVD) [5], and elevated oxidative stress [6, 7].

The role of nuts in the improvement of metabolic health, weight management, and glucose/insulin homeostasis markers and prevention of insulin resistance, hyperinsulinemia, dyslipidemia, and hypertension, the main characteristics of MetS, was suggested but studies are quite rare [8, 9]. In the protection of CVD, walnuts have the leading role [10], with the highest amount of a polyunsaturated omega-3 fatty acids (n-3 PUFAs), which have

antioxidant and anti-inflammatory/immunomodulatory effects on the heart [11, 12]. They can be easily used in nutrition and could be essential for use in low-marine food intake countries. It has been shown that several different n-3 PUFA derivatives, docosahexaenoic acid (DHA), and alpha-linolenic acid (ALA) decrease ROS and NO production in LPS-stimulated macrophages [13, 14]. On the other hand, omega-6 fatty acids (arachidonic acid (AA)) are the precursor of inflammatory agents such as PGE2, cytokines, and interleukins and may have proinflammatory effects [15]. An unbalanced omega-6/omega-3 ratio in favor of omega-6 PUFAs contributes to MetS-related diseases [16] and have effects on immune cells [11]. An elevated AA/eicosapentaenoic acid (EPA) ratio represents an inflammatory biomarker in certain chronic diseases [17]; however, its capacity related to MetS-related diseases and diverse nutritional treatments is not fully understood.

Recent research suggests a strong link between the cellular energy homeostasis and immune cell activation and triggering of inflammation in response to cell and tissue damage [18]. It is supported by recent findings of the AMP-activated protein kinase (AMPK) role in inflammation and immunity [19], through AMPK repression of aerobic glycolysis and activation of mitochondrial oxidative metabolism. This role of AMPK in the inhibition of oxidative stress and inflammation seems to be closely related to a group of fuel-sensing molecules, the sirtuins, both involved in metabolic syndrome-associated diseases [20]. AMPK and sirtuin 1 (SIRT1) activate each other, suggesting the existence of an AMPK-SIRT1 cycle that links the cell's energy and redox states [20]. SIRT1 deacetylates the transcriptional regulator, forkhead box O3 (FoxO3a), thereby promoting the initiation of FoxO3a-dependent gene transcription [21] and upregulation of the expression of genes involved in antioxidative defence, such as mitochondrial manganese superoxide dismutase (MnSOD) and catalase [22, 23]. Recent studies have established a central role of SIRT1 in the relationship of the immune response to metabolism that are closely dependent on each other. SIRT1-mediated regulation of cellular metabolism reprogramming [24] is closely linked to a SIRT1 role in the appropriate dendritic cell function and innate immunity. Namely, the absence of SIRT1 alters the mitochondrial function and metabolic phenotype, resulting in the induction of fatty acid synthesis and leading to dysregulation of innate and adaptive immunity [25]. Recent findings [26] support a role of SIRT1 in the switch from early to late inflammation. SIRT1 inactivates NADPH oxidase 4 (Nox4) in cardiomyocytes [27] and rat aorta [28], which is of utmost importance for cardiomyocytes, as Nox4 is the major source of mitochondrial oxidative stress [29]. SIRT1 could be repressed by direct binding of the carbohydrate response element-binding protein (ChREBP) to its promoter, in metabolic active tissues [30]. ChREBP regulates gene transcription in glycolysis/fructolysis and de novo lipogenesis [31], which suggests its important role in the pathogenesis of metabolic diseases. Recent data [32] establish a critical role for ChREBP in preventing macrophage inflammation and apoptosis in atherosclerosis and demonstrate the importance of immune metabolic flux in chronic inflammatory diseases.

Based on the pointed relationship between mitochondria metabolism and inflammation/immunity and our previous findings [33] regarding fructose effects on target molecules in the heart, we hypothesized that walnut-enriched diet should have the capacity to revert the fructose-rich diet-induced changes in (1) metabolic stress axis mitochondrial molecule SIRT1-FoxO3a-MnSOD/catalase in the rat heart and Nox4 and ChREBP, as its unfavorable regulators, and (2) harmful ratios of proinflammatory/anti-inflammatory plasma PUFAs (omega-6/omega-3 fatty acid ratio), to achieve cardioprotective effects. This work will give a new insight into the relationship between nutrients, cellular energy homeostasis, and the modulators of the inflammatory/immune response in MetS, emphasizing that the heart as the molecular background of walnut supplementation in metabolic disorders has not been fully addressed, yet.

2. Materials and Methods

2.1. Walnut Characterization. Walnuts (*Juglans regia*) used in this study were purchased from a local market. A recent study described the complete fatty acid, macronutrient, and mineral composition of the walnuts [34]. In terms of fatty acid content, the most abundant n-3 fatty acid in the walnuts was ALA (C18:3 *n*-3, 11.2%), while linoleic acid (C18:2 *n*-6, 63.2%) was the most abundant n-6 fatty acid identified by gas chromatography, similar to the data reported in the European Food Information Resource [35].

2.2. Animal Model and Treatment. Twenty-one-day-old male Wistar rats were randomly divided into two groups according to diet regime—control group (C) ($n = 18$), with free access to tap water and standard commercial rat chow, and the fructose-fed group (F) ($n = 18$), with free access to the same food and 10% (w/v) fructose solution instead of tap water. Rats were housed in individual cages (3 rats per cage) and maintained under standard temperature (22°C) and 12 h light/dark cycles. This diet regime lasted for nine weeks. After that period, half of the control (CW) and fructose-fed rats received 2.4 g of dietary walnuts daily (FW), an amount which corresponds to half of the kernel. To ensure the original PUFA content in the walnuts, they were given to animals as whole kernels ensuring that they were eaten by each animal. After six weeks of this diet regime, all rats were sacrificed by decapitation and their hearts were removed, washed in saline, and stored at −70°C until analysis, while blood samples were collected in EDTA-containing tubes for biochemical measurements. A total of 36 animals participated in the experiment (9 animals per group), corresponding to the standards of statistics and ethics. Experimental protocols were approved by the Ethical Committee of the "Vinča" Institute of Nuclear Sciences for the Use of Laboratory Animals and performed in accordance with the guidelines of Directive 2010/63/EU of the European Parliament.

2.3. Feeding Behavior, Metabolic Parameters, and Blood Pressure of Experimental Animals. Food intake and liquid intake were recorded daily, while body mass was recorded weekly during the study period. Energy intake from the

standard food, fructose solution, and walnuts was calculated and expressed as daily intake in kJ per rat.

The heart mass was weighted after removing from the body (absolute) and expressed relative to total body mass. Systolic blood pressure (SBP) and diastolic blood pressure (DBP) as well as heart rate frequency (HRF) were measured after dietary intervention in conscious rats by a noninvasive, computerized tail-cuff method BP system (Rat Tail Cuff Method Blood Pressure Systems (MRBP-R), IITC Life Science Inc., USA) with external preheating [36]. Mean arterial pressure (MAP), the average pressure in arteries during one cardiac cycle, was calculated as DBP plus 1/3 (SBP minus DBP). Pulse pressure (PP) was calculated as the difference between SBP and DBP.

2.4. Fatty Acid Analysis in Total Plasma Lipids. Blood samples were collected in EDTA tubes following overnight fasting, and fatty acids were analyzed as described before [37]. Briefly, plasma was separated by centrifugation ($1600 \times g$, 10 min), aliquoted, and stored at −20°C until analysis. Total plasma lipids were extracted by the method of Folch et al. [38] using a chloroform-methanol mixture (2 : 1) with 0.05% (w/v) butylated hydroxytoluene. Fatty acids were esterified to methyl esters which were reconstituted in hexane and separated by gas chromatography on the Shimadzu chromatograph (GC-2014, Kyoto, Japan) equipped with a flame ionization detector and an RTX 2330-fused silica gel capillary column (60 m × 0.25 mm id × 0.2 μm film thickness) (Restek Co., Bellefonte, PA, USA). For the purposes of the current study, arachidonic acid (AA) (20 : 4 n-6), eicosapentaenoic acid (EPA) (20 : 5 n-3), and docosahexaenoic acid (DHA) (22 : 6 n-3) were identified by comparing the peak retention times with a PUFA-2 standard mixture and Supelco 37 Component FAME Mix (Supelco Inc., Bellefonte, PA, USA). The amounts of individual fatty acids in plasma were presented as a percentage of the total identified fatty acids in the total lipid pool.

2.5. Cardiac Lysate Preparation. Cardiac tissue from three animals of the same group was pooled to prepare lysate, cytosolic, and nuclear fractions. Frozen pooled hearts were thawed and homogenized on ice with an Ultra-Turrax Homogenizer in modified RIPA buffer (pH 7.4) containing 50 mM Tris–HCl, pH 7.4, 150 mM NaCl, 1% Triton X-100, 0.2% Na-deoxycholate, 0.2% SDS, 1 mM EDTA, pH 7.4, protease inhibitors (1 mM PMSF, 10 μg/mL leupeptin, and 10 μg/mL aprotinin), and phosphatase inhibitors (1 mM activated sodium orthovanadate and 10 mM sodium fluoride). The homogenates were centrifuged at $15000 \times g$ for 30 min at 4°C. Supernatants were boiled in Laemmli sample buffer and used as a cardiac cell lysate for Western blot analysis.

2.6. Preparation of Cytosolic and Nuclear Fractions. The rest of the total pooled heart weight was homogenized on ice with an Ultra-Turrax Homogenizer in homogenization TEMG buffer (pH 7.5) containing 50 mM Tris–HCl, 1 mM EDTA, 12 mM monothioglycerol, 10% glycerol (v/v), protease, and phosphatase inhibitors. The cell lysate was filtered through gauze and centrifuged ($1000 \times g$, 15 min). Cytosolic proteins were isolated from the original supernatant (Sn1), while nuclear proteins were isolated from the original pellet. The original supernatant (Sn1) was centrifuged at $12000 \times g$ for 30 min. The upper phase containing cytosolic proteins was collected by centrifugation of the supernatant (Sn2) at $100000 \times g$ for 1 h. The original pellet was washed twice in TMG + 0.2% Triton X-100 buffer and once in TMG buffer, pH 7.5 (20 mM Tris–HCl, 12 mM monothioglycerol, and 10% glycerol (v/v)), followed by centrifugation ($1000 \times g$, 15 min) after each wash. The resulting pellet was resuspended in TEMG + 0.5 M KCL buffer and incubated on ice for 1 h with frequent vortexing. The supernatant containing nuclear proteins was collected by centrifugation of this resuspended pellet (34 200 rpm, 1 h). Samples were boiled in Laemmli sample buffer and used as a cardiac cytosolic and nuclear fraction for Western blot analysis.

2.7. Western Blot Analysis. Cardiac proteins (50 μg/lane) were separated by electrophoresis on 10% SDS polyacrylamide gels and transferred to polyvinylidene fluoride (PVDF) membranes. The uniformity of protein loading in each lane was assessed by staining the membranes with Ponceau S (Sigma-Aldrich, P3504), and this total protein staining quantified by ImageJ software was used as a loading control [39]. After destaining, membranes were blocked with 5% (w/v) milk in TBST and incubated with primary antibody for AMPK (sc-25792), SIRT1 (sc-74465), FoxO3a (sc-11351), MnSOD (sc-30080), catalase (ab16731), Nox4 (ab133303), or ChREBP (NB400-135) overnight. Unbound and nonspecifically bound antibodies were washed with TBST, and membranes were incubated with horseradish peroxidase- (HRP-) conjugated secondary anti-rabbit antibody (for AMPK, FoxO3a, MnSOD, catalase, and ChREBP antibody) or anti-mouse antibody (for SIRT1 antibody) (Santa Cruz Biotechnology) for 1.5 h at room temperature. After washing, the proteins were visualized by the enhanced chemiluminescence (ECL) method. The films were scanned, and quantitative analyses based on densitometry of protein bands on X-ray film were performed by ImageJ software (NIH, USA). As AMPK, FoxO3a, and ChREBP shuttle between the nucleus and the cytoplasm, protein levels of their total forms were determined in the cytosolic and nuclear fractions of cardiac tissue. The levels of SIRT1, MnSOD, catalase, and Nox4 were determined in the cardiac cell lysate. All Western blot experiment results were expressed as the protein/total protein staining ratio. The levels of proteins are presented as a fold of the appropriate control value.

2.8. Statistical Analysis. Statistical analysis was performed using Statistica software package. Data were expressed as mean ± standard deviation (SD) for 9 animals per experimental group (a total of 36 animals). The results were analyzed using two-way analysis of variance (ANOVA) (evaluating fructose and walnut factors, as well as mutual interactions), followed by the Tukey's post hoc test to evaluate differences between groups. A value of $p < 0.05$ was considered as statistically significant.

Table 1: Effects of fructose-rich diet and walnut supplementation on total body mass, relative heart mass, and blood pressure in experimental rats.

	C	CW	F	FW	Two-way ANOVA		
					W	F	F × W
Total body mass (g)	463.22 ± 34.3	513.33 ± 36.54*	485.44 ± 30.78	554.44 ± 33.22***,$$$	<0.001	<0.01	NS
Heart mass/total body mass (×100)	0.25 ± 0.02	0.23 ± 0.02	0.24 ± 0.01	0.22 ± 0.03*	<0.01	NS	NS
SBP (mm·hg)	147.4 ± 3.36	149.8 ± 3.49	150.8 ± 5.54	138.8 ± 4.97*,$$,##	<0.05	NS	<0.01
DBP (mm·hg)	84.6 ± 6.8	91 ± 9.49	88.8 ± 13.81	84.6 ± 5.03	NS	NS	NS
HRF (beats/min)	359.6 ± 29.31	323.2 ± 29.52	390.4 ± 42.17	336.6 ± 27.02	<0.01	NS	NS
MAP (mm·hg)	103.17 ± 6.3	107.06 ± 10.21	106.06 ± 12.39	107.17 ± 9.33	NS	NS	NS
PP (mm·hg)	62.5 ± 9.89	58.17 ± 10.15	62.67 ± 10.98	54.50 ± 15.67	NS	NS	NS

Data are presented as mean ± SD for 9 animals per group. A value of $p < 0.05$ was considered as statistically significant. C: animals on standard laboratory chow; CW: animals on standard laboratory chow and walnut supplementation; F: animals fed a fructose-rich diet; FW: fructose-fed animals on walnut supplementation; SBP: systolic blood pressure; DBP: diastolic blood pressure; HRF: heart rate frequency; MAP: mean arterial pressure; NS: not significant. Significantly different from *control, #walnuts, and $fructose. Significance is *$p < 0.05$, ##$$$ $p < 0.01$, and ***$$$ $p < 0.001$.

3. Results

3.1. Relative Heart Mass, Blood Pressure, and Heart Rate Frequency in Experimental Treatments. We calculated the energy intake in kJ/day/rat and expressed intake from each source (chow food, fructose solution, and walnut) as a percentage of the total. Control animals had 100% chow energy intake. The total energy intake of CW rats was the sum of chow energy intake (90.66%) and walnut energy intake (9.34%); while in the F group, it was the sum of the chow energy intake (63.27%) and liquid energy intake (36.73%). The FW group had a total energy intake from all three sources: chow energy intake (59.13%), liquid energy intake (33.43%), and walnut energy intake (7.44%). There was no significant difference in liquid energy intake in the F and FW groups yet; as previously published in the current animal model, the significant main effect of fructose ($p < 0.001$) and walnut supplementation ($p < 0.01$) on total energy intake was detected [40].

We detected significant main effects of walnut supplementation on relative heart mass (two-way ANOVA, $p < 0.01$), but post hoc comparisons showed a significant difference only between control animals and combined fructose and walnut treatment ($p = 0.04$) (Table 1). Total body mass at the end of the study was affected by both factors, FRD ($p < 0.01$) and walnut supplementation ($p < 0.001$).

We also demonstrated the significant main effects of walnut supplementation and fructose × walnut interaction ($p < 0.01$, partial eta-squared 0.45, observed power 0.93 for alpha = 0.05) on systolic blood pressure, while these factors did not show any significant effect on diastolic blood pressure (Table 1). Walnut supplementation gained the significant main effect on the heart rate frequency ($p < 0.01$) (Table 1). Post hoc test revealed no effect of walnut-enriched diet on blood pressure and heart rate frequency of control rats; but in fructose-fed rats, walnut supplementation was associated with a significant reduction in systolic blood pressure (F vs FW, $p < 0.01$, and C vs FW, $p < 0.05$) and showed trend toward a decrease in heart rate frequency (F vs FW, $p = 0.08$). However, fructose and walnut consumption and their interaction did not have a significant effect on either MAP or PP.

3.2. Effects of Fructose-Rich Diet and Walnut Supplementation on AA/EPA and AA/DHA in Total Plasma Lipids. Our results showed that the intake of walnuts reversed the fructose-induced increase in AA/EPA (p for interaction < 0.001, partial eta-squared 0.39, and observed power 0.99 for alpha = 0.05). On the other hand, regardless of the metabolic burden associated with fructose intake, walnut supplementation decreased AA/DHA levels ($p = 0.013$, Table 2).

3.3. Effects of Fructose-Rich Diet and Walnut Supplementation on the Protein Content of AMPK-SIRT1-FoxO3a-MnSOD/Catalase, ChREBP, and Nox4 in the Heart of Male Rats. Our results did not show any significant effect of fructose/walnut supplementation or fructose × walnut interaction on the cytosolic or nuclear AMPK protein level in the rat heart (Figures 1(a) and 1(b)).

The results showed the significant main effects of fructose ($p < 0.05$) and fructose × walnut interaction ($p < 0.001$, partial eta-squared 0.30, and observed power 0.98 for alpha = 0.05) on the SIRT1 protein level (Figure 2). FRD significantly decreased the SIRT1 protein level in rat hearts compared to control animals (C vs F, $p < 0.001$), while the walnut supplementation of fructose-fed animals elevated its level compared to rats fed only fructose (F vs FW, $p < 0.01$).

The results demonstrated a significant effect of fructose × walnut interaction on the cytosolic FoxO3a protein level ($p < 0.05$, partial eta-squared 0.10, and observed power 0.54 for alpha = 0.05) and significant main effects of fructose ($p < 0.05$) and walnut supplementation ($p < 0.001$) on the nuclear FoxO3a protein level (Figures 3(a) and 3(b)). FRD significantly increased the cytosolic FoxO3a protein level (C vs F, $p < 0.05$), while walnut supplementation elevated the nuclear FoxO3a protein level in the hearts of both, control (C vs CW, $p < 0.001$) and fructose-fed rats (F vs FW, $p < 0.001$, and C vs FW, $p < 0.001$, respectively).

Table 2: Effects of fructose-rich diet and walnut supplementation on the total plasma AA/EPA and AA/DHA ratio in experimental rats.

	C	CW	F	FW	Two-way ANOVA		
					F	W	F × W
AA/EPA	116 ± 58	87.09 ± 20.31	204.50 ± 46.87	58.92 ± 17.09	0.032	0.000	0.000
AA/DHA	15.17 ± 7.35	8.28 ± 2.61	12.36 ± 3.80	11.17 ± 2.35	0.977	0.013	0.071

Data are presented as mean ± SD for 9 animals per group. A value of $p < 0.05$ was considered as statistically significant. C: animals on standard laboratory chow; F: animals fed a fructose-rich diet; CW: animals on standard laboratory chow and walnut supplementation; FW: fructose-fed animals on walnut supplementation; AA: arachidonic acid (20 : 4 *n*-6); EPA: eicosapentaenoic acid (20 : 5 *n*-3); DHA: docosahexaenoic acid (22 : 6 *n*-3).

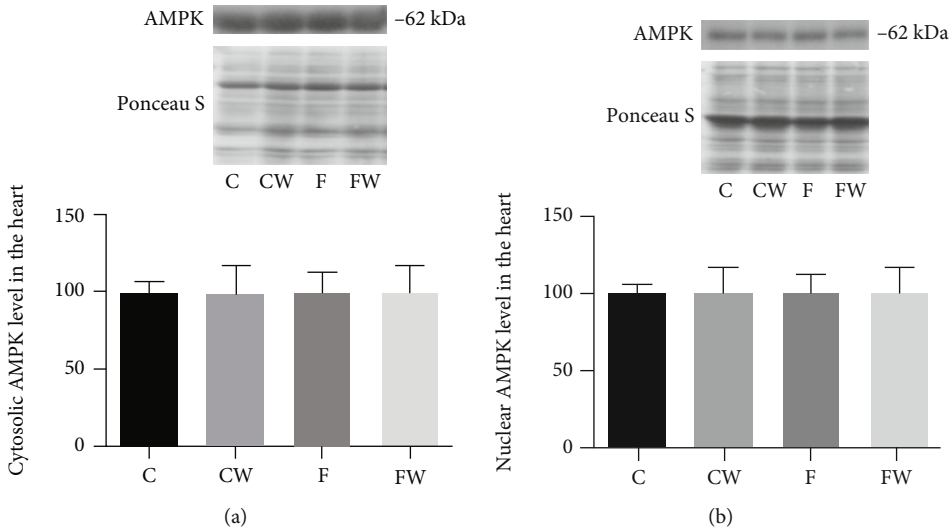

Figure 1: Effects of fructose-rich diet and supplementation with walnuts on the (a) cytosolic and (b) nuclear AMPK protein levels in the heart of experimental rats. Values are means with standard deviations represented by vertical bars for 9 animals per group. C: animals on standard laboratory chow; F: animals fed a fructose-rich diet; CW: animals on standard laboratory chow and walnut supplementation; FW: fructose-fed animals on walnut supplementation.

Significant main effects of fructose and walnut supplementation on the MnSOD ($p < 0.001$ and $p < 0.01$, respectively) and catalase ($p < 0.001$ and $p < 0.001$, respectively) protein levels were detected (Figures 4(a) and 4(b)). FRD decreased the MnSOD and catalase protein levels (C vs F, $p < 0.01$, for both), while walnut supplementation reverted these changes (F vs FW, $p < 0.05$ and $p < 0.01$, respectively). Walnut-enriched diet significantly increased the catalase level even in control animals (C vs CW, $p < 0.05$).

The significant main effects of fructose ($p < 0.001$) and walnut supplementation ($p < 0.01$) as well as a significant effect of fructose × walnut interaction ($p < 0.05$, partial eta-squared 0.15, and observed power 0.72 for alpha = 0.05) on the Nox4 protein level were detected (Figure 5). Post hoc analyses revealed a significant increase in Nox4 protein expression after both FRD (C vs F, $p < 0.001$) and walnut supplementation (C vs CW, $p < 0.01$, and C vs FW, $p < 0.001$) compared to the control group.

A significant main effect of fructose on the cytosolic ChREBP protein level ($p < 0.01$) as well as a significant effect of fructose × walnut interaction on the nuclear ChREBP protein level ($p < 0.001$, partial eta-squared 0.25, and observed power 0.99 for alpha = 0.05) was demonstrated (Figures 6(a) and 6(b)). Post hoc analyses revealed that FRD increased the ChREBP protein level in the

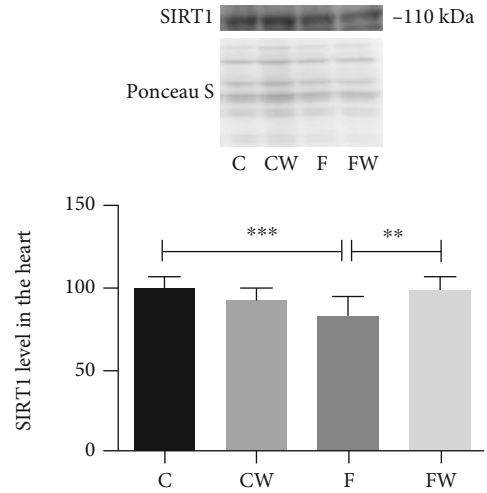

Figure 2: Effects of fructose-rich diet and supplementation with walnuts on the SIRT1 protein level in the heart of experimental rats. Values are means with standard deviations represented by vertical bars for 9 animals per group. C: animals on standard laboratory chow; F: animals fed a fructose-rich diet; W: animals fed a dietary walnut; CW: animals on standard laboratory chow and walnut supplementation; FW: fructose-fed animals on walnut supplementation; $^{**}p < 0.01$; $^{***}p < 0.001$.

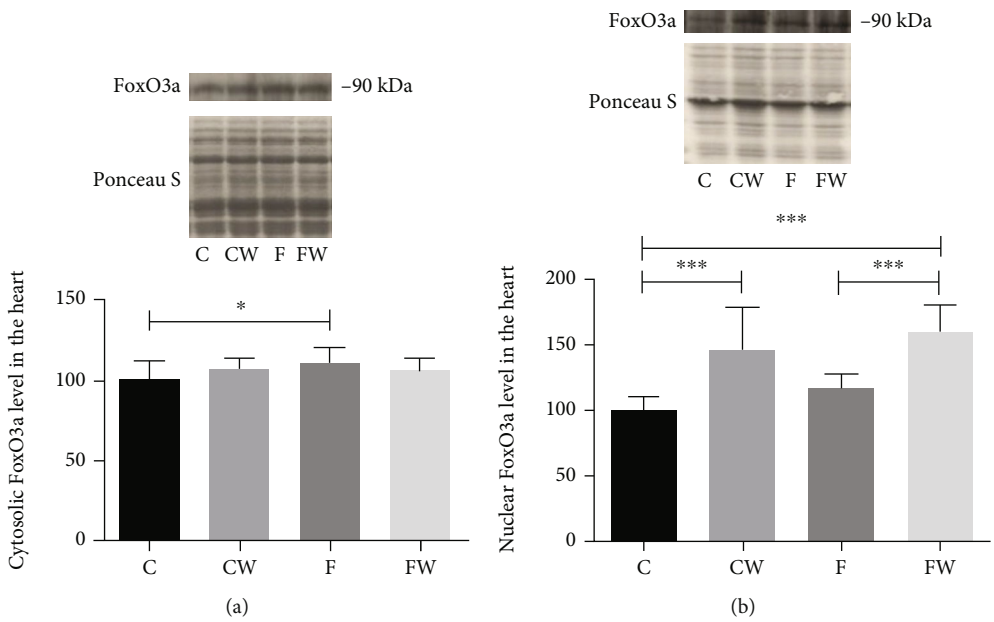

Figure 3: Effects of fructose-rich diet and walnuts on the (a) cytosolic and (b) nuclear FoxO3a protein levels in the heart of experimental rats. Values are means with standard deviations represented by vertical bars for 9 animals per group. C: animals on standard laboratory chow; F: animals fed a fructose-rich diet; CW: animals on standard laboratory chow and walnut supplementation; FW: fructose-fed animals on walnut supplementation; $^{*}p < 0.05$; $^{***}p < 0.001$.

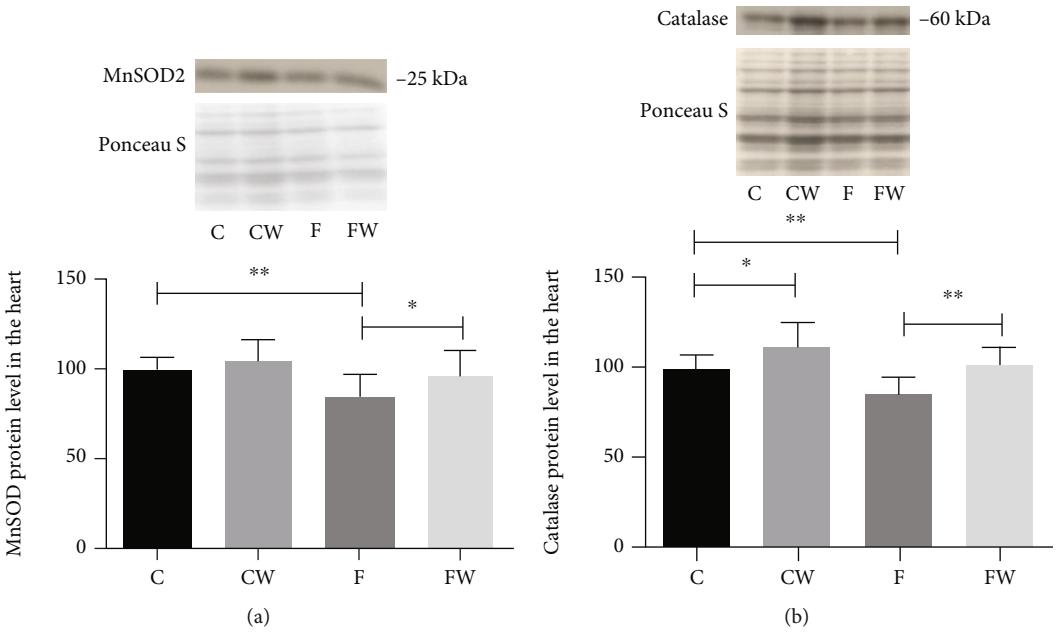

Figure 4: Effects of fructose-rich diet and walnuts on the (a) MnSOD and (b) catalase protein levels in the heart of experimental rats. Values are means with standard deviations represented by vertical bars for 9 animals per group. C: animals on standard laboratory chow; F: animals fed a fructose-rich diet; CW: animals on standard laboratory chow and walnut supplementation; FW: fructose-fed animals on walnut supplementation; $^{*}p < 0.05$; $^{**}p < 0.01$.

cytosolic fraction (C vs F, $p < 0.01$) and decreased its level in the nuclear fraction compared to the control group (C vs F, $p < 0.01$). Walnut consumption significantly decreased the nuclear ChREBP protein level in control rats (C vs CW, $p < 0.001$) and showed a trend toward an increase in the cytosolic ChREBP protein level of control rats (C vs CW, $p = 0.07$). In the cytosolic fraction, walnut consumption significantly increased the ChREBP protein level in fructose-fed rats compared to the control group (C vs FW, $p < 0.01$).

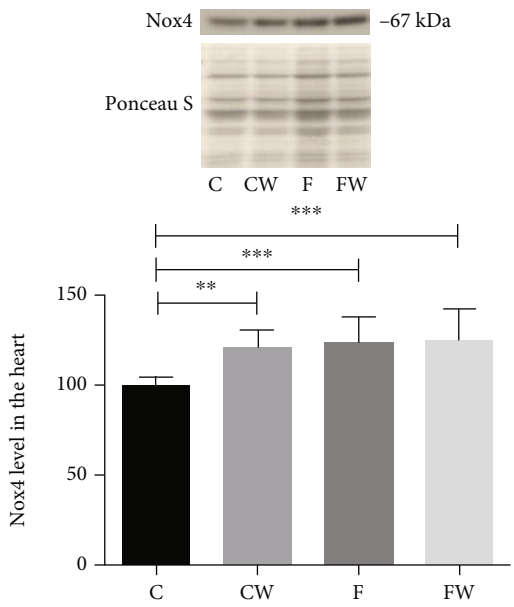

Figure 5: Effects of fructose-rich diet and walnut supplementation on the Nox4 protein level in the heart of experimental rats. Values are means with standard deviations represented by vertical bars for 9 animals per group. C: animals on standard laboratory chow; F: animals fed a fructose-rich diet; CW: animals on standard laboratory chow and walnut supplementation; FW: fructose-fed animals on walnut supplementation; $^{**}p < 0.01$; $^{***}p < 0.001$.

4. Discussion

Among other nuts, walnuts could be promising for use in dietary supplementation as they contain high levels of n-3 PUFAs, dietary fiber, antioxidants, and phytosterols [10, 41]. Our study suggests a beneficial role of walnuts in the improvement of the metabolic status that is mainly impaired by high fructose intake, a common component of the modern lifestyle. In addition, we demonstrated an increased omega-6/omega-3 ratio in FRD rats, which has been suggested to be highly prothrombotic and proinflammatory and to contribute to the prevalence of atherosclerosis and MetS-related diseases [16, 42]. The tissue-specific omega-6/omega-3 decrease after walnut consumption in high-fructose-fed Wistar rats was recently demonstrated [37]. An increase in the AA/EPA ratio as a result of fructose feeding in our study could be deleterious for the heart; previously, it has been suggested that higher levels of the AA/EPA ratio are associated with a greater risk for CVD and has been proposed as a biochemical marker of CVD events [16, 42]. We demonstrated a decrease in the AA/EPA and AA/DHA ratio in plasma as a result of walnut consumption and walnut × fructose interaction, which confirms that walnut consumption could be beneficial in dietary regime especially in MetS and in the prevention of CVD associated with MetS. The additional beneficial effect of walnut consumption in our study was the reduction of systolic BP in FRD rats, another risk factor for CVD. In the literature, the effect of walnuts or other nuts on BP was inconsistent yet but our result is in line with studies that have found a reduction in BP [9, 43]. Effects of walnut consumption on BP lowering in FRD rats may be related to the rich cation content, such as magnesium and potassium [44] and high content of ALA [10], which induces coronary VSMC relaxation [45]. The observed effect of walnut consumption on BP could be in association with its beneficial effect on the vascular tone, through the ATP-sensitive potassium channel, recently presented in the same model of FRD rats [40].

The main results of our study about the beneficial effects of walnuts on the antioxidant AMPK-SIRT1-FoxO3a-MnSOD/catalase axis in the heart of fructose-fed male rats are in line with previous evidence that n-3 PUFAs induce significant cardiovascular benefits, which appear to be achieved via its antioxidant and anti-inflammatory/immunomodulatory effects on the heart [11, 12]. The decrease of the omega-6/omega-3 fatty acid ratio, which is in our study related to walnut consumption, has been previously associated with a decrease of circulating inflammatory markers [46, 47]. Several recent studies have connected inflammation with fatty acids as important providers of nutritional needs of immune cells after sensing metabolic stress [48]. Two nutrient sensors, AMPK and SIRT1, interact to inhibit oxidative stress and macrophage inflammation, which appear to be involved in the pathogenesis of MetS [20]. Decreased nuclear SIRT1 levels/activity increases NF-κB activity and amplifies proinflammatory gene expression during chronic inflammation [49]. On the other hand, activation of SIRT1 by polyphenol fisetin [50] or by n-3 PUFA [51] was observed to be anti-inflammatory through inhibition of downstream expression of cytokines, chemokines, prostaglandins, and MMP-s. This guided us to investigate SIRT1 and AMPK in the heart of FRD rats, as well as the potential of walnuts to rebalance sirtuins as molecules that integrate metabolism, bioenergetics, and immunity during inflammation in MetS. Previously, we have detected that fructose could contribute to inflammation through the changes of MMP-9 expression that could be mediated via the NF-κB pathway in the heart [2]. In addition, we showed that estrogen replacement exerted beneficial effects on the AMPK-SIRT1-FoxO3a-MnSOD/catalase axis in the heart of FRD rats, which has been compromised by fructose overload [33]. The effects of walnut supplementation on this axis and related molecules, Nox4 and ChREBP, in the heart of FRD rats have not been previously determined. We hypothesized that reduced oxidative stress in the heart, as a result of walnut supplementation, could be also mediated by suppression of ROS production by Nox4. It has been demonstrated that n-3 PUFA could disrupt Toll-like receptor 4- (TLR4-) induced activation of Nox [52] and inhibit ROS-dependent activation of the proinflammatory transcription factor NF-κB in endothelial cells [53]. It was documented that a diet enriched with 60% fructose increased the levels of Nox4 mRNA in the rat heart and aorta [6]. In the current study, a diet enriched with 10% fructose increased the protein level of Nox4 in the rat heart. As previously denoted, Nox-mediated ROS production has a central role in vascular inflammatory responses during nutritional excess [54]. Vascular Nox production could be additionally enhanced by Ang II [55], which is the main effector molecule of the activated unfavorable arm of the

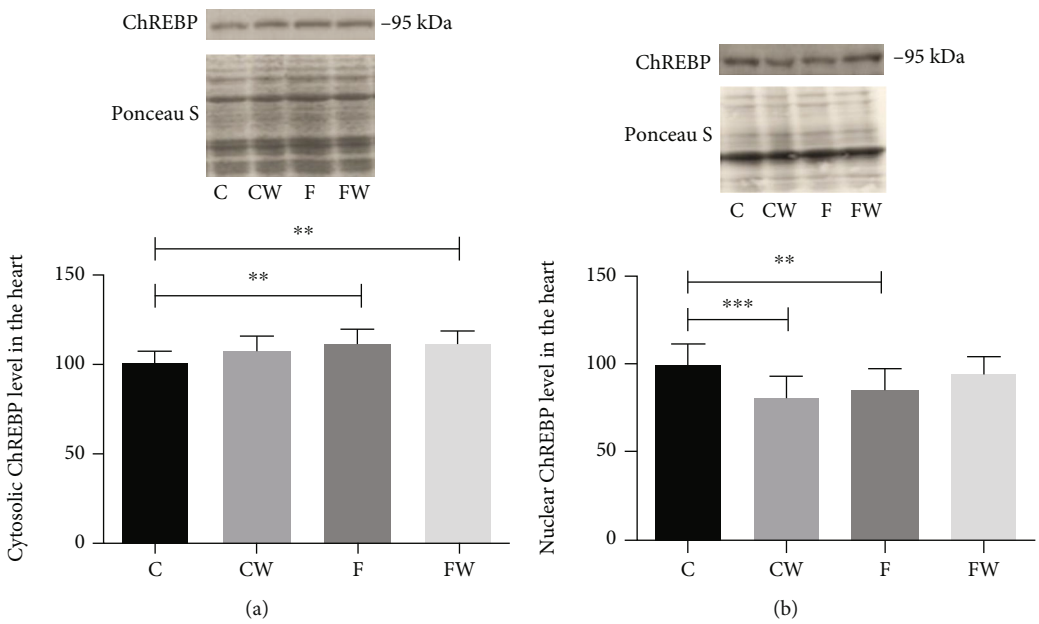

Figure 6: Effects of fructose-rich diet and walnut supplementation on the (a) cytosolic and (b) nuclear ChREBP protein levels in the heart of experimental rats. Values are means with standard deviations represented by vertical bars for 9 animals per each group. C: animals on standard laboratory chow; F: animals fed a fructose-rich diet; CW: animals on standard laboratory chow and walnut supplementation; FW: fructose-fed animals on walnut supplementation; $^{**}p < 0.01$; $^{***}p < 0.001$.

RAS in the heart/aorta of a fructose-fed rat model [56]. Activated NADPH oxidase leads to the generation of ROS, which activate NF-κB to increase the transcription of cytokines (TNF and IL-6). The binding of these cytokines to their sarcolemmal receptors induce serine kinases that phosphorylate IRS-1 and inhibit cardiac insulin signaling, providing a novel interaction path between Ang II and insulin signaling [57]. In the present study, elevated Nox4 protein levels induced by FRD contribute to inflammation in the heart, possibly through Ang II- and ROS-dependent mechanisms. However, recent data also suggested a possible atheroprotective role of Nox4 [58, 59], as well as its role in maintaining the cardiac energetic status [60]. In line with this, we could suggest that increased Nox4 protein levels in control animals after walnut supplementation, detected in our study, indicate its possible role in cardiovascular homeostasis and adaptation to chronic inflammatory stress. Even so, this should be further investigated.

While both FRD and walnut supplementation did not affect AMPK, they did significantly alter the SIRT1 protein level, indicating the possibility that SIRT1 expression in the heart is not regulated via AMPK, at least in current experimental conditions, which is in agreement with our previous study [33] and recent results in the aorta in the same FRD model [40]. Herein, FRD decreased the SIRT1 protein level in the rat heart, in line with the findings that MetS, obesity, and chronic inflammation have been associated with reduced levels of SIRT1 [61]. SIRT1-deficient *ob*/*ob* mice show exaggerated microvascular inflammation in comparison with lean mice [62]. In addition, SIRT1 deletion in myeloid cells increased the infiltration of M1 macrophages and decreased M2 macrophages in adipose tissue in mice on high-fat diets, resulting in insulin resistance [63] that is present in our FRD model. The studies of Yoshizaki et al. directly linked the anti-inflammatory effects of SIRT1 in adipocytes and macrophages with improved insulin sensitivity [64]. SIRT1 has been located in the nuclei of a significant fraction of cardiomyocytes [65] and could yield protection of cardiomyocytes. In alignment with our hypothesis, walnut supplementation restored the SIRT1 protein level in the FRD rat heart, indicating protection of the heart and a probable decrease of inflammation. The pluripotent regulatory role of sirtuins, which we previously discussed, leads to their recognition as new therapeutic targets. Thus, the determined effect of walnuts on SIRT1 represents the basis for further investigation of nutritional treatments regarding the metabolic state and inflammatory/immunomodulatory processes in the heart.

The downstream effects of SIRT1 include promotion of FoxO3a dephosphorylation and consequent initiation of FoxO3a-dependent gene transcription [28]. Our results suggest that a decrease in SIRT1 by FRD might underline the increased FoxO3a phosphorylation and downregulation of dependent genes. As FoxO3a regulates gene expression of MnSOD [22] and catalase [23], their decreased protein content in fructose-fed rats in the current study might be related to increased cytosolic FoxO3a in FRD. Importantly, our study revealed a significant increase in the nuclear protein level of FoxO3a following walnut supplementation, and consequently, we detected an increase in the MnSOD and catalase protein content in walnut-enriched diet groups.

Fructose activates ChREBP, which could repress SIRT1 expression in metabolic-active tissues [30], but data about the heart are missing. Moreover, in the rat liver, ChREBP

activity was markedly higher in rats fed with high fructose compared with isocaloric high-glucose diets [66]. During fasting, the nuclear import and transactivity of ChREBP were inactivated [67] while these processes are activated by the products of carbohydrate metabolism [68]. In our study, however, FRD significantly increased the cytosolic and decreased nuclear ChREBP protein levels in the heart. The lack of studies dealing with ChREBP in the heart and the complexity of tissue-specific expression suggest probable differential expression of ChREBP in the heart compared to metabolic active tissues [31, 69]. It is feasible that SIRT1 expression in the heart is not regulated via ChREBP and that ChREBP is important to regulate gene transcription in glycolysis/fructolysis in tissues that preferentially oxidize carbohydrates, to provide ATP for energy-expensive metabolic processes [70]. Fatty acid oxidation provides 60–70% of the energy requirements in the heart [71], but fructose can also be used as an energy substrate in the heart, considering that cardiomyocytes express the fructose-specific GLUT5 transporter [72]. Our results suggest that ChREBP is also more prevalent in the cytosol after walnut supplementation of fructose-fed animals, indicating the suppression of ChREBP activity in the heart of walnut-fed rats. A decreased level of nuclear localization of ChREBP in the heart after walnut supplementation, similar to the previously shown in the liver on high-fat diet [67], could be due to elevated amounts of fatty acids in the heart. Fatty acid-rich diets have been shown to suppress ChREBP expression by accelerating ChREBP mRNA decay [67, 73] and inhibit the nuclear localization of ChREBP [73]. Decreased DNA-binding activity of ChREBP has been observed in rats fed a high-fat diet, compared to a high-carbohydrate diet, which also implicates ChREBP in the mechanism of fatty acid inhibition of glycolysis and lipogenesis [67, 69]. However, further results on the ChREBP in the heart should be provided to bring us closer to understand its role upon nutritional treatment.

5. Conclusions

The current study has confirmed the benefits of walnut consumption and suggested the mechanisms underlying their cardioprotective effects, emphasizing the role of SIRT-1 as the nutritional sensor that transmits molecular signals responsible for the metabolic state and inflammatory/immunomodulatory processes in the heart. The SIRT1-FoxO3a-MnSOD/catalase axis, compromised by fructose overload, was balanced upon walnut treatment. The anti-inflammatory effect of walnut fatty acids, expressed in the form of a decreased AA/EPA and AA/DHA ratio, is likely mediated through negative regulation of NF-κB signaling and downstream cytokine expression, which should be investigated in the future study. Intriguing results of a decrease in nuclear ChREBP in the heart upon walnut supplementation, resembling changes in the metabolic tissue on high-fat diet, should be further deepened as the available data about this molecule in the heart are scarce. Nevertheless, this study provides novel data regarding the molecular background of anti-inflammatory and antioxidative effects of walnuts in the heart, which may be translated into modulation of nutrition and dietary therapeutic approaches against metabolic disease.

Data Availability

Data are available upon request (contact the corresponding author).

Conflicts of Interest

The authors declare that there is no conflict of interest regarding the publication of this paper.

Acknowledgments

The research was supported by the Ministry of Education, Science and Technological Development, Republic of Serbia, contract nos. 451-03-68/2020-14/200017 and 451-03-68/2020-14/200015.

Supplementary Materials

Supplementary 1. Graphical abstract.

Supplementary 2. ARRIVE checklist.

References

[1] M. R. Taskinen, C. J. Packard, and J. Borén, "Dietary fructose and the metabolic syndrome," *Nutrients*, vol. 11, no. 9, p. 1987, 2019.

[2] M. Bundalo, M. Zivkovic, T. Culafic, M. Stojiljkovic, G. Koricanac, and A. Stankovic, "Oestradiol treatment counteracts the effect of fructose-rich diet on matrix metalloproteinase 9 expression and NFκB activation," *Folia Biologica (Praha)*, vol. 61, pp. 233–240, 2015.

[3] R. Medzhitov, "Origin and physiological roles of inflammation," *Nature*, vol. 454, no. 7203, pp. 428–435, 2008.

[4] A. R. Aroor, S. McKarns, V. G. Demarco, G. Jia, and J. R. Sowers, "Maladaptive immune and inflammatory pathways lead to cardiovascular insulin resistance," *Metabolism*, vol. 62, no. 11, pp. 1543–1552, 2013.

[5] S. M. Haffner, "Pre-diabetes, insulin resistance, inflammation and CVD risk," *Diabetes Research and Clinical Practice*, vol. 61, pp. S9–S18, 2003.

[6] M. D. Nyby, K. Abedi, V. Smutko, P. Eslami, and M. L. Tuck, "Vascular angiotensin type 1 receptor expression is associated with vascular dysfunction, oxidative stress and inflammation in fructose-fed rats," *Hypertension Research*, vol. 30, pp. 451–457, 2007.

[7] T. Senoner and W. Dichtl, "Oxidative stress in cardiovascular diseases: still a therapeutic target?," *Nutrients*, vol. 11, p. 2090, 2019.

[8] N. Ibarrola-Jurado, M. Bulló, M. Guasch-Ferré et al., "Cross-sectional assessment of nut consumption and obesity, metabolic syndrome and other cardiometabolic risk factors: the PREDIMED study," *PLoS One*, vol. 8, no. 2, article e57367, 2013.

[9] N. Scott, L. Ellmers, A. Pilbrow et al., "Metabolic and blood pressure effects of walnut supplementation in a mouse model of the metabolic syndrome," *Nutrients*, vol. 9, no. 7, p. 722, 2017.

[10] A. Croitoru, D. Ficai, L. Craciun, A. Ficai, and E. Andronescu, "Evaluation and exploitation of bioactive compounds of walnut, Juglans regia," *Current Pharmaceutical Design*, vol. 25, pp. 119–131, 2019.

[11] S. Gutiérrez, S. L. Svahn, and M. E. Johansson, "Effects of omega-3 fatty acids on immune cells," *International Journal of Molecular Sciences*, vol. 20, no. 20, p. 5028, 2019.

[12] F. Oppedisano, R. Macrì, M. Gliozzi et al., "The anti-inflammatory and antioxidant properties of n-3 PUFAs: their role in cardiovascular protection," *Biomedicine*, vol. 8, p. 306, 2020.

[13] N. Kumar, G. Gupta, K. Anilkumar et al., "15-Lipoxygenase metabolites of α-linolenic acid, [13-(S)-HPOTrE and 13-(S)-HOTrE], mediate anti-inflammatory effects by inactivating NLRP3 inflammasome," *Scientific Reports*, vol. 6, no. 1, article 31649, 2016.

[14] J. Sung, H. Jeon, I. H. Kim, H. S. Jeong, and J. Lee, "Anti-inflammatory effects of stearidonic acid mediated by suppression of NF-κB and MAP-kinase pathways in macrophages," *Lipids*, vol. 52, pp. 781–787, 2017.

[15] P. C. Calder, "N-3 polyunsaturated fatty acids, inflammation, and inflammatory diseases," *The American Journal of Clinical Nutrition*, vol. 83, pp. 1505S–1519S, 2006.

[16] M. Takahashi, J. Ando, K. Shimada et al., "The ratio of serum n-3 to n-6 polyunsaturated fatty acids is associated with diabetes mellitus in patients with prior myocardial infarction: a multicenter cross-sectional study," *BMC Cardiovascular Disorders*, vol. 17, no. 1, p. 41, 2017.

[17] V. Tutino, V. De Nunzio, M. G. Caruso et al., "Elevated AA/EPA ratio represents an inflammatory biomarker in tumor tissue of metastatic colorectal cancer patients," *International Journal of Molecular Sciences*, vol. 20, no. 8, p. 2050, 2019.

[18] S. E. Weinberg, L. A. Sena, and N. S. Chandel, "Mitochondria in the regulation of innate and adaptive immunity," *Immunity*, vol. 42, no. 3, pp. 406–417, 2015.

[19] L. A. O'Neill and D. G. Hardie, "Metabolism of inflammation limited by AMPK and pseudo-starvation," *Nature*, vol. 493, no. 7432, pp. 346–355, 2013.

[20] N. B. Ruderman, X. Julia Xu, L. Nelson et al., "AMPK and SIRT1: a long-standing partnership?," *American Journal of Physiology Endocrinology and Metabolism*, vol. 298, no. 4, pp. E751–E760, 2010.

[21] Y. Olmos, F. J. Sánchez-Gómez, B. Wild et al., "SirT1 regulation of antioxidant genes is dependent on the formation of a FoxO3a/PGC-1α complex," *Antioxidants and Redox Signaling*, vol. 19, no. 13, pp. 1507–1521, 2013.

[22] G. J. Kops, T. B. Dansen, P. E. Polderman et al., "Forkhead transcription factor FoxO3a protects quiescent cells from oxidative stress," *Nature*, vol. 419, pp. 316–321, 2002.

[23] W. Q. Tan, K. Wang, D. Y. Lv, and P. F. Li, "Foxo3a inhibits cardiomyocyte hypertrophy through transactivating catalase," *The Journal of Biological Chemistry*, vol. 283, no. 44, pp. 29730–29739, 2008.

[24] H. C. Chang and L. Guarente, "SIRT1 and other sirtuins in metabolism," *Trends in Endocrinology and Metabolism*, vol. 25, no. 3, pp. 138–145, 2014.

[25] S. Elesela, S. B. Morris, S. Narayanan, S. Kumar, D. B. Lombard, and N. W. Lukacs, "Sirtuin 1 regulates mitochondrial function and immune homeostasis in respiratory syncytial virus infected dendritic cells," *PLoS Pathogens*, vol. 16, no. 2, article e1008319, 2020.

[26] B. Raud, P. J. McGuire, R. G. Jones, T. Sparwasser, and L. Berod, "Fatty acid metabolism in $CD8^+$ T cell memory: challenging current concepts," *Immunological Reviews*, vol. 283, no. 1, pp. 213–231, 2018.

[27] L. Cheng, A. Tanaka, C. Chiribau, Q. Qin, and D. Sorescu, "Nox4 regulates cellular survival by modulating FoxO3a activity and SIRT1 expression," *Journal of Cardiac Failure*, vol. 16, no. 8, p. S35, 2010.

[28] M. J. Zarzuelo, R. López-Sepúlveda, M. Sánchez et al., "SIRT1 inhibits NADPH oxidase activation and protects endothelial function in the rat aorta: implications for vascular aging," *Biochemical Pharmacology*, vol. 85, no. 9, pp. 1288–1296, 2013.

[29] J. Kuroda, T. Ago, S. Matsushima, P. Zhai, M. D. Schneider, and J. Sadoshima, "NADPH oxidase 4 (Nox4) is a major source of oxidative stress in the failing heart," *Proceedings of the National Academy of Sciences of the United States of America*, vol. 107, no. 35, pp. 15565–15570, 2010.

[30] L. G. Noriega, J. N. Feige, C. Canto et al., "CREB and ChREBP oppositely regulate SIRT1 expression in response to energy availability," *European Molecular Biology Organization reports*, vol. 12, pp. 1069–1076, 2011.

[31] K. Iizuka, R. K. Bruick, G. Liang, J. D. Horton, and K. Uyeda, "Deficiency of carbohydrate response element-binding protein (ChREBP) reduces lipogenesis as well as glycolysis," *Proceedings of the National Academy of Sciences of the United States of America*, vol. 101, no. 19, pp. 7281–7286, 2004.

[32] V. Sarrazy, S. Sore, M. Viaud et al., "Maintenance of macrophage redox status by ChREBP limits inflammation and apoptosis and protects against advanced atherosclerotic lesion formation," *Cell Reports*, vol. 13, no. 1, pp. 132–144, 2015.

[33] M. Boskovic, M. Bundalo, M. Zivkovic et al., "Estradiol ameliorates antioxidant axis SIRT1-FoxO3a-MnSOD/catalase in the heart of fructose-fed ovariectomized rats," *Journal of Functional Foods*, vol. 52, pp. 690–698, 2019.

[34] G. Petrovic-Oggiano, J. Debeljak-Martacic, S. Rankovicc et al., "The effect of walnut consumption on n-3 fatty acid profile of healthy people living in a non-Mediterranean West Balkan country, a small scale randomized study," *Nutrients*, vol. 12, p. 192, 2020.

[35] EuroFIR FoodExplorer, 2013, Available at: http://www.eurofir.org/foodexplorer/ (Accessed: 16 May 2018).

[36] M. Feng, S. Whitesall, Y. Zhang, M. Beibel, L. D'Alecy, and K. DiPetrillo, "Validation of volume-pressure recording tail-cuff blood pressure measurements," *American Journal of Hypertension*, vol. 21, pp. 1288–1291, 2008.

[37] M. Zec, I. Krga, M. Takic et al., "Walnut consumption induces tissue-specific omega-6/omega-3 decrease in high-fructose-fed Wistar rats," *ACS Omega*, vol. 5, pp. 28136–28145, 2020.

[38] J. Folch, M. Lees, and G. H. S. Stanley, "A simple method for the isolation and purification of total lipides from animal tissues," *The Journal of Biological Chemistry*, vol. 226, no. 1, pp. 497–509, 1957.

[39] I. Romero-Calvo, B. Ocón, P. Martínez-Moya et al., "Reversible Ponceau staining as a loading control alternative to actin in Western blots," *Analytical Biochemistry*, vol. 401, no. 2, pp. 318–320, 2010.

[40] J. Stanisic, T. Ivkovic, S. Romic et al., "Beneficial effect of walnuts on vascular tone is associated with Akt signalling, voltage-dependent calcium channel LTCC and ATP-sensitive potassium channel Kv1.2," *International Journal of Food Sciences and Nutrition*, vol. 21, pp. 1–11, 2021.

[41] C. Y. Chen and J. B. Blumberg, "Phytochemical composition of nuts," *Asia Pacific Journal of Clinical Nutrition*, vol. 17, pp. 329–332, 2008.

[42] T. Ninomiya, M. Nagata, J. Hata et al., "Association between ratio of serum eicosapentaenoic acid to arachidonic acid and risk of cardiovascular disease: the Hisayama Study," *Atherosclerosis*, vol. 231, no. 2, pp. 261–267, 2013.

[43] C. L. Rock, S. W. Flatt, H. S. Barkai, B. Pakiz, and D. D. Heath, "Walnut consumption in a weight reduction intervention: effects on body weight, biological measures, blood pressure and satiety," *Nutrition Journal*, vol. 16, no. 1, p. 76, 2017.

[44] R. J. Elin and J. M. Hosseini, "Is the magnesium content of nuts a factor for coronary heart disease?," *Archives of Internal Medicine*, vol. 153, no. 6, pp. 779-780, 1993.

[45] S. I. Pomposiello, M. Alva, D. W. Wilde, and O. A. Carretero, "Linoleic acid induces relaxation and hyperpolarization of the pig coronary artery," *Hypertension*, vol. 31, no. 2, pp. 615–620, 1998.

[46] L. Ferrucci, A. Cherubini, S. Bandinelli et al., "Relationship of plasma polyunsaturated fatty acids to circulating inflammatory markers," *The Journal of Clinical Endocrinology and Metabolism*, vol. 91, pp. 439–446, 2006.

[47] N. Kalogeropoulos, D. B. Panagiotakos, C. Pitsavos et al., "Unsaturated fatty acids are inversely associated and _n-6/n-3_ ratios are positively related to inflammation and coagulation markers in plasma of apparently healthy adults," *Clinica Chimica Acta*, vol. 411, no. 7-8, pp. 584–591, 2010.

[48] T. F. Liu, C. M. Brown, M. El Gazzar et al., "Fueling the flame: bioenergy couples metabolism and inflammation," *Journal of Leukocyte Biology*, vol. 92, no. 3, pp. 499–507, 2012.

[49] V. Vachharajani, T. Liu, X. Wang, J. J. Hoth, B. K. Yoza, and C. E. McCall, "Sirtuins link inflammation and metabolism," *Journal of Immunology Research*, vol. 2016, Article ID 8167273, 2016.

[50] W. Zheng, Z. Feng, S. You et al., "Fisetin inhibits IL-1β-induced inflammatory response in human osteoarthritis chondrocytes through activating SIRT1 and attenuates the progression of osteoarthritis in mice," *International Immunopharmacology*, vol. 45, pp. 135–147, 2017.

[51] B. Xue, Z. Yang, X. Wang, and H. Shi, "Omega-3 polyunsaturated fatty acids antagonize macrophage inflammation via activation of AMPK/SIRT1 pathway," *PLoS One*, vol. 7, no. 10, article e45990, 2012.

[52] H. S. Park, J. N. Chun, H. Y. Jung, C. Choi, and Y. S. Bae, "Role of NADPH oxidase 4 in lipopolysaccharide-induced proinflammatory responses by human aortic endothelial cells," *Cardiovascular Research*, vol. 72, pp. 447–455, 2006.

[53] E. Maloney, I. R. Sweet, D. M. Hockenbery et al., "Activation of NF-kappaB by palmitate in endothelial cells: a key role for NADPH oxidase-derived superoxide in response to TLR4 activation," *Arteriosclerosis, Thrombosis, and Vascular Biology*, vol. 29, pp. 1370–1375, 2009.

[54] T. Inoguchi, P. Li, F. Umeda et al., "High glucose level and free fatty acid stimulate reactive oxygen species production through protein kinase C-dependent activation of NAD(P)H oxidase in cultured vascular cells," *Diabetes*, vol. 49, no. 11, pp. 1939–1945, 2000.

[55] D. G. Harrison, H. Cai, U. Landmesser, and K. K. Griendling, "Interactions of angiotensin II with NAD(P)H oxidase, oxidant stress and cardiovascular disease," *Journal of the Renin-Angiotensin-Aldosterone System: JRAAS*, vol. 4, pp. 51–61, 2003.

[56] M. Bundalo, M. Zivkovic, S. Romic et al., "Fructose-rich diet induces gender-specific changes in expression of the renin-angiotensin system in rat heart and upregulates the ACE/AT1R axis in the male rat aorta," *Journal of the Renin-Angiotensin-Aldosterone System*, vol. 17, article 1470320316642915, 2016.

[57] V. C. Calegari, M. Alves, P. K. Picardi et al., "Suppressor of cytokine signaling-3 provides a novel interface in the cross-talk between angiotensin II and insulin signaling systems," *Endocrinology*, vol. 146, pp. 579–588, 2005.

[58] K. Schröder, M. Zhang, S. Benkhoff et al., "Nox4 is a protective reactive oxygen species generating vascular NADPH oxidase," *Circulation Research*, vol. 110, pp. 1217–1225, 2012.

[59] S. P. Gray, E. Di Marco, K. Kennedy et al., "Reactive oxygen species can provide atheroprotection via NOX4-dependent inhibition of inflammation and vascular remodeling," *Arteriosclerosis, Thrombosis, and Vascular Biology*, vol. 36, pp. 295–307, 2016.

[60] A. A. Nabeebaccus, A. Zoccarato, A. D. Hafstad et al., "Nox4 reprograms cardiac substrate metabolism via protein O-GlcNAcylation to enhance stress adaptation," *Journal of Clinical Investigation Insight*, vol. 2, no. 24, article e96184, 2017.

[61] M. M. Poulsen, J. O. Jørgensen, N. Jessen, B. Richelsen, and S. B. Pedersen, "Resveratrol in metabolic health: an overview of the current evidence and perspectives," *Annals of the New York Academy of Sciences*, vol. 1290, pp. 74–82, 2013.

[62] V. Vachharajani, J. M. Russell, K. L. Scott et al., "Obesity exacerbates sepsis-induced inflammation and microvascular dysfunction in mouse brain," *Microcirculation*, vol. 12, no. 2, pp. 183–194, 2005.

[63] Z. Yang, X. Wang, Y. He et al., "The full capacity of AICAR to reduce obesity-induced inflammation and insulin resistance requires myeloid SIRT1," *PLoS One*, vol. 7, no. 11, article e49935, 2012.

[64] T. Yoshizaki, S. Schenk, T. Imamura et al., "SIRT1 inhibits inflammatory pathways in macrophages and modulates insulin sensitivity," *American Journal of Physiology Endocrinology and Metabolism*, vol. 298, no. 3, pp. E419–E428, 2010.

[65] G. Bolasco, R. Calogero, M. Carrara et al., "Cardioprotective mIGF-1/SIRT1 signaling induces hypertension, leukocytosis and fear response in mice," *Aging (Albany NY)*, vol. 4, no. 6, pp. 402–416, 2012.

[66] H. Y. Koo, M. Miyashita, B. H. Cho, and M. T. Nakamura, "Replacing dietary glucose with fructose increases ChREBP activity and SREBP-1 protein in rat liver nucleus," *Biochemical and Biophysical Research Communications*, vol. 390, no. 2, pp. 285–289, 2009.

[67] T. Kawaguchi, K. Osatomi, H. Yamashita, T. Kabashima, and K. Uyeda, "Mechanism for fatty acid "sparing" effect on glucose-induced transcription:," *The Journal of Biological Chemistry*, vol. 277, no. 6, pp. 3829–3835, 2002.

[68] T. Kabashima, T. Kawaguchi, B. E. Wadzinski, and K. Uyeda, "Xylulose 5-phosphate mediates glucose-induced lipogenesis by xylulose-5-phosphate-activated protein phosphatase in rat liver," *Proceedings of the National Academy of Sciences of the United States of America*, vol. 100, no. 9, pp. 5107–5112, 2003.

[69] H. Yamashita, M. Takenoshita, M. Sakurai et al., "A glucose-responsive transcription factor that regulates carbohydrate metabolism in the liver," *Proceedings of the National Academy of Sciences of the United States of America*, vol. 98, no. 16, pp. 9116–9121, 2001.

[70] S. M. Logan and K. B. Storey, "Tissue-specific response of carbohydrate-responsive element binding protein (ChREBP) to mammalian hibernation in 13-lined ground squirrels," *Cryobiology*, vol. 73, no. 2, pp. 103–111, 2016.

[71] L. Bertrand, S. Horman, C. Beauloye, and J. L. Vanoverschelde, "Insulin signalling in the heart," *Cardiovascular Research*, vol. 79, pp. 238–248, 2008.

[72] A. Karaca, O. Palabıyık, E. Taştekin, F. N. Turan, and S. Arzu Vardar, "High-fructose diet suppresses exercise-induced increase in AQP7 expression in the rat heart in vivo," *Anatolian Journal of Cardiology*, vol. 16, pp. 916–922, 2016.

[73] R. Dentin, F. Benhamed, J. P. Pégorier et al., "Polyunsaturated fatty acids suppress glycolytic and lipogenic genes through the inhibition of ChREBP nuclear protein translocation," *Journal of Clinical Investigation*, vol. 115, no. 10, pp. 2843–2854, 2005.

Hindawi
Oxidative Medicine and Cellular Longevity
Volume 2021, Article ID 5599997, 16 pages
https://doi.org/10.1155/2021/5599997

Research Article

Epigallocatechin-3-Gallate Alleviates High-Fat Diet-Induced Nonalcoholic Fatty Liver Disease via Inhibition of Apoptosis and Promotion of Autophagy through the ROS/MAPK Signaling Pathway

Dongdong Wu,[1,2] **Zhengguo Liu**,[1] **Yizhen Wang**,[1] **Qianqian Zhang**,[1] **Jianmei Li**,[1] **Peiyu Zhong**,[1] **Zhongwen Xie**,[3] **Ailing Ji**,[1] **and Yanzhang Li**[1]

[1]*Henan International Joint Laboratory for Nuclear Protein Regulation, School of Basic Medical Sciences, Henan University, Kaifeng, Henan 475004, China*
[2]*School of Stomatology, Henan University, Kaifeng, Henan 475004, China*
[3]*State Key Laboratory of Tea Plant Biology and Utilization, Anhui Agricultural University, Hefei, Anhui 230036, China*

Correspondence should be addressed to Zhongwen Xie; zhongwenxie@ahau.edu.cn, Ailing Ji; ailingji@163.com, and Yanzhang Li; yanzhang206@163.com

Received 21 January 2021; Revised 22 March 2021; Accepted 28 March 2021; Published 17 April 2021

Academic Editor: Stefania D'Adamo

Nonalcoholic fatty liver disease (NAFLD) represents one of the most common chronic liver diseases in the world. It has been reported that epigallocatechin-3-gallate (EGCG) plays important biological and pharmacological roles in mammalian cells. Nevertheless, the mechanism underlying the beneficial effect of EGCG on the progression of NAFLD has not been fully elucidated. In the present study, the mechanisms of action of EGCG on the growth, apoptosis, and autophagy were examined using oleic acid- (OA-) treated liver cells and the high-fat diet- (HFD-) induced NAFLD mouse model. Administration of EGCG promoted the growth of OA-treated liver cells. EGCG could reduce mitochondrial-dependent apoptosis and increase autophagy possibly via the reactive oxygen species- (ROS-) mediated mitogen-activated protein kinase (MAPK) pathway in OA-treated liver cells. In line with *in vitro* findings, our *in vivo* study verified that treatment with EGCG attenuated HFD-induced NAFLD through reduction of apoptosis and promotion of autophagy. EGCG can alleviate HFD-induced NAFLD possibly by decreasing apoptosis and increasing autophagy via the ROS/MAPK pathway. EGCG may be a promising agent for the treatment of NAFLD.

1. Introduction

Tea, made from the leaves of *Camellia sinensis*, has long been considered a popular beverage worldwide [1–3]. Tea can be mainly classified into three types according to the manufacturing processes, including green tea (nonfermented), oolong tea (semifermented), and red and black teas (fermented) [4]. The functional constituents of tea can be attributable to the polyphenolic compounds, particularly catechins [1]. Four main catechins have been identified in green tea, such as epigallocatechin-3-gallate (EGCG), epigallocatechin, epicatechin-3-gallate, and epicatechin, with EGCG as the most active and abundant compound [3, 5]. These catechins have different hydroxyl groups on the B-ring with the presence/absence of a galloyl moiety [4]. EGCG exhibits strong binding to bioactive macromolecules, such as DNA and proteins via π-π stacking interaction, hydrogen bonding, and hydrophobic interaction [5, 6].

EGCG, a flavone-3-ol phenolic compound, has eight free hydroxyl groups [2], which might contribute to its diverse

biological and pharmacological properties, such as antiamyloidogenic [7], chemopreventive [8], renoprotective [9], anticancer [10], antiaging [11], antiautoimmune [12], and antiviral [13] activities. Nonalcoholic fatty liver disease (NAFLD), a common chronic liver disease, has been considered one of the leading causes of end-stage liver disease, liver transplantation, and hepatocellular carcinoma [14–16]. The prevalence of NAFLD is growing in parallel with the global obesity epidemics, hypertension, type 2 diabetes, hyperlipidemia, and metabolic syndromes [15, 16]. It has been shown that EGCG could attenuate high-fat diet- (HFD-) induced NAFLD in rats and mice [17–19]. Nevertheless, the inhibitory effects and detailed mechanisms of EGCG in the initiation and progression of NAFLD need to be further investigated.

In this study, the mechanism of action of EGCG on the growth, apoptosis, and autophagy of oleic acid- (OA-) treated liver cells was elucidated. The HFD-induced NAFLD mouse model was further adopted to confirm the effect and mechanism of EGCG on NAFLD.

2. Materials and Methods

2.1. Cell Culture. Human liver cell lines L02 and QSG-7701 were purchased from Feiya Biological Technology Co., Ltd. (Yancheng, Jiangsu, China). The cells were cultured in Dulbecco's modified Eagle's medium (DMEM) with 10% fetal bovine serum (FBS) and 1% streptomycin/penicillin. Before each experiment, the cells were starved for 12 h in serum-free DMEM. Then, the cells were treated with the medium containing the 0.5 mM OA-bovine serum albumin (BSA; fatty acid-free, low endotoxin) complex (4 : 1, molar ratio), with or without a concentration of 50 μM EGCG for 24 h. The medium with only BSA was selected as the control [20].

2.2. Oil Red O (ORO) Staining. Cells were fixed in 4% paraformaldehyde for 15 min, incubated with isopropyl alcohol for 20 min, and stained with ORO solution for 20 min, followed by being counterstained with hematoxylin at room temperature. The staining intensity of ORO was measured by ImageJ software (National Institutes of Health, Bethesda, MD, USA) [21].

2.3. Cell Growth Assay. The 5-ethynyl-2′-deoxyuridine (EdU) experiment was carried out using economical kits (RiboBio, Guangzhou, China). The cell proliferation rate was calculated as the percentage of positive cells to total cells. In addition, the cell counting kit-8 (CCK-8) detection kits (Beyotime, Shanghai, China) were used to detect cell viability. Cell viability was expressed as a percentage to the control group [22].

2.4. Flow Cytometry Assay. Cells were incubated with propidium iodide (PI)/RNase A mixture for 20 min. A FACSVerse flow cytometer (BD, San Jose, CA, USA) was adopted to analyze the cell cycle. The apoptotic level was examined by Annexin V-FITC/PI assay kits (KeyGen, Nanjing, Jiangsu, China) and further analyzed using a FACSVerse flow cytometer.

2.5. Immunofluorescence Staining. The green fluorescent protein- (GFP-)-red fluorescent protein- (RFP-) microtubule-associated protein 1 light chain 3 (MAP1LC3/LC3) plasmid has been used to detect the autophagic level [23]. Then, the GFP-RFP-LC3 plasmid (Hanbio, Shanghai, China) was transfected into the cells. After 48 h of incubation, the cellular fluorescence was determined using an Eclipse Ti fluorescent microscope (Nikon, Melville, NY, USA). The autophagosomes (yellow dots) and autolysosomes (red dots) were calculated as the ratios of positive-stained cells to total cells [24].

2.6. Monodansylcadaverine (MDC) Staining. Morphologically, the formation of autophagic vacuoles in the cytoplasm is a typical characteristic of autophagy. MDC is a key marker for autophagic vacuoles [25]. Briefly, the liver cells were stained with 50 μmol/L MDC for 30 min at 37°C. Then, the cells were fixed with 5% paraformaldehyde and immediately observed under an Eclipse Ti fluorescent microscope (Nikon).

2.7. Measurement of Reactive Oxygen Species (ROS). Cellular ROS levels were measured by 2′,7′-dichlorodihydrofluorescein diacetate (Beyotime).

2.8. Determination of Antioxidant Activity. The total superoxide dismutase (SOD) activity was determined using the kit with WST-8 (Beyotime). The catalase (CAT) activity was analyzed using the CAT assay kit (Beyotime). The glutathione peroxidase (GSH-Px) activity was detected by the GSH-Px assay kit with nicotinamide adenine dinucleotide phosphate (Beyotime).

2.9. Western Blot. Western blot assay was adopted to determine the expression levels of proteins. The primary antibodies, such as anti-cyclin D1/E1, anti-cyclin-dependent kinase (CDK) 2/4, anti-p21, anti-p27, anti-beclin-1, anti-P62, anti-LC3A/B, anti-extracellular signal-regulated protein kinase 1/2 (ERK1/2), anti-phospho- (p-) ERK1/2 (Thr202/Tyr204), anti-c-Jun N-terminal kinase (JNK), anti-p-JNK (Thr183/Tyr185), anti-p38, and anti-p-p38 (Thr180/Tyr182), and the horseradish peroxidase-conjugated secondary antibody were purchased from Cell Signaling Technology (CST, Danvers, MA, USA). Anti-B-cell lymphoma-2 (Bcl-2), anti-Bcl-2-associated X protein (Bax), anti-B-cell lymphoma-extra large (Bcl-xl), anti-Bcl-xl/Bcl-2-associated death promoter (Bad), anti-cleaved caspase-3/9, anti-cleaved poly-ADP-ribose polymerase (PARP), and anti-β-actin were obtained from Proteintech (Chicago, IL, USA). The bands were detected with a chemiluminescence system (Thermo, Rockford, IL, USA). Band intensities were analyzed by densitometry using ImageJ software.

2.10. Animals. The animal experiment was approved by the Committee of Medical Ethics and Welfare for Experimental Animals of Henan University School of Medicine (HUSOM-2017-208). C57BL/6J mice (8 weeks old, male), HFD (60% kcal as fat), and low-fat diet (LFD, 10% kcal as fat) were obtained from Vital River Laboratory Animal Technology Co., Ltd. (Beijing, China). All mice were maintained on a 12 h light/dark cycle and allowed access to food and water *ad libitum*. Mice were fed either HFD ($n = 12$) or LFD ($n = 6$) for a total of 14 weeks. After feeding for 10 weeks, HFD-fed mice were assigned to the HFD group ($n = 6$) and HFD +EGCG (50 mg/kg/day) group ($n = 6$). The mice were treated

for an additional 4 weeks. Food/water intakes and body weights of the mice were measured. Then, the mice were killed and blood samples were collected. The liver, brown fat, and white fat were removed and weighed.

2.11. Biochemical Analysis. The concentrations of triglyceride (TG), total cholesterol (TC), alanine aminotransferase (ALT), and aspartate aminotransferase (AST) in the plasma were examined by an automated hematology analyzer (BC-6900, Mindray, Shenzhen, Guangdong, China). The contents of TG and TC in liver cells and tissues, as well as nonesterified fatty acid (NEFA) in liver tissues were detected by commercial enzyme-linked immunosorbent assay kits (Jiancheng Bioengineering Institute, Nanjing, Jiangsu, China).

2.12. Hematoxylin and Eosin (HE) Staining. Liver tissues were fixed in 10% neutral formalin, embedded in paraffin wax, sectioned at 4 μm, and then stained with HE.

2.13. Immunohistochemistry (IHC). Liver samples were respectively stained with anti-Ki67 (CST), anti-beclin-1, and anti-cleaved caspase-3 antibodies. The proliferation index, autophagic index, and apoptotic index were determined by the ratios of positive cells to total cells.

2.14. Statistics. All data were presented as the mean ± standard error of the mean. Differences between the two groups were determined by the two-tailed Student's t-test and one-way analysis of variance using GraphPad Prism 6 software. $P < 0.05$ was considered to indicate a statistically significant difference.

3. Results

3.1. EGCG Promotes the Growth of OA-Treated Liver Cells. As shown in Figures 1(a) and 1(b), OA induced the accumulation of lipid in OA-treated liver cells, as further evidenced by the increased levels of TC and TG (Figures 1(c) and 1(d)). Treatment with EGCG reduced the lipid level in OA-treated liver cells (Figures 1(a)–1(d)). The viability and proliferation of liver cells were decreased by OA; nevertheless, EGCG promoted the viability and proliferation of OA-treated liver cells (Figures 1(e)–1(g)). In addition, the results showed that OA triggered cell cycle arrest at the G1 phase and EGCG reversed the trend (Figures 2(a) and 2(b)). Many cell cycle-related proteins have been identified in mammals, such as cell cycle regulatory proteins, including cyclin D1/E1 and CDK2/4, as well as inhibitory cell cycle regulators, including p21 and p27 [26, 27]. Our data suggested that OA increased the expressions of cyclin D1, cyclin E1, CDK2, and CDK4 but downregulated the protein levels of p21 and p27; however, administration of EGCG exhibited reverse trends (Figures 2(c) and 2(d)). Taken together, the data indicate that EGCG can promote the growth of OA-treated liver cells through promoting G1 phase cell cycle progression.

3.2. EGCG Decreases Apoptosis in OA-Treated Liver Cells. As shown in Figures 3(a) and 3(b), the data suggested that OA increased the early and late apoptotic cell populations, whereas EGCG decreased the early and late apoptosis in OA-treated liver cells. The ratios of Bax/Bcl-2 and Bad/Bcl-xl are regarded as key factors in regulating apoptosis. Increased ratios of Bax/Bcl-2 and Bad/Bcl-xl are key phenomena in mitochondrial-dependent apoptosis in mammals [28, 29]. Furthermore, cleaved caspase-3/9 could induce apoptosis through the mitochondrial-mediated pathway [30]. PARP, a nuclear enzyme involved in DNA repair, is an important target for caspases during apoptosis [31]. The data showed that OA increased both the Bax/Bcl-2 and Bad/Bcl-xl ratios and the expression levels of cleaved caspase-3/9 and cleaved PARP, which were reversed by the administration of EGCG (Figures 3(c) and 3(d)). The results suggest that OA can induce mitochondrial-dependent apoptosis in liver cells and EGCG could reduce the apoptotic levels in OA-treated liver cells.

3.3. EGCG Increases Autophagy in OA-Treated Liver Cells. Autophagy is responsible for the degradation of intracellular protein aggregates, invasive pathogens, and damaged organelles and therefore is essential in maintaining cellular homeostasis and responding to stress conditions [32, 33]. A crucial step in autophagy is the conversion of LC3 from the nonlipidated form (LC3-I) to the lipid-conjugated form (LC3-II) [33, 34]. Autophagic turnover could be molecularly monitored using a GFP-conjugated LC3 and the conversion of LC3-I to LC3-II [35]. In the present study, the GFP-RFP-LC3 plasmid was transfected into liver cells and further detected by fluorescence microscopy. Treatment with OA decreased the numbers of free red dots (autolysosomes) and yellow dots (autophagosomes), whereas administration of EGCG showed the opposite effects (Figures 4(a) and 4(b)). A similar trend was observed in MDC staining (Figures 4(c) and 4(d)). Apart from LC3, beclin-1 and P62 have also been considered specific markers of autophagy [33, 36]. The expression levels of beclin-1 and LC3 in the OA group were lower than those in the control group, but the protein levels of these two factors were higher in the OA+EGCG group than in the OA group. Furthermore, the expression level of P62 exhibited a reverse trend (Figures 4(e) and 4(f)). These results together suggest that the autophagic level is downregulated in OA-treated liver cells and treatment with EGCG could upregulate the autophagy machinery.

3.4. EGCG Suppresses the ROS/Mitogen-Activated Protein Kinase (MAPK) Pathway in OA-Treated Liver Cells. ROS such as hydroxyl radical, hydrogen peroxide, and superoxide anion are normally generated as by-products of aerobic metabolism [37, 38]. ROS can be scavenged by the antioxidant defense system that mainly includes GSH-Px, SOD, and CAT [37–39]. Compared with the control group, the ROS levels were increased, but GSH-Px, SOD, and CAT activities were downregulated in the OA group, which can be reversed by the administration of EGCG (Figures 5(a) and 5(b)). The results suggest that EGCG can reduce OA-induced oxidative stress in liver cells. It has been shown that ROS can activate the MAPK pathway and attenuation of ROS by ROS scavengers could deactivate MAPK signaling [40, 41]. As shown in Figures 5(c) and 5(d), OA reduced the

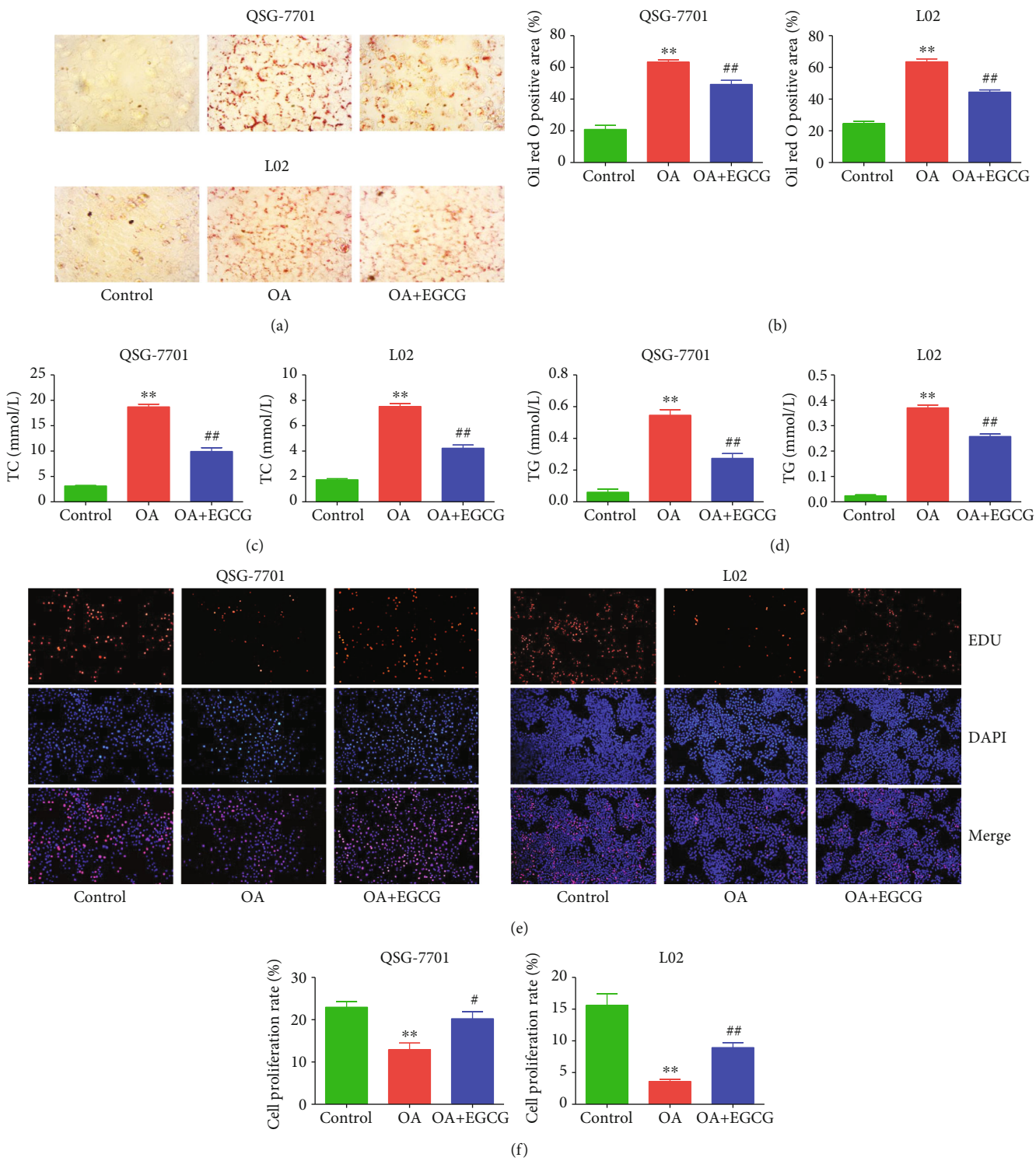

Figure 1: Continued.

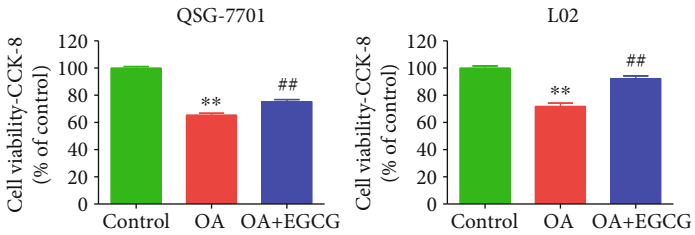

(g)

Figure 1: Effects of EGCG on lipid droplet formation and the growth of OA-treated QSG-7701 and L02 cells. (a) Representative photographs of ORO-stained QSG-7701 and L02 cells; original magnification ×400. (b) ORO-positive area was calculated. (c) The levels of TC were measured. (d) The levels of TG were measured. (e) DNA replication activities were examined by EdU assay; original magnification ×200. (f) The proliferation rate of each group was analyzed. (g) The percentages of viable cells were determined using CCK-8 assay, and the cell viability of control cells was normalized as 100%. Data are presented as mean ± SEM of three independent experiments; $^{**}P < 0.01$ compared with the control group; $^{\#}P < 0.05$, $^{\#\#}P < 0.01$ compared with the OA group.

expression of p-ERK1/2 but increased the levels of p-JNK and p-p38, while administration of EGCG exhibited reverse effects on the kinases. The data suggest that EGCG may suppress the ROS/MAPK pathway in OA-treated liver cells.

3.5. EGCG Attenuates HFD-Induced NAFLD in Mice. Compared with the mice fed with LFD for 10 weeks, HFD-fed mice exhibited increased body weight, indicating that an alimentary obesity model had been successfully established. In addition, compared to the LFD group, HFD-fed mice showed decreased food and water intakes, as well as increased weights of liver, white fat, and brown fat. Treatment with EGCG reversed these changes except for the food intake (Figures 6(a)–6(h)). Furthermore, HFD-fed mice exhibited increased levels of TC, TG, ALT, and AST when compared to the LFD group, which could be reversed by the treatment with EGCG (Figures 6(i)–6(l)). Moreover, HFD-fed mice showed upregulated levels of TC, TG, and NEFA in the liver when compared with the LFD group, which were reduced by the administration of EGCG (Figures 6(m)–6(o)). Compared to the LFD group, the HFD group exhibited a higher apoptotic index, as well as a lower proliferation index and autophagic index, which could be reversed by the administration of EGCG (Figures 7(a)–7(d)). These results indicate that EGCG can attenuate HFD-induced NAFLD in mice.

4. Discussion

NAFLD, the most common chronic liver disease, leads to end-stage liver disease, liver transplantation, and hepatocellular carcinoma [14–16]. It has been shown that EGCG plays important biological and pharmacological roles in mammals. Nevertheless, the effect and mechanism of EGCG in the process of NAFLD are largely unknown. Human normal liver cells QSG-7701 and L02 have been widely adopted to investigate the mechanism of action of novel drugs and donors [42, 43]. OA, a monounsaturated fatty acid, has been successfully used in the establishment of the NAFLD model [44]. In this study, QSG-7701 and L02 cells were adopted to examine the effects of EGCG on NAFLD induced by OA *in vitro*. A recent study has revealed that epoxy stearic acid, a type of oxidative product from OA, can induce cytotoxicity and G0/G1 phase cell cycle arrest in HepG2 cells [45]. Our data indicated that OA decreased the viability and proliferation of liver cells and induced G1 phase cell cycle arrest. The changes could be reversed by the administration of EGCG. These data together indicate that EGCG acts as an effector molecule in promoting the growth of OA-treated liver cells.

Apoptosis is a conserved cell death pathway which can play key roles in the maintenance of organismal homeostasis and normal eukaryotic development [46, 47]. Two main apoptotic pathways have been identified in mammals: the mitochondrial-mediated intrinsic pathway and the death receptor-mediated extrinsic pathway [48]. Bcl-2 family proteins are involved in the regulation of apoptosis, such as Bax, Bad, Bcl-2, and Bcl-xl [49]. Many apoptotic stimuli can activate caspases, and PARP is activated by cleaved caspase-3, leading to the occurrence of apoptosis [31, 38, 49]. It has been reported that OA could induce apoptosis by increasing the levels of Bax and PARP but decreasing the level of Bcl-2 in HepG2 cells [50]. Another study shows that OA can promote the expressions of both cleaved caspase-3 and PARP1 [51]. Similarly, our data indicated that OA induced the early and late apoptosis, as well as increased the ratios of both Bax/Bcl-2 and Bad/Bcl-xl and the expressions of cleaved caspase-3/9 and cleaved PARP in liver cells. EGCG significantly reduced the apoptotic levels in the OA group. The data suggest that the apoptotic levels are increased in OA-treated liver cells and treatment with EGCG could reduce apoptosis.

Autophagy, an evolutionarily conserved catabolic pathway, serves to deliver cytoplasmic materials to lysosomes for recycling and degradation, leading to macromolecular synthesis and energy production [36, 52]. Autophagy is activated by many environmental factors, including cytokines, hormones, and nutrients [53]. Recent studies have indicated that autophagy is impaired in lipid-overloaded hepatocytes and in the liver from the NAFLD murine model and NAFLD patients [54–56]. In line with the above studies, we observed that the autophagic levels were decreased in OA-treated liver cells. Another study has reported that EGCG can increase the autophagic level by increasing lysosomal acidification and

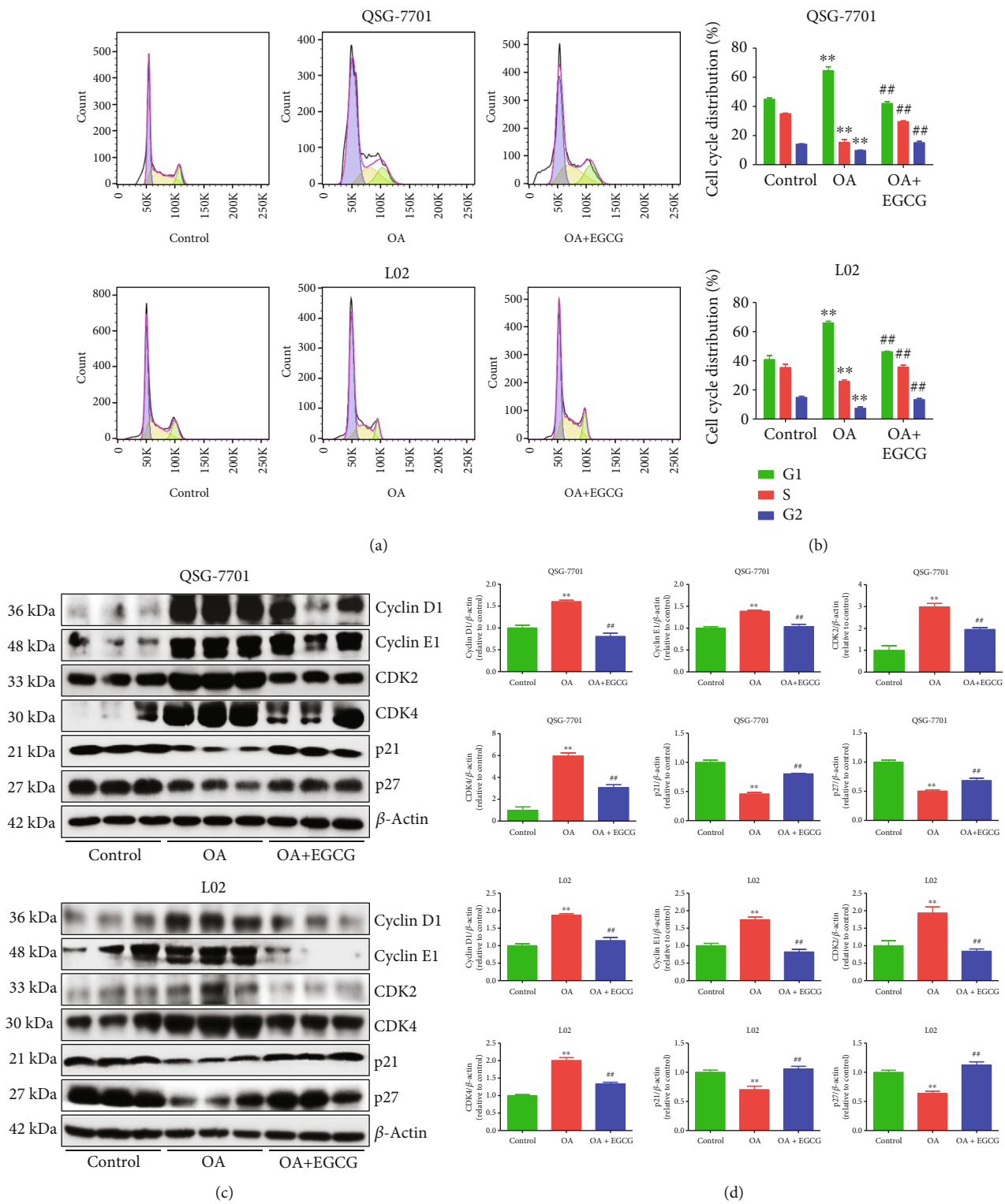

Figure 2: Effects of EGCG on cell cycle progression of OA-treated QSG-7701 and L02 cells. (a) Flow cytometry assay was used to determine cell cycle distribution. (b) Cell cycle distribution was analyzed. (c) Western blot analysis for the expression levels of cyclin D1, cyclin E1, CDK2, CDK4, p21, and p27 in each group. β-Actin was used as the loading control. (d) The densitometry analysis of each factor was performed in each group, normalized to the corresponding β-actin level. Data are presented as mean ± SEM of three independent experiments; $^{**}P < 0.01$ compared with the control group; $^{\#\#}P < 0.01$ compared with the OA group.

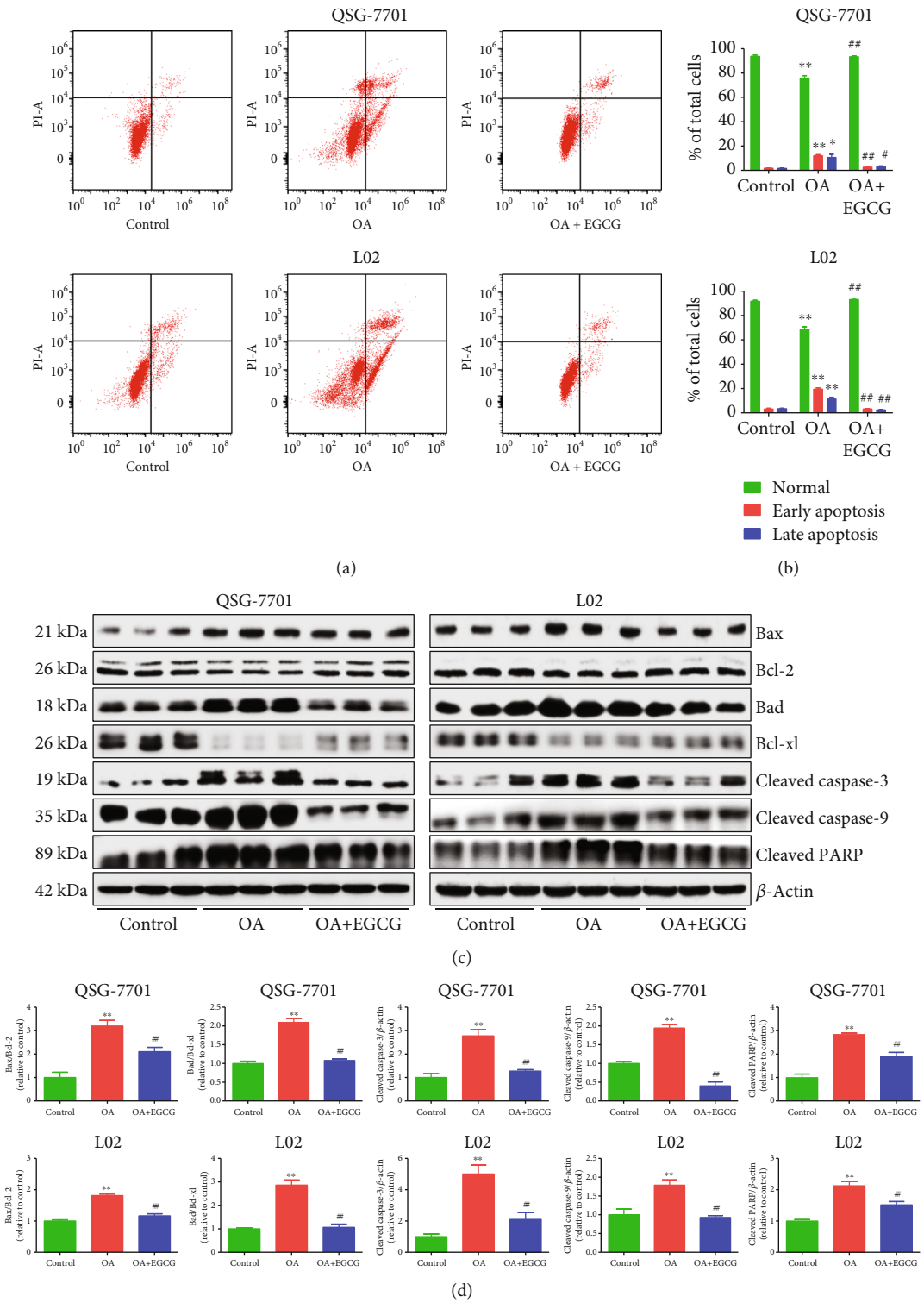

Figure 3: Effects of EGCG on the apoptosis of OA-treated QSG-7701 and L02 cells. (a) Flow cytometry assay was used to determine the apoptotic level. (b) The results of flow cytometry were analyzed. (c) Western blot analysis for the expression levels of Bax, Bcl-2, Bad, Bcl-xl, cleaved caspase-3/9, and cleaved PARP in each group. β-Actin was used as the loading control. (d) The densitometry analysis of each factor was performed in each group, normalized to the corresponding β-actin level. Data are presented as mean ± SEM of three independent experiments; $^{*}P < 0.05$, $^{**}P < 0.01$ compared with the control group; $^{\#}P < 0.05$, $^{\#\#}P < 0.01$ compared with the OA group.

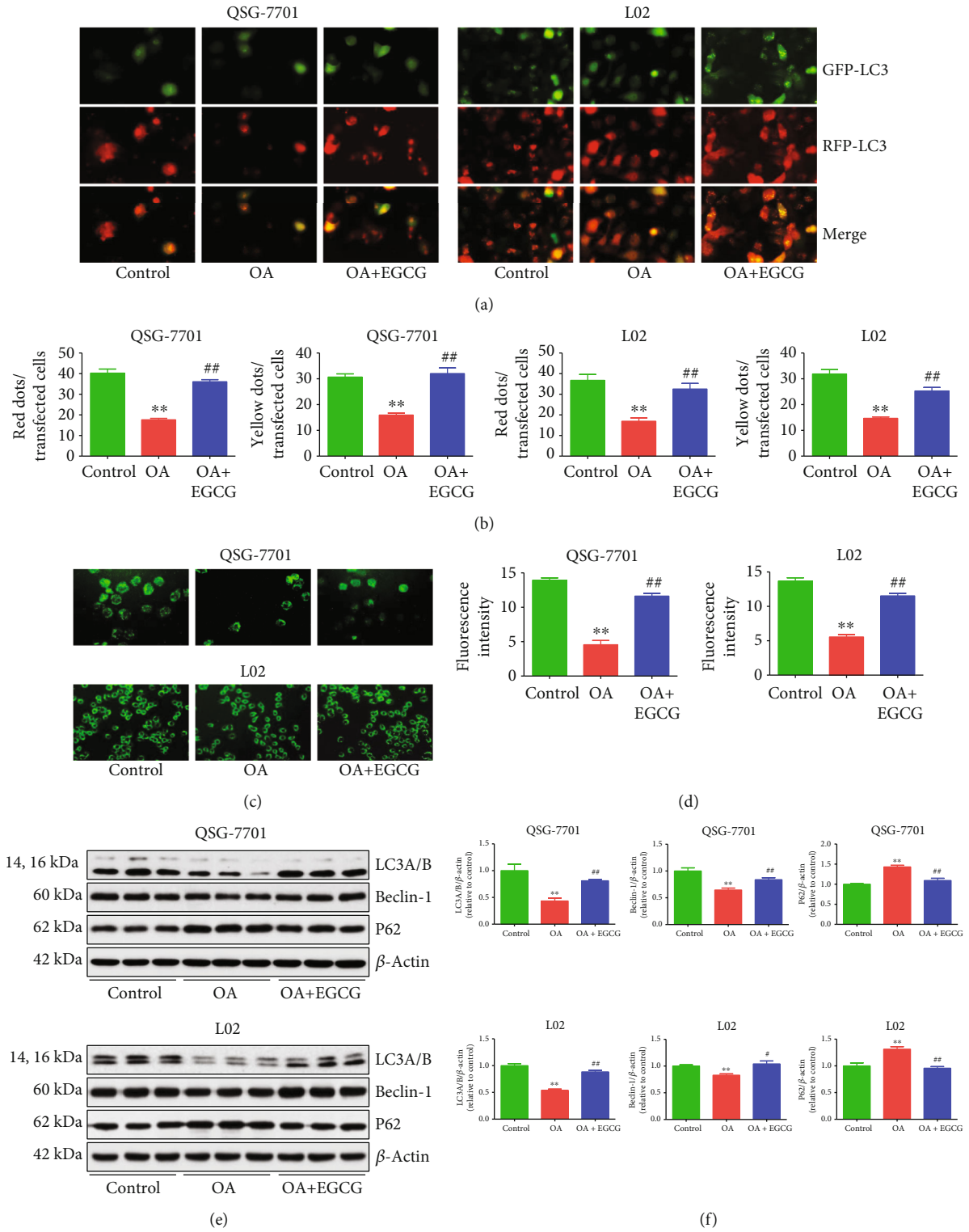

Figure 4: Effects of EGCG on the autophagy of OA-treated QSG-7701 and L02 cells. (a) GFP-RFP-LC3-transfected QSG-7701 and L02 cells were examined by fluorescence microscopy; original magnification ×1000. (b) The ratios of red and yellow dots to transfected cells were calculated. (c) Representative photographs of MDC staining. (d) The fluorescence intensity was analyzed. (e) Western blot analysis for the expression levels of LC3A/B, beclin-1, and P62 in each group. β-Actin was used as the loading control. (f) The densitometry analysis of each factor was performed in each group, normalized to the corresponding β-actin level. Data are presented as mean ± SEM of three independent experiments; $^{**}P < 0.01$ compared with the control group; $^{\#}P < 0.05$, $^{\#\#}P < 0.01$ compared with the OA group.

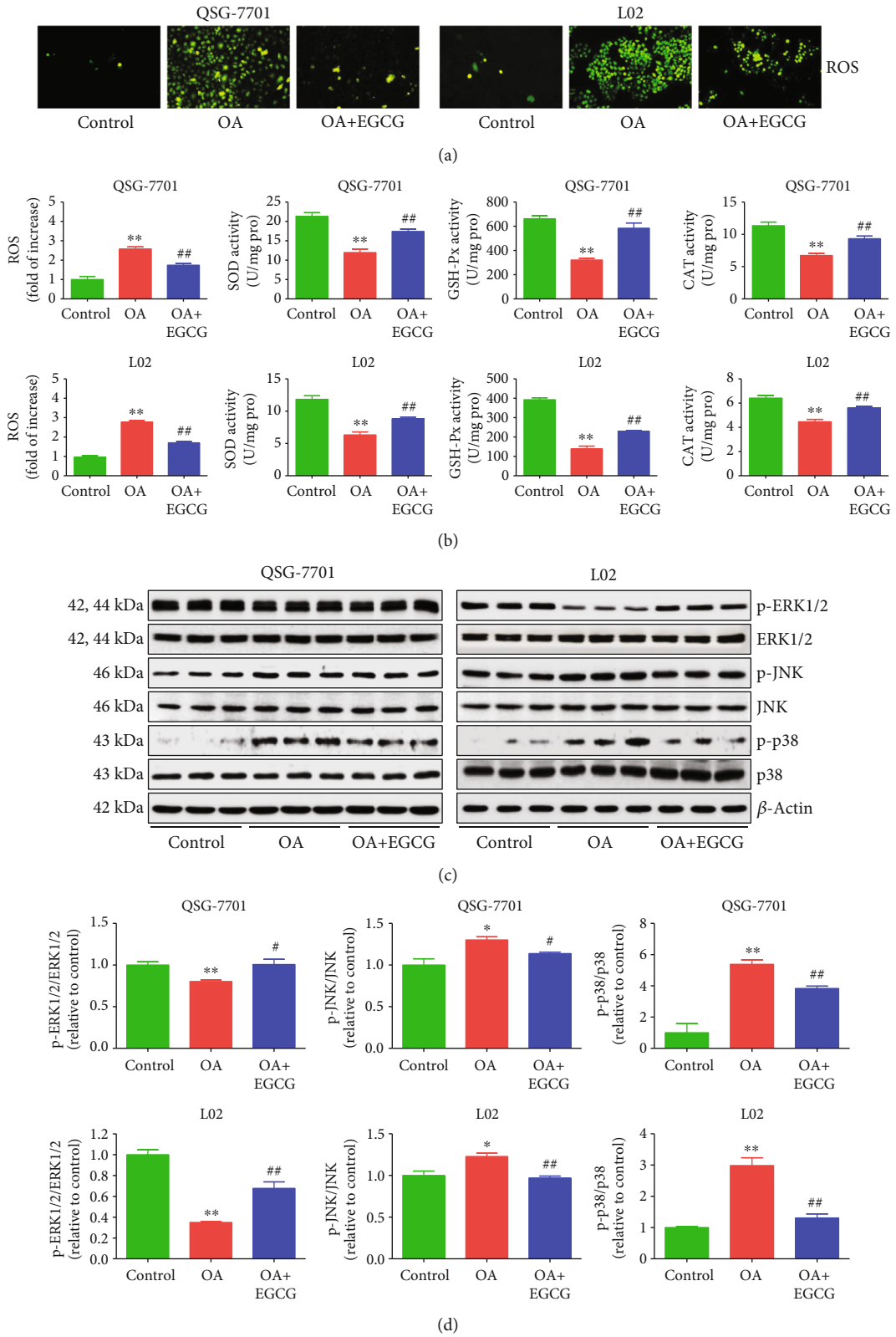

Figure 5: Effects of EGCG on the ROS/MAPK signaling pathway in OA-treated QSG-7701 and L02 cells. (a) The intracellular ROS production was detected using the fluorescent probe DCF-DA (shown in green; original magnification, ×400). (b) The intracellular ROS production and the activities of SOD, GSH-Px, and CAT were measured. (c) The protein expressions of ERK1/2, p-ERK1/2, JNK, p-JNK, p38, and p-p38 were analyzed by Western blot. β-Actin was used as the loading control. (d) The densitometry analysis of each factor was performed in each group, normalized to the corresponding β-actin level. Data are presented as mean ± SEM of three independent experiments; $^{*}P < 0.05$, $^{**}P < 0.01$ compared with the control group; $^{\#}P < 0.05$, $^{\#\#}P < 0.01$ compared with the OA group.

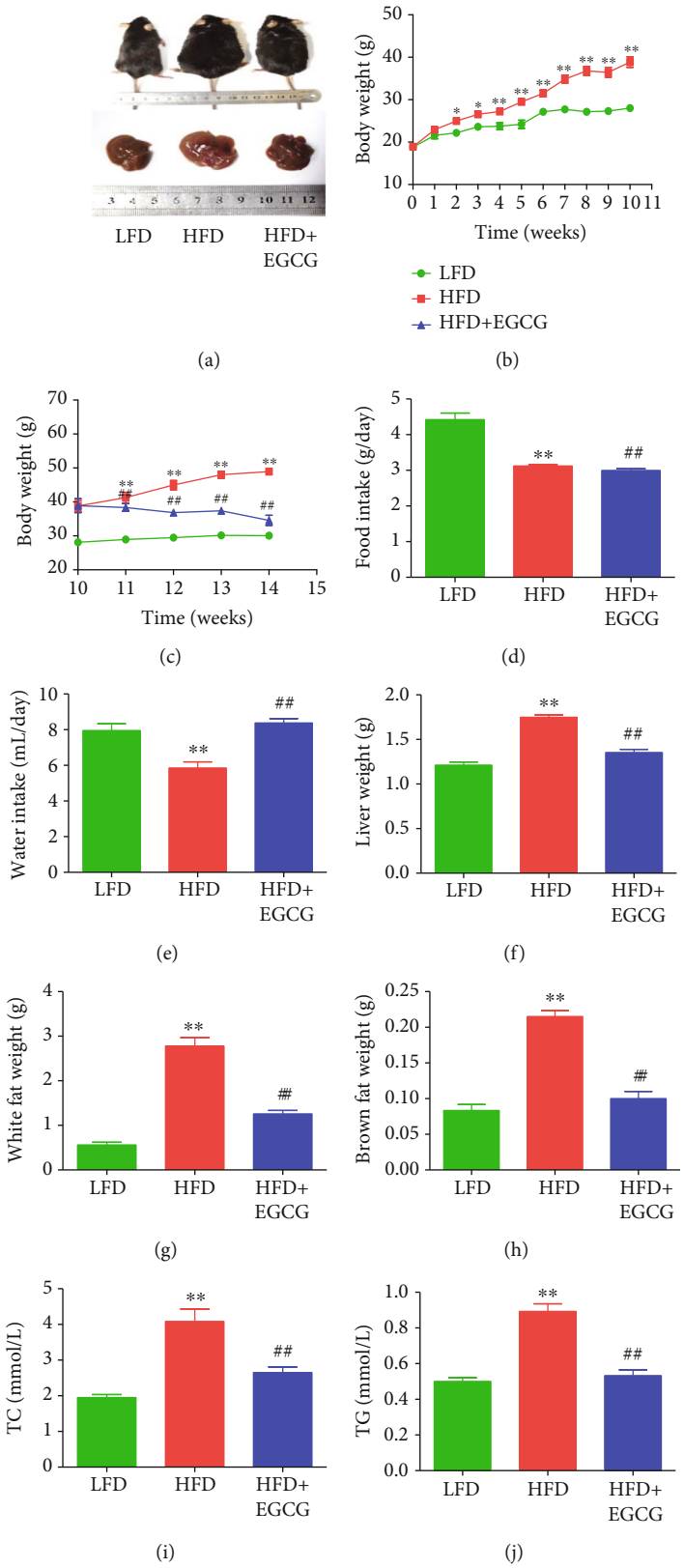

Figure 6: Continued.

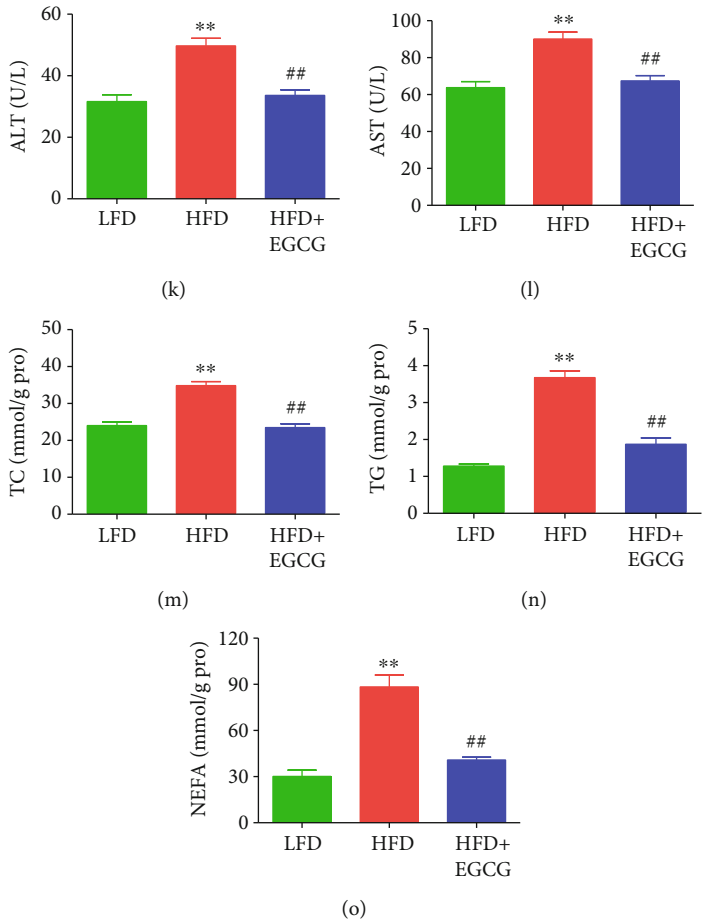

Figure 6: Effects of EGCG on HFD-induced NAFLD in mice. (a) Representative photographs of mice in each group. (b, c) The body weights of mice were measured. (d, e) Food intake and water intake were determined. (f–h) The liver weight, white fat weight, and brown fat weight were calculated. (i–l) The levels of TC, TG, ALT, and AST in the plasma of mice were detected. (m–o) The expression levels of TC, TG, and NEFA in the liver of mice were detected. Data are presented as mean ± SEM ($n = 6$). $^{*}P < 0.05$, $^{**}P < 0.01$ compared with the control group; $^{\#\#}P < 0.01$ compared with the OA group.

stimulating autophagic flux in liver cells and the mouse liver [57]. Our data showed that EGCG could increase autophagy in OA-treated liver cells, indicating that autophagic activation can serve as a potential therapeutic target for NAFLD.

It has been shown that low concentrations of intracellular ROS are necessary for many physiological roles including signal transduction and cell proliferation. Nevertheless, ROS overproduction can induce oxidative stress and cellular redox imbalance, thus ultimately affecting many cellular functions [41, 58]. Our data indicated that OA increased ROS levels and decreased the activities of GSH-Px, SOD, and CAT, which were consistent with the results of a previous study [59]. The effects were significantly reversed by the treatment with EGCG. In mammalian cells, three major types of MAP kinases are present: ERK, p38, and JNK, which are associated with EGCG interaction in the MAPK pathway [60, 61]. MAPK cascades play key roles in the progression of NAFLD, and elevation of ROS activates the MAPK pathway [38, 41, 62]. It has been revealed that intraperitoneal administration of EGCG (5 mg/kg) for 14 days inhibits phosphorylation of ERK, JNK, and p38 in animals with artificial unilateral ureteral obstruction [63]. Another study indicates that MAPK and hypoxia-inducible factor-1α are decreased after the treatment with EGCG, suggesting that EGCG could suppress MAPK-related oxidative stress [64]. A recent study has shown that EGCG can increase the expression levels of antioxidant enzymes, reverse the increase of ROS production, and regulate mitochondrial-involved autophagy [65]. Furthermore, EGCG could prevent αTC1-6 cells from H_2O_2-induced ROS production via the activation of Akt signaling and suppression of the p38 and JNK pathway [66]. In this study, OA upregulated the expression levels of p-JNK and p-p38 but downregulated the levels of p-ERK1/2. However, administration of EGCG remarkably reversed the levels of the proteins. Furthermore, the ROS/MAPK pathway is an important signaling cascade which can mediate the processes of apoptosis and autophagy in mammalian cells [67, 68]. In sum, the data suggest that EGCG can reduce apoptosis and induce autophagy possibly through the ROS/MAPK pathway in OA-treated liver cells.

In this study, a mouse model of HFD-induced NAFLD was used to imitate unhealthy dietary habits. Our results

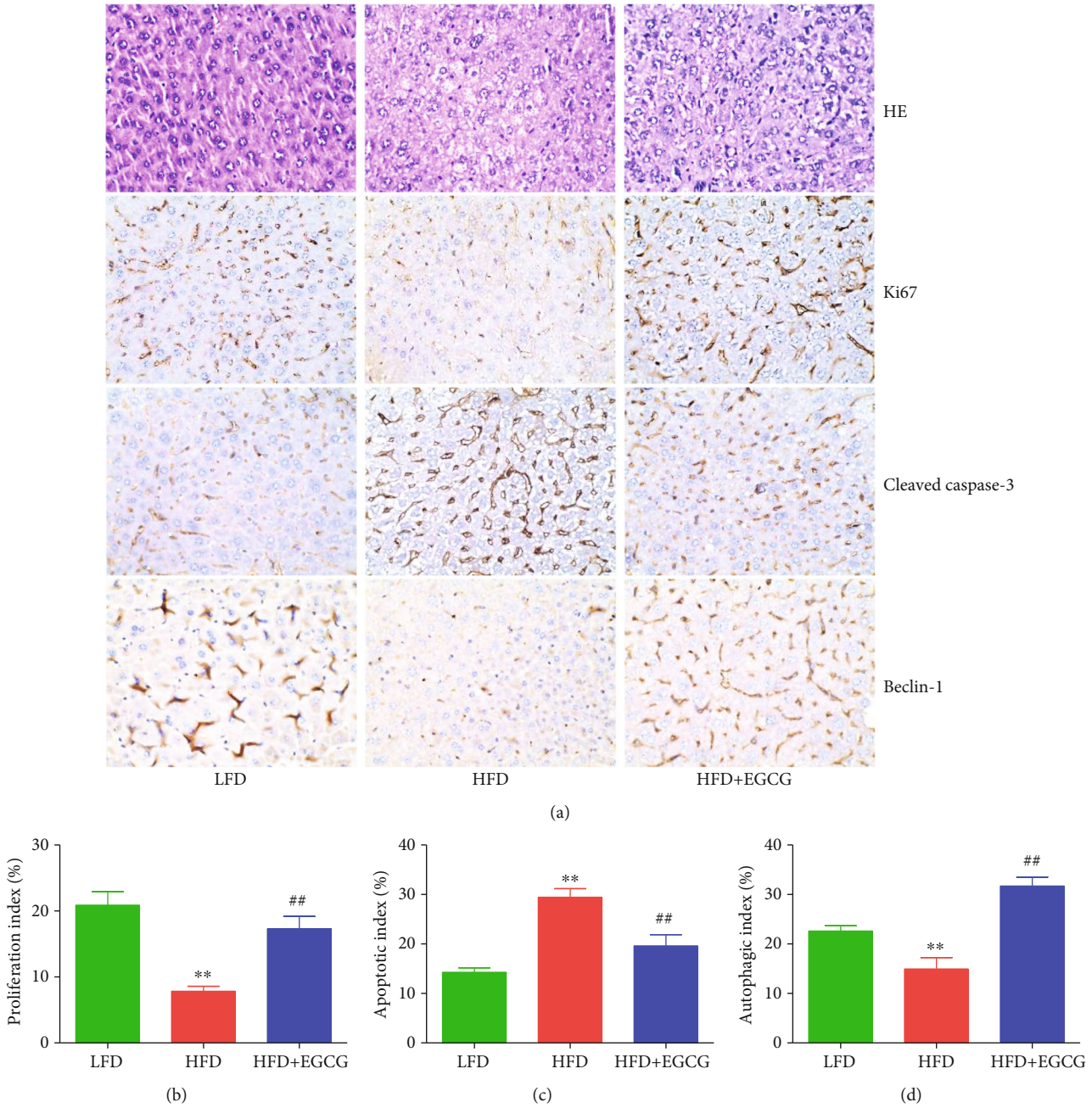

Figure 7: Effects of EGCG on the proliferation, apoptosis, and autophagy in liver tissues of the NAFLD mice. (a) Representative photographs of HE, Ki67, cleaved caspase-3, and beclin-1 staining in the liver of mice; original magnification ×400. (b–d) The proliferation index, apoptotic index, and autophagic index were calculated. Data are presented as mean ± SEM ($n = 3$). $^{**}P < 0.01$ compared with the control group; $^{\#\#}P < 0.01$ compared with the OA group.

suggested that HFD feeding induced obvious increases in body weight, liver weight, white fat weight, and brown fat weight, as well as the levels of TC, TG, ALT, and AST in the plasma of mice, indicating the successful establishment of the NAFLD model. It has been reported that NAFLD patients tend to have higher TC and TG levels [69]. EGCG markedly decreased the levels of TG and TC in both the plasma and the liver. Furthermore, ALT and AST are important indicators of liver damage in NAFLD [70]. Administration of EGCG significantly alleviated liver damage in HFD-fed mice by reducing ALT and AST levels. The flux of NEFA can be delivered to hepatocytes for TG synthesis, resulting in the development of NAFLD [71]. Treatment with EGCG decreased the level of NEFA in the liver of HFD-fed mice. Moreover, EGCG can increase the proliferation and autophagy but decrease the apoptosis in the liver of HFD-fed mice. The data together indicate that EGCG might alleviate HFD-induced NAFLD by inhibiting apoptosis and promoting autophagy.

In summary, our data suggest that EGCG can alleviate HFD-induced NAFLD through inhibition of apoptosis and promotion of autophagy possibly via the ROS/MAPK pathway. EGCG could be developed as an effective agent for the treatment of NAFLD.

Abbreviations

EGCG:	Epigallocatechin-3-gallate
NAFLD:	Nonalcoholic fatty liver disease
HFD:	High-fat diet
OA:	Oleic acid
DMEM:	Dulbecco's modified Eagle's medium
FBS:	Fetal bovine serum
BSA:	Bovine serum albumin
ORO:	Oil red O
EdU:	5-Ethynyl-2′-deoxyuridine
CCK-8:	Cell counting kit-8
PI:	Propidium iodide
GFP:	Green fluorescent protein
RFP:	Red fluorescent protein
MAP1LC3/LC3:	Microtubule-associated protein 1 light chain 3
MDC:	Monodansylcadaverine
ROS:	Reactive oxygen species
SOD:	Superoxide dismutase
CAT:	Catalase
GSH-Px:	Glutathione peroxidase
CDK:	Cyclin-dependent kinase
ERK1/2:	Extracellular signal-regulated protein kinase 1/2
p:	Phospho
JNK:	Jun N-terminal kinase
CST:	Cell Signaling Technology
Bcl-2:	B-cell lymphoma-2
Bax:	Bcl-2-associated X protein
Bcl-xl:	B-cell lymphoma-extra large
Bad:	Bcl-xl/Bcl-2-associated death promoter
PARP:	Poly-ADP-ribose polymerase
LFD:	Low-fat diet
TG:	Triglyceride
TC:	Total cholesterol
ALT:	Alanine aminotransferase
AST:	Aspartate aminotransferase
NEFA:	Nonesterified fatty acid
HE:	Hematoxylin and eosin
IHC:	Immunohistochemistry
MAPK:	Mitogen-activated protein kinase.

Data Availability

All data generated or analyzed in this study are included in this published article.

Ethical Approval

The animal experiment was approved by the Committee of Medical Ethics and Welfare for Experimental Animals of Henan University School of Medicine (HUSOM-2017-208).

Conflicts of Interest

The authors declare that there is no conflict of interests.

Authors' Contributions

D. W., Z. X., A. J., and Y. L. conceived and designed the experiments; Z. L., Y. W., Q. Z., J. L., and P. Z. performed the experiments and prepared the figures; and D. W. wrote the main manuscript text. All authors reviewed and approved the manuscript.

Acknowledgments

The study was supported by grants from the National Natural Science Foundation of China (Nos. 81802718, U1504817, and 81870591), the Foundation of Science & Technology Department of Henan Province, China (Nos. 202102310480, 182102310335, and 192102310151), the Training Program for Young Backbone Teachers of Institutions of Higher Learning in Henan Province, China (No. 2020GGJS038), and the Science Foundation for Young Talents of Henan University College of Medicine, China (No. 2019013).

References

[1] D. Wang, Y. Wei, T. Wang et al., "Melatonin attenuates (-)-epigallocatehin-3-gallate-triggered hepatotoxicity without compromising its downregulation of hepatic gluconeogenic and lipogenic genes in mice," *Journal of Pineal Research*, vol. 59, no. 4, pp. 497–507, 2015.

[2] R. Y. Gan, H. B. Li, Z. Q. Sui, and H. Corke, "Absorption, metabolism, anti-cancer effect and molecular targets of epigallocatechin gallate (EGCG): an updated review," *Critical Reviews in Food Science and Nutrition*, vol. 58, no. 6, pp. 924–941, 2018.

[3] H. S. Kim, M. J. Quon, and J. A. Kim, "New insights into the mechanisms of polyphenols beyond antioxidant properties; lessons from the green tea polyphenol, epigallocatechin 3-gallate," *Redox Biology*, vol. 2, pp. 187–195, 2014.

[4] J. Steinmann, J. Buer, T. Pietschmann, and E. Steinmann, "Anti-infective properties of epigallocatechin-3-gallate (EGCG), a component of green tea," *British Journal of Pharmacology*, vol. 168, no. 5, pp. 1059–1073, 2013.

[5] K. Liang, J. E. Chung, S. J. Gao, N. Yongvongsoontorn, and M. Kurisawa, "Highly augmented drug loading and stability of micellar nanocomplexes composed of doxorubicin and poly(ethylene glycol)-green tea catechin conjugate for cancer therapy," *Advanced Materials*, vol. 30, no. 14, article e1706963, 2018.

[6] K. Liang, K. H. Bae, F. Lee et al., "Self-assembled ternary complexes stabilized with hyaluronic acid-green tea catechin conjugates for targeted gene delivery," *Journal of Controlled Release*, vol. 226, pp. 205–216, 2016.

[7] S. J. Hyung, A. S. DeToma, J. R. Brender et al., "Insights into antiamyloidogenic properties of the green tea extract (-)-epigallocatechin-3-gallate toward metal-associated amyloid-β species," *Proceedings of the National Academy of Sciences*, vol. 110, no. 10, pp. 3743–3748, 2013.

[8] S. Chikara, L. D. Nagaprashantha, J. Singhal, D. Horne, S. Awasthi, and S. S. Singhal, "Oxidative stress and dietary

phytochemicals: role in cancer chemoprevention and treatment," *Cancer Letters*, vol. 413, pp. 122–134, 2018.

[9] R. Kanlaya and V. Thongboonkerd, "Protective effects of epigallocatechin-3-gallate from green tea in various kidney diseases," *Advances in Nutrition*, vol. 10, no. 1, pp. 112–121, 2019.

[10] J. E. Chung, S. Tan, S. J. Gao et al., "Self-assembled micellar nanocomplexes comprising green tea catechin derivatives and protein drugs for cancer therapy," *Nature Nanotechnology*, vol. 9, no. 11, pp. 907–912, 2014.

[11] L. G. Xiong, Y. J. Chen, J. W. Tong, Y. S. Gong, J. A. Huang, and Z. H. Liu, "Epigallocatechin-3-gallate promotes healthy lifespan through mitohormesis during early-to-mid adulthood in Caenorhabditis elegans," *Redox Biology*, vol. 14, pp. 305–315, 2018.

[12] Z. S. Liu, H. Cai, W. Xue et al., "G3BP1 promotes DNA binding and activation of cGAS," *Nature Immunology*, vol. 20, no. 1, pp. 18–28, 2019.

[13] N. Calland, A. Albecka, S. Belouzard et al., "(-)-Epigallocatechin-3-gallate is a new inhibitor of hepatitis C virus entry," *Hepatology*, vol. 55, no. 3, pp. 720–729, 2012.

[14] G. Targher and C. D. Byrne, "Non-alcoholic fatty liver disease: an emerging driving force in chronic kidney disease," *Nature Reviews. Nephrology*, vol. 13, no. 5, pp. 297–310, 2017.

[15] E. Vilar-Gomez, L. Calzadilla-Bertot, V. Wai-Sun Wong et al., "Fibrosis severity as a determinant of cause-specific mortality in patients with advanced nonalcoholic fatty liver disease: a multi-national cohort study," *Gastroenterology*, vol. 155, no. 2, pp. 443–457.e17, 2018.

[16] Z. M. Younossi, "Non-alcoholic fatty liver disease - a global public health perspective," *Journal of Hepatology*, vol. 70, no. 3, pp. 531–544, 2019.

[17] N. Kuzu, I. H. Bahcecioglu, A. F. Dagli, I. H. Ozercan, B. Ustündag, and K. Sahin, "Epigallocatechin gallate attenuates experimental non-alcoholic steatohepatitis induced by high fat diet," *Journal of Gastroenterology and Hepatology*, vol. 23, no. 8, pp. e465–e470, 2008.

[18] L. Gan, Z. J. Meng, R. B. Xiong et al., "Green tea polyphenol epigallocatechin-3-gallate ameliorates insulin resistance in non-alcoholic fatty liver disease mice," *Acta Pharmacologica Sinica*, vol. 36, no. 5, pp. 597–605, 2015.

[19] Y. Ding, X. Sun, Y. Chen, Y. Deng, and K. Qian, "Epigallocatechin gallate attenuated non-alcoholic steatohepatitis induced by methionine- and choline-deficient diet," *European Journal of Pharmacology*, vol. 761, pp. 405–412, 2015.

[20] S. Vidyashankar, R. Sandeep Varma, and P. S. Patki, "Quercetin ameliorate insulin resistance and up-regulates cellular antioxidants during oleic acid induced hepatic steatosis in HepG2 cells," *Toxicology In Vitro*, vol. 27, no. 2, pp. 945–953, 2013.

[21] T. Qiu, P. Pei, X. Yao et al., "Taurine attenuates arsenic-induced pyroptosis and nonalcoholic steatohepatitis by inhibiting the autophagic-inflammasomal pathway," *Cell Death & Disease*, vol. 9, no. 10, p. 946, 2018.

[22] D. Wu, J. Li, Q. Zhang et al., "Exogenous hydrogen sulfide regulates the growth of human thyroid carcinoma cells," *Oxidative Medicine and Cellular Longevity*, vol. 2019, no. 6927298, 18 pages, 2019.

[23] Y. Zhai, P. Lin, Z. Feng et al., "TNFAIP3-DEPTOR complex regulates inflammasome secretion through autophagy in ankylosing spondylitis monocytes," *Autophagy*, vol. 14, no. 9, pp. 1629–1643, 2018.

[24] Y. Wang, H. Nie, X. Zhao, Y. Qin, and X. Gong, "Bicyclol induces cell cycle arrest and autophagy in HepG2 human hepatocellular carcinoma cells through the PI3K/AKT and Ras/Raf/MEK/ERK pathways," *BMC Cancer*, vol. 16, no. 1, p. 742, 2016.

[25] Y. Yuan, D. Ding, N. Zhang et al., "TNF-α induces autophagy through ERK1/2 pathway to regulate apoptosis in neonatal necrotizing enterocolitis model cells IEC-6," *Cell Cycle*, vol. 17, no. 11, pp. 1390–1402, 2018.

[26] Y. Xie, S. Li, L. Sun et al., "Fungal immunomodulatory protein from Nectria haematococca suppresses growth of human lung adenocarcinoma by inhibiting the PI3K/Akt pathway," *International Journal of Molecular Sciences*, vol. 19, no. 11, p. 3429, 2018.

[27] Q. Shen, J. W. Eun, K. Lee et al., "Barrier to autointegration factor 1, procollagen-lysine, 2-oxoglutarate 5-dioxygenase 3, and splicing factor 3b subunit 4 as early-stage cancer decision markers and drivers of hepatocellular carcinoma," *Hepatology*, vol. 67, no. 4, pp. 1360–1377, 2018.

[28] P. Pitchakarn, S. Suzuki, K. Ogawa et al., "Induction of G1 arrest and apoptosis in androgen-dependent human prostate cancer by Kuguacin J, a triterpenoid from Momordica charantia leaf," *Cancer Letters*, vol. 306, no. 2, pp. 142–150, 2011.

[29] M. Chen, X. Wang, D. Zha et al., "Apigenin potentiates TRAIL therapy of non-small cell lung cancer _via_ upregulating DR4/DR5 expression in a p53-dependent manner," *Scientific Reports*, vol. 6, no. 1, article 35468, 2016.

[30] S. M. Man and T. D. Kanneganti, "Converging roles of caspases in inflammasome activation, cell death and innate immunity," *Nature Reviews. Immunology*, vol. 16, no. 1, pp. 7–21, 2016.

[31] D. Wu, W. Tian, J. Li et al., "Peptide P11 suppresses the growth of human thyroid carcinoma by inhibiting the PI3K/AKT/mTOR signaling pathway," *Molecular Biology Reports*, vol. 46, no. 3, pp. 2665–2678, 2019.

[32] J. Li, R. Zhu, K. Chen et al., "Potent and specific Atg8-targeting autophagy inhibitory peptides from giant ankyrins," *Nature Chemical Biology*, vol. 14, no. 8, pp. 778–787, 2018.

[33] L. Galluzzi, E. H. Baehrecke, A. Ballabio et al., "Molecular definitions of autophagy and related processes," *The EMBO Journal*, vol. 36, no. 13, pp. 1811–1836, 2017.

[34] S. Lépine, J. C. Allegood, M. Park, P. Dent, S. Milstien, and S. Spiegel, "Sphingosine-1-phosphate phosphohydrolase-1 regulates ER stress-induced autophagy," *Cell Death and Differentiation*, vol. 18, no. 2, pp. 350–361, 2011.

[35] D. J. Klionsky, K. Abdelmohsen, A. Abe et al., "Guidelines for the use and interpretation of assays for monitoring autophagy (3rd edition)," *Autophagy*, vol. 12, no. 1, pp. 1–222, 2016.

[36] D. Y. Wang, Y. Hong, Y. G. Chen et al., "PEST-containing nuclear protein regulates cell proliferation, migration, and invasion in lung adenocarcinoma," *Oncogene*, vol. 8, no. 3, p. 22, 2019.

[37] B. Nuvoli, E. Camera, A. Mastrofrancesco, S. Briganti, and R. Galati, "Modulation of reactive oxygen species via ERK and STAT3 dependent signalling are involved in the response of mesothelioma cells to exemestane," *Free Radical Biology & Medicine*, vol. 115, pp. 266–277, 2018.

[38] G. Y. Zhang, D. Lu, S. F. Duan et al., "Hydrogen sulfide alleviates lipopolysaccharide-induced diaphragm dysfunction in rats by reducing apoptosis and inflammation through ROS/-MAPK and TLR4/NF-κB signaling pathways," *Oxidative*

Medicine and Cellular Longevity, vol. 2018, no. 9647809, 15 pages, 2018.

[39] C. Y. Li, H. S. Hao, Y. H. Zhao et al., "Melatonin improves the fertilization capacity of sex-sorted bull sperm by inhibiting apoptosis and increasing fertilization capacitation via MT1," *International Journal of Molecular Sciences*, vol. 20, no. 16, p. 3921, 2019.

[40] Z. Zhang, Z. Ren, S. Chen et al., "ROS generation and JNK activation contribute to 4-methoxy-TEMPO-induced cytotoxicity, autophagy, and DNA damage in HepG2 cells," *Archives of Toxicology*, vol. 92, no. 2, pp. 717–728, 2018.

[41] D. Wu, N. Luo, L. Wang et al., "Hydrogen sulfide ameliorates chronic renal failure in rats by inhibiting apoptosis and inflammation through ROS/MAPK and NF-κB signaling pathways," *Scientific Reports*, vol. 7, no. 1, p. 455, 2017.

[42] Z. Liu, J. Wang, C. Guo, and X. Fan, "MicroRNA-21 mediates epithelial-mesenchymal transition of human hepatocytes via PTEN/Akt pathway," *Biomedicine & Pharmacotherapy*, vol. 69, pp. 24–28, 2015.

[43] D. Wu, M. Li, W. Tian et al., "Hydrogen sulfide acts as a double-edged sword in human hepatocellular carcinoma cells through EGFR/ERK/MMP-2 and PTEN/AKT signaling pathways," *Scientific Reports*, vol. 7, no. 1, p. 5134, 2017.

[44] Q. Chu, S. Zhang, M. Chen et al., "Cherry anthocyanins regulate NAFLD by promoting autophagy pathway," *Oxidative Medicine and Cellular Longevity*, vol. 2019, no. 4825949, 16 pages, 2019.

[45] Y. Liu, Y. Cheng, J. Li, Y. Wang, and Y. Liu, "Epoxy stearic acid, an oxidative product derived from oleic acid, induces cytotoxicity, oxidative stress, and apoptosis in HepG2 cells," *Journal of Agricultural and Food Chemistry*, vol. 66, no. 20, pp. 5237–5246, 2018.

[46] R. Singh, A. Letai, and K. Sarosiek, "Regulation of apoptosis in health and disease: the balancing act of BCL-2 family proteins," *Nature Reviews. Molecular Cell Biology*, vol. 20, no. 3, pp. 175–193, 2019.

[47] D. Wu, W. Si, M. Wang, S. Lv, A. Ji, and Y. Li, "Hydrogen sulfide in cancer: friend or foe?," *Nitric Oxide*, vol. 50, pp. 38–45, 2015.

[48] D. Wu, Y. Gao, Y. Qi, L. Chen, Y. Ma, and Y. Li, "Peptide-based cancer therapy: opportunity and challenge," *Cancer Letters*, vol. 351, no. 1, pp. 13–22, 2014.

[49] Q. Dong, B. Yang, J. G. Han et al., "A novel hydrogen sulfide-releasing donor, HA-ADT, suppresses the growth of human breast cancer cells through inhibiting the PI3K/AKT/mTOR and Ras/Raf/MEK/ERK signaling pathways," *Cancer Letters*, vol. 455, pp. 60–72, 2019.

[50] L. Pang, K. Liu, D. Liu et al., "Differential effects of reticulophagy and mitophagy on nonalcoholic fatty liver disease," *Cell Death & Disease*, vol. 9, no. 2, p. 90, 2018.

[51] T. P. Patel, K. Rawal, S. Soni, and S. Gupta, "Swertiamarin ameliorates oleic acid induced lipid accumulation and oxidative stress by attenuating gluconeogenesis and lipogenesis in hepatic steatosis," *Biomedicine & Pharmacotherapy*, vol. 83, pp. 785–791, 2016.

[52] D. Wu, H. Wang, T. Teng, S. Duan, A. Ji, and Y. Li, "Hydrogen sulfide and autophagy: a double edged sword," *Pharmacological Research*, vol. 131, pp. 120–127, 2018.

[53] A. J. Clarke and A. K. Simon, "Autophagy in the renewal, differentiation and homeostasis of immune cells," *Nature Reviews. Immunology*, vol. 19, no. 3, pp. 170–183, 2019.

[54] A. González-Rodríguez, R. Mayoral, N. Agra et al., "Impaired autophagic flux is associated with increased endoplasmic reticulum stress during the development of NAFLD," *Cell Death & Disease*, vol. 5, no. 4, article e1179, 2014.

[55] L. Zhang, Z. Yao, and G. Ji, "Herbal extracts and natural products in alleviating non-alcoholic fatty liver disease via activating autophagy," *Frontiers in Pharmacology*, vol. 9, p. 1459, 2018.

[56] T. Ueno and M. Komatsu, "Autophagy in the liver: functions in health and disease," *Nature Reviews. Gastroenterology & Hepatology*, vol. 14, no. 3, pp. 170–184, 2017.

[57] J. Zhou, B. L. Farah, R. A. Sinha et al., "Epigallocatechin-3-gallate (EGCG), a green tea polyphenol, stimulates hepatic autophagy and lipid clearance," *PLoS One*, vol. 9, no. 1, article e87161, 2014.

[58] H. Cui, S. Wu, Y. Shang et al., "Pleurotus nebrodensis polysaccharide (PN50G) evokes A549 cell apoptosis by the ROS/AMPK/PI3K/AKT/mTOR pathway to suppress tumor growth," *Food & Function*, vol. 7, no. 3, pp. 1616–1627, 2016.

[59] H. Su, Y. Li, D. Hu et al., "Procyanidin B2 ameliorates free fatty acids-induced hepatic steatosis through regulating TFEB-mediated lysosomal pathway and redox state," *Free Radical Biology & Medicine*, vol. 126, pp. 269–286, 2018.

[60] J. S. Arthur and S. C. Ley, "Mitogen-activated protein kinases in innate immunity," *Nature Reviews Immunology*, vol. 13, no. 9, pp. 679–692, 2013.

[61] M. Sharifi-Rad, R. Pezzani, M. Redaelli et al., "Preclinical pharmacological activities of epigallocatechin-3-gallate in signaling pathways: an update on cancer," *Molecules*, vol. 25, no. 3, p. 467, 2020.

[62] X. Shen, H. Guo, J. Xu, and J. Wang, "Inhibition of lncRNA HULC improves hepatic fibrosis and hepatocyte apoptosis by inhibiting the MAPK signaling pathway in rats with nonalcoholic fatty liver disease," *Journal of Cellular Physiology*, vol. 234, no. 10, pp. 18169–18179, 2019.

[63] Y. Wang, N. Liu, X. Bian et al., "Epigallocatechin-3-gallate reduces tubular cell apoptosis in mice with ureteral obstruction," *The Journal of Surgical Research*, vol. 197, no. 1, pp. 145–154, 2015.

[64] J. Chen, J. Xu, J. Li et al., "Epigallocatechin-3-gallate attenuates lipopolysaccharide-induced mastitis in rats via suppressing MAPK mediated inflammatory responses and oxidative stress," *International Immunopharmacology*, vol. 26, no. 1, pp. 147–152, 2015.

[65] E. Casanova, J. Salvadó, A. Crescenti, and A. Gibert-Ramos, "Epigallocatechin gallate modulates muscle homeostasis in type 2 diabetes and obesity by targeting energetic and redox pathways: a narrative review," *International Journal of Molecular Sciences*, vol. 20, no. 3, p. 532, 2019.

[66] T. Cao, X. Zhang, D. Yang et al., "Antioxidant effects of epigallocatechin-3-gallate on the aTC1-6 pancreatic alpha cell line," *Biochemical and Biophysical Research Communications*, vol. 495, no. 1, pp. 693–699, 2018.

[67] K. Wang, B. Chen, T. Yin et al., "N-Methylparoxetine blocked autophagic flux and induced apoptosis by activating ROS-MAPK pathway in non-small cell lung cancer cells," *International Journal of Molecular Sciences*, vol. 20, no. 14, p. 3415, 2019.

[68] Y. Liu and D. Fan, "Ginsenoside Rg5 induces G2/M phase arrest, apoptosis and autophagy via regulating ROS-mediated MAPK pathways against human gastric cancer," *Biochemical Pharmacology*, vol. 168, pp. 285–304, 2019.

[69] X. Zheng, L. Gong, R. Luo et al., "Serum uric acid and non-alcoholic fatty liver disease in non-obesity Chinese adults," *Lipids in Health and Disease*, vol. 16, no. 1, p. 202, 2017.

[70] M. Lazo, J. Rubin, J. M. Clark et al., "The association of liver enzymes with biomarkers of subclinical myocardial damage and structural heart disease," *Journal of Hepatology*, vol. 62, no. 4, pp. 841–847, 2015.

[71] H. S. Jeong, K. H. Kim, I. S. Lee et al., "Ginkgolide A ameliorates non-alcoholic fatty liver diseases on high fat diet mice," *Biomedicine & Pharmacotherapy*, vol. 88, pp. 625–634, 2017.